The Stabilisation of Low-Coordinate and Heteroleptic Transition Metal Complexes

Gareth Ashworth, MSci (Hons)

Thesis submitted to the University of Nottingham for the degree of

Doctor of Philosophy

June 2018

Declaration

The work in this thesis was carried out at the University of Nottingham between October 2014 and June 2018, under the supervision of Dr Deborah L. Kays. All the work is my own unless stated to the contrary and has not been previously submitted for any degree at this or any other university.

Gareth Ashworth

Abstract

Since the middle of the last decade, many *m*-terphenyl *d*-block complexes have been reported in the literature. Some of these have been shown to possess the qualities of single molecule magnets whilst others have been applied in the activation of small molecules and as catalysts in organic and inorganic transformations. Heteroleptic, *m*-terphenyl, *d*-block complexes are underrepresented in the literature, despite the potential such complexes could have in the applications detailed above.

In the development, described herein, of reliable synthetic and purification procedures toward heteroleptic, transition metal complexes a range of previously reported *m*-terphenyl ligands has been utilised. In some instances, attempts have been made to combine these ligands with N-heterocyclic carbene ligands such as 1,3-diisopropyl-4,5-dimethylimidazol-2-ylidene (IPrMe) and 1,3-bis(2,6-diisopropylphenyl)imidazol-2-ylidene (IPr).

A series of *d*-block and Group 12 complexes bearing one *m*-terphenyl or NHC ligand and a halide has been synthesised and have been characterised in the solid state and in solution. These Grignard analogues have been developed as intermediates in the multistep synthesis of heteroleptic complexes.

The complexes [2,6-$Ar_2C_6H_3$]Hg[2,6-$Ar^*_2C_6H_3$] (Ar = 2,6-Xyl, Pmp or Dcp; Ar* = Mes or Tmp) have been synthesised, utilising [2,6-$Ar^*_2C_6H_3$]HgBr as an intermediate. The diamagnetic nature of mercury(II) allowed study using NMR techniques. ^{1}H NMR spectroscopy suggests that the opposing ligands interact through space. Application of the synthetic route developed to other *d*-block and Group 12 metals affords [2,6-$Dcp_2C_6H_3$]M[2,6-$Mes_2C_6H_3$] (M = Mn and Zn) in low yields. The homoleptic by-products isolated through from the synthesis of these latter complexes and attempt synthesis of others indicates that ligand

exchange occurs over the course of the reaction. This was confirmed through the study of reactions towards heteroleptic cadmium complexes using ^{1}H and ^{113}Cd NMR spectroscopy.

Complexes of the type [2,6-$Dcp_2C_6H_3$]M[2,6-$Mes_2C_6H_3$] (M = Fe and Co) could not be isolated in our hands. Attempts to isolate the homoleptic complexes [2,6-$Dcp_2C_6H_3$]$_2$M (M = Mn, Fe or Co) result in the desired [2,6-$Dcp_2C_6H_3$]$_2$Mn (M = Mn), the biphenylene 1-[2,6-$Dcp_2C_6H_3$]-7-$DcpC_{12}H_6$ (M = Fe) and the Grignard analogue [2-{2,6-($Dcp_2C_6H_3$)$_2$$C_6H_3$}-6-$DcpC_6H_3$]CoBr (M = Co). These results demonstrate that iron and cobalt halides are able to couple the aryl halide flanking groups to the central lithium aryl of the ligand precursor.

A series of metal(I) complexes, supported by one *m*-terphenyl ligand and one NHC ligand has been envisioned. It was hoped that this ligand system would alleviate the issues caused by the exchange of *m*-terphenyl ligands in the reaction mixture. To this end, complexes of the type [(2,6-$Ar_2C_6H_3$)MX(IPrMe)]$_n$ (Ar = Mes, n = 2, M = Mn; Ar = Mes, n = 1, Fe, Co, Zn, Cd, Hg; Ar = Dipp, n = 1, M = Fe, Co, Zn) have been developed. The reaction between [2,6-$Dipp_2C_6H_3$]CoBr[PrMe] and KC_8 affords the heteroleptic, two-coordinate cobalt(I) complex [2,6-$Dipp_2C_6H_3$]CoBr[PrMe], the first such complex stabilised by two different ligands binding through a carbon. Studies of the complex using Evans' NMR techniques demonstrate that this complex possessed a magnetic moment at room temperature that is significantly higher than the value of the spin only d^8 ion.

Preliminary investigations into the ability of the complexes disclosed in this work to promote small molecule reactivity have been conducted and the results are discussed herein.

Acknowledgements

I wish to thank my supervisor Dr Deborah Kays for giving me the opportunity to work under her guidance for the last four years. I will always be grateful for her patience, willingness to pass on knowledge and magnanimity when Wales beat England at rugby. Thanks must also go to Prof. Neil Champness for his supervision during Dr Kays' maternity leave.

I would like to express my gratitude to Dr Ana Geer for her encouragement and advice throughout this project. Ana's tireless enthusiasm for chemistry and life improves the world for all those who meet her. I would also like to thank Dr Toby Blundell, who laid the groundwork for this project, Dr Allie Gower. I am also indebted to Grace Lowe for helping me with electrochemical analysis. Dr William Lewis has made a huge contribution to this work, not only through trying to teach me the dark arts of crystallography, but by being making me answer the difficult questions. I would like to thank him for this contribution.

Several project students have been involved in the work described in this thesis, namely Yu Liu, Andrew Smith, Jessica Dove and Jennifer Grist. I would like to thank them for their help over the course of this project. I would also like to thank Olivia Churchill for continuing this work in her research project: I wish her the best of luck for the future.

This project would not have got far without the support of the technical staff at the University of Nottingham; Dr Adriene Davis, Shazad Aslam and Kevin Butler for NMR, Dr Mick Cooper and Ben Pointer-Gleadhill for mass spectrometry, and Dr Sandy Blake and Dr William Lewis for X-ray crystallography, Tong Liu from the University of Nottingham and Stephen Boyer from London Metropolitan University for running elemental analysis. I wish to thank them all for their contribution. I would also like to thank Mark Guyler for keeping the lab working and always being willing to solve an unsolvable problem.

I would like to extend my gratitude to all the members of the Kays group, past and present, who have filled the last four years with laughter and fond memories. In particular, Dr Helen Sharpe who taught me how to use a Schlenk line and put up with me thinking that I knew better than her, Dr Alex Reid who has made me fear for my life on several occasions, Charlotte Gidman for her relentless friendship and Rob Nolla for his advice and camaraderie.

I would like to thank my friends and family for their support over at least the last four years if not longer. In particular, I would like to thank Thomas Clarke and Edward Anderson for the laughter, Ben Jones and Jasmin Ashworth for being inspirational, and Heather and Tony Ashworth for their constant support.

Finally, I would like to thank Isabel Cope, now Isabel Ashworth. Her support is unyielding, her proof reading is ruthless, her love is priceless, and her decision to marry me whilst I was still preparing this thesis was foolish. I love her with all of my heart.

Contents

Declaration....2
Abstract....3
Acknowledgements....5
Contents....7
Abbreviations....11
Characterised Complexes....13
Chapter I - Introduction....18
1.1 Organometallic Chemistry....18
1.2 Early Developments in Low-Coordinate, Transition Metal Chemistry....20
1.2.1 Aryl Ligand Systems....23
1.3 Sterically Bulky Ligand Systems: 1996 Onwards....26
1.3.1 *m*-Terphenyl Chemistry....28
1.3.2 Low-Coordinate, *m*-Terphenyl Complexes....30
1.3.3 N-Heterocyclic Carbene Chemistry....32
1.3.4 N-Heterocyclic Carbene Chemistry of First Row Transition Metals....35
1.4 Applications of Low-Coordinate, Transition Metal Complexes....46
1.4.1 Reactivity….....46
1.4.2 Single Molecule Magnetism....56
1.5 Global Aims....59
Chapter II - A Study of *m*-Terphenyl and N-Heterocyclic Carbene, Halide-Bridged Complexes....62
2.1 Introduction....62
2.2 Aims....68
2.3 Results and Discussion....70
2.3.1 N-Heterocyclic Carbene Complexes....70
2.3.2 *m*-Terphenyl Complexes....86
2.3.2.1 Transition Metal Complexes....87
2.3.2.2 Group 12 Complexes....104
2.4 Conclusions….....113
2.5 Future Work....114
2.6 General Experimental....115
2.6.1 Glove Box and Schlenk Line Techniques....115
2.6.2 Analytical Measurments....116

2.6.3 Preparation and Purification of solvents and reagents....119
2.6.4 Preparation of Pro-Ligands....120
2.7 Synthetic Experimental....123
2.7.1 $[(IPrMe)CoBr_2]_2$ **II.30**....123
2.7.2 $[(IPrMe)ZnCl_2]_2$ **II·31**....123
2.7.3 $[IPrMe]_2CoBr_2$ **II·32**....124
2.7.4 $[IPrMe]_2NiBr_2$ **II·34**....125
2.7.5 $[IPrMe]_2CuCl$ **II·35**....125
2.7.6 $[IPrMe]_2ZnCl_2$ **II·33**....126
2.7.7 $[2,6\text{-}Dipp_2C_6H_3MBr]_2\cdot[LiBr(OEt_2)]_2$ [M = Mn (**II·36**), Co (**II·37**)]....126
2.7.8 $[2,6\text{-}Mes_2C_6H_3MBr]_2\cdot[LiBr(OEt_2)]_2$ [M = Mn (**II·38**), Fe (**II·39**), Co (**II·40**)]....127
2.7.9 $[2,6\text{-}Mes_2C_6H_3ZnCl]_2$ **II·41**....128
2.7.10 $[2,6\text{-}Mes_2C_6H_3CdCl]_3LiCl(Et_2O)$ **II·42**....129
2.7.11 $[2,6\text{-}Mes_2C_6H_3]HgBr$ **II·43**....130
2.5.12 $[2,6\text{-}Tmp_2C_6H_3]HgBr$ **II·44**....131
Chapter III – A Heteroleptic *m*-Terphenyl Complexes....132
3.1 Introduction....132
3.1.1 Heteroleptic Aryl Complexes....132
3.1.2 Halogenated *m*-Terphenyl Complexes....136
3.2 Aims....141
3.3 Results and Discussion....142
3.3.1 Mercury Complexes....142
3.3.2 Ligand Exchange....153
3.3.3 Ligand Exchange Studies....155
3.3.4 $[2,6\text{-}Dcp_2C_6H_3]^-$ Heteroleptic Products....162
3.3.5 $[2,6\text{-}Dcp_2C_6H_3]^-$ Homoleptic Products....166
3.4 Conclusions....181
3.5 Future Work....183
3.6 Experimental....185
3.6.1 Heteroleptic, Diaryl Complexes....185
3.6.1.1 $[2,6\text{-}Tmp_2C_6H_3]Hg[2,6\text{-}Ar_2C_6H_3]$ Ar = Pmp (**III·21**), 2,6-Xyl (**III·22**), Dcp (**III·23**)....185

3.6.1.2 [2,6-$Mes_2C_6H_3$]Hg[2,6-$Pmp_2C_6H_3$] **III·24**.....187
3.6.1.3 [2,6-$Dcp_2C_6H_3$]M[2,6-$Mes_2C_6H_3$] [M = Mn (**III·30**), Zn (**III·31**)].....187
3.6.2 Scrambling Experiments.....189
3.6.2.1 [2,6-$Mes_2C_6H_3$]$_2$Cd **III·32**.....189
3.6.2.2 [2,6-$Dipp_2C_6H_3$]$_2$Cd **III·33**.....190
3.6.2.3 [2,6-$Mes_2C_6H_3$]Cd[2,6-$Dipp_2C_6H_3$].....190
3.6.2.4 [2,6-$Mes_2C_6H_3$]$_2$Cd + [2,6-$Pmp_2C_6H_3$]$_2$Cd 190
3.6.2.5 [2,6-$Pmp_2C_6H_3$]$_2$Cd + [2,6-$Mes_2C_6H_3Li$]$_2$Cd 191
3.6.3 [2,6-$Dcp_2C_6H_3$]$^-$ Complexes.....191
3.6.3.1 [2,6-$Dcp_2C_6H_3$]$_2$Mn **III·35**.....191
3.6.3.2 1-[2,6-$Dcp_2C_6H_3$]-7-Dcp$C_{12}H_6$ **III·36**.....192
3.6.3.3 [2-{2,6-($Dcp_2C_6H_3$)$_2$$C_6H_3$}-6-Dcp$C_6H_3$]CoBr **III·37**.....194
Chapter IV - The Development of Heteroleptic Complexes Stabilised by *m*-Terphenyl and N-Heterocyclic Carbene Ligands.....195
4.1 Introduction.....195
4.2 Aims.....201
4.3 Results and Discussion.....202
4.3.1 [2,6-$Mes_2C_6H_3$]$^-$ Group 12 Complexes.....202
4.3.2 [2,6-$Mes_2C_6H_3$]$^-$ Transition Metal Complexes.....211
4.3.3 Attempted Reductions of [2,6-$Mes_2C_6H_3$]MX[IPrMe] [MX = ZnCl (**IV·10**), FeCl (**IV·14**) and CoBr (**IV·15**)].....220
4.3.4 [2,6-$Dipp_2C_6H_3$]$^-$ Complexes.....223
4.3.5 Two Coordinate, Heteroleptic, Transition Metal Complexes.....232
4.3.6 IPr Complexes.....240
4.3.7 Small Molecule Activation with Mixed Ligand Species.....245
4.4 Conclusions.....249
4.5 Future Work.....251
4.6 Experimental.....254
4.6.1 [2,6-$Mes_2C_6H_3$]ZnCl[IPrMe] **IV·10**.....254
4.6.2 [2,6-$Mes_2C_6H_3$]CdCl[IPrMe] **IV·11**.....255
4.6.3 [2,6-$Mes_2C_6H_3$]HgBr[IPrMe] **IV·12**.....256
4.6.4 [2,6-$Dipp_2C_6H_3$]ZnCl[IPrMe] **IV·19**.....257
4.6.5 [(2,6-$Mes_2C_6H_3$)MnBr(IPrMe)]$_2$ **IV·13**.....257

4.6.6 [2,6-$Ar_2C_6H_3$]FeX[IPrMe] [Ar = Mes, X = Br (**IV·14**) or Ar = Dipp, X = Cl (**IV·16**)] 258
4.6.7 [2,6-$Ar_2C_6H_3$]CoBr[IPrMe] [Ar = Mes (**IV·15**) or Dipp (**IV·18**)].....259
4.6.9 $[(IPrMe)_2Fe(\mu_3\text{-}O)]_2[(2,6\text{-}Mes_2C_6H_3)_2Fe(\mu_3\text{-}O)]_2Fe$ **IV·16**.....261
4.6.9 [2,6-$Dipp_2C_6H_3$]Co[IPrMe] **IV·20**.....261
4.6.10 Attempted Synthesis of [2,6-$Mes_2C_6H_3$]MBr[IPr] [M = Fe (**IV·24**),Co (**IV·25**)].....262
4.6.11 Hydrosilylation of Phenylacetylene Promoted by [2,6-$Dipp_2C_6H_3$]ZnCl[IPrMe] **IV·26**.....262
4.6.12 Synthesis of 1,3-diphenyl-5-(hexa-ylidene)imidazolidine-2,4-dione Promoted by [2,6-$Dipp_2C_6H_3$]Co[IPrMe] **IV·28**.....264
Chapter V - Global Conclusions.....265
5.1 Global Conclusions.....265
Appendices.....273
6.1 Appendix A – Solid State Structures of Ligand Scrambled Products.....273
6.2 Appendix B – Crystallographic Tables.....275
6.2 Appendix C – UV/Vis Spectra.....286
6.3 References.....288

Abbreviations

2,2,2-crypt	4,7,13,16,21,24-hexaoxa-1,10-diazabicyclo[8.8.8]hexacosane
Ad	adamantyl, $C_{10}H_{15}^-$
Ar	aryl
br	broad
COD	cycloocta-1,5-diene, C_8H_{12}
CV	cyclic voltammetry
d	doublet (NMR)
DCM	dichloromethane
Dcp	2,6-dichlorophenyl, 2,6-$Cl_2C_6H_3^-$
dd	double doublet (NMR)
DFT	density functional theory
Dipp	2,5-diisopropylphenyl, 2,6-*i*$Pr_2C_6H_3$
EI	electron ionisation
ESI	electrospray ionisation
Et	ethyl, $CH_3CH_2^-$
GED	gas electron diffraction
HOMO	highest occupied molecular orbital
i	*ipso*, iso
*i*Pr	isopropyl, Me_2CH^-
IPr	1,3-bis(2,6-diisopropylphenyl)imidazoline-2-ylidene (NHC)
IPrMe	1,3-Diisopropyl-4,5-dimethylimidazol-2-ylidene (NHC)
IR	infrared
J	coupling constant (NMR)
LUMO	lowest unoccupied molecular orbital
m	*meta*
m	multiplet (NMR)
Me	methyl, CH_3^-
Mes	mesityl, 2,4,6-$Me_3C_6H_2^-$
Mes*	supermesityl, 2,4,6-*t*$Bu_3C_6H_2^-$
MS	Mass spectrometry

n	normal
Naph	naphthyl, $C_{10}H_7^-$
*n*Bu	*n*-butyl, $Me(CH_2)_2CH_2^-$
NHC	N-heterocyclic carbene
NMR	nuclear magnetic resonance
o	*ortho*
p	*para*
Ph	phenyl, $C_6H_5^-$
Pmp	2,3,4,5,6 pentamethylphenyl, $Me_5C_6^-$
ppm	parts per million
q	quartet (NMR)
R	alkyl
s	singlet (NMR)
SQUID	superconducting quantum interference device
t	triplet (NMR)
*t*Bu	*tert*-butyl, Me_3C^-
THF	tetrahydrofuran, C_4H_8O
Tmp	2,4,5-trimethylphenyl, 2,4,5-$Me_3C_6H_3^-$
TMS	trimethylsilyl, Me_3Si^-
Tol	tolyl, $MeC_6H_3^-$
Tripp	2,4,6-triisopropylphenyl, 2,4,6-*i*$PrC_6H_3^-$
UV/vis	ultraviolet/visible
XRD	X-ray diffraction
Xyl	xylyl, $Me_2C_6H_3^-$
δ	Chemical shift (NMR), delta (orbital symmetry)
$\Delta\nu_{1/2}$	half-height peak width
μ_{eff}	effective magnetic moment
π	pi (orbital symmetry)
σ	sigma (orbital symmetry)

Characterised Complexes

Chapter II:

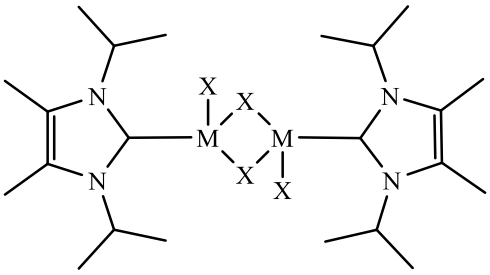

II·30 M = Co, X = Br
II·31 M = Zn, X = Cl

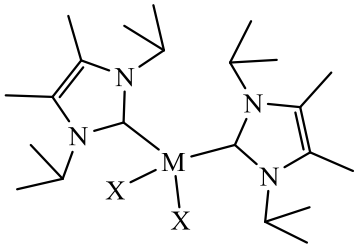

II·32; M = Co; X = Br
II·33; M = Zn; X = Cl
II·34; M = Ni; X = Cl

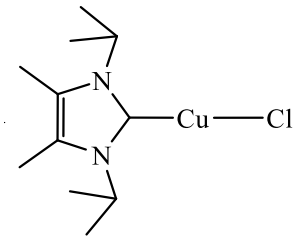

II·35

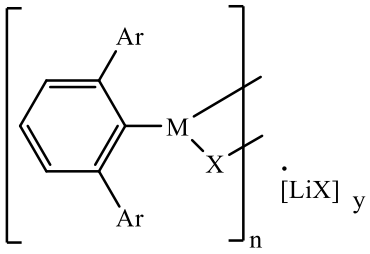

II·36, **II·38**; M = Mn; X = Br; Ar = Mes, Dipp; n = 2; y = 2
II·39; M = Fe; X = Br; Ar = Mes; n = 2; y = 2
II·37, **II·40**; M = Co; X = Br; Ar = Mes, Dipp; n = 2; y = 2

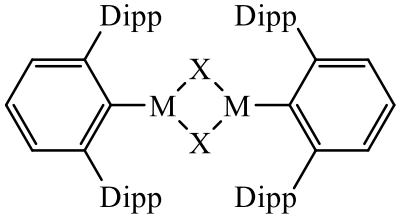

III·36b, M = Mn, X = Br
III·37b, M = Co, X = Br

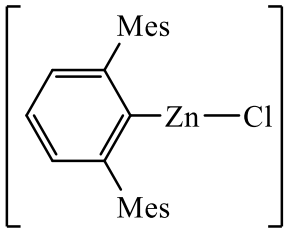

II·41

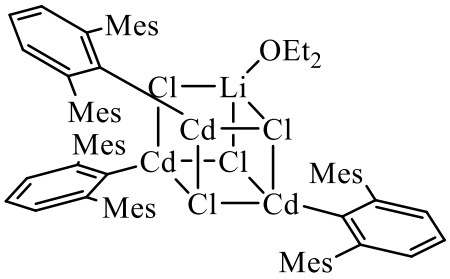

II·42

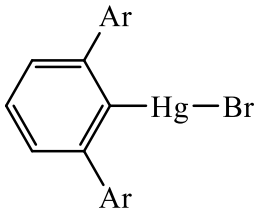

II·43, Ar = Mes
II·44, Ar = Tmp

Chapter III:

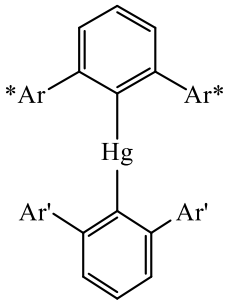

II•21; Ar* = Pmp, Ar' = Tmp
II•22; Ar* = 2,6-Xyl, Ar' = Tmp
II•23; Ar* = Dcp, Ar' = Tmp
II•24; Ar* = Pmp, Ar' = Mes

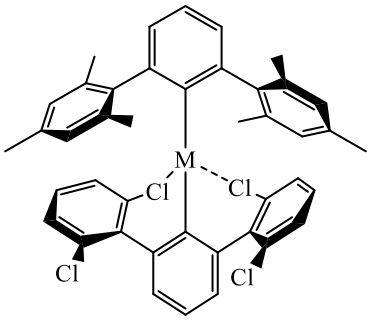

III•30, M = Mn
III•31, M = Zn

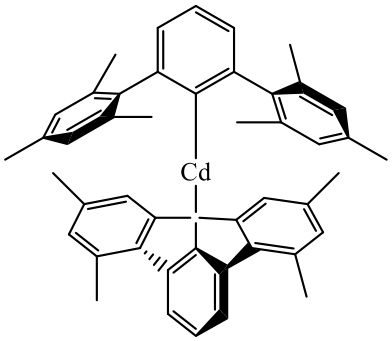

III•32

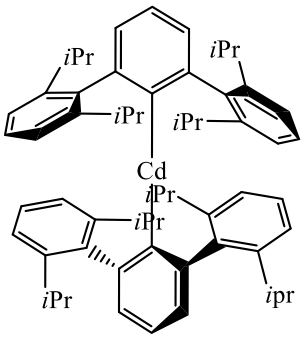

III•33

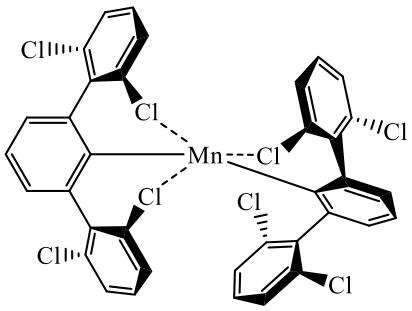

III•35

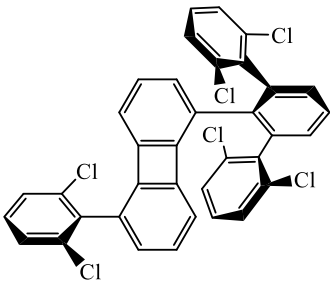

III•36

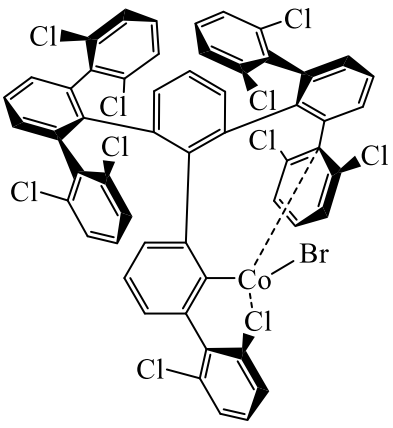

III•37

Chapter IV:

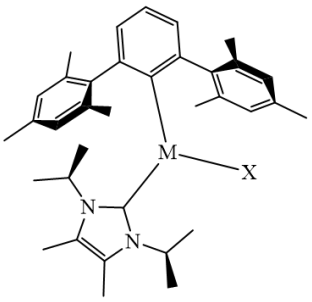

IV·10: M = Zn, X = Cl
IV·11: M = Cd, X = Cl
IV·12: M = Hg, X = Br
IV·14: M = Fe, X = Br
IV·15: M = Co, X = Br

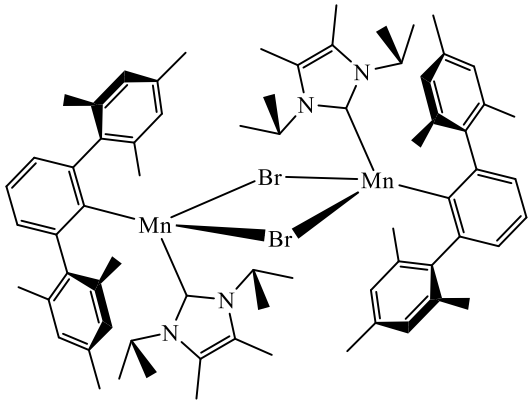

IV·13

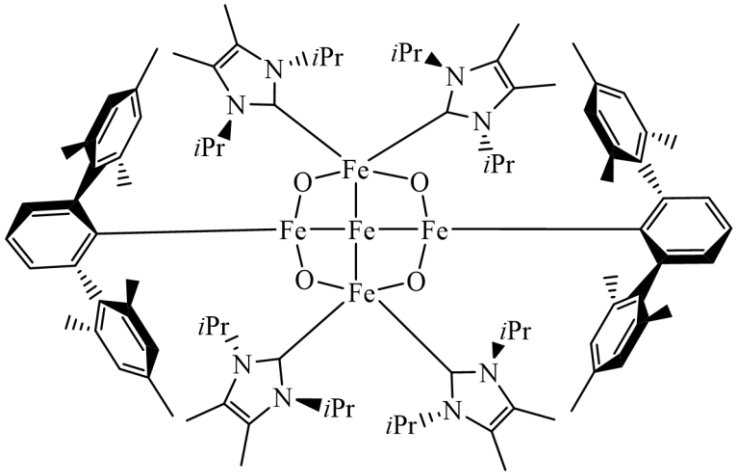

IV·16

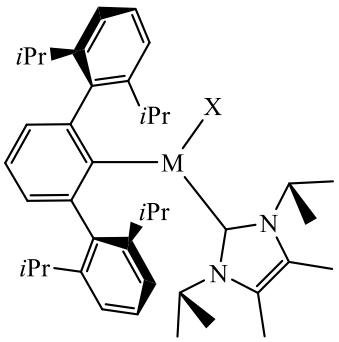

IV·17; M = Fe, X = Cl
IV·18; M = Co, X = Br
IV·19; M = Zn, X = Cl

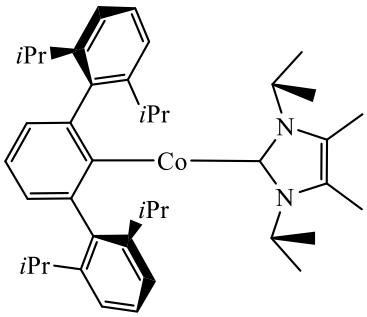

IV·20

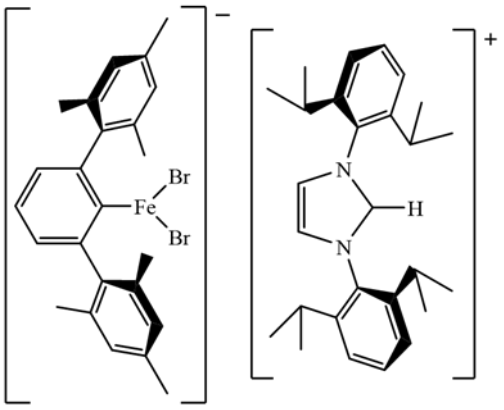

IV·23

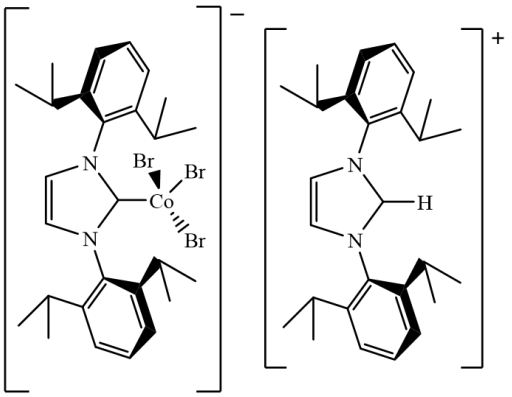

IV·24

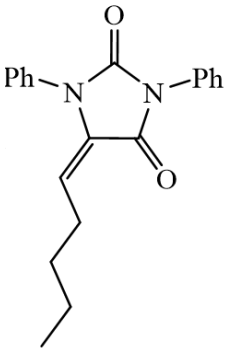

IV·26

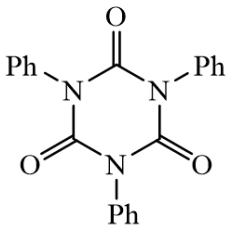

IV·27

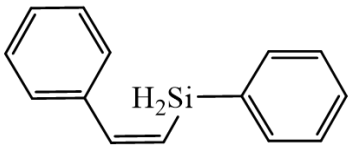

IV·25

Chapter I

Introduction

1.1 Organometallic Chemistry

In 1963, Karl Ziegler and Giulio Natta were awarded the Nobel Prize in Chemistry for their work on the development and use of organoaluminium complexes as catalysts for polymerisation. Mindful of the earlier work on organomagnesium reagents by Grignard, this was the first direct mention of the field of organometallic chemistry in a Nobel Prize award speech.[1]

Having announced itself independently on the scientific stage the field grew rapidly. The Prize of 1973 was awarded for “pioneering work, performed independently, on the chemistry of the organometallic, so called sandwich compounds" to Ernst Otto Fischer and Geoffrey Wilkinson. The press release of that year described the work as “chemistry for chemists” as the practical considerations were not obvious. Indeed, whilst the previous two Nobel Prizes that can be claimed by organometallic chemistry both recognised the contributions of the scientists to other fields (Grignard to organic synthesis and, Ziegler and Natta to polymerisation), the Prize of 1973 was awarded for the contributions, while of no particular use, to “the basic concepts and structure of the chemistry”.

Since this award, the field of organometallic chemistry has made significant practical contributions to the world. Organometallic complexes and the catalyses that they promote have

become a vital tool in synthetic chemistry through the work of, amongst others, Grubbs,[2–4] Schrock,[5,6] Negishi[7] and Suzuki.[8] The field continues to provide notable developments in chemistry. One such example is the recent synthesis of a dysprosium complex, [Dy(1,2,4-^{t}BuC$_5$H$_2$)][BAr$^F_4$] (**I·1, Figure 1·1**), able to retain its magnetisation up to a temperature of 60 K.[9,10]

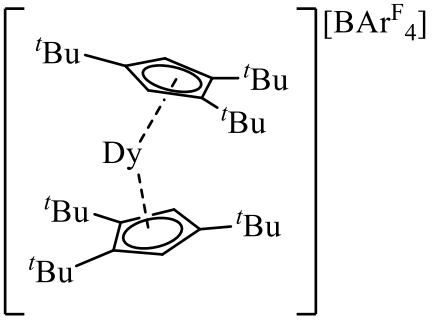

Figure 1·1. Dysprosium complex **I·1**

Since the 1970s, there has been an interest in developing low-coordinate, organometallic, transition metal chemistry. This was motivated, in the first instance, by a desire to understand such complexes and the insight that they provide into transition metal chemistry.[11,12] Initially, transition metal complexes stabilised solely by alkyl or aryl ligands were thought to be thermally unstable.[13] This was ascribed to an inherent weakness in the transition metal-carbon bonds due to the promotion of high energy d-electrons into anti-bonding orbitals causing the irreversible decomposition of the complex. It was suggested that this could be alleviated through the use of accompanying, strong field ligands that lowered the energy of the d-orbitals making this decomposition less energetically favourable.

This view held sway until 1972 when it became apparent that the experimental evidence on metal-carbon bond strengths did not fit this theory.[11,14] It was suggested that organometallic, transition metal complexes were not stable because there existed a variety of low-energy decomposition pathways and that the accompanying ligands of earlier studies did not prevent decomposition electronically but instead occupied orbitals around the metal centre.[11,14–16]

It was Wilkinson who proposed that β-hydride elimination was the cause of instability, when he published a number of complexes featuring σ-bound carbon ligands which bore no β-hydrogens.[17] He further developed this theory with the synthesis of hexamethyltungsten, a coordinatively saturated complex featuring no β-hydrogens but also no strong field ligands to support the supposedly weak transition metal-carbon bonds.[18] Heat of hydrolysis studies on this compound found the energy of dissociation of the W−Me bond to be 159 kJ ± 7 kJ mol^{-1}, comparable with the energy of dissociation of a W−CO bond 178.2 ± 3.3 kJ mol^{-1} kJ mol^{-1}.[19] The understanding developed from these studies facilitated the development of low-coordinate, organometallic, transition metal chemistry, as researchers could now design ligands that were not susceptible to β-hydride elimination.

1.2 Early Developments in Low-Coordinate, Transition-Metal Chemistry

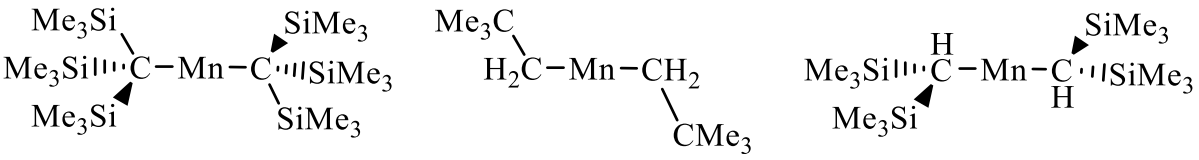

I·2 **I·4** **I·5**

Figure 1.2. The structures of **I·2**, **I·4** and **I·5**.

The design and application of increasingly bulky ligands that were β-hydride elimination resistant facilitated access to low-coordinate transition metal complexes. The early complexes published were, on the whole, three-coordinate.[12,20–22] However, in 1985 Eaborn *et al.* published $Mn[C(SiMe_3)_3]_2$ (**Figure 1.2**), the first crystallographically characterised example of a two-coordinate, transition metal compound.[23] This complex was prepared by addition of a solution of $Li[C(SiMe_3)_3]$ in tetrahydrofuran (THF) to a slurry of $MnCl_2$ in THF cooled to −78°C under anaerobic conditions. Single crystal X-ray diffraction studies of **I·2** found the structure to be strictly linear around the C−Mn−C core with the ligands arranged in an interlocking geometry that filled the available space around the manganese. The compression of the Si−C−Si angles to 112.3(3)° demonstrated the high degree of steric congestion required

to stabilise the complex. The analogous and isostructural $Fe[C(SiMe_3)_3]_2$ (**I·3**) was synthesised in 2001 but similar first-row transition metal analogues have yet to be reported.[24,25]

At the same time as Eaborn's discovery, Anderson *et al*. were able to demonstrate the two-coordinate nature of $Mn[CH_2CMe_3]_2$ (**I·4**, Figure 1.2) *via* gas electron diffraction studies. Subsequently, $Mn[CH(SiMe_3)_2]_2$ (**I·5**, **Figure 1.2**), was also shown to adopt a strictly linear, two-coordinate geometry.[26]

The syntheses of the first crystallographically characterised examples of two-coordinate iron and cobalt complexes required an N-based ligand with greater steric bulk and were reported by Power *et al*. in 1987.[27] $[N(SiMePh_2)_2]_2M$ [M = Fe (**I·6**) or Co (**I·7**)] feature a bent geometry around the N−M−N core [Fe 169.0(1)°, Co 147.0(1)°] as well as long range, secondary interactions between the metal and the phenyl groups of the ligand. The authors discuss the effects of increasing the steric bulk of the ligand on the coordination number of the metal. It is suggested that the steric bulk of $[N(SiMePh_2)_2]^-$, compared with the three-coordinate structures supported by $[N(SiMe_3)_2]^-$[20] or $[NPh_2]^-$,[21] prevents oligomerisation in the solid state and therefore allowed access to mononuclear, two-coordinate complexes.[27,28]

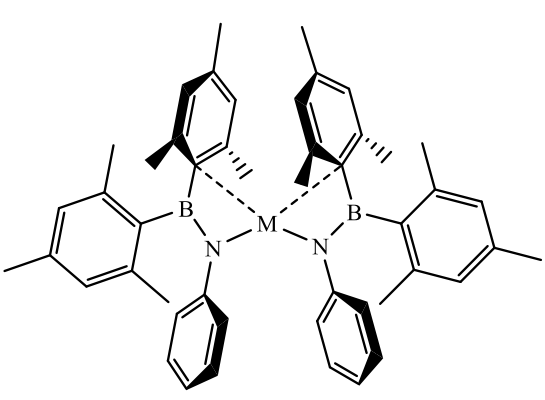

M = Cr (**I·9**), Co (**I·10**), or Ni (**I·11**)

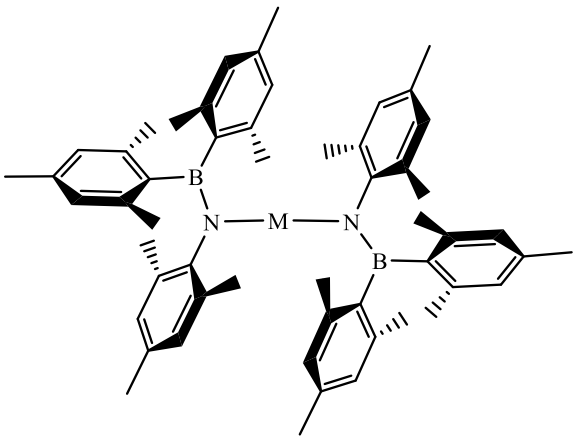

M = Fe (**I·13**), Co (**I·14**), or Ni (**I·15**)

Figure 1·3. The structures of **I·9**–**I·11** and **I·13**–**I·15**.

This theme was further continued by Power and co-workers through the use of the $[NPhBMes_2]^-$ ligand (Mes = 2,4,6-trimethylphenyl). The ligand was designed to combine high steric bulk with the reduced Lewis basicity of the coordinating nitrogen. The aim of the latter was to reduce the ability of the ligand to bridge two metal centres. This approach afforded $Mn[NMesBMes]_2$ (**I·8**), only the fourth solid state example of a two-coordinate manganese centre and the first stabilised by two ligands bound *via* a nitrogen.[29] Unlike previous examples, the structure displays a bent geometry around the metal centre [N−Mn−N = 160.4(2)°] which is attributed to secondary, long range interactions between the manganese moiety and phenyl groups. This methodology was further applied to isolate $M[NAr(BMes_2)]_2$ [Ar = Ph, M = Cr (**I·9**), Co (**I·10**), Ni (**I·11**); Ar = Mes, M = Cr (**I·12**), Mn (**I·8**), Fe (**I·13**), Co (**I·14**) or Ni (**I·15**), **Figure 1·3**].[30] Complexes **I·9** and **I·12**, and **I·11** and **I·15** are the first crystallographically characterised examples of two-coordinate chromium and nickel respectively.[30,31] **I·9** displays a highly bent geometry [N−Cr−N = 110.8(1)° (Ph), 112.3(3)° (Mes)] attributed to long range interactions between the chromium centre and phenyl groups causing a pseudo-square planar geometry. X-ray diffraction studies of **I·11** and **I·15** demonstrate a N−Ni−N angle of 135.7(1)° (**I·11**) and 167.9(1)° (**I·15**). The almost linear nature of **I·15** is attributed to the increased steric bulk of the $[NMes(BMes_2)]^-$ ligand, the covalent radius of the nickel centre encouraging a larger angle, and the relative electron richness of the nickel centre discouraging long range interactions with the ligand.

The first example of a two-coordinate copper(II) complex was isolated and characterised in 2016. $[N(SiMe_3)Dipp]_2Cu$ (**I·16**) was obtained through the reaction of four equivalents of $[N(SiMe_3)Dipp]Li$ and two equivalents of CuCl to give the proposed intermediate $\{[N(SiMe_3)Dipp]_2Cu\}^-$, which decomposes *in situ* to afford two equivalents of **I·16**.[32] The structure is strictly linear and the two ligands adopt a planar arrangement. The complex has a magnetic moment of 1.52 μ_B at 300 K, which is comparable with the spin-only value for a

single unpaired electron as expected for a linear d^9 complex. London Dispersion Forces (LDF) are significant in the stabilisation of this complex and the disproportionation of the copper(I) intermediate. This assertion is supported by Density Functional Theory (DFT) studies that put the contribution of LDF from the ligands to the stabilisation of the complex at 20.8 kcal mol^{-1}.

1.2.1 Aryl Ligand Systems

Aside from $Mn[C(SiMe_3)_3]_2$ (**I·2**), $Mn[CH_2CMe_3]_2$ (**I·4**) and $Mn[CH(SiMe_3)_2]_2$ (**I·5**), organometallic examples of two-coordinate, late-transition metal complexes took longer to develop. In 1995, Power *et al*. published a study of $M[Mes^*]_2$ [M = Mn (**I·17**, **Figure 1·4**) or Fe (**I·18**), Mes* = $(2,4,6\text{-}t\text{Bu}_3C_6H_3)^-$].

Prior to this development, a number of examples of three or four-coordinate late-transition metal complexes featuring aryl ligands had been reported, all demonstrating some degree of oligomerisation. The earliest example was "diphenyl manganese", $[MnPh_2]_\infty$(**I·19**, **Figure 1·4**), first reported in 1937 as a mixture with phenylmanganese iodide.[33] The solid state structure of **I·19** was confirmed by X-ray diffraction studies in 2009 following the publication of a method of purification in 1959.[34,35]

The use of Mes and Tripp as ligands decreases the degree of oligomerisation observed. Guastini *et al*. published Mes_6Mn_3 (**I·20**, **Figure 1·4**), produced from the reaction of MesMgBr with $MnCl_2$ in THF at −30°C and obtained as deep maroon crystals.[36] The complex has three manganese(II) centres in two different coordination geometries. The central manganese atom adopts a tetrahedral geometry coordinated by four bridging Mes units, whilst the terminal manganese centres adopt trigonal planar geometries, each being coordinated by two bridging Mes ligands and one terminal Mes ligand. Magnetic data suggested a degree of magnetic interaction between the metal centres as the magnetic moment, 3.65 μ_B, is lower than expected.

Structural data puts the Mn···Mn distance at 2.851(3) Å, which the authors suggest is too long for this interaction to be a metal-metal bond.[36]

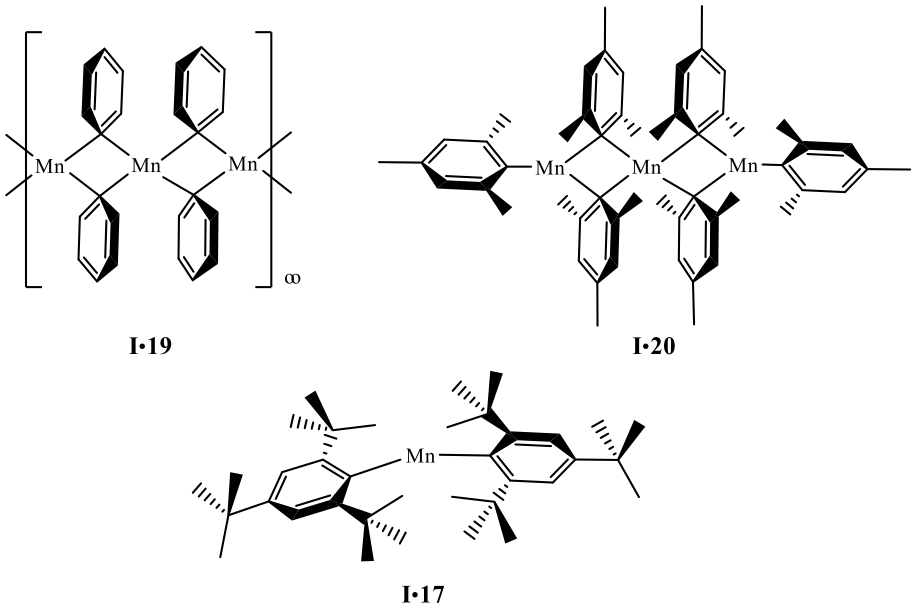

I·19 **I·20**

I·17

Figure 1·4. The structures of manganese complexes **I·17**, **I·19** and **I·20** stabilised by aryl ligands.

Five years later, Power *et al*. reported a similar complex, $[Li(THF)_4][MnMes_3]$ (**I·21**). The different reaction stoichiometry and the presence of a bulky anion, introduced through the use of MesLi as a starting material, seemed to prevent oligomerisation. Therefore, a different structure to that isolated by Guastini *et al.* was obtained. Complex **I·21** features a rare example of a three-coordinate manganese centre. In the same year Siedel and Kriesel published the analogous cobalt complex (**I·22**), which was further characterised and used by Richeson *et al*. as a starting material in the synthesis of $[CoMes_2]_2$ (**I·23**), a dimeric complex featuring two trigonal planar cobalt centres that decomposes slowly at room temperature (**Scheme 1·1**).[37,38] The solid-state structure of this complex shows close contacts between the cobalt centres and the methyl groups of the Mes ligands. The authors demonstrated the presence of a relatively strong Co−Co interaction using magnetic studies, Hückel calculations and examination of the Co−Co distances [2.512(2) and 2.519(2) Å].

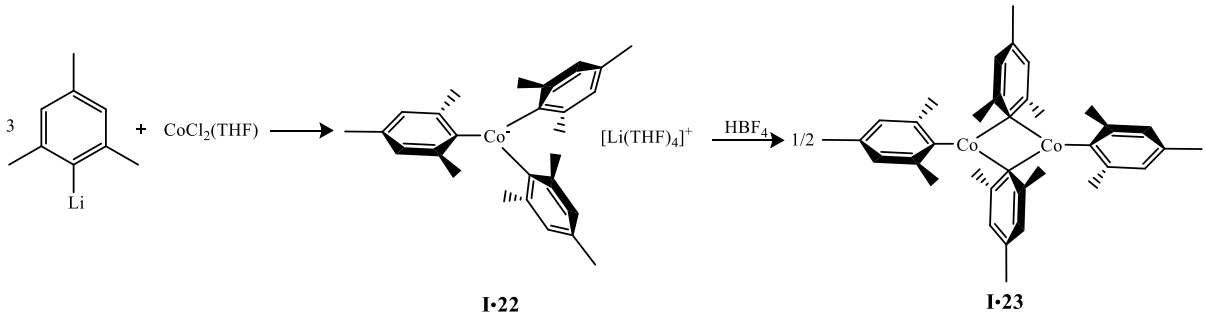

I·22 **I·23**

Scheme 1·1. The synthetic route developed by Richeson *et al*. toward **I·23**.

The iron analogue, $[FeMes_2]_2$ (**I·24**, **Figure 1·5**), reported first in 1976 and fully characterised seventeen years later, is also dimeric.[39,40] A study by Floriani *et al.* suggested **I·24** demonstrates a degree of metal−metal interaction. The short Fe−Fe bond distance of 2.614(1) Å is less than the sum of the Van der Waals radii and magnetic studies indicated the pairing of an electron from each iron centre. The coupling constant of this interaction is too high for a carbon bridged interaction therefore a supported Fe−Fe bond must exist.[41]

Increasing the steric bulk of the ligand through the substitution of the *ortho* and *para* positions of the phenyl ring with *i*Pr (Tripp) also produce the dimer $[FeTripp_2]_2$ (**I·25**, **Figure 1·5**). Whilst similar in structure to **I·24** there is a higher degree of steric strain, manifesting in larger Fe−Fe [2.666(3) Å] and Fe−C [2.083(9)–2.188(8) Å] distances.[41] The manganese analogue $[MnTripp_2]_2$ was published in 2010 and exhibits a slight contraction of the Mn···Mn distance [2.7783(4) Å] when compared with trimeric, $[MnMes_2]_3$ [**I·20**, Mn···Mn = 2.851(2) Å]. This is presumably due to a reduction in steric strain moving from a trimeric to a dimeric structure.[42]

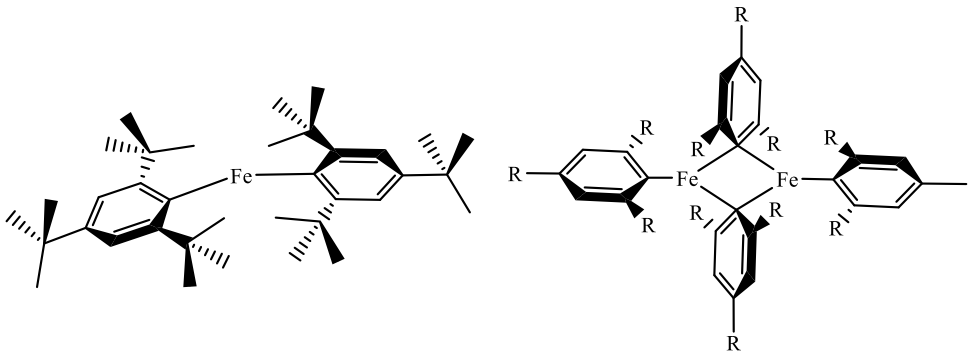

I·18 R = Me (**I·24**), *i*Pr (**I·25**)

Figure 1·5. The structures of **I·18**, **I·24** and **I·25**.

The application of [2,4,6-^{t}Bu$_3$C$_6$H$_3$]$^-$ (Mes*) as a ligand afforded M[Mes*]$_2$ (M = Mn (**I·17**) or Fe (**I·18**, **Figure 1·5**). These are the first examples of two-coordinate, transition metal, diaryl complexes in the literature to be crystallographically characterised.[43] They were synthesised through the reaction of the corresponding metal halide ($MnCl_2$ or $FeBr_2$) with [Mes*]$_2$Mg. Both structures are similar, with a significant deviation from linearity along the C−M−C bond [**I·17** = 159.66(10)°, **I·18** = 157.9(2)°] attributed to secondary interactions between the electron poor metal centre and the *ortho t*Bu groups. In both complexes the torsion angles between the ligands approach 90° [**I·17** = 74.5°, **I·18** = 75.5°], this occurs to reduce steric strain but also creates a steric pocket around the metal which prevents oligomerisation of the complexes. Magnetic studies of both complexes revealed magnetic moments of 5.90 μ_B (**I·17**) and 5.18 μ_B (**I·18**), suggesting high spin d^5 and d^6 electron configurations. A similar synthetic methodology was applied in efforts to isolate the chromium and cobalt analogues, which the authors report to be significantly less stable.[43] It would require an *m*-terphenyl ligand to stabilise a similar cobalt complex, whilst a two-coordinate, diaryl chromium(II) species has yet to be reported.

1.3 Sterically Bulky Ligand Systems: 1996 Onwards

As the development of low-coordinate transition metal complexes demonstrates, the steric bulk of the ligands employed is vital in the isolation of these highly reactive complexes.[12,44,45] Developments have thus far been limited to the 3d transition metals because their small size allows easier blocking of coordination sites with sterically bulky ligands.[44] There has been a focus in recent years in developing new mono- or bidentate ligands of increasing bulk. For example, extensive studies with β-diketiminato,[46–48] hetero-coordinating *m*-terphenyls,[49–52] and bulky amide ligands[53–55] have yielded an array of novel complexes featuring previously unknown bonding modes. Chief amongst these was the synthesis of the Group 12 series LZn^{I}M^{0}Zn^{I}L (L = N(2,6-{C(H)Ph$_2$}$_2$-4- *i*PrC$_6$H$_2$)(SiMe$_3$), M = Zn (**I·26**), Cd (**I·27**) or Hg (**I·28**), **Figure 1·6**). The authors point to the extreme steric bulk of the ligand as the factor that

allows the Zn_3 species to exist at room temperature. Such structures were previously thought unstable with respect to the elimination of Zn metal.[54]

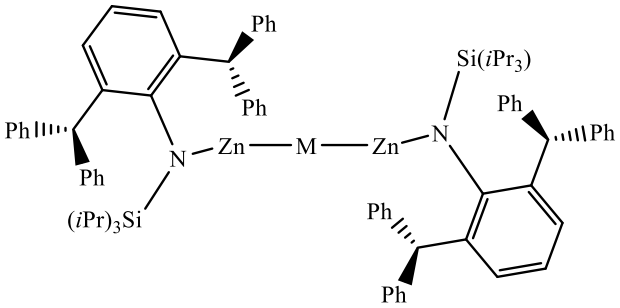

M = Zn (**I·26**), Cd (**I·27**) or Hg (**I·28**)

Figure 1·6. The structures of **I·26**–**I·28**.

With respect to organometallic species, *m*-terphenyl, N-heterocyclic carbenes (NHC) and cycloalkyl amino carbene (CAAC) ligand systems have made a significant impact on the field since their introduction. The impact of *m*-terphenyl and NHC ligands will be discussed below, CAAC complexes will be discussed briefly where relevant to the discussion. An important factor in the success of these ligands has been the ease with which the steric bulk of the ligands can be tailored through the alteration of flanking groups.[45]

Several methods have been developed for measuring the steric bulk of a ligand. One of the earliest, the Tolman Cone Parameter, was designed to assess the properties of tertiary phosphine ligands.[56] This is measured by taking a space-filling model of the M-PR_3 group and folding back the substituents. A cone that contains the ligand is then drawn from the metal and the angle of this cone is recorded. Computational methods are available for this process. Tolman also reported a methodology to measure the electronic properties of tertiary phosphines through the infra-red (IR) signals of CO groups in $Ni(CO)_3R$ (R = a tertiary phosphine) with the lowest ν_{CO} denoting the most strongly donating phosphine. Through the combination of these two techniques Tolman was able to create a ligand map to describe a range of tertiary phosphines.[56]

The Tolman model is less reliable with ligands that do not have a symmetric steric profile, such as NHCs.[16] Alterations to the methodology were attempted by Nolan *et al*.[57] before the same authors proposed a new method of comparing steric bulk known as percent buried volume ($\%V_{Bur}$). This was based initially on DFT optimised geometries and then directly on crystallography data.[58,59] This technique quantified the percentage of the Van der Waals radius of a metal atom obscured by a ligand, allowing for comparison across ligand systems. A web application, known as SambVca, is available for general use.[60]

1.3.1 *m*-Terphenyl Chemistry

m-Terphenyl ligands, a generalised structure of which is given in **Figure 1·7**, are widely used across the periodic table.[61] In the field of organometallic chemistry they have been involved in the stabilisation of the first observed quintuple bonding interaction and have been used in magnetism and catalysis.[62–66]

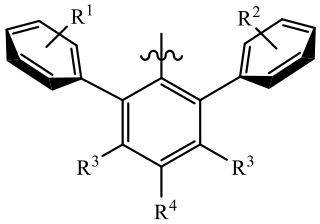

R^1, R^2 = H, Halo, O, Alkyl
R^3 = H, Alkyl
R^4 = H, Halo, Alkyl, OMe, $SiMe_3$,

Figure 1·7. A general schematic of the m-terphenyl ligand.

A foundation for the success of the *m*-terphenyl ligand was laid by the publication of a readily scalable and flexible synthesis by Hart *et al*. in 1986.[67,68] A revised synthesis, shown in **Scheme 1·2**, was developed by the same group in a later publication.[69] Both syntheses allows for the ready alteration of all three phenyl moieties either through altering the Grignard complex used (R^1 and R^2, **Figure 1·7**) or the substitution of the dichlorobenzene (R^3 and R^4, **Figure 1·7**). Accordingly, the steric and electronic properties of the ligand can be altered to fulfil a range of roles.

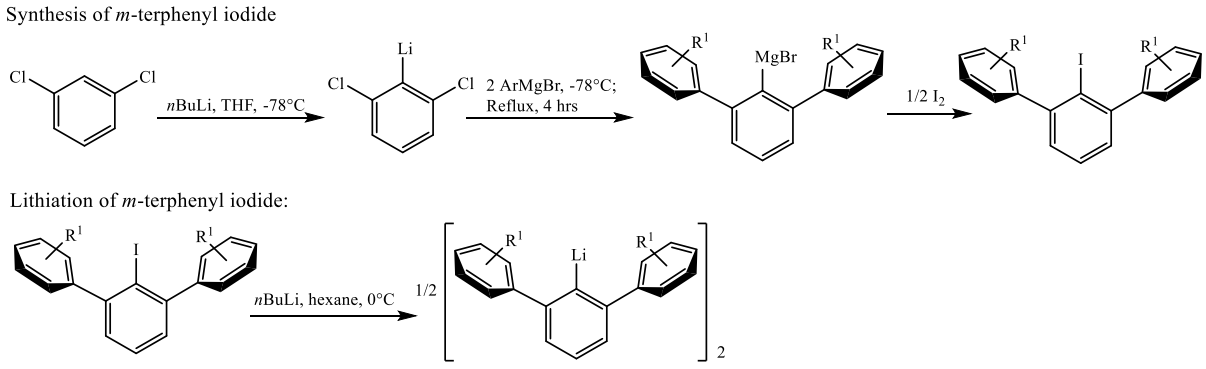

Scheme 1·2. The Hart method of synthesising *m*-terphenyls.[69]

The Hart method, shown in **Scheme 1·2**, provides access to large amounts of a wide array of *m*-terphenyl ligands. However, there are some substitution patterns that it cannot access. For this reason, several alternative methods exist.[70–72] Most pertinent to the work discussed herein is the synthesis of $[2,6\text{-}Dcp_2C_6H_3]^-$ (Dcp = Dichlorophenyl) (**Scheme 1·3**) published in 2002.[71]

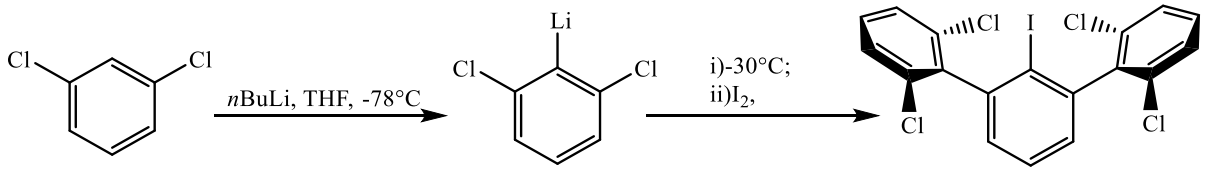

Scheme 1·3. The synthesis of the Dcp *m*-terphenyl ligand.

Through the lithiation of 2,6-dichlorobenzene and careful control of the temperature the trimeric complex can be isolated as the lithium salt, before being converted to the iodide through the addition of a slight excess of iodine. The authors note that phosphorus is able to insert into the C−Cl bonds of the flanking group. This may indicate that the ligand is unsuitable for the stabilisation of certain, highly reactive, species. Even so, a series of two-coordinate Group 12 species have been stabilised using $[2,6\text{-}Dcp_2C_6H_3]^-$ as the sole ligand.[73] These highly symmetrical complexes exhibit a strictly linear C−M−C bond and are stable at room temperature indicating that the C−Cl bond is not activated under mild conditions.

1.3.1 Low-Coordinate, *m*-Terphenyl Complexes

The first use of an *m*-terphenyl ligand in a transition metal complex was reported in 1996.[74,75] Through the reaction of [2,6-$Mes_2C_6H_3$]MgBr and $CoCl_2$ in THF, Power *et al*. were able to isolate [2,6-$Mes_2C_6H_3$(μ-Br)Co(THF)]$_2$ (**I·29**) as dark blue crystals. This four-coordinate, binuclear cobalt complex is a rare example of an aryl-bound cobalt species. Compared with the previous example of such a compound, [Mes_2Co]$_2$ (**I·23**),[38] **I·29** has a longer Co−Co distance [2.516(4) and 3.520(2) Å, for **I·23** and **I·29** respectively] and a larger magnetic moment (3.80 and 4.7 μ_B, respectively). The larger magnetic moment for **I·29** indicates less antiferromagnetic coupling and therefore a weaker metal-metal bond than **I·23**. Attempts to access a two-coordinate, cobalt(II) complex through the use of two equivalents of 2,6-$Mes_2C_6H_3$MgBr were unsuccessful.[74]

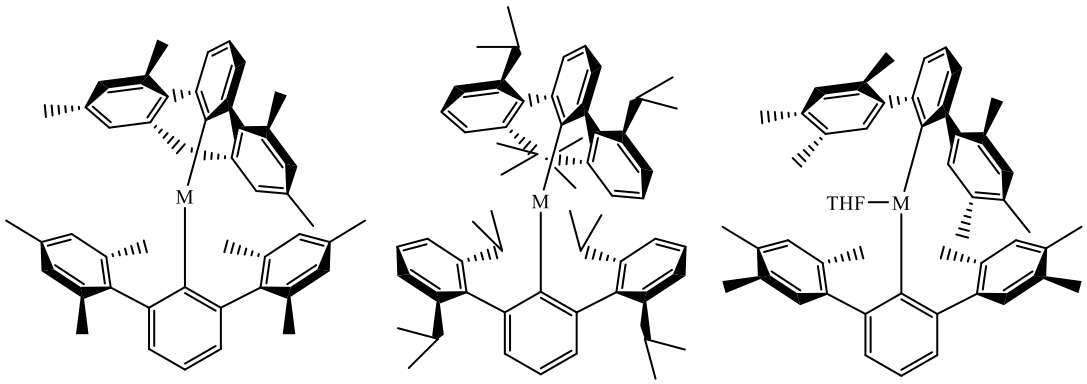

M = Mn (**I·31**), Fe (**I·32**), Co (**I·30**) M = Mn (**I·33**), Fe (**I·34**), Co (**I·35**) M = Mn (**I·36**), Fe (**I·37**)

Figure 1·8. The structures of two-coordinate, m-terphenyl manganese, iron, and cobalt complexes, **I·30**–**I·37**.

[2,6-$Mes_2C_6H_3$]$_2$Co (**I·30**, **Figure 1·8**), was later synthesised through the reaction of the lithium salt, [2,6-$Mes_2C_6H_3Li$]$_2$, with $CoBr_2$(DME).[76] Complex **I·30** is the first example of a crystallographically characterised, two-coordinate cobalt(II) complex stabilised by Co−C bonds. The manganese and iron analogues (**I·31** and **I·32**, **Figure 1·8**) were published alongside this complex; structural and magnetic characteristics for these complexes are featured in **Table 1·1**. Each complex crystallised with two crystallographically distinct molecules in the unit cell

and all showed a deviation from linearity along the C−M−C axis. However, the differences in this angle between the two molecules in each unit cell (*ca*. 7.5−8.8°) indicated that the angle is relatively soft and may be influenced by packing effects or secondary interactions.[27,76] The magnetic moments of the complexes [5.89 (Mn), 4.90 (Fe) and 3.81 (Co) μ_B] suggest no significant ligand contribution to the value. The zinc analogue, [2,6-$Mes_2C_6H_3$]$_2$Zn was published in 2014 and demonstrated a more linear C−M−C axis (177.1(1)°) in the solid state.[77]

Table 1·1. Selected bond lengths, angles, and magnetic moments for *m*-terphenyl complexes of the first-row transition metals. ^ indicates an averaged value.

	[2,6-$Ar_2C_6H_3$]$_2$Mn			[2,6-$Ar_2C_6H_3$]$_2$Fe			[2,6-$Ar_2C_6H_3$]$_2$Co	
Ar =	Mes	Dipp	Tmp	Mes	Dipp	Tmp	Mes	Dipp
	I·31	**I·33**	**I·36**	**I·32**	**I·34**	**I·37**	**I·30**	**I·35**
C−M (Å)	2.095(3) ^	2.113(2)	2.1395(11)	2.040(3) ^	2.059(1)	2.0734(19), 2.073(2)	2.001(3) ^	2.014(2)
C−M−C (°)	173.00(13), 166.41(13)	160.19(9)	138.14(3)	164.44(12), 172.17(11)	159.34(6)	133.89(8)	162.84(10), 172.17(11)	159.34(8)
μ_{eff} (μ_B)	5.89	-	5.59	4.90	4.82	5.58	3.81	4.38

Since this development, a range of similar Group 7-9 complexes have been reported that feature the alternative *m*-terphenyl ligands [2,6-$Dipp_2C_6H_3$]$^-$ and [2,6-$Tmp_2C_6H_3$]$^-$ (Dipp = 2,6-*i*$Pr_2C_6H_3$, Tmp = 2,4,5-$Me_3C_6H_3$).[42,52,63–65] These structures are summarised in **Figure 1·8** and key structural and magnetic characteristics reported in **Table 1·1**.

[2,6-$Dipp_2C_6H_3$]$^-$ has a greater steric bulk relative to [2,6-$Mes_2C_6H_3$]$^-$. In the [2,6-$Dipp_2C_6H_3$]$_2$M (M = Mn (**I·33**), Fe (**I·34**) and Co (**I·35**)) structures this manifests in longer C−M bond lengths and greater deviation from linearity relative to the [2,6-$Mes_2C_6H_3$]$_2$M analogues.[63]

In contrast, the [2,6-$Tmp_2C_6H_3$]$^-$ ligand is less bulky relative to the other two ligands detailed in **Table 1·1**. The complexes, [2,6-$Tmp_2C_6H_3$]$_2$M(THF) [M = Mn (**I·36**) and Fe (**I·37**)], included a THF moiety coordinated to the metal centre as a result of this reduced steric bulk.

The structures adopt a distorted trigonal planar geometry which increases the steric strain around the metal centre. This, in turn, results in slightly longer C−M bond lengths than those seen in the other *m*-terphenyl complexes. The cobalt analogue of these complexes has yet to be published.

Despite many advances in aryl ligands, manganese, iron, and cobalt remain the only open shell transition metals for which two-coordinate, diaryl complexes have been isolated.

1.5 N-Heterocyclic Carbene Chemistry

Despite extensive study throughout the 20th century, free, uncoordinated carbenes were not isolated and characterised until the late 1980s.[78–82] At this point Bertrand *et al*. published the synthesis of phosphino(silyl)carbene (**I·38**, **Figure 1·9**).[83] This complex did not, however, show great affinity with transition metals.[59] The huge growth in the transition metal chemistry of carbenes observed over the last two decades was delayed until the synthesis and characterisation of 1,3-di-1-adamantylimidazol-2-ylidene (IAd, **I·39**, **Figure 1·9**) by Arduengo III *et al*. in 1991.[84]

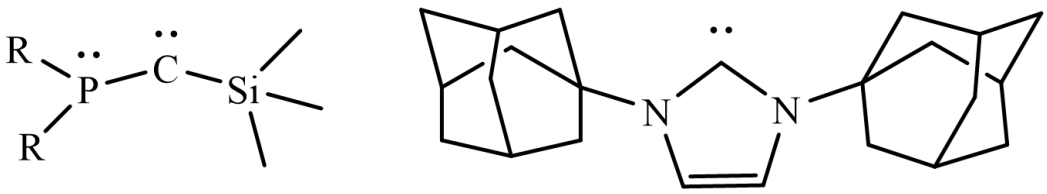

I·38 **I·39**

Figure 1·9. The structures of phosphino(silyl)carbene (**I·38**) and 1,3-di-1-adamantylimidazol-2-ylidene (IAd, **I·39**)

Several factors contribute to the stability of the Fischer carbene. They include the contribution from the nitrogen atoms in the 1- and 3-positions, which stabilise the structure through inductive and mesomeric means. The nitrogen atoms inductively lower energy of the σ-orbital of the carbon whilst they donate electron density to the empty π-orbitals. For a time, the degree of π-electron donation from the nitrogen atoms to the carbon atom was disputed due to

differences in computational studies.[85–87] There is now agreement that there is significant electronic charge from the nitrogen atoms in the formally empty p-orbital of the lone pair bearing carbon.[88] Also, the cyclic nature of the imidazole core has been cited as stabilising the carbene through the enforcement of an sp^2-like configuration. The steric bulk of the flanking groups is said to protect the lone-pair and the partial aromaticity of the core contributes *ca*. 25 kcal mol^{-1} to the stability of the system.[82,85,87] These stabilising characteristics are not vital for the existence of "bottleable" carbenes: NHCs have been synthesised that lack one or more of these later stabilising characteristics.[89–92]

Various synthetic routes to NHCs have been published. A simple, one-pot method to obtain the 1,3-disubstitued imidazolium salt is the subject of a patent, listing the inventor as Arduengo III.[93] This method involves the combination of two equivalents of a primary amine bearing the desired flanking group (R) and glyoxal to afford the corresponding Schiff base *via* two condensation reactions. This is then combined with formaldehyde in acidic (HX) conditions where a further condensation reaction affords the 1,3-disubstitued imidazolium salt. This can then be deprotonated using a strong base to afford the desired NHC (**Scheme 1·4a**). It was through deprotonation of 2,4-diadamantylimidazolium chloride with sodium hydride in the presence of a catalytic amount of the dimsyl ion that Arduengo *et al.* isolated the first free carbene.[84] Other methods have been reviewed by Herrmann[94] and Nolan.[95]

Scheme 1·4 details other examples pertinent to this work; examples of a synthesis that affords non-symmetric substitution of the 1- and 3-positions (**Scheme 1·4b**),[96] and examples providing different substitution patterns of the back bone (**Scheme 1·4c and 1·4d**).[97–99] In **1·4c** and **1·4d** the carbene is formed through the reduction of a thione with a Group 1 metal (**1·4c**) or Na/K (**1·4d**). The flexibility of the structure of NHCs has led to a huge range of different examples being synthesised and applied, which contributes to their popularity in organometallic chemistry.

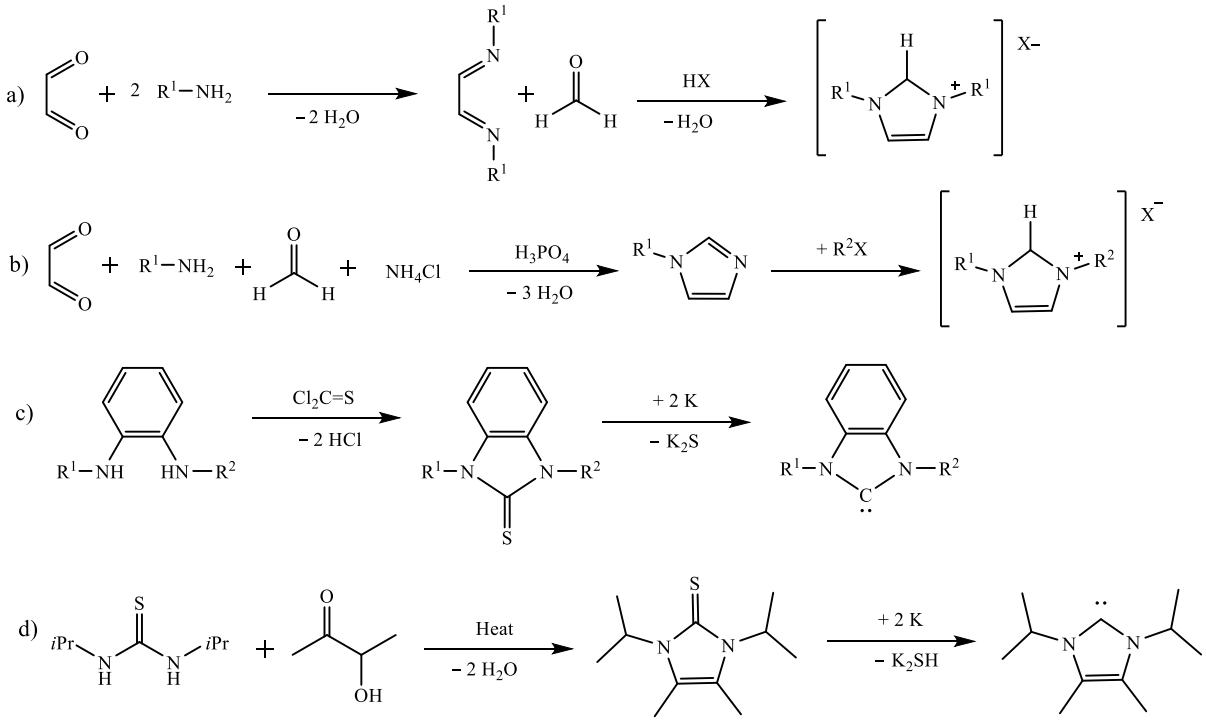

Scheme 1·4. Examples of the many synthetic routes to N-heterocyclic carbenes that have been developed.

As ligands, NHCs are nucleophilic and have been shown to coordinate to transition metals predominantly through σ-bonds, with π-back bonding from the metal discouraged by donation of the α-nitrogen atoms into the empty p-orbital of the carbene.[100] Later studies suggested that the ligands do engage in a degree of π bonding behaviour, either donating or accepting electron density from the metal depending on the environment.[101] A degree of π-π interaction in NHC−M bonds is now accepted, however, they are often represented as single bonds.[82] At first, NHCs were considered tertiary phosphine mimics due to their strong σ-donation. However, rigorous investigation into the steric and electronic properties of these ligands has shown them to differ significantly from tertiary phosphines, displaying a complex and novel chemistry of their own.[102] For example, theoretical studies show that they are significantly stronger σ-donors than even the most basic tertiary phosphines.[103] Investigations by Nolan *et al.* (*vide infra*) demonstrate the differences in the steric profiles of the two ligand classes.[57]

1.3.5 N-Heterocyclic Carbene Complexes of First Row Transition Metals

Whilst *m*-terphenyl chemistry struggles to find purchase among the 4d and 5d transition metals,[61] the application of NHCs quickly spread across the periodic table. In particular, NHC complexes of all the transition metals were published by the turn of the century,[104] with the exclusion of a technetium complex, which was published in 2005.[105] NHCs were found to be excellent spectator ligands and are often employed as ligands of 4d and 5d metals in the catalysis of organic reactions, such complexes and their applications have been recently reviewed.[4,95,106,107] Similarly, extensive work on the chemistry of NHCs with main group and f-block elements has been the subject of reviews by Robinson and Wang, and Arnold and Casely, respectively.[108,109]

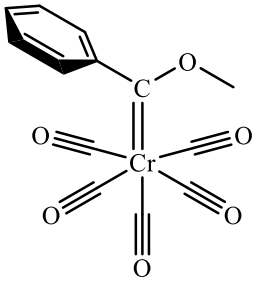

I·40

Figure 1·10. The structure of $(CO)_5Cr(C_6H_5COCH_3)$.

The earliest first row transition metal carbene complexes were isolated before Arduengo published his landmark synthesis. In 1965 $(CO)_5Cr(C_6H_5COCH_3)$ (**I·40**, **Figure 1·10**), synthesised by Fischer and Maasböl, was characterised using X-ray diffraction analysis by Mills and Redhouse.[110] The study demonstrated that the Cr−carbene distance was longer [2.05(3) Å] than the $Cr-C_{carbonyl}$ distance [1.88(3) Å]. This suggests that π-backbonding, which is possible in a Fischer carbene, was less pronounced in the Cr−carbene than in the $Cr-C_{carbonyl}$. The authors note that the phenyl group α to the carbene is perpendicular to the chromium carbene plane and so the π-systems are presumed not to interact. In a later review Fischer notes

that the O−carbene bond is shorter at 1.33 Å than would be expected for a single C−O bond (1.44 Å), indicating a degree of π−π interaction between the two elements.[80]

The first two-coordinate chromium complex stabilised solely by carbon-based ligands was isolated in 2015. $[(cAAC)_2Cr][BAr^F{}_4]$ (**I·41**) exhibits a strictly linear geometry around the chromium(I) centre and was synthesised through chloride abstraction from $[cAAC\text{-}Dipp]_2CrCl$.[111]

Previous to this development, the low-coordinate, carbene chemistry of chromium was restricted to $Cr[IPr][Bz]_2$ [**I·42**, Bz = $CH_2(C_6H_5)$, IPr = 1,3-bis(2,6-diisopropylphenyl)imidazoline-2-ylidene].[112] This is despite NHC−chromium complexes being some of the earliest NHC complexes isolated before 1991 and having a rich chemistry thereafter.[113,114]

$Cr[IPr][Bz]_2$ (**I·42**) was synthesised through the coordination of IPr to $CrCl_2{\cdot}THF_2$ followed by a metathesis reaction with an equivalent of $Mg[Bz]_2{\cdot}THF_2$. The synthesis of the four-coordinate analogue, $Cr[IPrMe]_2[Bz]_2$ (**I·43**), was also described. The geometry of **I·42** is heavily distorted from a trigonal planar geometry with the $C_{carbene}$−Cr−C_{benzyl} angles compressed to 100.66(12)° and 103.64(12)°, which demonstrates the large steric profile of the IPr ligand. The authors note that both complexes are paramagnetic however magnetic studies were not reported.

I·42 and **I·43** were used to investigate the effects of Polarisation Induced Metal Arene (PIMA) interactions between electron poor $3d^4$ metal centres and the π-system of the benzyl fragment. These interactions led to very acute Cr−C−C_{aryl} angles (<101°), which grew more acute when the coordination number of the chromium(II) dropped from four to three. It is suggested this is because the chromium centres become more electron poor. Extensive DFT and *ab initio* investigations were conducted to confirm the presences of PIMA interactions, including comparison with a similar $3d^0$ structure.

The NHC chemistry of manganese is also limited compared with the later transition metals. This is especially true with respect to low-coordinate complexes.[115] Three-coordinate NHC chemistry of manganese currently consists of the four complexes shown in **Figure 1·11**. [IPr]$Mn^{II}[CH_n(SiMe_3)_{3-n}]_2$ [n = 1 (**I·44**) or 2 (**I·45**)] were synthesised through the combination of equivalent amounts of the polymeric $Mn[CH(SiMe_3)_2]$ or $Mn[CH_2(SiMe_3)]\cdot THF$ and IPr in warm hexane. Both structures adopt slightly distorted trigonal planar arrangements. The planes of the NHC N−C−N and C_{alkyl}−Mn−C_{alkyl} moieties are also distorted from planarity with dihedral angles of 16.15(4)° (**I·44**) and 45.42(7)° (**I·45**), the degree of distortion corresponds with the steric bulk of the ligands, which indicates the absence of π-π interactions between the manganese centre and NHC fragments.

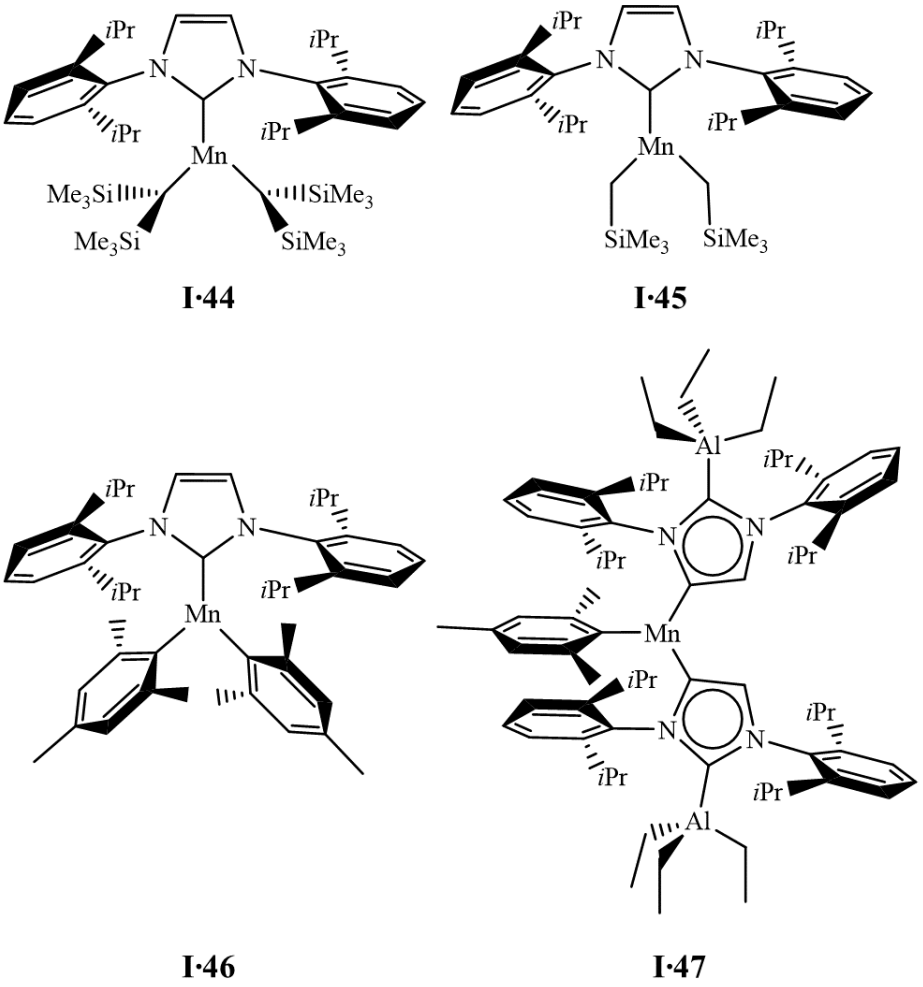

Figure 1·11. Three-coordinate manganese complexes stabilised by NHC ligands.

[IPr]Mn[Mes]$_2$ (**I·46**) and [K(2,2,2-crypt)][{(Et$_3$Al)C(NDipp)$_2$(CH)C}$_2$MnMes] (**I·47**), where [C(NDipp)$_2$(CH)C] represents an anionic, dicarbene ligand, were synthesised by Goicoechea *et al*. (**Figure 1·11**).[116] **I·46** was obtained in near quantitative yield through the addition of three equivalents of IPr to one equivalent of Mn$_3$Mes$_6$ (**I·20**) dissolved in diethyl ether. As in **I·44** and **I·45**, the complex adopts a trigonal planar geometry, however, there is minimal distortion from idealised trigonal planar. Superconducting Quantum Interference Device (SQUID) measurement of the magnetic moment gave a value of 6.042(6) μ_B, comparable to the spin only value (5.92 μ_B).

Reduction of **I·46** with KC$_8$ affords K[C(NDipp)$_2$(CH)C]$_2$Mn[Mes][THF]·THF (**I·48**). A coordination polymer featuring a four-coordinate manganese(II) centre bound by a mesityl group, a THF molecule and two carbenes through the abnormal bonding mode. The normal bonding positions of these carbenes interact with potassium cations to give a neutral species. Reaction of **I·48** with two equivalents of the Lewis acid, triethylaluminium, in the presence of 2,2,2-cryptand results in **I·47**. This complex is a discrete, monomeric complex featuring a three coordinate, manganese(II) centre. A coordinating THF is not present despite the crystals of **I·47** being grown from a THF/hexane mixture. This was attributed by the authors to the THF being unnecessary to stabilise either **I·47** or **I·46**. The magnetic moment of **I·47** is 5.903(6) μ_B. It is noteworthy that the NHC ligand is non-innocent in these reactions, being reduced instead of the manganese centres and adopting an abnormal coordination mode.

The first examples of two-coordinate iron complexes with solely NHC ligation were published by Deng *et al.* in 2015. They are anionic species that feature an iron(I) centre coordinated by two 1,3-bis(2′,6′-diethylphenyl)-4,5-(CH$_2$)$_4$-imidazol-2-yli-dene (CyIDep) (**I·49**,**Figure 1·12**) or two 1,3-bis(2′,6′-diethylphenyl)-imidazolin-2-yli-dene (sIDep) (**I·50**, **Figure 1·12**) moieties and balanced by [BAr$^F_4$]$^-$ (Ar^F = 3,5-ditrifluoromethylphenyl).[117] This study was preceded by the publication of [(R$_2$-cAAC)$_2$Fe][BAr$^F_4$] [R = Me[118,119] (**I·51**) or Et[120] (**I·52**)] the previous

year and the iron(I) species [(IPr)Fe(N(SiMe$_3$)Dipp)][121] (**I·53**, **Figure 1·12**) in the same year. The properties of complex **I·53** will be discussed further in Chapter IV.

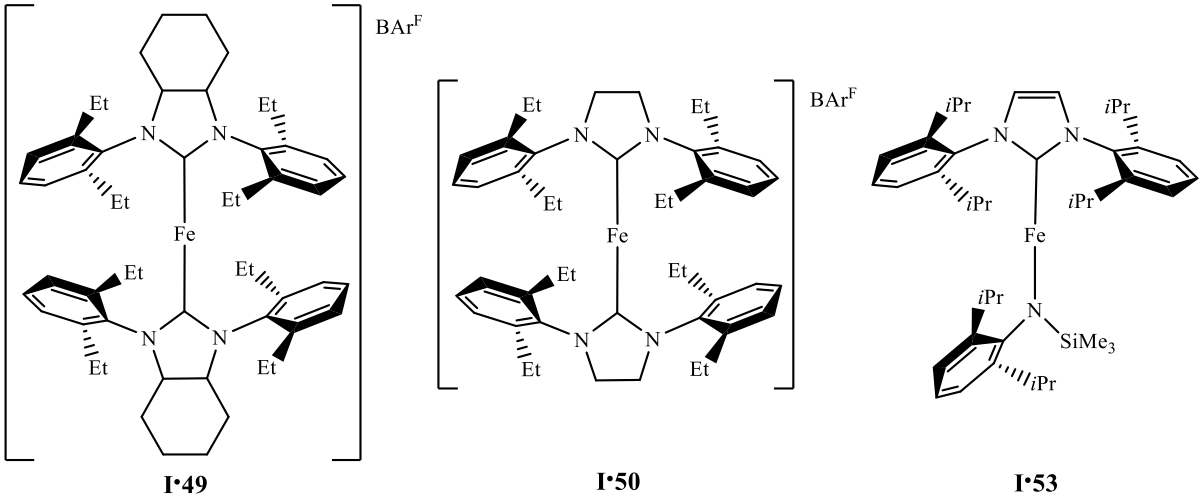

I·49 **I·50** **I·53**

Figure 1·12. Two-coordinate iron complexes stabilised by NHC ligands.

[(CyIDep)$_2$Fe][BAr$^F_4$] (**I·49**) and [(sIDep)$_2$Fe][BAr$^F_4$] (**I·50**) were synthesised through the halide abstraction of [NHC]$_2$FeBr with Na[BAr$^F_4$] in diethyl ether.[117] Both structures are linear [C−Fe−C = 178.4(3)° (**I·49**), 175.8(2)° (**I·50**)] and the magnetic moment of **I·49** was found to be 5.5 μ_B, again this is significantly higher than the spin-only coupling. Measurement of an accurate magnetic moment of **I·50** *via* Evans' method was prevented by the reversible coordination of THF to the complex. Attempts to isolate analogous complexes featuring the IPr, IAd and 1,3-di-1-^{t}butyl-2-ylidene (I^{t}Bu) ligands were unsuccessful whilst attempts to prepare the precursor [sIMes]$_2$FeBr (sIMes = 1,3-bis(Mes)-4,5-dihydroimidazol-2-ylidene) were frustrated as the complex readily undergoes disproportionation. This necessitated the development of a one-pot synthetic route to the three-coordinate, T-shaped complex [(sIMes)$_2$Fe(THF)][BAr$^F_4$] that by-passed this precursor. The coordinated THF could not be removed from this molecule. The authors therefore concluded that the steric properties of the NHC were vital to the isolation of these complexes.

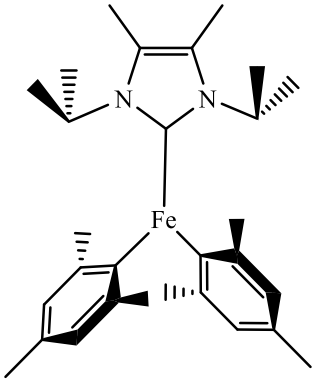

I·54

Figure 1·13. [IPrMe]Fe[Mes]$_2$.

Prior to the publication of two-coordinate, NHC-coordinated iron complexes, several three-coordinate examples existed in the literature. The first of these was the "propeller like" complex [IPrMe]Fe[Mes]$_2$ (**I·54**, **Figure 1·13**) published in 2011.[122] **I·54** was obtained *via* two methods: either through the reaction of [IPrMe]$_2$FeCl$_2$ with two equivalents of MesMgBr, which forces the dissociation of one of the IPrMe moieties, or through the coordination of IPrMe to Mes$_4$Fe$_2$. The latter is similar to the method that produces the manganese analogue (**I·46**).[116]

I·54 features trigonal planar geometry and has a magnetic moment of 5.4 μ_B, indicating a high spin configuration. Exposure of this complex to an equivalent of 2,6-diisopropylaniline results in the species [(IPrMe)Fe(μ_2-NDipp)$_2$Fe(IPrMe)] (**I·55**).[123] The significantly lower magnetic moment of this complex (2.9 μ_B), compared with **I·54**, is indicative of antiferromagnetic coupling between the two iron nuclei. This, together with the short Fe−Fe distance of 2.424(4) Å, suggests the existence of a Fe−Fe bond, similar to that seen in the early work with aryl ligands.

It was found that **I·54** could be selectively oxidised to either the mixed valence [X(IPrMe)Fe^{III}(μ_2-NDipp)$_2$Fe^{II}(IPrMe)X(BF$_3$)$_n$] [X = Cl, n = 0 (**I·56**) or X = F, n = 1 (**I·57**)] or [X(IPrMe)Fe^{III}(μ_2-NDipp)$_2$Fe^{III}(IPrMe)X] [X = Cl (**I·58**) or (**I·59**)] through the reaction with one or two equivalents (respectively) of PhCH$_2$Cl or BF$_3$.

Low-coordinate cobalt complexes with NHC ligation appeared in the literature around the same time as their iron analogues. These complexes have been investigated for their magnetic[124–126] and catalytic[127–129] properties, both of which have been shown to be significant.

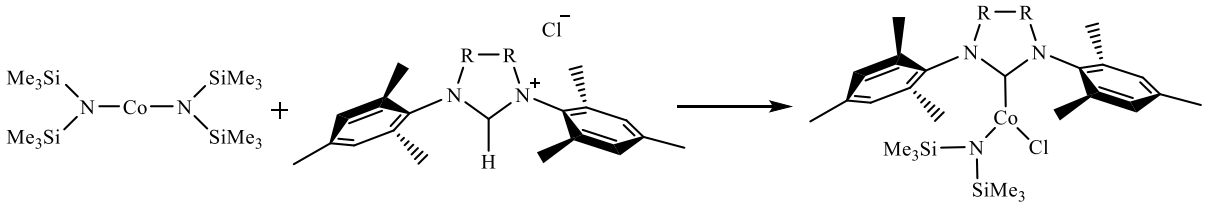

Scheme 1·5. The synthesis of **I·60** and **I·61**.

The first examples of a three-coordinate species were published by Danopoulos *et al*., in the same year as the first examples of three-coordinate iron complexes.[130] [NHC][$N(SiMe_3)_2$]CoCl (NHC = sIMes (**I·60**) or 1,3-di-mesitylimidazol-2-ylidene (IMes, **I·61**)) were synthesised *via* aminolysis of $Co[N(SiMe_3)_2]_2$ using the appropriate NHC hydrochloride salt (**Scheme 1·5**) . This contrasted with the method used by Deng *et al*. to synthesise [IPrMe]Fe[Mes]$_2$ (**I·54**), in which $FeCl_2$·tmeda was exposed to the free carbene followed by a metathesis reaction with MesMgBr. The products have magnetic moments of 4.9 μ_B and 4.8 μ_B, respectively, within the expected range for a high spin, trigonal planar, cobalt(II) structure.

The following year a study by Deng *et al*. into the chemistry of [IMes]$_2$CoCl (**I·62**, **Scheme 1·6**) described the synthesis of [$(IMes)_2$Co][BPh_4] (**I·63**, **Scheme 1·6**), the first example of a two-coordinate cobalt(I) complex. **I·62** was synthesised through the reaction of $Co[PPh_3]_3Cl$ with two equivalents of IMes in THF. It adopts a trigonal planar geometry, distorted by the steric demands of the IMes ligands. The magnetic moment of 4.4 μ_B is similar to that of complexes **I·62** and **I·63** (*vide supra).* Treatment of **I·62** with $NaBPh_4$ in THF resulted in complex **I·63**. This displays a linear C−Co−C geometry [178.57(7)°] and possesses a magnetic moment of 4.1 μ_B.

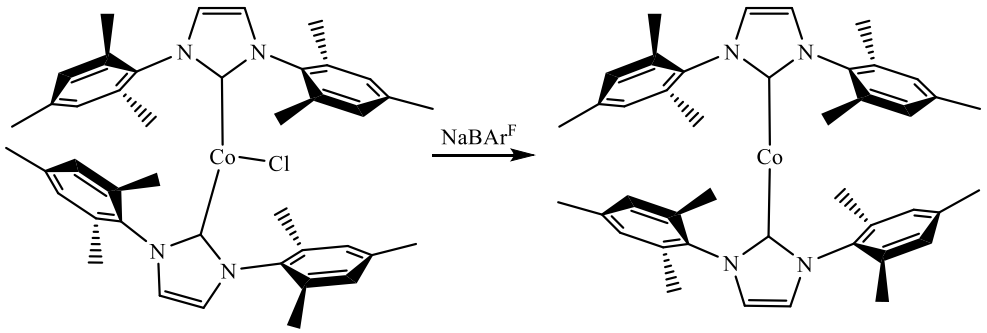

Scheme 1·6. The synthetic route to a two-coordinate cobalt species (**I·63**) stabilised by NHC ligands from a three-coordinate precursor (**I·62**).

Many examples of two and three-coordinate cobalt complexes with NHC ligation feature cobalt in the I or II oxidation state. Examples where this is not true is the three-coordinate, dimido complex, $[IMes]Co^{IV}[NDipp]_2$ (**I·64**), and the oxidised form, $[(IMes)Co^{V}(NDipp)_2][BAr^F_4]$ (**I·65**).[131]

Table 1·2. Key bond lengths, bond angles and magnetic moments of cobalt NHC complexes.

Two-coordinate cobalt complexes						
Complex	Co–L^1 (Å)	Co–L^2 (Å)	L^1–Co–L^2 (°)	μ_{eff} (μ_B)	Ref
$[(IMes)_2Co][BAr^F_4]$	1.937(2)	1.937(2)	178.57(7)	4.2(1)	[132]
[IPr]Co[N(2,6-$Mes_2C_6H_3$)]	1.691(6)	1.953(6)	173.0(3)	4.8(1)	[133]
[cyIPr]Co[N(2,6-$Mes_2C_6H_3$)]	1.675(3), 1.677(3)	1.949(4), 1.959(4)	177.5(2), 179.3(2)	5.1(1)	[124]
[sIPr]Co[N(2,6-$Mes_2C_6H_3$)]	1.682(4)	1.971(5)	175.7(2)	4.6(1)	[124]
$[(sIMes)_2Co][BAr^F_4]$	1.936(2)	1.936(2)	178.4(1)	5.40*	[126]
$[(IAd)_2Co][BAr^F_4]$	1.943(3)	1.943(3)	180	3.94*	[126]
Ar*N[IPrMe]	1.879(2)	1.962(3)	175.2(1)	2.6(1)	[53]

Three-coordinate complexes							
Complex	Co–L^1 (Å)	Co–L^2 (Å)	Co–L^3 (Å)	L^1–Co–L^2 (°)	L^1–Co–L^3 (°)	μ_{eff} (μ_B)	Ref
$[IMes]_2CoCl$	2.244(2)	1.955(5)	1.953(5)	114.9(2)	115.2(2)	4.4(1)	[132]
$[IAd]CoCl[PPh_3]$	2.2358(5)	2.0407(18)	1.9999(16)	110.77(5)	110.30(5)	4.1(1)	[127]
$[IAd]Co[PPh_3][CH_2TMS]$	2.2294(3)	2.2448(3)	1.970(12)	121.195(14)	110.60(3)	3.7(1)	[127]
$[IMes]Co[NDipp]_2$	1.665(3)	1.665(3)	1.879(5)	147.0(20	106.50(12)	2.2(1)	[131]
$[IMes]Co[NDipp]_2[BAr^F]$	1.640(3)	1.642(3)	1.941(4)	141.10(16)	109.70(16)	–	[131]
[η^2-IMesNHDipp]Co[NH Dipp]	1.883(2)	1.885(2)	2.034(3)	131.2(1)	100.8(1)	3.9(1)	[131]
$[IPr]Co[CH_2SiMe_3]_2$	2.099(2)	2.099(2)	2.097(3)	122.66(16)	118.67(8)	5.1(2)	[134]
$[IPr]Co[N(SiMe_3)_2]_2$	1.966(4)	1.958(3)	2.119(3)	122.7(1)	119.9(1)	4.69	[135]
$[IMes]Co[N(SiMe_3)_2]_2$	1.952(6)	1.950(6)	2.105(6)	122.8(2)	118.4(2)	5.08	[135]
[I*t*Bu]Co[$N(SiMe_3)_2$]$_2$	1.971(4)	1.964(5)	2.064(5)	131.6(2)	111.2(2)	4.69	[135]
[aIPr]Co[$N(SiMe_3)_2$]$_2$	1.960(2)	1.930(2)	2.059(2)	124.7(1)	130.4(1)	4.79	[135]

I·64 was isolated from the reaction between $DippN_3$ and $[IMes]Co^0[\eta^2{:}\eta^2\text{-dvtms}]$ (dvtms = divinyltetramethylsiloxane) with the evolution of dinitrogen. It is paramagnetic (μ_{eff} = 2.2 μ_B) and has a trigonal planar geometry with symmetrically equivalent Co=N bonds of 1.665(3) Å. These shorten to 1.640(3) and 1.642(3) Å upon the oxidation of **I·64** to **I·65** with $[Cp_2Fe][BAr^F{}_4]$ whilst the Co−C bond lengthens [1.879(5) Å (**I·64**), 1.941(4) Å (**I·65**)]. The authors propose that this is due to a strengthening of the trans-effect of the imido ligands as a consequence of removing an electron from an antibonding orbital. DFT calculations were employed to confirm this. The development of this dimido ligation of carbene complexes has led to some key developments in single molecule magnetism (*vide infra*).

The compounds discussed here are just a sample of the low-coordinate NHC complexes of cobalt present in the literature. The bond angles and lengths, oxidation states and magnetic moments of these complexes and others are given in **Table 1·2**.

The first example of a two-coordinate nickel complex was synthesised by Arduengo III *et al*. in 1994 alongside the platinum analogue.[136] The complex, $[IMes]_2Ni$ (**I·66**), was synthesised through the displacement of two equivalents of 1,5-cyclooctadiene (cod) from $(cod)_2Ni^0$ by IMes and exhibits a linear geometry along the C–Ni–C axis. Similar complexes of all the Group 10 metals, featuring similar geometry and the I*t*Bu ligand, were synthesised *via* co-condensation reactions by Cloke *et al*. in 1999.[137] These linear, d^{10} complexes are diamagnetic and NMR studies, combined with the short Ni-C distances observed, suggests a degree of π back-bonding demonstrating the flexibility of the electronics in the NHC ligand systems.[136,137]

$[IPr]Ni^I[L]$ [where L = $N(SiMe_3)_2^-$ (**I·67**) or 2,6-*i*$Pr_2C_6H_3NH^-$ (**I·68**)] were synthesised by Hillhouse *et al*. in 2008,[138] and were, at the time, unique examples of two-coordinate nickel(I) amides. **I·67** was isolated in high yields as yellow crystals following a metathesis reaction (**Scheme 1·7**) and exhibits a magnetic moment of 1.9 μ_B. This value is characteristic of a one

electron paramagnet. Complex **I·68** was isolated as bright purple crystals *via* a similar method but possesses a magnetic moment of 2.4 μ_B which, being larger than expected, suggests an orbital contribution to the magnetism.

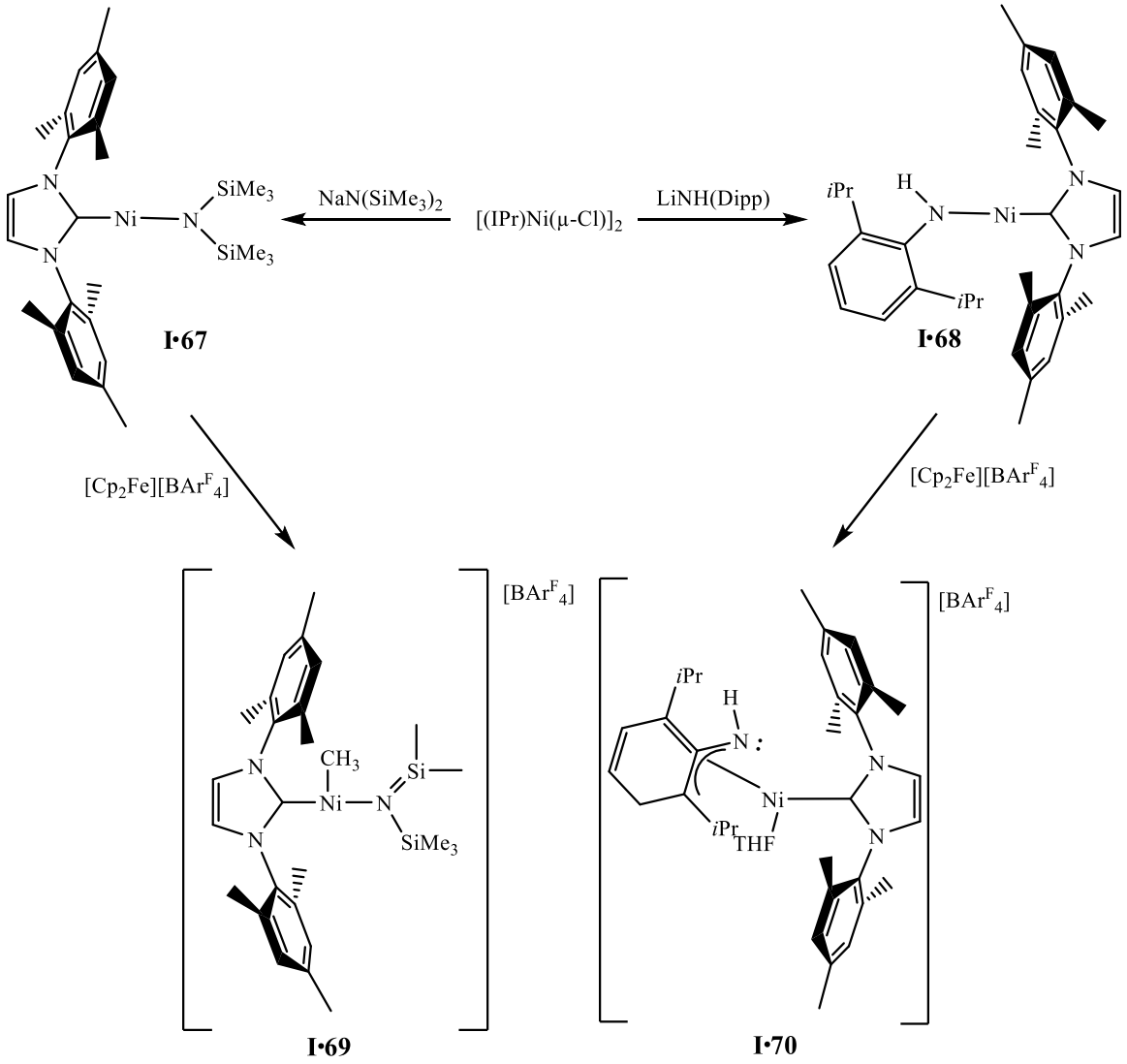

Scheme 1·7. Synthetic routes towards, and structures of, low-coordinate nickel complexes bearing NHC ligands.

Attempts to oxidise to the two-coordinate nickel(II) complexes, both through electronic and chemical means, resulted in ligand rearrangement. In the case of **I·67**, the reaction with $[Cp_2Fe][BAr^F_4]$ results in the translation of one of the methyl groups from a $[N(SiMe_3)_2]^-$ moiety to the nickel centre which was itself reduced to nickel(II). The amide ligand becomes a neutral donor to the nickel centre which adopts a T-shaped geometry with the charge balanced by $[BAr^F_4]^-$ (**I·69**, **Scheme 1·7**). This is a unique example of a three-coordinate, nickel(II) alkyl

cation. The reaction of **I·68** with $[Cp_2Fe][BAr^F_4]$ results in [IPr]Ni[THF][η^3-(2,6-C_6H_4NH)] (**I·70**) in which the aniline moiety adopts η^3 ligation with concomitant coordination of a THF molecule (**Scheme 1·7**). In the solid state, this complex dimerised with loss of the THF and coordination of the imine to the nickel(II) centre. All three of the oxidised species were found to be low-spin diamagnetic complexes.

The NHC chemistry of nickel was given a major boost when Sigman *et al*. isolated $[IPrNi^ICl]_2$ (**I·71**, **Figure 1·14**) and $[sIPrNi^ICl]_2$ (**I·72**) in 2005.[139] These complexes were formed by the coordination of $Ni^{II}Cl_2$(DME) to $Ni^0(cod)_2$ in the presence of the relevant NHC ligand. The nickel complexes equilibrated to afford the complexes which are rare examples of nickel(I) complexes bearing neutral, monodentate ligands. The complexes possess a planar, four-membered core unit with Ni−Ni distances of 2.5194(5) Å (**I·71**) and 2.5099 Å (**I·72**) which are short enough to suggest a metal-metal bond. Attempts to expand the range of NHCs utilised to less bulky but electronically similar analogues were unsuccessful, leading the authors to comment on the importance of the steric pocket in these complexes. Complexes **I·71** and **I·72**, now known as Sigman's dimers, are used as starting materials in metathesis reactions and provide a useful NHC coordinated nickel(I) source.[138,140,141]

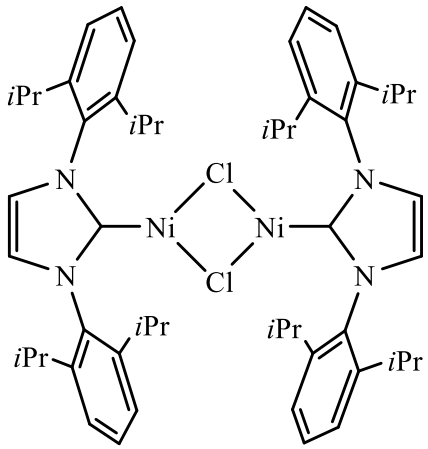

I·71

Figure 1·14. $[IPrNi^ICl]_2$ (Sigman's Dimer).

1.4 Applications of Low-Coordinate, Transition Metal Complexes

The electron deficiency, presence of unpaired electrons and coordinative unsaturation of the metal centres in low-coordinate, transition metal complexes makes them highly reactive. This reactivity has been put to use by a number of groups to activate small molecules such as carbon monoxide[52,142], ammonia,[143] oxygen[52] and isocyanates,[64,65] and they also behave as Lewis acids with several Lewis base-stabilised complexes being published.[12,144]

The magnetic properties of these complexes are also of interest. As has been highlighted above, the majority of these complexes are paramagnetic and exhibit magnetic moments larger than those expected when applying a spin only perspective. Fewer ligands around the metal centre leads to fewer interactions between metal orbitals and these ligands. This reduces the quenching of the first-order orbital magnetic moment arising from the presence of unpaired electrons in these orbitals. Detailed investigation into the magnetic properties of some transition-metal complexes has shown that they can behave as single-molecule magnets (SMMs) and this has become a major driving force for research in this field.

1.4.1 Reactivity

The conversion of small molecules into products of commercial or societal value is a focus of many areas of chemistry. Low-coordinate, transition metal complexes have found application in this field. Stoichiometric reactions between these complexes and small molecules have led to a variety of metal containing or organic complexes.[52,142,143] The promotion of organic and inorganic transformations using catalytic amounts of these complexes has also been investigated.[64–66]

Following the crystallographic characterisation of the quintuple bond in 2005, Power and co-workers developed a series of d^5-d^8 metal(I) species, some of which were sterically prevented from dimerising. The cobalt complex [2,6-(2,4,6-*i*Pr$_3$C$_6$H$_3$)$_2$-3,5-*i*Pr$_2$C$_6$H]Co[η^6-Tol] (**I·73**)

was investigated for its ability to activate carbon monoxide and nitric oxide (**Scheme 1·8**).[145] Exposure of **I·73** to an atmosphere of carbon monoxide resulted in the crystallisation of the paramagnetic complex [2,6-(2,4,6-*i*Pr$_3$C$_6$H$_3$)$_2$-3,5-*i*Pr$_2$C$_6$H]C(O)CoCO (**I·74**), from the insertion of one equivalent of carbon monoxide into the Co−C bond and coordination of a further equivalent to the metal centre. The cobalt(I) moiety features an η^6 interaction between the cobalt and one of the flanking aryl rings. The bond between the terminal carbon monoxide and the cobalt centre was shown to involve a high degree of π-back bonding by infra-red spectroscopy and X-ray diffraction studies.

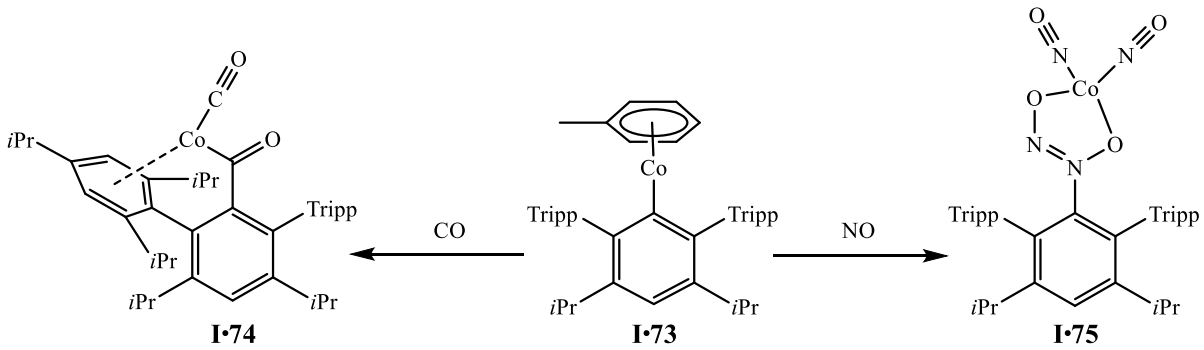

Scheme 1·8. The reactivity **I·73** with carbon monoxide to afford **I·74**, and with nitric oxide to afford **I·75**.

The reaction with nitric oxide afforded the red complex [2,6-(2,4,6-*i*Pr$_3$C$_6$H$_3$)$_2$-3,5-*i*Pr$_2$C$_6$H]N(NO)OCo(NO)$_2$ (**I·75**) in 19% yield. The complex features a cobalt(I) centre with tetrahedral geometry bound to two equivalents of nitric oxide and by the bidentate ligand [2,6-(2,4,6-*i*Pr$_3$C$_6$H$_3$)$_2$-3,5-*i*Pr$_2$C$_6$H]N(NO)O]$^{2-}$. The latter was formed by the insertion of nitric oxide into the Co−C bond and formation of an N−N bond. The authors note that such nitric oxide insertion products are known for early transition metal complexes but rare in the later transition metals.

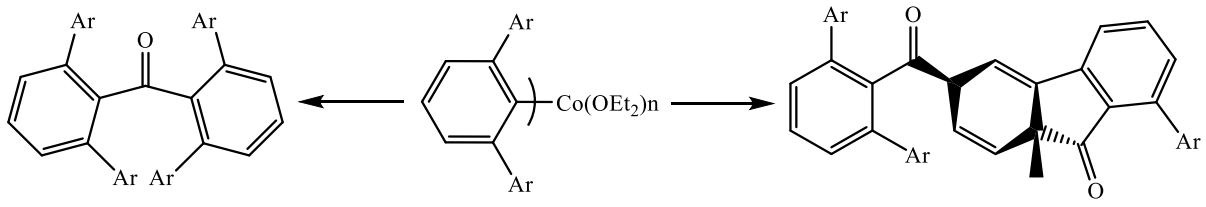

I·77 Ar = Naph **I·76** Ar = Naph, n = 1 **I·30** Ar = Mes, n = 0 **I·78** Ar = Naph

Scheme 1·9. The reactivity of cobalt diaryls with carbon monoxide.

Similar reactivity of carbon monoxide with cobalt(II) diaryls was reported by Kays and co-workers. It was found that the nature of the aryl ligand had a strong influence over the reaction products (**Scheme 1·9**).[142] Exposure of [2,6-(1-Naph)$_2$C$_6$H$_3$]$_2$Co(OEt$_2$) (**I·76**) to an atmosphere of dry carbon monoxide resulted in the formation of the sterically bulky benzophenone, [2,6-(1-Naph)$_2$C$_6$H$_3$]$_2$CO (**I·77**). This was the first example of a benzophenone featuring substituents in the *meta*-positions. Exposure of [2,6-Mes$_2$C$_6$H$_3$]$_2$Co (**I·30**) to dry carbon monoxide resulted in a terphenyl substituted keto-fluorenone, 3-Mes-9,11,13-trimethyl-10-ArCO-fluorenone (where Ar = 2,6-Mes$_2$C$_6$H$_3$, **I·78**). Both complexes are formed with concomitant elimination of Co$_2$(CO)$_8$.

The proposed mechanisms feature the coordination of carbon monoxide to the cobalt centre, followed by insertion into the Co−C$_{ipso}$ bond and reductive elimination of the organic molecules **I·77** and **I·78**. The fluorenone complex forms *via* the dearomatisation of one of the mesityl flanking groups and the generation of two steric centres, either in the *R,R* or *S,S* configurations but not in the *meso* configuration. These examples demonstrate the ability of small molecule activation by transition metals to access molecules that could not be obtained by other means.

The reduction of [2,6-(2,4,6-*i*Pr$_3$C$_6$H$_3$)$_2$-3,5-*i*Pr$_2$C$_6$HCoCl]$_2$ with KC$_8$ in hexafluorobenzene affords K[2,6-(2,4,6-*i*Pr$_3$C$_6$H$_3$)$_2$-3,5-*i*Pr$_2$C$_6$H]CoF[Ph] (**I·79**).[146] In this reaction the cobalt centre inserts into the C-F bond, through a mechanism the authors were unable to establish, to give a three-coordinate cobalt(II) centre. Activation of C–F bonds is common in nickel chemistry[147] but relatively rare with cobalt as the active metal species.[148–150] This study was

conducted to investigate η^6-binding in analogues of **I·73** coordinated by electron poor aromatic systems. Other fluoride bearing aromatics, C_6H_5F and $C_6H_5CF_3$, were found to be stable and mask the cobalt centre effectively.

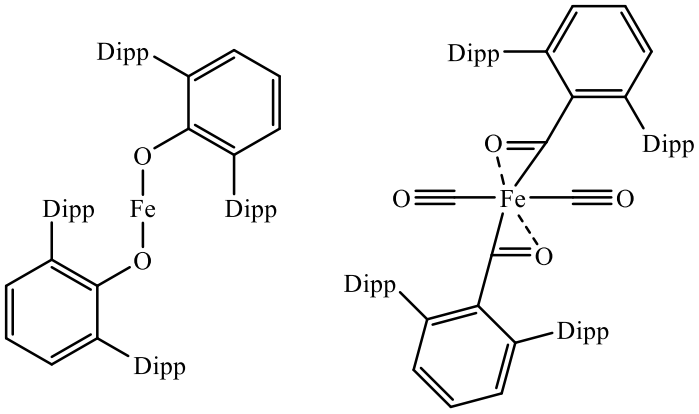

I·80 **I·81**

Figure 1·15. Complexes obtained from the reaction between **I·34** and oxygen (**I·80**) or carbon monoxide (**I·81**).

The reactivity of manganese and iron diaryls toward small molecules has also been investigated. Oxygen and carbon monoxide were found to insert into the Fe–C bond of [2,6-$Dipp_2C_6H_3]_2Fe$ (**I·34**) to afford [2,6-$Dipp_2$-$C_6H_3O]_2Fe$ (**I·80**) and [η^2-2,6-$Dipp_2$-$C_6H_3CO]_2Fe(CO)_2$ (**I·81**) respectively (**Figure 1·15**).[52] Complex **I·80** is a rare example of a two-coordinate iron acyl complex and is notable for the fact that it is resistant to further oxidation to an iron(III) species in the presence of excess dry oxygen. The complex is strictly linear around the metal centre and has a magnetic moment of 5.28 μ_B, suggesting significant orbital contributions to the magnetism. **I·81** is the product of two instances of carbon monoxide insertion into Fe–C bonds and the coordination of two further equivalents of the small molecules. This affords a diamagnetic six-coordinate iron(II) centre that provides a significant amount of π-back bonding to the carbonyl groups, according to infra-red studies and inspection of the crystal structure.

Power *et al*. found that **I·34** shows no reactivity towards nitrogen dioxide.[52] However, both **I·34** and the manganese analogue (**I·32**) were able to form amido complexes, [2,6-

$Dipp_2C_6H_3Fe(NH_3)]_2$ (**I·82**) and $[2,6\text{-}Dipp_2C_6H_3Mn(NH_3)(\mu_2\text{-}NH_3)]_2$ (**I·83**) respectively, through the activation of dry ammonia.[143] It was postulated that the mechanism of formation involved coordination of one equivalent of ammonia, which is then deprotonated in conjunction with the loss of a terphenyl ligand. The two-coordinate aryl-amido complexes then dimerises. Complex **I·83** does not react further whilst the formation of **I·82** requires further coordination by one equivalent of ammonia. The magnetic moments of both complexes [4.41 μ_B (**I·82**) and 5.62 μ_B (**I·83**)] are lower than the spin-only values for two high spin d^6 or d^5 respectively. This indicates a degree of antiferromagnetic coupling between the metal centres. Both complexes are rare examples of first row-transition metals with bridging amido ligands.

More recently, transition metal *m*-terphenyl species have been shown by Kays *et al*. to catalytically promote a variety of reactions. $[2,6\text{-}Ar_2C_6H_3]_2M(THF)n$ [Ar = tmp, n = 1, M = Mn (**I·36**) or Fe (**I·37**), Ar = Mes, n = 0, M = Mn (**I·31**) or Fe (**I·32**)] were shown to catalyse the cyclotrimerization of primary aliphatic isocyanates at low temperatures and low catalyst loadings.[65] The efficacy of the catalysts was limited by the sterics of the system; secondary and tertiary aliphatic or aryl isocyanates did not cyclise in the presence of diaryl complexes **I·31**, **I·32**, **I·36** or **I·37**, except as mixtures with primary aliphatic isocyanates.

Complexes **I·32** and **I·37** were also found to catalyse the hydrophosphination of isocyanates.[64] This was the first example of a transition metal catalyst promoted hydrophosphination of isocyanates which results in both the mono- and di-insertion of isocyanates into the P−H bond. The scope of the substrates is again affected by steric factors: bulkier isocyanates selectively afford the mono-insertion product. The authors were able to promote the formation of the double insertion product almost exclusively for aryl isocyanates through the addition of the weak acid $NEt_3{\cdot}HCl$ to the reaction when **I·37** was used as the catalyst. The proposed mechanism for this catalytic cycle is given in **Scheme 1·10** and involves the insertion of the isocyanate into the Fe−C bond before subsequent attack and rearrangement of the secondary

phosphine. Finally, the authors demonstrated that this process was able to combine two different isocyanates into the di-insertion product, albeit as a minor product of the reaction.

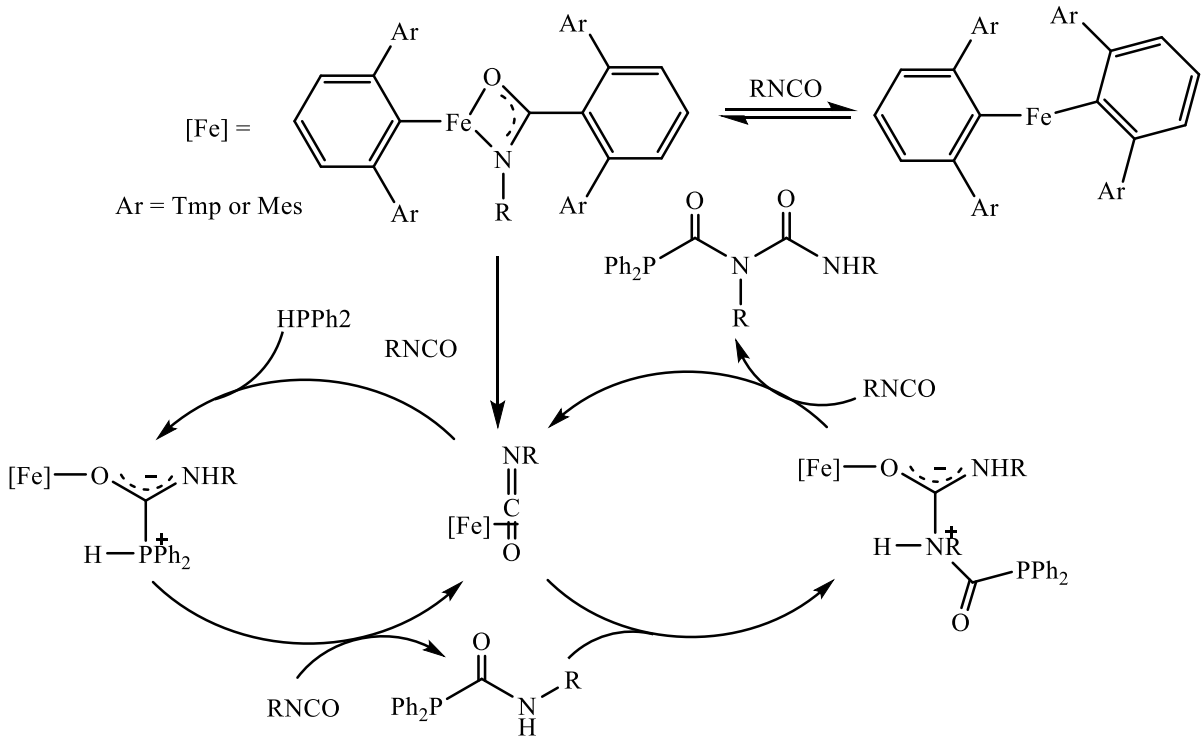

Scheme 1·10. The proposed mechanism for the hydrophosphination of isocyanates.[64]

The same group demonstrated that manganese complexes **I·31**, **I·36** and [2,6-(2,6-Xyl)$_2$C$_6$H$_3$]$_2$Mn (**I·83**) effectively promote the dehydrocoupling of dimethylamine-borane at 60 °C and 5 mol% loading, generating hydrogen gas in the process.[66] Such reactions are of importance to the development of new fuel storage materials. The ability to liberate dihydrogen from stable, hydrogen rich molecules at low temperatures using cheap, abundant and non-toxic metals is of great value.[151] The authors found that **I·31** and **I·83** promoted the reaction through a homogeneous mechanism that affords [Me$_2$N-BH$_2$]$_2$ in yields greater than 95% in 3.8 and 1.7 hours respectively. **I·36** promotes the reaction through a heterogeneous route. Upon addition of Me$_2$NH-BH$_2$ to a solution of **I·36**, manganese nanoparticles were observed to form immediately. These nanoparticles were found to be the active catalyst through the mercury drop test and their character was determined *via* a variety of imaging techniques.

Whilst the catalytic potential of *m*-terphenyl complexes of first row transition metals is only now being explored, the NHC ligand system has been viewed as an organometallic co-ligand for catalytic processes since the 1990s.[4,94,152,153] However, with respect to low-coordinate complexes the chemistry is less developed with the majority of late, open shell, transition metal complexes appearing within the last decade. Much of this chemistry is limited to that of Groups 8-10, with nickel(I)-mediated cross couplings accounting for the majority.

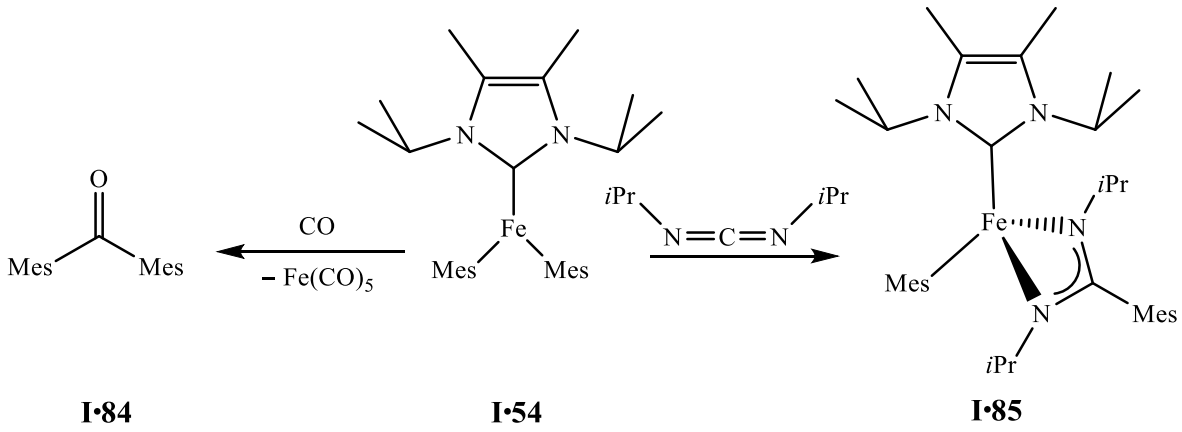

I·84 **I·54** **I·85**

Scheme 1·11. The reactivity of **I·54** with carbon monoxide (**I·84**) and carbodiimide (**I·85**).

Deng *et al*. demonstrated that the reactivity of low-coordinate iron NHC complexes can be exploited to promote several reactions (**Scheme 1·11**). Exposure of [IPrMe]Fe[Mes]$_2$ (**I·54**) to carbon monoxide results in the formation of a substituted benzophenone, Mes$_2$CO (**I·84**), similar to the benzophenone (**I·77**) isolated by Kays and coworkers.[122] The proposed mechanism involves consecutive insertion-reduction cycles followed by elimination which is consistent with literature examples.[154,155] Exposure of the same complex to two equivalents of the carbodiimide, *i*PrNCN*i*Pr, again resulted in insertion of the small molecule into the Fe−C$_{Ar}$ bond to form [IPrMe]Fe[Mes][η^2-(*i*PrNC{Mes}N*i*Pr)](**I·85**). This complex was resistant to further insertion of a carbodiimide moiety into the remaining Fe−C$_{Ar}$ bond.

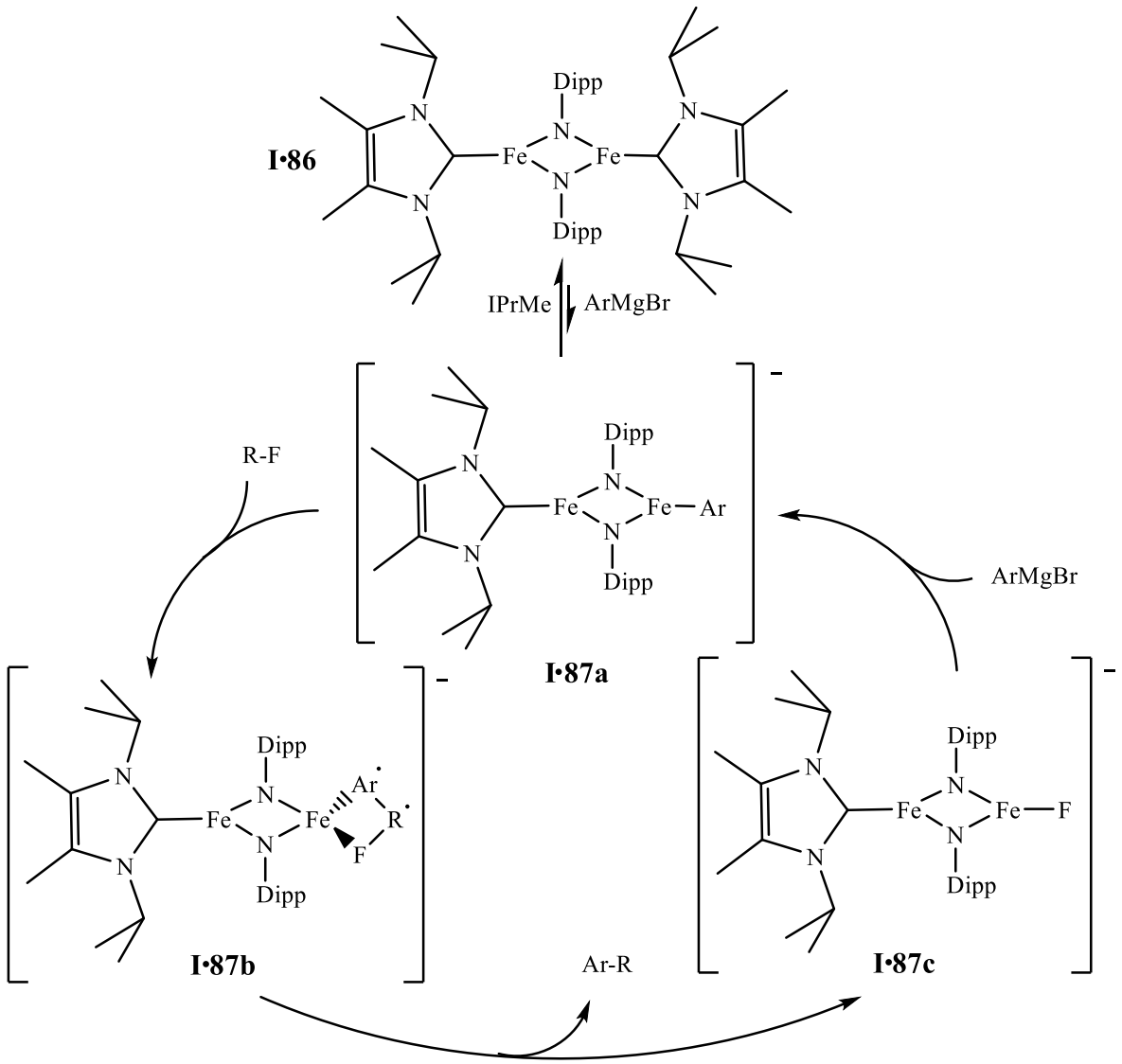

Scheme 1·12. The proposed catalytic mechanism for the coupling of primary alkyl fluorides with aryl-Grignard reagents proposed by Deng and coworkers.[156]

Deng *et al.* also demonstrated the ability of these complexes to promote cross-coupling reactions. The reaction of [IPrMe]Fe[Mes]$_2$ (**I·54**) with one equivalent of iodobenzene was shown to result, following hydrolysis, in the organic molecule Ph-Mes. This product was isolated in yield of 35% and suggested that the reaction between the organoiron-NHC species and an aryl-halide is the C−C formation step of the Kumada coupling reaction.[122] A later, more in-depth study by the same group demonstrated the ability of [(IPrMe)Fe(NDipp)]$_2$ (**I·86**) and of [(IPrMe)Fe(μ-NDipp)$_2$FeF] (**I·87c**) to catalytically promote the coupling of primary alkyl fluorides with aryl-Grignard reagents.[156] This reaction progresses over 48 hrs in THF at room

temperature with a catalyst loading of 5 mol% to afford isolated yields of over 65% for a wide range of substrates bearing different steric profiles and functional groups. Investigations into the mechanism found that a reaction between just one of the substrates and **I·86** does not occur which led the authors to suggest that **I·86** is actually the pro-catalyst, converted into the active catalytic species [(IPrMe)Fe(μ-NDipp)$_2$FeAr] (**I·87a**) *in-situ* as demonstrated in **Scheme 1·12**. The mechanism proposed by the authors and shown in **Scheme 1·12** proceeds *via* an iron species bearing two radical organic fragments. These then couple to give the iron-fluoride species (**I·87c**).

The same group has used three-coordinate cobalt complexes with NHC ligation as hydrosilylation catalysts.[127] This work was based on an earlier observation that four-coordinate NHC-cobalt complexes were able to activate the Si−H bond of H_2SiPhR (R = H, Me or Ph), with concomitant formation of gaseous hydrogen.[157] [IAd]Co[PPh_3][CH_2SiMe_3] (**I·90**) was found to catalyse the hydrosilylation of terminal alkynes at catalyst concentrations as low as 0.01 mol%, exclusively yielding the *trans*-isomer (**Scheme 1·13**). At catalyst loadings of 2 mol% the reaction affords *E*-$C_6H_{13}CHCHSiHPh_2$, from the reaction of H_2SiPh_2 and 1-octyne, in yields of 96%. The selectivity is lower and the reaction time longer with H_3SiPh as the silane and the reaction does not progress at all when this is replaced with $HSiPh_3$, even at 70 °C.

The catalyst tolerated a range of functional groups on the alkyne without a significant loss of yield. Furthermore, at higher temperatures and within equivalent timeframes, **I·88** is able to promote the hydrosilylation of internal, symmetrical alkynes in more than 90% yields (**Scheme 1·13**).

Investigations into internal, asymmetric alkynes found the production of possible trans-isomers in *ca*. 1:1 ratios except when trimethylsilyl (TMS) groups were present. In these cases, hydrosilylation exclusively affords the complex with the silyl group germinal to the TMS

group. The authors suggest that this is a steric affect. Investigations into the mechanism found that the active catalytic species is actually [IAd]Co[PPh_3][$SiHPh_2$] (**I·89**). The authors note that the selectivity achieved in this process is rare and signifies the uniqueness of this cobalt catalyst.

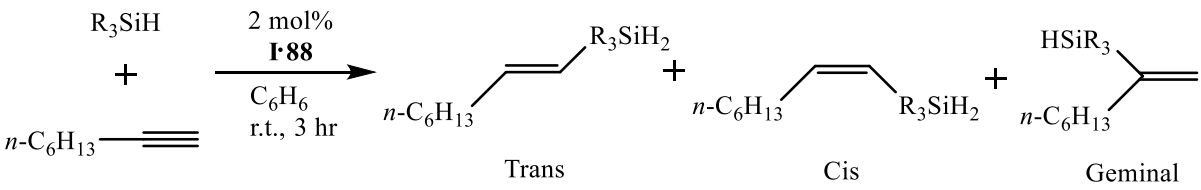

Scheme 1·13. The hydrosilylation of terminal alkynes promoted by **I·88**.

Deng et al. employed similar complexes Co[$N(SiMe_2)_2]_2$ (**I·90**) and the NHC adducts [NHC]Co[$N(SiMe_2)_2]_2$ [NHC = IPr (**I·91**), IMes (**I·92**), IMesPr (**I·93**) or IMesMe (**I·94**)] in the hydrosilylation of alkenes.[129] Initial experiments with 1-octene found that whilst all the complexes are able to promote the reaction with $HSi(OEt)_3$, all but the **I·94**, which contains the least bulky NHC, afford significant amounts of by-products. These by-products were the dehydrogenative silylation product *n*-$C_6H_{13}CH{=}CHSi(OEt)_3$, isomers of 1-octene and *n*-octane. **I·94** gave 99% conversion to *n*-$C_7H_{15}CHSi(OEt)_3$. This demonstrates neatly the benefit a readily alterable ligand system can have to catalytic studies. The efficacy of **I·94**, in loadings of 1 mol%, was investigated for a range of functional groups and the process proved sensitive to the steric profile of the substrates. For example, the conversion rate of the *t*-Bu substituted alkene was much lower than that of 1-octene. The reaction also does not progress with styrene which the authors attribute to the complexation of the low-coordinate cobalt species with aryl systems. This was supported by the observation that the reaction between **I·91** and $HSi(OEt)_3$ in benzene affords [NHC]CoH[η^6-C_6D_6], which is not catalytically active. This catalytic process is notable for the lack of external activator, such as $NaBHEt_3$, in the initiation of the reaction.

Further reactivity towards small molecules promoted by similar cobalt species is limited to intramolecular CH_3-activations[131,132] and ligand cleavage.[133] A notable example of the latter is the reaction between the amido complex [IPr]Co[N(2,6-$Mes_2C_6H_3$)] (**I·95**) and excess carbon monoxide in Et_2O which affords the bulky isocyanate (2,6-$Mes_2C_6H_3$)NCO (**I·96**) and the unusual cobalt(0) dimer, [IPrCo$(CO)_3]_2$ (**I·97**). **I·95** is the first imido complex of cobalt to be isolated. This molecule also possesses unique qualities as a single molecule magnet.[124,133]

1.4.2 Single Molecule Magnetism

The paramagnetism of open-shell d-block complexes is an area of intense scrutiny due to their potential to act as single molecule magnets (SMMs). SMMs were described by Layfield as displaying slow relaxation of the magnetisation, purely of molecular origin, in the absence of an applied magnetic field.[158]

SMMs have potential applications in quantum computing and high density data storage and could play a major role in the continued miniaturisation of technology.[159,160] To find wide application in real-world scenarios SMMs need to exhibit magnetic hysteresis at readily accessible temperatures, such as those of liquid nitrogen. A strong aspect of research in this area is therefore angled toward isolating complexes that display such behaviour. The key parameters by which SMM behaviour is measured and some basic aspects of SMM design will be discussed below.

A key property of SMMs is magnetic anisotropy, defined as the magnetic moment of a discrete complex has a favoured orientation, also described as the easy axis. The energy barrier that must be overcome for this spin to relax is known as the anisotropy barrier, U_{eff}. As the energy required to overcome this barrier increases so does the temperature at which the spin relaxes, although this relationship is not linear. This temperature is known as the blocking temperature (T_B).

Initial research efforts focused on developing transition metal clusters with a high total spin (*S*) due to the high number of metal centres. This approach was related to the origins of the field with the cluster complex, $[Mn_{12}O_{12}(CH_3COO)_{16}(H_2O)_4]$ being the first SMM identified. A natural limit to the approach was found in that the anisotropy of the system was inversely proportional to the total spin of the system.[161] Research in recent years has therefore focused on SMMs that contain a single magnetic centre and methods of raising the blocking temperature and anisotropy of such complexes.[162]

One method of increasing anisotropy is through the reduction of the coordination number of the metal centre. This decreases the crystal field splitting, reducing the gap between the ground and excited states, allowing better mixing of the excited states. This reduces the quenching of the orbital angular moment which contributes significantly to the anisotropy of the system. As has been alluded to, this contributes to the magnetic moment of complexes being higher than the spin-only value.[162] SMMs featuring metals in low-coordination numbers exhibit some of the highest anisotropy barriers, and therefore blocking temperatures, observed for transition metal complexes.[163]

In 2013 Long *et al*. published what was, at the time, the transition metal complex with the highest U_{eff}.[164] The complex, $[K(crypt\text{-}222)][Fe(C(SiMe_3)_3)_2]$ (**I·98**), was synthesised through the reduction of $[Fe(C(SiMe_3)_3)_2]$ with KC_8 in the presence of 222-cryptand (crypt-222). X-ray diffraction studies revealed the complex to be linear [C−Fe−C = 179.2(2)°] and the iron(I) oxidation state was confirmed by Mössbauer spectroscopy. Complex **I·98** demonstrated an U_{eff} of 226(4) cm^{-1} and exhibited slow relaxation of magnetisation below 29 K. The blocking temperature of the complex was 4.5 K. This U_{eff} is significantly higher than the next highest value of 181 cm^{-1} reported for a transition metal complex at that time.[165] Above 20 K the magnetisation in **I·98** was reversed by thermally activated processes. Below 20 K, however, there was a reduced dependence of relaxation time on temperature indicating a tunnelling

relaxation pathway was present. The authors attributed this to the linear nature of the two-coordinate complex and the d^7 electron configuration which afforded a $S = 3/2$ spin state.

A later development by Deng *et al*. currently possesses the record for the highest anisotropy barrier among first row transition metals. It was found that the d^7 complexes, [NHC]Co[N(2,6-$Mes_2C_6H_3$)] [NHC = IPr (**I·95**), CyIPr (**I·99**) or sIMes (**I·100**)], described in **Table 1·2**, exhibited anisotropy barriers (U_{eff}) as high as 413 cm^{-1}. It was theorised by Long *et al*. that increased rigidity of a two-coordinate core would reduce vibronic coupling, which would in turn reduce the opportunity for the magnetisation of a complex to relax.[166] Deng *et al*. therefore suggested that increasing the covalency of the metal−ligand bonds might raise the U_{eff} of the complex and therefore the blocking temperature. Selecting an imido ligand achieved this. All three complexes broke the previous U_{eff} record [U_{eff} = 297 (**I·95**), 288 (**I·99**), 413 (**I·100**) cm^{-1} respectively]. The highest performing complex, **I·100**, exhibited a blocking temperature of 9.5 K.

1.5 Global Aims

Given the range of uses that have been found for low-coordinate, transition metal systems, and the contribution to the general understanding of fundamental chemical concepts, there is a motivation to explore these systems further. Therefore, the broad aim of this work is to expand the range of low-coordinate, transition metal complexes available for study. This will be achieved by developing two-coordinate, transition metal complexes supported by an organic, heteroleptic ligand framework. The complexes developed will then be investigated for their catalytic capabilities and magnetic properties.

The heteroleptic ligand framework will be formed from either a combination of two different *m*-terphenyl ligands or a combination of one *m*-terphenyl ligand with a second organic ligand type. In the first instance, this second ligand will be a N-heterocyclic carbene, but the desire is to develop a synthetic route that will be applicable to multiple organic ligand types.

Expanding the range of available two-coordinate, transition metal complexes will provide a greater variety of complexes for use in catalytic and magnetic studies. Synthetic routes toward heteroleptic ligand systems, to be developed in this work, will also enhance the tuning of such complexes to suit specific purposes.

Heteroleptic ligand systems will enhance the design potential of two-coordinate, transition metal complexes. For instance, it will be possible to design complexes that can be tethered to a surface through a substituent on one ligand. Another foreseeable use is the combination of *m*-terphenyl ligands that interact with one another to form a stabilising cage around a metal ion. Through this method the isolation of a chromium(II) diaryl complex may be achieved.

The first stage of this project is to isolate a series of Grignard analogues, bearing one organic ligand each, for use as starting materials. With these isolated, it will be possible to investigate the combination of this first ligand with alternative organic ligands. The two-coordinate,

heteroleptic, open-shell transition metal complexes that are successfully isolated will be tested for their magnetic and catalytic properties. Analogous Group 12 complexes will be developed to facilitate structural NMR studies of the ligand systems.

Chapter II

A Study of *m*-Terphenyl and N-Heterocyclic Carbene, Halide-Bridged Complexes

2.1 Introduction

Organometallic complexes with the general motif RMX (R = alkyl or aryl, M = any metal, X = any halide) have great synthetic utility in metathesis or reductive methodologies.[167,168] A late transition metal, *m*-terphenyl example is the dimeric complex [2,6-$Mes_2C_6H_3$(μ-Br)Co(THF)]$_2$ (**I·29**) published by Power and co-workers.[74] A related, chromium complex was fundamental in the synthesis of [2,6-$Dipp_2C_6H_3Cr]_2$, containing the first crystallographically observed quintuple bonding interaction.[62] [2,6-$Dipp_2C_6H_3Cr]_2$ was synthesised by the reduction of the halide bridged dimer, [2,6-$Dipp_2C_6H_3$Cr(μ-Cl)]$_2$ with KC_8.

A series of halide bridged, transition metal and Group 12 complexes have been reported, of which [2,6-$Dipp_2C_6H_3$Zn(μ-I)]$_2$ (**Figure 2·1**, **II·1**) is an example.[169–171] The halide bridged complexes of manganese, iron and cobalt adopt a similar structure to that of **II·1** but further incorporate two equivalents of lithium iodide into the structure, each supported by a diethyl ether molecule, to form a central cubic unit and a general formula [2,6-$Dipp_2C_6H_3$M(μ-I)·(LiI)]$_2$.[170] This synthetic methodology was expanded to a variety of different *m*-terphenyl ligands, facilitating investigations into the nature of metal-metal bonds,[172,173] alternate bridging

ligands,[174] and low-coordinate metal(I) species stabilised by a *m*-terphenyl ligand and a masking arene ligand (**Figure 2·1**, **II·2**)[175] or tertiary phosphine.[176]

Jones *et al*. reported the use of [LM(μ-X)(THF)]$_2$ (L = [(2,6-{C(H)Ph$_2$}$_2$-4-MeC$_6$H$_3$)(SiMe$_3$)N]

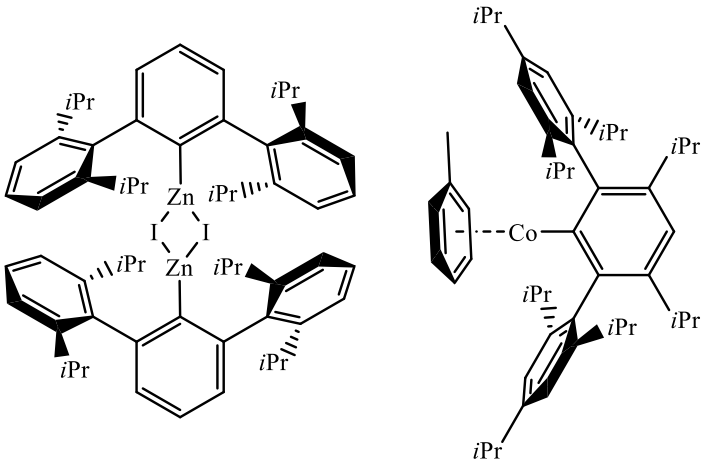

II·1 **II·2**

Figure 2·1. The halide bridged, dimeric complex, [2,6-Dipp$_2$C$_6$H$_3$Zn(μ-I)]$_2$ (**II·1**) and the toluene masked, cobalt(I) complex, [3,5-*i*Pr$_2$-2,6-Tripp$_2$C$_6$H$_3$]Co[η^6-C$_6$H$_7$] (**II·2**), synthesised through the reduction of [3,5-*i*Pr$_2$-2,6-Tripp$_2$C$_6$H$_3$Co(μ-Cl)]$_2$ in toluene.

(L*) or [(2,6-{C(H)Ph$_2$}$_2$-4-*i*PrC$_6$H$_3$)(Si*i*Pr$_3$)N] (L$^\#$); M = Mn, X = Br (**II·4**, **II·5** respectively, **Figure 2·2**) or L = L$^\#$, M = Cr, X = Cl (**II·3**) or M = Mn, X = Br (**II·4**, **II·5** respectively, **Figure 2·2**))[177] as a precursor to a heterobimetallic complex bridged by two ligands, Mn^{II}(μ-L*)(μ-L$^\#$)Cr^0 (**II·6**), and the first examples of two-coordinate, manganese(I) dimers, L*MnMnL* (**II·7**) and L*MnMnL$^\#$ (**II·8**, **Figure 2·2**).[55]

II·7 and **II·8** were accessed through the reduction of **II·4** and **II·5**, respectively, with [(^{Mes}NacNac)Mg]$_2$.[178] In the case of **II·4**, the L*Mn^I fragment generated by this reaction dimerises, affording **II·7**. In contrast, upon reduction of **II·5** with [(^{Mes}NacNac)Mg]$_2$, the fragment is prevented from dimerising by the greater steric bulk of the ligand. The L$^\#$Mn^I fragment is therefore reduced further to afford L$^\#$Mn^{0}Mg[^{Mes}NacNac]. Exposure of L$^\#$Mn^{0}Mg[^{Mes}NacNac] to half an equivalent of [L*Mn(μ-Br)] (**II·4**) affords **II·8** through the reduction of **II·4** (**Figure 2·2**).

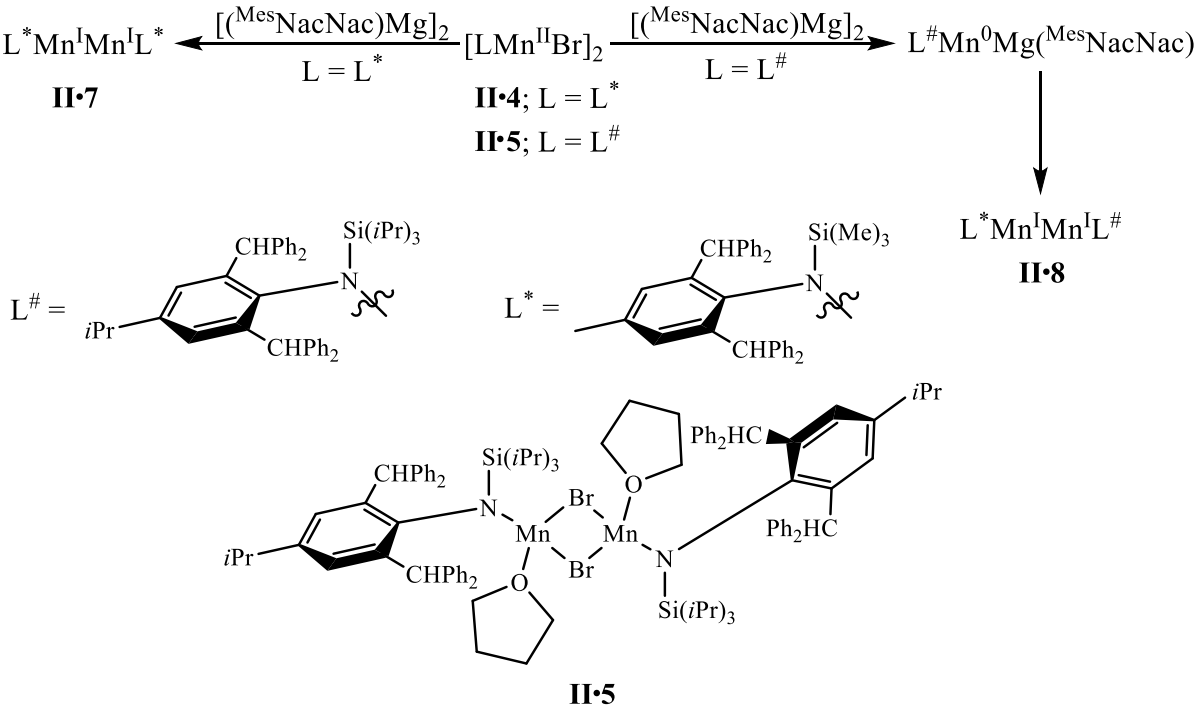

Figure 2·2. A summary of the synthetic routes to the first examples of a two-coordinate manganese(I) dimer featuring a metal-metal interaction (**II·7** and **II·8**, top) and structure of the halide bridged, dimeric structure (**II·5**) from which (**II·8**) was synthesised.

A structural and magnetic study of a series of halide-bridged, dimeric, transition metal complexes of the type $[LM(\mu\text{-}X)(THF)]_2$ (where L = L* or $[(2,6\text{-}\{C(H)Ph_2\}_2\text{-}4\text{-}MeC_6H_3)(SiPh_3)N]^-$ (L^), X = Br, M = Mn (**II·4** and **II·9**, respectively), Fe (**II·10** and **II·11**, respectively); X = Cl, M = Cr (**II·12** and **II·13**, respectively), Co (**II·14** and **II·15**, respectively) was conducted by Jones and Co-workers.[177] The manganese, iron and cobalt complexes, **II·4**, **II·9**–**II·11, II·14** and **II·15**, adopt a tetrahedral geometry, whilst the chromium complexes **II·12** and **II·13** adopt a square planar geometry.

Table 2·1 The magnetic moments (μB) of the halide bridged complexes of the formula $[LM(\mu\text{-}X)(THF)]_2$ where L = L* or L^.

Complex no.	Metal	Magnetic moment/μ_B
II·12	Chromium	5.81
II·4	Manganese	5.90
II·9		6.85
II·10	Iron	5.38
II·11		6.61
II·14	Cobalt	4.86
II·15		5.20

These complexes have magnetic moments which are lower than the spin-only values,[179] and has been proposed that this demonstrates antiferromagnetic coupling between the bridged metal centres. The magnetic moments are summarised in **Table 2·1**.

In complexes containing more than one metal centre magnetic investigations provide valuable information about the degree of magnetic coupling, and therefore interaction, between these centres. Antiferromagnetic coupling between metal centres manifests as a depression of the magnetic moment, relative to the spin only values. This has been used, alongside structural data, to infer the existence of bonds between metal ions.[41] Examples where this is the case are the investigations of the early, three-coordinate, organometallic complexes of manganese, iron, and cobalt.[38,41,180]

Close contact between metal ions can result in direct interaction between metal centres, which occurs when the metal centres are close enough for the d-orbitals of each to overlap. There is then possibility for the unpaired electrons from each paramagnetic centre to interact with the other and for their spins to align or adopt opposing spin orientations, according to Hund's rules.[41,179]

There are other mechanisms for magnetic interaction between two paramagnetic metal ions in one complex. These are known as indirect methods and describe a situation where magnetic coupling is transmitted between two paramagnetic moieties by a diamagnetic, bridging moiety. This allows a ferromagnetic or antiferromagnetic effect to be observed in structures where the metal centres concerned are too far apart to directly couple. This type of coupling is often observed in metal-oxides where the transmission takes place through the bridging oxo groups.[181,182]

The two types of indirect coupling are superexchange and semicovalent. Superexchange coupling involves the promotion of one electron from the ground state of a bridging

diamagnetic ion to an excited state of the paramagnetic ion.[183] The nature of this coupling, ferromagnetic or antiferromagnetic, depends on the occupancy of the d-orbitals of the metal ions.

Semi-covalent coupling describes the different covalent bonding scenarios within a bridged system. More precisely, this is how a bonding electron pair of the bridging ion is shared between the two bridged paramagnetic centres. Alignment of individual electrons within the bonding pair with the electrons of the separate metal centres effectively transmits the spin of one paramagnet to the other. A covalent interaction between the bridging ion and two identical metal ions results in antiferromagnetic coupling. Covalent interaction between the bridging ion and just one metal centre, with an ionic interaction between a second, identical metal centre results in ferromagnetic coupling.[184]

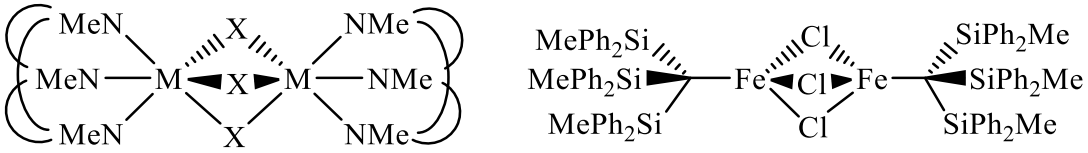

II·16 - II·22 **II·23**

Figure 2·3. The structures of **II·16–II·22** and **II·26**. The amide of **II·16–II·22** are joined by ethyl fragments.

Trautwein *et al*. demonstrated that indirect magnetic coupling can occur in discrete molecules containing two paramagnetic centres bridged by halide moieties, through a magnetic study of a series of first row, transition metal species, $[\{Cyc(MeNC_2H_4)\}M^{II}(\mu\text{-}X)_3M^{II}\{Cyc(MeNC_2H_4)\}][BPh_4]$ (X = Cl, M = Mn (**II·16**), Fe (**II·17**), Co (**II·18**), Ni (**II·19**); X = Br, M = Mn (**II·20**), Co (**II·21**), Ni (**II·22**), **Figure 2·3**).[185] Power *et al.* reported the related complex, $[\{C(SiMe_2Ph)_3\}Fe_2(\mu\text{-}Cl)_3][Li(THF)_4]$ (**II·23**, **Figure 2·3**)[186]

In these complexes both metal centres adopt a, sometimes distorted, octahedral geometry. M···M distances were *ca.* 3.0 Å where X = Cl, well within the sum of the Van der Waals radii, this presents the possibility of a metal-metal bond.[187] Through solid-state measurements of the

magnetic susceptibility Trautwein *et al.* observed that the coupling between the metal centres is antiferromagnetic. However, Power *et al.* did not observe this phenomenon in the iron complex **II·23**.

Trautwein *et al.* noted in this study that coupling is often a function of both direct and indirect pathways. The exceptions to this are the nickel complexes **II·19** and **II·22** where direct exchange is not possible due to the filled t_{2g} orbitals. Therefore, any coupling observed must be occurring by indirect pathways.

To return to the *m*-terphenyl supported, halide bridged complexes of the type [2,6-$Dipp_2C_6H_3$(μ-Cl)Cr]$_2$ **II·24** and [2,6-$Dipp_2C_6H_3$(μ-I)M]$_2$[LiI(OEt_2)]$_2$ [M = Mn (**II·26**), Fe (**II·27**), **Co** (**II·28**); **Figure 2·4**] discussed previously, Power *et al*. reported a detailed study into the origin of the antiferromagnetic coupling observed in the complexes.[170] The dominant exchange pathway in these complexes was direct coupling between the metal centres. Weak, indirect coupling was observed however, transmitted *via* the bridging halides.

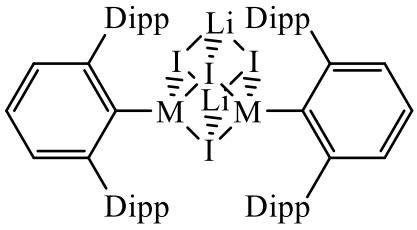

Figure 2·4. A general structure of the cubic, halide bridged dimeric complexes of later transition metals synthesised by Power *et al*. Diethyl ether molecules, bound to the lithium moieties, are omitted for clarity. M = Mn – Co (**II·26**- **II·28**)

2.2 Aims

The aim of this project is to develop two-coordinate, heteroleptic complexes bearing two different organic ligands. It was envisioned these complexes could be accessed *via* transition metal or Group 12 complexes in the +II oxidation state, coordinated by a single organic ligand and at least one halogen. This synthetic route is outlined in **Scheme 2·1**.

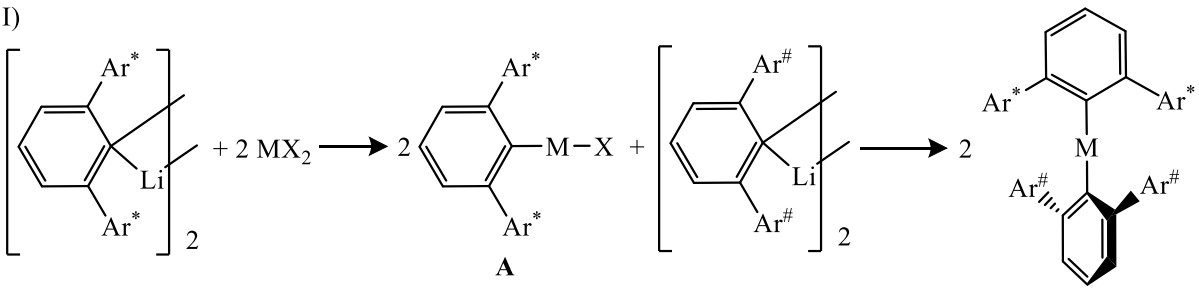

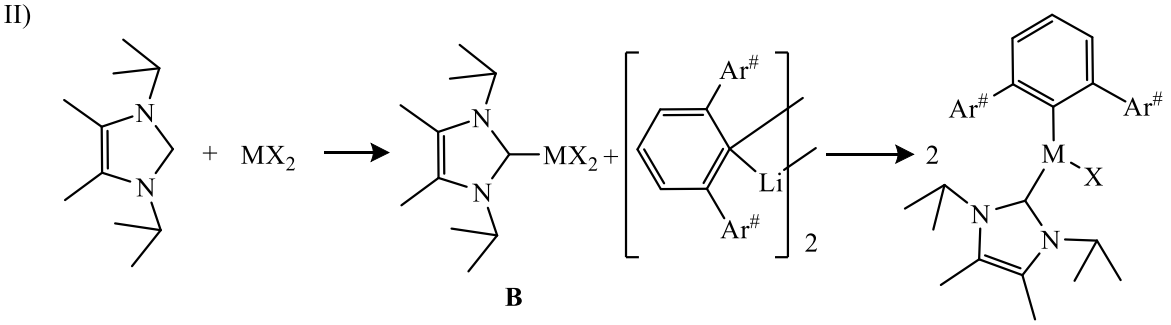

Scheme 2·1. Showing the proposed synthetic routes to two-coordinate, heteroleptic, transition metal and group 12 complexes.

It is necessary to synthesise, isolate and characterise a series of complexes that fit this description (complexes **A** and **B** in **Scheme 2·1**). Two types of complex are envisioned: one type in which the metal centre is coordinated by an *m*-terphenyl ligand and a single halogen in a two-coordinate metal(II) complex (**A**); and a second type in which the metal centre is coordinated by an NHC and two halogens in a three-coordinate, metal(II) complex (**B**). From examples of similar complexes in the literature, it is thought likely that these complexes will dimerise through halogen bridges.[170,188]

The Group 12 metals, manganese, iron, and cobalt will be investigated as these have been shown to form stable, two-coordinate complexes supported by *m*-terphenyls.[76,189] Chromium, nickel and copper will also be investigated.[62,140] The complexes synthesised will be characterised using mass spectrometry and single-crystal X-ray diffraction.

2.3 Results and Discussion

A series of halogen-bearing, transition metal and Group 12 complexes supported by one type of ligand were synthesised for use as precursors for heteroleptic, two-coordinate species. These complexes typically dimerised to fulfil their electronic requirements indicating that the ligands used do not provide enough steric bulk to prevent dimerisation.

These complexes are ideal as starting materials for heteroleptic, two-coordinate complexes as a second, bulky ligand can be introduced to break up the oligomerisation and provide the desired complexes. To access these products kinetic control of the reaction is required to prevent the reaction of the metal halide with two ligands where only one was required.

2.3.1 N-Heterocyclic Carbene complexes

1,3-bis(2,6-Diisopropylphenyl)imidazoline-2-ylidene (IPrMe) was synthesised *via* a literature procedure, described in general experimental section 2.6.3.[97] Complexes of the type $[(IPrMe)MX_2]_2$ [X = Br, M = Co (**II·30**); X = Cl, M = Zn (**II·31**)] were synthesised by slow addition of two equivalents of IPrMe to two equivalents of an appropriate metal halide, dissolved in THF (**Scheme 2**).

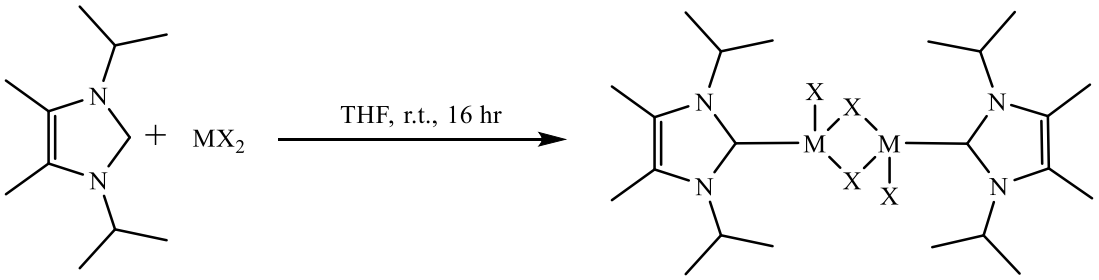

Scheme 2·2. Synthetic route to **II·30** and **II·31**.

$[(IPrMe)CoBr_2]_2$ (**II·30**) was isolated as a blue solid, which was sparingly soluble in non-polar, aromatic solvents such as benzene and toluene. Crystals of the compound were grown by layering pentane onto a saturated solution of the complex in benzene, followed by storage at

7°C. The crystals were shown to be **II·30** by X-ray diffraction experiments and elemental analysis, which confirmed the empirical formula.

The broadening and shift of the ligand signals in the ^{1}H NMR spectrum of **II·30** (**Figure 2.5**) compared with that of the uncoordinated ligand indicates a paramagnetic species, as expected for a d^7-d^7 dimeric complex. The signal for the CH of the *i*Pr group moved from 1.51 ppm to −15.93 ppm and the signal for the methyl groups of the backbone moved from 1.74 ppm to 28.83 ppm.

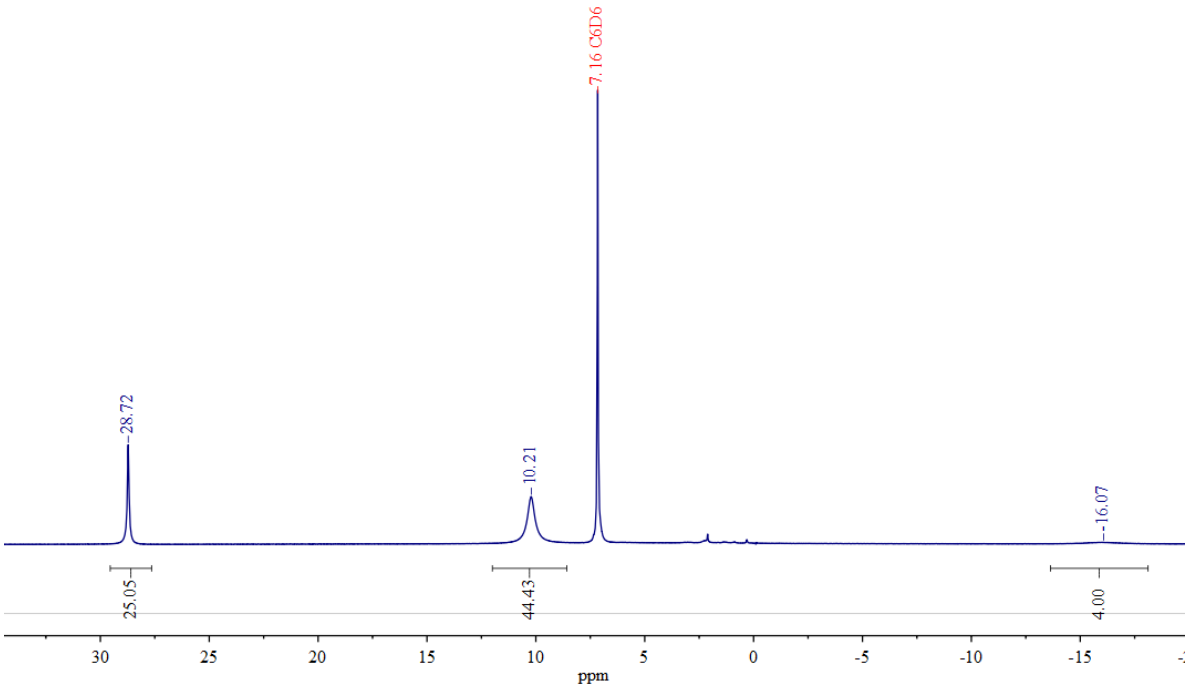

Figure 2·5. ^{1}H NMR spectrum of **II·30**.

The magnetic moment for **II·30** was not determined *via* Evans' method due to the lack of solubility in benzene-d_6 and instability in chloroform-*d*. THF-d_8 or solid-state methods such as SQUID magnetometry could be used to determine the magnetic moment.

$[(IPrMe)ZnCl_2]_2$ (**II·31**) was extracted into dichloromethane. Removal of this solvent and washing with pentane afforded a white solid. Crystals were grown by diffusion of pentane vapour into a saturated solution of the complex in chloroform-*d* and shown to be **II·31** by X-

ray diffraction studies and elemental analysis. The compound was further analysed by high resolution mass spectrometry and ^{1}H and ^{13}C NMR spectroscopy studies.

The ^{1}H NMR spectrum of **II·31** shows the three signals from IPrMe are shifted compared to the free ligand. The largest shift is of the CH of the *i*Pr group, the signal for which moves downfield from 3.95 ppm for uncoordinated IPrMe to 5.35 ppm in **II·31**. This shift could be attributed to inductive effects from the zinc centre, CH···Cl interactions or a combination of both.[190] That there is only one peak for the *i*Pr CH proton in the spectrum and that it shows no evidence of broadening suggests that any CH···Cl interactions are transient, forming and breaking on a timescale shorter than that of NMR spectroscopy. The signal representing the CH_3 groups of the *i*Pr in the ^{1}H NMR spectrum was also shifted downfield compared with the free ligand, though not by as significant an amount (1.74 ppm for uncoordinated IPrMe to 2.24 ppm for **II·31**).

Table 2·2. The unit cell parameters of **II·30** and **II·31**.

	II·30	**II·31**
Space Group	$P2_1/c$	$P2_1/c$
a/Å	19.2472(5)	19.0012(3)
b/Å	14.5080(4)	14.15029(17)
c/Å	11.2499(4)	11.10419(13)
$\alpha=\gamma$/°	90	90
β/°	105.803(3)	105.2982(12)

In the solid-state, the structures of **II·30** and **II·31** are isomorphous. **Table 2·2** contains the unit cell parameters of the complexes and the structures are shown in **Figure 2·8** and **Figure 2·6** respectively. Both complexes adopt the monoclinic space group $P2_1/c$. The asymmetric unit contains two halves of the dimeric species, each with a different morphology.

The metal centres in **II·31** adopt distorted tetrahedral geometries (τ'_4 = 0.79, 0.86)[191] and feature bonds to two bridging halides, one terminal halide and an IPrMe ligand. Of the four *i*Pr groups, three are orientated so the CH moiety is pointing toward the metal centre, whilst one [C15] is rotated *ca.* 180° from this position.

An analysis of the CH···Cl contacts in **II·31** suggested that long range interactions are present in the solid state. In a review of hydrogen bonds in the solid state, Steiner proposes the hydrogen bond definition "XH···A interaction is called a 'hydrogen bond' if (1) It constitutes a local bond, and (2) X–H acts as a proton donor to A". Steiner also suggests a more technical definition of a hydrogen bond as an H···X distance of 3.2 Å and an angular cut off set at >90°.[192] These technical criteria are used to assess hydrogen bonding in this work.

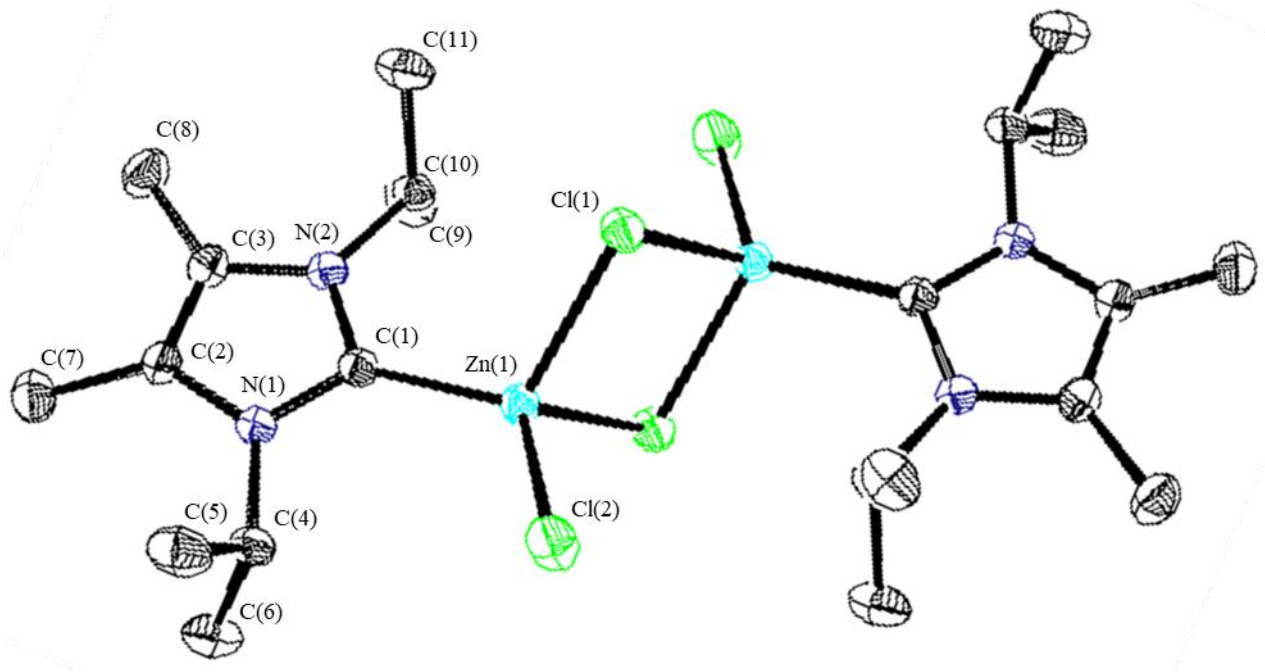

Figure 2·6. The structure of one morphology within the asymmetric unit of **II·31**, grown to represent the full molecule. Hydrogens omitted for clarity and ellipsoids set at 50% probability.

One of the intramolecular *i*Pr-CH···Cl distances in **II·31** approaches a value comparable with a long-range interaction [C4H···Cl1 2.71(2) Å, 155.5(19)°]; a full list of values is given in **Table 2·3**.[191–193] Two additional protons, from *i*Pr-CH_3 groups, are in close contact with a chloride, both on the same flanking group of the second morphology, rotated 180° from the position of the other three [C17H_3···Cl3 2.85(3) Å, 151(2)° and C16H_3···Cl3 2.87(3) Å, 147(2)°]. The flanking group is orientated such that the CH···Cl distances are minimised [C12−N−C15−C16 = 45.65(25)°]. The four types of hydrogen bonding with the halides in **II·30** and **II·31** are shown in **Figure 2·7**.

Though care must be taken when using solid-state evidence to interpret solution state observations, the conclusion that CH···Cl interactions can form in this structure can be drawn. It is therefore possible that these interactions also form in solution and are the cause of the significant ppm shifts of the signals in the ^{1}H NMR spectrum for the flanking *i*Pr groups. Further ^{1}H NMR spectroscopy experiments involving solvents capable of interrupting CH···Cl interactions could help to clarify the situation.[190]

Table 2·3. Key bond lengths and angles for **II·30** and **II·31**.

	II·30 (M = Co, X = Br)		**II·31** (M = Zn, X = Br)	
CH···X interactions	Atom Label		Atom Label	
$C_{i\text{Pr}}H\cdots X$/Å[°]	C4, Br2a	2.17(3) [174(8)]	C4, Cl1	2.71(2) [155.5(19)]
	C4, Br2	2.65(3) [169(7)]	C20, Cl4	3.19(2) [142.5(18)]
	C9, Br1a	3.14(6) [141(6)]	C9, Cl2	3.14(2) [146.5(17)]
	C9, Br1a	3.43(6) [143(6)]		
	C20, Br3	3.36(7) [131(7)]		
	C20, Br3a	3.47(7) [139(7)]		
$C_{i\text{Pr}}H_3\cdots X$/Å[°]	C17, Br4	2.88(3) [167(9)]	C17, Cl3	2.85(3) [151(2)]
	C17, Br4	2.90(4) [156(7)]	C16, Cl3	2.87(3) [147(2)]
Bond geometry				
M···M/Å	Co1, Co1	3.407(3)	Zn1, Zn1	3.3776(4)
	Co2, Co2	3.327(2)	Zn2, Zn2	3.2960(4)
M−C/Å	Co1, C1	2.033(7)	Zn1, C1	2.0215(19)
	Co2, C12	2.045(8)	Zn2, C2	2.0195(18)
$M-X_{terminal}$/Å	2.209(12) − 2.445(15)		Zn1, Cl1	2.2199(5)
			Zn2, Cl4	2.2230(6)
$M-X_{bridging}$/Å	2.444(7) − 2.517(13)		2.2230(6) − 2.3954(5)	
$C-N-C_{i\text{Pr}}-CH_3$/°	C1, C9, C11	105.58(80)	C1, C9, C11	111.43(19)
	C12, C15, C16	41.7(12)	C1, C4, C5	110.76(19)
	C12, C20, C22	101.47(82)	C12, C20, C22	107.10(19)
	C1, C4, C5	105.51(90)	C12, C15, C16	45.65(25)
Plane deviation				
NHC−M/Å	Co1	0.283(13)	Zn1	0.295(3)
	Co2	0.230(13)	Zn2	0.231(3)
τ' values				
τ'_4	Co1	0.86	Zn1	0.79
	Co2	0.85	Zn2	0.86

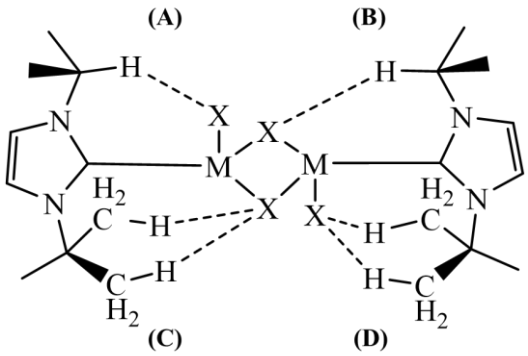

Figure 2·7. The four types of hydrogen bonding (A-D) that can occur in **II·30** and **II·31**.

The solid-state structure of **II·30** (**Figure 2·8**) contains two crystallographically distinct morphologies of one half of the full molecule. Bromides Br1 (bridging), and Br2 and Br3 (terminal) in the structure are disordered over two positions. The lower occupancy position in each set is labelled BrXa where X is the number of the higher occupancy bromide. CH···Br interactions are evident.[192] The shortest contact is between one of the CH protons of the *i*Pr and a disordered terminal bromide. Of the two possible distances the shortest was between the proton and the lowest occupancy bromide however, both are within the parameters of a H···Br hydrogen bond [C4H···Br2a/2 2.17(3), 2.65(3) Å, 174(8), 169(7)°] (a list of geometric parameters is given in **Table 2·3**). As in **II·31**, the next shortest contact existed between the *i*Pr-CH_3 groups and the bridging halide of the alternate morphology [C17H···Br4 2.88(3), Å, 167(9); C16H···Br4 2.90(4) Å, 156(7)°]. This functional group also deviates significantly from what can be assumed to be the most sterically favourable conformation, where C_{ipso}–N–C_{iPr}–CH_3 = 120°, to facilitate this interaction [C12–N3–C15–$C16H_3$ = 41.7(12)°].

The Co···Co distances in **II·30** [3.327(2) and 3.407(3) Å] are shorter than the structurally similar [2,6-$Mes_2C_6H_3$(μ-Br)Co(THF)]$_2$ (**I·29**) [3.520(2) Å] in which antiferromagnetic coupling was observed. Therefore, it is possible that some Co···Co interactions occur in **II·30**.

The Zn···Zn distances of 3.2960(4) and 3.3776(4) Å in **II·31** are shorter than the equivalent distances in **II·30**. The C_{ipso}–M distances [2.033(7) and 2.045(8) Å (Co–C), 2.0195(18) and 2.0215(19) Å (Zn–C)] are consistent with similar Co–NHC and Zn–NHC complexes in the

literature. These include 2.032(4) Å in $[(IPr)CoBr(\mu\text{-}Br)]_2$ and 2.040 Å in $[(IMes)(\mu\text{-}OCH_2Ph)ZnCl]_2$.[167,194,195]

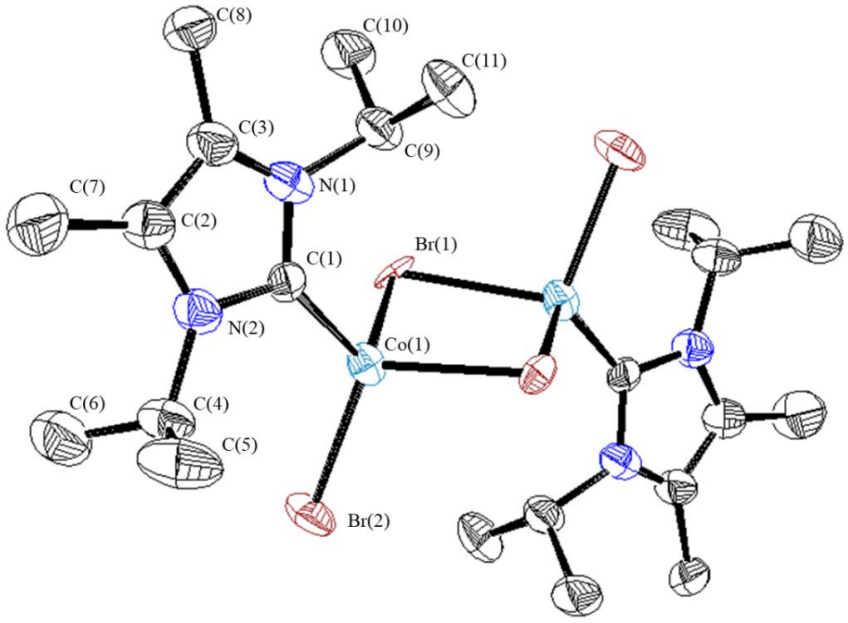

Figure 2·8. The structure of one morphology within the asymmetric unit of **II·30**, grown to represent the full molecule. Hydrogens omitted for clarity and ellipsoids set at 50% probability.

Attempts to synthesise $[(IPrMe)MnBr_2]_2$ and $[(IPrMe)FeCl_2]_2$ were unsuccessful. Repeated reactions between one equivalent of $MnBr_2$ and one equivalent of IPrMe afforded crystals of $[MnBr_4][IPrMeH]_2$ despite the rigorous exclusion of air. The uncoordinated NHC presumably scavenges a proton either from the solvent or another equivalent of IPrMe whilst the extra bromides must be taken from $MnBr_2$. Combination of $FeCl_2(THF)_{1.5}$ and one equivalent of IPrMe resulted in the isolation of $[IPrMe]_2FeCl_2$ as a crystalline solid. This structure has previously been reported by Grubbs and coworkers.[196]

Reactions between IPrMe and MX_2 often afforded $[IPrMe]_2MX_2$ (MX = CoBr, ZnCl or NiCl) as a by-product, where MX = CoBr or ZnCl, or the major product, where MX = NiCl. A magnetic study of $[IPrMe]_2CoCl_2$ was conducted by Deng *et al*. which revealed a magnetic moment of *ca.* 4.2 μ_B. X-ray diffraction experiments were not performed.[197]

$[IPrMe]_2CoBr_2$ (**II·32**) and $[IPrMe]_2ZnCl_2$ (**II·33**) were synthesised and characterised so that they could be identified in reaction mixtures. $[IPrMe]_2NiCl_2$ (**II·34**) was the exclusive product of attempts to synthesise $[IPrMeNiCl_2]_2$. [IPrMe]CuCl (**II·35**) was isolated as a product from an attempt to synthesise $[IPrMeCuCl_2]_2$. Addition of THF to a 2:1 mixture of IPrMe and an appropriate metal(II) halide at room temperature afforded the complexes **II·32**, **II·33** and **II·34** as shown in **Scheme 2·3**.

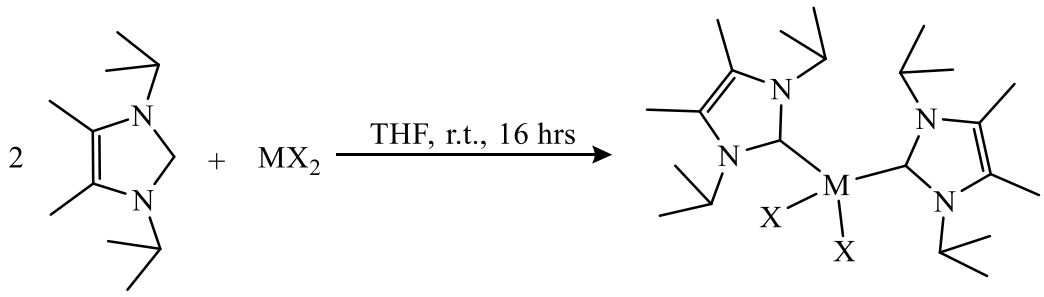

II·32; M = Co; X = Br
II·33; M = Zn; X = Cl
II·34; M = Ni; X = Cl

Scheme 2·3. A generic synthetic route to $[IPrMe]_2CoBr_2$ (**II·32**), $[IPrMe]_2ZnCl_2$ (**II·33**) and $[IPrMe]_2NiCl_2$ (**II·34**).

II·32 was extracted into toluene. Crystallisation was induced by concentration of the resultant blue solution followed by layering with *iso*-hexane. The purity of the blue crystals was established by elemental analysis and the structure by X-ray diffraction studies (**Figure 2·9**).

^{1}H NMR spectroscopic analysis of **II·32** demonstrates that the complex is paramagnetic with nine broad signals between 0.30 and 24.90 ppm. The signals could not be assigned accurately due to the paramagnetic nature of the complex.

The magnetic moment of **II·32** was shown to be 4.7 μ_B using Evans' method.[198] This value is higher than the spin only value for a tetrahedral d^7 complex (3.87 μ_B) and the value of 4.2 μ_B reported for $[IPrMe]_2CoCl_2$.[197] The UV/Vis spectrum of **II·32** contains three absorbance bands at 626, 667 and 699 nm (ε = 285, 402 and 347 $dm^3\ mol^{-1}\ cm^{-1}$, respectively). This is consistent with the d-d transitions of a tetrahedral, d^7 complex.[179,199]

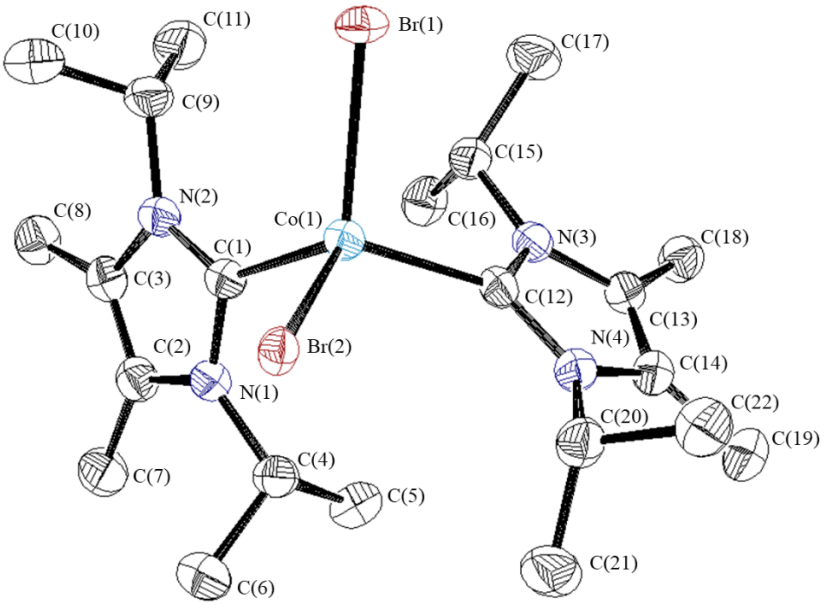

Figure 2·9. The X-ray diffraction derived structure of **II·32**. Hydrogens are omitted for clarity and ellipsoids are set at 50% probability.

II·33 (**Figure 2·10**) was obtained as a white solid. Colourless crystals were grown by diffusion of pentane into a saturated solution of the complex in benzene-d_6.

II·33 was characterised with ^{1}H and ^{13}C{^{1}H} NMR spectroscopy. CH···Cl interactions are evident in the ^{1}H NMR spectrum, with the *i*Pr CH proton shifted downfield to 6.00 ppm.[190,200,201] This effect is also evident in **II·34**, with the same signal shifted to 7.55 ppm.

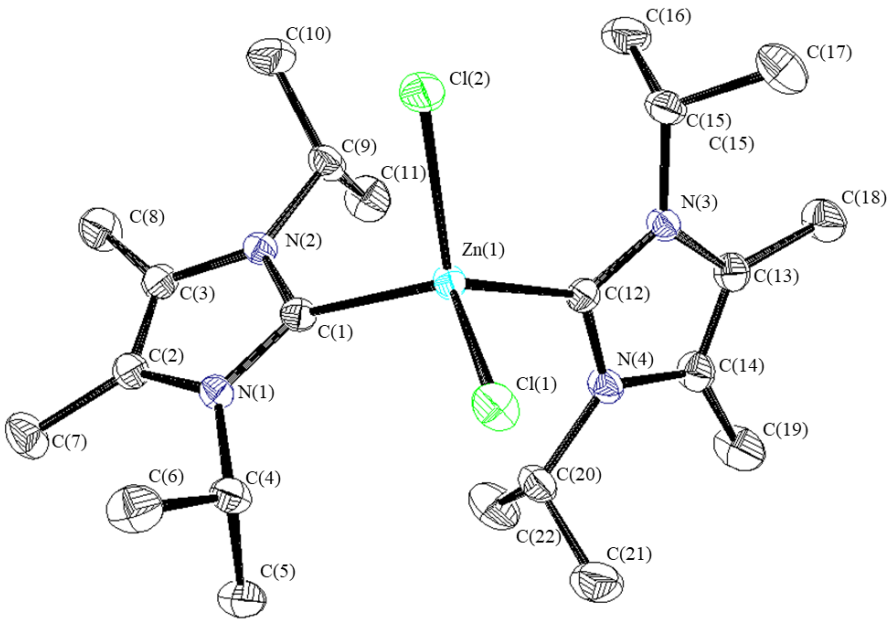

Figure 2·10. The structure of **II·33**. Hydrogens are omitted for clarity and ellipsoids are set at 50% probability.

II·34 (**Figure 2·11**) was isolated as orange crystals by cooling a saturated solution of the complex in toluene from room temperature to −30°C. H^1 and C^{13} NMR spectroscopic studies showed the complex to be diamagnetic which suggested a low spin, d^8 complex with square planar geometry. This was confirmed with UV/Vis studies which demonstrated a single transition at 370 cm^{-1} ($\varepsilon = 7524\ dm^3\ mol^{-1}\ cm^{-1}$), which is consistent with a single d-d transition.

II·32, **II·33** and **II·34** adopt a monoclinic crystal morphology. **II·32** and **II·34** crystallise in the $P2_1/n$ space group, **II·34** with one half of the molecule and one equivalent of C_6D_6 in the asymmetric unit. **II·33** adopts the $P2_1/c$ space group with two molecules of C_6D_6 in the asymmetric unit. X-ray diffraction studies confirm that **II·32** and **II·33** are distorted tetrahedral complexes whilst **II·34** adopts a square planar geometry.

Table 2·4. Key bond lengths and angles for **II·32** and **II·33**.

	II·32 (M = Co, X = Br)		**II·33** (M = Zn, X = Cl)	
CH···X interactions	Atom Label		Atom Label	
C*i*PrH···X/Å[°]	C15, Br2	2.50(6) [177(4)]	C20, Cl2	2.48(3) [164(2)]
	C4, Br2	2.91(6) [141(4)]	C10, Cl1	2.62(3) [167(2)]
	C9, Br1	2.76(6) [165(4)]	C4, Cl2	2.87(3) [133(2)]
	C20, Br1	3.05(6) [139(4)]	C15, C11	3.24(3) [125(2)]
Bond geometries				
M−C/Å	Co1, C1	2.074(4)	Zn1, C1	2.067(2)
	Co1, C12	2.079(4)	Zn1, C12	2.070(2)
M−X/Å	Co1, Br1	2.5120(8)	Zn1, Cl1	2.2872(6)
	Co1, Br2	2.4903(8)	Zn1, Cl2	2.3158(6)
C−N−C*i*Pr−CH3/°	C12, C20, C12	124.74(47)	C1, C4, C5	128.58(24)
	C12, C15, C17	110.06(49)	C1, C10, C11	121.19(24)
	C1, C9, C11	117.70(45)	C12, C20, C22	129.92(23)
	C1, C4, C5	119.86(45)	C12, C15, C17	111.50(26)
IPrMe− IPrMe/°	C1, C12	85.61(14)	C1, C12	79.730(96)
Plane deviations				
NHC−M/Å		0.0637(75)		0.1778(41)
τ' values		0.1765(75)		0.1296(38)
τ'_4	Co1	0.91	Zn1	0.93

Key bond lengths and angles for **II·32** and **II·33** are given in **Table 2·4**. Both **II·32** and **II·33** show evidence of CH···X interactions in the solid-state. In **II·32**, all the CH protons of the *i*Pr groups are in close contact with a bromide moiety. This does not coincide with any significant

deviation in the orientation of these flanking groups. Through inspection of the angle of these CH···Br interactions it can be seen that one from each ligand approaches a CH···X angle of 180°. The size of this angle correlates with the length of the hydrogen bond, with a more acute angle leading to a longer interaction. This suggests that each ligand can only orientate to fully satisfy one of these interactions.

The solid-state structure of **II·33** is similar to that of **II·32** and a similar hydrogen bonding pattern is observed, with the longest CH···X interaction [C(15)H···Cl(1) = 3.24(3) Å] approaching the limits of what can be reasonably termed an interaction and the angle of this interaction deviating significantly from the ideal angle of 180° [125(2)°].[192] In **II·33**, however, there is a greater deviation of the flanking *i*Pr groups from the idealised torsion angle of 120° (**Table 2·4**). This suggests that the structure is flexible enough to maximise these interactions. Possibly this is due to the size of the chloride ion, compared with the bromide ion, reducing the steric strain in the structure of **II·33** with respect to **II·32**.

Noltemeyer *et al*. observed the effect of the steric strain on C−Mn−X angles when they reported the synthesis and characterisation of $[IPrMe]_2MnX_2$ (X = Cl or I).[179] Less steric congestion around the metal centre allows the flanking groups to manoeuvre and maximise the favourable interactions.

The C−M bonds in **II·32** are slightly longer than those in **II·30** and the equivalent bonds in **II·33** are longer than those in **II·31**. This is most likely a function of the tension placed on this bond by the extra IPrMe ligand coordinated to the metal centre in **II·32** and **II·33**.

As mentioned previously, attempts to synthesise $[IPrMeNiCl_2]_2$ were unsuccessful as the reaction exclusively affords $(IPrMe)_2NiCl_2$ (**II·34**) in our hands. The reason for this is unclear. It should be noted that while a number of nickel complexes analogous to **II·34** exist in the

literature[202] and complexes of the form $[(NHC)NiCl_2]_2$ have not been reported, implying that they are difficult to isolate.

The absence of such complexes may be due to the *trans*-effect, which is often present in d^8 complexes. NHC ligands are known to be strong σ-donors and as such can weaken the *trans* metal-ligand interaction in a square planar complex.[59,179] Where only one NHC was coordinated to nickel(II) chloride the monomeric complex may dimerise, as in **II·30** and **II·31**. A strong *trans*-effect could weaken this process making the coordination of a bridging halide less favourable. Unable to dimerise to increase stability, the monomers may react in solution to afford **II·34** and a unit of nickel(II) chloride. A strong *trans*-effect could also explain why the cis-isomer of **II·34** was not isolated in this work.

This theory presumes that the $[(NHC)NiCl_2]_2$ would have a square planar geometry around the nickel centre which may not be the case. Further study of this reaction, potentially at low temperature, would be required to investigate this theory and establish why nickel equivalents of **II·32** and **II·33** could not be isolated in our hands.

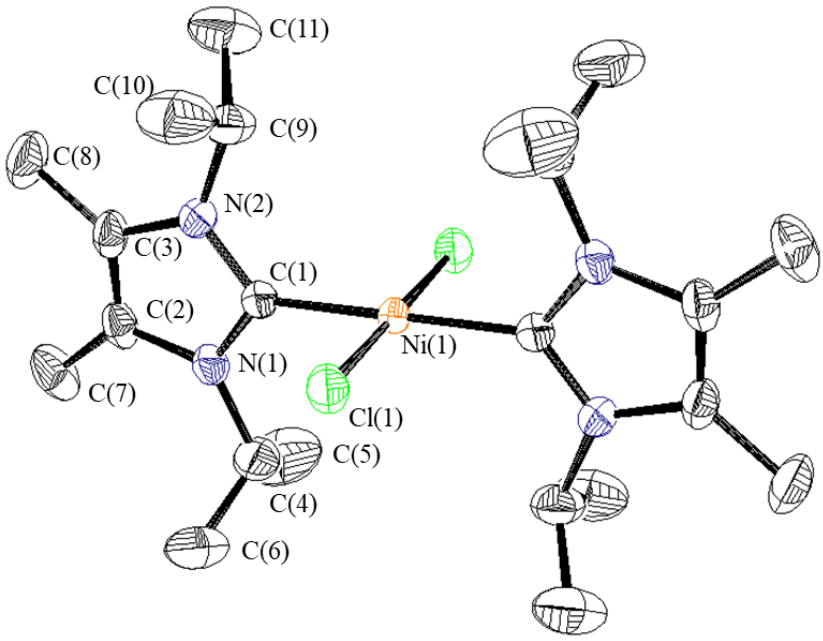

Figure 2·11. The solid-state structure of **II·34**, grown to show the whole molecule. Hydrogens and solvent molecules are omitted for clarity, and ellipsoids are set at 50% probability.

Sigman *et al*. found a synthetic route to a dimeric, NHC bearing, nickel(I) complex *via* a disproportionation reaction that produced (NHC)NiCl, which dimerised to afford $[(NHC)NiCl]_2$, with trigonal planar geometry around the metal centres.[139] This complex requires the NHC to be IPr. A similar complex, with the less steric bulky IMes ligand, could not be isolated. This demonstrates that steric bulk is essential to the stability of the complex.

The solid-state structure of **II·34** (**Figure 2·11**) contains one half of the molecule in the asymmetric unit with an inversion centre located on the nickel moiety. The complex adopts a square planar geometry ($\tau'_4 = 0.00$), with each of the *i*Pr groups of the ligand orientated so the CH moiety points toward the metal centre. The IPrMe ligands are co-planar and the nickel centre does not deviate significantly from the plane (out-of-plane deviation = 0.0183(26) Å). The ^{1}H NMR spectrum shows a large downfield shift of this proton from the CH group of the *i*Pr flanking groups, consistent with the presence of CH···X interactions. This contrasts with the solid-state structure which shows the same protons are not in close contact with the chloride whilst a proton of the CH group of the *i*Pr group is (**Table 2·5**).

Table 2·5.Key bond lengths and angles for **II·34** and **II·35**.

	II·34·C_6D_6 (M = Ni)		**II·35** (M = Cu)	
CH···Cl interactions	Atom Label		Atom Label	
$C_{i\text{Pr}}H\cdots Cl$/Å[°]	C9, Cl1	3.33(2) [120.6(15)]		n/a
	C4, Cl1	3.48(2) [106.5(14)]		
$C_{i\text{Pr}}H_3\cdots Cl$/°	C6, Cl1	3.01(4) [140(3)]		n/a
Bond geometries				
M−C/Å	Ni1, C1	1.9165(15)	Cu1, C1	1.893(3)
$M-Cl_{terminal}$/Å	Ni1, Cl1	2.1832(4)	Cu1, Cl1	2.1061(10)
$C-N-C_{i\text{Pr}}-CH_3$/°	C1, C9, C10	118.70(22)	C1, C4, C5	175.67
	C1, C4, C5	98.93(22)		
Plane deviations				
NHC−M/Å		0.0183(26)		0.0011(33)
τ' values				
$\boldsymbol{\tau'_4}$		0.00		N/a

The ^{1}H NMR spectrum of **II·34** (**Figure 2·12**) does not show a significant shift for this proton away from the free ligand (1.47 to 1.83 ppm). This serves to highlight the difference between solid state and solution structures. These differences can be enforced by crystal packing or arise

from electronic effects that occur only when degrees of freedom or solvent interactions are removed.[203,204]

II·34 bears a geometric similarity to $[ICyc]_2NiCl_2$ reported by Herrmann *et al.*[202] and $[NHC]_2NiCl_2$ (NHC = IPr or IMes) reported by Matsubara and coworkers.[205] These complexes were synthesised through displacement of a neutral ligand, either a tertiary phosphine or THF, from the corresponding nickel(II) chloride adduct by the relevant carbene. The authors report attempts to synthesise a complex coordinated by just one NHC, maintaining the ligation of one triphenylphosphine. It was found that this was possible with IPr, the largest NHC in the study, but not with the slightly smaller IMes. Addition of less than two equivalents of IMes resulted in the formation of $[IMes]_2NiCl_2$ and recovery of the starting material $[PPh_3]_2NiCl_2$. This bears similarity to the attempted synthesis of $[(IPrMe)NiCl_2]_2$ in this work.

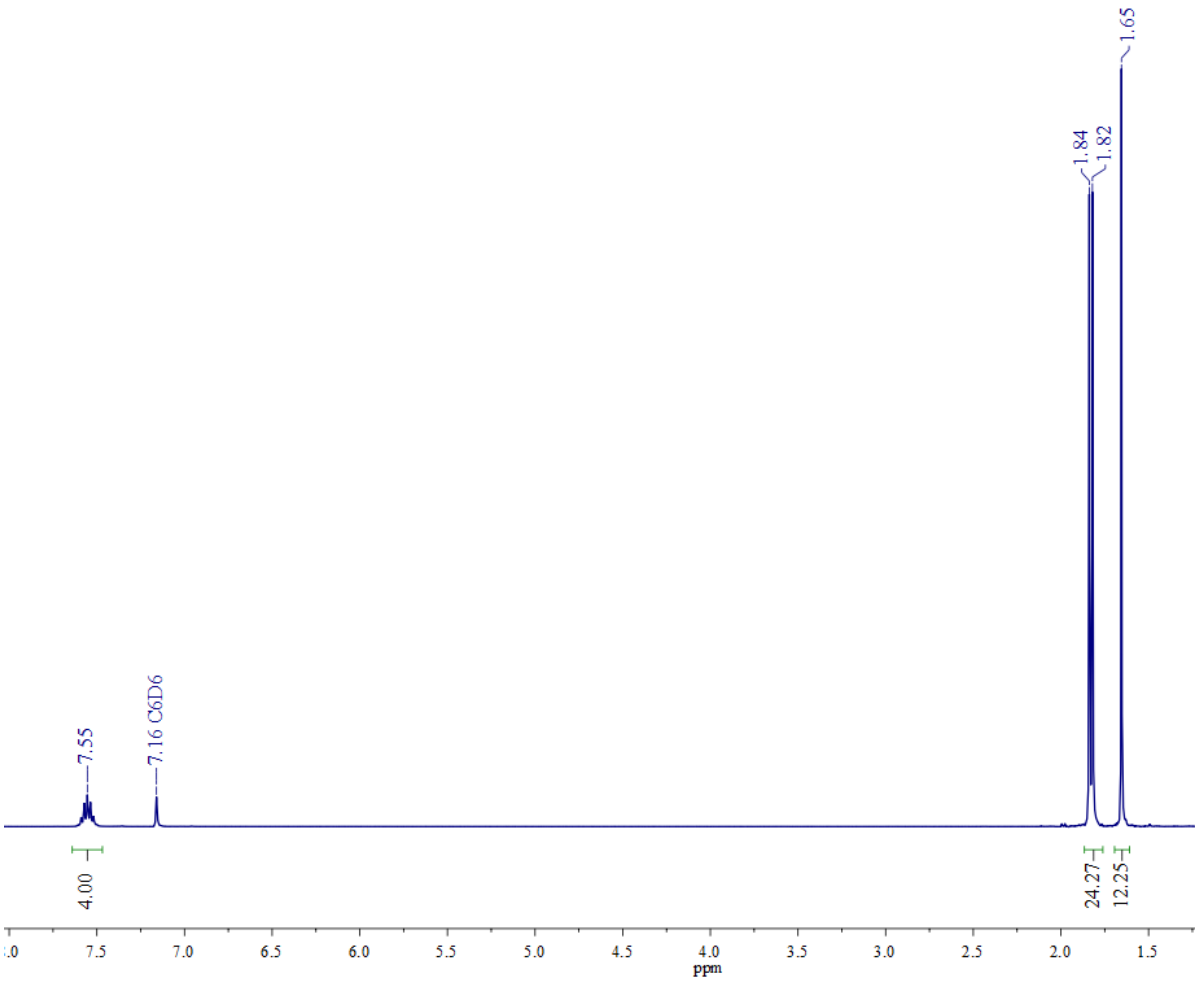

Figure 2·12. The H^1 NMR spectrum of **II·34**.

Matsubara *et al.* attribute the observed difference to the steric profiles of the ligand with the second coordination of IMes occurring too quickly to isolate [IMes][PPh_3]$NiCl_2$. Herrmann *et al*. note that the ^{1}H NMR spectrum of $[ICyc]_2NiCl_2$ showed a downfield shift of 2.73 ppm in the signal of the α-CH_2 of the cyclohexyl ring compared with the free ligand. This is attributed not to the formation of CH···X interactions but to the inductive effects as the nitrogen donates to the carbene−metal bond, which may explain the downfield shifts in the ^{1}H NMR spectra of **II·34** and the other complexes discussed previously. All these complexes were square planar and exhibited similar C−M distances (*ca.* 1.91 Å) and ligand orientation despite the drastic differences in the steric profile of the ligands.

[IPrMe]CuCl (**II·35**) was isolated as a product of the reaction between one equivalent of IPrMe and $CuCl_2$ (**Scheme 2·4**). The product most likely formed *via* a disproportionation reaction with the concomitant formation of $CuCl_3$. The ^{1}H NMR spectrum of this complex contained three signals at 1.33 ppm ($C_{iPr}H_3$), 1.39 ppm (backbone CH_3) and 3.86 ppm ($C_{iPr}H$). There was no evidence in the ^{1}H NMR spectrum of any hydrogen bonding in solution.

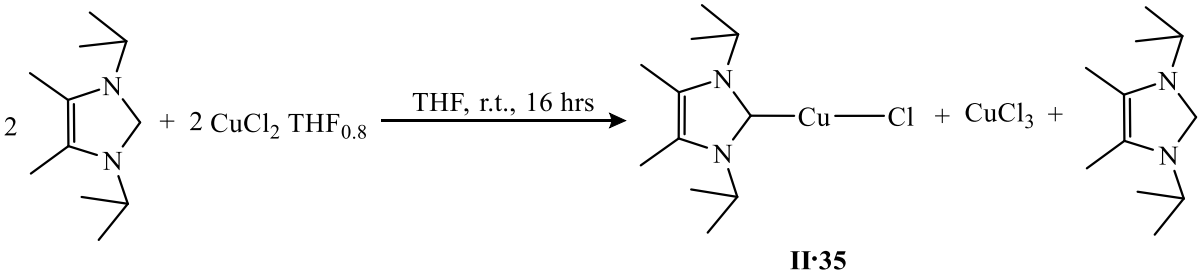

Scheme 2·4. The synthetic route that afforded [IPrMe]CuCl (**II·34**).

II·35 was previously reported by Barry *et al*. as a precursor for the complex [IPrMe]Cu[N($SiMe_3$)] but was not crystallographically characterised.[206] In this report, **II·35** was synthesised through the coordination of the free IPrMe to CuCl, a method also employed by Nolan and co-workers to synthesise [NHC]CuX (X = Cl, Br, and I) complexes.[207]

II·35 (**Figure 2·13**) crystallises in the tetragonal space group $P4_12_12$ and is isomorphous with the silver analogue.[208] The asymmetric unit contains one half of the molecule with a centre of

rotation along the Cu−Cl bond. The *i*Pr group is orientated so the CH bond points away from the metal centre and the CH_3 groups toward it. The distances between the chloride and the protons of this group are too long to suggest a hydrogen bonding interaction.[192] Concomitant with this, the *i*Pr groups also show no evidence of twisting to maximise such interactions. The Cu1−C1 bond is 1.893(3) Å in length, consistent with the wide range of copper−NHC bonds reported in the literature.[207] The C1−Cu1−Cl1 bond angle is strictly linear at 180.0(0)° which is consistent with literature examples of Group 11 analogues.[207,209,210]

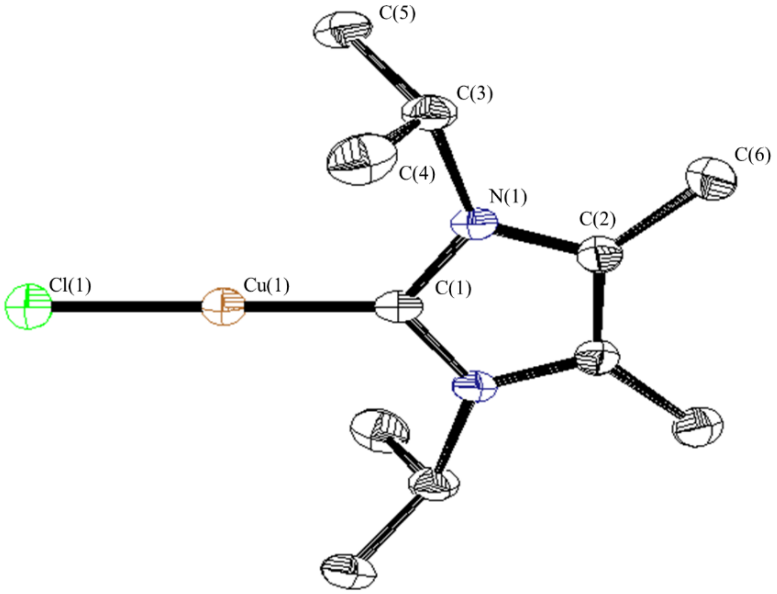

Figure 2·13. The solid-state structure of **II·35**, grown to represent the full molecule. Hydrogens are omitted for clarity and ellipsoids are set at 50% probability.

There are numerous examples of copper(I) complexes supported by NHC ligands in the literature.[211–213] The number of copper(II) complexes is more limited. Willans attributes this to the mismatch between the soft carbon donors and hard copper(II) cations.[214] Of the copper(II) NHC complexes reported, many require stabilisation by NHC ligands featuring a chelating nitrogen donor, possibly to prevent disproportionation pathways.[214–216] Those that are stabilised by monodentate NHC ligands also feature oxygen based ligands, as in the complex [IPr]Cu[OAc]$_2$.[217,218] In one study Nechaev *et al*. attempted to synthesise [(NHC)CuX_2]$_2$ (NHC = IPr, SIPr, 6-Mes, 6-Dipp, 7-Mes or 7-Dipp; X = Cl or Br) through coordination of the free carbene to CuX_2. They described a decomposition pathway whereby [(NHC)CuX_2]$_2$ formed

briefly before decomposition into [NHC]$Cu^{I}X$ and $[Cu^{II}X_2]^-[NHCBr]^+$.[218] This is presumably the decomposition pathway that prevents isolation of $[(IPrMe)CuCl_2]_2$ in this work.

2.3.2 *m*-Terphenyl Complexes

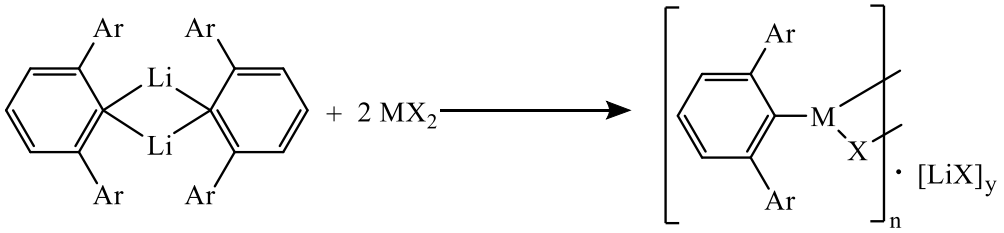

II·36, **II·38**; M = Mn; X = Br; Ar = Mes, Dipp; n = 2; y = 2
II·39; M = Fe; X = Br; Ar = Mes; n = 2; y = 2
II·37, **II·40**; M = Co; X = Br; Ar = Mes, Dipp; n = 2; y = 2
II·41; M = Zn; X = Cl; Ar = Mes; n = ?; y = ?
II·42; M = Cd; X = Cl; Ar = Mes; n = 3; y = 1
II·43, **II·44**; M = Hg; X = Br, Ar = Mes, Tmp; n = 1; y = 0

Scheme 2·5. A synthesis of transition metal and Group 12 Grignard analogues bearing *m*-terphenyl ligands.

A series of dimeric, late transition metal and Group 12 *m*-terphenyl complexes were synthesised. A modified literature synthesis, reported by Power *et al*., was used which involved the slow addition of a solution of an *m*-terphenyl lithium salt (synthesised using literature methods as described in Section 2.5.1.4) in diethyl ether to the relevant metal(II) halide suspended/dissolved in the same solvent at 0°C (**Scheme 2.5**).[170] The products were extracted into non-polar organic solvents such as toluene or hexane. Crystallisation was induced by concentrating the solutions and slowly cooling them to either 7°C or −30°C.

As has been discussed, Power *et al*. reported a series of complexes of the form $[2,6\text{-}Dipp_2C_6H_3MI]_2[LiI(Et_2O)]_2$ (M = Mn, Fe or Co).[170] These complexes feature a halide-bridged, dimeric species with the incorporation of two equivalents of lithium iodide.

Similar complexes were required for this study, however, bridging chlorides or bromides were required to avoid a bulky iodide moiety in what would be sterically congested final products. $[2,6\text{-}Ar_2C_6H_3MX]_2[LiX(Et_2O)]_2$ [Ar = Dipp, MX = MnBr (**II·36**), CoBr (**II·37**); Ar = Mes, MX = MnBr (**II·38**), FeBr (**II·39**) and CoBr (**II·40**)] were therefore synthesised.

A series of Group 12 complexes [2,6-$Ar_2C_6H_3MX]_2$ [Ar = Mes, MX = ZnCl (**II·41**), CdCl (**II·42**), HgBr (**II·43**); Ar = 2,5,6-trimethylphenyl (Tmp), MX = HgBr (**II·44**)] was also synthesised. These complexes are similar to the $[2,6\text{-}Dipp_2C_6H_3]^-$ series of complexes reported by Power *et al*.[169] and $[2,6\text{-}Tripp_2C_6H_3ZnI]_2$ reported by Robinson and coworkers.[219]

2.3.2.1 Transition Metal Complexes

$[2,6\text{-}Dipp_2C_6H_3MnBr]_2[LiBr(Et_2O)]_2$ (**II·36**) and $[2,6\text{-}Dipp_2C_6H_3CoBr]_2[LiBr(Et_2O)]_2$ (**II·37**, **Figure 2·14**) were isolated as crystals from *iso*-hexane. Both structures adopt the space group $P2_1/n$ and contain one moiety of disordered *iso*-hexane in the crystal lattice. These complexes crystallised alongside $[2,6\text{-}Dipp_2C_6H_3MBr]_2$ [M = Mn, (**II·36b**) or Co (**II·37b**)].

Crystals of **II·36** are colourless and slowly adopted a brown tinge upon storage under an argon atmosphere. Key bond lengths and angles for **II·36** are given in **Table 2·6**. The UV/Vis spectrum of **II·36** features an absorption at 345 nm (ε = 137 $dm^3\ mol^{-1}\ cm^{-1}$), consistent with a high spin, d^5 complex.[179,199]

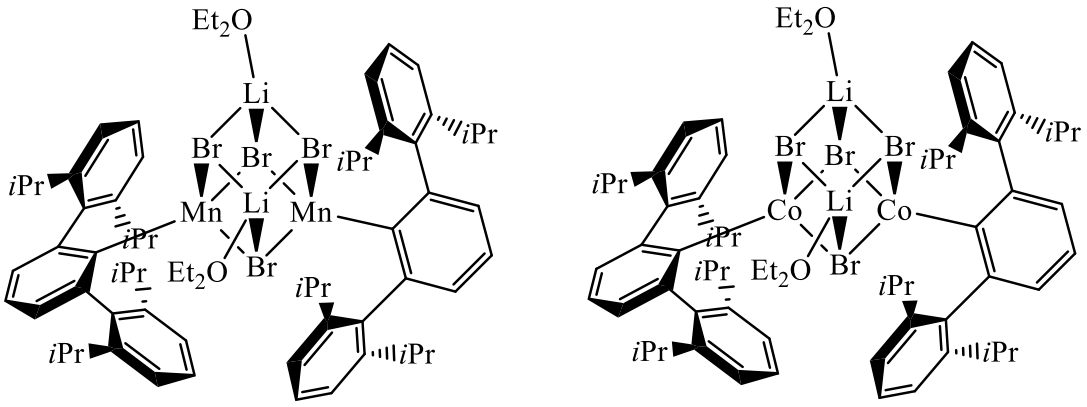

II·36 **II·37**

Figure 2·14. The structures of **II·36** and **II·37**

The ^1H NMR spectrum is consistent with a high spin manganese *m*-terphenyl complex with broad signals over a wide spectral range.[76] The magnetic moment is 3.5 μ_B, lower than would be expected for two high spin, d^5 centres (spin only value = 5.92 μ_B), suggesting a degree of antiferromagnetic coupling between the two manganese(II) centres. Antiferromagnetic

coupling was reported by Power *et al*. in $[2,6\text{-}Dipp_2C_6H_3MnI]_2[LiI(Et_2O)]_2$. However, the complex $[(IPr)(Ph)MnCl]_2$ had an inter-metal distance of 3.393(1) Å and a magnetic moment of 7.0 μ_B;[220] the Mn−Mn distance in **II·36** was 3.8174(9) Å. This suggests that indirect coupling pathways may play a significant role in the magnetic coupling.

Complex **II·37** is dark green in colour and forms crystals when a saturated *iso*-hexane solution is cooled slowly to −30°C and stored for several days. The purity of these crystals was confirmed by elemental analysis. The UV/Vis spectrum of II·37 showed one absorbance at 362 nm (ε = 1197 $dm^3\ mol^{-1}\ cm^{-1}$) from $\pi^*\leftarrow\pi$ transitions. Three weaker absorbances at 816, 645, and 600 nm (ε = 367, 203, and 147 $dm^3\ mol^{-1}\ cm^{-1}$, respectively) correspond to the d←d transitions of a tetrahedral d^7 complex.[179,199]

Table 2·6. Key bond lengths and angles for **II·36** and **II·37**.

	II·36·Et_2O (M = Mn)		**II·37** (M = Co)	
Bond Lengths				
M−C/Å	Mn1, C1	2.119(4)	Co1, C31	2.007(4)
	Mn2, C31	2.112(4)	Co2, C1	2.009(4)
M−Br/Å	Mn1, Br1	2.6498(7)	Co1, Br1	2.5677(8)
	Mn2, Br1	2.6706(7)	Co1, Br2	2.5693(8)
	Mn1, Br2	2.6548(6)	Co1, Br4	2.4900(8)
	Mn2, Br2	2.7364(7)	Co2, Br1	2.6054(7)
	Mn1, Br3	2.6045(7)	Co2, Br2	2.5369(8)
	Mn2, Br4	2.5967(8)	Co2, Br3	2.4867(8)
Br−Li/Å	Br1, Li1	2.6106(71)	Br1, Li2	2.636(9)
	Br3, Li1	2.5761(71)	Br2, Li1	2.631(8)
	Br4, Li1	2.5507(71)	Br3, Li1	2.520(8)
	Br2, Li2	2.6548(79)	Br3, Li2	2.614(9)
	Br3, Li2	2.5592(75)	Br4, Li1	2.560(9)
	Br4, Li2	2.5993(75)	Br4, Li2	2.575(8)
Li−O/Å	Li1, O1	1.901(8)	Li2, O1	1.905(9)
	Li2, O2	1.898(7)	Li1, O2	1.898(9)
M−M/Å	Mn1, Mn2	3.8174(9)	Co1, Co2	3.6151(9)
Bond Angles				
C−M−Br/°	C1, Mn1, Br1	128.71(10)	C31, Co1, Br1	123.47(11)
	C1, Mn1, Br2	124.40(9)	C31, Co1, Br2	127.72(12)
	C1, Mn1, Br3	117.81(9)	C31, Co1, Br4	114.55(11)
	C2, Mn2, Br1	121.74(10)	C1, Co2, Br1	126.05(12)
	C2, Mn2, Br2	128.00910)	C1, Co2, Br2	121.37(12)
	C2, Mn2, Br4	120.01(10)	C1, Co2, Br3	117.22(12)
M−Br−Li/°	Mn1, Br1, Li1	85.41(16)	Co1, Br1, Li2	80.85(20)
	Mn2, Br1, Li1	80.92(16)	Co2, Br1, Li2	84.27(19)
	Mn1, Br2, Li2	81.07(16)	Co1, Br2, Li1	84.29(18)
	Mn2, Br2, Li2	83.88(16)	Co2, Br2, Li1	79.33(19)
	Mn1, Br3, Li1	87.49(16)	Co2, Br3, Li1	82.44(18)
	Mn1, Br3, Li2	85.00(18)	Co2, Br3, Li2	87.12(19)
	Mn2, Br4, Li1	83.09(16)	Co1, Br4, Li1	87.09(18)
	Mn2, Br4, Li2	87.84(18)	Co1, Br4, Li2	83.84(20)
M−Br−M/°	Mn1, Br1, Mn2	91.70(2)	Co1, Br1, Co2	88.66(2)
	Mn1, Br2, Mn2	88.948(19)	Co1, Br2, Co2	90.14(2)
Plane−Plane				
$[Ar_{Central}]-[Ar_{Central}]$ /°		64.89 (13)		63.33(12)
$[Ar_{Dipp}]-[Ar_{Central}]$/°	C1, C7	85.68(48)	C1, C7	75.46(55)
	C1, C19	86.69(48)	C1, C19	90.98(50)
	C31, C37	89.96(48)	C31, C37	95.74(47)
	C31, C49	106.05(48)	C31, C49	91.71(49)
τ' values				
τ'_4	Mn1	0.74	Co1	0.76
	Mn2	0.76	Co2	0.78

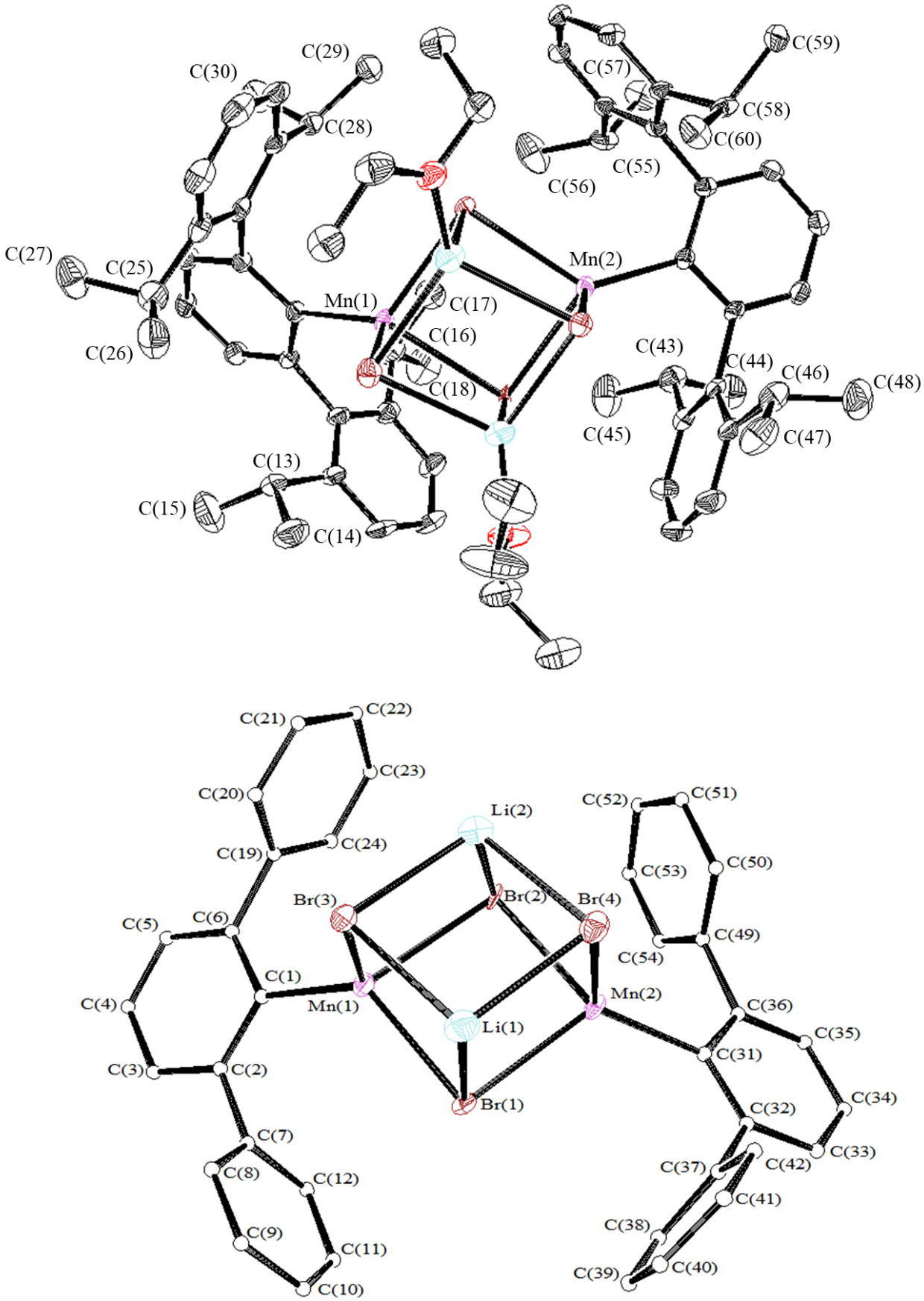

Figure 2·15. The solid-state structure of **II·36**. Hydrogens are omitted for clarity. Ellipsoids are set at 50% probability where shown. Top: Full structure with iPr groups labelled, Bottom: *i*Pr and diethyl ether groups have been omitted for clarity and the terphenyl scaffold labels are shown.

The ^{1}H NMR spectrum of **II·37** showed a paramagnetic complex with broad signals ranging from −43.93 to 48.34 ppm. The magnetic moment, 5.2 μ_B, was slightly less than the spin only value for two cobalt(II) centres (7.45 μ_B) which again suggested a degree of antiferromagnetic coupling between the two metal centres. The magnetic moment is comparable with that observed for [2,6-$Mes_2C_6H_3CoBr(THF)]_2$ (4.7 μ_B).[74] In this complex the Co−Co bond [3.520(2) Å] is slightly shorter than that in **II·37** [3.6151(9) Å], which would be consistent with a slightly greater degree of direct antiferromagnetic coupling.

II·36 and **II·37** are isomorphous in the solid-state. Both exhibit a distorted, cubane motif comprised of two transition metal centres on one face, each bound to three bromide moieties, two of which bridge both transition metal centres to form one face of the cube, and the other bridges the metal and lithium ions. The other two bromides bridge the two lithium centres to form the second face. The lithium ions themselves are each coordinated by one diethyl ether moiety. Finally, the transition metal centres are each coordinated by one *m*-terphenyl ligand. The structures of **II·36** and **II·37** are shown in **Figures 2·15** and **2·16**, respectively, key bond lengths, angles and geometric parameters are summarised in **Table 2·6**.

In both structures the transition metal centres adopt a geometry somewhere between tetrahedral and see-saw to facilitate the cubane structure [τ'_4 = 0.74 (Mn1), 0.76 (Mn2; **II·36**) and 0.76 (Co1), 0.78 (Co2; **II·37**)]. The M−Br−Li angles (M = Mn or Co) are between 80 and 100° whilst the C_{ipso}−M−Br angles are *ca.*120°. As the ligands were forced together by the cubane geometry the planes of the central aryl rings of these ligands are rotated with respect to each other by 64.89(13)° (**II·36**) and 63.33(12)° (**II·37**). In both structures, all but one of the flanking aryl groups are roughly perpendicular to the central aryl rings. The outlying plane to plane angles are 106.05(48)° (**II·36**) and 75.46(55)° (**II·37**). Inspection of the $C_{i\mathrm{Pr}}H\cdots X$ distances shows that this angle is concomitant with the longest of these distances

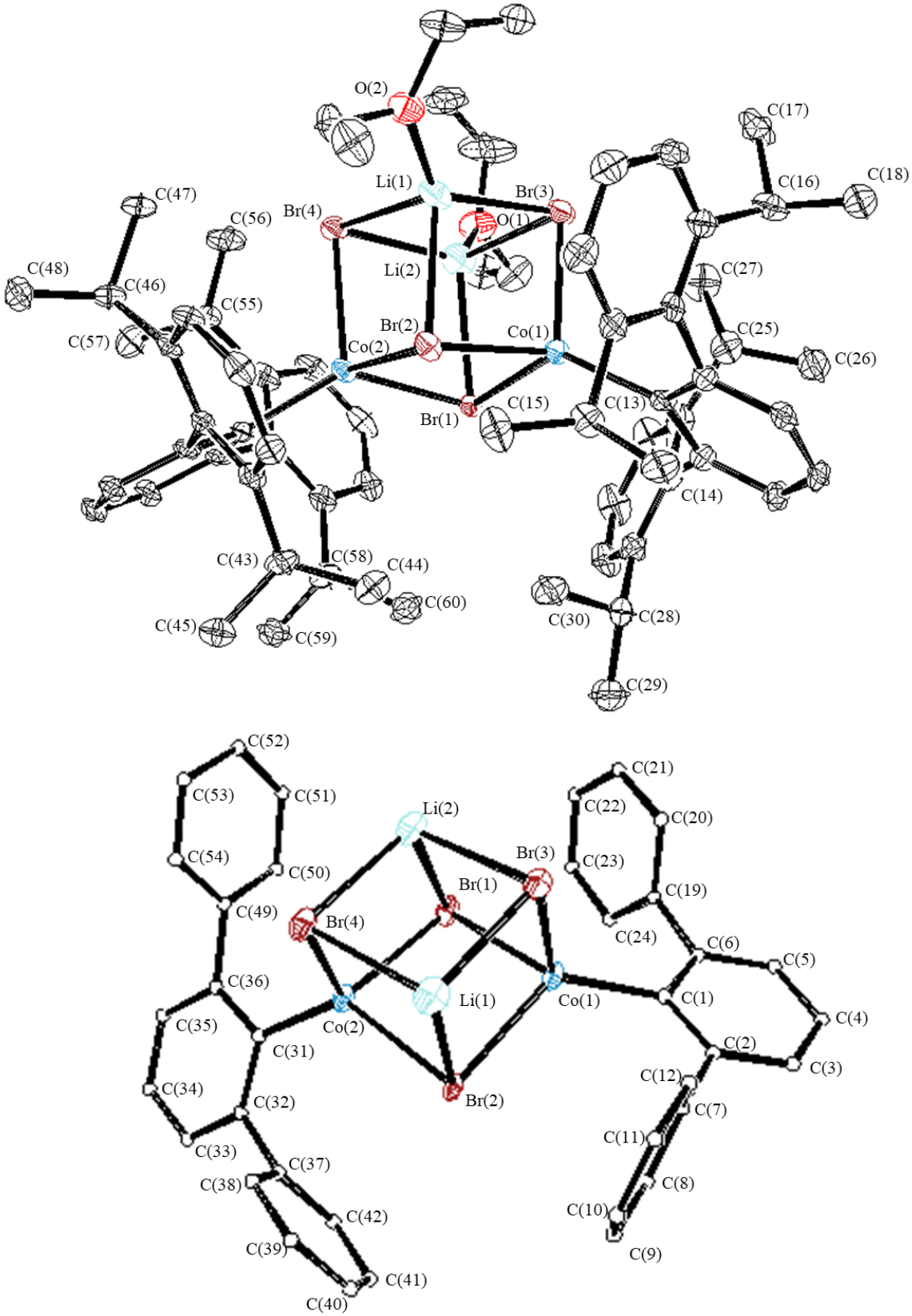

Figure 2·16. The solid-state structure of **II·37**. Hydrogens are omitted for clarity. Ellipsoids are set at 50% probability where shown. Top: Full structure with *i*Pr groups labelled, Bottom: *i*Pr and diethyl ether groups have been omitted for clarity and the terphenyl scaffold labels are shown.

and the only one that cannot be considered an interaction. That these features of the solid-state structures correlate, does not mean that one causes the other. However, it could be envisioned that steric strain in the structure causes the aryl ring to tilt causing a large $C_{iPr}H\cdots X$ distance.

II·36 and **II·37** occasionally crystallise alongside $[2,6\text{-}Dipp_2C_6H_3MBr]_2$ [M = Mn (**II·36b**) or Co (**II·37b**) respectively]. In the case of **II·37**, **II·37b** occurs when the crude product is dried *in vacuo* for longer than 4 hrs before extraction into hexane.

Table 2·7. Key bond lengths and angles for **II·36b** and **II·37b** where _$ indicates an atom related to another by reflection.

	II·36b (M = Mn)		**II·37b** (M = Co)	
Bond Lengths				
M−C/Å	Mn1, C1	1.966(10)	Co1, C31	1.954(5)
	Mn2, C2	1.969(12)	Co2, C1	1.947(4)
M−Br/Å	Mn1, Br1	2.6207(18)	Co1, Br1	2.445(5)
	Mn2, Br2	2.6253(15)	Co1, Br1a	2.5727(11)
	Mn1, Br1_$1	2.6141(15)	Co2, Br1	2.5556(11)
	Mn2, Br2_$2	2.6274(18)	Co2, Br1a	2.5077(84)
M−M/Å	Mn1, Mn1	3.490(3)	Co1, Co2	3.1756(13)
	Mn2, Mn2	3.528(3)		
Bond Angles				
C−M−Br/°	C1, Mn1, Br1_$1	131.3(3)	C1, Co1, Br1	129.8(2)
	C1, Mn1, Br	132.1(3)	C1, Co1, Br1a	127.5(2)
	C31, Mn2, Br2	132.4(3)	C31, Co2, Br1	124.5(2)
	C31, Mn2, Br2_$2	131.9(3)	C31, Co2, Br1a	123.3(2)
M−Br−M/°	Mn1, Br1, Mn1_$1	83.62(5)	Co1, Br1, Co2	76.52(3)
	Mn2, Br2, Mn2_$1	84.38(6)	Co1, Br1a, Co2	79.4(3)
Br−M−Br /°	Br1, Mn1, Br1_$1	96.38(5)	Br1, Co1, Br1a	102.3(2)
	Br2, Mn2, Br2_$2	95.62(6)	Br1, Co2, Br1a	100.7(1)
Plane−Plane				
$Ar_{Central}$−$Ar_{Central}$ /°	C1	co-planar	C1, C31	22.83(15)
	C31	co-planar		
Ar_{Dipp}−$Ar_{Central}$ /°	C31, C54	77.6 (12)	C31, C54	92.11(63)
	C1, C20	78.0 (13)	C1, C20	99.73(53)
	C31, C42	95.1 (12)	C31, C49	77.51(60)
	C1, C12	97.0(12)	C1, C8	95.03(58)
$Ar_{Central}$–MBr core/°	C1	37.84(86)	C1	58.41 (26)
	C31	32.71(88)	C31	80.97(24)
τ_3 values				
τ_3	Mn1	0.79	Co1	0.76
	Mn2	0.80	Co2	0.84

II·36b (**Figure 2·17**) crystallises in the space group *P*-1 and features two halves of the molecule, each with a distinct morphology, in the asymmetric unit. **II·37b** crystallises in the monoclinic space group $P2_1/c$ and features one full molecule. The complexes feature a four-membered ring that consists of the metal moieties bridged by two bromide moieties. The metal ions adopt a trigonal planar geometry, distorted slightly by the steric demands of the bridging groups. In both structures some of the *i*Pr groups of the Dipp flanking group and bromide moieties are disordered. Key bond lengths and angles are given in **Table 2·7**.

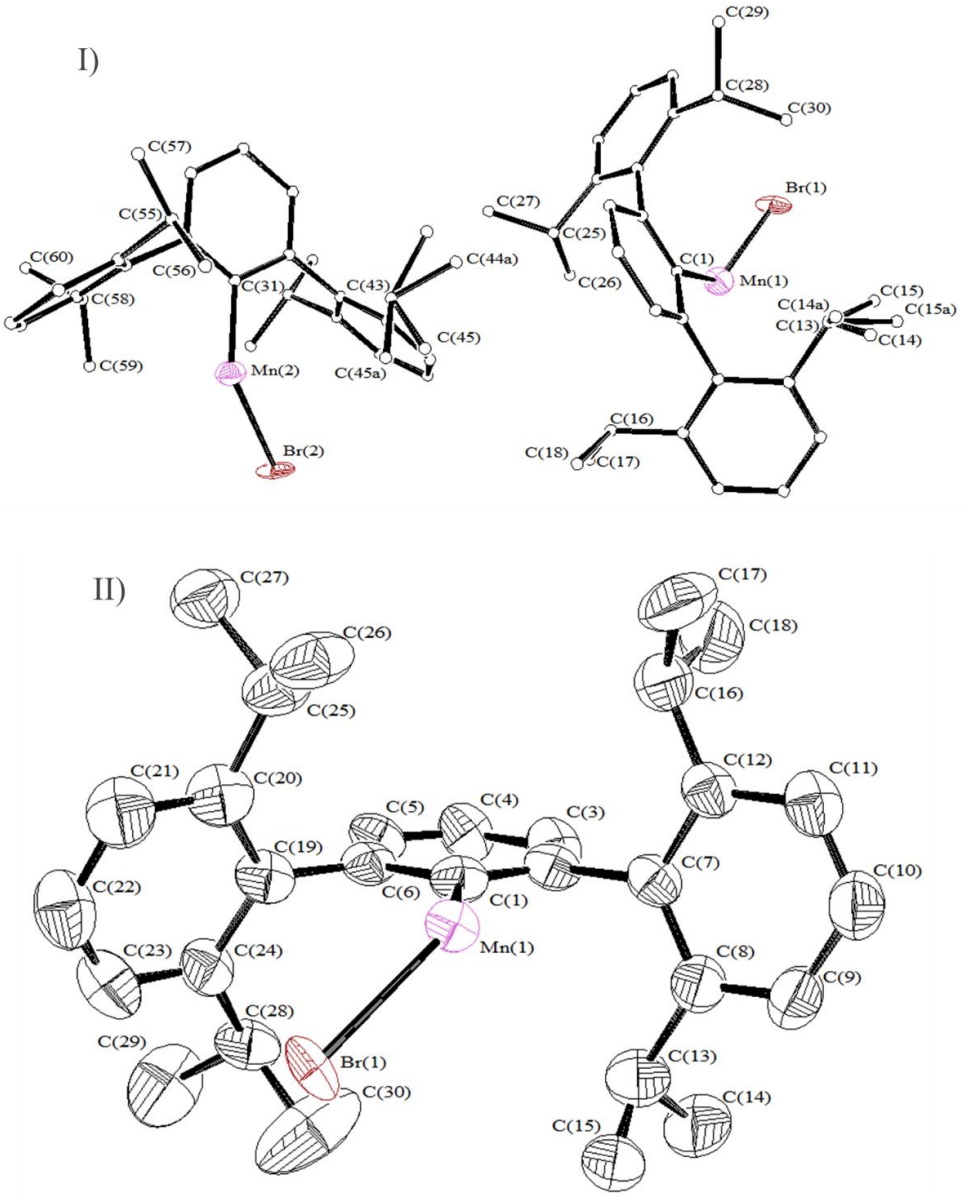

Figure 2·17. Hydrogens and disordered carbons are omitted for clarity, and, unless otherwise stated, ellipsoids are set at 50% probability. I) The solid-state structure of **II·36b**, containing two distinct morphologies, each representing half of the full structure. The carbons of the *i*Pr groups, manganese, bromides have been labelled, carbons are represented as spheres for clarity. II) One distinct morphology of **II·36b**.

In both morphologies of **II·36b** the opposing *m*-terphenyl ligands are orientated co-planar to one another with the plane of the Mn_2Br_2 core offset from this plane by 37.84(86)° (Mn1) and 32.71(88)° (Mn2). The Mn···Mn distances, at 3.490(3) Å (Mn1) and 3.528(3) Å (Mn2), are shorter than the equivalent distance in **II·36** and other bromide bridged examples in the literature [M···M 3.574(1) Å ({L'MBr}$_2$) 3.724(1) Å ({L"MBr}$_2$) (L'/L" = N{C_6H_2(C{H}-Ph_2)$_2$Me-2,6,4}{SiR_3} [R = Me (L'), Ph (L")]).[177] The manganese centres in these examples are four-coordinate and possibly it is the three-coordinate nature of **II·36b** that causes this shorter distance, due to less steric congestion or to increase the Mn···Mn interaction.

The flanking aryl groups of **II·36b** show some deviation from a geometry perpendicular to the central aryl rings, however, there is no evidence of CH···Br interactions in the solid-state structure. The shortest interaction is 3.2(2) Å with an angle of 118(15)°. Whilst this is within the realms of a hydrogen bond, the measurement is imprecise due to the quality of the data.[192]

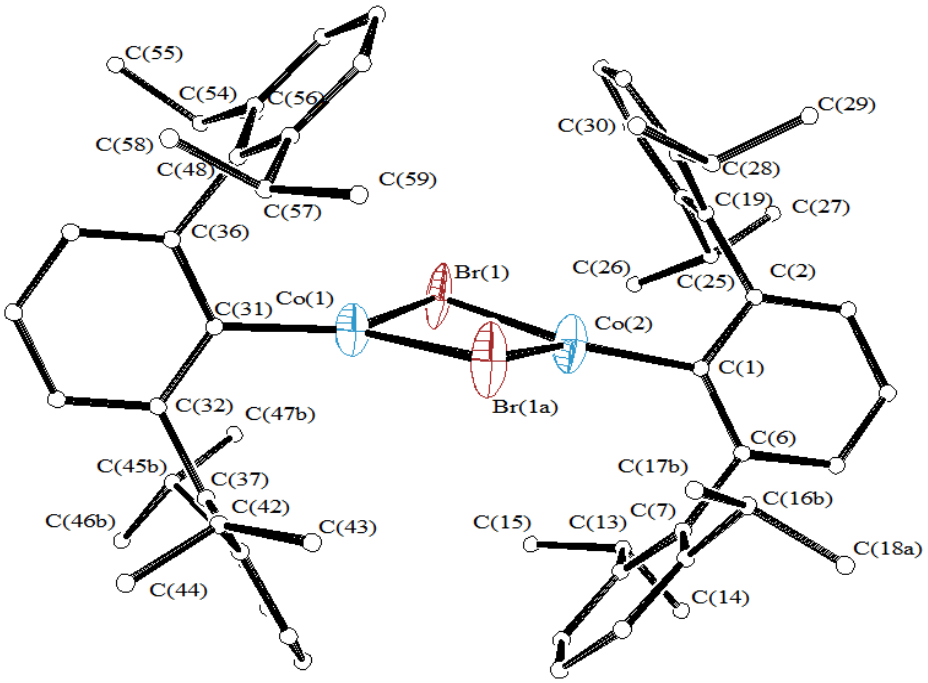

Figure 2·18. The solid-state structure of **II·37b**. Carbons are represented as spheres, all other atoms are represented as ellipsoids, the probability of which is set to 50%. Key atoms are labelled. Hydrogens are omitted for clarity.

The two *m*-terphenyl ligands in **II·37b** (**Figure 2·18**) are offset with a plane to plane angle of 22.83(15)° and the plane of the central $[CoBr]_2$ was offset from these two planes by 58.41(25) (C1) and 80.93(24)° (C31). The ligands in **II·37b** are closer than in **II·36b** as demonstrated by the shorter M···M distance [3.1756(13) Å]. This leads to an offset orientation of the *m*-terphenyl ligands to avoid steric clashing.

On each *i*Pr group, one of the methyl groups is in close contact with one of the bromide moieties. This could indicate an array of hydrogen bonds in the structure. The shortest of these interactions [CH···Br 2.57(8) Å; 164(7)°] correlates with a torsion angle of 96.69° (CH_3–C_{iPr}–C_{ortho}– C_{ipso}, the sterically optimal position is 120°), the *i*Pr group is presumably rotated to maximise this interaction, and this is typical of the *i*Pr groups in the structure with most rotated at an angle that brings a methyl group in contact with a bromide. The orientation of the flanking Dipp groups deviated significantly from the perpendicular in two instances [77.51(60) and 99.73(53)°]. The degree of deviation correlates with the strength (inferred from interaction distance) of the hydrogen bonding on both sides of the flanking group. Where this is unbalanced the flanking group deviates the most from the perpendicular.

Manganese (**II·38**), iron (**II·39**) and cobalt (**II·40**) analogues of **II·36** and **II·37** with $[2,6\text{-}Mes_2C_6H_3]^-$ as the *m*-terphenyl ligand were synthesised using a similar methodology. Complex $[2,6\text{-}Mes_2C_6H_3MnBr]_2{\cdot}[LiBr(OEt_2)]_2$ (**II·38**) could not be isolated in a crystalline form and was used and analysed as a powder, but $[2,6\text{-}Mes_2C_6H_3FeBr]_2{\cdot}[LiBr(OEt_2)]_2$ (**II·39**) and $[2,6\text{-}Mes_2C_6H_3CoBr]_2{\cdot}[LiBr(OEt_2)]_2$ (**II·40**) were obtained as crystals suitable for X-ray diffraction experiments. Both **II·39** and **II·40** crystallised in the monoclinic space group $P2_1/n$. The asymmetric units each contain a single molecule morphology. The structures obtained demonstrate that they adopt similar, cubic structures to the $[2,6\text{-}Dipp_2C_6H_3]^-$.

Various, unsuccessful attempts were made to crystallise **II·38** *via* slow cooling and diffusion methods in a variety of solvents. Instead the product was isolated by extraction of the crude product into cyclohexane, to produce a pale pink solution, and removing this solvent in vacuo to afford **II·38** as a white powder.

The UV/visible spectrum of **II·38** is similar to that of **II·36**. The only feature of the spectrum is an absorbance at 332 nm (ε = 139 dm^3 mol^{-1} cm^{-1}), which can be attributed to $\pi^* \leftarrow \pi$ transitions. ^{1}H NMR spectroscopic analysis of **II·38** (**Figure 2·19**) showed signals broadened and shifted significantly downfield (11.64 and 16.22 ppm) by the paramagnetic behaviour of **II·38**. These signals could not be assigned with any certainty.

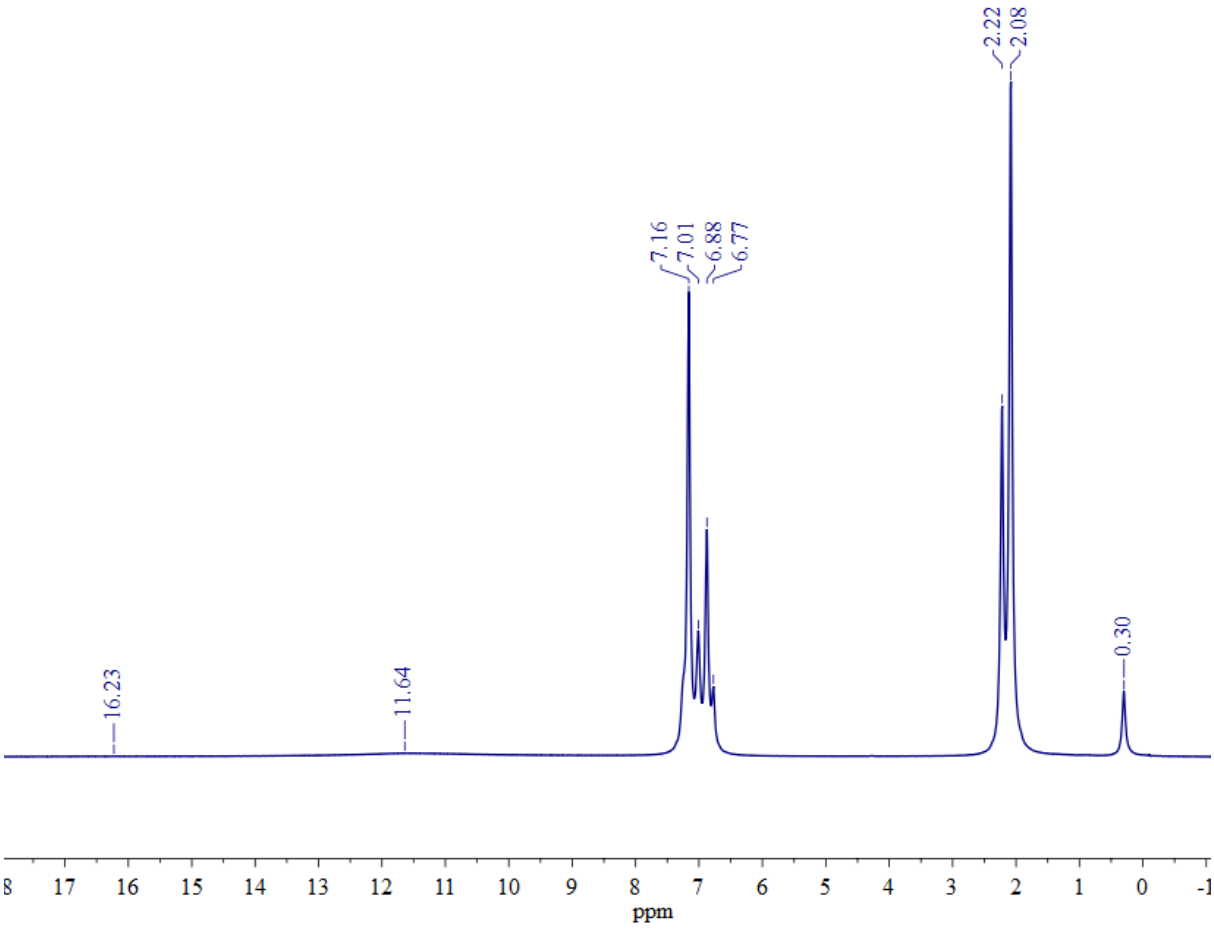

Figure 2·19. The H[1] NMR spectrum of **II·3**

Identification of **II·38** proved difficult due to its paramagnetic nature, the absence of crystals and because the parent ion could not be observed by mass spectrometry. The ^{1}H NMR spectrum does not suggest the presence of the previously isolated [2,6-$Mes_2C_6H_3$]$_2$Mn.[76] Combining **II·38** with IPrMe afforded [(IPrMe)MnBr(2,6-$Mes_2C_6H_3$)]$_2$, which suggested that the structure contains [2,6-$Mes_2C_6H_3$]MnBr. This would presumably dimerise as similar transition metal complexes do.[170]

The incorporation of two equivalents of lithium bromide could not be confirmed. If it was assumed that **II·38** was similar in structure to **II·36**, the magnetic moment could be calculated, using Evans' method, as 3.7 μ_B. This is similar in magnitude to the magnetic moment of **II·36** (3.5 μ_B). This value is, however, based on conjecture and further structural data is required to characterise this complex.

[2,6-$Mes_2C_6H_3FeBr$]$_2$·[$LiBr(OEt_2)$]$_2$ (**II·39**) was obtained as yellow crystals, the purity of which was confirmed by elemental analysis. UV/Vis analysis showed a broad absorbance between 430 and 640 nm with a distinct peak at 505 nm (ε = 1772 dm^3 mol^{-1} cm^{-1}). The peak at 505 nm is consistent with what would be expected for a tetrahedral d^6 system and represents a single d←d transition.[179,199] **II·39** is extremely air and moisture sensitive and a solution of the complex in toluene was observed to change colour from yellow to a light brown in a sealed UV/Vis cell. This decomposition *in situ* was most likely responsible for the broad absorbance observed in the spectrum.

^{1}H NMR spectroscopic analysis of **II·39** shows a series of paramagnetically shifted signals from −23.14 to 8.34 ppm, which were broadened and overlapping. The magnetic moment was calculated to be 5.1 μ_B, half that of the spin only value for two iron(II) centres (spin only value for one iron(II) = 4.90 μ_B).[179]

[2,6-$Mes_2C_6H_3CoBr]_2$·[$LiBr(OEt_2)]_2$ **II·40** was first isolated as a deep blue powder in a yield of 56% through extraction into *iso*-hexane. It was found that slow cooling of a saturated solution of the complex in cyclohexane resulted in lower yields (18 %) of a crystalline solid that was blue-green in colour. Elemental analysis of the sample found the crystals obtained *via* the latter method to be impure with a discrepancy of 0.9% carbon between the expected and experimental values. UV/Vis analysis afforded a spectrum with three absorbances at 602, 640, and 805 nm (ε = 531, 340, and 311 $dm^3\ mol^{-1}\ cm^{-1}$, respectively), ascribed to the expected three d←d transitions, and one stronger absorbance at 364 nm (ε = 1246 $dm^3\ mol^{-1}\ cm^{-1}$), ascribed to a π*←π transition.

^{1}H NMR spectroscopic analysis of **II·40** shows a range of paramagnetically shifted peaks from −11.62 to 22.68 ppm, a narrower range than observed in the spectrum of **II·37**.

Key bond lengths, angles, and geometric parameters of **II·39** and **II·40** can be found in **Table 2·8** and images of both structures are contained in **Figure 2·20** and **2·21**. The core unit in each is similar to the cubic structure observed in the [2,6-$Dipp_2C_6H_3]^-$ analogues. In **II·39** and **II·40** the cubic structures are distorted, with the $[MBr]_2$ face puckering to raise the bromides away from the body of the cube. This coincides with the transition metal centres adopting a more tetrahedral geometry that the transition metal centres in the equivalent [2,6-$Dipp_2C_6H_3]^-$ as shown by the τ'_4 values (e.g. **II·37**; τ'_4 = 0.76, 0.78, **II·40**; τ'_4 = 0.82, 0.83). The tetrahedral geometry of the metal centres and the demands of the cubic core place the ligands close to one another [$Ar_{Central}$–$Ar_{Central}$ = 80.663(61)° (**II·39**), 79.821(91)° (**II·40**)].

The characteristics of the solid-state structure **II·39** and **II·40** are similar to those of the [2,6-$Dipp_2C_6H_3]^-$ analogues. Where they differ is in the presence of CH···Br contacts. In the [2,6-$Dipp_2C_6H_3]^-$ ligand the *i*Pr groups are flexible and bulky. Therefore, they are able to form CH···Br contacts, impacting how the flanking groups arrange themselves in the solid-state.

Table 2·8. Key bond lengths and angles for the solid-state structures of **II·39** and **II·40**

	II·39 (M = Fe)		**II·40** (M = Co)	
Bond Lengths	Atom Label		Atom Label	
M−C/Å	Fe1, C1	2.0303(18)	Co1, C9	1.991(1)
	Fe2, C25	2.0395(17)	Co2, C33	1.997(2)
M−Br/Å	Fe1, Br4	2.5185(3)	Co1, Br4	2.4777(5)
	Fe2, Br1	2.5802(4)	Co2, Br2	2.5363(5)
	Fe1, Br1	2.5615(3)	Co1, Br1	2.5029(5)
	Fe2, Br2	2.5559(3)	Co2, Br1	2.5255(5)
	Fe1, Br2	2.5776(3)	Co1, Br2	2.5120(5)
	Fe2, Br3	2.5404(4)	Co2, Br3	2.4968(5)
Br−Li/Å	Br2, Li1	2.572(4)	Br1, Li1	2.590(6)
	Br3, Li1	2.590(4)	Br3, Li1	2.573(5)
	Br4, Li1	2.592(4)	Br4, Li1	2.592(6)
	Br1, Li2	2.582(4)	Br4, Li2	2.556(5)
	Br3, Li2	2.566(4)	Br2, Li2	2.607(6)
	Br4, Li2	2.550(4)	Br3, Li2	2.582(6)
Li−O/Å	Li1, O1	1.988(5)	Li1, O1	1.834(10)
	Li1, O1A	1.901(4)	Li1, O1A	1.522(11)
	Li2, O2	1.751(8)	Li2, O2	1.895(6)
M−M/Å	Fe1, Fe2	3.5899(4)	Co1, Co2	3.4534(6)
Bond Angles				
C−M−Br/°	C1, Fe1, Br1	116.83(5)	C9, Co1, Br1	123.27(9)
	C1, Fe1, Br2	124.84(5)	C9, Co1, Br2	116.58(8)
116.83(5)	C1, Fe1, Br4	123.24 (5)	C9, Co1, Br4	120.51(7)
	C25, Fe2, Br1	125.63(5)	C33, Co2, Br1	120.57(8)
	C25, Fe2, Br2	122.15(5)	C33, Co2, Br2	123.83(8)
	C25, Fe2, Br3	118.37(5)	C33, Co2, Br3	116.67 (8)
M−Br−Li/°	Fe1, Br1, Li2	79.83(8)	Co1, Br1, Li1	84.77(14)
	Fe2, Br1, Li2	84.34(9)	Co2, Br1, Li1	80.77(12)
	Fe1, Br2, Li1	82.62(9)	Co1, Br2, Li2	78.86(12)
	Fe2, Br2, Li2	85.79(9)	Co2, Br2, Li2	83.33(13)
	Fe2, Br3, Li1	82.56(8)	Co2, Br3, Li1	81.24(13)
	Fe2, Br3, Li2	85.49(8)	Co2, Br3, Li2	84.64(13)
	Fe1, Br4, Li1	81.26(9)	Co1, Br4, Li1	85.71(12)
	Fe2, Br4, Li2	86.57(8)	Co2, Br4, Li2	80.49(13)
M−Br−M/°	Fe1, Br1, Fe2	88.564(11)	Co1, Br1, Co2	86.749(17)
	Fe1, Br2, Fe2	88.740(11)	Co1, Br2, Co2	86.324(17)
Plane−Plane				
$[Ar_{Central}]-[Ar_{Central}]$ /°		80.663(61)		79.821(91)
$Ar_{Dipp}- Ar_{Central}$ /°	C1, C7	79.30(23)	C9, C16	95.33(33)
	C1, C16	94.69(22)	C9, C29	101.16(33)
	C25, C31	83.29(22)	C33, C53	83.56(34)
	C25, C40	92.11(22)	C33, C40	91.71(33)
Metal Geometry				
τ'_4	Fe1	0.79	Co1	0.82
	Fe1	0.79	Co2	0.83

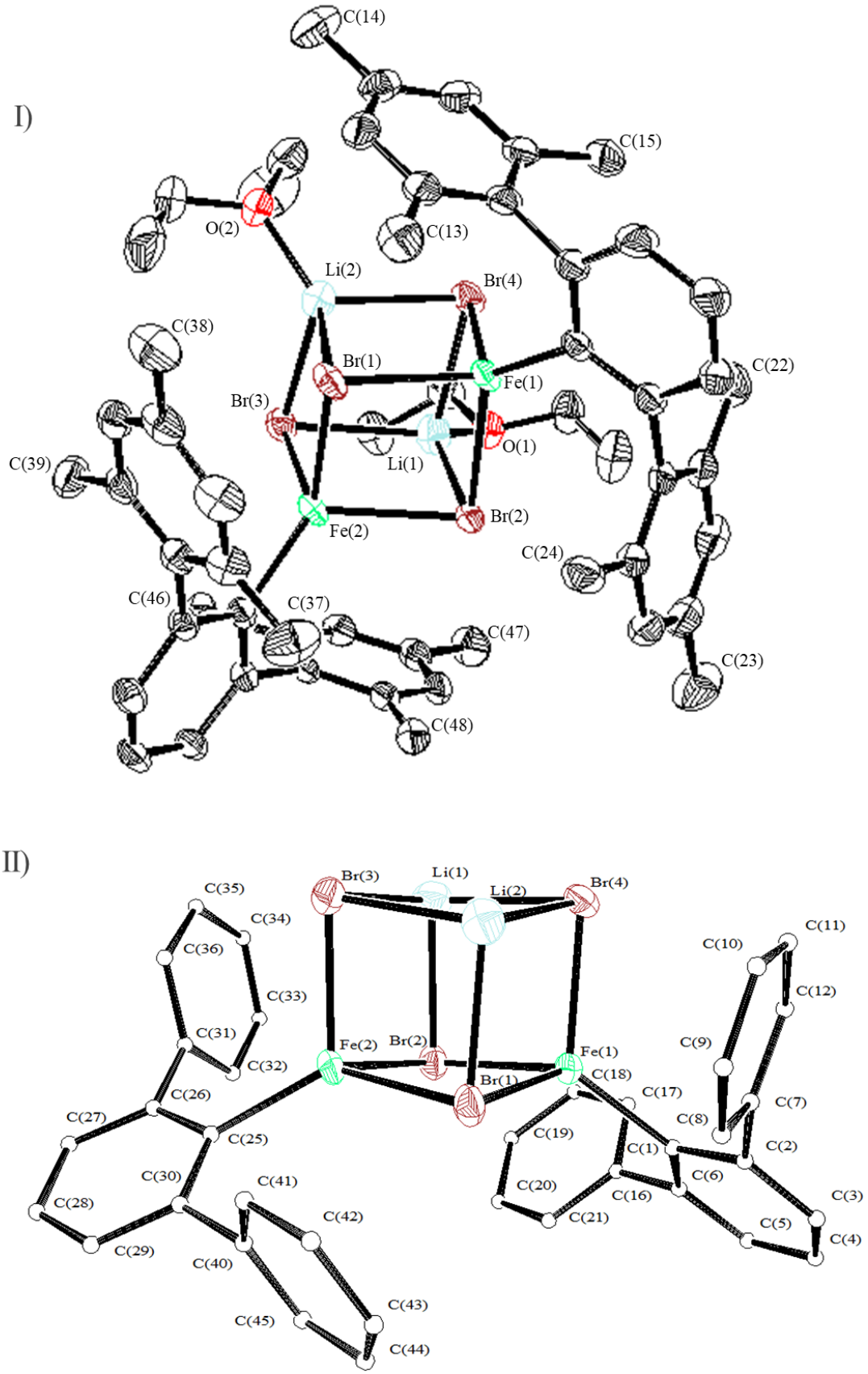

Figure 2·20. The solid-state structure of **II·39** with ellipsoids set at 50% probability, unless otherwise specified. I) the full structure with key atoms labelled and hydrogens and disordered diethyl ether substituent omitted for clarity. II) The core molecule with aryl substituents and diethyl ether molecules omitted for clarity and the remaining *m*-terphenyl carbons represented as spheres.

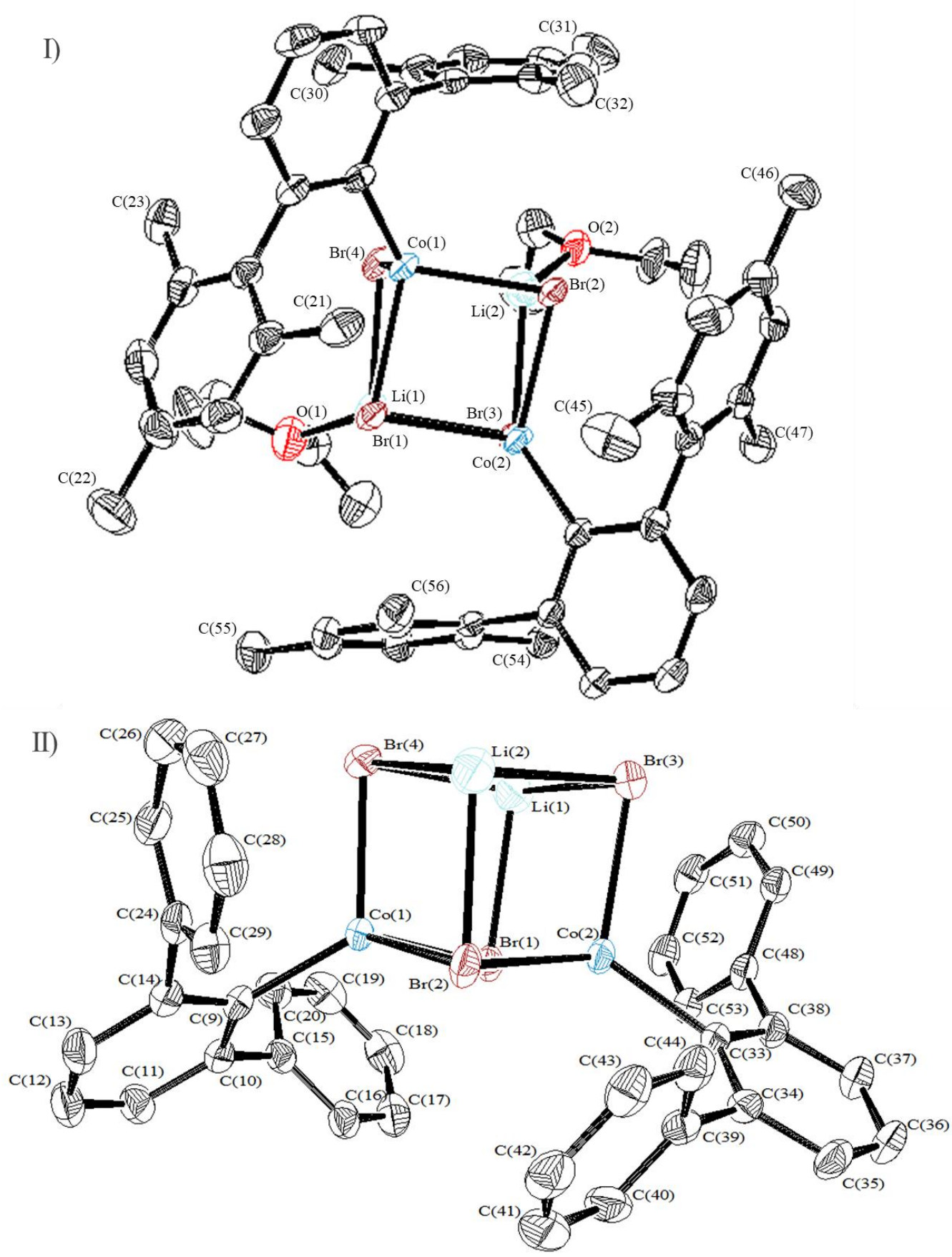

Figure 2·21. The solid-state structure of **II·40** with ellipsoids set at 50% probability unless otherwise specified. I) the full structure with key atoms labelled and hydrogens and disordered diethyl ether substituent omitted for clarity. I) The core molecule with aryl substituents and diethyl ether molecules omitted for clarity and the remaining m-terphenyl carbons represented as spheres.

In the $[2,6\text{-}Mes_2C_6H_3]^-$ moiety, the methyl groups that replace the *i*Pr groups are significantly smaller. Instances of close CH···Br contacts are few in **II·39** and non-existent in **II·40**. Some distortion of the flanking groups away from perpendicular is apparent. In both structures, two flanking groups are distorted from perpendicular to the central aryl ring by *ca.* 7-10°. These flanking groups are positioned flat to two of the M−Br−Li−Br faces of the structure; the reason for this is unclear. The distance between the aryl group and the M−Br−Li−Br face in both structures is greater than 3.5 Å. Therefore, it is unlikely to be an interaction between any component of the cubic face and the π-system of the flanking aryl groups. This bending of the torsion angles of the flanking aryl groups is therefore likely to be a result of crystal packing effects forcing the two faces close to one another, which results in a distortion of the angle to reduce repulsive effects.

All of the $[2,6\text{-}Mes_2C_6H_3MX]_2{\cdot}[LiX(OEt_2)]_2$ complexes show lower magnetic moments than would be predicted by a spin only consideration. As has already been discussed the magnetic moments of the manganese complexes **II·36** and **II·38** are similar. Without a crystal structure we can assume a similar degree of antiferromagnetic coupling in the complexes.

The magnetic moment of **II·39** (5.1 μ_B) suggests the presence of antiferromagnetic coupling between the two metal centres. A similar depression of the magnetic moment is seen in the literature. $[FeMes_2]_2$ has a magnetic moment of 3.5 μ_B and an Fe···Fe distance of 2.614(1) Å.[41] $[\{2,6\text{-}Tripp_2C_6H_3\}Fe\{\mu\text{-}R\}]_2$ [where R = Me (**II·45**) or Ph (**II·46**)] has a magnetic moment of 3.30 μ_B (**II·45**) or 5.32 μ_B (**II·46**) with Fe···Fe distances of 2.5832(3) and 2.7207(14) Å, respectively.[174] In the literature to higher magnetic moments occur with Fe···Fe distance increases due to a weakening of antiferromagnetic coupling. **II·39** fits into this trend.

Floriani *et al*. note, however, that "the nature of the bridging ligand is essential in determining the type of antiferromagnetic coupling".[41] The importance of indirect coupling to magnetic

moments in binuclear complexes is demonstrated by the increase in magnetic moment by *ca.* 2 μ_B despite only a small increase in the Fe···Fe distance between **II·46** and **II·47** and that, despite the much greater Fe···Fe distance of 3.9855(4) Å in **II·39**, the magnetic moment of 5.1 μ_B is slightly less than that of **II·46**.

The magnetic moment of **II·40** (3.6 μ_B) is lower than the spin only value (3.87 μ_B), and the values for $[2,6\text{-Dipp}_2C_6H_3CoBr]_2{\cdot}[LiBr(OEt_2)]_2$ (**II·37**, 5.1 μ_B) and $[2,6\text{-Mes}_2C_6H_3CoBr(THF)]_2$ (4.7 μ_B).[74] The latter examples have Co···Co distances of 3.6151(9) and 3.520(2) Å, respectively.[74] It is greater than that of $[CoMes_2]_2$ (2.7 μ_B) which has a Co···Co distance of 2.512(2), which the authors show to be a bonding interaction. The Co···Co distance in **II·40** is 3.4534(6) Å, indicating a greater Co···Co interaction than **II·37** and therefore greater magnetic coupling. The difference between the magnetic moments of **II·40** and **II·37** of 1.5 μ_B is significant and suggests that other interactions are depressing the magnetic moment.

2.3.2.2 Group 12 complexes

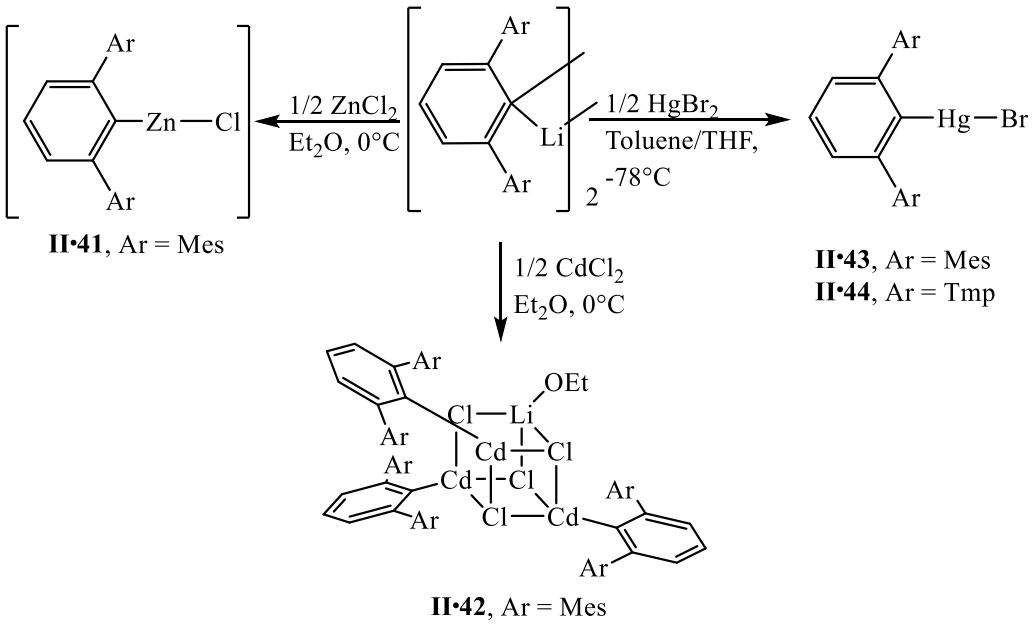

Scheme 2·6. The synthetic routes to **II·41**–**II·44**.

Group 12 *m*-terphenyl complexes [2,6-$Mes_2C_6H_3ZnCl$] (**II·41**, the precise structure is as yet unknown) and [2,6-$Mes_2C_6H_3CdCl]_3$·[$LiCl(Et_2O)$] (**II·42**) were synthesised *via* a similar procedure to the transition metal analogues (**Scheme 2·6**).

The mercury complexes, [2,6-$Mes_2C_6H_3$]HgBr (**II·43**) and [2,6-$Tmp_2C_6H_3$]HgBr (**II·44**), were synthesised through slow addition of a solution of the relevant *m*-terphenyl lithium salt in toluene/THF (5:1) to a solution of mercury bromide in the same solvent mix cooled to −78°C (**Scheme 2·6**)

II·42-**II·44** were isolated as crystalline products that could be investigated using X-ray diffraction experiments. **II·41** could not be crystallised, despite employing various methodologies, and was isolated as an impure, white powder. Analysis of this complex therefore relied on NMR spectroscopy and reaction products.

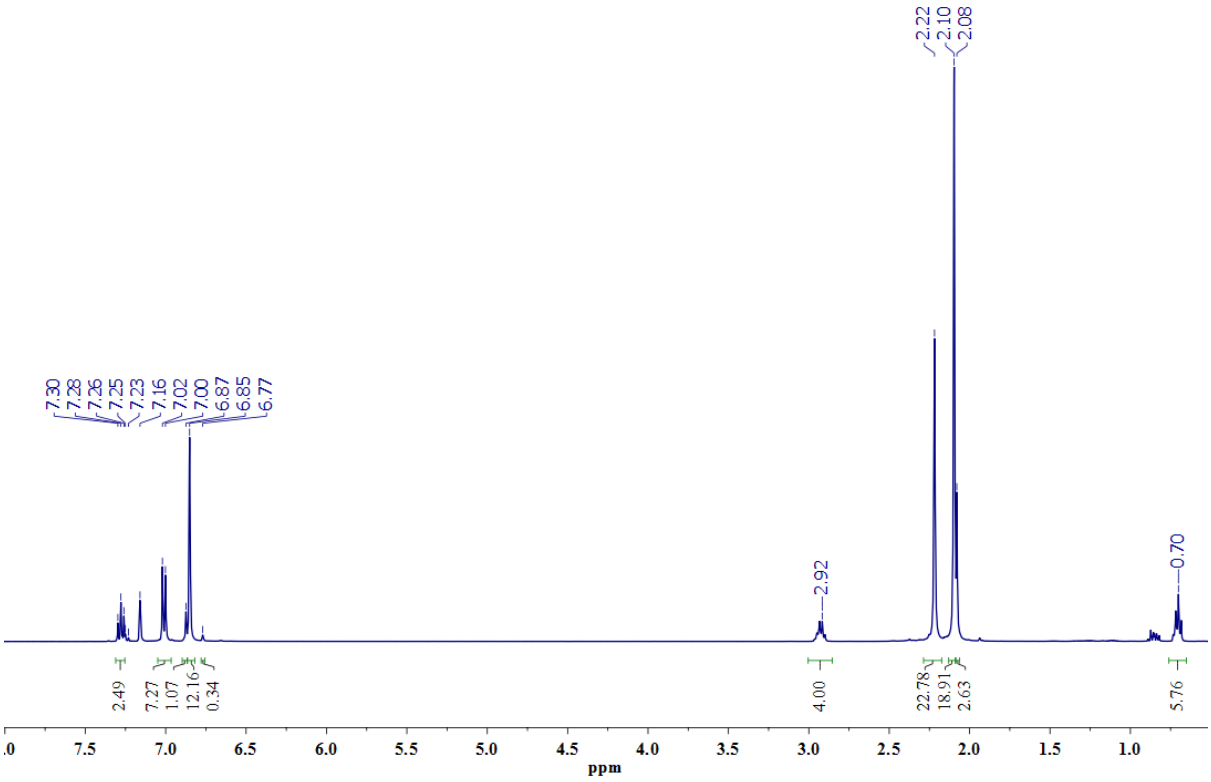

Figure 2·22. The ^{1}H NMR Spectrum of **II·41**

The ^{1}H NMR spectrum of **II·41** (**Figure 2·22**) shows that the reaction mixture contained two products. Roughly 5% of the sample was found to be [2,6-$Mes_2C_6H_3]_2Zn$ (**II·47**). **II·47** has

been previously reported by Beckmann and co-workers.[77] The remaining seven signals correspond to a compound containing a $[2,6\text{-}Mes_2C_6H_3]^-$ ligand and one equivalent of diethyl ether. These signals show a shift from either the lithium salt $[2,6\text{-}Mes_2C_6H_3Li]_2$ or unbound diethyl ether.[68,221] This indicates a fourth species containing an *m*-terphenyl ligand. $^{13}C\{^1H\}$ NMR spectroscopy supported this conclusion.

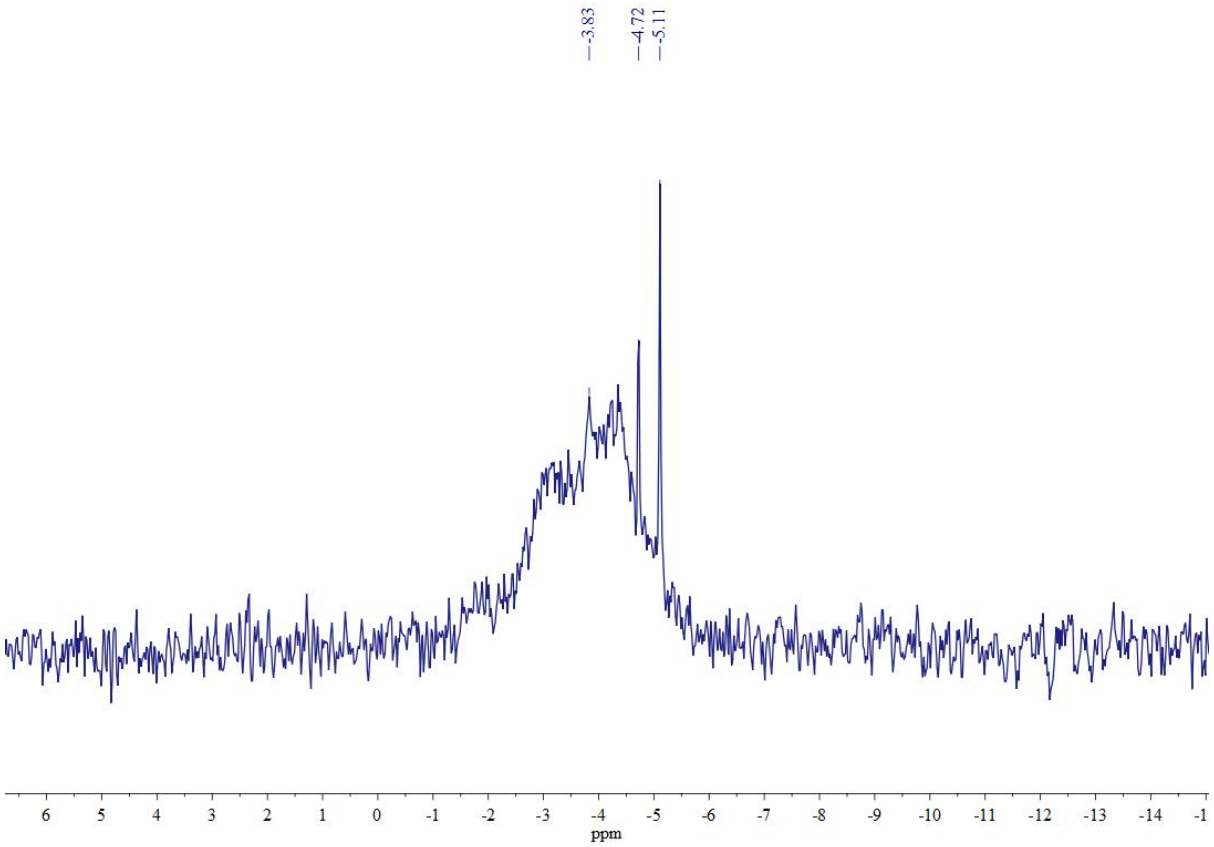

Figure 2·23. The ^7Li NMR spectrum of **II·41**.

Investigation of the complex with ^7Li NMR spectroscopy demonstrated the presence of three lithium environments in the sample, one of which gives a very broad signal. This suggests either a degree of fluxionality in the lithium containing species, more than one lithium containing species or multiple lithium environments within one species. It is possible that lithium chloride produced in the metathesis reaction is carried into the final product. As this lithium halide often aggregates, this could account for the broad signal at −4.01 ppm. The two sharper signals could signify discreet molecules.[222]

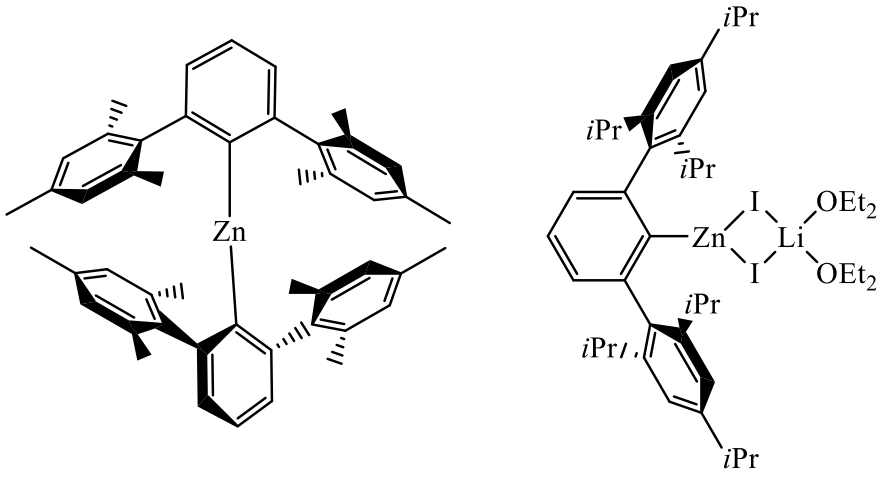

II·48 **II·49**

Figure 2·24. The structures of $[2,6\text{-}Mes_2C_6H_3]_2Zn$[77] (**II·48**) and $[2,6\text{-}Tripp_2C_6H_3]ZnI[LiI(Et_2O)_2]$[219] (**II·49**) reported in the literature.

In the literature there is precedent for a zinc terphenyl that incorporates a lithium halide moiety. Robinson *et al*. reported the complex $[2,6\text{-}Tripp_2C_6H_3]ZnI[LiI(Et_2O)_2]$ (**II·49**, **Figure 2·24**) in which one equivalent of lithium iodide was incorporated in the structure and stabilised by two equivalents of diethyl ether.[219] An equivalent structure for **II·41** does not fit with the observation that there is only one equivalent of diethyl ether in the structure relative to the *m*-terphenyl ligand. A cubic structure, similar to those of **II·36**–**II·40**, would fit the evidence (**Figure 2·24**). However, there is no literature precedent for this. A procedure reported by Power *et al*. affords the halide bridged dimer, $[2,6\text{-}Dipp_2C_6H_3ZnI]_2$ (**II·1**), with no lithium iodide incorporation.[169] A proposed structure of **II·41** is shown in **Figure 2·25**.

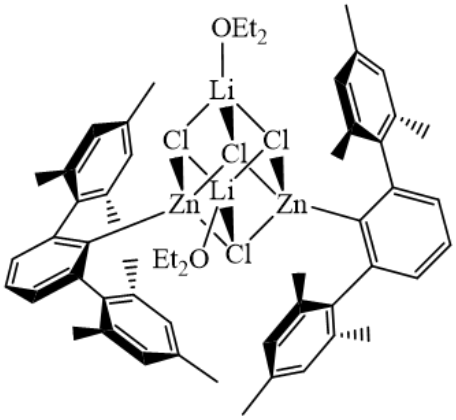

II·41

Figure 2·25. The proposed structure of **II·41**

The reaction between **II·41**, treated as $[2,6\text{-}Mes_2C_6H_3ZnCl]_2$, and two equivalents of IPrMe afforded $[2,6\text{-}Mes_2C_6H_3]ZnCl[IPrMe]$ as a crystalline product. This product was fully characterised and will be discussed further in Chapter V. Isolation of this product demonstrates that **II·41** contains a $[2,6\text{-}Mes_2C_6H_3ZnCl]$ moiety.

The reaction to produce the cadmium analogue afforded $[2,6\text{-}Mes_2C_6H_3CdCl]_3{\cdot}[LiCl(Et_2O)]$ (**II·42**) which crystallised alongside $[2,6\text{-}Mes_2C_6H_3]_2Cd$ (**III·32**). A full characterisation of **III·32** will be given in Chapter III. **II·42** was characterised *via* X-ray diffraction and NMR spectroscopic analysis. ^1H NMR spectroscopic analysis demonstrated a roughly 1:1 distribution of **II·42** to **III·32**. X-ray diffraction investigations revealed the complex to be similar to $[2,6\text{-}Mes_2C_6H_3CdCl]_3{\cdot}[LiCl(THF)]$ reported by Kays and co-workers.[223] The composition was identical except for the solvent coordinated to the lithium moiety. The complexes crystallise in different space groups [*C*2/*c* (**II·41**) and *P*-1 (**II·42**)], despite having similar solid-state structures.

The mercury analogues, $[2,6\text{-}Ar_2C_6H_3]HgBr$ [Ar = Mes (**II·43**) and Tmp (**II·44**)] were both monomeric and crystallised in moderate yields from *iso*-hexane (47% and 64% respectively).

Accurate mass EI-MS demonstrated the presence of **II·43** and the purity of the crystals of both complexes was confirmed with elemental analysis. As would be expected, the ^1H NMR spectrum of the complex contains four signals between 1.99 and 7.12 ppm, each shifted from the lithium salt[65,68] and the ^{13}C NMR spectrum contains nine signals between 20.9 and 147.2 ppm.

The elemental analysis of crystals of **II·44** gave the values within acceptable limits of the theoretical value, demonstrating the purity of the sample. The ^1H NMR spectrum of **II·44** contains six signals between 2.00 and 7.31 ppm. The signals attributed to the protons of the methyl groups are broad. This is a result of the asymmetric nature of the flanking group allows

two possible conformational isomers, *syn* or *anti* (**Figure 2·26**), which alter the shielding of the protons.

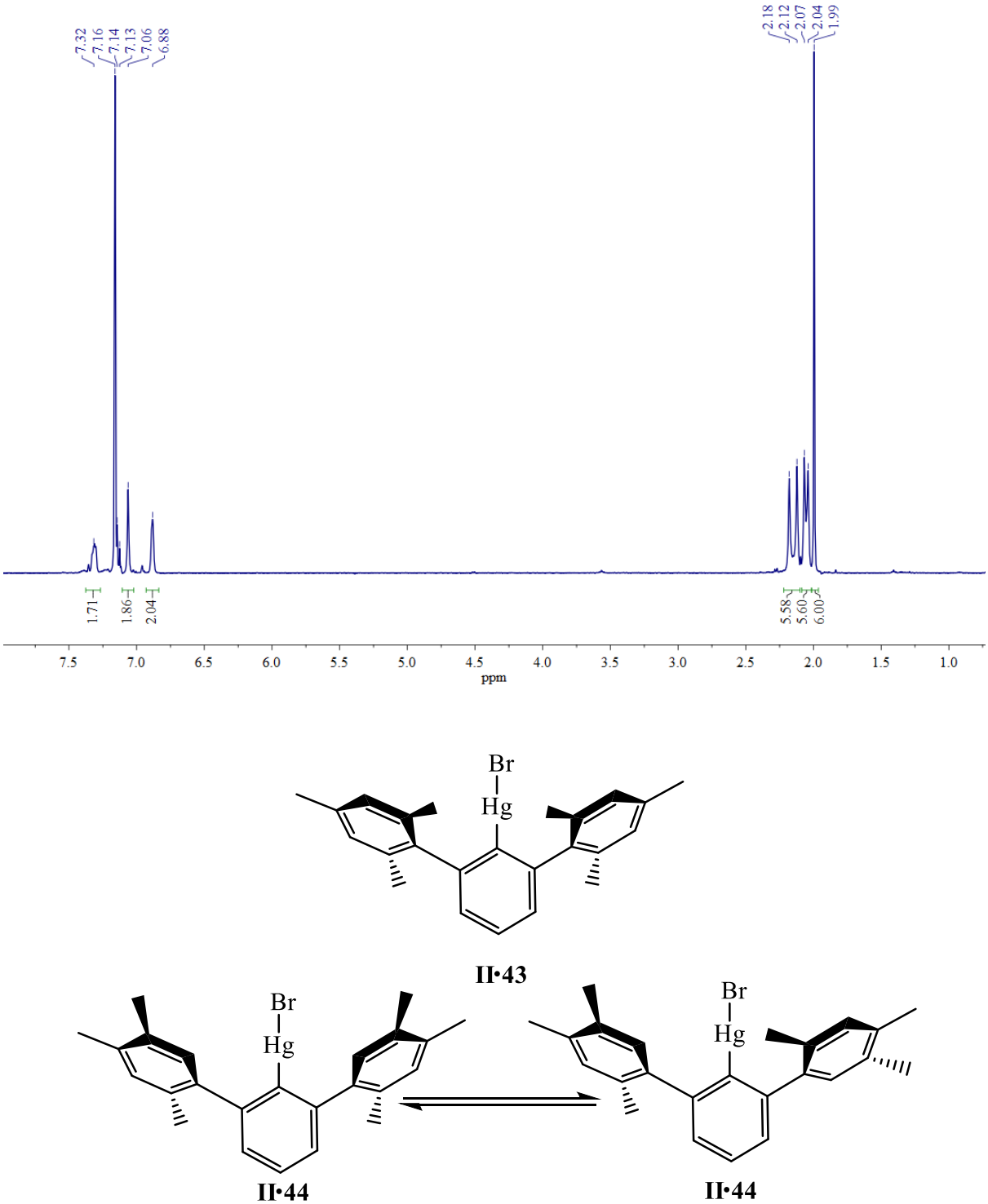

Figure 2·26. Top: the ^{1}H NMR spectrum of **II·44**. Bottom: the structure of **II·43**, and the two possible conformations of **II·44**.

The ^{199}Hg{^{1}H} NMR spectra of the complexes show signals at −1186 ppm (**II·43**), and −1157 and −1153 ppm (**II·44**); values that are similar to related complexes 9-chloromercurio-

anthracene (−1100 ppm)[224] and 2,6-Dipp$_2$C$_6$H$_3$HgBr (−1293.6 ppm).[169] The two signals in the spectrum of **II·44** are a consequence of the asymmetric nature of the Tmp flanking groups. The different conformations alter the electronic environment around the mercury centre. Interconversion of these conformational isomers must be slow, as they are observable without significant broadening on an NMR spectroscopy timescale. Presumably the methyl group in the *ortho* position of the flanking group acts as a barrier to rotation that is present but not observed for similar, rotationally symmetric, flanking groups.

The effect of conformational isomerism on heteronuclear NMR spectra was observed for the complexes, [2,6-Naph$_2$C$_6$H$_3$]$_2$M[OEt$_2$] (M = Cd or Hg).[189] Here, the asymmetric naphthyl flanking group (Naph) allows six possible conformations, which in turn gives rise to multiple signals in the ^{199}Hg NMR spectrum.

Table 2·9. Key bond lengths and angles for **II·43** and **II·44**.

	II·43		**II·44**	
Bond Lengths	Atom Labels		Atom Labels	
Hg−C/Å	Hg1, C1	2.049(4)	Hg1, C1	2.10(2)
Hg−Br/Å	Hg1, Br1	2.4145(5)	Hg1, Br1	2.466(3)
Bond Angles				
C−Hg−Br/°	C1, Hg1, Br1	178.71(14)	C1, Hg1, Br1	179.3(6)
Plane−Plane				
$Ar_{flanking}$−$Ar_{Central}$ /°	C1, C7	83.84(55)	C1, C7	56.95 (83)
	C1, C16	91.80(53)	C1, C16	
$Ar_{Central}$–Hg/Å		0.0837(67)		0.206 (38)

X-ray diffraction experiments on the two complexes allowed for a structural analysis. key bond lengths and angles are given in **Table 2·9**. Both complexes crystallise in tetragonal space groups. **II·43** adopts the space group *Pbca*, whilst **II·44** adopts the space group *Pnma*. The complexes are close to linear along the C−Hg−Br axis [178.71(14)° (**II·43**) and 179.5(6)° (**II·44**)]. This linearity is seen in other arylmercury halide complexes in the literature such as 9-chloromercurio-anthracene [175.4(2)°][224] and 2,6-Dipp$_2$C$_6$H$_3$HgBr [178.14(14)°].[169,225,226]

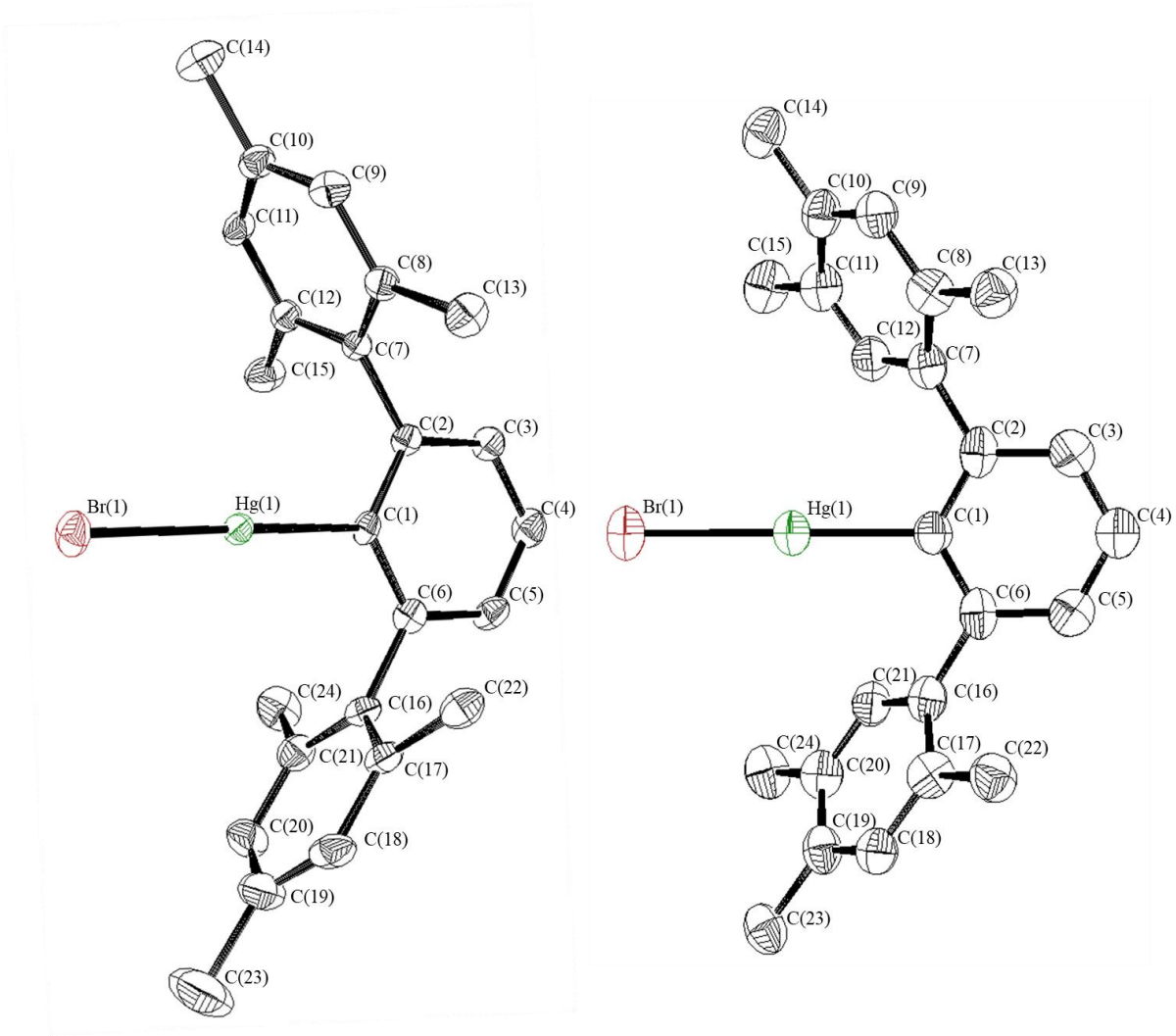

Figure 2·27. The solid-state structures of **II·43** and **II·44**. Hydrogens are omitted for clarity and ellipsoids are set at 50%.

The mesityl flanking groups in **II·43** (**Figure 2·27**) are orientated nearly perpendicular to the central aryl ring of the *m*-terphenyl ligand. The mercury moiety deviates only slightly from the plane of the aryl ring and no long-range interactions, either inter- or intramolecular, are observed.

In **II·44**, the plane-to-plane angle between the flanking aryl group and the central aryl ring is offset by 56.95(83)°. This morphology is such that the *ortho* methyl group is orientated away from the mercury centre. This could be predicted through a purely steric consideration of the system. However, the distance between the *ortho* proton of the flanking groups and the mercury centre is 2.99(3) Å, a distance that could indicate a secondary interaction which may also

contribute to the rotation of the flanking group. Such secondary interactions between aryl protons and two-coordinate mercury centres have been proposed previously in a report by Kays *et al.*[188]

It is also possible that there are intermolecular interactions in the structure. The interatomic distance between mercury of one structure and the nearest bromide moiety of another is 3.519(3) Å, which is within the combined van der Waals radii of the two atoms.[187] There is also a deviation of the mercury moiety from the plane of the aryl ring of 0.206(28)° toward this interaction, as shown in **Figure 2·28**.

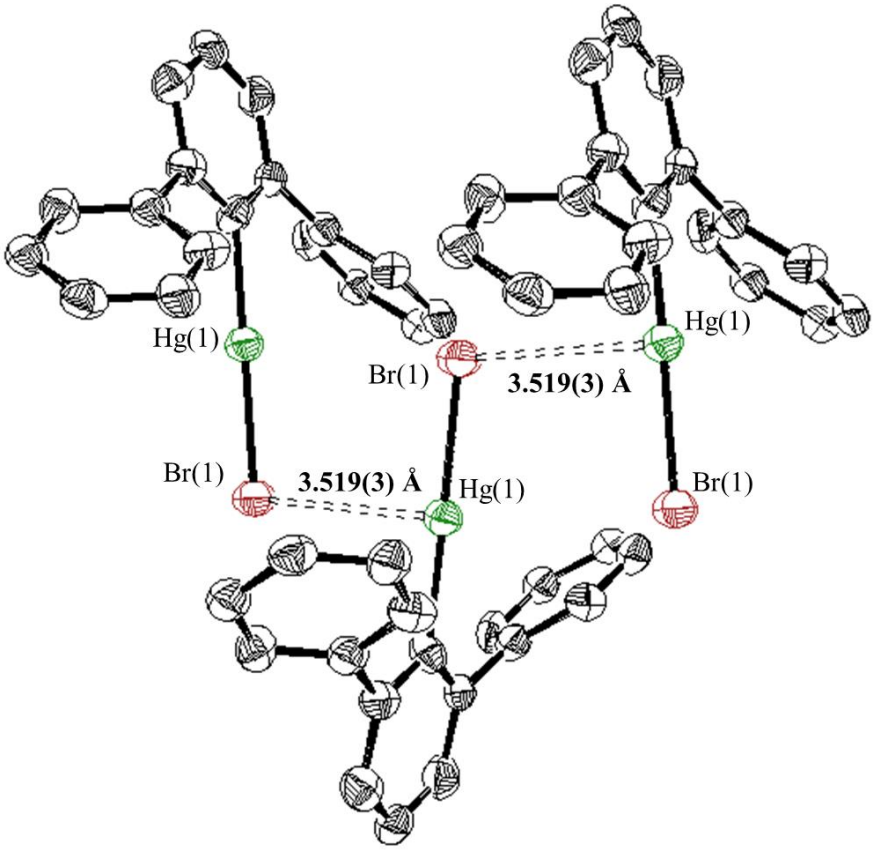

Figure 2·28. The intramolecular interactions in the crystal structure of **II·44**. Methyl groups and hydrogens are omitted for clarity. Ellipsoids are set at 50%.

2.4 Conclusions

A series of transition metal and Group 12 Grignard analogues, supported by *m*-terphenyl ligands, have been synthesised and characterised. This has shown that the family of Grignard analogues first published by Power *et al.*[169,170] can be expanded to contain different halogens and *m*-terphenyl ligands.

Two NHC complexes, in which each metal centre is coordinated by just one NHC, have also been characterised. These complexes will provide intermediates in the synthesis of two-coordinate, heteroleptic complexes. We were unable to isolate manganese(II), iron(II), nickel(II) and copper(II) complexes coordinated by a single NHC. Instead these metals formed four-coordinate monomers (iron and nickel), two-coordinate disproportionation products (copper) or salt complexes (manganese).

^{1}H NMR spectroscopic investigations of the diamagnetic complexes of ligands with *i*Pr groups show large shifts of the *i*Pr signals upon complexation. Similarly, in the solid-state, it was observed that in some complexes the ligands are orientated such that the CH···X contacts are shorter than in the sterically optimal position. We suggest that in the complexes with *i*Pr groups a network of intermolecular hydrogen bonds formed between the flanking groups and halogens. This effect is not observed when the *i*Pr groups are replaced with methyl groups. These hydrogen bonding networks have not been previously observed in the literature.

The dimeric, paramagnetic species possessed magnetic moments that are lower than the spin only values. This has been attributed to antiferromagnetic coupling between the two metal ions. The mechanism for this coupling could not be examined with the available techniques. Where complexes could be compared, the magnitude of the magnetic moment decreased with the distance between the metals, a pattern that has been observed in the literature, and indicates that the interaction between the metals contains a direct coupling component.

2.5 Future Work

An important aspect of future work would be to increase the range of NHC and *m*-terphenyl ligands used. This would facilitate the production of a wide range of complexes bearing multiple types of organometallic ligand, and so expand the scope of this investigation. With respect to *m*-terphenyls, this would involve the use of different flanking groups, many of which have been reported in the literature.[71,144,227] Expanding the range of NHCs investigated would involve different synthetic methods such as *in situ* deprotonation of an NHC precursor. There could also be scope to investigate the use of heavy tetrylenes as ligands in the place of NHCs (**Figure 2·29**).[228]

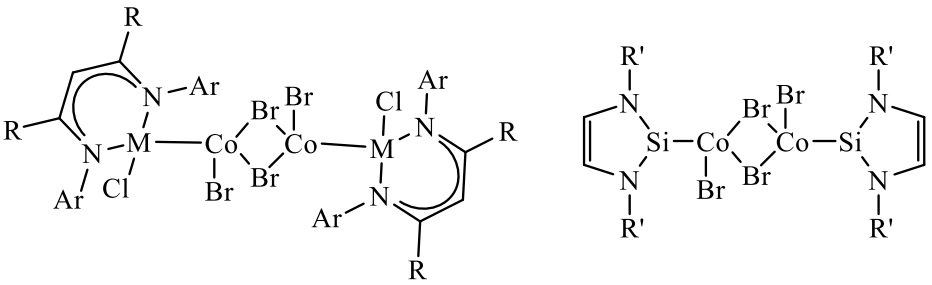

Figure 2·29. Possible halide bridged, dimeric structure coordinated by selected tetrylenes.

Exchange of one or more of the bridging halides for alternative anions would give more scope to the study, and possibly facilitate the isolation of bridged zinc and manganese species bearing the $[2,6\text{-}Mes_2C_6H_3]^-$ ligand. The introduction of bridging groups such as methylene and phenyl groups would not add much steric bulk to the system but could be exchanged with a weak acid.[174] Substitution of the halides for hydrides, possibly using a similar methodology to Power *et al*. in the synthesis of $[2,6\text{-}Dipp_2C_6H_3Zn(\mu\text{-}H)]_2$, could allow the introduction of very bulky, secondary ligands.[229] Such complexes would also be worth investigating as hydrosilylation catalysts in their own right.[217] Finally, altering the bridging moiety would give further insight into the effects of indirect coupling in these complexes.[185,220] Bridged complexes with a range of organic and inorganic bridging ligands would provide a lot of scope to this work and would be worth future investigation.

2.6. General Experimental

2.6.1. Glove Box and Schlenk Line Techniques

Low-coordinate, transition metal compounds are prone to readily reacting with atmospheric gases such as H_2O and O_2. Preparation and manipulation of such compounds was therefore undertaken under an inert atmosphere (N_2 or Ar) with the use of standard Schlenk line and glove box techniques. Such techniques prevent decomposition of the compounds and unwanted side reactions.

Schlenk line apparatus consists of a dual manifold of thick-walled borosilicate glass. The first manifold was connected to a cylinder of argon gas at a pressure of *ca.* 0.5 bar while the second was connected to an Edwards RV5 rotary vane two stage mechanical pump capable of achieving a dynamic vacuum of 10^{-4} mbar. The vacuum was measured by an Edwards pirani 10 thermal conductivity vacuum gauge. A liquid nitrogen cooled low-temperature trap was used to capture volatiles and prevent contamination of the vacuum pump.

A range of apparatus, including Schlenk tubes and Youngs tap ampoules, were connected to the Schlenk line *via* neoprene pipes and exposed to vacuum/argon atmospheres *via* two-way ground glass taps.

To prevent leaks all glass joints were lubricated with Dow-Corning high vacuum grease prior to use which allowed an inert atmosphere to be achieved by cycling between vacuum and inert gas three times before finally being refilled with inert gas. Typically, the hot glassware was connected to the system and placed under vacuum until a vacuum of *ca.* 10^{-3} mbar was achieved. The glassware was then heated with a blue Bunsen flame for one minute under a dynamic vacuum, allowed to cool slightly and subjected to three refill and evacuation cycles before a final refill to give an inert atmosphere within the glassware. Liquids were transferred *via* stainless steel cannulae or using glass/plastic syringes.

A MBraun UNIlab glove box of stainless steel construction fitted with a strengthened viewing panel and neoprene gloves was used for storage and manipulation of anhydrous reagents. An inert atmosphere was maintained within the glove box by continuous recirculation of the dinitrogen atmosphere through a copper-based catalyst in order to maintain O_2 and H_2O levels below 0.1 ppm (parts per million). Apparatus was admitted *via* an ante-chamber using four, two-minute evacuation and refill cycles.

2.6.2 Analytical Measurements

NMR Spectroscopy

NMR spectroscopy samples were prepared using standard techniques under an atmosphere of dinitrogen using Youngs tap modified borosilicate glass NMR tubes. The spectra were collected on Bruker DPX 300, DPX 400, AV400, AV(III)400, or AV(III)500 spectrometers. Chemical shifts are quoted in ppm relative to neat TMS (tetramethylsilane) (^{1}H and $^{13}C\{^{1}H\}$) or a $LiCl/D_2O$ solution ($^{7}Li\{^{1}H\}$). $^{113}Cd\{^{1}H\}$ and $^{199}Hg\{^{1}H\}$ spectra were collected on AV400 or AV(III)400 spectrometers with chemical shifts quoted in ppm relative to Me_2Cd and Me_2Hg, using internal calibrants of 0.1 M $Cd(ClO_2)_2/H_2O$ and 1.0 M $Hg(ClO_4)_2/H_2O$, respectively.

Evans' Magnetic Measurements

Diamagnetic constants were calculated *via* Evans' method at 298 K in Benzene-d_6 using **Equation 1**. Diamagnetic corrections were calculated according to pascals constants.[198,230]

$$\chi = \frac{3\Delta f}{2\pi f m} + \chi_0 + \frac{\chi_0(d_o + d_s)}{m}$$

Equation 1 *χ = magnetic susceptibility, f = frequency at which the proton resonances were studied (Hz), Δf = the frequency separation between two lines (Hz), m = mass of substance in 1 mL of solution, χ_0 = susceptibility of solvent, d_0 = density of solvent and d_s = density of the solution.*

Mass Spectrometry

Air sensitive samples for mass spectrometry were prepared under a dinitrogen atmosphere in a glove box and sealed in glass capillary tubes. EI-MS measurements were recorded by Dr Mick Cooper (University of Nottingham) on a Bruker Apex IV FTICR-MS with heptacosafluorotributylamine (FC43) as mass calibrant or at the EPSRC National Mass Spectrometry Service Centre on a Finnigan MAT 95 XP spectrometer using a perfluorotributylamine standard. ASAP-MS measurements were recorded at the EPSRC National Mass Spectrometry Service Centre on a Waters Xevo-G2-S. For high resolution measurements this machine was calibrated against external standards also run on an LTQ Orbitrap XL.

Elemental Analysis

Elemental analysis samples were measured either at London Metropolitan University by Stephen Boyer or at the University of Nottingham by Tong Liu. In both cases the samples were prepared under a dinitrogen atmosphere in a glove box. For measurement at London Metropolitan University samples were sealed in glass tubes and measured using a CE1108 Elemental Analyser. For the measurement at the University of Nottingham samples were sealed in nickel capsules and measured using a CE-440 Elemental Analyzer, Exeter Analytical Inc..

Cyclic Voltammetry

Cyclic Voltammetry measurements were carried out with the assistance of Grace Lowe at the University of Nottingham using a CHI700 potentiostat and a three-electrode system in a single compartment cell using a glassy carbon working electrode, a platinum wire secondary electrode and a silver wire refence electrode. Experiments were conducted in a glove box under a dinitrogen atmosphere. Solution concentrations are given in the relevant experimental entry

and redox potentials are referenced to the Standard Calomel Electrode (SCE) by an internal calibration.

UV/Vis Spectroscopy

UV/Vis spectroscopy samples were prepared under a dinitrogen atmosphere in a glove box as solutions of known concentration in a 10 mL quartz cell modified with a Young's tap. UV/Vis spectra were recorded over a 350-1100 nm range on a Perkin Elmer Lamda 25 UV/Vis Spectrophotometer.

X-ray Diffraction Analysis

Crystals suitable for X-ray diffraction analysis were either coated in Fomblin® PFPE (YR-1800 perfluoropolyether oil, Lancaster) under a dinitrogen atmosphere in a glove box or removed from the crystallisation vessel under a flow of dinitrogen and placed in Fomblin® PFPE on a glass slide. A suitable crystal was then mounted on a polymer tipped MiTeGen MicroMount^{TM} and frozen rapidly in a stream of nitrogen cooled to 120 K using an Oxford Cryostreams open flow cryostat in line with the X-ray source.[231] Single crystal X-ray diffraction data was collected on either an Agilent SuperNova diffractometer with an Atlas CCD area detector and Cu/Mo microfocus X-ray sources, one of two Agilent SuperNova II diffractometers equipped with a copper microfocus X-ray source and either an Atlas S2 or Titan S2 CCD area detector or a Rigaku diffractometer equipped with an air-cooled Dectris Pilatus 200K CCD area detector and an MM07 rotating anode copper X-ray source. Cell parameters were refined from the observed positions of all strong reflections in each data set and absorption corrections were applied using a Gaussian numerical method with beam profile correction.

Data sets were solved either by direct or iterative methods and where possible non-hydrogen atoms were refined by full-matrix least-squares on all unique F^2 values with anisotropic displacement parameters. Details of the rare instances in which this was not possible, where

the atoms were refined isotopically are contained within the .cif files of the relevant structures. Hydrogen atoms were refined with constrained geometries and riding thermal parameters. Programs used include CrysAlisPro[232] (control and integration of Supernova), SHELXL (structure solution), SHELXD[233], SHELXS[234], SHELXT[235], SUPERFLIP[236] and OLEX2[237]. CIF files were checked using CheckCIF and by Dr William Lewis at the University of Nottingham.

2.6.3 Preparation and Purification of solvents and reagents

Solvents

All solvents were dried, degassed *in vacuo* using standard Schlenk line techniques, and stored in ampoules over potassium mirrors, save for THF which was stored over 4 Å molecular sieves, prior to use. Diethyl ether and THF were both pre-dried over sodium wire then thoroughly dried *via* refluxing over sodium-potassium alloy (diethyl ether) or sodium/benzophenone (THF) for a minimum of three days. Toluene, cyclohexane, and benzene were dried by refluxing over potassium, again for a minimum of three days. *iso*-Hexane and pentane were passed through a drying column fitted with 4 Å molecular sieves.

Benzene-d_6 and THF-d_6 were dried over potassium in sealed ampoules at 90°C for five days before vacuum transfer to ampoules containing a potassium mirror (C_6D_6) or 4 Å molecular sieves. $CDCl_3$ was dried over calcium hydride before vacuum transfer to ampoules containing molecular sieves. Deuterated solvents were thoroughly degassed prior to use using three freeze-pump-thaw-degas cycles.

Reagents

Where necessary solid reagents were dried *in vacuo* using standard Schlenk line techniques before use. When required, solvent adducts of commercially available metal halides were prepared by minor modifications of literature methodologies[238]. All anhydrous solid reagents

were stored in a glove box prior to use. Liquid reagents were either dried over 4 Å molecular sieves and degassed prior to use or used as delivered.

Carbon monoxide was used as purchased. A cylinder fitted with a gas regulator was attached *via* neoprene tubing to the gas manifold of a Schlenk line, and the whole apparatus purged with carbon monoxide using three fill-evacuate cycles, before admittance to reaction vessels.

2.6.4 Preparation of Pro-Ligands

1,3-Diisopropyl-4,5-dimethylimidazol-2-ylidene (IPrMe)

1,3-Diisopropyl-4,5-dimethylimidazol-2-ylidene (IPrMe) was prepared from commercially available starting materials and purified according to the synthesis published by Kuhn and Kratz in 1992.[97] ^{1}H NMR (C_6D_6, 400 MHz, 300K) δ_H/ppm; 1.51 (d, 12 H, J_{HH} = 8.1 Hz, CH_3 of *i*Pr flanking group), 1.74 (s, 6 H, CH_3 of backbone), 3.96 (sept, 4 H, J_{HH} = 8.1 Hz, CH of *i*Pr flanking group). ^{13}C{^{1}H} NMR (C_6D_6, 100 MHz, 300 K) δ_c/ppm; 9.11 (CH_3 of backbone), 25.0 (CH_3 of *i*Pr flanking group), 48.8 (CH of *i*Pr flanking group), 121.7 (C=C), 207.9 (N-C-N).

1,3-bis(2,6-diisopropylphenyl)imidazol-2ylidene (IPr)

1,3-bis(2,6-diisopropylphenyl)imidazol-2-ylidene (IPr) was prepared *via* the HCl salt from commercially available starting materials. The HCl salt was synthesised using the procedure published by Huang and Nolan in 1999.[239] This product was then deprotonated using potassium hydride.[240] ^{1}H NMR (C_6D_6, 400 MHz, 300K) δ_H/ppm; 1.17 (d, 24 H, J_{HH} = 9.2 Hz, CH_3 of Dipp flanking group), 2.90 (sept, 4 H, J_{HH} = 9.2 Hz, CH of *i*Pr flanking group), 6.55 (s, 2 H, CH of backbone), 7.09 (d, 4 H, J_{HH} = 7.7 Hz, *m*-H_{Ar} on flanking group), 7.21 (t, 2 H, J_{HH} = 7.7 Hz, *p*-H_{Ar} on flanking group).

Lithium *m*-Terphenyl Compounds

m-Terphenyl iodides were prepared *via* literature procedures and purified by recrystallisation from hot ethanol.[69,71,188,241] 2,6-$Dcp_2C_6H_3I$ was further purified by sublimation at 140°C under a vacuum of 10^{-2} mbar. Starting materials were used as purchased except 2,6-*i*PrC_6H_3Br which was synthesised using a Sandmeyer synthesis and purified by distillation at 80°C under a vacuum of *c*. 10^{-2} mbar.

m-Terphenyl iodides were converted to lithiated species *via* a lithium-halogen exchange reaction for use in metathesis reactions. This was performed using modified literature syntheses.[68,188] *m*-Terphenyl iodide (1 equivalent) was suspended in 20 mL of hexane and cooled to 0°C. *n*-BuLi (2.5 M in hexane, 1.5 equivalents) was added dropwise *via* syringe over 1 minute. The reaction stirred at 0°C for 1 hr and then allowed to warm to room temperature and stirred for a further 2 hrs before the stirring was switched off and the reaction allowed to settle. The supernatant was then filtered from the reaction to leave behind a white product which was then washed twice with cold hexane (2 × 10 mL) before being dried *in vacuo* and transferred to a glove box. The purity of the product was assessed *via* $^7Li\{^1H\}$ and ^1H NMR spectroscopy. In the lithium halogen exchange reaction of 2,6-$Dcp_2C_6H_3I$ only 1.1 equivalents of *n*-BuLi was used to prevent side reactions from occurring.

$[2,6\text{-}Mes_2C_6H_3Li]_2$: ^1H NMR (C_6D_6, 400 MHz, 300 K) δ_H/ppm; 1.83 (s, 12 H, *p*-CH_3), 2.17(s, 24 H, *m*-CH_3), 6.82 (d, 2 H, *m*-H_{Ar}), 6.84 (s, 4 H, *m*-H_{Ar} of the flanking groups), 7.24 (t, 1 H, *p*-H_{Ar}). $^{13}C\{^1H\}$ NMR (C_6D_6, 100 MHz, 300 K) δ_c/ppm; 21.5 (CH_3), 21.9 (CH_3), 124.1 (CH_{Ar}), 126.5 (CH_{Ar}), 130.1 (CH_{Ar}), 136.1 (quaternary-C_{Ar}), 136.7 (quaternary-C_{Ar}), 143.7 (quaternary-C_{Ar}), 151.2 (quaternary-C_{Ar}). $^7Li\{^1H\}$ NMR (C^6D^6, 155 MHz, 300 K): δ_{Li}/ppm; 1.64.

$[2,6\text{-}Dipp_2C_6H_3Li]_2$: ^1H NMR (C_6D_6, 400 MHz, 300 K) δ_H/ppm; 1.20 (d, 12 H, J_{HH} = 6.8 Hz, CH_3 of *i*Pr), 1.38 (d, 12 H, J_{HH} = 6.8 Hz, CH_3 of *i*Pr), 3.52 (sept, 4 H, J_{HH} = 6.8 Hz, CH of *i*Pr),

7.17 (d, 2 H, J_{HH} = 7.5 Hz, *m*-CH_{Ar} of central aryl), 7.29 (d, 4 H, J_{HH} = 7.9 Hz, *m*-CH_{Ar} of flanking group), 7.42 (d, 2 H, J_{HH} = 7.9 Hz, *p*-CH_{Ar} of flanking group), 7.45 (J_{HH} = 7.5 Hz, *p*-CH_{Ar} of central aryl). $^{13}C\{^1H\}$ NMR (C_6D_6, 100 MHz, 300 K) δ_c/ppm; 24.3 (CH_3 of *i*Pr), 24.9 (CH_3 of *i*Pr), 32.8 (CH of *i*Pr), 110.8 (CH_{Ar}), 122.8 (CH_{Ar}), 127.6 (CH_{Ar}), 128.2 (CH_{Ar}), 128.5 (quaternary-C_{Ar}), 142.6 (quaternary-C_{Ar}), 145.9 (quaternary-C_{Ar}), 146.4 (quaternary-C_{Ar}). $^7Li\{^1H\}$ NMR (C_6D_6, 155 MHz, 300 K): δ_{Li}/ppm; 2.38.

[2,6-(2,6-Xyl)$_2$C$_6$H$_3$Li]$_2$: ^1H NMR (C_6D_6, 400 MHz, 300 K) δ_H/ppm; 1.98 (s, 12 H, CH_3 of the flanking groups), 6.95 (d, 2 H, J_{HH} = 7.5 Hz, *m*-H_{Ar}), 7.34 (m, 6 H, H_{Ar}), 7.37 (t, 1H, J_{HH} = 7.60 Hz, *p*-H_{Ar}). $^{13}C\{^1H\}$ NMR (C_6D_6, 100 MHz, 300 K) δ_c/ppm; 21.52 (CH_3), 123.4 (CH_{Ar}), 126.1 (CH_{Ar}), 127.1 (CH_{Ar}), 128.73 (CH_{Ar}), 136.1 (quaternary-C_{Ar}), 146.2 (quaternary-C_{Ar}), 151.7 (quaternary-C_{Ar}). $^7Li\{^1H\}$ NMR (C_6D_6, 155 MHz, 300 K): δ_{Li}/ppm; 1.58.

[2,6-Pmp$_2$C$_6$H$_3$Li]$_2$: ^1H NMR (C_6D_6, 400 MHz, 300 K) δ_H/ppm; 1.88 (s, 12H, *o*-CH_3 of Pmp), 2.13 (s, 6H, *p*-CH_3 of Pmp), 2.19 (s, 12H, *m*-CH_3 of Pmp), 6.81 (d, 2H, J_{HH} = 7.5 Hz, *m*-H of C_6H_3), 7.25 (t, 1H, J_{HH} = 7.6 Hz, *p*-H of C_6H_3). $^7Li\{^1H\}$ NMR (C_6D_6, 155 MHz, 300 K): δ_{Li} / ppm; 1.82.

[2,6-Dcp$_2$C$_6$H$_3$Li]$_2$: ^1H NMR (C_6D_6, 400 MHz, 300 K) δ_H/ppm; 6.51 (t, 2 H, J_{HH} = 8.0 Hz, *p*-$C_{Ar}H$,), 6.91 (d-overlapping, 2 H, J_{HH} = 8.1, *m*-$C_{Ar}H$), 6.93 (d-overlapping, 1 H, J_{HH} = 8.5 Hz, *m*-$C_{Ar}H$), 7.22 (t, 1 H, J_{HH} = 7.6 Hz, *p*-$C_{Ar}H$,). $^{13}C\{^1H\}$ NMR (C_6D_6, 100 MHz, 300 K): δ_C/ppm; 126.92 (CH_{Ar}), 127.65 (CH_{Ar}), 128.75 (CH_{Ar}), 129.57 (CH_{Ar}), 134.20 (quaternary-C_{Ar}), 145.58 (quaternary-C_{Ar}), 150.32 (quaternary-C_{Ar}). $^7Li\{^1H\}$ NMR (C_6D_6, 155 MHz, 300 K): δ_{Li}/ppm; 2.95.

[2,6-Tmp$_2$C$_6$H$_3$Li]$_2$: ^1H NMR (C_6D_6, 400 MHz, 300 K) δ_H/ppm; 1.90 (s, 6 H, *o*-CH_3), 2.02 (s, 6 H, *p*-CH_3), 2.03 (s, 6 H, *m*-CH_3), 6.74 (s, 2 H, H_{Ar}), 7.12 (s, 1 H, H_{Ar}), 7.22 (s, 2 H, H_{Ar}). $^{13}C\{^1H\}$ NMR (C_6D_6, 100 MHz, 300 K) δ_c/ppm 19.50 (CH_3), 19.71 (CH_3), 20.66 (CH_3), 124.5

(tertiary-C_{Ar}), 125.0 (tertiary-C_{Ar}), 130.1 (tertiary-C_{Ar}), 133.5 (quaternary-C_{Ar}), 133.9 (quaternary-C_{Ar}), 135.3 (quaternary-C_{Ar}), 135.6 (quaternary-C_{Ar}), 143.6 (quaternary-C_{Ar}), 151.5 (*ipso*-C_{Ar}). ^{7}Li{^{1}H} NMR (C_6D_6, 155 MHz, 300 K): 1.86.

2.7.1 Synthetic Experimental

2.7.1 [(IPrMe)$CoBr_2$]$_2$ (II·30)

$CoBr_2$(DME) (822 mg, 2.66 mmol) and IPrMe (400 mg, 2.22 mmol) were dissolved separately in THF (2 × 20 mL). The solution of IPrMe was added dropwise to the dark blue solution of $CoBr_2$ (cooled to 0°C) over 10 mins. The reaction was stirred at room temperature for 16 hrs before all volatiles were removed *in vacuo*. The blue solid was washed with pentane (2 × 10 mL) to give [(IPrMe)$CoBr_2$]$_2$. Yield 200 mg, 23%. Crystals suitable for X-Ray diffraction investigations were grown by vapour diffusion of pentane into a concentrated solution of the compound in C_6D_6. A reliable value for the magnetic moment of the complex could not be obtained due to the low of solubility in C_6D_6 and instability in chloroform-*d*. ^{1}H NMR (C_6D_6, 400 MHz, 300 K) δ_H/ppm; −15.93 (4H, CH of *i*Pr flanking group), 10.33 (24H, CH_3 of *i*Pr flanking group), 28.83 (12H, backbone CH_3). Elemental analysis $C_{22}H_{40}N_4Co_2Br_4$: calcd. C 33.03, H 5.29, N 7.00; found C 32.84, H 4.86, N 6.88. EI-MS (positive ion mode) *m/z* = 577.1 [$C_{22}H_{40}N_4CoBr_2$]$^+$ (6%), 498.1 [$C_{22}H_{40}N_4BrCo$]$^+$ (20%), 396.9 [M – $C_{11}H_{20}N_2Co_1Br_2$]$^+$ (15%), 318.0 [M − $C_{11}H_{20}N_2Co_1Br_3$]$^+$ (42%), 275.9 (20%), 243.1 (60%), 180.1 [IPrMe]$^+$ (55%), 138.1 [IPrMe – *i*Pr] (100%),

2.7.2 [(IPrMe)$ZnCl_2$]$_2$ (II·31)

$ZnCl_2$ (181 mg, 0.133 mmol) and IPrMe (195 mg, 1.08 mmol) were dissolved separately in THF (2 × 20 mL). The solution of IPrMe was added dropwise to the colourless solution of $ZnCl_2$ (cooled to 0°C) over 10 mins. The reaction was stirred at 0°C for 1 hr before being allowed to warm to room temperature with stirring. All volatiles were removed *in vacuo* and

the resulting white solid was extracted into dichloromethane (1 × 10 mL). All volatiles were removed from this extraction *in vacuo* and the white solid washed with pentane (10 mL) to afford $[(IPrMe)ZnCl_2]_2$. Yield 196 mg, 48%. Crystals suitable for X-ray diffraction investigations were grown by vapour diffusion of pentane into a concentrated solution of the compound in $CDCl_3$. ^1H NMR ($CDCl_3$, 400 MHz, 300 K) δ_H/ppm; 1.55 (d, 24H, J_{HH} = 7.03, CH_3 of *i*Pr flanking group), 2.24 (s, 12H, backbone CH_3), 5.35 (sept, 4H, J_{HH} = 7.02 Hz, CH of *i*Pr flanking group). $^{13}C\{^1H\}$ NMR ($CDCl_3$, 100 MHz, 300 K) δ_C/ppm; 10.5 (CH_3 of IPrMe backbone), 22.3 (CH_3 of *i*Pr group), 53.6 (CH of *i*Pr group), 126.5 (*quaternary* C of IPrMe backbone), 166.4 (*ipso*-C of IPrMe). Elemental analysis $C_{22}H_{40}N_4Zn_2Cl_4$: calcd. C 41.73, H 6.37, N 8.85; found C 41.47, H 5.93, N 8.76), EI-MS *m/z* accurate mass $[M - Cl]^+$: calcd. 279.0601; found 279.0530. TOF ASAP MS *m/z*; 279.0 $[M – Cl]^+$ (28%), 180.1 $[IPrMe]^+$ (98%), 138.1 [IPrMe – *i*Pr]$^+$, 95.0 [IPrMe – 2*i*Pr]$^+$ (50%).

2.7.3 $[IPrMe]_2CoBr_2$ (II·32)

THF (30 mL) was added to a mixture of $CoBr_2$(DME) (0.554 mmol, 171 mg) and IPrMe (1.10 mmol, 199 mg) at room temperature. The blue solution was stirred for 16 hrs before the solvent was removed *in vacuo* to afford a blue solid. This solid was extracted into toluene (3 × 10 mL) to give a blue solution, the volume of which was reduced by 1/2. Crystallisation was induced by layering with *iso*-hexane (30 mL) onto the solution before storage at 7°C to give deep blue crystals of pure product suitable for X-ray diffraction investigations. 24.5 mg, 7.7%. ^1H NMR (C_6D_6, 400 MHz, 300K) δ_H/ppm; 0.30 (s), 2.88 (s, $\Delta\nu$½ = 237 Hz), 6.23 (s, $\Delta\nu$½ = 396 Hz), 9.26 (s, $\Delta\nu$½ = 370 Hz), 11.52 (s, $\Delta\nu$½ = 267 Hz), 16.52 (s, $\Delta\nu$½ = 198 Hz), 17.36 (s), 18.36 (s, $\Delta\nu$½ = 224 Hz), 24.90 (s, $\Delta\nu$½ = 331 Hz). μ_{eff} = 4.7 μ_B. Elemental analysis: $C_{22}H_{40}N_4CoBr_2$ calcd: C 45.61, H 6.96, N 9.67; found C 45.37, H 6.83, N 9.50. UV/Vis: 1.45×10^{-5} M (THF) λ_{max}/nm (ε/dm^3 mol^{-1} cm^{-1}) broad absorption 600 – 740 nm, 626 (285), 667 (402), 699 (347). EI-MS (positive ion mode) *m/z* = 579.2 $[M]^+$ (2%), 578.1 $[M - Br]^+$ (2%). Fragment ion peak

at *m/z* = 498.2 $[M - 2Br]^+$ (4%) 399.0 $[M - IPrMe]^+$ (2%), 355.1 $[M - IPrMe - iPr]^+$ (1%), 218.0 $[M - IPrMe - Br]^+$ (5%), 260.1 $[IPrMe + Br]^+$ (7%), 180.1 $[IPrMe]^+$ (50%), 139.1 $[IPrMe - iPr]^+$ (100%), 95.0 $[IPrMe - 2iPr]^+$ (77%).

2.7.4 $[IPrMe]_2NiCl_2$ (II·33)

THF (30 mL) was added to a mixture of IPrMe (556 mg, 3.08 mmol) and $NiCl_2$ (200 mg, 1.54 mmol) at room temperature to give a deep orange solution. The reaction was stirred for 16 hrs, during which time the reaction became orange/pink in colour, before all volatiles were removed *in vacuo* to give an orange/pink solid. This was extracted into toluene (4 × 5 mL) to give an orange/pink solution which was reduced in volume by *ca.* 1/3. The solution was then stored at −30°C for 16 hrs to afford large orange/red crystals suitable for X-ray diffraction investigations. 405 mg, 54%. ^1H NMR (C_6D_6, 400 MHz, 300K) δ_H/ppm; 1.65 (s, 12H, backbone CH_3), 1.83 (d, 24H, J_{HH} = 7.1 Hz, CH_3 of *i*Pr flanking group), 7.55 (sept, 4H, J_{HH} = 7.1 Hz, CH of *i*Pr flanking group). $^{13}C\{^1H\}$ NMR (C_6D_6, 100 MHz, 300K) δ_C/ppm; 9.83 (backbone CH_3) 22.56 (CH_3 of *i*Pr flanking group), 53.26 (CH of *i*Pr flanking group), 124.52 (olefinic C_q), 167.94 (C_q bound to Ni). Elemental analysis $C_{22}H_{40}Cl_2N_4Ni$: calcd. C 53.91, H 8.23, N 11.43; found 53.72, H 8.07, N 11.33. EI-MS (positive ion mode) *m/z* = 488.2 $[M]^+$ (10%) fragment ion peaks at *m/z* 237.1 $[M - C_{11}H_{21}N_2Cl_2]$ (6%), 215.1 $[M - NiN_2C_{11}H_{20}Cl]^+$ (100%), 181.1 (18%) $[M - NiN_2C_{11}H_{20}Cl_2]^+$, accurate mass $C_{22}H_{40}ClN_4Ni$: calcd. 453.2295; found 453.2295. UV/Vis: 9.302×10^{-6} M (toluene) λ_{max}/nm (ε/dm^3 mol^{-1} cm^{-1}, shoulder): 307 (7524, 490). Melting point: 288°C (the sample decomposed at 300°C).

2.7.5 [IPrMe]CuCl (II·34)

THF (30 mL) was added to $CuCl_2 \cdot THF_{0.8}$ (206 mg, 1.07 mmol) at room temperature to give an orange slurry. IPrMe (196 mg, 1.09 mmol), dissolved in THF (10 mL) was added dropwise. The reaction became beige/green over the course of the addition and the reaction cleared as

$CuCl_2$ dissolved. The reaction was stirred for 16 hrs before all volatiles were removed *in vacuo* to give a pale yellow solid. This was extracted into toluene (2 × 10 mL) to give a golden solution from which all volatiles were removed *in vacuo*. Crystals suitable for X-ray diffraction experiments were grown by vapour diffusion of pentane into C_6D_6. ^{1}H NMR (C_6D_6, 400 MHz, 300K) δ_H/ppm; 1.33 (d, 12H, J_{HH} = 6.8 Hz, CH_3 of *i*Pr flanking group) 1.39 (s, 6H, CH_3 of backbone) 3.86 (sept, 2H, J_{HH} = 6.8 Hz, CH of *i*Pr flanking group).

2.7.6 [IPrMe]$_2$ZnCl$_2$ (II·35)

THF (20 mL) was added to a mixture of $ZnCl_2$ (19 mg, 0.139 mmol) and IPrMe (50 mg, 0.277 mmol) at room temperature. The colourless solution was stirred for 16 hrs, during which time the solution became cloudy, before the solvent was removed *in vacuo* to give a white solid. 28.6 mg, 42%. Crystals of suitable for X-ray diffraction investigations were grown by pentane diffusion into a saturated C_6D_6 solution of $[IPrMe]_2ZnCl_2$ at room temperature. ^{1}H NMR (C_6D_6, 400 MHz, 300K) δ_H/ppm; 1.27 (d, 24H, J_{HH} = 7.1 Hz, CH_3 of *i*Pr flanking group), 1.65 (s, 12H, backbone CH_3), 6.00 (sept, 4H, J_{HH} = 7.0 Hz, CH of *i*Pr flanking group). ^{13}C{^{1}H} NMR (C_6D_6, 100 MHz, 300K) δ_C/ppm; 10.10 (backbone CH_3), 22.25 (CH_3 of *i*Pr flanking group), 52.40 (CH of *i*Pr flanking group), 67.84 (C_q bound to Zn), 125.56 (olefinic C_q).

2.7.7 [2,6-Dipp$_2$C$_6$H$_3$MBr]$_2$·[LiBr(OEt$_2$)]$_2$ [M = Mn (II·36), Co (II·37)]

$[2,6\text{-}Dipp_2C_6H_3Li]_2$ (400 mg, 0.494 mmol) and MBr_2 (1.20 mmol) were separately dissolved in Et_2O (2 × 20 mL). Both solutions were cooled to 0°C and the solution of $[2,6\text{-}Dipp_2C_6H_3Li]_2$ was then added dropwise to the suspension of MBr_2. The reaction was stirred at 0°C for 1 hr and then allowed to warm to room temperature. Stirring was continued for 16 hrs after which time all volatiles were removed *in vacuo*. This solid was dried *in vacuo* for a further 1 hr before it was extracted in into *iso*-hexane (4 × 10 mL). Reduction of the volume of this solution by

half followed by storage of the solution at −30°C afforded large crystals suitable for X-ray diffraction studies.

[2,6-$Dipp_2C_6H_3MnBr]_2$·[$LiBr(OEt_2)]_2$ (**II·36**) was obtained as pale pink crystals of suitable quality for X-ray diffraction investigations. (31%, 214 mg). ^{1}H NMR (C_6D_6, 400 MHz, 298 K) δ_H/ppm; 0.41 (*s*), 0.97 (*s*), 1.25 (*s*), 3.01 (*s*), 7.27 (*s*), 7.47 (*s*). μ_{eff} = 3.5 μ_B. UV/Vis: 2.86 × 10^{-3} M (toluene) λ_{max}/nm (ε/dm^3 mol^{-1} cm^{-1}) 345 (137).

[2,6-$Dipp_2C_6H_3CoBr]_2$·[$LiBr(OEt_2)]_2$ (**II·37**) was obtained as dark green crystals of suitable quality for X-ray diffraction investigations. (16%, 110 mg). ^{1}H NMR (C_6D_6, 400 MHz, 298 K) δ_H/ppm; -43.93 (*s*, $\Delta\nu$½ = 209 Hz), -38.49 (*s*, $\Delta\nu$½ = 144 Hz), -26.31 (*s*), -25.68 (*s*), -20.47 (*s*), -20.24 (*s*), -11.57 (*s*), -8.80 (*s*), 0.11 (*s*), 0.86 (*s*), 1.13 (*s*), 2.11 (*s*), 3.82 (*s*), 4.46 (*s*), 6.02 (*s*), 6.54 (*s*), 7.58 (*s*, $\Delta\nu$½ = 207 Hz, 10.53 (*s*), 16.03 (*s*), 18.83 (*s*), 26.42 (*s*, $\Delta\nu$½ = 274 Hz, 28.63 (*s*), 32.23 (*s*), 32.87 (*s*, $\Delta\nu$½ = 723 Hz, 40.15 (*s*), 48.34 (*s*). μ_{eff} = 5.2 μ_B. Elemental analysis [2,6-$Dipp_2C_6H_3CoBr]_2$·[$LiBr(OEt_2)]_2$: calcd C 58.55, H 6.79; found C 58.50, H 6.71. UV/Vis: 8.03 × 10^{-4} M (toluene) λ_{max}/nm (ε/dm^3 mol^{-1} cm^{-1}) 816 (367), 645 (203), 600 (147) (br); 3.30 × 10^{-4} M (toluene) λ_{max}/nm (ε/dm^3 mol^{-1} cm^{-1}) 362 (1197) shoulder.

2.7.8 [2,6-$Mes_2C_6H_3MBr]_2$·[$LiBr(OEt_2)]_2$ [M = Mn (II·38), Fe (II·39), Co (II·40)]

[2,6-$Mes_2C_6H_3Li]_2$ (400 mg, 0.624 mmol) and MBr_2 (1.87 mmol) were separately dissolved in Et_2O (2 × 20 mL). Both solutions were cooled to 0°C and the solution of [2,6-$Mes_2C_6H_3Li]_2$ was then added dropwise to the suspension of MBr_2. The reaction was stirred at 0°C for 1 hr and then allowed to warm to room temperature. Stirring was continued for 16 hrs after which time all volatiles were removed *in vacuo*. This solid was dried *in vacuo* at room temperature for a further 1 hr.

[2,6-$Mes_2C_6H_3MnBr]_2$·[$LiBr(OEt_2)]_2$ (**II·38**) was extracted into cyclohexane (2 × 10 mL) to give a pale pink solution. All volatiles were removed *in vacuo* to give [2,6-

$Mes_2C_6H_3MnBr]_2{\cdot}[LiBr(OEt_2)]_2$ as a pale pink powder. (33%, 253 mg). ^{1}H NMR (C_6D_6, 400 MHz, 300K) δ_H / ppm; 0.30 (s), 2.08 (s), 2.22 (s), 6.77 (s) 6.88 (s), 7.01 (s), 11.64 (s), 16.22 (s). μ_{eff} = 3.7 μ_B. UV/Vis: 7.1 × 10^{-4} M (toluene) λ_{max}/nm (ε/dm^3 mol^{-1} cm^{-1}) 332 (139). TOF MS ASAP (positive ion mode) *m/z*; 441.1 (5%), 345.2 (13%), 331.2 (60%), 316.2 (100%), 300.2 (60%), 271.1 (17%), 239.1 (13%).

$[2,6\text{-}Mes_2C_6H_3FeBr]_2{\cdot}[LiBr(OEt_2)]_2$ (**II·39**) was extracted into cyclohexane (2 × 10 mL) to give a pale yellow solution. Reduction of the volume of this solution by half followed by storage at 7°C afforded yellow crystals of suitable quality for X-xay diffraction investigations. (21%, 158 mg). ^{1}H NMR (C_6D_6, 400 MHz, 300K) δ_H / ppm; −23.14 (*s*), −15.04 (*b*), −10.16 (*s*), −4.40 (*s*), −0.52 (*s*), 0.54 (*b*), 1.50 (*s*), 2.58 (*s*), 3.27 (*s*), 3.39 (*s*), 8.06 (*s*) 8.34 (*b*). μ_{eff} = 5.1 μ_B. Elemental analysis: $C_{56}H_{70}Br_4Fe_2Li_2O_2$ Calc. C 55.12, H 5.83; found C 55.23, H 5.83. UV/Vis: Sample began to decompose in the UV/Vis cell, 2.29 × 10^{-4} M (toluene) λ_{max}/nm (ε/dm^3 mol^{-1} cm^{-1}) broad absorbance from 640-430 nm, 505 (1772). TOF MS ASAP *m/z*; 671.4 (3%), 627.4 (5%), 347.2 (8%), 331.2 (55%), 315.2 (100%), 263.2 (25%).

$[2,6\text{-}Mes_2C_6H_3CoBr]_2{\cdot}[LiBr(OEt_2)]_2$ (**II·40**) was extracted into *iso*-hexane (2 × 10 mL) to give a blue green solution. The solvent was removed *in vacuo* to give $[2,6\text{-}Mes_2C_6H_3CoBr]_2{\cdot}[LiBrOEt]_2$ as a blue powder. (56%, 429 mg). Alternatively, the solid was extracted into cyclohexane (1 × 5 mL) and stored at 7°C to blue-green crystals of suitable quality for X-ray diffraction investigations (18%, 139 mg). ^{1}H NMR (C_6D_6, 400 MHz, 300K) δ_H / ppm −11.62 (s), −10.66 (s), −3.59 (s), 0.30 (s), 2.09 (s), 2.21 (s), 4.82 (b), 6.88 (s), 7.16 (s), 22.68 (s). μ_{eff} = 3.6 μ_B. Elemental analysis $C_{56}H_{70}Co_2Br_4Li_2O_2$: calcd. C 54.84, H 5.74; found C 55.69, H 5.68. UV/Vis: 3.42 × 10^{-4} M (toluene) λ_{max}/nm (ε/dm^3 mol^{-1} cm^{-1}) 805 (531), 640 (340), 602 (311), 364 (1246) (shoulder).

2.7.9 [2,6-$Mes_2C_6H_3ZnCl]_2$ (II·41)

A solution of $[Mes_2C_6H_3Li]_2$ (400 mg, 1.248 mmol) in Et_2O (20 mL) was added dropwise to a suspension of $ZnCl_2$ (340 mg, 2.49 mmol) in Et_2O (30 mL) cooled to −78°C. The reaction was allowed to warm to room temperature for 16 hrs before all volatiles were removed *in vacuo* to give a white solid. This was extracted into *iso*-hexane (3 × 10 mL) to give a colourless solution from which all volatiles were removed *in vacuo* to give a white powder. Crystals of the product suitable for X-ray diffraction studies could not be obtained. 340 mg, 66%. According to ^{1}H NMR spectrometry, roughly 5% of the sample was $[2,6\text{-}Mes_2C_6H_3]_2Zn$[77]. ^{1}H NMR ($C_6D_6$, 100 MHz, 300K) δ_H / ppm; 0.70 (*t*, *J* = 7.1 Hz, 6H, CH_3 of Et_2O), 2.10 (*s*, 48H, *o*-CH_3), 2.22 (*s*, 24H, *p*-CH_3), 2.92 (*q*, *J* = 7.2 Hz, 4H, CH_2 of Et_2O), 6.85 (*s*, 16H, *m*-$C_{Ar}H$ of mes), 7.01 (*d*, *J* = 7.6 Hz, 8H, *m*-$C_{Ar}H$ of central phenyl ring), 7.22 (*t*, *J* = 7.6, 4H, *p*-$C_{Ar}H$ of central phenyl ring). $^{13}C\{^1H\}$ NMR; (C_6D_6, 100 MHz, 300K) δ_C / ppm 14.3 (CH_3 of Et_2O), 21.1 (*o*-CH_3), 21.3 (*p*-CH_3), 66.2 (CH_2 of Et_2O), 126.0 (*m*-$C_{Ar}H$ of central phenyl ring), 128.8 (*m*-$C_{Ar}H$ of Mes), 128.9 (*p*-$C_{Ar}H$ of central phenyl ring), 136.0 (*o*-C_{Ar} of Mes), 136.2 (*p*-C_{Ar} of mes), 143.3 (*i*-C_{Ar} of Mes), 149.9 (*o*-C_{Ar} of central phenyl ring), 152.6 (*i*-C_{Ar} of central phenyl ring). $^7Li\{^1H\}$ NMR (C_6D_6, 155 MHz, 298 K): δ_{Li} / ppm; −5.11, −4.72, −4.01 (broad).

2.7.10 [2,6-$Mes_2C_6H_3CdCl]_3LiCl(Et_2O)$ (II·42)

A solution of $[Mes_2C_6H_3Li]_2$ (200 mg, 0.624 mmol) in Et_2O (10 mL) was added dropwise over 5 mins to a suspension of $CdCl_2$ (229 mg, 1.25 mmol) in Et_2O (20 mL) cooled to −78°C. The reaction was allowed to warm to room temperature for 16 hrs before all volatiles were removed *in vacuo* to afford a white solid. This was extracted into *iso*-hexane (3 × 10 mL) to give a colourless solution, the volume of which was reduced by *ca.* half, stored at room temperature for 16 hrs and at 7°C for a further 48 hrs to afford white crystals of two distinct shapes, both of suitable quality for X-ray diffraction investigations. Further investigation showed to product to

be a mixture of $[Mes_2C_6H_3]_2Cd$ and $[2,6\text{-}Mes_2C_6H_3CdCl]_3LiCl(Et_2O)$ in roughly a 1:1 molar ratio. Yield = 59 mg, . ^{1}H NMR (C_6D_6, 100 MHz, 300 K) δ_H / ppm (* indicates a peak that can be attributed to $[Mes_2C_6H_3]_2Cd$); 0.95 (*t*, *J* = 7.0 Hz, 6H, CH_3 of Et_2O), 1.81* (*s*, 23H, o-CH_3), 2.15 (*s*, 36H, o-CH_3), 2.20* (*s*, overlapping, p-CH_3), 2.21 (*s* (*br*), overlapping, p-CH_3), 6.85* (*s*, 8H, *m*-H of mes), 6.88 (*s*, 12 H, *m*-H of mes), 6.92* (*d*, *J* = 7.50 Hz, 4H, *m*-CH of C_6H_3), 7.05 (*d*, *J* = 7.5 Hz, 6H, *m*-CH of C_6H_3), 7.17* (*t*, *J* = 7.35 Hz, 2H, *p*-CH of C_6H_3), 7.28 (*t*, *J* = 7.4 Hz, 3H, *p*-CH of C_6H_3). $^{13}C\{^1H\}$ NMR (C_6D_6, 100 MHz, 298 K) δ_C / ppm 14.7 (CH_3 of Et_2O) , 20.9* (*p*-CH_3), 21.0* (o-CH_3), 21.2 (*p*-CH_3), 21.3 (o-CH_3), 65.5 (CH_2 of Et_2O), 125.0* (m-CH of central aryl), 128.5* ($C_{Ar}H$ of flanking group), 135.5* (*quaternary*-C_{Ar} of flanking group), 135.8* (o-C_{Ar} of central aryl), 144.0*(*quaternary*-C_{Ar} of Mes), 149.4* (*ipso*-C of flanking group), 162.6* (*ipso*-C of C_6H_3).

2.7.11 $[2,6\text{-}Mes_2C_6H_3]HgBr$ (II·43)

$[2,6\text{-}Mes_2C_6H_3Li]_2$ (200 mg, 0.624 mmol) and $HgBr_2$ (448 mg, 1.24 mmol) were dissolved separately in toluene/THF (10/2 mL). The solution of $HgBr_2$ was then cooled to -78°C before the solution of $[2,6\text{-}Mes_2C_6H_3Li]_2$ was added dropwise over 5 mins. The reaction was allowed to warm slowly to room temperature for 16 hrs before all volatiles were removed *in vacuo* to give a white solid. This was extracted with warm *iso*-hexane (3 × 10 mL). Storage of this solution at room temperature for 4 hrs followed by storage at 7°C for 16 hrs afforded colourless crystals of suitable quality for X-ray diffraction investigations. (170 mg, 47%). ^{1}H NMR (C_6D_6, 100 MHz, 300K) δ_H / ppm; 1.99 (*s*, 12H, *o*-Me) 2.11 (*s*, 6H, *p*-Me), 6.80 (*s*, 4H, *m*-H_{Ar} on flanking group), 7.01 (*d*, 2H, *m*-H_{Ar} on central phenyl) , 7.12 (*t*, 1H, *p*-H_{Ar} on central phenyl). $^{13}C\{^1H\}$ NMR (C_6D_6, 400 MHz, 300K) δ_C / ppm; 20.9 (*o*-Me), 21.2 (*p*-Me), 127.90 (*m*-$C_{Ar}H$ of central phenyl), 129.1 (*m*-$C_{Ar}H$ of flanking group), 129.8 (*p*-$C_{Ar}H$ of central phenyl), 135.6 (*o*-C_{Ar} of flanking group), 137.8 (*p*-C_{Ar} of flanking group), 141.1 (*i*-C_{Ar} of flanking group),

147.2 (*o*-C_{Ar} of central phenyl), 162.0 (*i*-C_{Ar} of central phenyl). $^{199}Hg\{^{1}H\}$ NMR (C_6D_6, 71.7 MHz, 300K) δ_{Hg} / ppm; −1186. Elemental analysis $C_{24}H_{25}HgBr$: calcd. C 48.53, H 4.24; found C48.48, H 4.00. EI-MS *m/z* (accurate mass); calcd. 594.08404, found 594.08338. EI-MS (positive ion mode) *m/z*; 594.1 $[M]^+$ (10%), 313.2 $[2,6\text{-}Mes_2C_6H_3]^+$ (100%). 141.1

2.7.12 [2,6-Tmp$_2$C$_6$H$_3$]HgBr (II·44)

$[2,6\text{-}Tmp_2C_6H_3Li]_2$ (400 mg, 1.25 mmol) and $HgBr_2$ (896 mg, 2.45 mmol) were dissolved separately in a mixture of toluene (10 mL) and THF (2 mL). The solution of $HgBr_2$ was then cooled to −78°C before the solution of $[2,6\text{-}Tmp_2C_6H_3Li]_2$ was added dropwise. The reaction was allowed to warm slowly to room temperature over 16 hrs before all volatiles were removed *in vacuo* to give an off-white solid. This was extracted with warm *iso*-hexane (2 × 10 mL). Storage of this solution at room temperature for 1 hr followed by storage at 7°C for 16 hrs and at −30°C for 24 hrs afforded colourless crystals of suitable quality for X-ray diffraction investigations. 477 mg, 64%. ^{1}H NMR (C_6D_6, 100 MHz, 300K) δ_H / ppm; 2.00 (s, 6H, *p*-CH_3), 2.05 (*d*, *J* = 10 Hz, 6H, *m*-CH_3), 2.12 (*d*, *J* = 22 Hz, ,*o*-CH_3), 6.88 (*s*, 2H, *m*-$C_{Ar}H$ of mes), 7.06 (*s*, 2H, *o*-$C_{Ar}H$ of mes), 7.14 (*t*, *J* = 7.7 Hz, partially obscured, 1H, *p*-$C_{Ar}H$ of central phenyl ring), 7.31 (*m*, 2H, *m*-$C_{Ar}H$ of central phenyl ring). $^{13}C\{^{1}H\}$ NMR (C_6D_6, 100 MHz, 300K) δ_C / ppm; $^{13}C\{^{1}H\}$ NMR (C_6D_6, 100 MHz, 298 K): δ_C / ppm = 19.1 (*p*-CH_3), 19.3 (*m*-CH_3), 19.9 (*m*-CH_3), 128.9 (*p*-$C_{Ar}H$ of central phenyl ring), 129.3 (*m*-$C_{Ar}H$ of central phenyl ring), 131.1 (*q*-C_{Ar}), 131.2 (*o*-$C_{Ar}H$ of mes), 132.5 (*q*-C_{Ar}), 132.6 (*m*-$C_{Ar}H$ of mes), 134.8 (*q*-C_{Ar}), 142.6 (*q*-C_{Ar}), 147.4 (*q*-C_{Ar}), 184.0 (*ipso*-C_{Ar} of central phenyl ring). $^{199}Hg\{^{1}H\}$ NMR (C_6D_6, 71.7 MHz, 298 K) δ_{Hg} / ppm; = −1157, −1153. Elemental analysis: $[2,6\text{-}Tmp_2C_6H_3]HgBr$ calcd. C 48.53, H 4.24 found. C 48.47, H 4.10.

Chapter III

Heteroleptic *m*-Terphenyl Complexes

3.1 Introduction

3.1.1 Heteroleptic, Aryl Complexes

Few examples of heteroleptic, two-coordinate, transition metal complexes have been reported and even fewer of these feature at least one aryl ligand.[242]

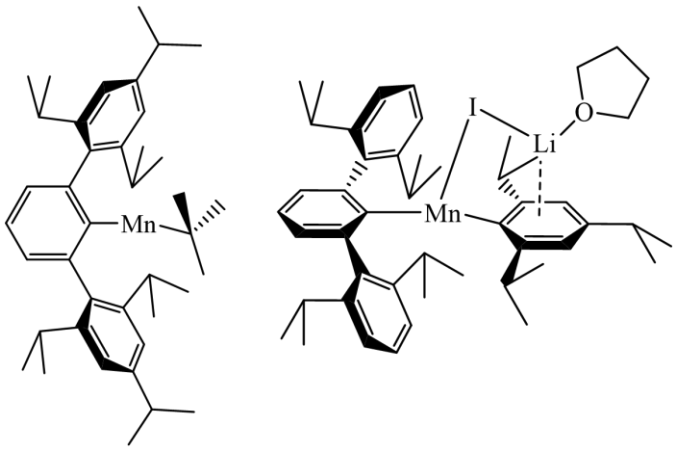

III·2 **III·3**

Figure 3·1. [2,6-Tripp$_2$C$_6$H$_3$]Mn*t*Bu (**III·2**) and [2,6-Dipp$_2$C$_6$H$_3$]Mn[Tripp][LiI(THF)] (**III·3**).

In 2010, a study by Power *et al.* detailed the reactivity of [2,6-Ar$_2$C$_6$H$_3$Mn(μ-I)]$_2$[LiI(OEt$_2$)]$_2$ [Ar = 2,4,6-*i*Pr$_3$C$_6$H$_3$ (Tripp, **III·1**) or Dipp (**II·26**)] with a wide range of organolithium species and Grignard reagents.[42] The authors reported one heteroleptic, two coordinate complex, [2,6-

Tripp$_2$C$_6$H$_3$]Mn*t*Bu (**III·2**, **Figure 3·1**), in which β-elimination of the *t*Bu$^-$ ligand was prevented by the steric bulk of the [2,6-Tripp$_2$C$_6$H$_3$]$^-$ ligand.

The same authors also an attempted to synthesise a heteroleptic diaryl complex through the reaction of **II·26** with two equivalents of [Tripp]MgBr(THF)$_2$. The reaction afforded [2,6-Dipp$_2$C$_6$H$_3$]Mn[Tripp][LiI(THF)] (**III·3**, **Figure 3·1**). Complex **III·3** features two different aryl ligands and one equivalent of LiI, which originates in the starting material, coordinated by a molecule of THF. The lithium forms an η^6-interaction with the aromatic system of the [Tripp]$^-$ ligand and the iodide ion is coordinated to the manganese ion. This demonstrated the steric issues relating to this synthesis with the bulk of the ligand system not able to prevent coordination of the lithium iodide moiety to the metal. **III·3** has a magnetic moment of 5.88 μ_B, consistent with a high spin, d^5 complex.

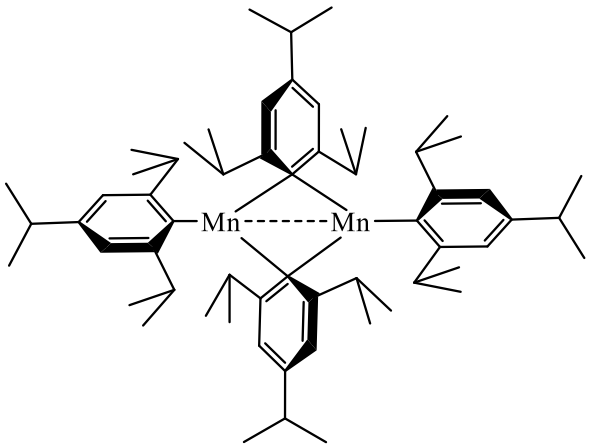

Figure 3·2. [Tripp]$_4$Mn$_2$ (**III·4**).

When **III·3** was reacted with a further equivalent of [Tripp]MgBr(THF)$_2$, the dimeric product [Tripp]$_4$Mn$_2$ (**III·4**, **Figure 3.2**) was isolated. The authors state that they were expecting the elimination of the iodide to afford [(2,6-Dipp$_2$C$_6$H$_3$)Mn(Tripp)$_2$]$^-$ with the charge balanced by the lithium ion. **III·4** forms through the elimination of the [2,6-Dipp$_2$C$_6$H$_3$]$^-$ ligand and the LiI(THF) moiety. The mechanism behind this exchange of aryl ligands was not obvious but it is a demonstration of the elimination of one aryl ligand by another.

The same group earlier reported a series of heteroleptic, quasi two-coordinate, transition metal complexes supported by an amido ligand and an *m*-terphenyl ligand.[242] These were the first examples of heteroleptic, two-coordinate transition metal complexes bearing an aryl ligand with the metal being in the +II oxidation state. They were synthesised through the reaction of [2,6-$Mes_2C_6H_3NH$]Li with [2,6-$Dipp_2C_6H_3M(\mu\text{-}X)]_2[LiX(OEt_2)]_2$, [M = Mn, X = I (**II·26**), M = Fe, X = Br (**III·5**), M = Co, X = Cl (**III·6**)] and take the form [2,6-$Mes_2C_6H_3NH$]M[2,6-$Dipp_2C_6H_3$] [M = Mn (**III·7**), Fe (**III·8**), Co(**III·9**), **Figure 3·3**].

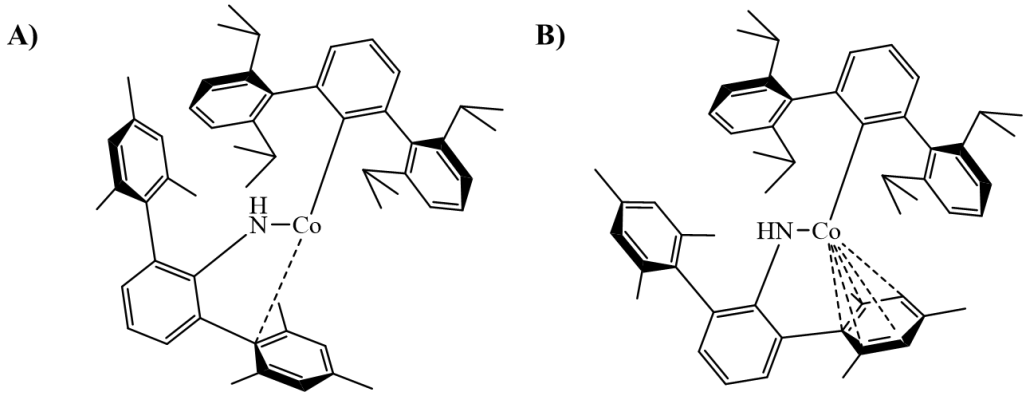

Figure 3·3. The solid-state structures of **III·9** at 240 K (A) and 90 K (B). The structure of **III·9** at 240 K (A) is similar to those of **III·7** and **III·9** at all temperatures.

The authors highlight the importance of the Grignard analogues, ArMX, as starting materials. Upon undergoing a metathesis reaction with a Grignard or organolithium reagent these complexes afford a two-coordinate product, acting as enabling materials for this study. The complexes are described as "quasi two-coordinate" due to the formation of weak, secondary M···C_{Ar} interactions in the structures. These are η^1-interactions (**III·7**, **III·8**, and **III·9** at 240 K, **Figure 3·3**) or η^6-interactions (**III·9** at 90 K, **Figure 3·3**) between the metal centre and a flanking group of the amido ligand.

A temperature change precipitates a structural change in **III·9**. The weak M···C interaction shifts to a strong Co···η^6-interaction as the temperature drops from 240 K to 90 K. This correlates with a spin crossover phenomenon in the complex around 229 K, a temperature identified through magnetic studies. Below this temperature the cobalt centre is in the high spin

state and this changes to a low spin state above this temperature prompting the change in coordination number. Amongst the other two complexes the magnetic moments, at 5.78(15) μ_B (**III·6**) and 5.36(15) μ_B (**III·7**) indicate high spin metal centres. The slight depression of the magnetic moment relative to the spin only value (5.92 μ_B) in **III·6** is attributed to a small amount of diamagnetic impurity in the species. The increased magnetic moment in **III·7** relative to the spin only value (4.90 μ_B) indicates an orbital contribution to the magnetic moment.

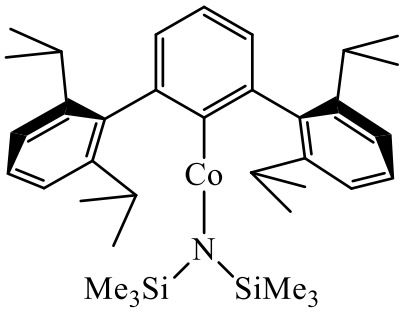

Figure 3·4. [2,6-Dipp$_2$C$_6$H$_3$]Co[N(SiMe)$_2$] (**III·10**).

Further examples of similar complexes are limited to [2,6-Tripp$_2$C$_6$H$_3$]Mn[*t*Bu] (**III·2**, **Figure 3·2**)[42] and [2,6-Dipp$_2$C$_6$H$_3$]Co[N(SiMe)$_2$] (**III·10**, **Figure 3·4**).[63] **III·3** is the only reported example of a heteroleptic, transition metal, aryl complex bound by two carbon containing ligands. Both **III·2** and **III·10** approach linearity along the L–M–L axis [169.68(9)°, **III·2** and 179.02(11)°, **III·10**].

In **III·10**, this linearity along the C–Co–N axis is credited with the complex possessing a larger magnetic moment than would be expected for a cobalt(II) complex. At 5.65 μ_B, it is significantly higher than the spin only value of 3.87 μ_B for a high spin, d^7, linear metal. This magnetic moment was determined by SQUID magnetometry and the authors note a 0.17 μ_B discrepancy between this value and the value determined by an initial investigation using the Evans' method. Detailed magnetic susceptibility measurements demonstrated that there is a strong orbital contribution to the magnetic moment arising from spin-orbit mixing of the

magnetic states. The authors attribute this effect to the linearity of the L–M–L axis and suggest that a systematic study of the magnetic behaviour of linearly coordinated complexes is required. **III·3** does not show any evidence of an orbital contribution to the magnetic moment. The magnetic moment determined for this complex is 5.73 μ_B which is similar to the spin only value of 5.92 μ_B.

3.1.2 Halogenated *m*-Terphenyl Ligands

The work herein describes a study on the use of the ligand $[2,6\text{-}Dcp_2C_6H_3]^-$ to stabilise heteroleptic and homoleptic, *m*-terphenyl, transition metal complexes. In this work it was found that some transition metals can activate the $Cl–C_{Ar}$ bond leading to the formation of coupled products. It is well documented that activation of an aryl chloride is hard to achieve relative to the aryl bromide and iodide analogues often used in coupling reactions.[243–247]

Several studies exist that feature complexes stabilised by halogenated *m*-terphenyl ligands. For example, Siegel *et al*. investigated the intramolecular interactions in the compound $[2,6\text{-}Ar_2C_6H_3]SiMe_2[B(C_6F_5)_4]$ [Ar = Dcp (**III·11**) or difluorophenyl (Dfp, **III·12**)].[248] They found that the ligand readily formed X···Si interactions with energies comparable to the interaction between silylium ion interactions and π-basic systems. The Cl···Si interactions were shown by NMR studies to be slightly weaker than the F···Si interactions. These measurements were made comparatively using ^{29}Si NMR investigations.

A later study directly compared these interactions within one complex through the development of silylium ions bearing asymmetric *m*-terphenyl ligands of the type $[2\text{-}Ar\text{-}6\text{-}DfpC_6H_3]SiMe_2][B(C_6F_5)_4]$ where Ar = Pmp, 2,6-Xyl, Mes and duryl.[70] The authors demonstrates that the interactions are finely balanced, with electron-rich aryl systems such as Pmp out-competing the F···Si interactions. Similar, Cl···Al, interactions were observed by Wehmschulte *et al*. in the solid-state structure of $[2,6\text{-}Dcp_2C_6H_3]AlEt_2$, **III·13**, **Figure 3·5**.[249]

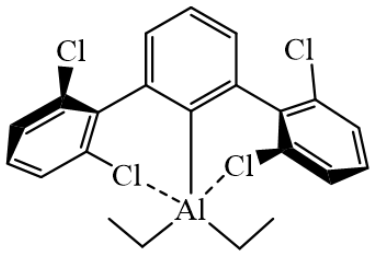

Figure 3·5. The solid-state structure of [2,6-$Dcp_2C_6H_3$]$AlEt_2$ (**III·13**).

Studies of transition metal complexes featuring halogens on the central aryl ring of the *m*-terphenyl ligands have demonstrated the effect of altering the electronics of the ligand on metal-metal bonding.[172]

Applications of the [2,6-$Dcp_2C_6H_3$]$^-$ ligand and its derivatives in transition metal complexes are limited to two studies by Figueroa *et al.*, who reported the effect that altering the electronic nature of terphenyl isocyanides, *via* substitution of the central and flanking aryl groups with halogens, had on the σ-donor/π-acid ratio of the isocyanides. This effect was studied in [ArCN]$Cr[CO]_5$ complexes and measured with ^{13}C NMR and IR spectroscopic methods.[250] The authors demonstrated the electron withdrawing substituents on the flanking groups in *m*-terphenyl groups such as [2,6-$Dcp_2C_6H_3$]$^-$ do not have a substantial impact on the σ-donor/π-acid ratio of the isocyanide. They surmise that the influence of the electron poor flanking groups is blocked by the central aryl ring. Contrastingly, introducing electron donating substituents to the flanking groups does change the ratio.

The 2,6-$Dcp_2C_6H_3CN$ ligand was developed in an earlier study by the same group. This study focused on methods of reducing the strength of intramolecular, η^6-interactions between the flanking groups of *m*-terphenyl isocyanides and the metal in zero-valent molybdenum complexes.[251] The authors found that the intramolecular η^6-interactions in complexes with 2,6-$Dcp_2C_6H_3CN$ are weaker and η^6-interactions with solvent molecules are favoured, compared with alkyl substituted analogues. This allowed isolation of [2,6-$Dcp_2C_6H_3CN$]$_3Mo[\eta^6$-Ar] [Ar = naphthyl (**III·14**), benzene (**III·15**, **Figure 3·6**), fluorobenzene (**III·16**)].

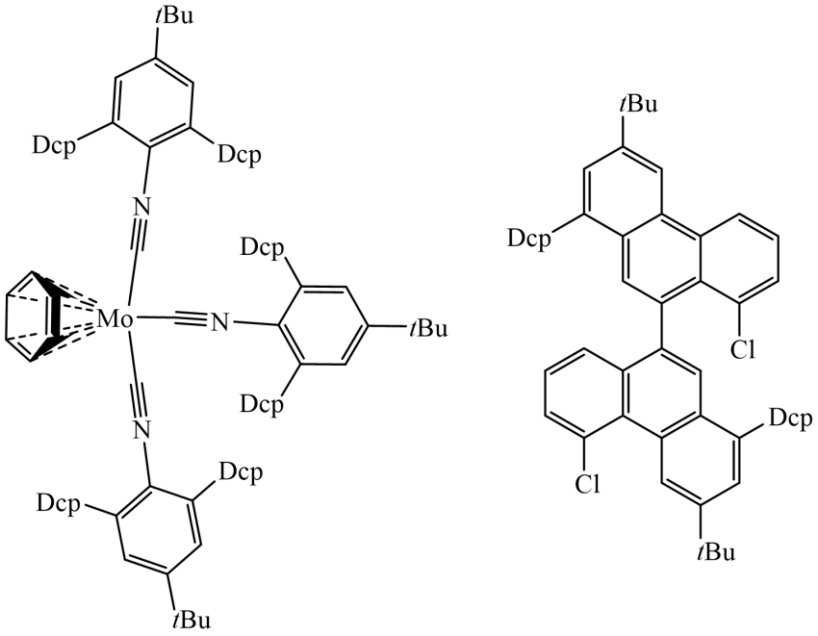

Figure 3·6. The solid-state structure of $[2,6\text{-}Dcp_2C_6H_3CN]_3Mo[\eta^6\text{-}C_6D_6]$ (**III·15**) and the coupled product 2,2′-di-tert-butyl-10,10′-dichloro-4,4′-bis(Dcp)-6,6′-biphenanthridine (**III·17**).

Removal of these aromatic solvents through trituration encourages η^6 interactions to form between the molybdenum centre and the ligand in 80% of the product. However, the remaining 20% decomposes into 2,2′-di-tert-butyl-10,10′-dichloro-4,4′-bis(Dcp)-6,6′-biphenanthridine (10%, **III·17**, **Figure 3·6**) and $[2,6\text{-}Dcp_2C_6H_3CN]_4MoCl_2$ (10%, **III·18**). Compound **III·17** is formed through the homo-coupling of two of the ligands and two instances of coupling of the ligand to itself. This affords two phenanthridine cores coupled to one another. The coupling of two ligands was also observed in this work when $[2,6\text{-}Dcp_2C_6H_3Li]_2$ was reacted with iron(II) chloride or cobalt(II) bromide.

Although aryl chlorides are more difficult to activate, their affordability as starting materials means there is a drive to develop catalysts that activate these materials under benign conditions.[246] Nickel and platinum catalysts have been developed to fulfil this role but the efficacy of simple manganese, iron and cobalt salts has also been heavily investigated.[252–255]

Iron and cobalt halides were shown to mediate cross-coupling reactions in the synthesis of Grignard reagents in 1941 by Kharasch and Fields.[256] These results were overshadowed by the

successes of Group 10 cross-coupling catalysts but, in recent years, iron mediated cross-coupling has come to the fore. Proponents highlight the sustainability, affordability, and diminished toxicity of iron based catalysts.[247,252,257,258] Simple iron salts have been demonstrated to act as effective, homogeneous catalysts for the cross-coupling of a wide range of aryl halides and Grignard or organolithium reagents.[252,259,260] Cobalt(II) halides have also found application as cross coupling catalysts that have demonstrated a high degree of chemoselectivity.[260] Comprehensive reviews of iron and cobalt mediated homo- and cross-coupling reactions have recently been published by Knölker and Bauer, and Cahiez and Moyeux respectively.[254,261] The catalytic activity of manganese salts in cross-coupling reactions is more limited and has begun to be investigated only relatively recently.[255,262,263]

Mechanistic studies of manganese, iron and cobalt mediated catalytic cycles have been stymied, relative to their Group 10 counterparts, by their complexity and the highly reactive, open-shell nature of the transient metal species.[257,264,265] Several mechanisms have been proposed that fall into distinct categories. Some of the mechanisms proposed involve radical species,[244,257,266,267] oxidative addition,[268–270] or organoferrate clusters with iron(−II) centres.[265,271]

Tonzetich *et al.* conducted an extensive study into the ability of $[(IPr)FeCl_2]_2$ to couple primary and secondary alkyl halides with aryl and alkyl Grignards.[244] They propose a catalytic cycle involving the abstraction of a halide from an aryl halide to form a radical species (**Scheme 3·1**). This mechanism is favoured over a concerted oxidative addition mechanism as aryl halides were found to be poor nucleophiles and avoided high iron oxidation states. Further investigations into the coupling of PhMgCl and 1-bromo-5-hexene, known to cyclise if a radical is formed in the 1-position, were used to support this proposal. The authors do not suggest that the catalytic cycle they propose is generic to all iron(II) halide mediated cross-coupling reactions.

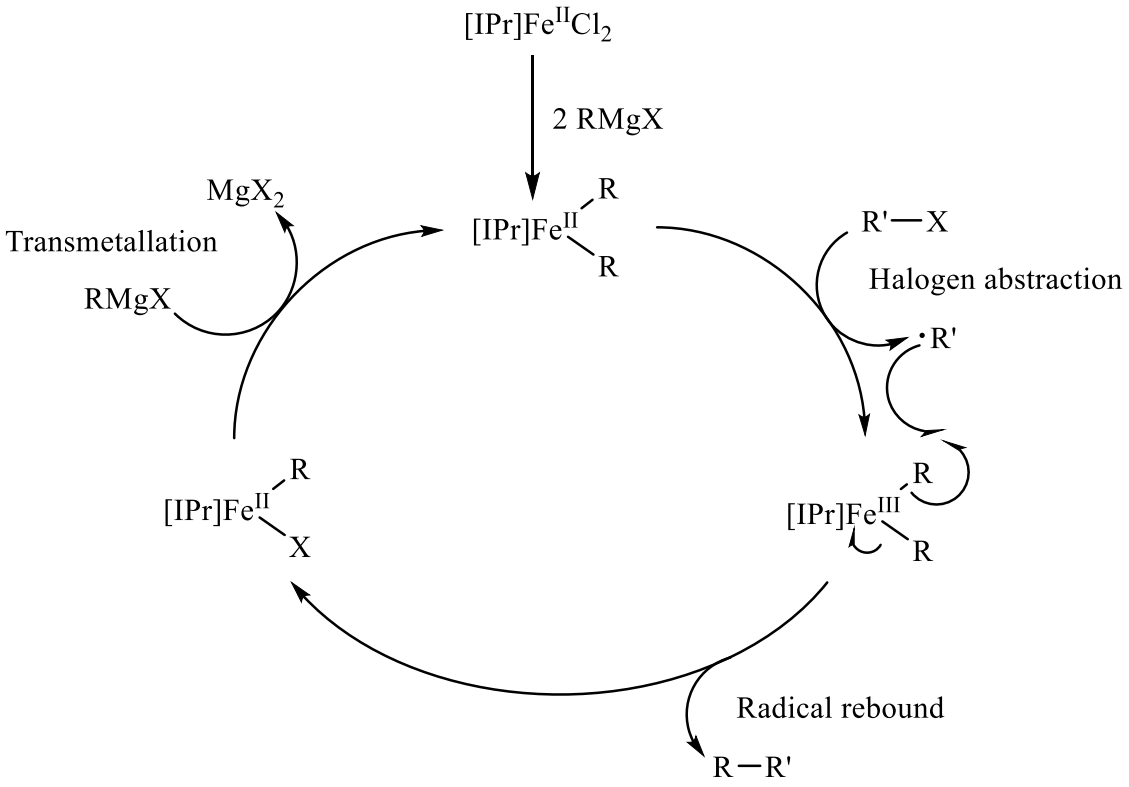

Scheme 3·1. The radical mechanism proposed by Tonzetich *et al.* for the coupling of primary and secondary alkyl halides with aryl and alkyl Grignards.[244]

When supporting ligands are not involved, species that contain low-valent iron centres in bimetallic clusters are thought to be key active species.[259] Fürstner *et al*. identified $[(Me_4Fe)(MeLi)][Li(OEt_2)]_2$ (**III·19**) as a product of the reaction between an excess of MeLi and iron(III) chloride. The iron ion is reduced to iron(II) and, along with the three lithium atoms, forms a tetrahedral metal framework. A similar reaction between four equivalents of PhLi and iron(II) chloride affords $[Ph_4Fe][Li(Et_2O)_2][Li(1,4\text{-dioxane})]$ (**III·20**). The authors note that **III·20** is effective at promoting cross-coupling between PhMgBr and cyclohexyl bromide and, upon heating, **III·20** decomposes into biphenyl. These examples illustrate the variety of possible reaction pathways proposed for iron promoted cross-coupling reactions.

3.2 Aims

The aim of the work described herein is to develop a heteroleptic complexes, featuring two different *m*-terphenyl ligands that can be used to stabilise two-coordinate, transition metal complexes. The intention was to investigate the application of the complexes developed in small molecule catalysis and reactivity and compare them with similar, homoleptic complexes that have already been developed.

The chosen methodology is to develop a synthesis of heteroleptic Group 12 complexes using the starting materials synthesised in Chapter I. The diamagnetic nature of the Group 12 metals allows the characterisation of the synthesised complexes with NMR spectroscopy. How different ligands interact with one another can therefore be investigated and the problems encountered with the synthesis can be analysed *in situ*. Once a suitable synthetic route is developed, the Group 12 metals can be substituted for the targeted first-row transition metals.

The first-row transition metals first selected to be investigated in the second stage of this methodology are manganese, iron and cobalt. These metals have been shown to form stable, homoleptic *m*-terphenyl complexes and so were considered suitable for this study.[76]

When applying this methodology to metals other than mercury it became apparent that they *m*-terphenyl ligands readily exchanged over the course of the synthesis. A statistical mixture of the two possible homoleptic products formed in the reaction mixture. The potential routes along which this ligand stage occurred were investigated and a ligand combination that partially overcame this problem is discussed.

3.3 Results and Discussion

3.3.1 Mercury Complexes

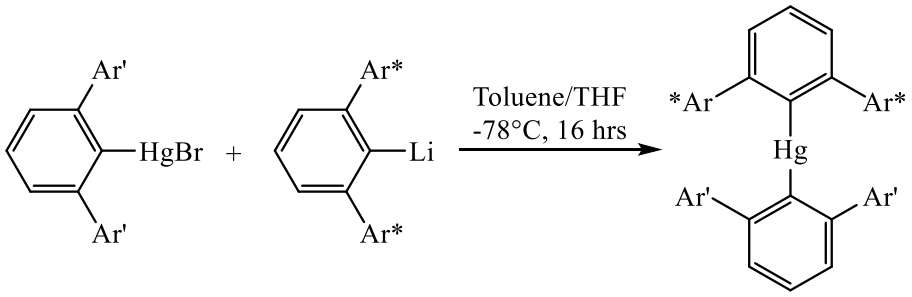

Scheme 3·2. The general synthesis of **III·21**–**III·24**. Ar' = Mes (**III·24**) or Tmp (**III·21**–**III·23**), Ar* = Pmp (**III·21**, **III·24**), 2,6-Xyl (**III·22**) and Dcp (**III·23**).

Through the reaction of either [2,6-$Mes_2C_6H_3$]HgBr (**II·43**) or [2,6-$Tmp_2C_6H_3$]HgBr [Tmp = $(2,4,5\text{-}Me_3C_6H_3)^-$, **II·44**] with one equivalent of an *m*-terphenyl metal salt, four heteroleptic mercury diaryls were synthesised and characterised (**Scheme 3·2**). These complexes are [2,6-$Tmp_2C_6H_3$]Hg[2,6-$Ar_2C_6H_3$] [Ar = Pmp (Pmp = $\{Me_5C_6\}^-$), **III·21**, 2,6-Xyl (2,6-Xyl = $\{2,6\text{-}Me_2C_6H_3\}^-$, **III·22**) and Dcp (Dcp = $\{C_6Cl_2H_3\}^-$) (**III·23**), **Figure 3·7**] and [2,6-$Mes_2C_6H_3$]Hg[2,6-$Pmp_2C_6H_3$] (**III·24**, **Figure 3·7**).

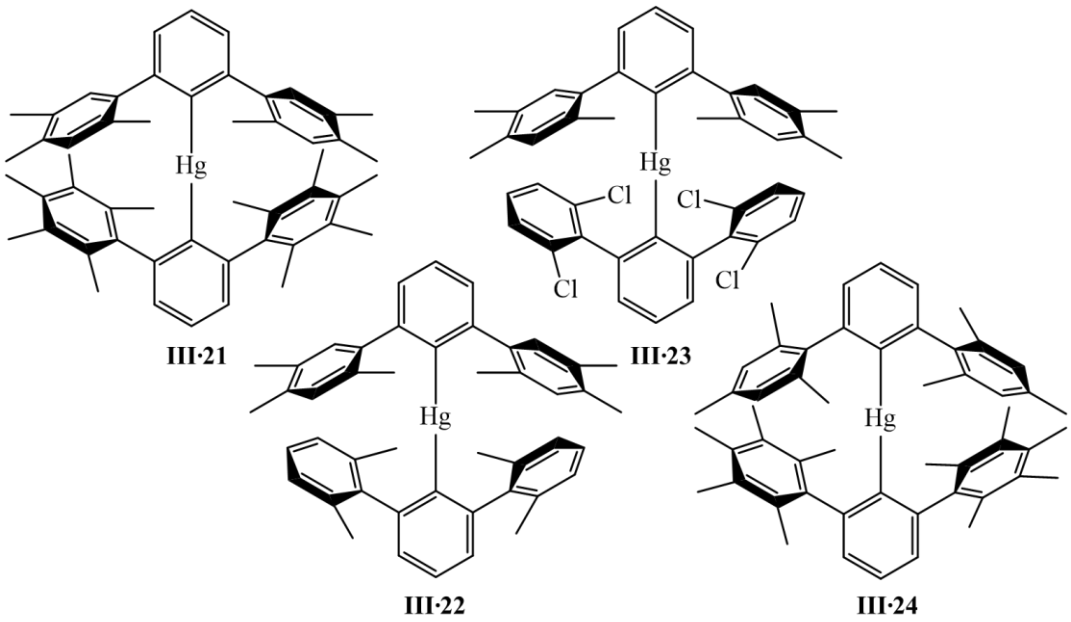

Figure 3·7. [2,6-$Tmp_2C_6H_3$]Hg[2,6-$Pmp_2C_6H_3$] (**III·21**), [2,6-$Tmp_2C_6H_3$]Hg[2,6-(2,6-Xyl)$_2C_6H_3$] (**III·22**), [2,6-$Tmp_2C_6H_3$]Hg[2,6-$Dcp_2C_6H_3$] (**III·23**), [2,6-$Mes_2C_6H_3$]Hg[2,6-$Pmp_2C_6H_3$] (**III·24**).

The complexes were isolated as crystalline products in varying yields. Only a single crystal of **III·23** was isolated, allowing characterisation by X-ray diffraction only. In contrast, **III·21** was isolated in a yield of 46%, **III·22** in a yield of 30%, and **III·24** in a yield of 17%. Complexes **III·21** and **III·24** were characterised using NMR spectroscopy, elemental analysis, X-ray diffraction, and ASAP-TOF mass spectrometry. **III·22** was characterised similarly however the parent ion was not visible in the EI-MS spectrum recorded.

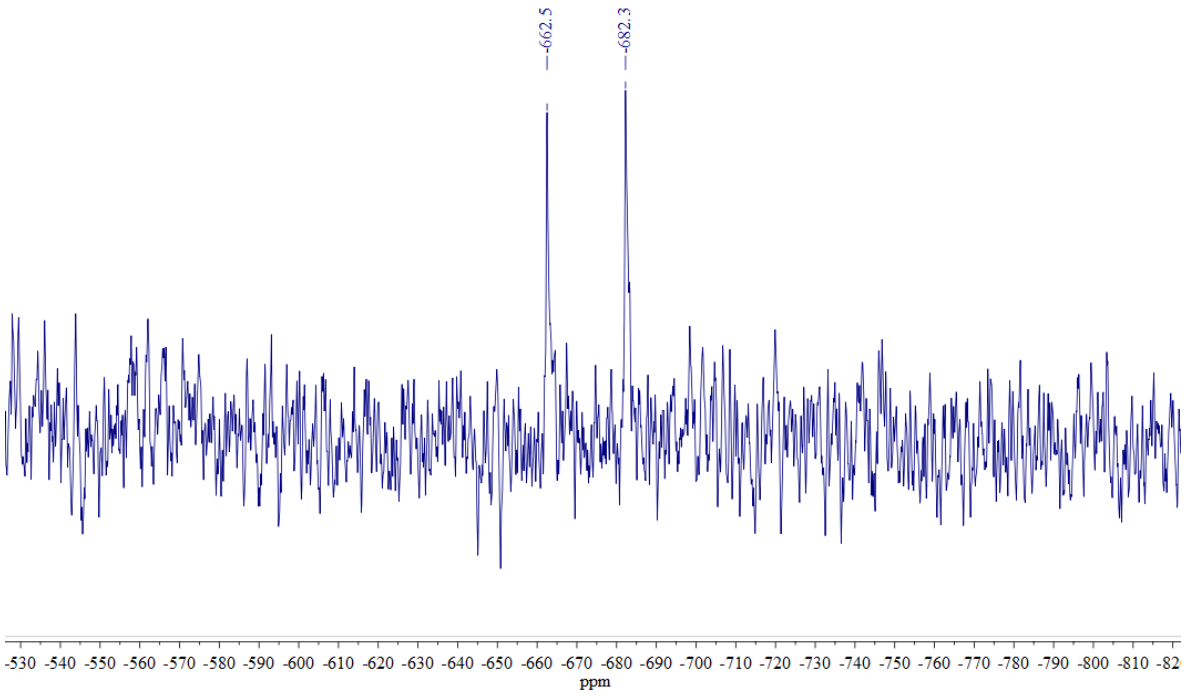

Figure 3·8. $^{199}Hg\{^{1}H\}$ NMR Spectrum of **III·22**.

The $^{199}Hg\{^{1}H\}$ NMR Spectra of **III·21**, **III·22** (**Figure 3·8**) and **III·24** contain signals in the region of −700 ppm, consistent with similar complexes in the literature.[188,189,272] Two signals are evident in the spectra of **III·21** and **III·22**. Elemental analysis and ASAP-TOF MS of **III·21** showed that the sample was pure. As with [2,6-$Tmp_2C_6H_3$]HgBr (**II·44**), the multiple signals in the $^{199}Hg\{^{1}H\}$ NMR spectrum can be attributed to the two possible conformations of the Tmp flanking groups (**Figure 3·9**).[189] Elemental analysis of **III·22** showed that the purity of the sample was not within generally accepted standards (calculated; C 69.11, H 5.80: found; C

70.68, H 5.67). Despite this, the most likely cause of two signals in the $^{199}Hg\{^{1}H\}$ NMR spectrum is conformational isomerism.

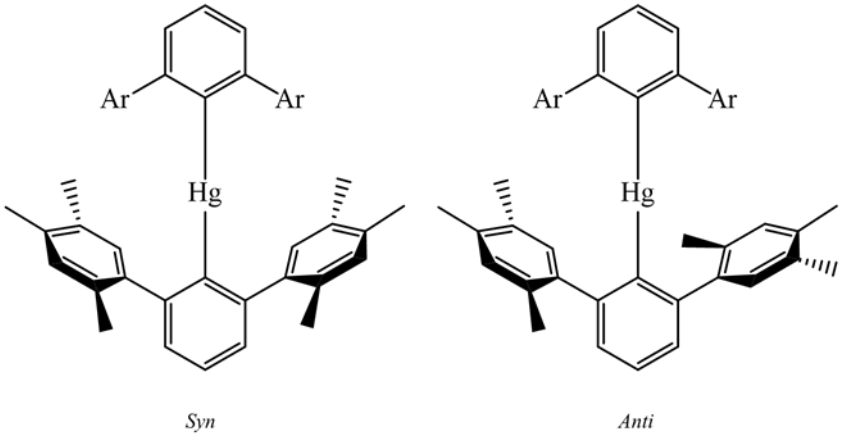

Figure 3·9. The two possible conformations of the $[2,6\text{-}Tmp_2C_6H_5]^-$ ligand in complexes **III·21**–**III·23**.

Conformational isomerism is also evident in the ^{1}H NMR spectra of these complexes. The spectra of **III·21** and **III·22** contain broad signals, assigned to the *ortho*- and *meta*-methyl groups of the $[2,6\text{-}Tmp_2C_6H_5]^-$ ligand. Unexpectedly, splitting of the signals assigned to the methyl groups of the Pmp and 2,6-Xyl flanking groups is also observed.

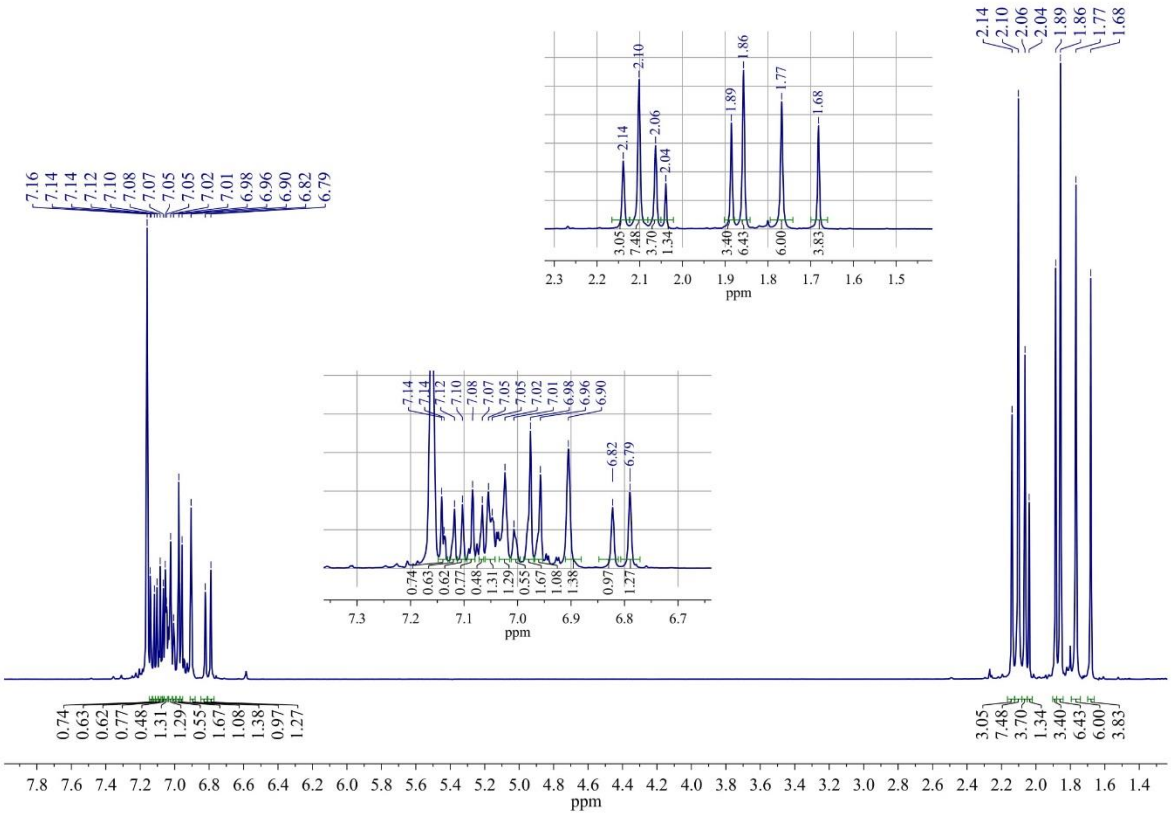

Figure 3·10. ^{1}H NMR spectrum of $[2,6\text{-}Tmp_2C_6H_3]Hg[2,6\text{-}(2,6\text{-}Xyl)_2C_6H_3]$ (**III·22**).

In the ^{1}H NMR spectrum for **III·22** (**Figure 3·10**) there are three distinct signals representing the methyl groups of the [(2,6-Xyl)$_2$C$_6$H$_3$]$^-$ ligand (1.68, 1.77 and 1.89 ppm). 2D NMR spectroscopic investigations show that one (1.77 ppm) represents two methyl groups on one flanking group. The other two signals (1.68 and 1.89 ppm), each of which integrates to three protons, represent the methyl groups on the second flanking group. This effect is not observed in [2,6-(2,6-Xyl)$_2$C$_6$H$_3$]$_2$Hg or other homoleptic mercury *m*-terphenyl complexes.[188] The effect is presumably a result of an interaction between the asymmetric flanking groups of [2,6-Tmp$_2$C$_6$H$_3$]$^-$ and of [2,6-(2,6-Xyl)$_2$C$_6$H$_3$]$^-$ creating differing electronic environments around the methyl groups of the latter ligand (**Figure 3·11**).

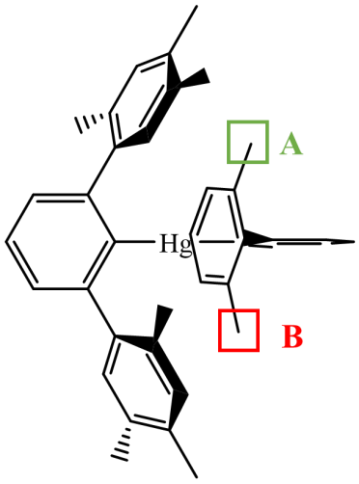

Figure 3·11. Showing the different steric environments (A and B) around the methyl groups of the 2,6-Xyl flanking group in **III·22**.

A similar effect is not observed for the aromatic protons of the flanking groups and no through space coupling constant could be determined for the split peaks which, at 1.68 and 1.89 ppm, are unlikely to be a doublet representing a single proton environment.[273] A NOESY NMR spectroscopy experiment could not resolve any through space interactions in the complex and so whether the splitting of the methyl peaks was a result of a through space or transmitted *via* the bonds was not clear. It should be noted that the [2,6-Tmp$_2$C$_6$H$_3$]$^-$ ligand causes two signals to appear in the ^{199}Hg NMR spectrum through the adoption of two conformations. This effect

could be transmitted through the structure to the $[2,6\text{-}(2,6\text{-Xyl})_2C_6H_3]^-$, though why it would cause splitting of just the methyl groups in one flanking group and not the other is uncertain.

In contrast, the expected number of signals is observed in the $^{13}C\{^1H\}$ NMR spectrum of **III·22**. This would suggest that the interaction that causes the splitting of the signal from the methyl protons is a through space interaction. A through bond interaction would have a similar effect on the signals of the methyl carbons. It is possible that the effect causes an imperceptible broadening of the methyl signals in the $^{13}C\{^1H\}$ NMR spectrum, however, no evidence of this is observed.

The $^{13}C\{^1H\}$ NMR spectrum of **III·21** contains more signals than expected, particularly in the methyl region. The reason for this is not obvious. Further investigation with 2D NMR spectroscopy experiments is required.

The NMR spectra of **III·24** are as expected and show no evidence of inter-ligand interaction. Mass spectrometric analysis demonstrated the presence of the molecular ion. The strongest signals coming from the ligand fragments. Elemental analysis results consistent with a pure sample of the complex could not be obtained.

Table 3·1 contains key bond lengths and angles for **III·21**–**III·24**. Complexes **III·22** and **III·23** (**Figure 3·12**) crystallise in the *P*-1 space group. Complex **III·21** crystallises in the monoclinic space group *C*2/*c*. **III·24** crystallises in the tetragonal, polar space group, $Pca2_1$. As with many two-coordinate mercury complexes, the C−Hg−C moieties are close to linear in all four complexes.[225,226,274]

Table 3·1. Key bond lengths and angles for **III·21**–**III·24**.

	III·21		**III·22**		**III·23**		**III·24**	
C– Hg/Å	C1	2.072(3)	C1	2.085(3)	C1	2.077(4)	C1	2.078(6)
	C14	2.080(3)	C23	2.083(3)	C19	2.072(4)	C29	2.081(6)
C– Hg – C/°	C1, C14	180.0	C1, C23	177.42(13)	C1, C19	177.97(13)	C1, C29	176.7(2)
Hg – C– C/°	C1, C2	120.63(13)	C1, C2	119.7(3)	C1, C6	119.3(3)	C29, C30	121.5(5)
	C14, C15	119.84(14)	C23, C28	120.7(3)	C1, C2	122.0(3)	C29, C34	118.7(6)
			C24, C28	117.8(3)	C19, C20	118.5(3)	C1, C6	120.5(4)
			C1, C6	123.1(3)	C19, C24	122.2(3)	C1, C2	120.4(4)
Plane – Plane								
$Ar_{central}$– $Ar_{central}$ /°	C1, C14	66.646(75)	C1, C23	73.49 (11)	C1, C19	68.58 (13)	C1, C29	82.87(17)
$Ar_{\textit{flanking}}$ –$Ar_{central}$/°	C2, C5	76.11(25)	C28, C38	73.26(46)	C20, C25	71.80(47)	C35, C30	101.83(73)
	C15, C18	98.42(22)	C24, C29	81.32(46)	C24, C34	99.81(46)	C44, C34	96.87(78)
			C6, C15	79.93(50)	C2, C7	79.44(52)	C19, C6	95.21(75)
			C2, C7	87.53(47)	C6, C13	91.63(53)	C7, C2	89.56(77)
Our-of-plane								
Ar – Hg/Å	C1	0.0191(25)	C1	0.0862(62)	C1	0.0019(68)	C1	0.0235(90)
	C14	0.0009(29)	C23	0.1244(54)	C19	0.0538(58)	C29	0.3239(96)

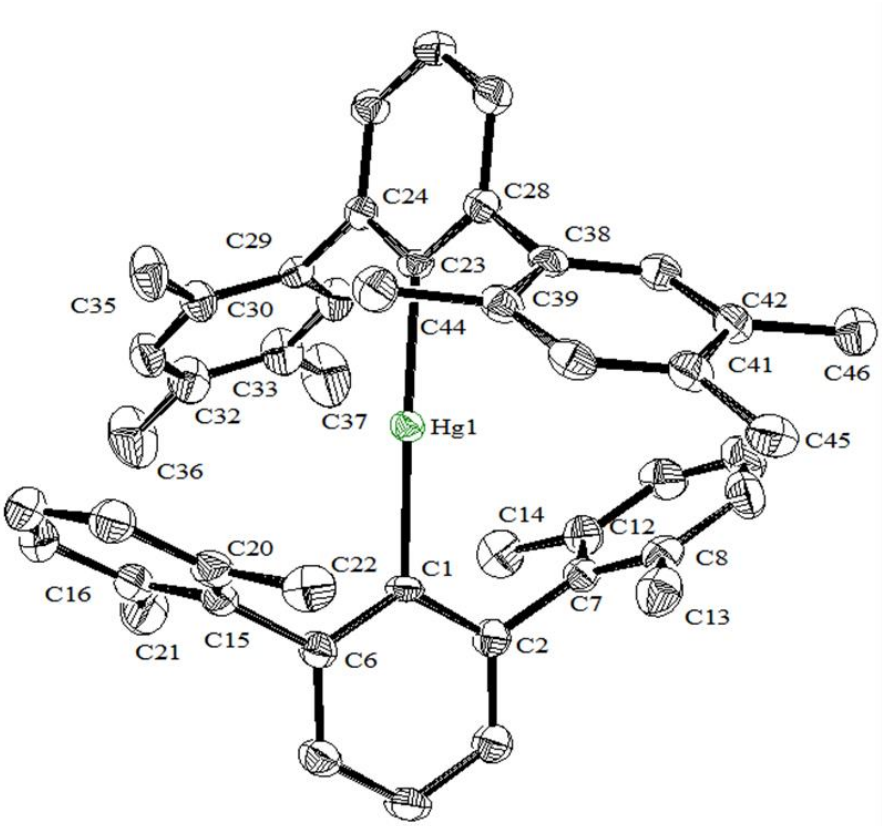

III·22

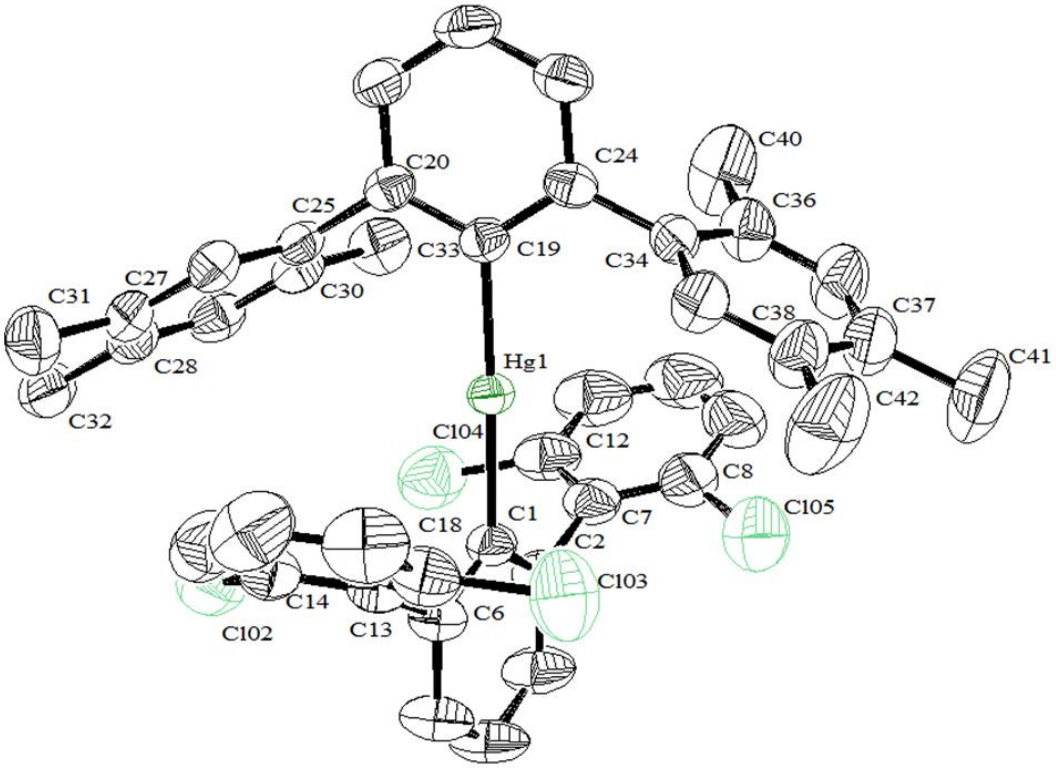

III·23

Figure 3·12. The solid-state structures of **III·22** and **III·23**. Hydrogens are omitted for clarity and ellipsoids are set at 50% probability. Significant atoms are labelled.

The Tmp flanking groups in complexes **III·22** and **III·23** (**Figure 3·12**) adopt a *syn* conformation as seen in **II·44**. In **III·22** this coincides with a tilting of the $[2,6\text{-}(2,6\text{-Xyl})_2C_6H_3]^-$ ligand away from the occupied *ortho*-positions of the opposing ligand. This can be measured through the distortion of the Hg−C_{ipso}−C_{ortho} angles away from 120° expected for an idealised sp^2 carbon. In **III·22** these angles are 117.8(3) (Hg−C24−C28) and 123.1(3)° (Hg−C1−C6).

Further distortion around the connectivity of the $[2,6\text{-}(2,6\text{-Xyl})_2C_6H_3]^-$ ligand with the mercury centre includes a tilting of the central aryl ring resulting in an out-of-plane distortion of the mercury centre by 0.1244(54) Å. There is a similar but smaller out-of-plane deviation of the mercury, with respect to the centre aryl plane of the $[2,6\text{-Tmp}_2C_6H_3]^-$ ligand [0.0862(62) Å]. These deviations are presumably enforced by the steric demands of the ligand system. Crystal packing forces may also have an influence.[203]

The torsion angle between the two ligands is 73.49(11)° and the flanking groups are slightly tilted from perpendicular. These angles, 73.26(46)° (C28, C38) and 81.32(46)° (C24, C29; $[2,6\text{-}(2,6\text{-Xyl})_2C_6H_3]^-$), and 79.93(50)° (C6, C15) and 87.53(47)° (C2, C7; $[2,6\text{-Tmp}_2C_6H_3]^-$), show that much of the steric strain in the ligand system is being accommodated by the flanking aryl groups and the flexibility of the ligand system, despite the steric bulk of the $[2,6\text{-}(2,6\text{-Xyl})_2C_6H_3]^-$ ligand. There was no evidence of a through space interaction to cause the splitting pattern observed in the ^{1}H NMR spectrum.

Complex **III·23** is similar, to **III·22** from a steric consideration; methyl and chloride moieties have similar van der Waals radii and the ligands $[2,6\text{-Dcp}_2C_6H_3]^-$ and $[2,6\text{-}(2,6\text{-Xyl})_2C_6H_3]^-$ therefore have similar steric profiles.[71] However, the electronics of the ligand system are different, with the inductive effects of the chlorides making the flanking groups of the $[2,6\text{-Dcp}_2C_6H_3]^-$ ligand electron-poor compared to the flanking groups of the $[2,6\text{-}(2,6\text{-Xyl})_2C_6H_3]^-$ ligand.[250,275] Differences between the two structures can therefore be attributed to electronic

effects. **III·22** and **III·23** adopt the same space group, with similar unit cell parameters, exhibit similar C_{ipso}–Hg distances [2.085(3) and 2.083(3) Å (**III·22**) and 2.077(4) and 2.072(4) Å (**III·23**)] and C–Hg–C angles [177.42(13)° (**III·22**) and 177.97(13)° (**III·23**)]. The distortion of the Hg−C−C angles [117.8(3)–123.1(3)° (**III·22**) and 118.5(3)–121.5(3)° (**III·23**)] differs slightly between the two complexes.

The major differences between the two complexes are that there is a smaller out-of-plane distortion of the mercury from the plane of both ligands in **III·23** than in **III·22** [0.0862(62) and 0.1244(54) Å (**III·22**) and 0.0019(68) and 0.0538(58) Å (**III·23**)], and the torsion angle between the two ligands in **III·23** is 68.58(13)°, *ca*. 5° wider than the equivalent angle in **III·22**.

The flanking groups deviate from a perpendicular orientation by similar amounts: 91.63(53)° (C6, C13) and 79.44(52)° (C19, C6; [2,6-$Dcp_2C_6H_3$]$^-$), and 71.80(47)° (C20, C25) and 99.81(46)° (C24, C34; [2,6-$Tmp_2C_6H_3$]$^-$). In **III·23** the [2,6-$Tmp_2C_6H_3$]$^-$ ligand shows the greatest distortion. This difference implies that the [2,6-$Dcp_2C_6H_3$]$^-$ is less flexible than [2,6-(2,6-$Xyl)_2C_6H_3$]$^-$ and imposes a geometry on the opposing [2,6-$Tmp_2C_6H_3$]$^-$ ligand. The reason behind this is unclear from the solid-state structures.

The Tmp flanking groups in **III·22** and **III·23** adopt a *syn*-conformation. In contrast, the flanking groups in [2,6-$Tmp_2C_6H_3$]Hg[2,6-$Pmp_2C_6H_3$] (**III·21**, **Figure 3·13**) adopt the *anti*-conformation. This is a function of the centre of rotation in the structure, as is the strictly linear geometry along the C–Hg–C axis. The interplanar torsion angle between the two ligands is similar at 66.646(75)° to that of **III·23**. The Tmp flanking groups in **III·21** are orientated such that the *ortho*-methyl group is further from the metal centre than the *meta*-methyl group and therefore out of contact with the Pmp flanking groups.

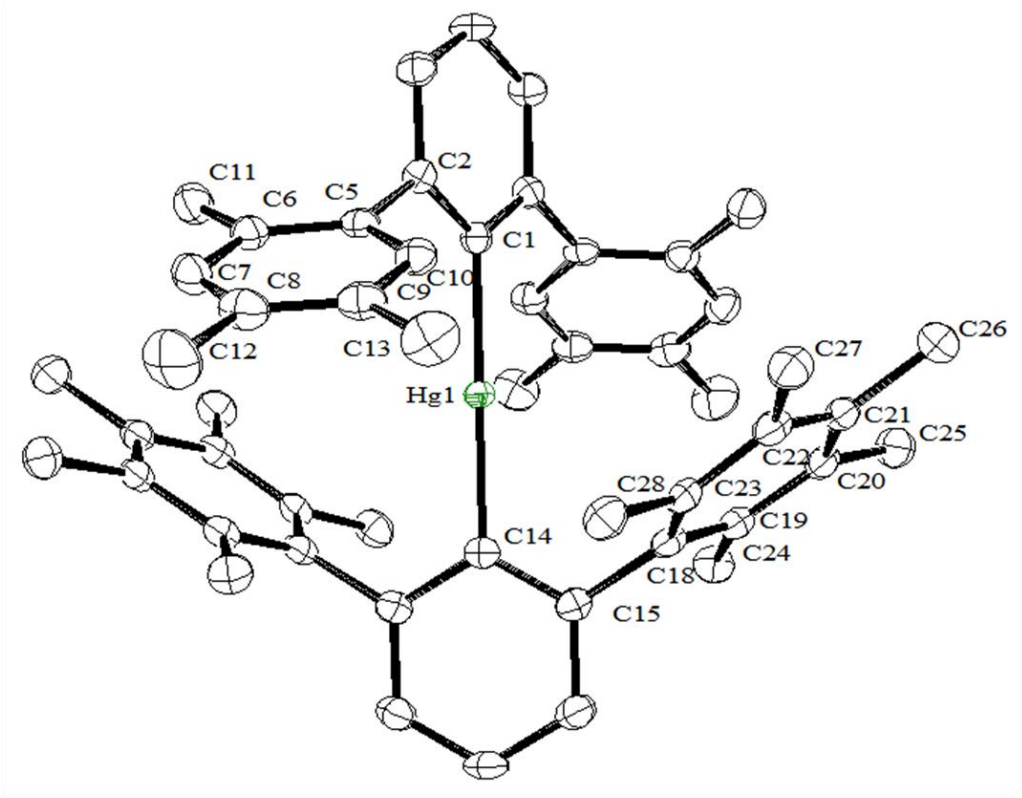

III·21

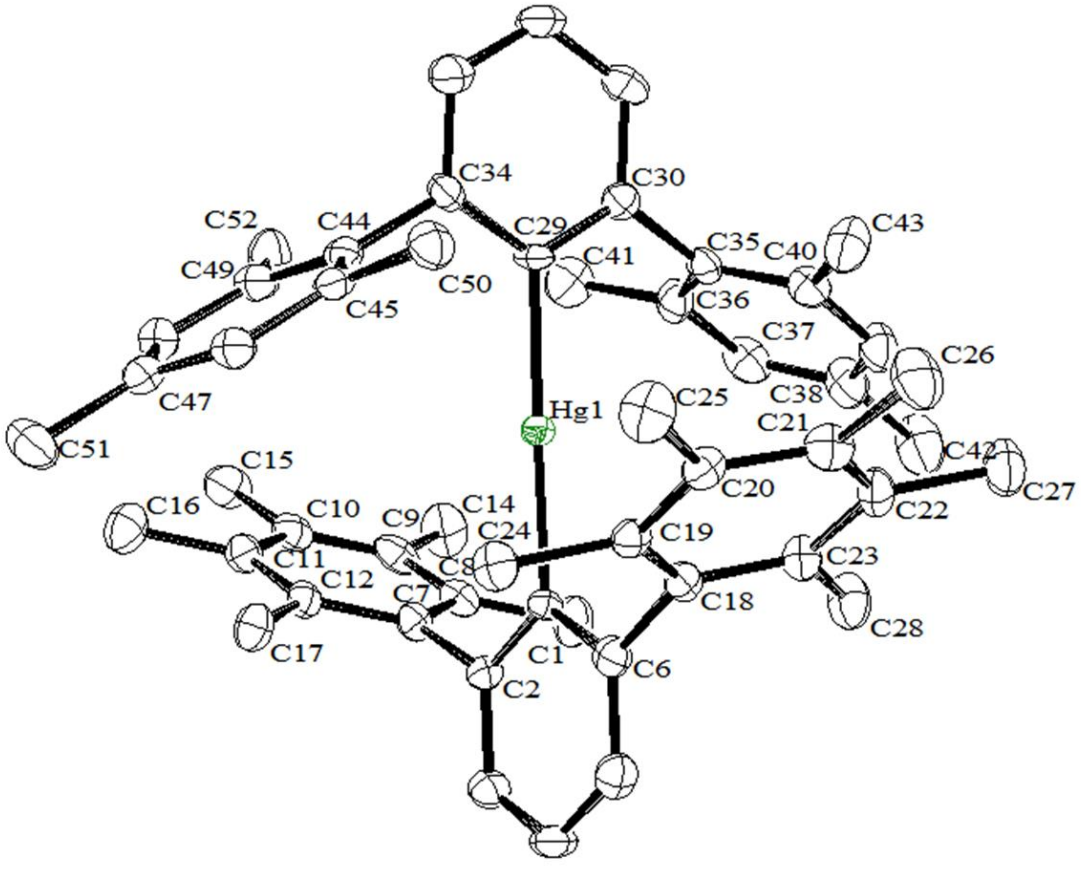

III·24

Figure 3·13. The solid-state structures of **III·21** and **III·24**. The full structure of **III·21**, the unit cell containing only half of the molecule. Hydrogens have been omitted for clarity and the ellipsoids are set at 50% probability.

The flanking groups tilt away from perpendicular to the central aryl ring by different amounts. The Tmp groups deviate the most with an angle of 76.11(25)° (C24, C29). The equivalent angle for the Pmp groups is 98.52(22)° (C15, C18). The greater distortion of the Tmp groups, when compared to the Pmp groups, is similar to the structure of **III·23** where the $[2,6\text{-}Tmp_2C_6H_3]^-$ ligand adjusts to accommodate the sterics of the system. In **III·21** this could be attributed to the greater and more evenly distributed steric bulk of the $[2,6\text{-}Pmp_2C_6H_3]^-$ ligand.

III·24 (**Figure 3·13**) is the only complex in this series that does not feature the $[2,6\text{-}Tmp_2C_6H_6]^-$ ligand. Attempts were made to synthesise $[2,6\text{-}Mes_2C_6H_6]Hg[2,6\text{-}(2,6\text{-}Xyl)_2C_6H_6]$ but it was not possible to isolate this complex. In comparison with **III·21**, the interplanar angle between the two ligands in **III·24** is less acute at 82.87(17)°. This is because the steric bulk of the methyl groups in the *ortho* position of the Mes flanking groups removes a degree of flexibility from the structure, an effect observed in previous work by Kays and coworkers.[188] The ligands therefore adopt a more perpendicular arrangement. An indicator of the increased steric strain in this structure is the deviation of the mercury centre from the plane of the $[2,6\text{-}Mes_2C_6H_6]^-$ ligand which, at 0.3239(96) Å, is larger than that in complexes **III·21–III·23**.

When compared with previously reported, homoleptic analogues, such as $[2,6\text{-}Ar_2C_6H_6]_2Hg$ [Ar = Tmp (**III·25**)[276], Dcp (**III·26**)[73], 2,6-Xyl (**III·27**), Pmp (**III·28**),[188] and Mes (**III·29**)[227]], the structures of **III·21**–**III·24** follow observable trends. For example, **III·25** and **III·27** are sterically dissimilar and the interplanar angles between the ligands are 86.62(18)° and 78.46(18)°, respectively. The steric bulk of the $[2,6\text{-}Mes_2C_6H_3]^-$ ligand can be compared with that of $[2,6\text{-}(2,6\text{-}Xyl)_2C_6H_6]^-$ and the interplanar angle in **III·24**, 82.87(17)°, falls between that in **III·25** and **III·27**. The comparison is imperfect but the necessary data to include **III·29** is not available.

The extreme deviation of the mercury centre from the plane of the central aryl ring in [2,6-$Mes_2C_6H_6$]$^-$ (**III·24**) or in [2,6-(2,6-Xyl)$_2C_6H_6$]$^-$ (**III·22**) is not observed in any of the homoleptic complexes.

A trend that does emerge is the general upfield shift of the signals in the $^{199}Hg\{^1H\}$ NMR spectra [−682.3 and −662.5 (**III·23**), −684.4 and −702.0 (**III·21**) −697.3 (**III·24**)] as the steric bulk of the ligand system increases. The same trend was observed by Kays *et al*. in a study of homoleptic complexes.[188] It is possible that this is due to the electronics of the ligand system with bulkier ligands that bear more methyl groups making the ligands more electron rich. More data points are required to fully establish this trend and determine the influences behind it.

3.3.2 Ligand Exchange

Attempts to expand the heteroleptic ligand systems developed for mercury to other metals, including first row, transition metals met with limited success. Initially, the halide bridged dimeric complexes, described in Chapter II and used as intermediates, were generated *in situ* and reacted with *m*-terphenyl lithium salts in a one pot reaction (**Scheme 3·3**). This approach afforded two complexes, [2,6-$Mes_2C_6H_6$]M[2,6-$Dcp_2C_6H_6$] [M = Mn (**III·30**) and Zn (**III·31**)].

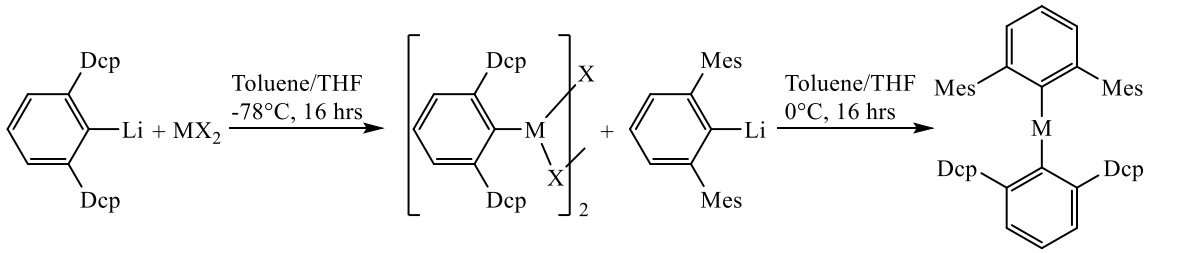

III·30 M = Mn, X = Br **III·31** M = Zn, X = Cl

Scheme 3·3. A one-pot scheme for the synthesis of heteroleptic, diaryl complexes [2,6-$Mes_2C_6H_6$]Mn[2,6-$Dcp_2C_6H_6$] (**III·30**) and [2,6-$Mes_2C_6H_6$]Zn[2,6-$Dcp_2C_6H_6$] (**III·31**).

Efforts to develop further heteroleptic complexes of manganese, iron, cobalt, zinc and cadmium using the ligand systems of complexes **III·21**–**III·24** or of the type [2,6-$Mes_2C_6H_3$]M[2,6-

$Dipp_2C_6H_3$]. Instead, the homoleptic analogues, featuring just one of the two ligands employed in the synthesis were repeatedly isolated from the reactions following **Scheme 3·3**.

To remove the possibility of a homoleptic contaminant being carried over from the generation of the halide bridged dimer, the complexes described in Chapter II and those developed by Power *et al*. and Kays *et al*. were isolated and purified for use in these reactions.[170,277] This did not alleviate the problem. Furthermore, homoleptic complexes bearing the second ligand added were isolated from the reaction mixture (Appendix I). Such complexes could not be generated in the synthesis of the halide bridged dimers. However, they could occur if the original metal salt contaminated the intermediate.

Occasionally, a crystal was isolated from the reaction mixture that X-ray diffraction studies revealed to be highly disordered. Such a crystal was isolated from the attempted synthesis of [2,6-$Mes_2C_6H_3$]Fe[2,6-$Dipp_2C_6H_3$]. In the X-ray diffraction data set obtained, the complex was disordered such that each ligand position was occupied by a mixture of either [2,6-$Mes_2C_6H_3$]$^-$ or [2,6-$Dipp_2C_6H_3$]$^-$ to such an extent that it was not possible to elucidate whether the crystal contained a roughly 50:50 mixture of the possible homoleptic complexes, purely the disordered heteroleptic complex, or a mixture of all three.

A similar phenomenon was observed by Trautwein *et al*. where conformational isomers co-crystallised. This resulted in the certain parts of the structure being unsolvable.[185]

This issue was not observed with **III·30** or **III·31**, complexes that bear the [2,6-$Dcp_2C_6H_3$]$^-$ ligand. The [2,6-$Dcp_2C_6H_3$]$^-$ ligand is electronically different to purely carbon based *m*-terphenyl ligands. It is, perhaps, the electronic differences that encourage the complex to crystallise in a regular fashion allowing structural characterisation. Several attempts were made to expand this ligand system to iron, cobalt, and cadmium but these were unsuccessful for reasons that will be discussed below.

It is apparent that there are two issues with expanding the ligand systems developed for the mercury complexes **III·21**–**III·24** to other metals. The first is that the ligands exchange during the reaction, providing a mixture of three possible products. Such exchange between aryl, transition metal complexes has been reported in the literature. Tonzetich *et al*. observed an exchange of alkyl and aryl ligands in mixtures of [IPr]Fe[Bn]$_2$ and either [IPr]Fe[*p*-MeBn]$_2$ or [IPr]Fe[*o*-tolyl]$_2$ to afford a statistical mixture of products.[244] The same authors also observed a similar effect in mixtures of [IPr]Fe[*p*-MeBn]$_2$ and BnMgCl. The authors suggest a mechanism based on the formation of a bimetallic species bridged by the alkyl or aryl ligands. A similar intermediate would be unlikely for the complexes in this work given the bulk of the *m*-terphenyl ligand.

The second issue is that the desired products are disordered in the solid state, preventing determination of the structure. The other analytical techniques that are available cannot provide the structural information that is required to characterise the reaction products. The lack of methods available to determine whether a sample was pure or not limits the usefulness of these compounds.

3.3.3 Ligand Exchange Studies

A series of experiments was designed to investigate the exchange of ligands in the reaction process. Cadmium was chosen as the test metal. Earlier experiments had demonstrated that the ligands exchange during the synthesis of heteroleptic cadmium complexes. Cadmium is diamagnetic and the isotopes ^{111}Cd and ^{113}Cd are NMR active, allowing NMR spectroscopic studies. This allows the number of cadmium environments to be assessed and therefore the number of cadmium complexes present to be inferred. By this method ligand exchange could be monitored the isotope. ^{113}Cd NMR spectroscopy was used through this work. Odom *et al*. highlight the suitability of ^{113}Cd NMR spectroscopy for such studies.[278]

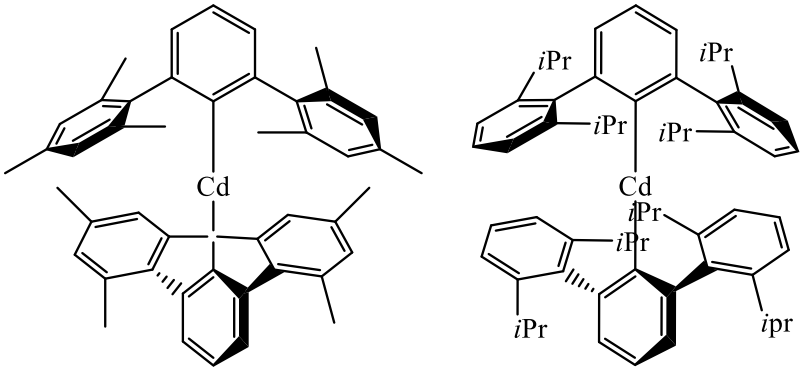

III·32 **III·33**

Figure 3·14. The Structures of [2,6-$Mes_2C_6H_3$]$_2$Cd (**III·32**) and [2,6-$Dipp_2C_6H_3$]$_2$Cd (**III·33**).

Before these experiments could be conducted it was necessary to characterise [2,6-$Mes_2C_6H_3$]$_2$Cd (**III·32**, **Figure 3·14**) and [2,6-$Dipp_2C_6H_3$]$_2$Cd (**III·33**, **Figure 3·14**). The other cadmium species used in these experiments was [2,6-$Pmp_2C_6H_3$]$_2$Cd (**III·34**), previously synthesised by Blundell *et al*.[188]

III·32 was synthesised according to standard literature procedures.[188] Crystals were obtained by slow cooling of a saturated hexane solution to −30°C for three days. **III·33** was synthesised on a smaller scale in an NMR tube. It was necessary to use [2,6-$Dipp_2C_6H_3Cd(\mu\text{-}I)]_2$, synthesised according to literature procedures,[169] as a starting material. and reacted with one equivalent of [2,6-$Dipp_2C_6H_3Li]_2$ in benzene-d_6 with a small amount of THF.[169] This is similar to the procedure for the synthesis of [2,6-$Dipp_2C_6H_3]_2$Mn.[42] NMR spectroscopic data was collected and crystals grown by the vapour diffusion of pentane into a saturated solution of the compound in benzene-d_6 before cooling of the solution to −30°C for 30 days. The solid-state structures of **III·32** and **III·33** are shown in **Figure 3·15**.

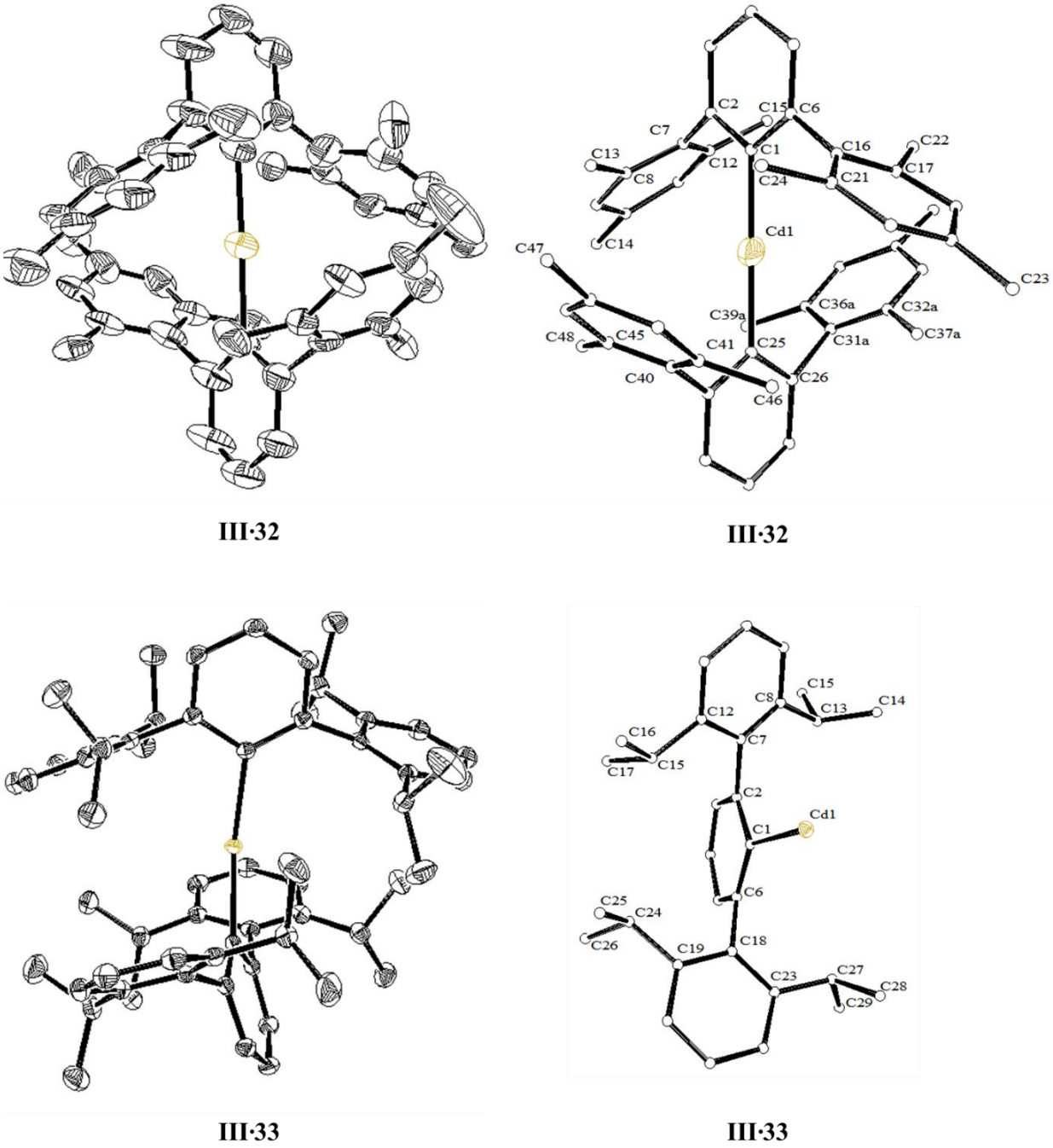

Figure 3·15. The solid-state structures of **III·32** and **III·33**. The full structure of each is shown on the left, Hydrogens are omitted for clarity and ellipsoids are set at 50% probability. The asymmetric units of **III·32** and **III·33** are shown on the right; Hydrogens are omitted for clarity, carbons are represented as spheres and significant atoms are labelled.

The $^{113}Cd\{^{1}H\}$ NMR spectra of **III·32** and **III·33** show peaks at 401 and 357 ppm respectively. These values are consistent with cadmium diaryl complexes in the literature.[188,189,278] The ^{1}H and $^{13}C\{^{1}H\}$ NMR spectra of **III·32** show the expected number of peaks, which were assigned using 2D experiments. The ^{1}H and $^{13}C\{^{1}H\}$ NMR spectra of **III·33** were more challenging to

assign due to the data being collected directly on the reaction mixture which contained THF and other solvents. In particular, the $^{13}C\{^{1}H\}$ NMR spectrum was dominated by THF signals. Attempts to scale up this reaction to obtain more data on **III·33** were unsuccessful.

X-ray diffraction studies on crystalline samples of **III·32** and **III·33** allowed structural elucidation. **III·33** crystallises in the monoclinic space group C2/*c* and half of the molecule is contained in the asymmetric unit. Key bond lengths and angles are recorded in **Table 3·2**.

Table 3·2. Key bond lengths and angles of **III·32** and **III·33**.

	III·32		**III·33**	
	Atom Label		Atom Label	
C–Cd1/Å	C1	2.093(10)	C1	2.1391(14)
	C25	2.106(10)		
C–Cd1–C/°	C1, C25	179.2(4)	C1, C1	169.17(8)
Cd1–C_{ipso}–C_{ortho}/°	C25, C26	121.3(9)	C1, C2	116.30(10)
	C25, C30	120.7(8)	C1, C6	125,46(10)
	C1, C2	120.4(8)		
	C1, C6	123.6(9)		
$C_{iPr}H$–C_{Ar}/°		n/a	C15, C12	76.89(17)
			C13, C8	111.61(17)
			C24, C19	107.07(16)
			C27, C23	109.06(19)
Plane–Plane/°	C1, C25	89.07(45)	C1, C1	73.29(7)
Plane–Plane/°	C25, C31a	88.6(30)	C6, C18	88.954(42)
	C25, C40a	95.8(28)	C2, C7	69.227(48)
	C1, C7a	87.0(21)		
	C1, C16a	84.9(26)		
	C25, C31	89.4(23)		
	C25, C40	90.3(28)		
	C1, C7	95.4(14)		
	C1, 16	90.9(23)		
Out-of-plane				
Ar–Cd1/Å	C25	0.102(17)	C1	0.6345(21)
	C1	0.030(21)		

The solid-state structure of **III·32** was disordered. Each of the four flanking groups is disordered over two positions. Competitive refinement demonstrated that each position was occupied between 40 and 60 %. The connectivity of the structure is as expected (**Figure 3·15**). What could be determined with accuracy was that the plane to plane angle between the two structures is close to perpendicular at 89.07(45)°. The C_{ipso}–Cd bond distances, 2.093(10) (C1)

and 2.106(10) (C25) Å, are comparable to examples in the literature. The complex is essentially linear with a C1–Cd1–C25 angle of 179.2(4)°.

The structure of **III·33** is distorted, presumably due to the steric bulk of the Dipp flanking groups around the cadmium centre. The cadmium moiety sits out of the plane of the central aryl ring of the ligand by 0.6245(21) Å (C1). This compares with 0.102(17) and 0.030(21) Å (C1 and C25, respectively) in **III·32**. Similarly, the *ipso*-carbon of the flanking group is distorted from the same plane by 0.1644(24) and 0.3930(23) Å (C7 and C18 respectively).

Unlike **III·32**, the C1–Cd–C1 angle in **III·33** is bent at 169.17(8)°. This compares with the smallest C_{ipso}–Cd–C_{ipso} angle in the literature for a diaryl complex, 174.10(9)° in [2,6-(3,5-Xyl)$_2$C$_6$H$_3$]$_2$Cd.[188] The authors that reported this complex suggest that the angle in the complex is small because the smaller 3,5-Xyl flanking group allows the complex to flex and reduce steric clashing. The deformations in the solid-state structure of **III·33** are evidence of steric strain in the structure. The [2,6-Dipp$_2$C$_6$H$_3$]$^-$ ligand places a lot of steric bulk around the metal centre which appears to cause the ligand to buckle and distort to fit. It would therefore seem that the bent structure of the complex is also a consequence of steric strain in the structure. **III·33** is isomorphous to the manganese,[42] iron,[52] and cobalt[63] analogues.

To investigate the conditions under which *m*-terphenyl ligands can exchange between diaryl complexes NMR spectroscopic studies were conducted. [2,6-Dipp$_2$C$_6$H$_3$Cd(μ-I)]$_2$ was combined with [2,6-Mes$_2$C$_6$H$_3$Li]$_2$ in a 1:1 ratio and dissolved in benzene-d_6 (0.7 mL) and THF (0.05 mL). The THF was necessary to solubilise [2,6-Mes$_2$C$_6$H$_3$Li]$_2$ and allow the reaction to take place efficiently. Unfortunately, as it was not deuterated, it made the ^{1}H and ^{13}C{^{1}H} NMR spectra difficult to accurately interpret. The reaction was sonicated for five minutes and then allowed to stand at room temperature for 16 hours at which point a ^{113}Cd{^{1}H} NMR spectrum (**Figure 3·16**) was collected.

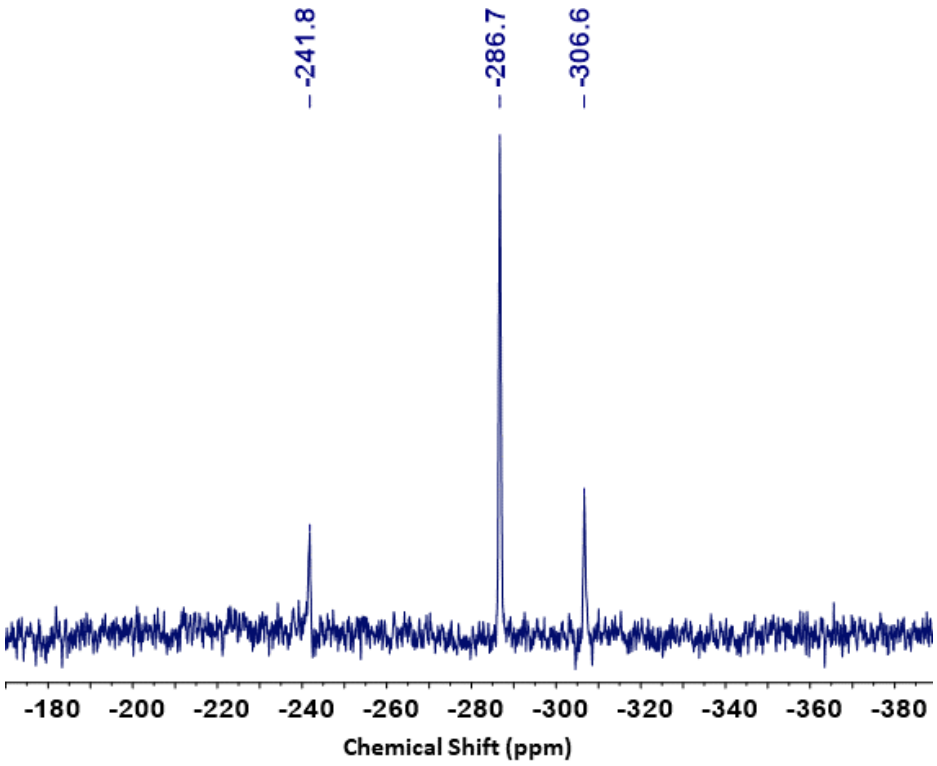

Figure 3·16.^{113}Cd{^{1}H} NMR spectrum of the reaction of [2,6-Dipp$_2$C$_6$H$_3$Cd(μ-I)]$_2$ and [2,6-Mes$_2$C$_6$H$_3$Li]$_2$.

The ^{113}Cd{^{1}H} NMR spectrum of this reaction contains three signals. The signals at 401 and 357 ppm can be attributed to **III·32** and **III·33**, respectively. The third, at 336 ppm, is a new species. This ppm value is consistent with a two-coordinate, diaryl cadmium complex.[188] This signal is not due to the starting material, [2,6-Dipp$_2$C$_6$H$_3$Cd(μ-I)]$_2$, which occurs at 853 ppm.[169] The spectrum of the starting material did not contain the three signals. It seems reasonable to assume in the absence of other candidates that the new signal belongs to the target complex [2,6-Dipp$_2$C$_6$H$_3$]Cd[2,6-Mes$_2$C$_6$H$_3$].

That the signal for [2,6-Dipp$_2$C$_6$H$_3$]Cd[2,6-Mes$_2$C$_6$H$_3$] lies upfield of both **III·32** and **III·33** is unexpected. The presence of **III·32** and **III·33** demonstrates that the reaction yields the three possible diaryl complexes which must occur *via* a ligand exchange.

To assess whether ligand exchange can occur between diaryl complexes, [2,6-Mes$_2$C$_6$H$_3$]$_2$Cd (**III·32**) and [2,6-Pmp$_2$C$_6$H$_3$]$_2$Cd (**III·34**)[188] were combined in equal proportions and dissolved in benzene-d_6. This solution was then heated to 50°C for twenty-four hours before ^{1}H, ^{13}C{^{1}H}

and $^{113}Cd\{^{1}H\}$ NMR spectra were collected. **III·34** was selected due to issues scaling up the synthesis of **III·33**. The spectra obtained contained the expected number of signals for a combination of **III·32** and **III·34** at the correct ppm. There is no suggestion of a third species indicating that ligand exchange does not occur under these conditions.

The second experiment involved combining **III·34** and one equivalent of $[2,6\text{-}Mes_2C_6H_3Li]_2$ in benzene-d_6. This sample was investigated with H^1 NMR spectroscopy at intervals of 1.5 hours, 27 hours, 6 days and 9 days. ^{113}Cd NMR spectra could not be obtained of these samples as the technique being unavailable due to technical issues at the time of this experiment. ^{1}H NMR spectra collected at each time interval contained the peaks of the starting materials and no evidence of a third species.

The ligands attached to the metal centre did not change in the presence of other diaryls species. This eliminated a potential pathway for ligand exchange identified by Odom and co-workers, in which $CdMe_2$ and $CdEt_2$ were shown to exchange ligands *via* a four-membered, cyclic transition state.[278] Ligands also do not exchange when a diaryl species and an *m*-terphenyl lithium salt are combined. Therefore, ligand exchange must occur between two diaryls in the presence of a lithium halide or between a diaryl, Ar_2Cd, and the starting material ArCdI in a Schlenk equilibrium style reaction.

Evans and Fazakerley demonstrated that the methyl groups in a mixture of dimethyl zinc and methyl zinc iodide exchange.[279] Woodward *et al*. later demonstrated the formation of EtZnMe from a reaction between Me_2Zn and EtZnCl.[280] They propose the pathway shown in **Scheme 3·4**.

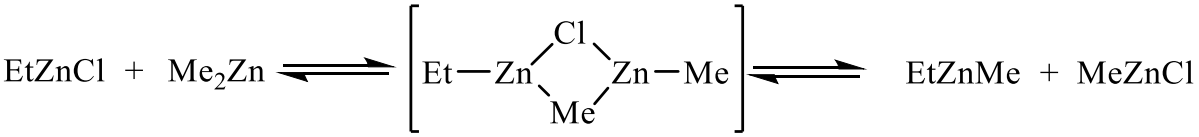

Scheme 3·4. The mechanism for alkyl group exchange in zinc complexes proposed by Woodward and co-workers.[280]

It is possible, despite the steric bulk of the *m*-terphenyl ligands, that this is the exchange mechanism observed in the synthesis of heteroleptic diaryl complexes. Such exchange could occur before [2,6-$Dipp_2C_6H_3Cd(\mu\text{-}I)]_2$ is consumed by the metathesis reaction.

Examples of this kind of exchange are limited to zinc species in the literature although, as mentioned, ligand exchange has been noted in cadmium systems.[278] Both metals are closed shell metals and the relevance of these observations to the open shell metals that are at the heart of this work can be questioned. However, in the absence of further evidence, the exchange mechanism proposed by Woodward *et al*. (**Scheme 3·4**) fits with most of the criteria currently known.

3.3.4 $[2,6\text{-}Dcp_2C_6H_3]^-$ Heteroleptic Complexes

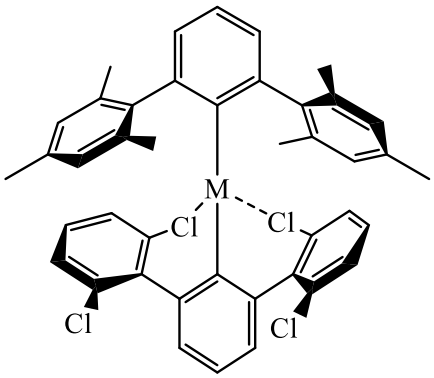

M = Mn (**III·30**) or Zn (**III·31**)

Figure 3·17. Schematic of [2,6-$Mes_2C_6H_3$]Mn[2,6-$Dcp_2C_6H_3$] (**III·30**) and [2,6-$Mes_2C_6H_3$]Zn[2,6-$Dcp_2C_6H_3$] (**III·31**).

Two heteroleptic, diaryl complexes featuring metals other than mercury were isolated. These complexes were [2,6-$Mes_2C_6H_3$]M[2,6-$Dcp_2C_6H_3$] [M = Mn (**III·30**) and Zn (**III·31**), **Figure 3·17**]. These complexes were characterised with X-ray diffraction studies. The structures are displayed in **Figure 3·18** and key bond lengths and angles are contained in **Table 3·3**.

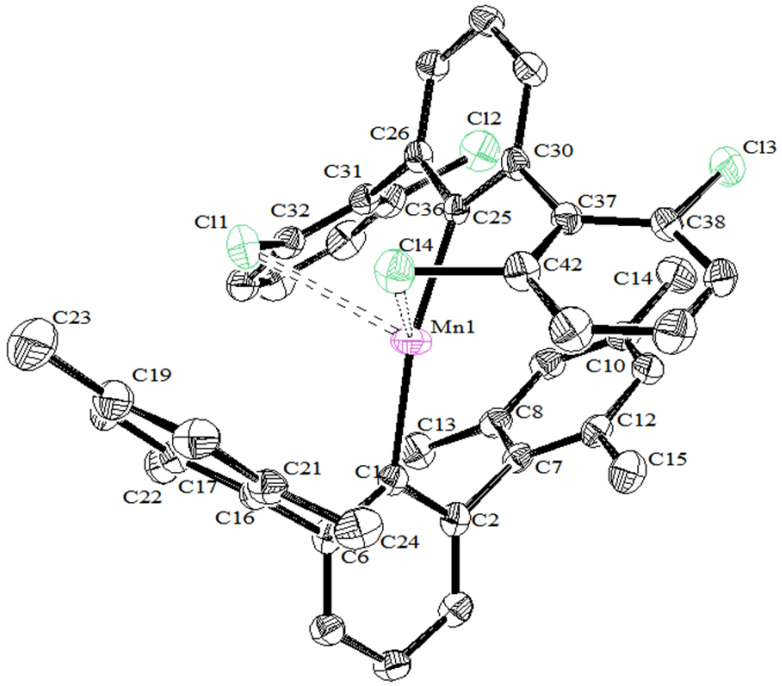

III·30

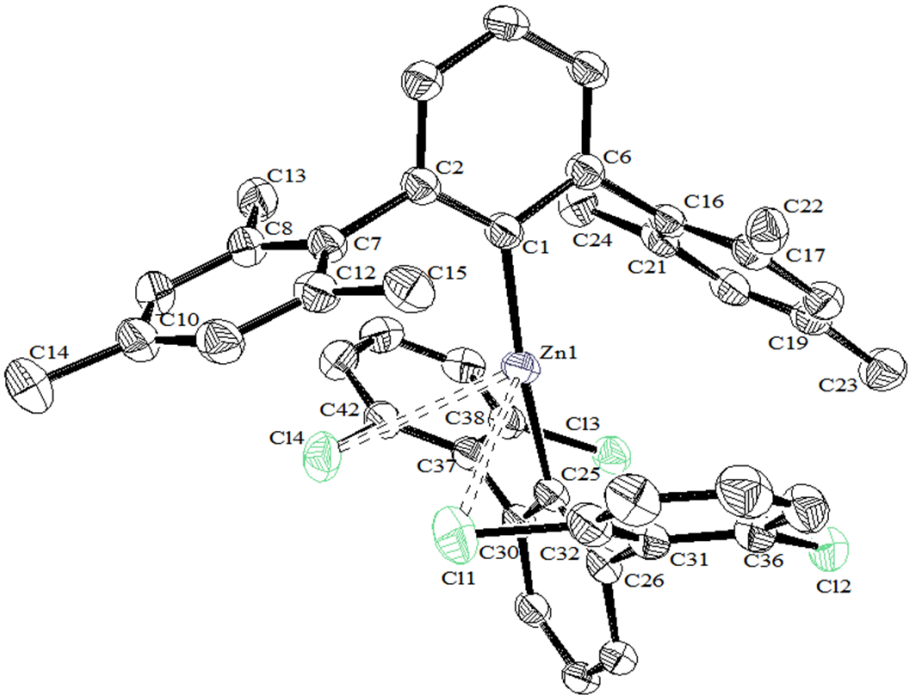

III·31

Figure 3·18. The solid-state structures of [2,6-$Mes_2C_6H_3$]Mn[2,6-$Dcp_2C_6H_3$] (**III·30**) and [2,6-$Mes_2C_6H_3$]Zn[2,6-$Dcp_2C_6H_3$] (**III·31**). Secondary M···Cl interactions are represented as dashed bonds. Hydrogens are omitted for clarity and ellipsoids are set at 50% probability.

A ^{1}H NMR spectrum of **III·31** was tentatively assigned. However, the purity of the sample could not be established and, as such, the spectrum could contain the three possible diaryl complexes or other impurities. EI-MS of the sample confirmed the presence of the parent ion.

III·30 and **III·31** crystallise in the space groups $P2_1/c$ and $P2_1/n$, respectively. The two complexes are structurally similar in the solid state but any distortion from an idealised *m*-terphenyl structure is more pronounced in the structure of **III·30**.

Table 3·3. Key bond lengths and angles for **III·30** and **III·31**.

	III·30 (M = Mn)		**III·31** (M = Zn)	
C_{ipso}–M/Å	C1	2.075(3)	C1	1.9471(18)
	C25	2.097(3)	C25	1.9501(18)
M···Cl/Å	Cl1	2.9021(11)	C1	3.2907(6)
	Cl4	2.8939(11)	Cl4	3.2397(6)
	Cl2	5.2669(11)	Cl2	4.8608(5)
	Cl3	5.3057(10)	Cl3	4.9124(5)
C_{ipso}–M–C_{ipso}/°	C1, C25	167.08(12)	C1, C25	173.51(7)
M–C_{ipso}–C_{ortho}/°	C1, C2	111.5(2)	C1, C2	128.53(13)
	C1, C6	130.4(2)	C1, C6	113.34(12)
	C25, C26	121.1(2)	C25, C26	121.28(13)
	C25, C30	121.8(2)	C25, C30	121.92(13)
Plane–Plane/°	C1, C25	87.49(10)	C1, C25	85.011(57)
Plane–Plane/°	C1, C16	84.88(39)	C1, C7	88.54(22)
	C1, C7	91.06(37)	C1, C16	96.31(20)
	C25, C31	61.72(44)	C25, C37	67.49(23)
	C25, C37	61.99(44)	C25, C31	69.64(24)
Out-of-plane				
Ar–MÅ	C1	0.0323(47)	C1	0.0211(26)
	C25	0.4519(46)	C25	0.1744(25)
τ'_4		0.40		0.34

Close contacts between the metal centre and two of the four chlorides are present in both structures. The Cl···M distances, 2.8939(11) Å (Cl1) and 2.9021(11) Å (Cl4) in **III·30** and 3.2397(6) Å (Cl1) and 3.2907(6) Å (Cl4) in **III·31**, are within the sum of the crystallographically determined van der Waals radii.[187] It is therefore likely that the chlorides form dative bonds with the electron poor metal centres. The Cl···M distances are shorter in **III·30** due to the manganese centre being more electron poor than the zinc centre. Therefore, the metal centres can be considered four-coordinate, with a distorted, "see-saw" geometry [t'_4 = 0.40 (**III·30**) and 0.34 (**III·31**), respectively].

These dative interactions involve the chloride groups of one side of the [2,6-$Dcp_2C_6H_3$]$^-$ ligand, with the remaining two chlorides held away from the metal centre by the geometry of the system. The aryl planes of the flanking groups are offset from the central plane of the ligand by *ca*. 61° in **III·31** and *ca*. 68° in **III·30**. This difference reflects the lengths of Cl···M interactions. The ligands in both complexes adopt a near perpendicular geometry to one another [87.49(10) (**III·30**) and 85.011(57) (**III·31**)] similar to the reported, homoleptic analogues.[76,77,188]

To accommodate these Cl···M secondary interactions the ligand structure deforms significantly. In both structures this manifests with a tilting of the [2,6-$Mes_2C_6H_3$]$^-$ ligand away from the two chlorides that interact with the metal centre, resulting in angles around the *ipso*-carbon of the [2,6-$Mes_2C_6H_3$]$^-$ ligand of 111.5(2)° and 130.4(2)° (**III·30**) and 128.53(13)° and 113.34(12)° (**III·31**). The metal centre is out of the plane of the central aryl ring of the [2,6-$Dcp_2C_6H_3$]$^-$ ligand by 0.4519(46) Å (**III·30**) and 0.1744(25) Å (**III·31**). This is due to the quasi four-coordinate nature of the complexes.

The slightly bent C1–M–C25 bonds of 167.08(12)° (**III·30**) and 173.51(7)° (**III·31**) could also be a function of these secondary interactions. The angles are not dissimilar from diaryl complexes in the literature, for example the C–Mn–C angles of 166.41(13)° and 173.52(7)° in [2,6-$Mes_2C_6H_3$]$_2$Mn reported by Kays and Cowley.[35] Relevant *m*-terphenyl literature complexes[52,76,188] are all two coordinate, Power *et al*. suggest that the bent C_{ipso}–M–C_{ipso} angles in such complexes could be a result of weak secondary interactions between the ligands and the metal centre.[43] This possibility has also been explored by Kays *et al*., who suggested that contacts between the metal centre and the *ipso*-carbons of the flanking groups are a likely cause of C_{ipso}–M–C_{ipso} distortion.[76]

The iron, cobalt, and cadmium analogues of **III·30** and **III·31** could not be isolated. Efforts to synthesise the cadmium analogue afforded co-crystals of the two homoleptic complexes [2,6-$Mes_2C_6H_3]_2Cd$ and [2,6-$Dcp_2C_6H_3]_2Cd$ (Appendix 1). The formation of these complexes provided further evidence of ligand exchange. No product could be isolated from attempts to synthesis the iron and cobalt analogues. The reason behind this was made clear through efforts to synthesise the homoleptic complexes.

3.3.5 [2,6-$Dcp_2C_6H_3]^-$ Homoleptic Complexes

Addition of one equivalent of [2,6-$Dcp_2C_6H_3Li]_2$ to a solution of MX_2 (MX_2 = $MnBr_2$, $FeCl_2{\cdot}THF_{1.5}$, and $CoBr_2$·DME) solubilised in a toluene/THF mixture resulted in three distinct products. The reaction with $MnBr_2$ resulted in the expected [2,6-$Dcp_2C_6H_3]_2Mn$ complex (**III·35**, **Scheme 3·5**).

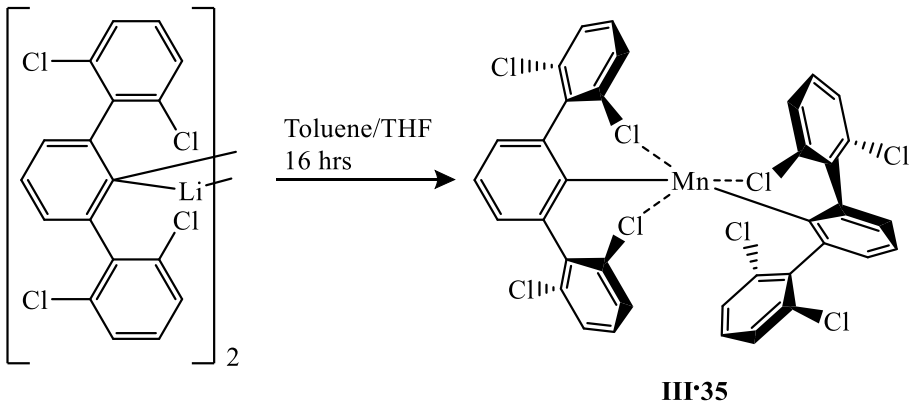

III·35

Scheme 3·5. The synthetic route to **III·35**.

Complex **III·35** was isolated as cream coloured crystals. The crystals were grown in a yield of 37% by slowly cooling a saturated solution of the complex in toluene to 7°C. These crystals were shown to be pure by elemental analysis. The ^1H NMR spectrum (**Figure 3·19**) contains broad peaks within a range of 37.17 to –0.96 ppm, consistent with literature examples of *m*-terphenyl manganese complexes and indicative of a paramagnetic product.[76] Magnetic susceptibility measurements demonstrated that the complex has a magnetic moment of 5.74 μ_B, which is consistent with the spin only value for high spin manganese(II) and indicates the

presence of five unpaired electrons.[179] The value is also consistent with the magnetic moments of reported compounds such as [2,6-$Mes_2C_6H_3$]$_2$Mn (5.81 μ_B).[76]

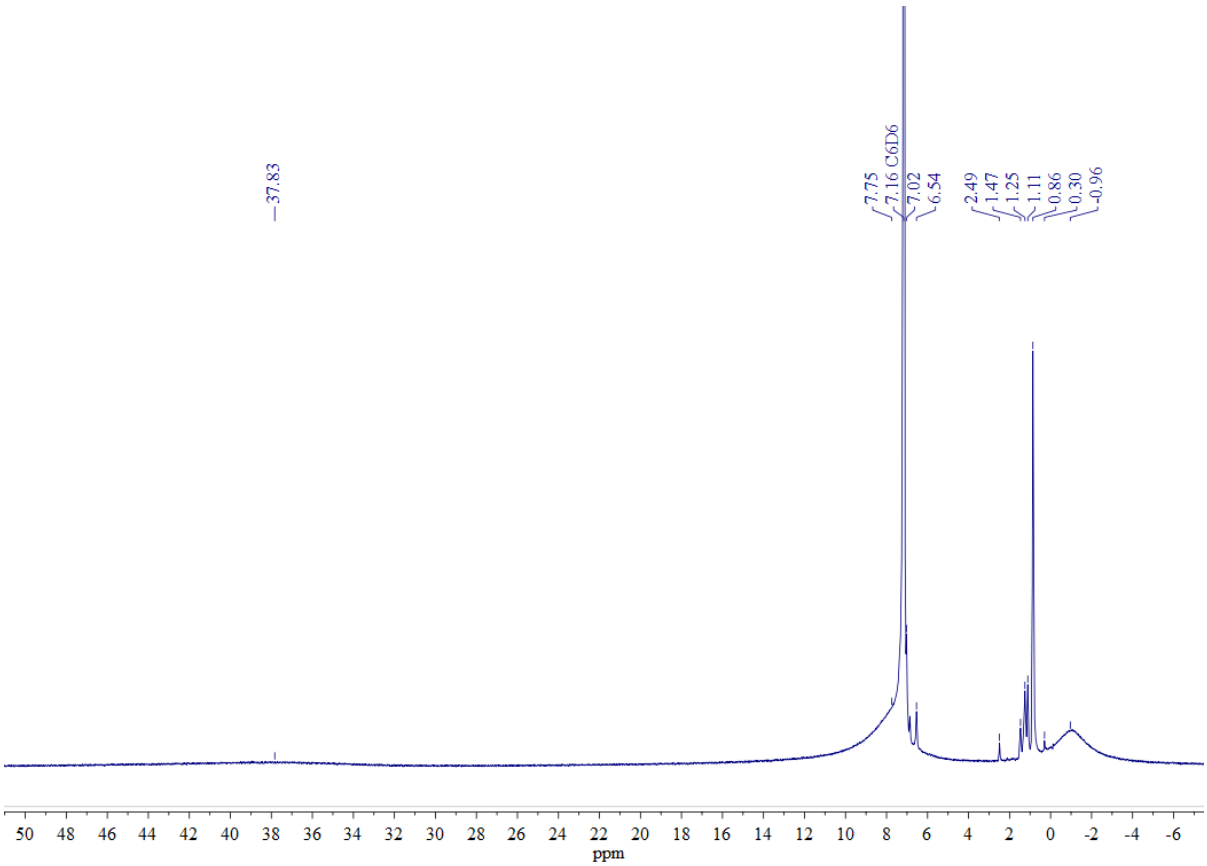

Figure 3·19. ^{1}H NMR spectrum of **III·35**.

Analysis of the crude product with EI-MS (**Figure 3·20**) showed evidence of the parent ion peak at 785.0 m/z. There are also signals that correspond to the m/z of coupled ligand species. The signal at 659.0 m/z could represent [(1-(2,6-$Dcp_2C_6H_3$)-7-$DcpC_{12}H_6$) – H]$^+$. Various fragment ions, resulting from the loss of a chloride, are observed.

Two solid-state structures of **III·35** were obtained through X-ray diffraction studies of crystals grown in two different environments. The first polymorph (**III·35a**) was grown as described above. The second polymorph (**III·35b**) was obtained through vapour diffusion of pentane into a solution of **III·35** in benzene-d_6, phenyl isocyanate, and *n*-hexyne followed by storage at room temperature for 1 month. This was as part of an investigation into the potential efficacy of **III·35** in catalysis.

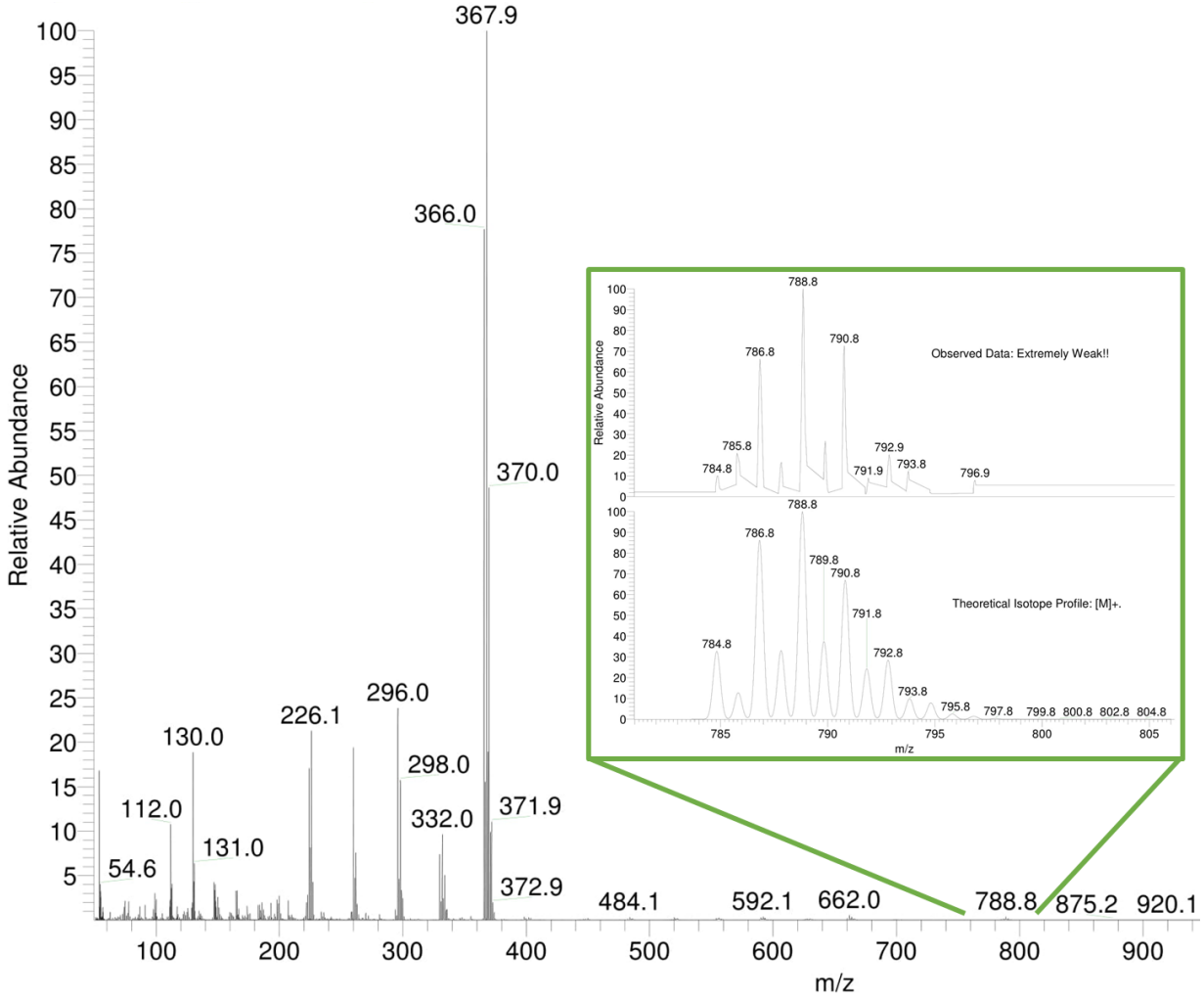

Figure 3·20. The EI-MS spectrum of **III·35** with an insert showing the parent ion.

Polymorph **III·35a** adopts the tetragonal space group *Pbca* whilst polymorph **III·35b** adopts the monoclinic space group *C*2/*c*. Both show two $[2,6\text{-}Dcp_2C_6H_3]^-$ moieties bound to a central manganese atom in a formally two-coordinate, quasi-linear arrangement. The structures are shown in **Figure 3·21** and key bond lengths and angles are contained within **Table 3·4**.

Surprisingly, despite the chelating nature of the $[2,6\text{-}Dcp_2C_6H_3]^-$ ligand, the Mn–C_{ipso} distances are not shorter than those observed in other diaryls in the literature.[65,66,76] The plane to plane angles between the two ligands are similar in both polymorphs at 75.287(67)° and 73.859(2)° respectively.

As in the structures of **III·30** and **III·31**, both polymorphs contain Cl···M interactions. In **III·35a** there are four Cl···Mn distances smaller than the sum of the van der Waals radii.[187]

Thee distances are 2.7208(8) (Cl1), 2.8043(8) (Cl4), 2.9474(8) (Cl5) and 3.7847(8) (Cl8) Å. The fourth distance is much longer than the others. The geometry around metal centre can be described as distorted square pyramidal (τ_5 = 0.30), with a long-range Mn···Cl interaction.

The manganese moiety is pulled out of the plane of the central aryl ring by 0.3723(37) Å towards the [2,6-$Dcp_2C_6H_3$]$^-$ moiety that provides the two shortest Cl···Mn interactions (Cl1 and Cl4). The other ligand tilts away from the two chlorides that form the closest interactions forcing Mn–C–C angles of 124.71(18)° (Mn1–C19–C24) and 119.35(18)° (Mn1–C19–C20) with the compression of the internal C_{ortho}–C_{ipso}–C_{ortho} to 115.9(2)° (C20–C19–C24). As similar angles are observed on the [2,6-$Mes_2C_6H_3Mn$]$^+$ moiety of **III·30** this is likely a steric effect rather than the ligand deforming to satisfy the longer Cl···Mn interaction (Cl8).

Table 3·4. Key bond lengths and angles for polymorphs **III·35a** and **III·35b**.

	III·35a		**III·35b**	
	Atom Label		Atom Label	
C–Mn/Å	C1	2.095(2)	C1	2.0886(18)
	C19	2.105(3)		
Mn···Cl/Å	Cl1	2.7208(8)	Cl1	2.9147(5)
	Cl4	2.8043(8)	Cl4	3.2838(7)
	Cl5	2.9476(8)	Cl3	4.9660(6)
	Cl8	3.7847(8)	Cl2	5.2295(7)
	Cl7	4.7660(8)		
	Cl6	5.1939(8)		
	Cl1	5.2719(8)		
	Cl2	5.3082(8)		
C–Mn–C/°	C1, C19	152.75(10)	C1, C1	150.34(11)
Mn–C–C/°	C1, C2	121.97(18)	C1, C2	120.79(14)
	C1, C6	121.12(18)	C1, C6	122.54(14)
	C19, C20	119.35(18)		
	C19, C24	124.71(18)		
$Ar_{central}$– $Ar_{central}$ /°	C1, C19	75.287(67)	C1, C1	73.859(2)
Plane–Plane/°	C6, C13	56.41(34)	C2, C7	56.448(61)
	C2, C7	58.24(34)	C6, C13	67.607(76)
	C24, C31	103.16(29)		
	C20, C25	122.22(27)		
Out-of-plane				
Ar–Mn/Å	C1	0.3723(37)	C1	0.1160
	C19	0.0480(35)		
τ_5		0.30		

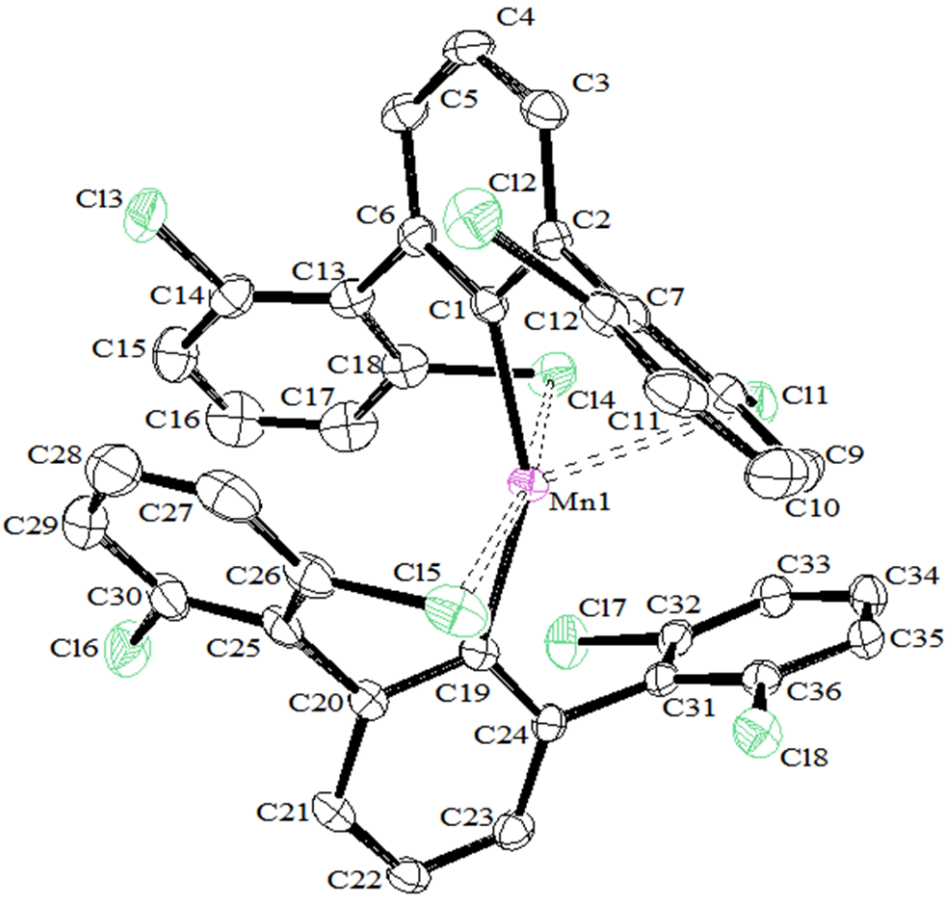

III·35a

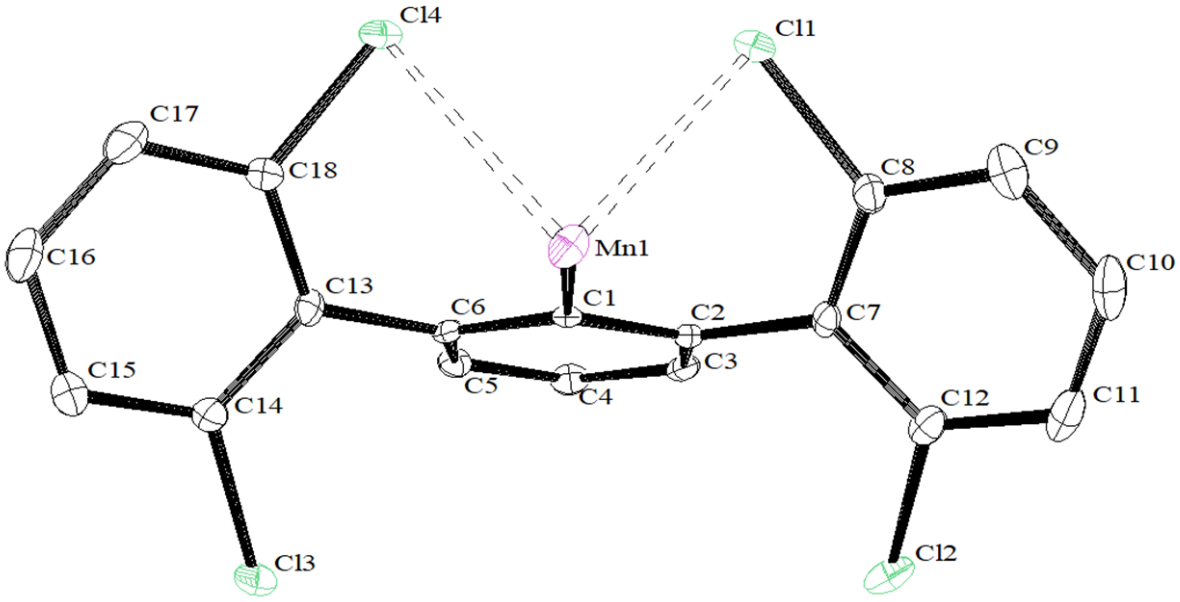

III·35b

Figure 3·21. The solid-state structures of **III·35**: the asymmetric units of polymorphs **III·35a** and **III·35b**. Hydrogens are omitted for clarity and ellipsoids are set at 50% probability.

These distortions are less pronounced in the second polymorph **III·35b**, in which only half of the molecule is in the asymmetric unit. The full structure again contains four Cl···Mn distances that are within the sum of the van der Waals radii. In this structure the distances are more equal, with two each at 2.9147(5) Å (Mn1···Cl1) and 3.2838(7) Å (Mn1···Cl4). This is the reason that the distortions of both the manganese centre from the central aryl ring and the Mn–C–C angles are less pronounced in **III·35b** as the strain of forming the Cl···Mn secondary interactions is spread over the whole structure. The metal centre in **III·35b** adopts a highly distorted, trigonal prismatic structure.

The reaction with $FeCl_2$ resulted in the two ligands coupling together to form a substituted biphenylene product, 1-[2,6-$Dcp_2C_6H_3$]-7-$DcpC_{12}H_6$ (**III·36**, **Scheme 3·6**), presumably with the concomitant expulsion of one equivalent of $FeCl_2$. It was found that yields greater than 90% could be achieved if the reaction was quenched with an excess of iodine and purified *via* a standard organic work up.

The reaction with $CoBr_2$ afforded a product featuring a ligand comprising three equivalents of the ligand, coupled together to form a *m*-terphenyl substituted *m*-terphenyl coordinated to a cobalt bromide moiety[2-{2,6-$(Dcp_2C_6H_3)_2C_6H_3$}-6-$DcpC_6H_3$]CoBr (**III·37**, **Scheme 3·6**). This final compound was isolated in low yield and may not be the major reaction product.

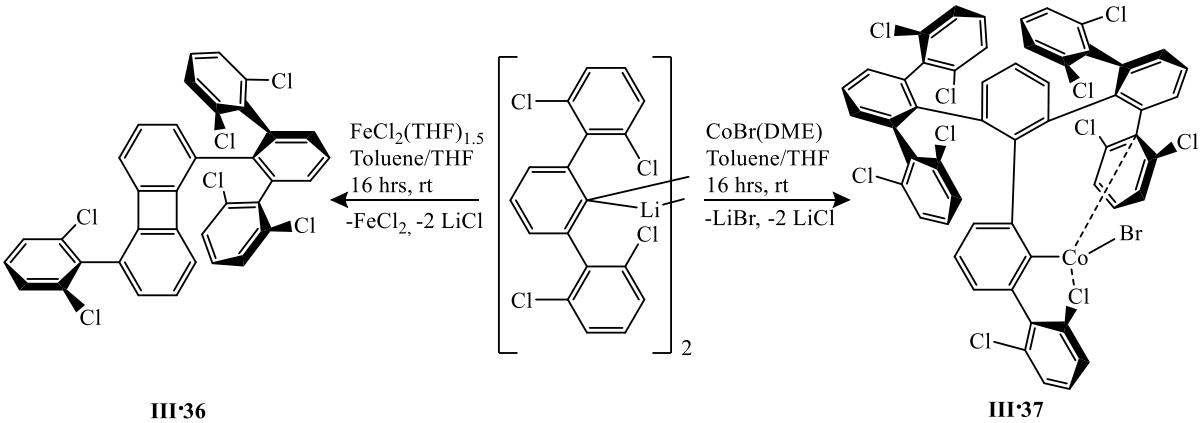

Scheme 3·6. The synthetic routes to **III·36** and **III·37**.

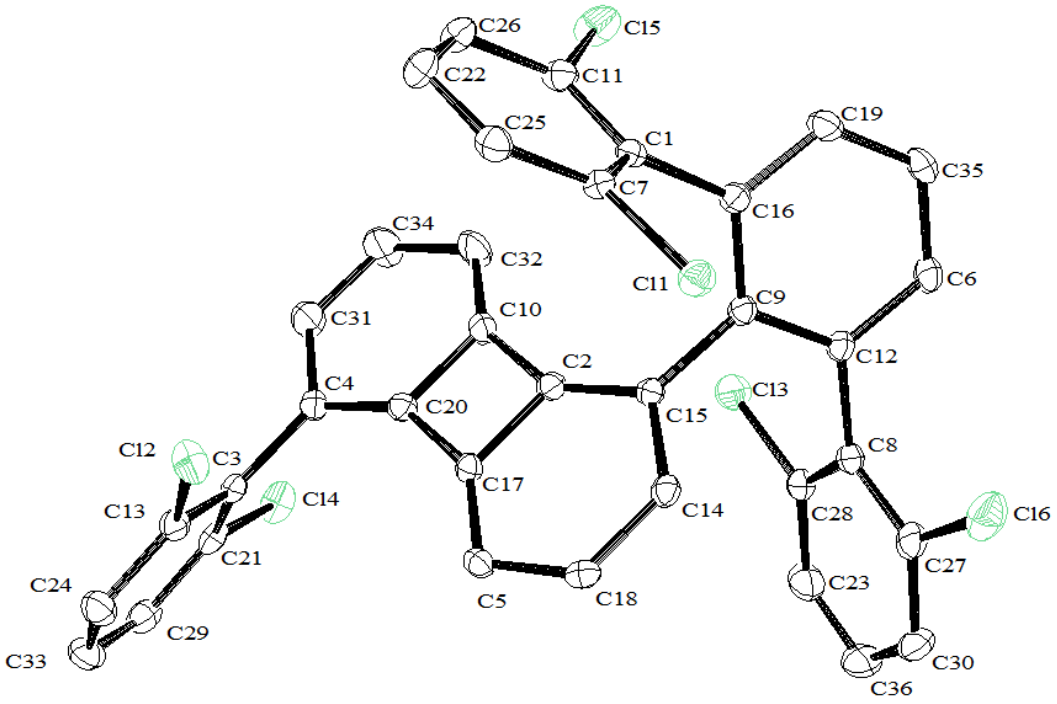

Figure 3·22. The solid-state structure of **III·36**. Hydrogens have been omitted for clarity and ellipsoids have been set at 50% probability.

The biphenylene product, **III·36**, is the result of the coupling of two $[2,6\text{-}Dcp_2C_6H_3]^-$ ligands. The biphenylene core is formed from a $[2,6\text{-}Dcp_2C_6H_3]^-$ moiety in which one of the *ortho* positions of a flanking group has been coupled to the *ipso* position of the central aryl ring; the same flanking group is then coupled to a further $[2,6\text{-}Dcp_2C_6H_3]^-$ moiety.

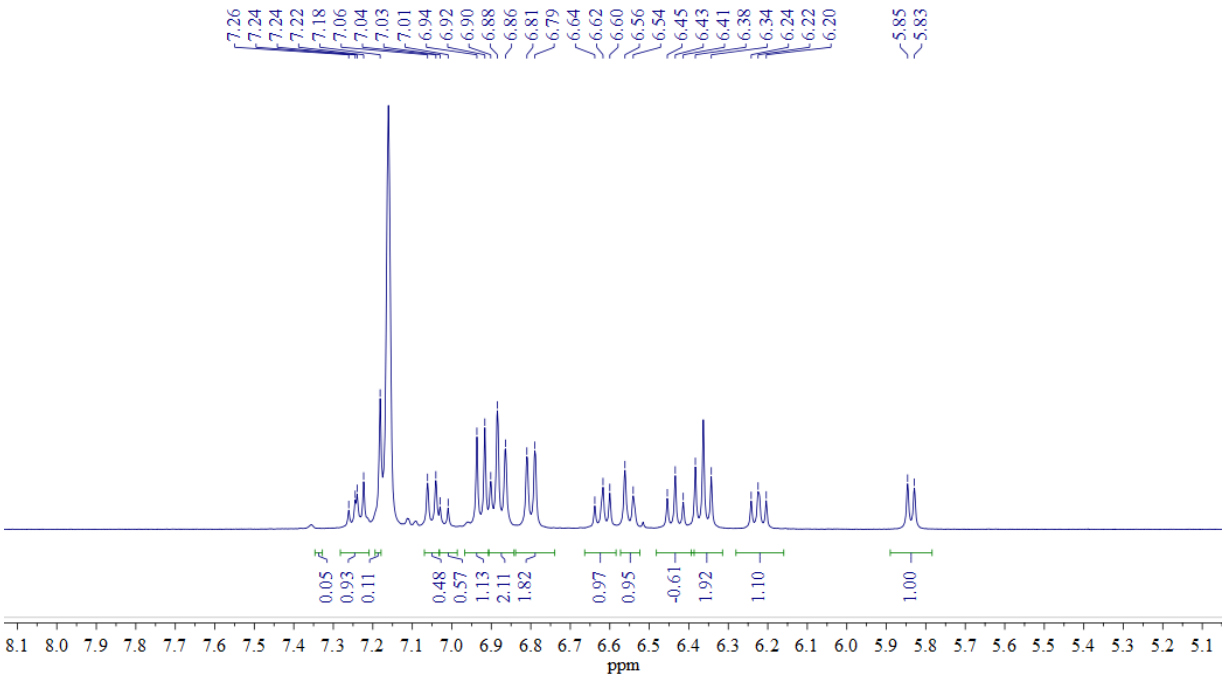

Figure 3·23. The peak containing region of the ^{1}H NMR spectrum of **III·36**.

The identity of **III·36** was confirmed by high resolution ASAP-MS, X-ray diffraction studies (**Figure 3·22**), elemental analysis of the crystalline product, and assignment of the ^{1}H (**Figure 3·23**) and ^{13}C{^{1}H} NMR spectra (**Figure 3·24**).

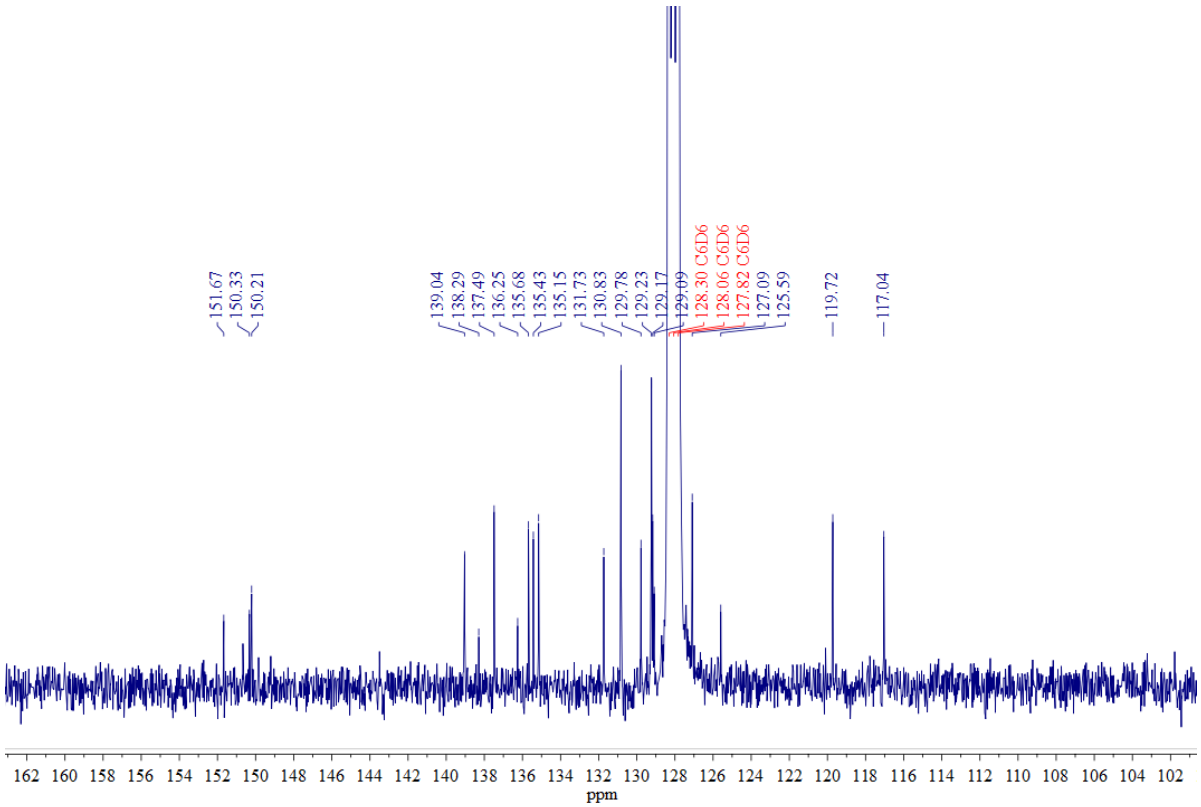

Figure 3·24. The peak containing region of the ^{13}C{^{1}H} NMR spectrum of **III·35**.

EI-MS analysis of the [2,6-Dcp$_2$C$_6$H$_3$Li]$_2$ starting material showed no evidence of **III·36**, excluding the possibility that the product forms through decomposition of the lithium salt. The ^{1}H NMR spectrum of the crude product contains no evidence of the expected, diamagnetic diaryl complex.

The fate of the metal halide has not been experimentally demonstrated. It is possible that it acts as a catalyst for the coupling reaction. EI-MS analysis of a reaction between [2,6-Dcp$_2$C$_6$H$_3$Li]$_2$ and two equivalents of iron(II) chloride showed no evidence of **III·36**. This can be interpreted to show that the formation of the diaryl complex, as opposed to a halide bridged, dimeric species, is necessary for the reaction that affords **III·36** to occur.

This reaction can be rationalised as the formation of [2,6-$Dcp_2C_6H_3$]$_2$Fe *via* metathesis reactions between the lithium salt and iron(II) chloride. A chloride substituent is then transferred from the ligand to the metal centre forming a phenyl radical, which then displaces the iron from the *ipso*-carbon of one of the aryl ligands. The mechanisms surrounding iron mediated cross coupling have proved problematic to identify. However, a proposed mechanism, based on the work of Tonzetich *et al.*, is shown in **Scheme 3·7**.[244]

A radical on an aryl ring can delocalise around the structure.[281] That yields of **III·36** above 90% are achieved suggests the radical reaction is very controlled with the radical reacting through the same position at least 90% of the time.[282] This could be because the radical is not long lived and cannot delocalise, or because reaction at this position is the most energetically favourable.

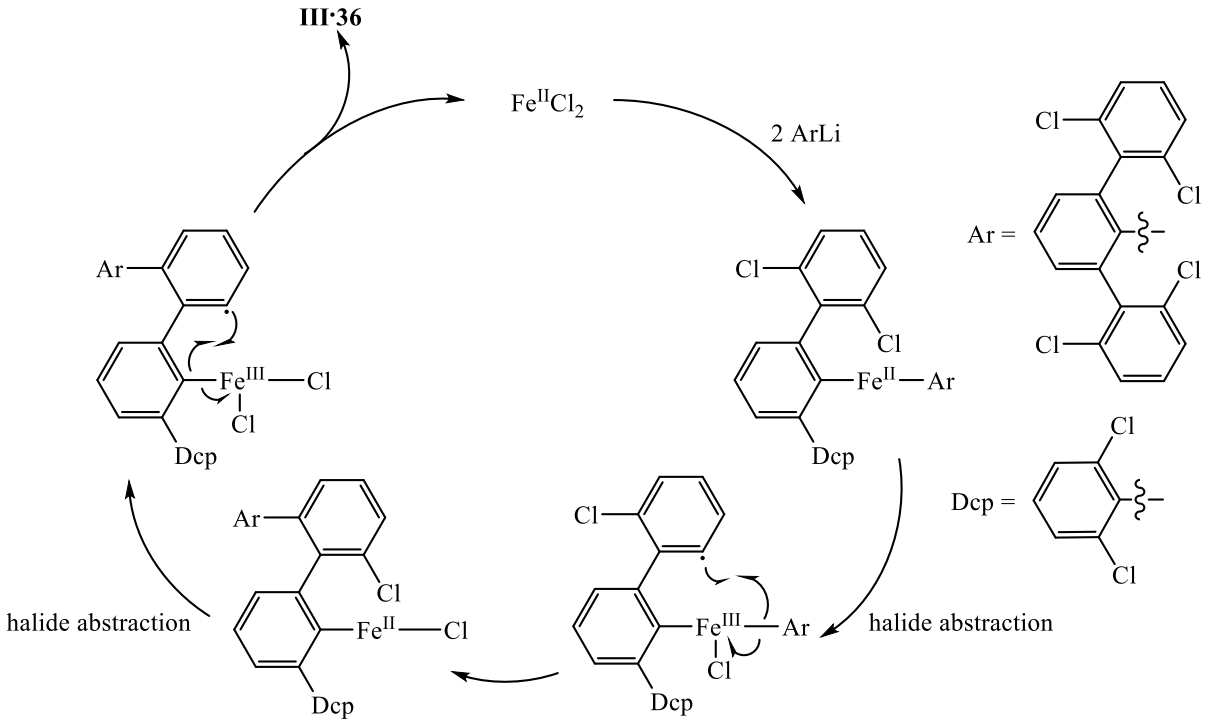

Scheme 3·7. A proposed mechanism for the formation of **III·36**.

A further alternative would be a two electron, oxidative addition mechanism involving an iron(IV) intermediate, however, examples of iron in the +IV oxidation state are rare, highly

reactive, and often involve multiple bonds to ligands such as oxygen or nitrogen.[283,284] On balance, a radical mechanism is more consistent with the literature for iron concerning cross-coupling reactions.[244,254,261,285] Further studies are required to elucidate the mechanism.

Several methods of synthesising biphenylenes have been reported. The oldest proceeds *via* an Ullmann coupling of 2,2'-dibromobiphenyl and was developed in 1941.[286] Since then methods that involve the generation of benzyne intermediates,[287] cobalt-catalysed coupling of alkynes,[288] and the coupling of self-reactive biphenyls[289,290] have been developed. To this author's knowledge this is the only example of an iron-mediated synthesis of biphenylene.

The reaction between $[2,6\text{-}Dcp_2C_6H_3Li]_2$ and $CoBr_2(DME)$ affords low yields of $[2\text{-}\{2,6\text{-}(Dcp_2C_6H_3)_2C_6H_3\}\text{-}6\text{-}DcpC_6H_3]CoBr$ (**III·37**, **Scheme 3·6**) as dark red crystals. The structure of this product was confirmed by X-ray diffraction analysis. A sufficient quantity of this product for analysis using other techniques could not be isolated.

III·37 can be envisioned as forming *via* two instances of reductive coupling that occur between three equivalents of the ligand to substitute one of the flanking aryl groups with two $[2,6\text{-}Dcp_2C_6H_3]^-$ moieties. The product forms very slowly and is not detectable by EI-MS immediately following the reaction but instead deep red crystals form from the green mother liquor alongside a blue powder, following storage of the reaction mixture in toluene at −30°C for 60 days.

X-ray diffraction studies revealed two polymorphs of **III·37**, labelled **a** and **b**. Both contain the full molecule in the asymmetric unit and molecules of toluene in the lattice. **III·37a** adopts the monoclinic space group $P2_1/n$ and contains half a molecule of highly disordered toluene. **III·37b** adopts the triclinic space group *P*-1 and contains three molecules of toluene, one of which is highly disordered. **Figure 3·25** shows the structure of **III·37a**. The atoms in **III·37b** follow the same numbering scheme as those in **III·37a**.

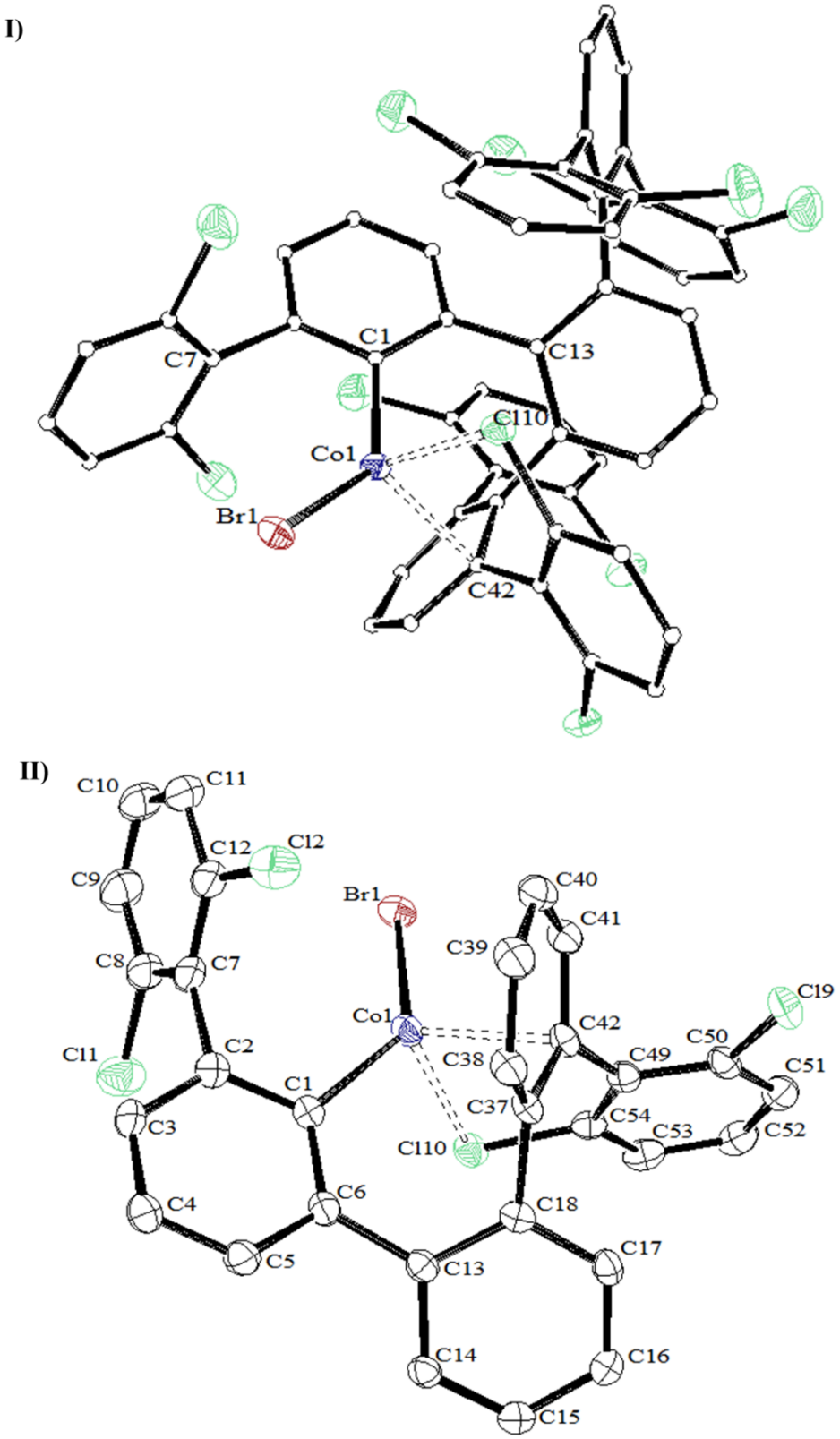

Figure 3·25. The solid-state structure of **III·37a**. I) The full structure with carbons represented as spheres, key atoms have been labelled. II) The core unit with all atoms labelled. Hydrogens have been omitted for clarity and, where applicable, ellipsoids have been set at 50%.

When the connectivity of the asymmetric units of the polymorphs is considered it can be seen that they are enantiomers of one another. Despite this, they do not crystallise in chiral or Schonke space groups, as they co-crystallise in an enantiomeric pair. The lability of the ligand is such that this chirality presumably interconverts in solution, meaning there is not enantiomeric excess, and can only be observed in the solid-state.

The structure of **III·37** contains a first $[2,6\text{-Dcp}_2C_6H_3]^-$ unit bound to a Co(II) centre, which is also bound to a bromide ion. One flanking aryl group of this first $[2,6\text{-Dcp}_2C_6H_3]^-$ unit is coupled to two further equivalents of $[2,6\text{-Dcp}_2C_6H_3]^-$ in the *ortho*-positions where chloride substituents originally resided. The coupling results in a ligand of significantly increased steric bulk over the original $[2,6\text{-Dcp}_2C_6H_3]^-$ ligand and it is presumably this bulk that prevents further coupling mediated by the still present cobalt moiety or the formation of halide-bridged, dimeric complexes similar to those in Chapter II. **Table 3·5** contains key bond lengths and angles for the structures.

Table 3·5. Bond lengths and angles for polymorphs **III·37a** and **III·37b**.

	III·37a		**III·37b**	
	Atom Labels		Atom Labels	
C_{ipso}–Co/Å	C1	1.982(3)	C1	1.994(2)
C_{ipso}··· Co /Å	C42	2.2951(32)	C42	2.2951(32)
Co–Br/Å	Br1	2.3802(6)	Br1	2.326(2)
Co–Cl/Å	Cl10	2.4983(10)	Cl10	2.4727(7)
	Cl12	3.6217(13)	Cl12	3.3228(7)
	Cl7	4.4588(13)	Cl7	4.6927(7)
			Cl8	4.8186(8)
C_{ipso}– Co –Br/°	C1, Br2	134.40(10)	C1, Br2	142.28(6)
Co –C_{ipso}–C_{ortho}/°	C1, C2	114.7(3)	C1, C2	115.11(15)
	C1, C6	118.2(3)	C1, C6	127.57(15)
Plane–Plane/°	C1, C7	80.24(12)	C1, C7	66.710(67)
	C1, C13	40.14(13)	C1, C13	40.438(85)
Out-of-plane				
Ar–Co/Å	C1	0.1280(52)	C1	0.1134(31)
Geometric indicators		$\tau'_4 = 0.73$		$\tau_5 = 0.33$

The cobalt centre is not two-coordinate. As with other $[2,6\text{-Dcp}_2C_6H_3]^-$ complexes the ligand forms additional Co···Cl interactions, increasing the coordination number. In **III·37a** the metal

centre is five-coordinate. One of these interactions is significantly longer than the others and the structure is best described as adopting a distorted tetrahedral geometry (τ'_4 = 0.73**)** with a long-range Co···Cl interaction. In **III·37b** the metal is five-coordinate and adopts a square pyramidal geometry.

In both structures, two secondary interactions form between the flanking group chlorides and the cobalt centre [Co···Cl = 2.4983(10) Å (Cl10), 3.6217(13) Å (Cl12), **III·37a** or Co···Cl = 2.4727(7) Å (Cl10), 3.3228(7) Å (Cl12), **III·37b**]. However, the shortest secondary interaction is with an *ipso* carbon of the central aryl ring of one of the $[2,6\text{-Dcp}_2C_6H_3]^-$ fragment that contributes a Co···Cl interaction. This creates a four membered metallacycle and has a pronounced effect on the geometry of this fragment.

The $[2,6\text{-Dcp}_2C_6H_3]^-$ fragment that contributes the *ipso* carbon secondary interaction is heavily distorted in both polymorphs. Both Dcp flanking groups in this fragment show a deviation from the plane of the central aryl ring away from the body of the structure. This deviation is large in both structures [0.3095(57) Å (C38) and 0.5825(53) Å (C42), (**III·37a**) and 0.1456(35) Å (C38) and 0.4728(35) Å (C42), (**III·37b**)]. Around the carbon that forms the secondary interaction with the cobalt centre, this could be interpreted as the formally sp^2 carbon adopting a sp^3 geometry to accommodate a secondary interaction with the cobalt ion. However, as this deviation is seen on both sides of the fragment (albeit being more pronounced on the side contributing the secondary interaction) and coincides with a puckering of the central aryl ring of the fragment, it is likely steric factors also contribute. The puckering is best represented through the rms deviation of the individual atoms within the plane of the ring. This stands at 0.0444 Å (**III·37a**) and 0.0416 Å (**III·37b**), respectively. In both cases this is more than double the average rms deviation of all the aryl rings in the structure.

Steric induced distortion is also seen in the second $[2,6\text{-}Dcp_2C_6H_3]^-$ fragment that is coupled to the flanking group of the central *m*-terphenyl moiety (i.e. the moiety bound *via* the *ipso*-carbon to the cobalt centre). This manifests as a movement of the chloride groups out of the plane of the respective flanking groups [0.1848(49) Å (Cl3), 0.2676(51) Å (Cl4), 0.1499(56) Å (Cl5) and 0.4584(58) Å (Cl6), **III·37a** and 0.1188(31) Å (Cl3), 0.2889(31) Å (Cl4), 0.2401(31) Å (Cl5) and 0.1756(31) Å (Cl6) **III·37b**]. These distortions demonstrate the large steric profile of the complex and the *m*-terphenyl substituted *m*-terphenyl ligand that has formed.

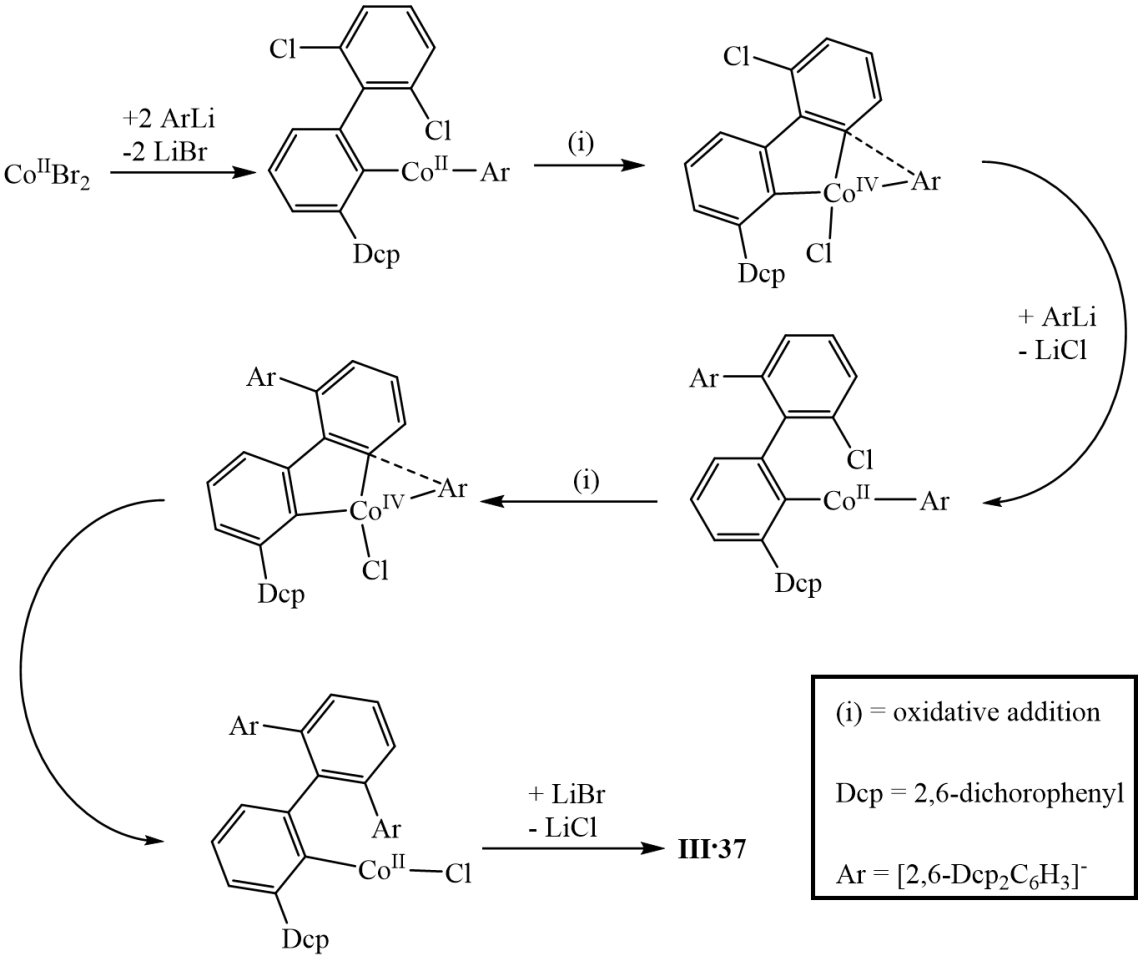

Scheme 3·8. A proposed mechanism for the formation of **III·37** *via* a cobalt(IV) intermediate.

The mechanism that affords **III·37** could be different from the reaction that affords **III·36**. That the ligand remains attached to the metal rather than eliminating as a biphenylene product indicates that a metathesis reaction occurs faster than the coupling reaction. This is because a third ligand must be provided for the reaction at the metal centre before a biphenylene forms.

Two possibilities for this reaction are a radical intermediate or a highly reactive cobalt(IV) intermediate.[131,291]

The mechanism proposed in **Scheme 3·8** involves a cobalt(IV) intermediate. Examples of cobalt inserting into an aryl halide bond *via* oxidative addition are present in the literature although they involve low-valent cobalt.[292,293] That the final product bears a bromide ligand does not necessarily mean that this is retained throughout the reaction. Power *et al*. observed that in the synthesis of $[2,6\text{-}Mes_2C_6H_3Co(\mu\text{-}Br)]_2$ from cobalt(II) chloride the bromides originate on the Grignard reagent and exchange with the chlorides.[74] Although this reaction utilises a lithium salt, possible halide exchange should be considered. **Scheme 3·8** represents a proposed sequence of events in the formation of **III·37** in the knowledge that the exact mechanisms for this transformation may be incorrect.

The coupling reactions, promoted by iron(II) chloride and cobalt(II) bromide, are the reason why heteroleptic complexes of the type $[2,6\text{-}Dcp_2C_6H_3]M[2,6\text{-}Mes_2C_6H_3]$ (M = Fe or Co) could not be isolated for these metals. If the desired products do form they must rapidly continue to react *via* the pathways described above to afford products that could not be isolated. In contrast, manganese and zinc are not known for cross coupling reactions.[255,294]

3.4 Conclusions

Four heteroleptic mercury complexes, **III·21–III·24**, have been synthesised *via* stepwise substitution of mercury bromide with two different *m*-terphenyl ligands. These complexes are the first examples of heteroleptic, two-coordinate diaryl complexes.

Characterisation of these complexes suggested that the ligands interacted with one another. NMR spectroscopic studies of **III·21** and **III·22** showed that, when in the presence of a ligand with asymmetric flanking groups, the methyl signals of ligands with symmetrical flanking groups are split. The mechanism for this manipulation of the chemical environment of one ligand by another could not be identified. Solid-state studies of these complexes also showed that heteroleptic complexes have radically different steric properties to the homoleptic analogues.

Through this investigation into a series of mercury complexes bearing two different *m*-terphenyl ligands, it has been shown that altering the steric pocket around the metal centre in a non-symmetric fashion can have a profound impact on the structures. Ligand combinations enforce solid-state structures that are distinct from the homoleptic analogues. The indication that through space interligand interactions occur further increases the complexity of these systems.

Efforts to stabilise low-coordinate, heteroleptic, transition metal complexes resulted in the isolation of complexes **III·30** and **III·31**. Secondary interactions between the chlorides of the $[2,6\text{-}Dcp_2C_6H_3]^-$ mean that the complexes are not truly two-coordinate. However, **III·30** is the first example of a quasi-two-coordinate transition metal complex stabilised by two different aryl ligands. Attempts to develop similar complexes encountered several issues. The first was the exchange of the *m*-terphenyl ligands in solution: resulting in a mixture of aryl products. The second was identification: disorder within the crystal structures prevented an accurate

structure determination. $^{113}Cd\{^{1}H\}$ NMR spectroscopy studies suggest that exchange may occur through the establishment of a Schlenk type equilibrium during the early stages of the reaction. Finally, iron and cobalt were able to activate the aryl chloride bonds in the [2,6-$Dcp_2C_6H_3]^-$ ligand resulting in cross-coupled products which could not be isolated.

This cross-coupling ability of $FeCl_2$ and $CoBr_2$ was demonstrated through the attempted preparation of the homoleptic products $[2,6\text{-}Dcp_2C_6H_3]_2M$ (M = Mn, Fe and Co). Whilst the manganese product, $[2,6\text{-}Dcp_2C_6H_3]_2Mn$ (**III·35**) was isolated in yields of 37%, the iron and cobalt reactions both resulted in the cross coupled products 1-[2,6-$Dcp_2C_6H_3$]-7-$DcpC_{12}H_6$ (**III·36**) and [2-{2,6-$(Dcp_2C_6H_3)_2C_6H_3$}-6-$DcpC_6H_3$]CoBr (**III·37**), respectively. The reaction that yields **III·36** is the first reported example of an iron mediated biphenylene synthesis.

3.5 Future Work

As demonstrated by complexes **III·30** and **III·31**, one method of overcoming the analytical problems with heteroleptic, *m*-terphenyl complexes is to have two ligands that are strikingly different either electronically or, potentially, sterically. Therefore, the use of ligands that have substituents of the central aryl ring that either alter the electronics or the sterics could serve to promote a more ordered crystal lattice. This could involve the introduction of CF_3 groups to the *para* position or buttressing *i*Pr groups to the *meta* positions and the combination of such ligands with the *m*-terphenyls used in this work.

Improving the yields of these heteroleptic products would involve reducing the time available for an exchange reaction between Ar*MX and $Ar^{\#}MAr^*$ to occur. Increasing the dilution of the reaction would help to slow this reaction and the use of a large excess of the *m*-terphenyl lithium salt might increase the speed of the metathesis reaction. Increasing the yield of these reactions is key to isolating a useful amount of heteroleptic diaryl and should be the focus of future work in this area.

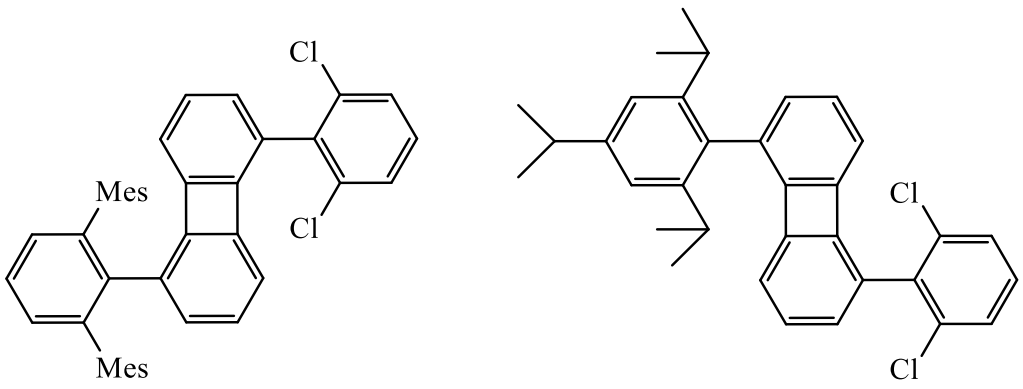

Figure 3·26. Potential asymmetrically substituted biphenylenes synthesised via the method that affords **III·36**.

There is potential to develop a simple biphenylene synthesis which allows the asymmetric substitution of the positions next to the butylene moiety. Complex **III·36** demonstrates this substitution pattern. It is possible that *via* the reaction of $[2,6\text{-}Dcp_2C_6H_3]^-$ with a halide bridged, dimeric species such as $[2,6\text{-}Mes_2C_6H_3Fe(\mu\text{-}Br)]_2{\cdot}[LiBr(OEt_2)]_2$ or $[TrippFeBr]_2$ the

substitution could be altered to afford complexes such as those shown in **Figure 3·26**. The ring opening, oxidative addition of metals to the biphenylene could be investigated to give access to asymmetrically bulky, chelating ligands.[295] Further reactivity with carbon monoxide could afford new, substituted fluorenones (**Figure 3·27**).

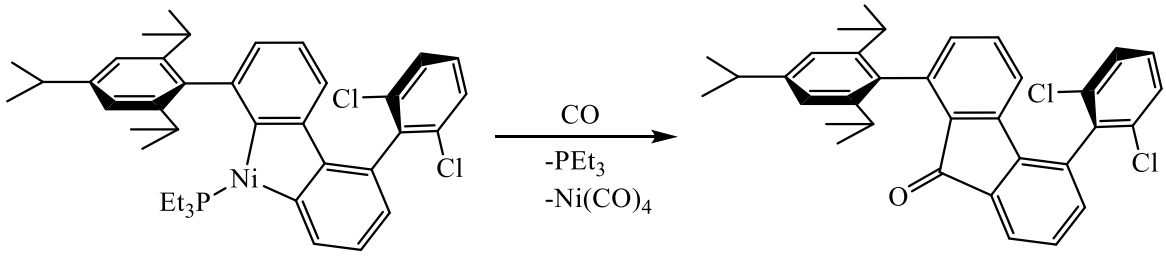

Figure 3·27. The result of addition of nickel(0) to the biphenylene (left) and the conversion of this product into a substituted fluorenone.

3.6 Experimental

3.6.1 Heteroleptic, Diaryl Complexes

3.6.1.1 [2,6-$Tmp_2C_6H_3$]Hg[2,6-$Ar_2C_6H_3$] Ar = Pmp (III·21), 2,6-Xyl (III·22), Dcp (III·23).

To a solution of 2,6-$Tmp_2C_6H_3HgBr$ (100 mg, 0.168 mmol) in toluene (10 mL) and THF (2 mL), cooled to 0°C, was added a solution of $[2,6\text{-}Ar_2C_6H_3Li]_2$ (0.168 mmol) in toluene (10 mL) and THF (2 mL) over 5 mins. The reaction was allowed to warm to room temperature over 16 hrs with stirring before all volatiles were removed *in vacuo*.

The off-white, impure solid [2,6-$Tmp_2C_6H_3$]Hg[2,6-$Pmp_2C_6H_3$] (**III·21**) was extracted into hexane (2 × 10 mL) to give a colourless solution. Storage of this solution at 7°C for 48 hrs afforded crystals of suitable quality for X-ray diffraction studies. 46%, 62 mg. ^{1}H NMR (C_6D_6, 400 MHz, 300 K) δ_H/ppm; 1.66 (s, 6H, *o*-CH_3 of Tmp), 1.76 (s, 6H, *m*-CH_3 of Tmp), 1.78 (s, 3H), 1.89 (s, 6H, *p*-CH_3 of Tmp), 2.13 (s, 6H, *m*-CH_3 of Pmp), 2.15 (s, 12H, *o*-CH_3 of Pmp), 2.18 (s, 6H, *m*-CH_3 of Pmp), 1.76 (m, broad, 6H) 2.27 (s, 6H, *p*-CH_3 of Pmp), 6.92 (s, 2H, *o*-H of Tmp), 6.94 (s, 2H, *m*-H of Tmp), 7.16 (m, 7H, *p*-H of both C_6H_3 and solvent). ^{13}C{^{1}H} NMR (C_6D_6, 100 MHz, 300 K) δ_C/ppm; 16.5 (CH_3), 16.6 (CH_3), 16.8 (CH_3), 17.0 (CH_3), 17.9 (CH_3), 18.3 (CH_3), 18.4 (CH_3), 18.9 (CH_3), 19.1 (CH_3), 19.17 (CH_3), 19.4 (CH_3), 19.8 (CH_3), 126.5 ($C_{Ar}H$), 127.0 ($C_{Ar}H$), 127.1 ($C_{Ar}H$), 127.3 ($C_{Ar}H$), 127.4 ($C_{Ar}H$), 127.6 ($C_{Ar}H$), 127.7 ($C_{Ar}H$), 130.5 ($C_{Ar}H$), 131.0 ($C_{Ar}H$), 131.0 (*q*-C_{Ar}), 131.5 ($C_{Ar}H$), 131.6 ($C_{Ar}H$), 131.7 (*q*-C_{Ar}), 132.8 (*q*-C_{Ar}), 133.0 (*q*-C_{Ar}), 133.1 (*q*-C_{Ar}), 133.1 (*q*-C_{Ar}), 133.3 (*q*-C_{Ar}), 134.5 (*q*-C_{Ar}), 134.8 (*q*-C_{Ar}), 170.8 (*q*-C_{Ar}), 171.8 (*q*-C_{Ar}), 172.9 (*q*-C_{Ar}), 173.3 (*q*-C_{Ar}). ^{199}Hg{^{1}H} NMR (C_6D_6, 71.7 MHz, 300 K) δ_{Hg}/ppm; −684.4, −702.0. Elemental analysis: [(2,6-$Tmp_2C_6H_3$)Hg(2,6-$Pmp_2C_6H_3$)] calcd. C 70.68, H 6.62; found C 70.57, H 6.55. TOF MS ASAP m/z (accurate mass); calcd. 881.4285, found 881.4293. ASAP-MS $[M]^+$ m/z: 885.4 [(2,6-$Tmp_2C_6H_3$)Hg(2,6-

$Pmp_2C_6H_3)]^+$ (100%), fragment ion peak: 371.3 $[(2,6\text{-}Pmp_2C_6H_3)]^+$ (60%), 313.2 $[(2,6\text{-}Tmp_2C_6H_3)]^+$ (7%).

The white, impure solid of $[2,6\text{-}Tmp_2C_6H_3]Hg[2,6\text{-}(2,6\text{-}Xyl)_2C_6H_3]$ (**III·22**) was extracted into warm hexane (10 mL) crystals suitable for X-ray analysis. 30%, 40 mg. ^1H NMR (C_6D_6, 400 MHz, 300 K) δ_H/ppm; 1.68 (s, 3H, Me^{42}), 1.77 (s, 6H, $Me^{33, 34}$), 1.86 (s, 6H, $Me^{11, 20}$), 1.89 (s, 3H, Me^{41}), 2.06 (s, 3H, Me^{13}), 2.10 (s, 6H, $Me^{12, 21}$), 2.14 (s, 3H, Me^{22}), 6.79 (s, 1H, $H_{Ar}{}^{10}$), 6.82 (s, 1H, H_{Ar} 19), 6.90 (s, 2H, $H_{Ar}{}^{16,7}$), 6.96 (s, 1H, $H_{Ar}{}^{25}$), 6.98 (s, 1H, $H_{Ar}{}^{37}$), 7.01 (s, 1H, $H_{Ar}{}^{25}$), 7.02 (s, 2H, $H_{Ar}{}^{31, 29}$) 7.06 (d, 1H, $H_{Ar}{}^{39}$, J = 2.5 Hz), 7.07 (m, 1H, $H_{Ar}{}^{38}$), 7.09, 7.10 (m, 1H, H_{Ar}) 7.12 (s, 1H, $H_{Ar}{}^{3}$), 7.15 (m, 1H, $H_{Ar}{}^{30}$). $^{13}C\{^1H\}$ NMR (C_6D_6, 100 MHz, 300 K): δ_C/ppm 19.7 ($Me^{12, 31}$), 19.9 (Me^{13}), 20.1 (Me^{22}), 20.6 ($Me^{11, 20}$), 21.2 ($Me^{33, 34, 41, 42}$), 21.2 ($Me^{33, 34, 41, 42}$), 127.1 ($C_{Ar}{}^{25}$) 127.2 ($C_{Ar}{}^{37}$), 127.6 ($C_{Ar}H^{39}$) 127.6 (C_{Ar}), 127.9 ($C_{Ar}H^{29,31}$), 127.9 ($C_{Ar}H^{30}$), 128.3 ($C_{Ar}{}^{36}$), 128.5 (q-C_{Ar}), 131.4 ($C_{Ar}H^{19}$) 131.6 ($C_{Ar}H^{10}$), 132.0 ($C_{Ar}H^{16,7}$), 132.2 (q-C_{Ar}), 133.5 (q-C_{Ar}), 133.6 (q-C_{Ar}), 133.8 (q-C_{Ar}), 133.8 (q-C_{Ar}), 136.2 (q-C_{Ar}), 136.5 (q-C_{Ar}), 136.7 (q-C_{Ar}). $^{199}Hg\{^1H\}$ NMR (C_6D_6, 71.67 MHz, 300 K) δ_{Hg}/ppm; −682.3, −662.5. Elemental analysis: $[(2,6\text{-}Tmp_2C_6H_3)Hg(2,6\text{-}(2,6\text{-}Xyl)_2C_6H_3)]$ calcd. C 69.11, H 5.80; found C 70.68, H 5.67.

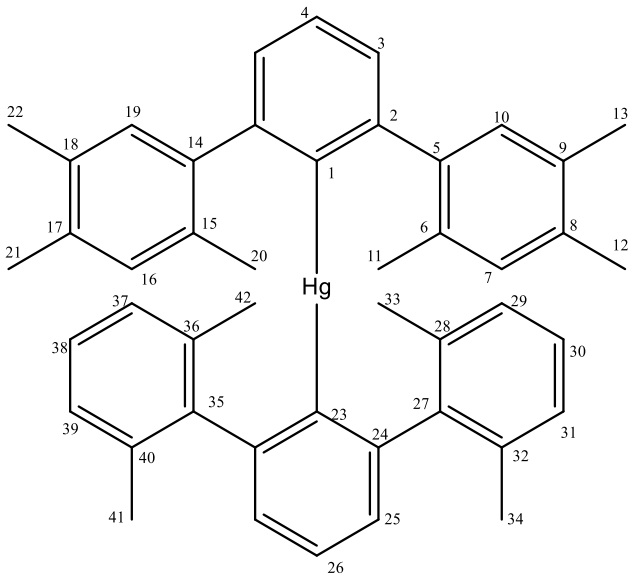

The beige, impure solid of [2,6-$Tmp_2C_6H_3$]Hg[2,6-$Dcp_2C_6H_3$] (**III·23**) was extracted into toluene (10 mL) to give a golden solution. Storage of this solution at −30°C for three days afforded a single crystal of suitable quality for X-ray diffraction studies.

3.6.1.2 [2,6-$Mes_2C_6H_3$]Hg[2,6-$Pmp_2C_6H_3$] (III·24)

[2,6-$Pmp_2C_6H_3Li]_2$ (129 mg, 0.171 mmol) and [2,6-$Mes_2C_6H_3$]HgBr (**II·43**, 100 mg, 0.169 mmol) were combined and the mixture dissolved in toluene (20 mL) and THF (5 mL) at room temperature to give an off-white solution. The reaction was stirred for 16 hrs before all volatiles were removed *in vacuo* to afford a yellow solid. The solid was extracted into hexane (3 × 10 mL) and the colourless solution stored at 7°C for 24 hrs to afford crystals of sufficient quality for X-ray diffraction studies. 17%, 50 mg. ^{1}H NMR (C_6D_6, 400 MHz, 300 K) δ_H/ppm; 1.74 (s, 12H, *o*-CH_3 of Pmp), 1.84 (s, 12H, *o*-CH_3 of Mes), 2.16 (s, 6H, *p*-CH_3 of Mes), 2.24 (s, 12H, *m*-CH_3 of Pmp), 2.25 (s, 6H, *p*-CH_3 of Pmp), 6.89 (s, 4H, *m*-H of Mes), 6.96 (d, 2H, J = 7.83 Hz, *m*-H of C_6H_3), 7.02 (d, 2H, J = 7.96 Hz, *m*-H of C_6H_3) 7.22 (m, 2H, *p*-H of both C_6H_3). ^{13}C{^{1}H} NMR (C_6D_6, 100 MHz, 300 K) δ_C/ppm; 16.42 (CH_3), 16.75 (CH_3), 18.0 (CH_3), 20.2 (CH_3), 20.85 (CH_3), 126.6 ($C_{Ar}H$), 127.0 ($C_{Ar}H$), 128.1 ($C_{Ar}H$), 128.9 ($C_{Ar}H$), 131.0 (*q*-C_{Ar}), 131.2 (*q*-C_{Ar}), 131.5 (*q*-C_{Ar}), 131.8 (*q*-C_{Ar}), 133.3 (*q*-C_{Ar}), 135.6 (*q*-C_{Ar}), 141.8 (*q*-C_{Ar}), 141.8 (*q*-C_{Ar}), 142.5 (*q*-C_{Ar}), 143.8 (*q*-C_{Ar}), 148.5 (*q*-C_{Ar}), 150.4 (*q*-C_{Ar}). ^{199}Hg{^{1}H} NMR (C_6D_6, 71.7 MHz, 300 K) δ_{Hg}/ppm; −697.3. ASAP-MS $[M]^+$ *m/z*: 884.6 [(2,6-$Mes_2C_6H_3$)Hg(2,6-$Pmp_2C_6H_3$)]$^+$ (15%), fragment ion peak: 368.3 [(2,6-$Pmp_2C_6H_3$)]$^+$ (100%), 312.2 [(2,6-$Mes_2C_6H_3$)]$^+$ (25%).

3.6.1.3 [2,6-$Dcp_2C_6H_3$]M[2,6-$Mes_2C_6H_3$] M = Mn (III·30), Zn (III·31).

To a solution of MX_2 (**III·30**: $MnBr_2$: 65 mg, 0.302 mmol, **III·31**: ZnI_2, 100 mg, 0.313 mmol) in toluene (20 mL) and THF (10 mL), cooled to −78°C, was added a solution of [2,6-$Dcp_2C_6H_3Li]_2$ (100 mg, 0.134 mmol) in toluene (20 mL) and THF (5 mL) dropwise

over 15 mins. The reaction was allowed to warm to room temperature with stirring over 16 hrs. The solvent was removed *in vacuo* to give a yellow oil which was extracted into toluene (2 × 10 mL), leaving behind a solid. Removal of all volatiles *in vacuo* from the toluene fraction afforded an oil to which [2,6-$Mes_2C_6H_3Li]_2$ (88 mg, 0.137 mmol) was added. Toluene (20 mL) and THF (5 mL) were added to the solid. The reaction was stirred at room temperature for a further 16 hrs. All volatiles were removed *in vacuo* to give an oil. Trituration with hexane (10 mL) afforded an off-white powder which was extracted into toluene (2 × 10 mL).

The golden brown solution of [2,6-$Mes_2C_6H_3$]Mn[2,6-$Dcp_2C_6H_3$] (**III·30**) was reduced in volume by one half and stored at −30°C for 5 d to give a small number of golden brown crystals of suitable quality for X-ray diffraction studies. Sufficient compound for further analysis could not be isolated.

The colourless solution of [2,6-$Mes_2C_6H_3$]Zn[2,6-$Dcp_2C_6H_3$] was cooled to 7°C for 5 d to give small crystals of [2,6-$Mes_2C_6H_3$]Zn[2,6-$Dcp_2C_6H_3$] amongst a glassy solid. A yield could not be determined. The crystals were of suitable quality for X-ray diffraction studies.

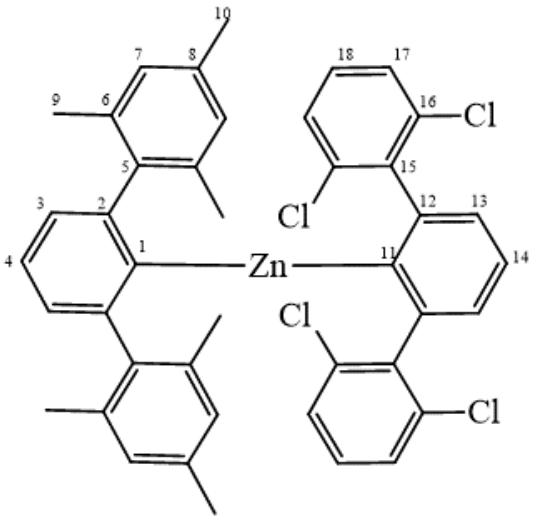

^{1}H NMR (C_6D_6 , 400 MHz, 300 K) δ_H/ppm; 1.80 (s, 2 H), 2.08 (s, 12H, Me^{10}), 2.22 (s, 6H, Me^{9}), 6.54 (t, 2H, H_{Ar}^{18}, *J* = 8.04 Hz), 6.77 (t, 1H, H_{Ar}^{14}, *J* = 1.32 Hz), 6.86 (m, 1H, H_{Ar}^{4}, *J* = 1.17 Hz), 6.87 (s, 4H, H_{Ar}^{7}), 7.00 (d, 1H, *J* = 1.75), 7.02 (d, 1H, *J* = 1.61 Hz), 7.02 (d, 4H, H_{Ar}^{17}, *J* = 1.75 Hz), 7.09 (dd, 1H, *J* = 0.73, *J* = 1.02 Hz) 7.11 (d, 1H, *J* = 1.75 Hz) 7.24 (d, 1H, *J* = 7.31 Hz). ^{13}C{^{1}H} NMR (C_6D_6, 100 MHz, 300 K) δ_C/ppm; 21.3 (CH_3^{10}), 21.5 (CH_3^{9}), 128.1 (C_{Ar}), 128.5 (C_{Ar}), 128.8 (C_{Ar}), 129.6 (C_{Ar}), 129.8 (C_{Ar}), 131.1 (C_{Ar}), 131.6 (C_{Ar}), 135.8 (C_{Ar}), 136.1 (C_{Ar}), 136.8 (C_{Ar}), 137.7 (C_{Ar}), 139.8 (C_{Ar}), 142.3 (C_{Ar}). EI-MS: [2,6-$Mes_2C_6H_3$]Zn[2,6-$Dcp_2C_6H_3$] (calcd: 744.07) m/z 744.2 (M+).

3.6.2 Scrambling Experiments

3.6.2.1 [2,6-$Mes_2C_6H_3$]$_2$Cd (III·32)

[2,6-$Mes_2C_6H_3Li$]$_2$ (100 mg, 0.156 mmol) was dissolved in toluene (10 mL) and THF (3 mL) and added dropwise to a solution of $CdCl_2$ (29 mg, 0.158 mmol) in toluene (10 mL) and THF (0.3 mL) cooled to −78°C. The solution was allowed to warm to room temperature with stirring over 16 hrs. All volatiles were removed *in vacuo* to afford a white solid. This solid was extracted into hexane (1 × 3 mL) and the resulting colourless solution was stored at −30°C for three days to afford colourless crystals of suitable quality for X-ray diffraction studies. ^{1}H NMR (C_6D_6, 400 MHz, 300 K) δ_H/ppm; 1.81 (*s*, 24H, *o*-CH_3), 2.20 (*s*, 12H, *p*-CH_3), 6.85 (*s*, 8H, *m*-H of Mes), 6.92 (*d*, *J* = 7.50 Hz, 4H, *m*-CH of C_6H_3), 7.17 (*t*, *J* = 7.35 Hz, 2H, *p*-H of C_6H_3). ^{13}C{^{1}H} NMR (C_6D_6, 100 MHz, 298 K) δ_C/ppm; 20.9 (*p*-CH_3), 21.01 (o-CH_3), 125.2 (*m*-CH of central aryl), 128.5 (C_{Ar}H of flanking group), 135.5 (*q*-C_{Ar} of flanking group), 135.79 (*o*-C_{Ar} of central aryl), 144.0 (*q*-C_{Ar} of Mes), 149.4 (*i*-C of flanking group), 162.6 (*i*-C of C_6H_3). ^{113}Cd{^{1}H} NMR (C_6D_6, 88.9 MHz, 300 K) δ_{Cd}/ppm; 401.0.

3.6.2.2 [2,6-$Dipp_2C_6H_3$]$_2$Cd (III·33)

To a solution of [2,6-$Dipp_2C_6H_3Cd(\mu\text{-}I)]_2[LiI(OEt_2)]_2$ (30 mg, 0.0178 mmol), synthesised *via* literature procedures,[169] in C_6D_6 (0.7 mL) was added $[Dipp_2C_6H_3Li]_2$ (20 mg, 0.0247 mmol) and THF (0.1 mL). The colourless solution was sonicated for 5 mins and stood at room temperature for 16 hrs. Following this ^{1}H and ^{113}Cd{^{1}H} data were collected. Crystals were grown by vapour diffusion of pentane into the filtered reaction mixture over 5 d, followed by storage at −30°C for *ca*. 50 d. 7%, 3 mg. ^{1}H NMR (C_6D_6, 400 MHz, 300 K) δ_H/ppm; 1.13 (*t*, *J* = 7.5 Hz, 2H, CH_3 of Et_2O) 1.20 (*d*, *J* = 7.0 Hz, 12H), 1.25 (*d*, *J* = 7.0 Hz, 6H), 1.50 (*m*, CH_2 of THF), 1.67 (*d*, *J* = 6.7 Hz, 9 H), 3.39 (*sept*, *J* = 7.4 Hz, 4H, CH of *i*Pr), 3.57 (*m*, OCH_2 of THF), 7.20 (*m*, 2H), 7.23 (*m*, 2H) 7.31 (*s* (br), 5H), 7.36 (m, 2H). ^{113}Cd{^{1}H} NMR (C_6D_6, 88.9 MHz, 300 K) δ_{Cd}/ppm; 356.2.

3.6.2.3 [2,6-$Mes_2C_6H_3$]Cd[2,6-$Dipp_2C_6H_3$]

To a solution of $[Dipp_2C_6H_3CdI]_2[LiI(OEt_2)]_2$ synthesised via literature procedures (30 mg, 0.0235 mmol) in C_6D_6 (0.7 mL) and THF (0.05 mL) was added $[2,6\text{-}Mes_2C_6H_3Li]_2$ (20 mg, 0.0247 mmol). The colourless solution was sonicated for 5 mins stood at room temperature for 16 hrs. Following this ^{113}Cd NMR data was collected. ^{113}Cd{^{1}H} NMR (C_6D_6, 88.9 MHz, 300 K) δ_{Cd}/ppm; 401.1, 356.2, 336.3.

3.6.2.4 [2,6-$Mes_2C_6H_3$]$_2$Cd + [2,6-$Pmp_2C_6H_3$]$_2$Cd

$[2,6\text{-}Mes_2C_6H_3]_2Cd$ (20 mg, 0.0271 mmol) and $[(2,6\text{-}Pmp_2C_6H_3)_2Cd]$ (20 mg, 0.0234 mmol) were combined and dissolved in C_6D_6 (*ca.* 0.7 mL). The solution was heated to 50°C for 24 hrs after which time ^{1}H, ^{13}C{^{1}H} and ^{113}Cd{^{1}H} NMR spectra were collected. ^{1}H NMR (C_6D_6, 400 MHz, 300 K) δ_H/ppm; 1.81 (m, *o*-CH_3 of Mes, *o*-CH_3 of Pmp), 2.16 (s, *p*-CH_3 of Mes), 2.20 (s, *m*-CH_3 of Pmp), 2.25 (s, *p*-CH_3 of Pmp), 6.85 (s, *m*-CH of Mes), 6.92 (d, *J* = 7.49 Hz, *m*-CH of C_6H_3 of Mes), 6.93 (d, *J* = 7.47 Hz, *m*-CH of C_6H_3 of Pmp), 7.17 (m, *p*-CH of C_6H_3 of

Pmp and Mes). $^{13}C\{^{1}H\}$ NMR (C_6D_6, 100 MHz, 300 K) δ_C/ppm; 16.5 (*p*-CH_3 of Pmp), 17.0 (*m*-CH_3 of Pmp), 17.8 (*o*-CH_3 of Pmp), 20.9 (*p*-CH_3 of Mes), 21.0 (*o*-CH_3 of Mes), 125.0 (*m*-CH of C_6H_3 of Mes), 125.7 (*m*-CH of C_6H_3 of Pmp), 128.5 (*m*-CH of Mes), 131.07 (*quaternary*-C_{Ar} of Pmp), 131.7 (*quaternary*-C_{Ar} of Pmp), 133.4 (*quaternary*-C_{Ar} of Pmp), 135.5 (*quaternary*-C_{Ar} of Mes), 135.8 (*o*-C of C_6H_3 of Mes), 144.0 (*quaternary*-C_{Ar} of Mes), 149.4 (*i*-C of Mes), 162.6 (*i*-C of C_6H_3 of Mes). $^{119}Cd\{^{1}H\}$ NMR (C_6D_6, 88.8 MHz, 300 K) δ_{Cd}/ppm; 399.25, 390.92.

3.6.2.5 [2,6-Pmp$_2$C$_6$H$_3$]$_2$Cd + [2,6-Mes$_2$C$_6$H$_3$Li]$_2$

[2,6-Pmp$_2$C$_6$H$_3$]$_2$Cd (21.3 mg, 0.0251mmol) was dissolved in C_6D_6 (*ca.* 0.7 mL). [2,6-Mes$_2$C$_6$H$_3$Li]$_2$ (17.04 mg, 0.0266 mmol) was dissolved in C_6D_6 (*ca.* 0.7 mL). The two solutions were combined and analysed *via* NMR at time (t) = 1.5 hrs, 27 hrs, 6 days, and 9 days.

1.5 hrs: ^{1}H NMR (C_6D_6, 400MHz, 298K) δ_H/ppm; 1.82 (s, 24H, *o*-CH_3 of Mes), 1.83 (s, 24H, *o*-CH_3 of Pmp), 2.16 (s, 12H, *p*-CH_3 of Pmp), 2.18 (s, 12H, *p*-CH_3 of Mes), 2.25 (s, 24H, *m*-CH_3 of Pmp), 6.84 (s, 8H, *m*-CH of Mes), 6.93 (d, J = 7.45 Hz, 4H, *m*-CH of C_6H_3), 7.19 (t, J = 7.4 Hz, 2H, *p*-CH of C_6H_3 of Mes), 7.24 (t, J = 7.4 Hz, 2H, *p*-CH of C_6H_3 of Pmp).

The ^{1}H NMR spectrum was no different at 27 hrs, 6 d, and 9 d.

3.6.3 [2,6-Dcp$_2$C$_6$H$_3$]$^-$ Complexes

3.6.3.1 [2,6-Dcp$_2$C$_6$H$_3$]$_2$Mn (III·35)

Toluene (30 mL) and THF (5 mL) were added to a mixture of [2,6-Dcp$_2$C$_6$H$_3$Li]$_2$ (200 mg, 0.267 mmol) and $MnBr_2$ (57 mg, 0.265 mmol) to give a golden coloured solution which was stirred at room temperature for 72 hrs. Following this, all volatiles were removed *in vacuo* and the remaining off-white solid was extracted into toluene (2 × 10 mL). The solution was concentrated by half and stored for seven days at 7°C to afford clear, off-white crystals suitable for X-ray diffraction studies. 79 mg, 37 %. A second polymorph was obtained by growing

crystals through vapour diffusion of pentane into a C_6D_6/phenylacetylene/phenyl isocyanate mixture. ^{1}H NMR (400 MHz, C_6D_6, 300 K) δ_H / ppm; −0.96 (br, $\Delta\nu$½ = 2546 Hz), 0.86 (br, s), 1.11 (br, s), 1.47 (br, s), 2.49 (s), 6.55 (br, s), 6.86 (br, s), 7.03 (br, s), 7.70 (br, s, $\Delta\nu$½ = 1785 Hz), 37.17 (br, s, $\Delta\nu$½ = 4605 Hz). μ_{eff} = 5.74 μ_B. EI MS: [2,6-Dcp$_2$C$_6$H$_3$]$_2$Mn *m/z* (%) = 785.0 (7%) [M$^+$], *coupled ligand* 659.0 (11%) [M(c)−Cl$^+$], 622.6 (4%) [M[c]−2Cl$^+$], 590.2 (14%) [M[c]−4Cl$^+$], 554.20 (13%) [M[c]−5Cl$^+$], 520.1 (11%) [M[c]−6Cl$^+$], 484.2 (9%) [M[c]−7Cl$^+$], 450.2 (5%) [M[c]−8Cl$^+$], *ligand* 366.0 (100%) [L$^+$], 330.0 (39%) [L-Cl$^+$], 296.1 (37%) [L-2Cl$^+$], 260.1 (76%) [L-3Cl$^+$], 223.1 (56%) [L-4Cl$^+$]. Elemental analysis $C_{36}H_{18}Cl_8Mn$ calcd: C 54.80, H 2.30; found C 54.67, H 2.14.

3.6.3.2 1-[2,6-Dcp$_2$C$_6$H$_3$]-7-DcpC$_{12}$H$_6$ (III·36)

Toluene (30 mL) and THF (5 mL) were added to a mixture of [2,6-Dcp$_2$C$_6$H$_3$Li]$_2$ (197 mg, 0.263 mmol) and $FeCl_2(THF)_{1.5}$ (53 mg, 0.225 mmol) to give a yellow solution which was stirred at room temperature for 24 hrs during which time a significant amount of pale yellow precipitate formed. All volatiles were removed *in vacuo* and the remaining cream solid was extracted into toluene (2 × 10 mL). The solution was concentrated by half and stored for seven days at −30°C to afford clear, colourless crystals, of suitable quality for X-ray diffraction studies, amongst a yellow powder.

Alternative workup: Following the stirring of the reaction at room temperature for 24 hrs, diiodine (320 mg, 1.26 mmol) was added to give a purple solution. The solution was then washed with $NaSO_3$ solution (5% w/w, 50 mL) and extracted into dichloromethane (3 × 100 mL). The organic washings were combined and washed with deionised water (2 × 100 mL) and brine (1 × 100 mL) before being dried over $MgSO_4$. All volatiles were removed in vacuo to afford an oil. Addition of petroleum (fraction 60-80) (10 mL) caused an off-white solid to

precipitate. The solid was isolated and recrystallised from hot dichloromethane. Storage at 7°C for 48 hrs afforded pale yellow crystals. 400 mg, 90%.

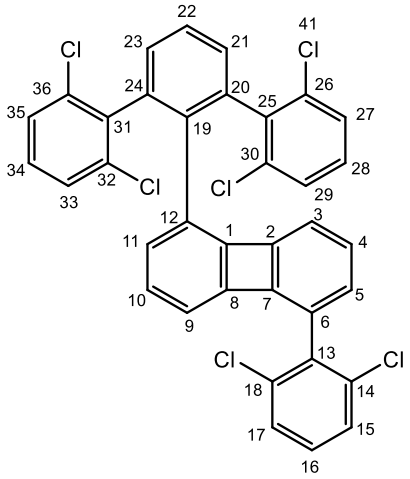

^{1}H NMR (400 MHz, C_6D_6, 300 K) δ_H/ppm; 5.85 (1H, d, *J* = 6.3 Hz, CH^{5}), 6.22 (1H, dd, *J* = 6.6 Hz, *J* = 1.1 Hz, CH^{5}), 6.36 (2H, t, *J* = 8.1 Hz, $CH^{28,34}$), 6.43 (1H, d, *J* = 8.1 Hz, CH^{16}), 6.55 (1H, d, *J* = 8.1 Hz, CH^{11}), 6.62 (1H, dd, *J* = 8.4 Hz, *J* = 6.7 Hz, CH^{10}), 6.80 (2H, d, *J* = 8.1 Hz, $CH^{35,27}$), 6.87 (2H, d, *J* = 8.1 Hz, CH^{5}), 6.89 (1H, d, *J* = 7.0 Hz, CH^{9}), 6.93 (2H, d, *J* = 8.2 Hz, $CH^{15,17}$), 7.05 (1H, d, *J* = 8.3 Hz, CH^{3}), 7.18 (2H, d, *J* = 8.4 Hz, $CH^{21,23}$), 7.24 (1H, d, *J* = 8.6 Hz, CH^{22}). ^{13}C{^{1}H} NMR (C_6D_6, 100 MHz, 300 K) δ_C/ppm; 117.04 ($C^{5}H$), 119.72 ($C^{9}H$), 125.59 (*q*-C_{Ar}) 127.09 ($C^{4}H$), 127.84 ($C^{10}H$), 128.17 (CH), 128.24 (CH), 128.36 (CH), 129.08 (*q*-C_{Ar}), 129.16 ($C^{16}H$), 129.23 ($C^{34,28}H$), 129.78 ($C^{11}H$), 130.83 ($C^{23}H$), 131.73 ($C^{3}H$), 135.15 (*q*-C_{Ar}), 135.43 (*q*-C_{Ar}), 135.68 (*q*-C_{Ar}), 136.25 (*q*-C_{Ar}), 137.48 (*q*-C_{Ar}), 138.29 (*q*-C_{Ar}), 139.04 (*q*-C_{Ar}), 150.21 (*q*-C_{Ar}^{8}), 150.33 (*q*-C_{Ar}^{7}), 151.67 (*q*-C_{Ar}^{9}), 151.67 (*q*-C_{Ar}^{1}). ASAP MS (accurate mass): $C_{36}H_{18}C_{l6}$ calculated 659.9550, found 660.9606 $[M+H]^+$. EI-MS 664.1 $[M]^+$ (3%), 503.2 (10%) $[M – Dcp – CH]^+$, 429.2 (12%) $[M – Dcp – C_6H_4 – CH]^+$, 368.0 (40%) $[2,6\text{-}Dcp_2C_6H_3]^+$, 281.1 (55%) $[M – 2\ Dcp – C_4H_3 – Cl]$, 207.0 (100%) $[M – 2,6\text{-}Dcp_2C_6H_3 – Dcp + Fe]^+$, 147.0 (12%) $[Dcp + H]^+$, 72.8 (22%) *potential impurity*. Elemental analysis $C_{36}H_{18}Cl_6$ calcd. C 65.19, H 2.74; found C 64.97, H 2.54.

3.6.3.3 [2-{2,6-(Dcp$_2$C$_6$H$_3$)$_2$C$_6$H$_3$}-6-DcpC$_6$H$_3$]CoBr (III·37)

Toluene (30 mL) and THF (5 mL) were added to a mixture of [2,6-Dcp$_2$C$_6$H$_3$Li]$_2$ (200 mg, 0.267 mmol) and CoBr$_2$(DME) (80 mg, 0.259 mmol) to give a blue solution, which was stirred at room temperature for 24 hrs. During this time the colour of the solution changed to deep green and a colourless precipitate formed. The product was filtered and the solvent subsequently removed *in vacuo*. The resulting green solid was extracted into toluene (3 × 10 mL) and the resulting green solution concentrated by half. Storage of this solution for *ca*. 60 d at −30°C resulted in a small amount of clear, red crystals of suitable quality for X-ray diffraction studies. Two polymorphs were obtained. Attempts to produce larger amounts of this product were unsuccessful.

Chapter IV

The Development of Heteroleptic Complexes Stabilised by *m*-Terphenyl and N-Heterocyclic Carbene Ligands

4.1 Introduction

Two-coordinate, heteroleptic, 3d metal complexes featuring an NHC ligand have been reported in the past decade. With the exception of species featuring metal–metal bonds,[62,169,171,177] the metals involved are limited to iron,[121,125] cobalt[53,125,126,129] and nickel.[138,140,296,297] Two-coordinate, monomeric manganese(I) complexes are currently not present in the literature. Significant examples are the previously discussed cobalt complexes, [NHC]Co[N(2,6-$Mes_2C_6H_3$)] [NHC = IPr (**I·95**), CyIPr (**I·99**) or sIMes (**I·100**)], reported by Deng *et al.*[124,133] and the nickel imido complexes [IPr]Ni[N($SiMe_3$)$_2$] (**I·67**) and [IPr]Ni[NHDipp] (**I·68**) reported by Hillhouse and co-workers.[138]

A notable development in this field was the synthesis by Hillhouse *et al.* of [Ipr*]Ni^0[N(2,6-$Mes_2C_6H_3$)] [**IV·1**, IPr* = 1,3-bis(2,6-bis(diphenylmethyl)-4-methylphenyl)imidazole-2-ylidene)],[296] a two-coordinate nickel(0) imido complex. The high steric demands of the IPr* ligand stabilised a masked nickel(0) complex, [IPr*]Ni^0[η^6-Tolyl], which was then reacted with

2,6-$Mes_2C_6H_3N_3$ to afford **IV·1** with the loss of dinitrogen (**Scheme 4·**1). The magnetic moment (2.77 μB) is indicative of a high spin, linear, d^8 species. The geometry around the metal centre is pseudo-linear with a C−Ni−N angle of 174.24(13)°, and the Ni−N bond is short at 1.663(3) Å [Ni-N in Ni[NMes{$BMes_2$}] (**I·15**) = 1.865(2) and 1.867(2) Å].

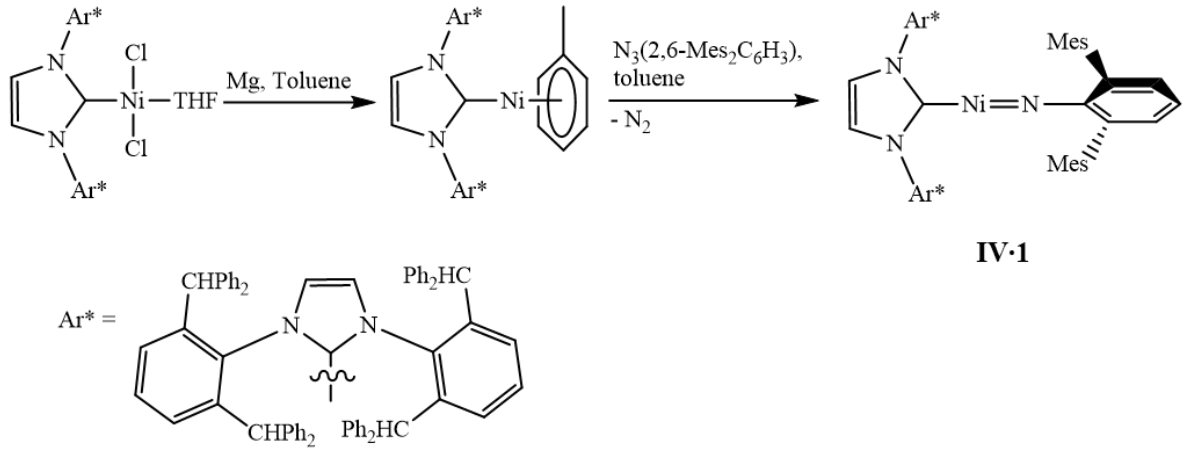

IV·1

1,3-bis(2,6-bis(diphenylmethyl)-4-methylphenyl)imidazol-2-ylidene

Scheme 4·1.The synthetic route to [Ipr^*]Ni^0[N(2,6-$Mes_2C_6H_3$)] [**IV·1**, IPr^* = 2,4-bis(2,6-bis(diphenylmethyl)-4-methylphenyl)imidazole-2-ylidene)].[140]

The same group later reported the two-coordinate complexes [IPr]Ni^I[$CH(SiMe_3)_2$] (**IV·2**) and [IPr]Ni^I[2,6-$Mes_2C_6H_3$] (**IV·3**).[140] The complexes were synthesised through the reaction of $ClMgCH(SiMe_3)_2$ or [2,6-$Mes_2C_6H_3Li]_2$, respectively, with Sigman's dimer [$(IPrNiCl)_2$, **Scheme 4·2**].[139] These complexes were the first examples of two-coordinate nickel alkyl and aryl complexes.[12]

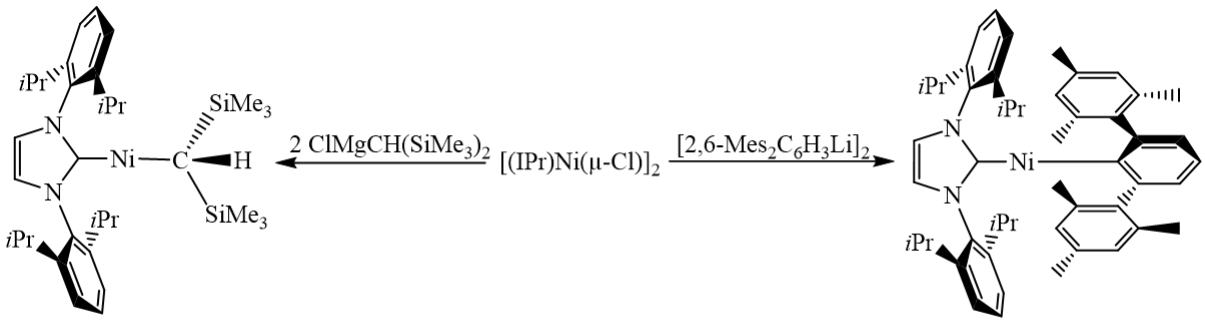

IV·2 **IV·3**

Scheme 4·2. The synthetic route to [IPr]Ni^I[$CH(SiMe_3)_2$] (**IV·2**) and [IPr]Ni^I[2,6-$Mes_2C_6H_3$] (**IV·3**).

IV·2 was found to couple primary and secondary alkyl halides such as 2-bromopropane in stoichiometric amounts. However, 1,1,2,2-$(SiMe_3)_4C_2$ and other compounds featuring a

coupled unit of the $[CH(SiMe_3)_2]^-$ ligand were also isolated from the reactions. **IV·3** is similar in structure to the target complexes of the work detailed below. Starting materials equivalent to Sigman's dimer, featuring manganese(I), iron(I) and cobalt(I), are less available.

Tilley *et al*. overcame the lack of an appropriate Fe(I) starting material in the synthesis of $[IPr]Fe^{I}[N(SiMe_3)(Dipp)]$ (**I·53**) *via* the *in situ* reduction of $[IPr]Fe^{I}Cl[N(SiMe_3)(Dipp)]$.[121] This was in turn produced through protonation of $[N(SiMe_3)(Dipp)]_2Fe^{II}$ using one equivalent of triethylamine hydrochloride followed by the introduction of the IPr ligand (**Scheme 4·3**).

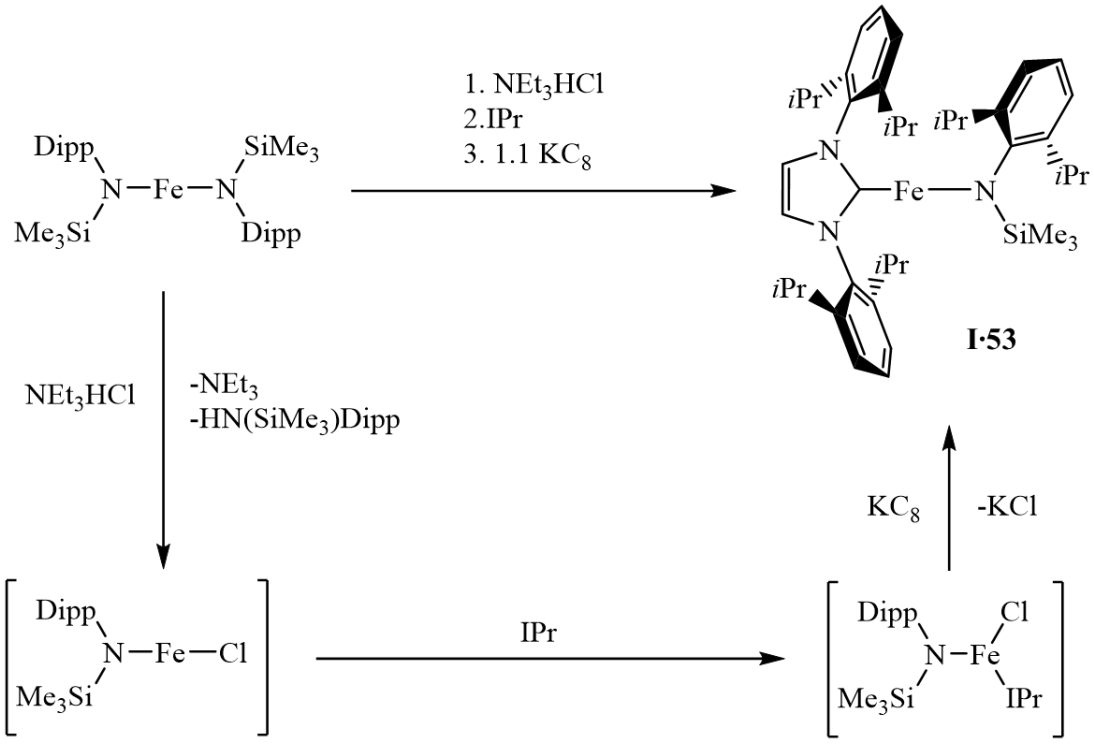

Scheme 4·3. The synthetic route affording $[IPr]Fe^{I}[N(SiMe_3)(Dipp)]$ (**IV·3**), along with the mechanism as proposed by the authors.

I·53 possesses a linear geometry [N−Fe−C = 176.94(6)°]. The authors suggest this geometry contributes to the magnetic moment of 5.0 μ_B found for the complex, which is greater than the spin-only value (3.87 μ_B). They tested this theory by coordinating one equivalent of XylNC to **I·53**. The magnetic moment of the resulting, three-coordinate species is significantly depressed to 4.1 μ_B.

I·53 was found to be an effective catalyst for the cyclotrimerisation of alkenes, both internal and terminal, at loadings of 2-5 mol%. The utility of this catalyst did not, however expand to alkynes bearing electron poor substituents.

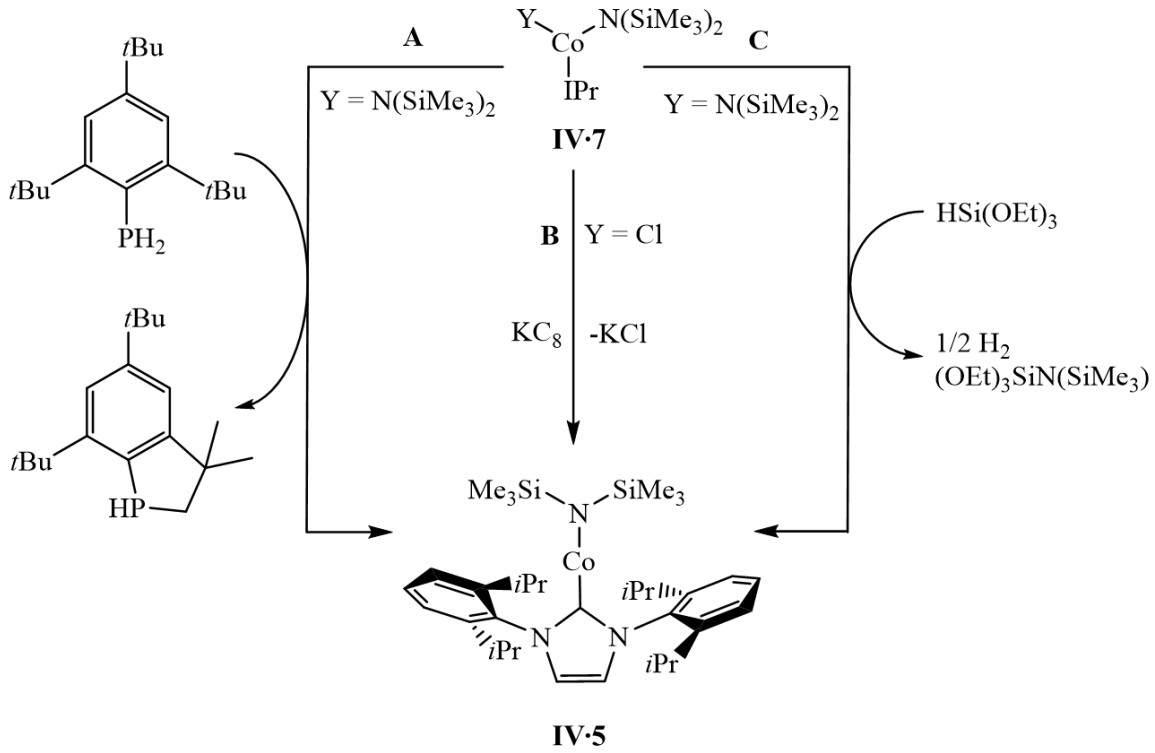

Scheme 4·4. Synthetic routes to **IV·5**. **A** and **B** were developed by Frison et al.,[18] **C** by Deng and co-workers.[130,298]

[IPr]Fe^{I}[$N(SiMe_3)$]$_2$ (**IV·4**) and the cobalt analogue [IPr]Co^{I}[$N(SiMe_3)$]$_2$ (**IV·5**, **Scheme 4·4**) were isolated by Frison *et al*. using a similar method to Tilley and co-workers. The complexes were synthesised through the reduction of the [IPr]M^{II}Cl[$N(SiMe_3)_2$] [M = Fe (**IV·6**) and Co (**IV·7**, **Scheme 4·4**, **B**)][130,298] with KC_8 afforded the target complexes. The authors found that the use of two equivalents of KC_8 in the reduction of **IV·6** afforded [(IPr)Fe^{0}(η^2-Tolyl)]$_2$[K(N{$SiMe_3$})]$_2$.

The yield of **IV·5** was improved through the reduction of **IV·7** with one equivalent of $Mes^{*}PH_2$ (**Scheme 4·4**, **A**). The same reaction with **IV·6** resulted in the IPr ligand adopting the abnormal bonding mode. Deng *et al*. isolated **IV·5** in the same year as Frison *et al*. *via* the reduction of

[IPr]$Co^{II}[N(SiMe_3)]_2$ using $HSi(OEt)_3$ (**Scheme 4·4**, **C**). Both alternative methods to reduction with KC_8 involve the concomitant formation of dihydrogen.

[IPr]$Fe[N(SiMe_3)_2]$ (**IV·4**) and [IPr]$Co^{I}[N(SiMe_3)]_2$ (**IV·5**) were also reported by Danopoulos and co-workers.[125] Both **IV·4** and **IV·5** have linear structures [C−M−C = 178.2(2)° (**IV·4**), 178.83(7)° (**IV·5**)] and the magnetic moments of these complexes are significantly higher than expected at 5.92 μ_B (**IV·4**) and 6.25 μ_B (**IV·5**). In the case of the latter, Danopoulos and co-workers note that 6.25 μ_B is higher than the value for the free d^8 ion (5.59 μ_B), the upper magnetic limit for the ion. Therefore **IV·5** cannot be a high spin cobalt(I) complex. A similar conclusion, that it cannot be an Fe(I) ion, is reached regarding **IV·4**, although the magnetic moment of this species is below that of the free-ion value (6.63 μ_B). The authors proposed that the electronic configuration is instead a metal(II) centre interacting with a single electron delocalised onto the NHC ligand and a range of experimental (XPS, XANES, EXAFS) and computational techniques were used to support this proposal. It is argued that the high energy of 3d metal orbitals, together with the low coordination number and weak ligand field could bring the metal and ligand orbitals closer in energy and promote non-innocent behaviour of the NHC. These observations are a radical contribution to the field of single molecule magnets and the ramifications for complex design have yet to be observed.

Another method of isolating a two-coordinate, heteroleptic cobalt complex, stabilised by an NHC, was developed by Jones and Hicks.[53] The method involves the isolation of [(2,6-$\{CHPh_2\}_2$-4-MeC_6H_3)$(SiPh_3)$N]Co[η^6-C_6H_6] (**IV·8**), a cobalt(I) species stabilised by an extremely bulky amide ligand and a masking, η^6-arene ligand, through the reduction of a halide bridged, dimeric starting material with KC_8. **IV·8** is then exposed to one equivalent of IPrMe to afford the two-coordinate complex [(2,6-$\{CHPh_2\}_2$-4-MeC_6H_3)$(SiPh_3)$N]Co[IPrMe] (**IV·9**, **Figure 4·1.** The two-coordinate isomer of **IV·9.**).

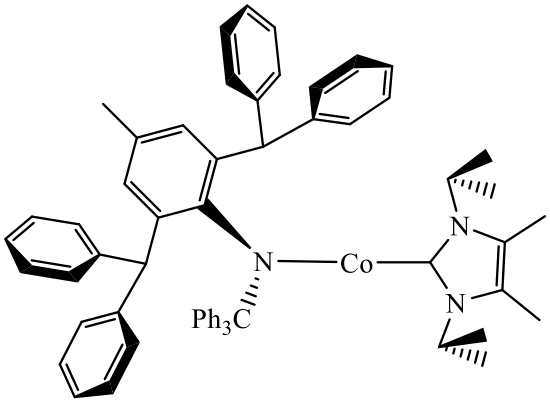

Figure 4·1. The two-coordinate isomer of **IV·9**.

This complex is the first example of a neutral, two-coordinate, cobalt(I) complex. Jones and Hicks also found that by changing the solvent from which crystals of **IV·9** were grown, two structural isomers could be obtained. Using pentane as the crystallisation solvent induced the formation of the two-coordinate species described above, whilst using diethyl ether induced the formation of an isomer that featured a secondary, η^6-interaction between the cobalt and a flanking phenyl group. The authors note that both isomers afford identical ^{1}H NMR spectra, suggesting that they converge structurally in solution. The two-coordinate isomer of **IV·9** (**Figure 4·1.** The two-coordinate isomer of **IV·9.**) is close to linear along the C–Co–N axis [175.2(1)°]. Unlike **IV·5**, the magnetic moment of **IV·9** (2.6 μ_B) is lower than the spin only value (2.83 μ_B).

The above examples represent several methods of synthesising two-coordinate, heteroleptic, 3d metal complexes supported by an NHC ligand. The synthesis of the imido complexes relies on the oxidation of a suitable metal(0) complex with bulky organo-azide reagents. Other nickel complexes have made use of Sigman's dimer as a starting material. As this is not available for iron and cobalt complexes, researchers have adopted two alternative methods; either a three-coordinate starting material bearing two amide ligands is reduced with concomitant protonation of one of the amide ligands or a suitable halogen bearing metal(II) complex is reduced with a

Group 1 metal to the metal(I) species. The latter option forms the basis of the work discussed below.

4.2 Aims

In attempting to synthesis and isolate a two-coordinate complex stabilised by two different *m*-terphenyl ligands it was found that the different ligands exchange to afford a mixture of products from which the desired product could not be identified.

To alleviate this problem, a combination of ligands was sought that allowed the isolation of a heteroleptic, two-coordinate, transition metal complex. Preferably a synthetic route could be developed that meant these ligands did not exchange to afford the mixture of products as found in Chapter III. If this was not possible, the ligands should be different enough, either sterically and/or electronically, such that the desired heteroleptic product could be easily isolated from any by-products.

N-heterocyclic carbenes (NHCs) were selected to be paired with *m*-terphenyl ligands. These two ligand types are sterically and electronically distinct. The NHCs are also neutral donors, in contrast to the negatively charged *m*-terphenyl ligands. Any by-products resulting from ligand exchange during the reaction would therefore have different geometries around the metal centres. It was hoped that these differences would ensure that the desired heteroleptic product could be isolated from any by-products formed.

Due to the neutral nature of this ligand and the II+ oxidation states of the commonly available starting materials, it was necessary to prepare a series of three-coordinate intermediates. These intermediates could then be isolated and purified before being reduced to afford neutral, two-coordinate, metal(I) species.

Products of the above study were investigated for their ability to activate small molecules. The goal was to determine whether the compounds behave similarly to the two-coordinate *m*-terphenyl complexes that have been previously reported in the literature.[64,65,142]

4.3 Results and Discussion

The NHC initially selected was 1,3-diisopropyl-4,5-dimethylimidazol-2-ylidene (IPrMe). This N-heterocyclic carbene has a small steric profile and is one of the most σ-donating NHCs available.[59] It was hoped that these characteristics would complement the sterically large *m*-terphenyl ligands already selected for this work.

4.3.1 $[2,6\text{-}Mes_2C_6H_3]^-$ Group 12 Complexes

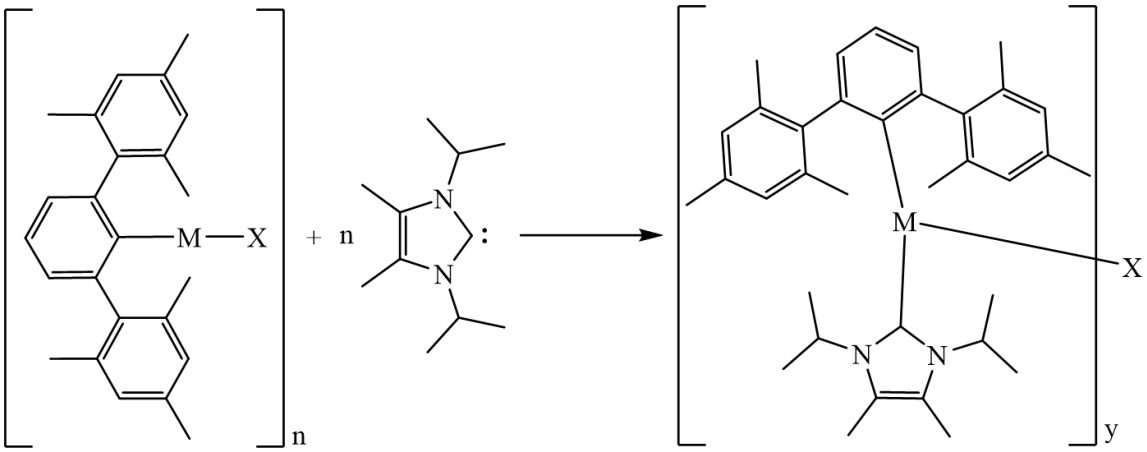

IV·10: M = Zn, X = Cl, n = 2 and y = 1; Conditions = benzene-d_6, room temperature, 16 hrs
IV·11: M = Cd, X = Cl, n = 3 and y = 1; Conditions = benzene-d_6, room temperature, 16 hrs
IV·12: M = Hg, X = Br, n = 1 and y = 1; Conditions = benzene-d_6, room temperature, 16 hrs
IV·13: M = Mn, X = Br, n = 2 and y = 2; Conditions = benzene-d_6, room temperature, 16 hrs
IV·14: M = Fe, X = Br, n = 3 and y = 1; Conditions = toluene, −30°C, 16 hrs
IV·15: M = Co, X = Br, n = 2 and y = 1; Conditions = toluene, −30°C, 16 hrs

Scheme 4·5. The synthetic route to complexes **IV·10**–**IV·15**.

A series of complexes of the type $[2,6\text{-}Mes_2C_6H_3]MX[IPrMe]$ were isolated and characterised. The synthetic route to these compounds is shown in **Scheme 4·5**. IPrMe was added to a solution of one of the *m*-terphenyl, halide bridged, dimeric complexes described in Chapter II. A variety of reaction conditions were investigated. Generally, slow addition of one equivalent of IPrMe and cooling the reaction to −30°C increased the yield. The solvent selected for the reaction was not seen to influence the yield. The Group 12 complexes, $[2,6\text{-}Mes_2C_6H_3]MX[IPrMe]$ [MX = ZnCl (**IV·10**), CdCl (**IV·11**) and HgBr (**IV·12**)], were synthesised through, and isolated from, NMR spectroscopic scale reactions in benzene-d_6.

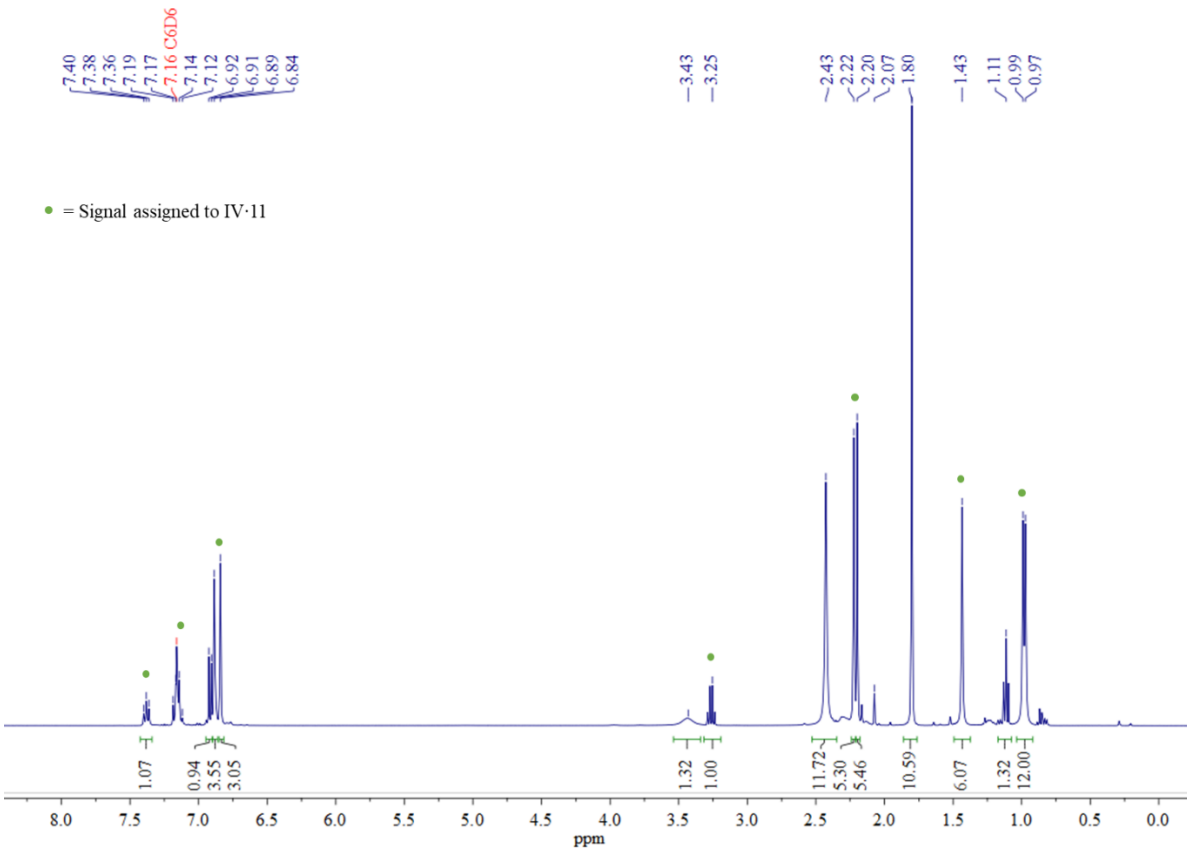

Figure 4·2. ^{1}H NMR Spectrum of **IV·11** with impurities.

IV·10 and **IV·11** were synthesised from [2,6-$Mes_2C_6H_3ZnCl]_2$ (**II·41**) and [2,6-$Mes_2C_6H_3CdCl]_3$[LiCl] (**II·42**) respectively. Both starting materials were contaminated with the relevant diaryl complex ([2,6-$Mes_2C_6H_3]_2$M, M = Zn (**IV·10**) or Cd (**IV·11**). The signals in the NMR spectra belonging to the target complexes were identified by comparing the spectra with those of the impurities (see, for example, **Figure 4·2**). There was no evidence of carbene coordination to these impurities. The ^{1}H and ^{13}C{^{1}H} spectra for both complexes contain the expected number of signals for the complexes. The same was true of the spectra of **IV·12**.

The signals in the ^{113}Cd{^{1}H} and ^{199}Hg{^{1}H} spectra of **IV·11** and **IV·12** [509.2 ppm (**Figure 4·3**) and −545.0 ppm, respectively] are both shifted downfield relative to the starting materials (−1186 ppm for [2,6-$Mes_2C_6H_3$]HgBr, **II·43**) and diaryl complexes (401.0 ppm for [$Mes_2C_6H_3]_2$Cd, **III·32**) as a result of the strong σ-donating properties of the NHC ligand.[59]

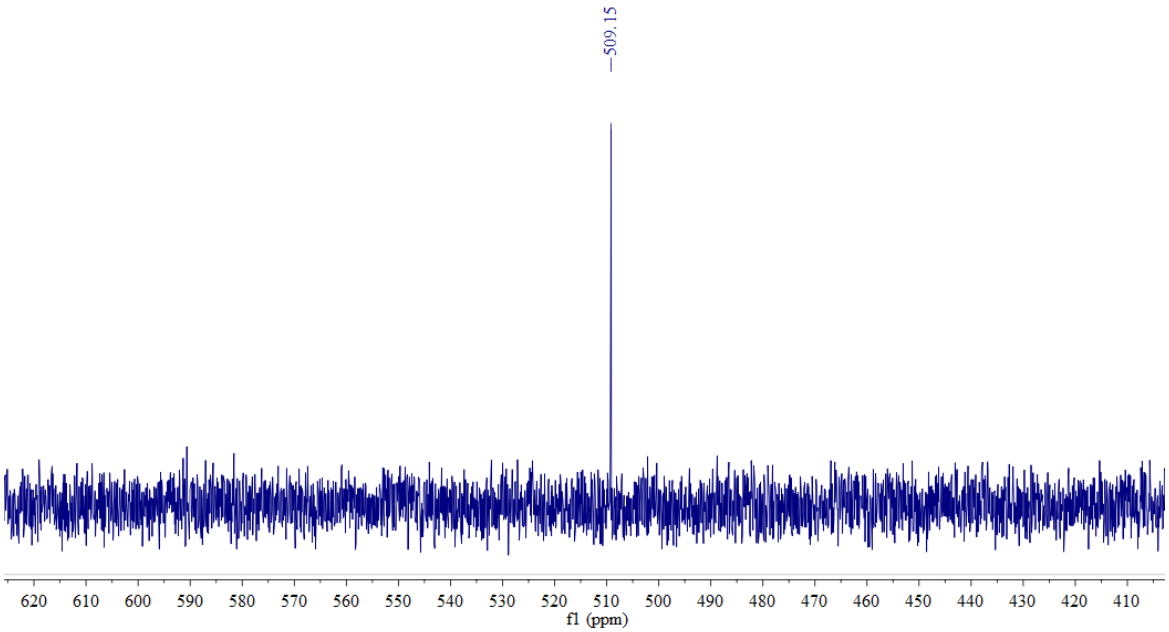

Figure 4·3. ^{113}Cd NMR spectrum of **IV·11**.

IV·10–**IV·12** were analysed by mass spectrometry (ASAP-MS for **IV·10** and **IV·11**, EI-MS for **IV·12**). Neither technique detected the parent ion. **IV·10**–**IV·12** appear to fragment in the spectrometer, losing the halide moiety so that the fragment [2,6-$Mes_2C_6H_3$]M[IPrMe]$^+$ [M = Zn , Cd or Hg, respectively] is detected (**Figure 4·4**). This suggests the M–X bond is weaker in **IV·10**–**IV·12** than in the transition metal analogues, where the parent ion is observed.

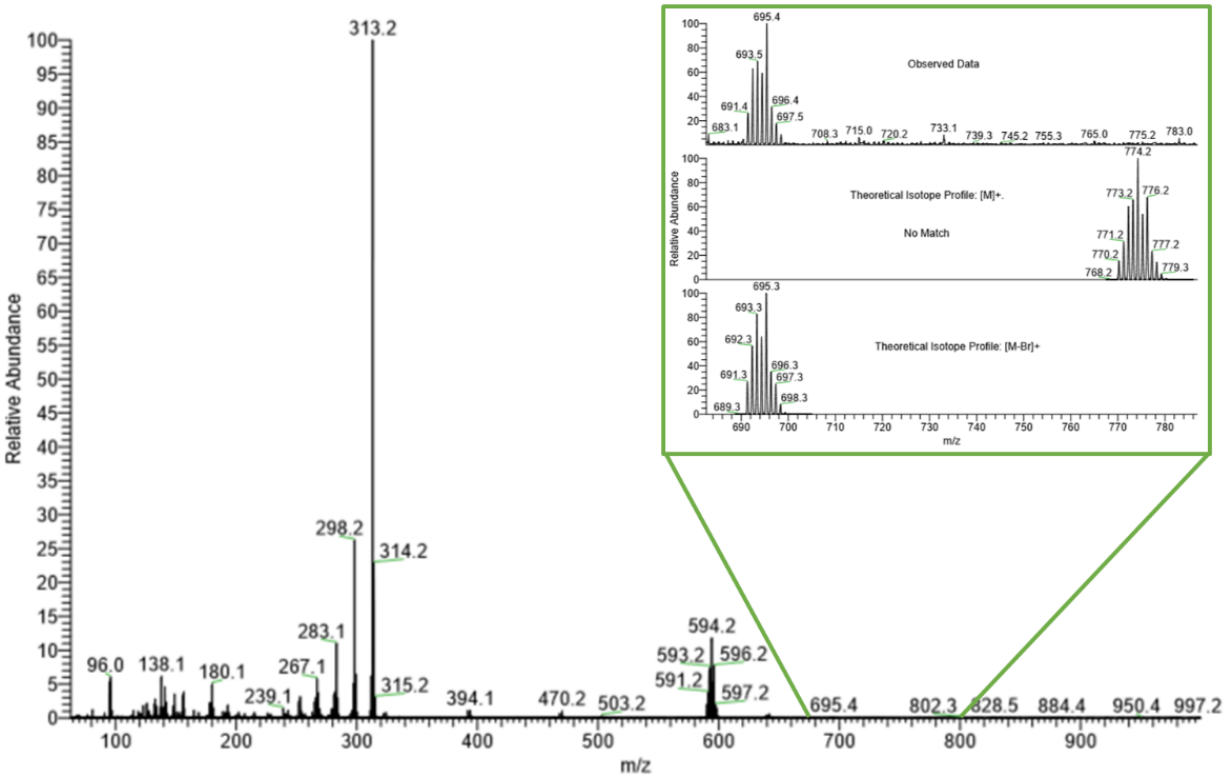

Figure 4·4. ASAP Mass Spectrum of **IV·12** ([M], m/z = 768.2).

Crystals of **IV·10** and **IV·11** were grown by vapour diffusion of pentane into a saturated solution of the complex in benzene-d_6, and **IV·12** crystallised at room temperature from benzene-d_6 upon synthesis. The purity of these crystals was investigated with elemental analysis. The analysis showed that the purity of **IV·10** was not within accepted limits with a carbon content of 0.5 % less than the calculated value. However, the elemental analysis of **IV·11** and **IV·12** demonstrated that they were pure within acceptable limits.

X-ray diffraction studies of **IV·10**, **IV·11**, and **IV·12** revealed the complexes to be three-coordinate. All three complexes are rare examples of three-coordinate Group 12 complexes stabilised by three different ligands.

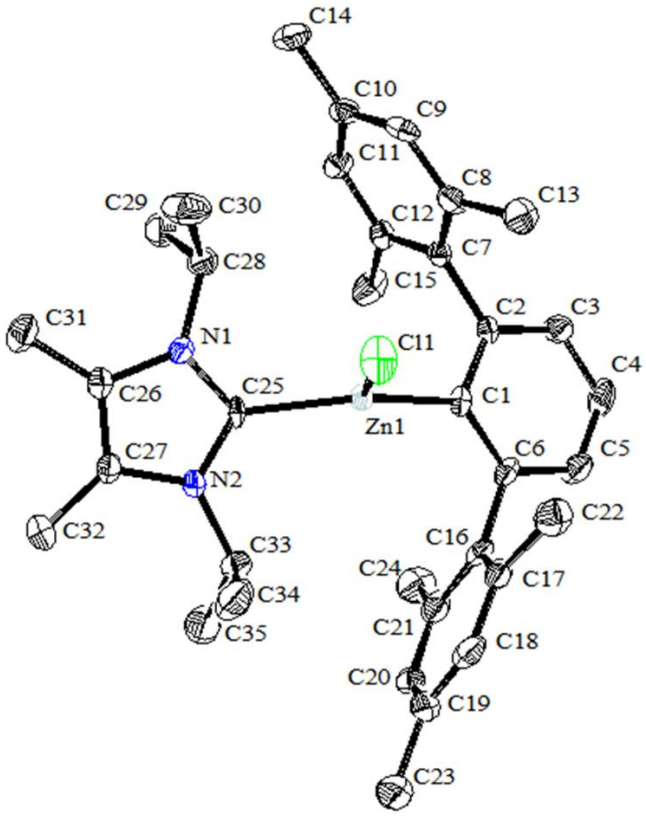

Figure 4·5. The solid-state structure of **IV·10**. Hydrogens are omitted for clarity and ellipsoids are set at 50% probability.

Complexes **IV·10** (**Figure 4·5**) and **IV·11** (**Figure 4·6**) crystallise in the enantiomorphic $P4_3$ space group as a tilt of the organic ligands in the solid state with respect to the plane defined around the trigonal planar metal centre makes the structures chiral. This chirality is not

observed in the NMR spectra of the complexes and is therefore unlikely to be maintained in solution. **IV·12** (**Figure 4·7**) crystallises in the *Pna*2_1 space group and the asymmetric unit of the structure contains the full molecule. Key bond lengths and angles of the structures are reported in **Table 4·1**.

Table 4·1. Key bond lengths, angles, and geometric parameters for **IV·10**–**IV·12**.

		IV·10 (MX = ZnCl)	**IV·11** (MX = CdCl)	**IV·12** (MX = HgBr)
	Atom Labels			
Bond Lengths				
C_{Ar}–M1/Å	C1	1.984(4)	2.135(6)	2.069(14)
C_{IPrMe}–M1/Å	C25	2.031(4)	2.194(6)	2.097(14)
X1–M1/Å		2.2896(11)	2.5260(17)	2.9586(15)
H - bonds				
$C_{iPr}H_3$–X1/Å[°]	C30	3.19(10) [136(7)]	4.676(12) [N/A]	3.15(15) [147(13)]
	C34	3.45(11) [144(7)]	3.27(16) [139(11)]	3.19(15) [148(13)]
$C_{Mes}H_3$–X1/Å[°]	C13	2.90(9) [136(7)]	2.84(12) [123(7)]	3.13(16) [150(15)]
	C22	2.83(8) [148(6)]	3.27(14) [138(11)]	2.86(14) [156(12)]
C_{iPr}H–Mes/Å[°]	C28	3.13(7) [168(5)]	3.15(10) [169(7)]	3.27(14) [164(9)]
	C33	2.99(8) [170(5)]	3.53(9) [162(7)]	3.36(14) [163(10)]
Bond Angles				
C1–M1–C25/°		142.53(17)	145.8(2)	171.2(4)
C–M1–X1/°	C1	118.30(13)	117.19(16)	105.7(3)
	C25	99.16(13)	97.03(16)	83.1(3)
Interplanar Angles				
NHC–[C1-M-X]/°		95.35(35)	101.83(54)	83.45(100)
Ar–[C25-M-X]/°		84.04(35)	94.31(51)	91.29(91)
Mes–$Ar_{central}$/°		82.07(61)	97.16(79)	89.10(140)
		86.71(57)	85.51(76)	93.75(150)
C–C–N–C25/°	C30, C28, N1	102.40(57)	100.55(78)	110.4(15)
	C34, C33, N2	117.63(59)	119.00(73)	112.5(13)
Ar–NHC /°		22.32(11)	23.80(15)	2.70(36)
Out of Plane Distortions		95.35(35)		
M–NHC /Å		0.4255(76)	0.202(11)	0.316(22)
M–Ar /Å		0.1960(66)	0.172(10)	0.085(19)
Geometry				
τ_3^{299}		0.62	0.57	0.15

The lattices of many of the [2,6-$Mes_2C_6H_3$]MX[IPrMe] complexes exhibit merohedral twinning facilitated by the tetragonal space group. The twinning is described according to the

twin law (0.0, 1.0, 0.0, 1.0, 0.0, 0.0, 0.0, 0.0, −1.0). In **IV·10** 45.5(2) % of the lattice obeys this law. By contrast only 1.35(16)% of the lattice obeys this law in **IV·11** and with 9.6(18) % of the lattice obeys the twin law in **IV·12**. **IV·12** (**Figure 4·7**) adopts an orthorhombic space group this twinning is pseudo-merohedral and can occur due to the two-unit cell lengths similar at 11.75702(3) and 11.91455(6) Å.

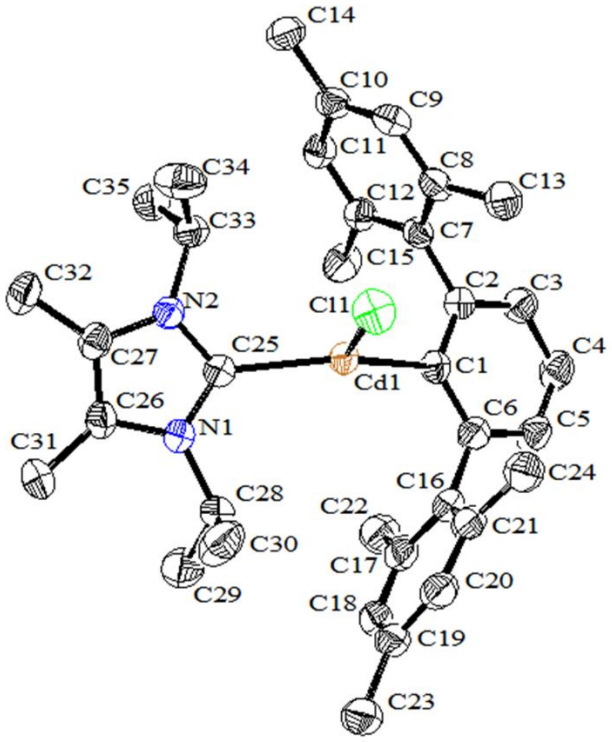

Figure 4·6. The solid-state structures of **IV·11**. Hydrogens are omitted for clarity and ellipsoids are set at 50 % probability.

The structures of **IV·10** and **IV·11** are similar. The three ligands are arranged around the metal centre in a distorted trigonal planar geometry (τ_3 = 0.62 and 0.57 respectively). The geometric parameter, τ_3 ($\tau_3 = [(\alpha + \beta + \gamma) / 360 - (\alpha - 120) / 60]$, where α = the largest angle between ligands coordinated to the metal centre, β = the next largest, and γ = the smallest), was developed by Khavasi and Tehrani to distinguish between T-shaped and trigonal planar structures.[299] A perfectly T-shaped complex has a τ_3 of 0.0 whilst a perfectly trigonal planar complex has a τ_3 of 1.0. The widest angle occurs between the $[2,6\text{-}Mes_2C_6H_3]^-$ and IPrMe ligands [142.53(17)° (**IV·10**) and 145.8(2)° (**IV·11**)], presumably as a result of the large steric profiles of these ligands compared with the chloride. As a result, the ligand–chloride angles are

compressed with the smallest angle occurring between the halide and the IPrMe ligand [99.16(13)° (**IV·10**) and 97.03(16)° (**IV·11**)]. This is caused by the steric bulk of the [2,6-$Mes_2C_6H_3$]$^-$ ligand out-competing the bulk of the NHC.

Both ligands have short CH_3···Cl interactions (see **Table 4·1**) which indicate the presence of hydrogen bonding.[300] Longer interactions occur between the *i*Pr methyl groups and the chloride than between the mesityl methyl groups and the chloride. The ^{1}H NMR spectra of these complexes show no evidence of splitting of the methyl signals or significant shift of the signals upfield from the region where methyl groups are observed in the unbound ligand.[97] This suggests that the close contacts are either not interactions, are not present in solution or that they are present but are transient and not strong. As always, inferring solution state behaviour from solid state observations must be done with caution.

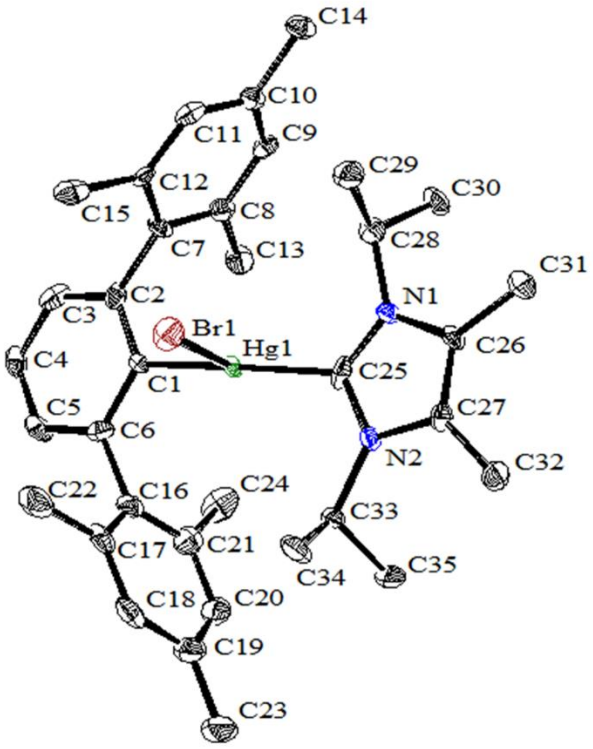

Figure 4·7. The solid-state structure of **IV·12**. Hydrogens are omitted for clarity and ellipsoids set at 50 % probability.

The solid-state structure of **IV·12** also shows long range, intramolecular interactions. The methyl groups of both the mesityl flanking groups, in the *ortho* position, and the *i*Pr groups are

at a distance from the bromide moiety that is less than the sum of the van der Waals radii (Br = 1.9 Å, C = 1.7 Å).[187] Again, in the ^{1}H NMR spectrum of this complex the signals for these groups do not show a significant shift from the free ligands which indicates that these interactions are likely to be transient in solution or crystallographically imposed.

In all three structures there are close contacts between the C$_{i\text{Pr}}$H and the aromatic ring of the *m*-terphenyl flanking groups as measured by the C$_{i\text{Pr}}$H···*i*C$_{\text{Mes}}$ distances [3.13(7) (C28, Cl1) and 2.99(8) (C33, Cl1) Å (**IV·10**), 3.15(10) (C28, Cl1) and 3.53(9) (C33, Cl1) Å (**IV·11**), 3.27(14) (C28, Br1) and 3.36(14) (C33, Br1) Å (**IV·12**)]. An attractive interaction between the ligands could contribute to the co-planar arrangement of the ligands [22.32(11)° (**IV·10**), 23.80(15)° (**IV·11**), 2.70(36)° (**IV·12**) (Ar–NHC)]. This arrangement is rare in the low-coordinate complexes discussed previously in this work and in the literature.[126,188]

The metal ions in complexes **IV·10**–**IV·12** are distinctly out of the plane of the central rings of the ligands. This distortion shifts the planes of the ligands toward the chloride moiety and makes central planes of the ligands more co-planar to one another. In **IV·11** the size of the distortion from both ligands is similar at 0.172(10) and 0.202(11) Å for [2,6-Mes$_2$C$_6$H$_3$]$^-$ and IPrMe respectively. This is not the case in the structure of **IV·10**. Whilst the distortion from the plane of the [2,6-Mes$_2$C$_6$H$_3$]$^-$ ligand is similar at 0.1960(66) Å, the deviation from the plane of IPrMe is more than double at 0.4255(76) Å. As has been discussed, hydrogen bond formation between the ligands and the chloride moiety is weak if present at all. Instead, this distortion is likely to be a result of repulsion between the ligands. This would explain why the effect is more pronounced in **IV·10**. The shorter C–M bond lengths, as a result of the smaller size of the zinc(II) ion relative to the cadmium(II) ion,[187] decrease the distances between the two ligands and therefore increase steric repulsion between them.

The mercury centre in **IV·12** (**Figure 4·7**) has a T-shaped geometry (τ_3 = 0.15) with the largest interligand angle, between the two carbon coordinating ligands, approaching linearity at 171.2(4)°. The C–Hg1–Br1 angles are 105.7(3) and 83.1(3)° for [2,6-$Mes_2C_6H_3$]$^-$ (C1) and IPrMe (C25) respectively. Again, the angle between the bromide moiety and NHC is compressed relative to the angle between the bromide and the *m*-terphenyl, reflecting the greater steric bulk of the *m*-terphenyl ligand.

T-shaped geometry is common in mercury complexes due to the tendency for mercury to maintain a linear geometry.[204,301–303] This generally results in two, strongly bound ligands in a linear geometry and a third ligand bound weakly at 90° to the linear axis. This can be seen through the large Hg–Br bond distance in **IV·10**, 2.9586(15) Å compared with 2.4145(4) Å in [2,6-$Mes_2C_6H_3$]HgBr (**II·43**). This effect is also observed to a lesser extent in the zinc and cadmium analogues. The M–Cl bond lengths in **IV·10** and **IV·11** are longer than many examples of terminal halides, in this work and in the literature, at 2.2896(11) and 2.5260(17) Å, respectively. They are, however, similar to the M–Cl lengths in bridged species.[185,277] This is probably as a result of the steric crowding around the metal centre. These long M–X distances, which can indicate a weak bond,[304] help to explain why this bond dissociates in a mass spectrometry ion stream.

The M–C distances in all complexes are consistent with equivalent bond lengths in this work and in the literature.[188,305,306] For example they are comparable with the M–C bond lengths in [2,6-(2,6-$Xyl)_2C_6H_3$]$_2$M (M = Zn, Cd and Hg) at 1.949(4), 2.115(5) and 2.087(6) Å, respectively. They also show an established trend in which the Cd–C distances are longer than Hg–C distances. This is due to relativistic effects and lanthanide contraction which results in a smaller van der Waals radius for mercury.[188]

4.3.2 [2,6-$Mes_2C_6H_3$]$^-$ Transition metal Complexes

Manganese, iron, and cobalt analogues of **IV·10–IV·12** were prepared (**Scheme 4·5**). [(2,6-$Mes_2C_6H_3$)MnBr(IPrMe)]$_2$ (**IV·13**, **Figure 4.8**) was isolated from an NMR spectroscopic scale reaction between [2,6-$Mes_2C_6H_3$MnBr]$_2$·[LiBr(OEt_2)]$_2$ (**II·38**) and two equivalents of IPrMe. [2,6-$Mes_2C_6H_3$]MBr[IPrMe] [M = Fe (**IV·14**) and Co (**IV·15**)] were isolated from the reaction between IPrMe and **II·39** or **II·40**, respectively, on a larger scale. The synthesis of **IV·15** also afforded a blue powder which ^{1}H NMR spectroscopy and X-ray diffraction analysis showed to be [IPrMe]$_2$$CoBr_2$ (**II·32**). This possibly forms through the displacement of an *m*-terphenyl ligand by free IPrMe or, more likely, *via* a Schlenk equilibrium as suggested in Chapter III. Attempts to isolate nickel and chromium analogues were unsuccessful.

A single, pale-pink crystal of **IV·13** was obtained from the reaction through vapour diffusion of pentane into the filtered reaction mixture. A ^{1}H NMR spectrum was collected after 10 hours at room temperature. This spectrum contains eighteen signals from 0.81 to 29.15 ppm. This distribution of peaks suggests a paramagnetic species is present, presumably **IV·13**. The number of signals in the spectrum, however, is more than the six that could be assigned to **IV·13**. These extra signals could arise from starting materials or by-products such as [IPrMe]$_2$$MnBr_2$ or [$MnBr_4$]$^{2-}$[IPrMeH]$^+_2$.

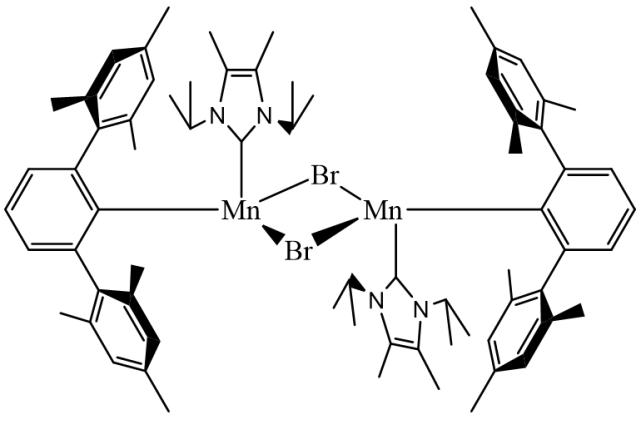

IV·13

Figure 4·8. The structure of the dimeric complex **IV·13**.

IV·13 crystallised in the monoclinic space group $P2_1/n$. X-ray diffraction studies (**Figure 4·9**) show **IV·13** to be a dimeric species with a $[MX]_2$ core, unlike **IV·10–IV·12**. Each manganese centre is four-coordinate with a distorted tetrahedral geometry (τ_4 = 0.76 and 0.76). The asymmetric unit contains one pentane molecule disordered almost equally over two sites. Key bond lengths and angles of **IV·13** are contained in **Table 4·2**.

Table 4·2. Key bond lengths, angles, and geometric parameters for **IV·13.**

		IV·13			
Bond Lengths	Atom Labels		**Interplanar Angles**	Atom Labels	
Ar–Mn/Å	C1, Mn1	2.150(2)	NHC–(C_{Ar}-Mn-Br)/°	C25	55.58(17)
	C36, Mn1	2.150(2)		C60	54.50(16)
NHC–Mn/Å	C25, Mn1	2.216(2)	Ar–(C_{NHC}-Mn-Br)/°	C1	19.32(18)
	C60, Mn1	2.212(2)		C33	21.63(20)
Br–Mn/Å	Mn1, Br1	2.6258(4)	Mes–Ar/°	C16, C6	100.96(26)
	Mn2, Br1	2.6340(4)		C7, C2	115.47(23)
	Mn1, Br2	2.6244(4)		C51, C37	115.03(23)
	Mn2, Br2	2.6421(4)		C42, C41	89.80(27)
H-bonds					
NHC CH_3–Br /Å[°]	C69, Br1	3.05(4) [120(2)]	C–C–N–C/°	C64, C63, N3, C60	105.84(24)
	C34, Br1	3.36(4) [110(2)]		C35, C33, N2, C25	122.09(23)
	C33, Br2	3.01(3) [127(2)]		C30, C28, N1, C25	114.23(24)
	C29, Br2	3.01(4) [123(3)]		C69, C68, N2, C60	102.29(25)
Mes CH_3–Br /Å[°]	C59, Br1	3.21(3) [104(2)]	Ar–NHC /°	C1, C25	39.523(56)
	C22, Br2	3.10(4) [125(3)]		C36, C60	37.289(62)
	C15, Br1	3.06(3) [122(2)]			
	C50, Br2	3.07(3) [117(2)]			
NHC CH–Br /Å[°]	C63, Br2	3.12(3) [117.4(19)]	**Out of Plane Distortions**		
	C28, Br2	3.24(3) [112.0(19)]			
	C33, Br1	3.01(3) [137(2)]			
Bond Angles			Mn–NHC/Å	Mn1, C25	0.3636(38)
				Mn2, C60	0.4277(38)
C–Mn–C /°	C1, Mn1, C25	129.50(7)	Mn–Ar /Å	Mn1, C1	0.4652(31)
	C36, Mn2, C60	127.80(8)		Mn2, C36	0.4121(32)
C–Mn–Br/°	C36, Mn2, Br1	106.68(6)	**Geometric Index**		
	C36, Mn2, Br2	123.68(6)			
	C1, Mn1, Br1	107.47(5)			
	C1, Mn1, Br2	118.99(6)			
C–Mn–Br/°	C25, Mn1, Br1	110.53(5)	τ_4	Mn1	0.76
	C25, Mn1, Br2	94.77(6)		Mn2	0.76
	C60, Mn2, Br1	113.10(6)			
	C60, Mn2, Br2	91.34(5)			

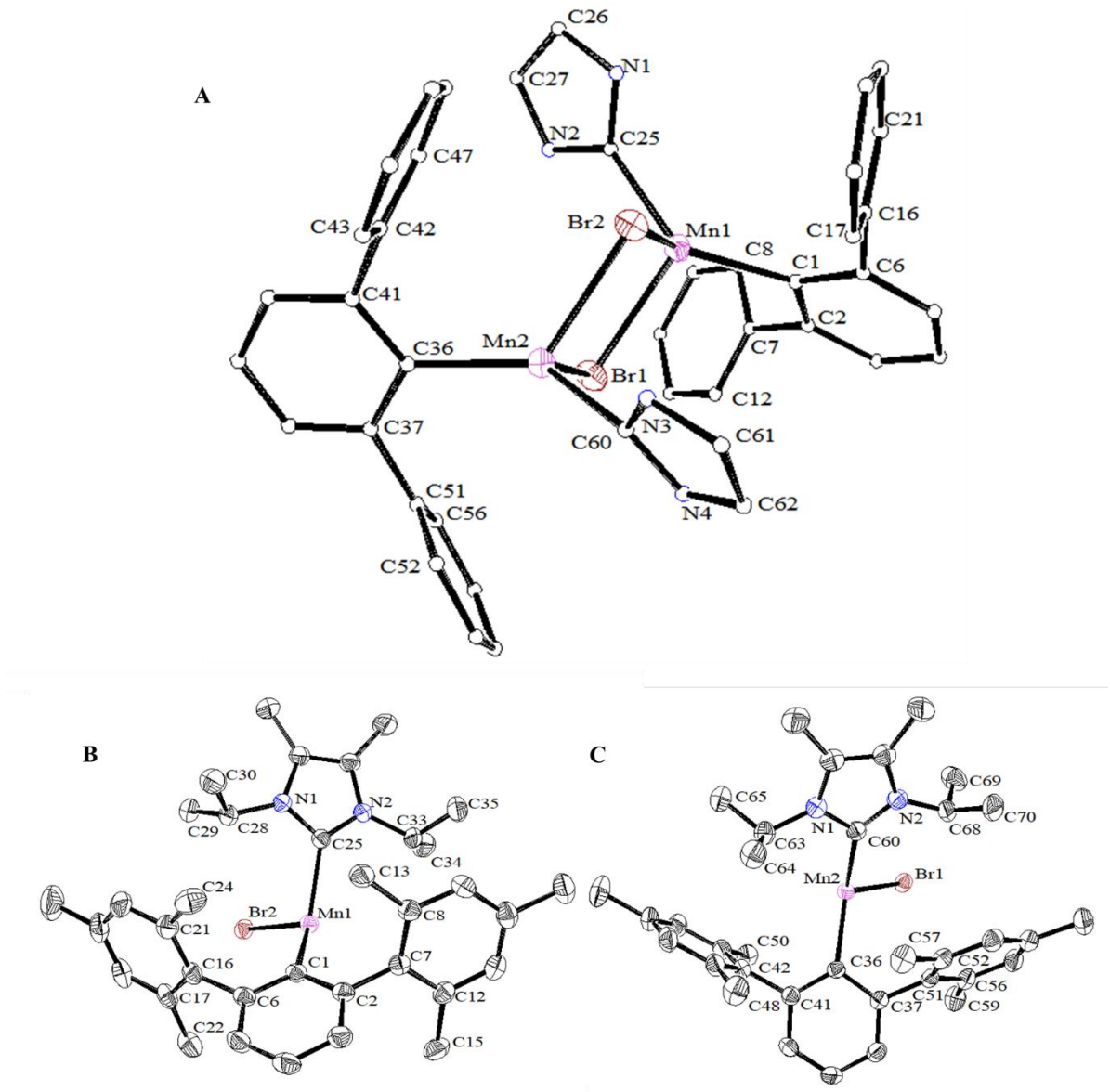

Figure 4·9. The dimeric structure of **IV·13** (A) and the monomers (B and C). Hydrogens, pentane molecules and flanking groups from (A) are omitted for clarity. Ellipsoids are set at 50 % probability.

IV·13 is similar in structure to $[2,6\text{-Mes}_2C_6H_3CoBr(THF)]_2$, synthesised by Power *et al.* with a similar $[MBr]_2$ core unit and IPrMe ligands replacing the coordinating THF molecules.[74] The Mn–Br–Mn angles are 92.739(12) (Mn1, Br1, Mn2) and 92.585(12)° (Mn1, Br2, Mn2) and the reciprocal Br–Mn–Br angles are 87.604(12) (Br1, Mn1, Br2) and 87.065(12)° (Br1, Mn2, Br2), giving a diamond shape to the core unit with an Mn1···Mn2 distance of 3.8071(5) Å. The extension and compression pattern is the opposite of that found in $[2,6\text{-Dipp}_2C_6H_3MnBr]_2$ (**II·36b**), which contains the same core unit. When compared with **II·36b** [Mn···Mn = 3.490(3)

and 3.528(3) Å], the Mn1···Mn2 distance in **IV·13** is significantly longer. This could be a result of increased steric congestion, caused by the IPrMe ligand, forcing the two monomers apart or decreased intermetal attraction in **IV·13** due to the four-coordinate nature. The latter theory is supported by the observation that the Mn···Mn distance in **II·36** is similar at 3.8174(9) Å.

The combined steric bulk of the IPrMe and $[2,6\text{-}Mes_2C_6H_3]^-$ ligands causes compression of the C–Mn–Br bond angles from an idealised 120° (**Table 4·2**). The two carbon-based ligands are forced closer to a bromide [C_{Ar}–Mn–Br = 106.68(6) (C36, Mn2, Br1) and 107.47(5)° (C1, Mn1, Br2), C_{NHC}–Mn–Br = 94.77(6) (C25, Mn1, Br2) and 91.34(5)° (C60, Mn2, Br2)] to accommodate the expansion of the C_{Ar}–Mn–C_{NHC} angles to 127.80(8) (C36, Mn2, C60) and 129.50(7)° (C1, Mn1, C25). The lengths of the C_{Ar}–Mn and Br–Mn bonds are consistent with similar complexes in this work, **II·36** and **II·36b**, and in the literature.[220,307]

IV·14 (**Figure 4·10**) was isolated as a pale yellow powder, through extraction of the reaction mixture into toluene and removal of all volatiles, in a yield of 63%. Crystals of this complex were obtained by vapour diffusion of pentane into a saturated solution of the complex in benzene. Lime green crystals of **IV·15** (**Figure 4·10**) were grown by layering pentane onto a saturated solution of the complex in toluene and were obtained in an 18% yield.

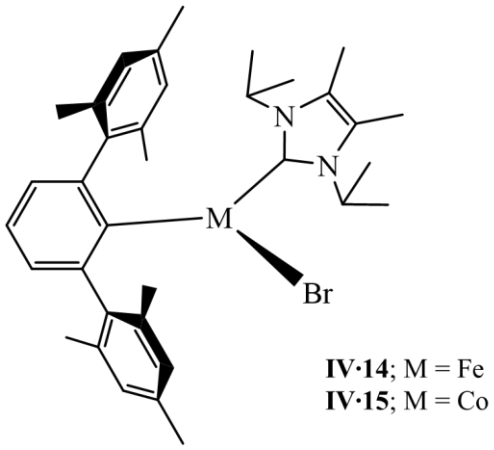

Figure 4·10. The structure of **IV·14** (M = Fe) and **IV·15** (M = Co).

Accurate mass EI-MS identified the parent ion of both complexes, and elemental analysis was able to confirm the purity of the crystals submitted for analysis. UV/Vis investigations of **IV·14** revealed one absorption peak at 338 nm (ε = 3501 dm^3 mol^{-1} cm^{-1}) at an intensity consistent with a $\pi^* \leftarrow \pi$ transition.[76] The absorbances giving rise to the pale yellow colour and consistent with a trigonal planar, d^6 species could not be detected. No evidence of such a signal was observed in the spectrum obtained, presumably this absorbance was weak and not observable at the concentration investigated. The same analysis of **IV·15** (Appendix C) revealed four absorbance peaks. The three weaker absorbances at 783, 673 and 480 nm (ε = 107, 166 and 171 dm^3 mol^{-1} cm^{-1}, respectively) were assigned to three d←d transitions. The stronger absorbance at 359 nm (ε = 1134 dm^3 mol^{-1} cm^{-1}) was assigned to a $\pi^* \leftarrow \pi$ transition.[64,74,76]

^{1}H NMR spectra of both complexes show that they are paramagnetic. The spectrum of **IV·14** contains eleven, broad signals between a range of −36.73 and 35.70 ppm. The extra signals observed may originate from an amount of protonated ligand in the sample. The magnetic moment of **IV·14** was measured as 4.8 μ_B, close to the spin only value of a d^6 ion (4.90 μ_B).

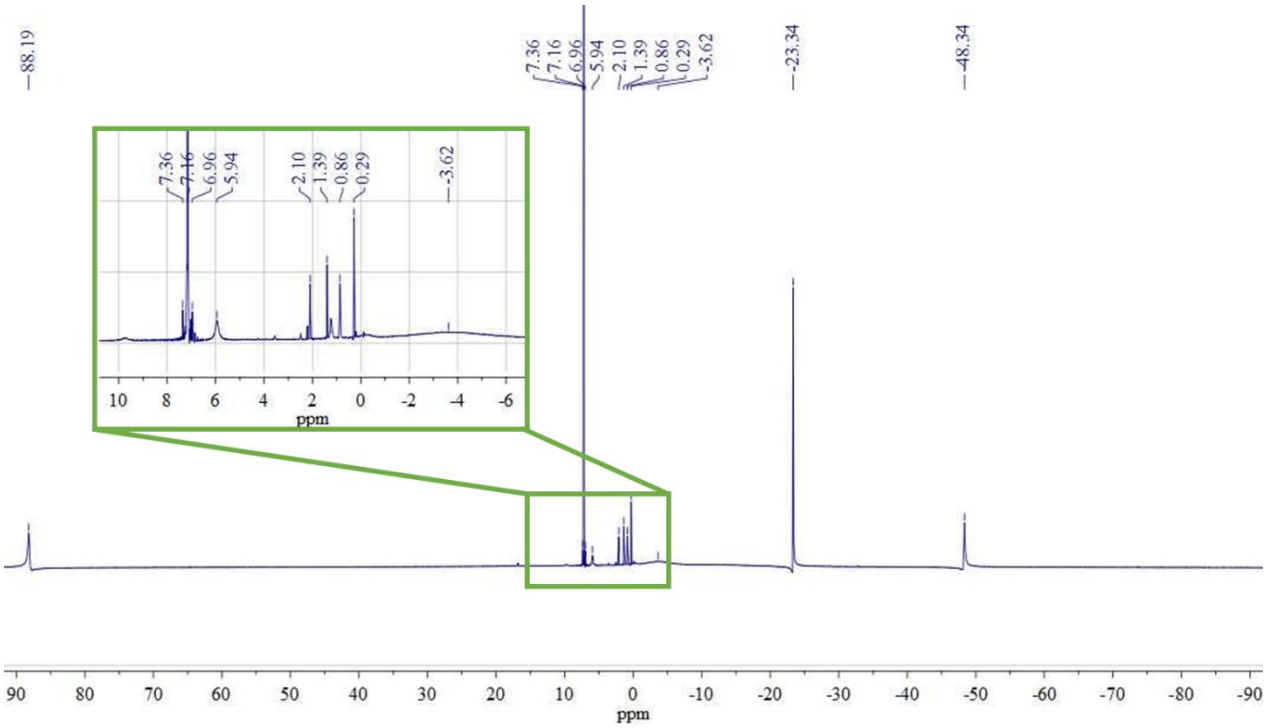

Figure 4·11. The ^{1}H NMR spectrum of **IV·15**.

The ^{1}H NMR spectrum of **IV·15** (**Figure 4·11**) contains five broad peaks between a range of −48.32 and 88.19 ppm. It is possible that some peaks overlap, leading to the lower than expected number in the spectrum. Small peaks, assignable to protonated ligand, were also observed. The magnetic moment of the complex was measured at 4.3 μ_B. This value is greater than the spin only value for a d^7 ion (3.87 μ_B), suggesting an orbital contribution, but lower than the value of 5.4 μ_B found by Danopoulos *et al*. for [cyIPr]FeCl[CH_2SiMe_3].[308] That the magnetic values for **IV·14** and **IV·15** are equal to or higher than the spin only values for the respective metal centres suggests that these complexes do not dimerise in solution.

Table 4·3. Key bond lengths, angles, and geometric parameters for complexes **IV·14** and **IV·15**.

		IV·14 (M = Fe)	**IV·15** (M = Co)
	Atom Labels		
Bond Lengths			
C1–M1/Å		2.054(5)	1.994(5)
C25–M1/Å		2.114(5)	2.031(6)
Br1–M1/Å		2.3961(11)	2.3791(9)
H - bonds			
$C_{i\text{Pr}}H_3\cdots$Br1 /Å[°]	C35	3.03(19) [141(14)]	3.32(12) [138(9)]
	C30		4.437(10) [N/A]
$C_{\text{Mes}}H_3\cdots$Br /Å[°]	C24	2.94(5) [170(15)]	2.79(10) [164(8)]
	C13	3.21(13) [118(10)]	2.94(11) [139(8)]
$CH_{i\text{Pr}}\cdots i\text{-}C_{\text{Mes}}$ /Å[°]	C28	3.09(19) [160(13)]	3.09(9) [169(7)]
	C33	3.00(17) [167(10)]	3.17(9) [168(6)]
Bond Angles			
C1–M1–C25 /°		137.5(2)	138.7(2)
C1–M1–Br1/°		120.11(17)	119.36(16)
C25–M1–Br1/°		102.38(17)	101.94(17)
Interplanar Angles			
NHC–(C1-M1-Br1) /°		68.8 (10)	68.16(53)
Ar–(C25-M1-Br1) /°		82.2(9)	83.58(47)
Mes–Ar_{central} /°		88.5(13)	97.65(82)
		81.2(16)	87.62(73)
C–C–N–C25/°	C35, C33, N2, C25	114.7(16)	116.24(72)
	C30, C28, N1, C25	101.0(15)	100.54(73)
NHC–Ar_{Central} /°		25.79(31)	23.643(146)
Out of Plane Distortions			
M1–NHC /Å		0.377(21)	0.439(10)
M1–Ar /Å		0.202(19)	0.2423(87)
Geometric Index			
τ_3		0.67	0.69

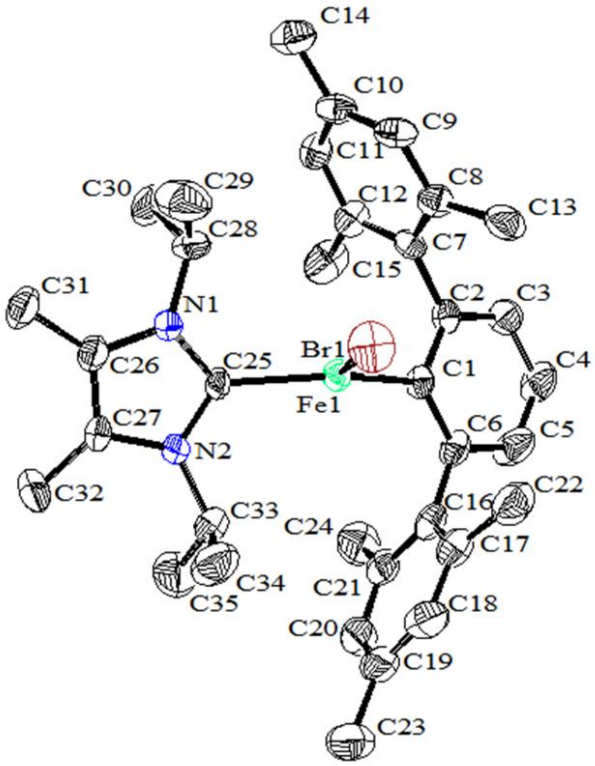

Figure 4·12. The solid-state structure of **IV·14**. Ellipsoids are set at 50 % probability and hydrogens are omitted for clarity.

X-ray diffraction analysis confirmed that **IV·14** (**Figure 4·12**) and **IV·15** (**Figure 4·13**) are not dimeric in the solid-state; the distance between a bromide and the second closest metal atom being greater than 9 Å in both structures.

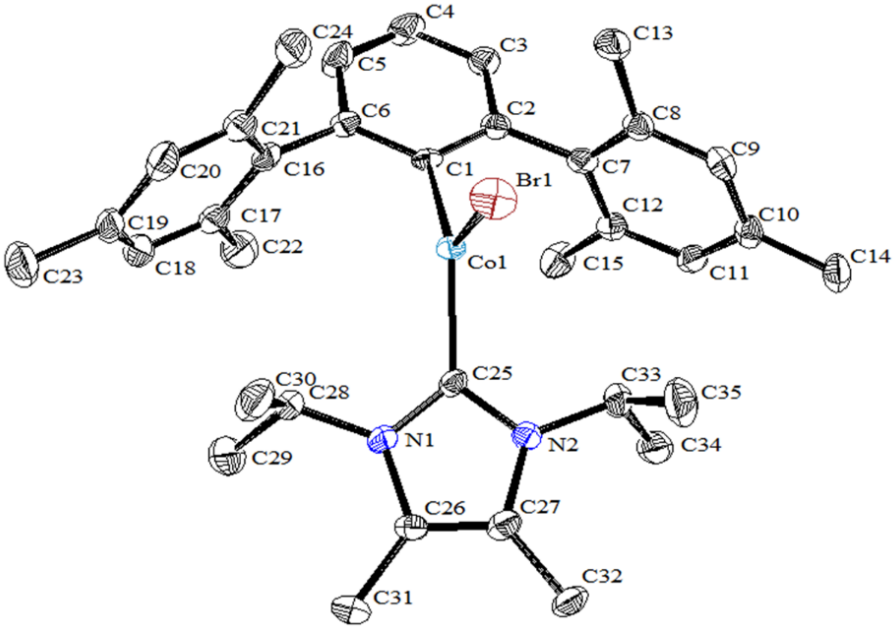

Figure 4·13. The solid-state structure of **IV·15**. Ellipsoids are set at 50 % probability and hydrogens are omitted for clarity.

As with **IV·10** and **IV·11**, **IV·14** crystallises in the $P4_3$ space group. **IV·15** crystallises in the $P4_1$ space group. These space groups contain an enantiomorphic pair. The chirality is again a result of a twist to the ligands in the solid state and is unlikely to be maintained in solution. The crystal structures of both complexes exhibit the merohedral twinning. Key bond lengths and angles are displayed in **Table 4·3**.

IV·14 and **IV·15** have geometry akin to that of **IV·10** and **IV·11**. The three ligands are arranged in a distorted, trigonal planar geometry around the metal (τ_3 = 0.67 and 0.69, respectively) with the largest angle occurring between the two organic ligands [C(1)–M–C(25) = 137.5(2)° (**IV·14**), 138.7(2)° (**IV·15**)]. This angle is the same, within error, in both complexes. The expansion of this angle is concomitant with a compression of the angle between the NHC and the bromide moieties [C25–M1–Br1 = 102.38(17)° and 101.94(17)°, respectively]. **IV·14** and **IV·15**, whilst not identical, are similar to one another in many structural aspects. This is including the positioning of the flanking groups and the ligands in space.

Both structures contain close contacts between the bromide moiety and the CH_3 groups of the two carbon-based ligands. Two interactions exist between the CH_3 groups of the mesityl moieties and the bromides [CH_3···Br = 2.94(5) and 3.21(13) Å (**IV·14**) and 2.79(10) and 2.94(11) Å (**IV·15**)]. The aryl flanking groups tilt toward this interaction away from an orientation perpendicular to the central aryl ring (**Table 4·3**). This suggests that these close contacts are not just the result of crystal packing but an active, electronic interaction that influences the geometry of the structure. Only one *i*Pr group of the NHC ligand participates in a short CH···Br interaction [CH_3···Br = 3.03(19) Å (IV·9) and 3.32(12) Å (IV·10)] and the group shows no resulting deviation toward this interaction. This suggests the $C_{i\mathrm{Pr}}H_3$···Br interactions are either weak or non-existent.

The CH moiety of the *i*Pr groups are in close contact with the π-system of the opposing mesityl rings, as in complexes **IV·10**–**IV·12**. Measured through the distance between the CH moiety and the *ipso*-carbons of the mesityl groups, these interactions are well within the van der Waals radii (C = 1.7 Å) of the atoms involved [CH···C = 3.09(19) (C28, C7) and 3.00(17) Å (C33, C16) (**IV·14**) and 3.09(9) (C28, C7) and 3.17(9) (C33, C16) Å (**IV·15**)].[187] Power *et al*. observe similar interactions in the solid state structure of $[2,6\text{-Dipp}_2C_6H_3]_2Co$.[63] One *i*Pr flanking group is lifted out of the plane of the IPrMe core by 0.165(24) and 0.218(11) Å (**IV·14** and **IV·15** respectively). This distortion demonstrates the impact of this interaction on the two structures and could have implications for any two-coordinate structures developed by the reduction of these complexes.

Finally, the metal ion in both **IV·14** and **IV·15** is significantly out of the plane of the core ring of both organic ligands, as calculated from the average plane of the atoms that form the core ring. The distortion is more pronounced from the IPrMe ligand [0.377(21) Å (**IV·14**) and 0.439(10) Å (**IV·15**)] than from the *m*-terphenyl ligand [0.202(19) Å (**IV·14**) and 0.2423(87) Å (**IV·15**)]. This is consistent with complex **IV·10**. The reason for this distortion remains unclear. It could be imposed by crystal packing forces or the result of favourable, intramolecular π-interactions between the ligands and the metal moiety.

The dimerisation of a low-coordinate manganese species whilst the iron and cobalt analogues remain as monomers has been observed by Bontemps and co-workers.[309,310] This study involved the metal(I) species $[(N\{SiMe_3\}_2)M^I]_n$[2,2,2-cryptK]$_n$[M = Fe and Co (n = 1), and Mn (n = 2)] however and the phenomena was attributed to the overlap of the partially occupied 4s orbitals in $[(N\{SiMe_3\}_2)Mn^I]_2$[2,2,2-cryptK]$_2$. This is not the case in **IV·13**, which dimerises through bridging bromide interactions. It is clear from the complexes investigated in Chapter II, as well as complexes in the literature, that low-coordinate, manganese, iron and cobalt complexes bearing halogens are prone to dimerise *via* this process.[170] This process can be

prevented through the use of ligands of extreme steric bulk.[167,220] Assuming the difference in the solid-state structures of **IV·13**, **IV·14**, and **IV·15** is not purely imposed solid-state effects, a difference in the enthalpy of dimerisation can be assumed. This could originate from a greater affinity of manganese for dimerisation or a reduction in the steric clashing that inhibits this process. Although the ionic radii of metals are dependent on coordination number and a comprehensive study of three-coordinate systems does not exist, it has been established that manganese(II) ions are generally larger than iron(II) and cobalt(II) ions.[311,312] It is reasonable to assume that this would be true in a three-coordinate system. There would therefore be more space around the manganese(II) ion in **IV·13** than around the iron(II) and cobalt(II) ions in **IV·14** and **IV·15**. This would reduce steric clashing in **IV·13**, making dimerisation more favourable than in **IV·14** and **IV·15**.

With the goal of producing a series of two-coordinate, transition metal complexes in mind, several methods of abstracting the halide from **IV·10**, **IV·14** and **IV·15** were investigated.

4.3.3 Attempted Reductions of [2,6-$Mes_2C_6H_3$]MX[IPrMe] [MX = ZnCl (IV·10), FeCl (IV·14) and CoBr (IV·15)]

Attempts were made to reduce the metal centres in **IV·10**, **IV·14**, and **IV·15** from the +II to the +I oxidation state using either a potassium mirror or potassium graphite or, in the case of **IV·10**, sodium shavings.[53,121,169] **IV·10**, **IV·14**, and **IV·15** were synthesised and reduced *in situ* due to the low yields associated with isolating the three-coordinate complexes. The reaction between **IV·10** and sodium shavings resulted in a colourless solution containing a grey powder assumed to be zinc metal. Crystals of **IV·10** were obtained by working up the reaction. Crystals of 2,6-$Mes_2C_6H_4$ were also isolated from this reaction, suggesting the reaction of the product with adventitious hydrogen. Upon addition of a reducing agent, solutions of **IV·14** and **IV·15** exhibited colour changes from yellow to colourless and lime green to dark green, respectively.

The only novel product isolated from these reactions was $[(IPrMe)_2Fe(\mu_3\text{-}O)]_2[(2,6\text{-}Mes_2C_6H_3)_2Fe(\mu_3\text{-}O)]_2Fe$ (**IV·16**, **Figure 4·14**).

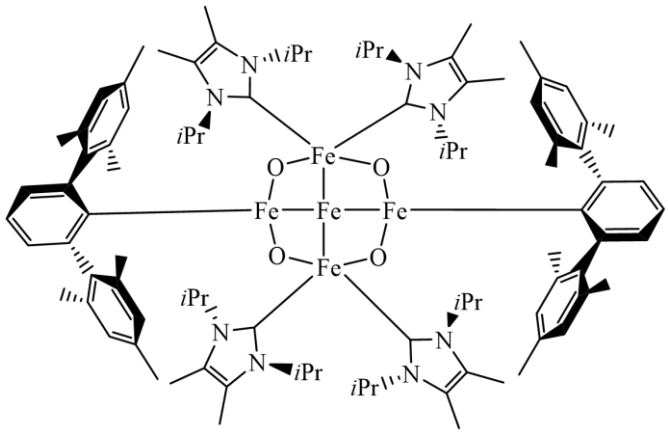

IV·16

Figure 4·14. The structure of $[(IPrMe)_2Fe(\mu_3\text{-}O)]_2[(2,6\text{-}Mes_2C_6H_3)_2Fe(\mu_3\text{-}O)]_2Fe$ (**IV·16**).

Table 4·4. Key bond lengths, angles, and geometric parameters of **IV·16**. AX_$1 indicates an atom related to atom AX by rotation.

		IV·16
	Atom Labels	
Bond Lengths		
Fe1–O/Å	O1	2.0195(18)
	O2	2.0038(17)
Fe2–O/Å	O1	1.8972(18)
	O2	1.8816(18)
Fe3–O/Å	O1	1.9184(18)
	O2	1.9155(18)
Fe1···Fe2/Å		2.6776(4)
Fe1···Fe3/Å		2.6572(4)
Fe2–C1/Å		2.083(2)
Fe2–C/Å	C25	2.125(3)
	C36	2.126(3)
Bond Angles		
O–Fe1–O/°	O1, O2	88.90(7)
	O1, O2_$1	91.10(7)
	O1, O1_$1	180.0
	O2, O2_$1	180.0
O1–Fe2–O2/°		97.03(8)
O1–Fe3–O2/°		96.42(8)
Fe2–O1–Fe3/°		162.84(12)
		166.77(12)
Geometric parameters		
Fe1 τ_4		0.00
Fe2 τ_4		0.79
Fe3 τ_3		0.80
O τ_3		0.16, 0.21

IV·16 is presumably formed by reduction of the iron centres, which are then oxidised by trace oxygen. Several instances of ligand loss and transfer must also occur. The complex was obtained as a small number of red crystals from a pentane solution of a reaction designed to afford [2,6-$Mes_2C_6H_3$]Fe^{I}[IPrMe], crystallising in the monoclinic space group $P2_1/n$ with one quarter of the molecule in the asymmetric unit (**Figure 4·15**). Key bond lengths, angles and geometric parameters are contained in **Table 4·4**.

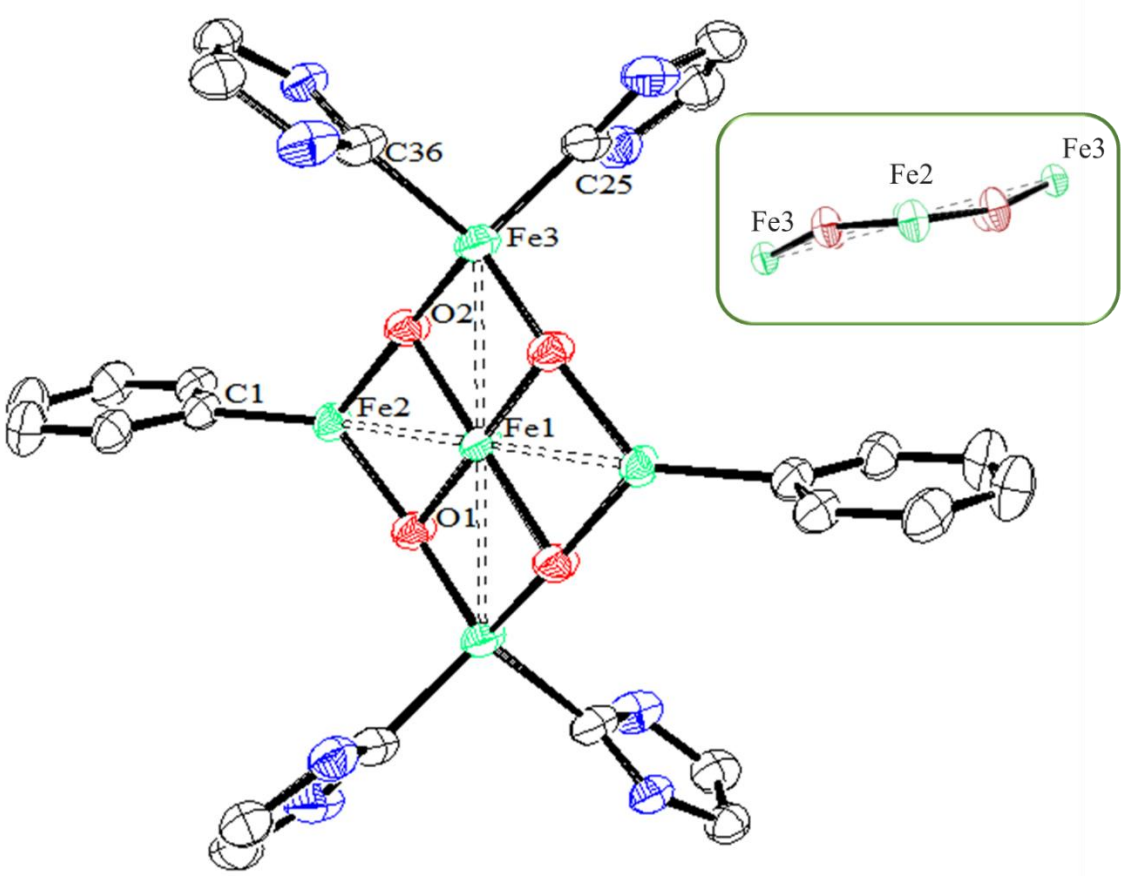

Figure 4·15. The solid-state structure of **IV·16**. The flanking mesityl groups of the *m*-terphenyl ligand, the *i*Pr and methyl groups of the NHC ligand and all hydrogens have been omitted for clarity. Short distances between the iron(II) ions are represented as dashed bonds. Ellipsoids are set at 50 % probability. The inset contains a side view to display the puckering of the iron-oxo core.

The complex features a central, square planar iron(II) ion [τ_4 = 0.00, Fe(1)] coordinated by four oxo-groups each of which bridges two further external iron(II) ions leading to a T-shaped geometry for the oxygens (τ_3 = 0.21, 0.16). The external iron centres are alternatively four-

coordinate, tetrahedral (τ_4 = 0.79), and bound by two IPrMe ligands [Fe(2)] or three-coordinate, trigonal planar (τ_3 = 0.80) and bound by a single *m*-terphenyl ligand [Fe(3)]. These units form a square Fe_5O_4 core, which is slightly puckered in a deck chair fashion with the trigonal planar iron units being shifted out of the plane (**Figure 4·15**, inset).

The oxidation states of each of the three iron moieties have been determined as +II through inspection of the ligand charges and the number of metal centres. It is likely that a more complicated electronic picture exists, which is beyond the reach of the crystallographic data obtained. The inter-ion distances between the central Fe1 and Fe2 or Fe3 [2.6776(4) and 2.6572(4)°, respectively] are similar to that in the complex Fe_2Mes_2 [2.614(1)°] in which significant antiferromagnetic coupling is present.[39,41] Whether these distances are indicative of an iron···iron interaction bond is unclear. Magnetic measurements would help to answer this question although the effect of an Fe···Fe interaction would have to be extricated from superexchange, antiferromagnetic coupling pathways which are known to take place across oxo-bridges.[41,184] Oxo-bridged, multinuclear iron complexes have been studied in depth due to their magnetic properties and their importance in biological systems.[313–315]

IV·16 is an uncommon example of a T-shaped oxygen bridging three iron centres.[316] A study of the magnetic and reactivity of the complex would give more of an insight into the complex and its applications. A reliable synthetic route would first have to be developed.

4.3.4 $[2,6\text{-}Dipp_2C_6H_3]^-$ Complexes

It was possible that the ligand system in **IV·10–IV·15** did not provide enough steric bulk to prevent the decomposition of the complex upon reduction to a metal(I) species. Analogues of **IV·10**–**IV·15**, supported by $[2,6\text{-}Dipp_2C_6H_3]^-$, a bulkier *m*-terphenyl ligand, were therefore developed.

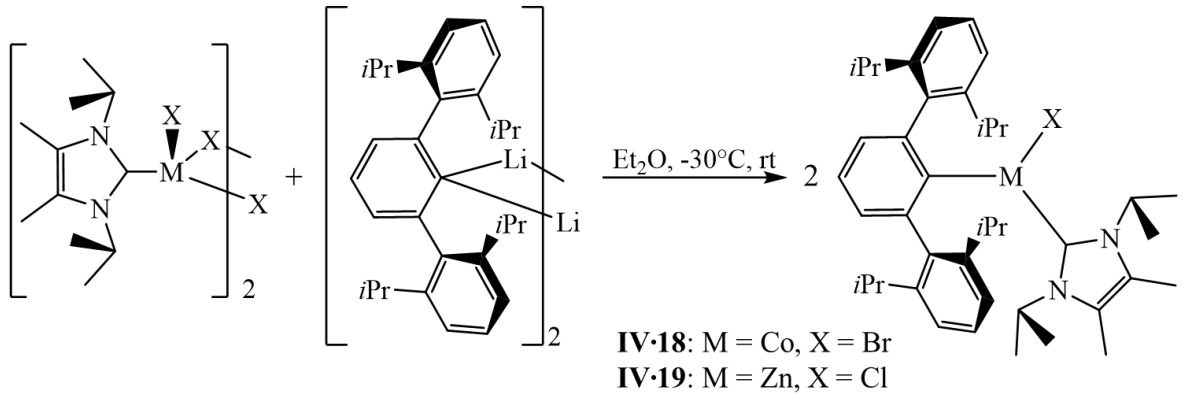

Scheme 4·6. The alternative synthetic route to **IV·18** and **IV·19** [MX = CoBr (**IV·18**) and ZnCl (**IV·19**)].

The $[2,6\text{-}Dipp_2C_6H_3]^-$ ligand was selected due to the increased steric presence provided by the *i*Pr groups in the *ortho* position on the flanking groups. It has also been shown by Power *et al*. to stabilise halide bridged, dimeric complexes that crystallise in high purity and yield.[170] The three-coordinate complexes $[2,6\text{-}Dipp_2C_6H_3]MX[IPrMe]$ [MX = FeCl (**IV·17**), CoBr (**IV·18**) and ZnCl (**IV·19**)] were synthesised. **IV·17** and **IV·18** were synthesised *via* the same method used to synthesis **IV·8**–**IV·13** (**Scheme 4·6**). An alternative synthesis was developed that used $[(IPrMe)MX_2]_2$ [MX = CoBr (**II·30**) and ZnCl (**II·31**)] as starting materials (**Scheme 4·6**). This alternative method was trialled with the aim of reducing or eliminating the occurrence of $[IPrMe]_2MX_2$ in the reaction mixture and to utilise an alternative starting material to $[2,6\text{-}Dipp_2C_6H_3ZnCl]_2$, which is difficult to isolate.[229]

This alternative method afforded **IV·18** in a yield of 25 % and still produced $[IPrMe]_2CoBr_2$ as a by-product. The standard method afforded a yield of 17 %. Despite this slightly increased yield, the standard method was used for the synthesis of **IV·18** as it requires less IPrMe, which is more expensive to synthesis than the *m*-terphenyl pro-ligands.

IV·18 was isolated as lime green crystals, again through layering of pentane onto a saturated solution of the complex in toluene. Accurate mass ASAP-MS established the presence of the complex. Elemental analysis showed that the purity was not within accepted limits with the theoretical and experimental carbon values differing by 0.88 %.

UV/Vis spectra at two different concentrations revealed three absorbances (Appendix C). Two, at 781 and 480 nm (ε = 133 and 145 $dm^3\ mol^{-1}\ cm^{-1}$, respectively), are of the correct intensity for d←d transitions. [179] There is a shoulder at 759 nm that could represent a third d←d transition giving the same number of absorbances as in **IV·15**. As in the spectrum of **IV·15** and many other *m*-terphenyl species there is an absorbance at 363 nm (ε = 2258 $dm^3\ mol^{-1}\ cm^{-1}$) which can be assigned to π*←π transitions within the *m*-terphenyl ligand.[76]

The ^{1}H NMR spectrum of **IV·18** (**Figure 4·16**) showed that the complex was paramagnetic. The spectrum contains six broad signals between −66.78 and 95.59 ppm. This is a similar range to that of complex **IV·15** (−48.32 to 88.19 ppm). As with **IV·15**, the spectrum of **IV·18** is also short of several peaks that are presumably subsumed into the broad peaks. The magnetic moment of the complex was determined to be 5.2 μ_B. This is significantly larger than the magnetic moment of **IV·15** (4.3 μ_B) and the spin only value (3.87 μ_B).

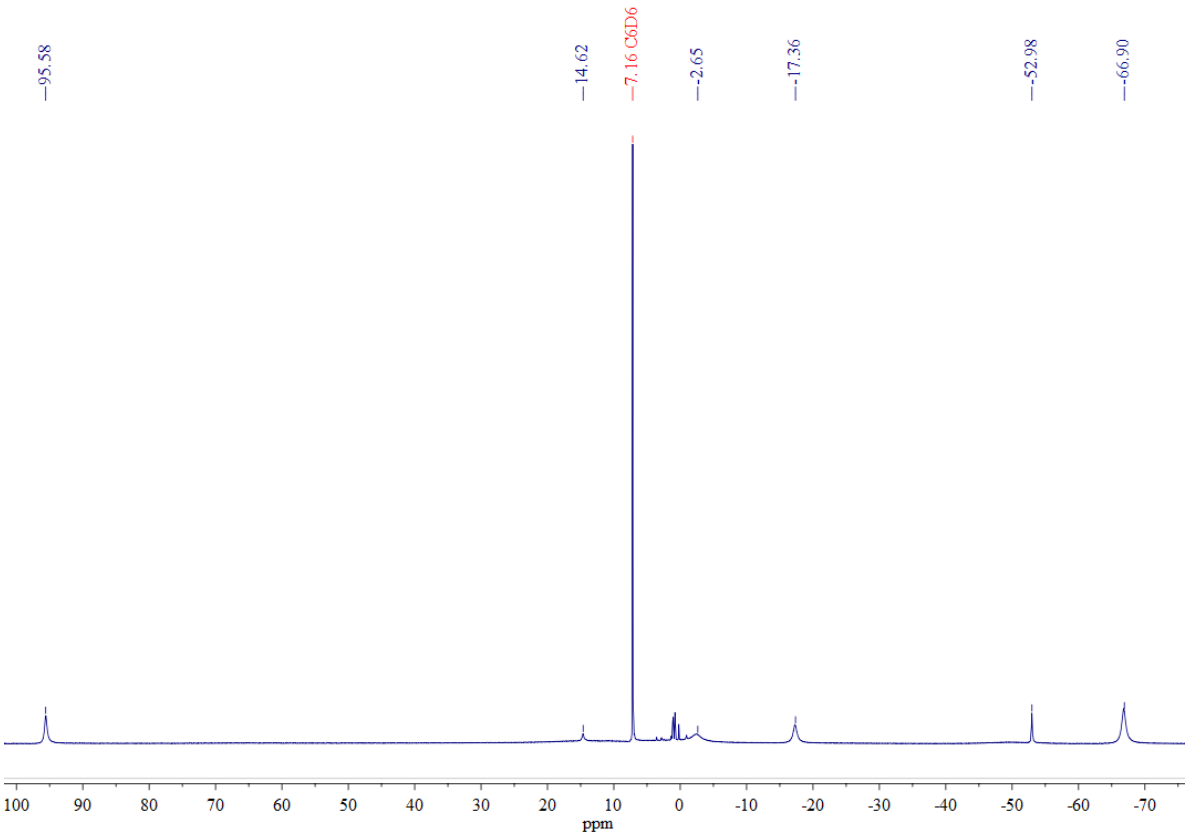

Figure 4·16. The ^{1}H NMR spectrum of **IV·18**.

As has been demonstrated, single ion species regularly exhibit larger magnetic moments than the spin only value, attributable to orbital contributions to the magnetic moment. That **IV·15** and **IV·18** have different magnetic moments is unexpected as they are similar complexes. The cause may be differences in the structures of **IV·15** and **IV·18**. However, both structures are similar in the solid-state despite of the increased bulk of the flanking groups in **IV·18**.

[2,6-$Dipp_2C_6H_3$]FeCl[IPrMe] (**IV·17**) was synthesised *via* the standard route using [2,6-$Dipp_2C_6H_3Fe(\mu\text{-}Cl)]_2\cdot[LiCl(OEt_2)]_2$, synthesised *via* literature methods, as a starting material.[170] **IV·17** was isolated as a brown-yellow powder in a yield of 18%. Yellow crystals were grown by vapour diffusion of pentane into a solution of **IV·17** in benzene-d_6. A satisfactory elemental analysis of the complex could not be obtained, either due to impurities in the product or decomposition during analysis. Accurate mass EI-MS demonstrated the presence of the parent ion (calculated 666.3743 m/z; found 666.3606). The UV/Vis spectrum contained one strong absorbance at 322 nm, attributed to a $\pi^*\leftarrow\pi$ transition and consistent with the spectrum of **IV·14**. The expected d←d transition of a d^6 species was not present.

The ^{1}H NMR spectrum of **IV·17** was similar to the spectrum of [2,6-$Mes_2C_6H_3$]FeCl[IPrMe] (**IV·14**). The complex is paramagnetic with ten signals between −59.48 and 28.09 ppm. Sharp signals at 0.24, 1.09, 2.11, 2.85 and 3.74 ppm could indicate a diamagnetic impurity, such as protonated ligand, that distorted the result of elemental analysis. The magnetic moment of the complex is 3.4 μ_B. This is lower than the spin only effective magnetic moment of a d^6 metal ion (4.90 μ_B) and of **IV·14** (4.8 μ_B). A likely reason for this is impurities in the samples used to establish this value as it is not consistent with the value for the other samples in this series.

The alternative synthesis shown in **Scheme 4·6** was used to synthesise **IV·19** due to the difficulty of isolating [2,6-$Dipp_2C_6H_3ZnCl]_2$.[229] This reaction yielded colourless crystals suitable for X-ray diffraction studies. ^{1}H NMR spectroscopic studies of the sample revealed

that the bulk sample contained several impurities and the resulting intractable series of signals could not be reliably assigned.

IV·18 crystallises in the monoclinic space group $P2_1/n$ (**Figure 4·17**). The asymmetric unit contains two crystallographically distinct molecules, each of which is disordered across two positions. Around 10% of each molecule is inverted, with the Co–Br unit projecting in the opposite direction to the other 90%. The disorder could only be modelled for the larger elements, cobalt and bromine leading to a large R_1 value of 0.1287 as the electron density for *ca*. 10% of the ligand system is not modelled.

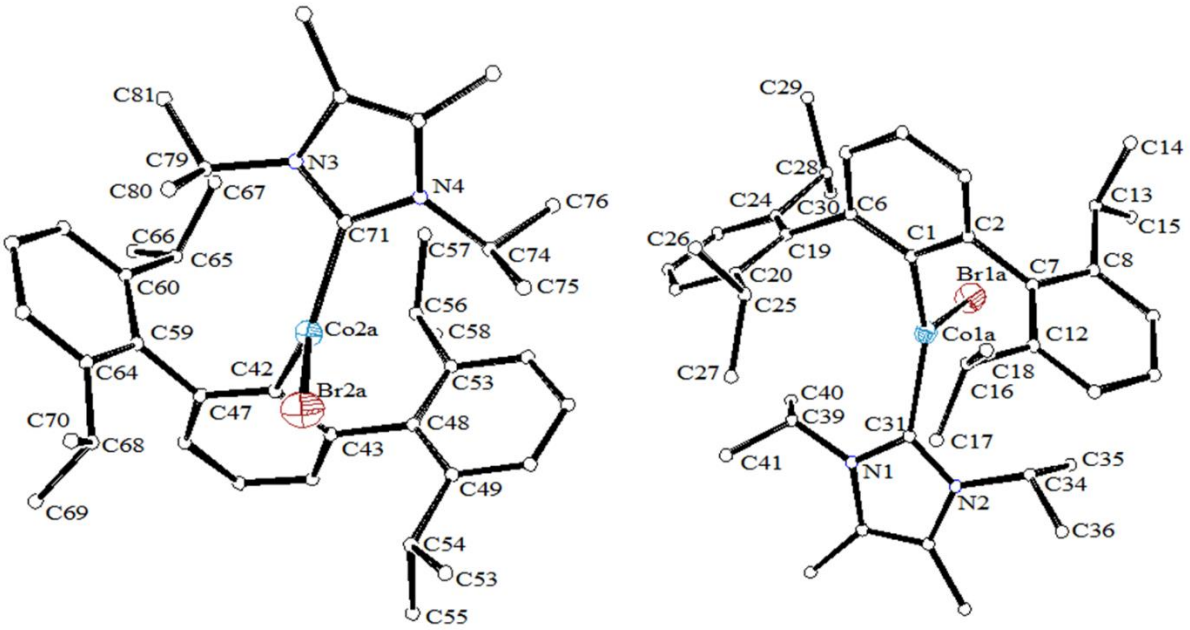

Figure 4·17. The solid-state structure of **IV·18** containing two crystallographically distinct molecules. Hydrogens and the disordered CoBr moieties are omitted, and carbon and nitrogen are represented as spheres, for clarity. Where present, ellipsoids are set at 50% probability.

The same disorder is observed in the structure of **IV·19** although only *ca*. 6% of the structure is disordered in this way leading to an R_1 value (0.0533). **IV·19** crystallises in the $Pna2_1$ space group. Key bond lengths, angles and geometric parameters of **IV·18** and **IV·19** are contained in **Table 4.5**. X-ray diffraction studies of **IV·17** revealed the crystals possess two degrees of disorder; a modular disorder as well as the M–X inversion disorder. A satisfactory solution for the data set obtained for **IV·17** could not be achieved.

Table 4.5. Bond lengths, bond angles and geometric parameters for **IV·18** and **IV·19**. (a/b atom notation refers to **IV·18** only).

	IV·18 (MX = CoBr)		**IV·19** (MX = ZnCl)	
	Atom Labels			
Bond Lengths				
C_{Ar}–M/Å	C1, Co1a	1.983(10)	C1, Zn1	1.980(5)
	C42, Co2a	2.003(11)	C42, Zn2	1.981(5)
C_{NHC}–M/Å	C31, Co1a	2.066(11)	C31, Zn1	2.028(5)
	C71, Co2a	2.041(11)	C72, Zn2	2.028(5)
X–M/Å	Br1a, Co1a	2.378(2)	Cl1, Zn1	2.3208(15)
	Br2a, Co2a	2.375(2)	Cl2, Zn2	2.3121(16)
	Br1b, Co1b	2.387(15)	Zn1A, Cl1A	2.30(2)
	Br2b, Co2b	2.373(14)	Zn2A, Cl2A	2.319(18)
H – bonds				
H_3C_{NHC}···X/Å[°]	C35, Br1a	3.10(17) [150(12)]	C34, Cl1	3.50(11) [138(8)]
	C40, Br1a	3.48(17) [134(12)]	C39, Cl1	3.03(10) [145(7)]
	C75, Br2a	3.30(17) [141(12)]	C75, Cl2	2.83(10) [160(7)]
	C80, Br2a	3.15(16) [144(11)]	C80, Cl2	3.17(10) [151(8)]
H_3C_{Dipp}···X/Å[°]	C30, Br1a	3.07(17) [119(11)]	C17, Cl1	2.70(9) [126(5)]
	C15, Br1a	2.94(10) [140(11)]	C30, Cl1	3.00(12) [122(8)]
	C53, Br2a	3.04(15) [125(10)]	C68, Cl2	2.92(9) [126(5)]
	C70, Br2a	3.18(17) [107(9)]	C56, Cl2	2.98(9) [122(6)]
HC_{Dipp}···X/Å[°]	C28, Br1a	3.18(13) [132(10)]	C28, Cl1	3.26(7) [122(5)]
	C13, Br1a	3.56(13) [109(8)]	C13, Cl1	3.24(7) [124(5)]
	C68, Br2a	3.16(13) [123(8)]	C69, Cl2	3.35(7) [116(5)]
	C54, Br2a	3.20(12) [119(8)]	C55, Cl2	3.29(8) [116(5)]
CH_{NHC}··· C_{Dipp} /Å[°]	C39, C19	2.94(13) [162(9)]	C39, C19	2.94(8) [159(5)]
	C34, C7	3.23(13) [163(10)]	C34, C7	3.10(8) [176(6)]
	C79, C59	2.80(13) [169(10)]	C80, C48	3.09(8) [163(6)]
	C74, C48	N/A	C75, C60	3.23(8) [168(6)]

	IV·18 (MX = CoBr)		**IV·19** (MX = ZnCl)	
Bond Angles				
C–M–C /°	C1, Co1a, C31	137.9(5)	C1, Zn1, C31	143.9(2)
	C42, Co2a, C71	141.2(5)	C42, Zn2, C72	143.5(2)
C–M–X/°	C42, Co2a, Br2a	114.4(3)	C1, Zn1, Cl1	114.52(15)
	C1, Co1a, Br1a	114.9(3)	C42, Zn2, Cl2	114.63(15)
	C71, Co2a, Br2a	104.3(3)	C31, Zn1, Cl1	101.55(16)
	C31, Co1a, Br1a	107.1(3)	C72, Zn2, Cl2	101.83(5)
Interplanar Angles				
NHC–(C_{Ar}-M-X)	C71, C42, Co2a, Br2a	85.87(97)	C72, C42, Zn2, Cl1	85.81(45)
/°	C31, C1, Co1a, Br2a	86.76(95)	C31, C1, Zn1, Cl1	89.85(48)
Ar–(C_{NHC}-M-X)	C42, C71, Co2a, Br2a	86.68(95)	C42, C72, Zn2, Cl1	97.49(45)
/°	C1, C31, Co1a, Br2a	89.16(89)	C1, C31, Zn1, Cl1	104.08(39)
Dipp–$Ar_{central}$/°	C24, C19, C6, C1	89.2(15)	C65, C60, C47, C42	83.89(62)
	C8, C7, C2, C1	98.3(13)	C53, C48, C43, C42	85.32(64)
	C49, C48, C43, C42	96.3(13)	C20, C19, C6, C1	84.34(62)
	C64, C59, C47, C42	88.1(14)	C8, C7, C2, C1	93.05(62)
$Plane_{Ar}$–	C42, C71	31.87 (33)	C1, C31	21.59(18)
$Plane_{NHC}$ /Å	C1, C31	35.35(31)	C42, C71	19.56(19)
Dihedral angles				
IPr Group (Ar)	C14, C13, C8, C7	91.9(13)	C14, C13, C8, C7	88.08(65)
CH_3–CH–C–C/°	C18, C16, C12, C7	107.3(13)	C18, C16, C12, C7	103.27(65)
	C29, C28, C24, C19	90.9(14)	C29, C28, C24, C19	90.85(68)
	C26, C25, C20, C19	105.5(12)	C26, C25, C20, C19	119.67(65)
	C53, C54, C49, C48	149.8(11)	C56, C54, C49, C48	104.10(62)
	C57, C56, C53, C48	125.4(41)	C59, C57, C53, C48	96.63(63)
	C70, C68, C64, C59	146.4(12)	C67, C66, C61, C60	110.96(63)
	C67, C65, C60, C59	119.4(13)	C71, C69, C65, C60	144.92(58)
IPr Group	C40, C39, N1, C31	98.8(13)	C40, C39, N1, C31	99.17(66)
(NHC)	C35, C34, N2, C31	100.1(13)	C96, C94, N2, C31	103.80(65)
CH_3–CH–N–C_I	C81, C79, N3, C71	132.4(12)	C81, C80, N4, C72	97.79(67)
/°	C76, C74, N4, C71	131.0(11)	C85, C75, N3, C72	98.10(67)
Out of Plane Distortions				
M–$Plane_{NHC}$ /Å	Co2a	0.406(20)	Zn1	0.4509(93)
	Co1a	0.460(20)	Zn2	0.3728(91)
M–$Plane_{Ar}$ /Å	Co2a	0.220(16)	Zn1	0.1801(71)
	Co1a	0.201(19)	Zn2	0.1628(77)
Geometric Index				
τ_3	Co2a	0.65	Zn1	0.60
	Co1a	0.70	Zn2	0.61

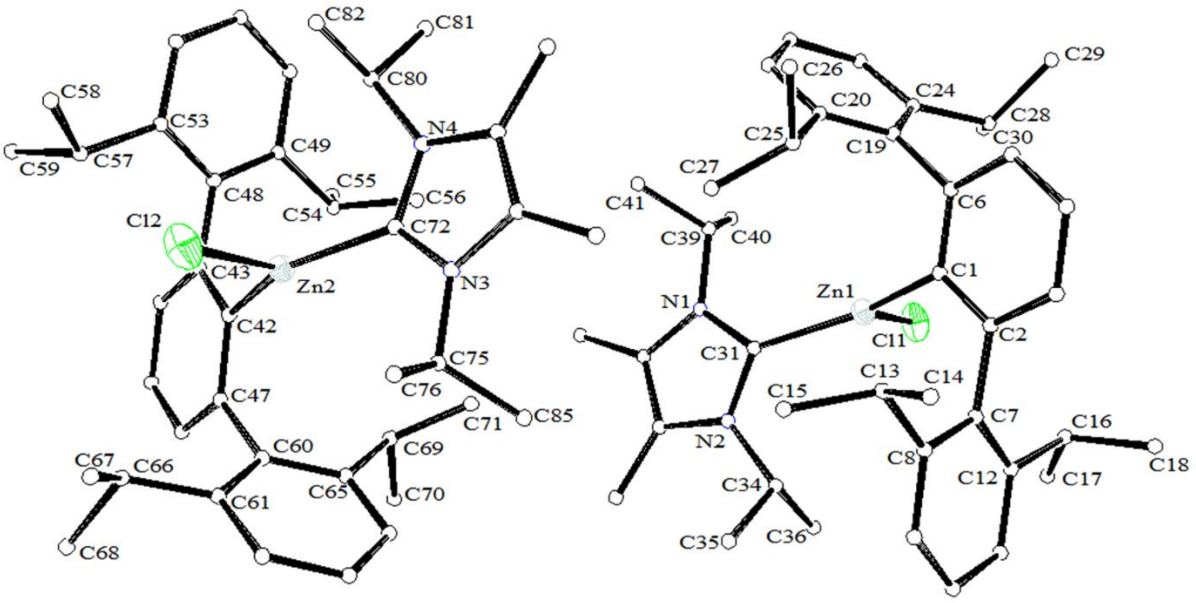

Figure 4·18. The solid-state structure of **IV·19** containing two crystallographically distinct molecules. Hydrogens and the disordered ZnCl moieties are omitted for clarity, and carbon and nitrogen are represented as spheres. Where present, ellipsoids are set at 50% probability.

IV·18 (**Figure 4·17**) and **IV·19** (**Figure 4·18**) have similar structures to **IV·15** and **IV·10**, respectively. The M–C and M–X distances in both comparative sets are within error of one another.

The angles between the ligands around the metal centre are also similar. The largest angle occurs between the *m*-terphenyl and NHC ligands, which is wider in [2,6-$Dipp_2C_6H_3$]MX[IPrMe] compared with [2,6-$Mes_2C_6H_3$]MX[IPrMe]. This reflects the increased steric bulk of the [2,6-$Dipp_2C_6H_3$]$^-$ ligand compared to the [2,6-$Mes_2C_6H_3$]$^-$ ligand. In both **IV·18** and **IV·19** this angle, within one of the crystallographically distinct units, is within error of the mesityl analogue [142.53(17) (**IV·10**) and 143.5(2)° (C42, Zn2, C72) (**IV·19**), 138.7(2) (**IV·15**) and 137.9(5)° (C1, Co1a, C31) (**IV·18**)]. However, in the other crystallographically distinct unit the angle is distinctly wider [143.9(2) (C1, Zn1, C31) (**IV·19**) and 141.2(5)° (C42, Co2a, C71) (**IV·18**)]. This demonstrates the flexibility of this angle and that it can be expanded by the [2,6-$Dipp_2C_6H_3$]$^-$ ligand compared with the [2,6-$Mes_2C_6H_3$]. However, only for the cobalt structures does this change the geometry of the complex

significantly according to the τ_3 parameter [0.62 (**IV·10**) and 0.60 (Zn1) or 0.62 (Zn2) (**IV·19**), 0.69 (**IV·15**) and 0.65 (Co2a) or 0.70 (Co1a) (**IV·18**)].

Unexpectedly, there is a distinct contraction of the *i*-C_{Ar}–M–X angles in **IV·18** and **IV·19** when compared with the mesityl analogues [118.30(13)° (**IV·10**) to 114.52(15) (Zn1) and 114.63(15)° (Zn2, **IV·19**), and 119.36(16)° (**IV·15**) to 114.4(3) (Co2a) and 114.9(3)° (Co1a, **IV·18**)]. This occurs with a concomitant expansion of the C_{IPrMe}–M–X angles [99.16(13)° (**IV·10**), to 101.55(16) (Zn1) and 101.83(5)° (Zn2, **IV·19**) and 97.03(16)° (**IV·15**) to 104.3(3) (Co2a) and 107.1(3)° (Co1a, **IV·18**)]. Given that steric bulk has been added to the *m*-terphenyl ligand the opposite pattern of expansion and contraction would be expected. These observations suggest that other factors influence this angle. An inspection of hydrogen bonding in the structure provides one possible explanation.

As in the mesityl analogues, there are close contacts between the *i*Pr CH groups of the IPrMe ligand and the aryl system of opposing, *m*-terphenyl flanking groups, [$C_{iPr}H\cdots i$-C_{Mes} 2.94(13)–3.23(13) Å (**IV·18**) and 2.94(8)–3.23(8) Å (**IV·19**)]. These have no noticeable impact on the structure. However, it is the interactions between the organic ligands and the halide that could be influencing the solid-state structure.

In the [2,6-$Mes_2C_6H_3$]MX[IPrMe] complexes there is evidence of the CH_3 groups of the [2,6-$Mes_2C_6H_3$]$^-$ forming close interactions with the halides. However, the number of interactions is balanced by the number of interactions between the *i*Pr groups of the IPrMe ligand. In **IV·18** and **IV·19** the *i*Pr groups of the [2,6-$Dipp_2C_6H_3$]$^-$ ligand allow the possible formation of four CH···X interactions from *m*-terphenyl ligand. The *i*Pr groups of the NHC ligand are twisted such that the CH_3 groups are brought closer to the halide moiety [$CH_3\cdots X$ = 3.10(17)–3.48(17) Å (**IV·18**), 2.83(10)–3.50(11) Å (**IV·19**, **Table 4.5**]. This indicates the short CH···X distance associated with this group is a hydrogen bond. This twist means that the tertiary CH group is

moved away from the halide moiety, preventing a CH···X interaction. In contrast, the *i*Pr groups of the *m*-terphenyl ligand are twisted such that the tertiary CH group is brought closer to the halide moiety [$C_{iPr}H\cdots X$ = 3.16(13)–3.56(13) Å (**IV·18**), 3.24(7)–3.35(7) Å (**IV·19**) (**Table 4.5**)], whilst the CH_3 group is still able to form interactions with the halide of the same length of those between the NHC *i*Pr group and the halide [$C_{iPr}H_3\cdots X$ = 2.94(10)–3.18(17) Å (**IV·18**), 2.70(9)–3.00(12) Å (**IV·19**), **Table 4.5**], contributing to the contraction of the C_{Ar}–M–X angles in these complexes when compared to the [2,6-$Mes_2C_6H_3$]MX[IPrMe] analogues.

The *m*-terphenyl ligands in complexes **IV·18** and **IV·19** are in a co-planar arrangement as they are in the mesityl analogues. In turn the metal is lifted out of the plane of the ligands (**Table 4·6**). This distortion may be an indicator of the steric strain in the system, the degree to which the structure is flexing to accommodate CH···X interactions or imposed by crystal packing forces. The degree of this distortion, measured in distance of the metal from an infinite plane, is similar and often within error between the cobalt and zinc complexes.

Table 4·6. The out of plane distortions of the metal from the ligands in complexes **IV·15** and **IV·18** (cobalt) and **IV·10** and **IV·18** (zinc).

	[2,6-$Mes_2C_6H_3$]MX[IPrMe]		[2,6-$Dipp_2C_6H_3$]MX[IPrMe]	
	NHC	***m*-Terphenyl**	**NHC**	***m*-Terphenyl**
Cobalt/Å	0.439(10)	0.2423(87)	0.406(20) 0.460(20)	0.220(16) 0.201(19)
Zinc/Å	0.4255(76)	0.1960(66)	0.4509(93) 0.3728(91)	0.1801(71) 0.1628(77)

4.3.5 Two-Coordinate, Heteroleptic, Transition Metal Complexes

IV·18 was investigated as a precursor to a two-coordinate heteroleptic, transition metal complex. The reduction of **IV·18** in toluene with a potassium mirror or two equivalents of KC_8 affords the two-coordinate metal complex [2,6-$Dipp_2C_6H_3$]Co[IPrMe] (**IV·20**, **Scheme 4·7**). **IV·20** was obtained as red crystals in a yield of 34% by cooling a saturated solution of the complex in pentane to 7°C.

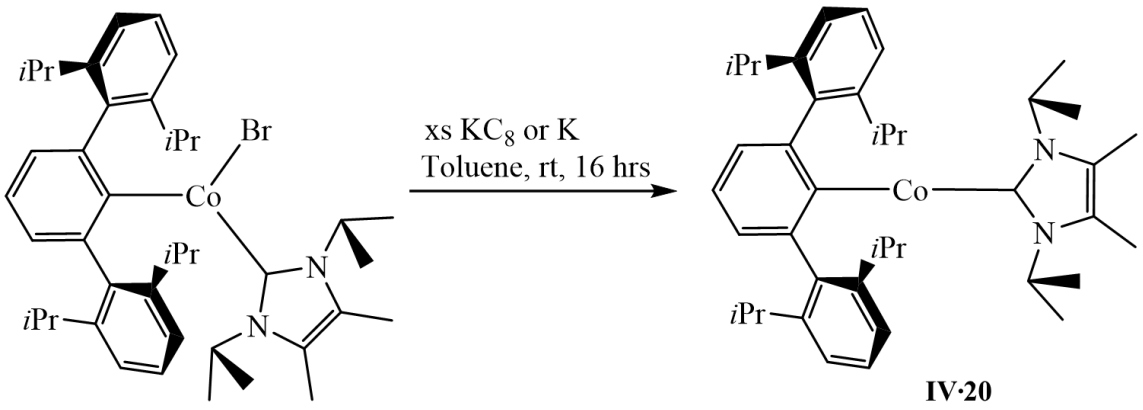

Scheme 4·7. The synthesis of [2,6-Dipp$_2$C$_6$H$_3$]Co[IPrMe] (**IV·20**).

Accurate mass ASAP-MS of **IV·20** demonstrated the presence of the parent ion. The spectrum also revealed the presence of a small amount of **IV·18** presenting the possibility that **IV·20** forms from the starting material *via* the loss of a halide in the spectrometer, as with **IV·10–IV·12**. However, the spectrum of the starting material contains a different ratio of the products, suggesting that **IV·20** is present before ionisation. X-ray diffraction and elemental analysis confirmed that the majority of the sample was **IV·20**.

The UV/Vis spectrum contains four absorbances (Appendix C). The three, highest wavelength absorbances, at 681, 514 and 442 nm (ε = 453, 892, and 2308 dm^3 mol^{-1} cm^{-1}, respectively), can be attributed to d←d transitions. X-ray diffraction studies revealed the complex to be almost linear along the ligand metal axis [*i*-C$_{Ar}$–Co–*i*-C$_{NHC}$ = 178.69(9)°]. This results in a splitting pattern that allows three distinct, d←d transitions to occur.[199] The fourth signal at 374 nm (ε = 3696 dm^3 mol^{-1} cm^{-1}) is consistent with the π^*←π transitions seen when an *m*-terphenyl ligand is present.[76]

The ^{1}H NMR spectrum of **IV·20** (**Figure 4·19**) contains six broad signals between −78.18 and 120.71 ppm. These could not be assigned due to the paramagnetism of the complex and the resulting broadening and shifting of the signals. The effective magnetic moment of the complex was determined to be 4.3 μ_B. This is larger than the spin only value for a d^8 complex (2.83 μ_B), which suggests an orbital contribution. This value is also larger than the magnetic moments of

[(2,6-{C(H)Ph$_2$}$_2$-4-MeC$_6$H$_3$)(SiPh$_3$)N]Co^{I}[IPrMe] (**IV·9**, 2.6 μ_B)[53] and [(IAd)$_2$Co^{I}][BAr$^{F}_4$] (**IV·21**, 3.94 μ_B), but smaller than those of [(sIMes)$_2$Co^{I}][BAr$^{F}_4$] (**IV·22**, 5.10 μ_B), [(IMes)$_2$Co^{I}][BAr$^{F}_4$] (**I·63**, 5.40 μ_B)[126] and [IPr]Co^{I}[N(SiMe$_3$)] (6.25 μ_B, **IV·5**).[125] As has been discussed a linear geometry around a metal centre can increase the magnetic moment of a species and explains the elevated magnetic moment. Danopoulos *et al*. demonstrated that an electron from the metal in a NHC, metal(I) species can disassociate to afford a metal(II) centre interacting with a single, delocalised electron onto the NHC ligand.[125]

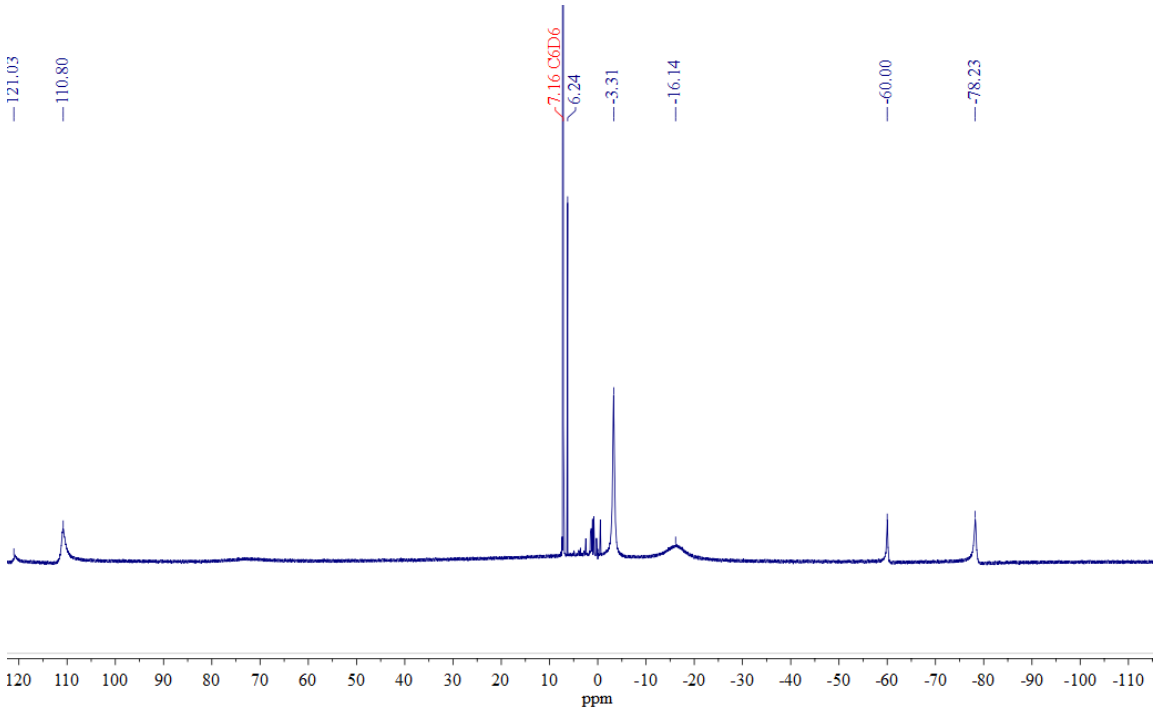

Figure 4·19. The ^{1}H NMR spectrum of **IV·20**.

Two polymorphs of **IV·20** were obtained. **IV·20a** (**Figure 4·20**) was isolated as previously described. The second polymorph, **IV·20b**, was obtained by vapour diffusion of pentane into a solution of **IV·20** in benzene-d$_6$ and methyl acrylate (0.0174 mmol). This was as part of an investigation into the application of **IV·20** as a catalyst for the hydrosilylation of alkenes.[127,129] No catalytic effect was identified. **IV·20a** crystallises in the monoclinic space group *Cc* whilst **IV·20b** crystallises in the triclinic space group *P*-1. Key bond lengths and angles can be found in **Table 4·7**.

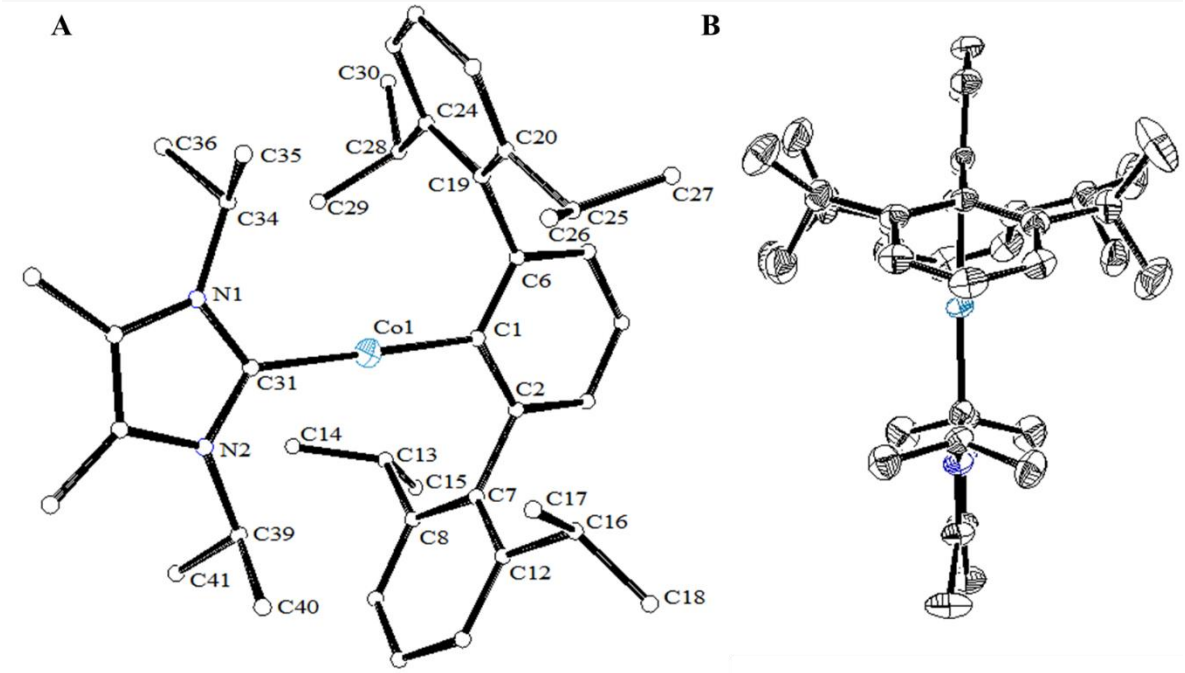

Figure 4·20. The solid-state structure of **IV·20a**. Hydrogens have been omitted for clarity and ellipsoids have been set at 50% probability where present. **A**) carbon and nitrogen are represented as spheres and key atoms are labelled. **B**) Showing the co-planar arrangement of the two ligands.

Table 4·7. Key bond lengths and angles for both polymorphs of **IV·20**.

		IV·20a	**IV·20b**
	Atom Labels		
Bond Lengths			
C–Co/Å	C1	1.966(2)	1.963(5)
	C31	1.976(2)	1.973(5)
H – bonds			
CH_{3iPr}···Co/Å[°]	C39, Co1	2.71(3) [126(2)]	2.58(7) [125(5)]
	C34, Co1	2.68(3) [124(2)]	2.73(8) [112(5)]
CH_{3Dipp}···Co/Å[°]	C14, Co1	3.23(6) [130(4)]	4.296(13) [N/A]
	C29, Co1	2.85(5) [158(4)]	3.03(15) [143(10)]
	C17, Co1	2.95(5) [148(4)]	3.58(16) [139(13)]
CH_{iPr}···*i*-C_{Dipp}/Å[°]	C34, C19	3.35(3) [172(2)]	3.23(8) [168(5)]
	C39, C7	3.28(3) [171(2)]	3.10(8) [178(5)]
Bond Angles			
C–Co–C/°	C1, Co1, C31	178.69(9)	179.1(2)
Dihedral Angles			
Dipp–$Ar_{Central}$/°	C1, C2, C7, C8	87.21(25)	94.73(60)
	C1, C6, C19, C24	98.60(25)	83.24 (64)
CH_3–CH–C–C/°	C29, C28, C24, C19	89.88(29)	118.32(80)
	C17, C16, C12, C7	131.87(24)	139.93(72)
	C27, C25, C20, C19	93.26	115.12(85)
	C14, C13, C8, C7	125.20	124.21(80)
CH_3–C–N–C/°	C36, C34, N1, C31	117.76(26)	118.60(73)
	C40, C29, N2, C31	117.14(24)	115.02(64)
Ar–NHC/°		4.08(15)	9.24(26)
Out of Plane Distortions			
Co–NHC /Å		0.0650(37)	0.0027(95)
Co–Ar/Å		0.0799(31)	0.0725(73)

The C1–Co1–C31 angle in **IV·20** is close to linear [178.69(9) (**IV·20a**) and 179.1(2) (**IV·20b**)]. Similar complexes bearing NHC ligands also possess this linear geometry, including **IV·19**-**IV·21** [178.6(1)°, 178.6(1)° and 180°, respectively].[126] Unlike these examples, the two ligands in **IV·20** approach a co-planar arrangement [4.09(15)° and 9.24(26)° (**IV·20a** and **b**) 39.55°, 35.02° and 90° (*sic*) (**IV·21**, **IV·22**, and **I·63**, respectively)]. Deng *et al*. note that the dihedral angle between the two ligands decreases with the steric bulk of the flanking groups and the dihedral angle in **IV·20** fits with this trend.[126] The total steric bulk of the ligands in **IV·20** is low when compared with the complexes in Deng's study. As well as this, because the two ligands in **IV·20** differ greatly in size and structure the flanking groups move in different spheres around the metal centre and so the steric clash between them, that presumably enforces the move away from co-planarity observed by Deng, is limited when compared with a homoleptic complex.

The reason that a planar arrangement of the ligands is preferred is less obvious. As discussed for the three-coordinate complexes above, the formation of favourable, hydrogen bonding interactions between the aryl system of the *m*-terphenyl flanking groups and the $C_{iPr}H$ of the IPrMe ligand may contribute to this arrangement. This would not, however, hold true for the ligand system employed by Deng and co-workers.[126] Another series of complexes by Deng *et al*., [NHC]Co^{II}[2,6-$Mes_2C_6H_3N$] [NHC = IPr (**I·95**), CyIPr (**I·99**) or sIMes (**I·100**)], features two sterically bulky ligands.[124] The imido linkage between the cobalt and *m*-terphenyl moiety enforces a greater distance between the two ligands allowing them to rotate freely. However, in this case the ligands adopt a perpendicular arrangement in contrast to the earlier observations by the same group. It is likely therefore that the nature of the cobalt-ligand bond contributes to the favourability of co-planarity.

The flanking Dipp and *i*Pr groups of the two ligands are orientated close to a sterically optimum geometry. Some of the *i*Pr groups of the *m*-terphenyl are twisted away from the idealised 120°,

such that the C$_{i\text{Pr}}$H axis points towards the metal centre. These distortions are greater where the CH$_3$···Co distances are shorter. For example, the CH$_3$–CH–C–C angle in **IV·20a** that deviates the most from an idealised 120° [89.88(29)°, C29–C28–C24–C19] correlates with the shortest CH$_{3i\text{Pr}}$···Co distance [2.71(3) Å (C39H$_3$···Co1)]. This raises the possibility of CH$_3$···Co interactions similar to those proposed by Kays and Power.[52,63,76] The Dipp flanking groups also create a steric pocket around the metal centre, as can be observed in **Figure 4·20**. This could also explain why it was possible to isolate **IV·20** but not [2,6-Mes$_2$C$_6$H$_3$]$_2$Co[IPrMe].

Several attempts were made to reduce [2,6-Dipp$_2$C$_6$H$_3$]$_2$FeCl[IPrMe] (**IV·17**) and [2,6-Dipp$_2$C$_6$H$_3$]$_2$ZnCl[IPrMe] (**IV·19**), using the same method**s** used for the [2,6-Mes$_2$C$_6$H$_3$]$_2$MX[IPrMe] analogues, to afford [2,6-Dipp$_2$C$_6$H$_3$]$_2$M[IPrMe] (M = Fe^{I} and Zn^{I} respectively). The reaction between **IV·19** and KC$_8$ or sodium shavings afforded a metallic, grey powder assumed to be zinc metal and a clear solution from which **IV·19** was isolated. The reaction between **IV·17** and KC$_8$ resulted in a colour change in the reaction mixture from a pale yellow to intense green. However, only 2,6-Mes$_2$C$_6$H$_4$ could be isolated from this reaction despite multiple attempts and the rigorous exclusion of air.

An electrochemical study of the reduction of **IV·18** was conducted to gain a greater insight into the reaction that affords **IV·20**. Cyclic voltammograms were measured at a glassy carbon electrode at 0.05 Vs^{-1} in a solution of **IV·18** (2 mM) and TBABF$_4$ (35 mM) in THF. A silver wire pseudo-reference was used for the electrochemical measurements and measurements were conducted under a dinitrogen environment. To obtain a reference potential the analyte solution was replaced at the end of the measurement with a blank solution containing ferrocene. Although this is not an ideal method for obtaining a reference potential, it was found that ferrocene, was able to react with **IV·18** upon addition to the test solution and could not clearly be detected in the resulting voltammogram. It was therefore necessary to use ferrocene to indirectly reference the cell in the absence of **IV·18**, introducing an error to the measurements

that must be considered when interpreting the data. The voltammetric data was referenced to ferrocene.[317]

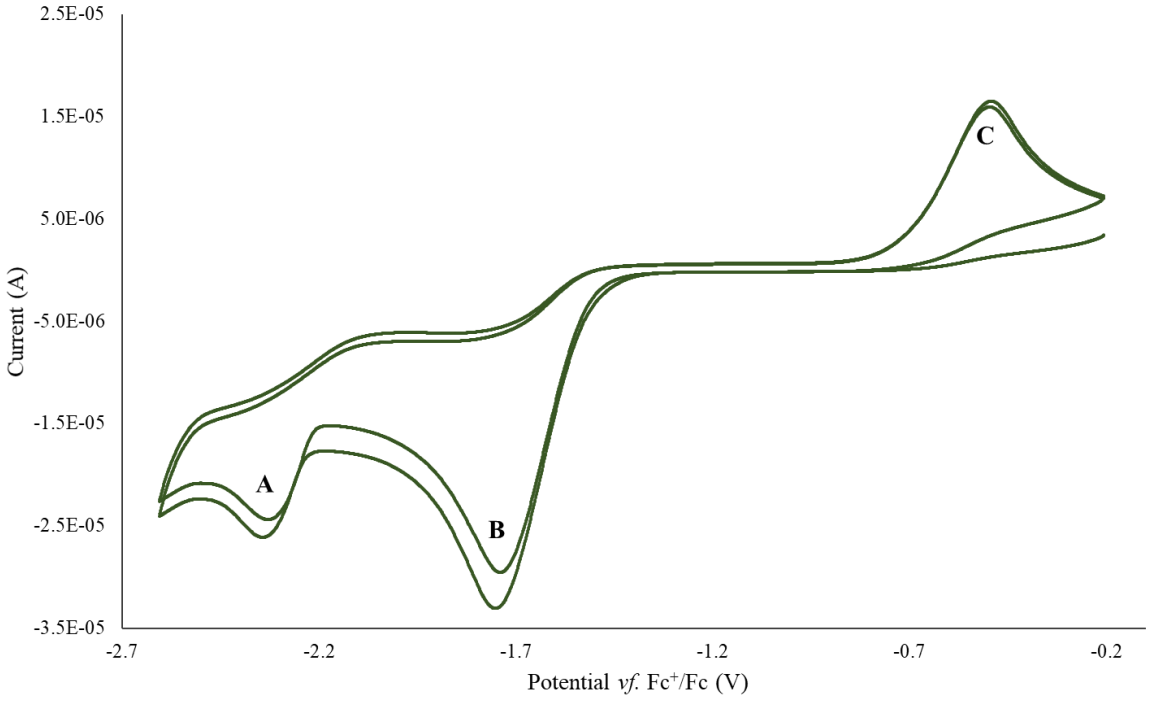

Peak	A	B	C
E (V)	−2.27	−1.61	−0.62
I_{pc}/I_{pa} (A)	-9.78×10^{-6}	-3.43×10^{-5}	1.658×10^{-5}

Figure 4·21. Cyclic voltammogram of **IV·18**. Init E = −0.19 V, High E = −0.19 V, Low E = −2.6 V, Scan rate = 0.05 Vs^{-1}. The table contains data for the three processes.

The study of **IV·18** revealed two reductions (reductions **A** and **B**) which occur between potentials of −1.2 and −2.6 V vs. Fc^+/Fc and an oxidation on the return sweep (oxidation **C**, **Figure 4·21**). Both reductions **A** and **B** are electrochemically irreversible. Reduction **B** is chemically reversible; the cyclic voltammogram shown in **Figure 4·22** links reduction **B** to oxidation **C**. This reductive reaction can be assigned to the reduction of the metal centre from Co(II)→Co(I) that occurs in the formation of **IV·20**, to afford the charged species $[(2,6\text{-}Dipp_2C_6H_3)CoBr(IPrMe)]^-$. It is likely that this species then reacts to form a compound with an oxidation potential at −0.62 V vs Fc^+/Fc. The reductive process occurs at a more positive potential than the reduction potential of KC_8, used to isolate **IV·20**.[179]

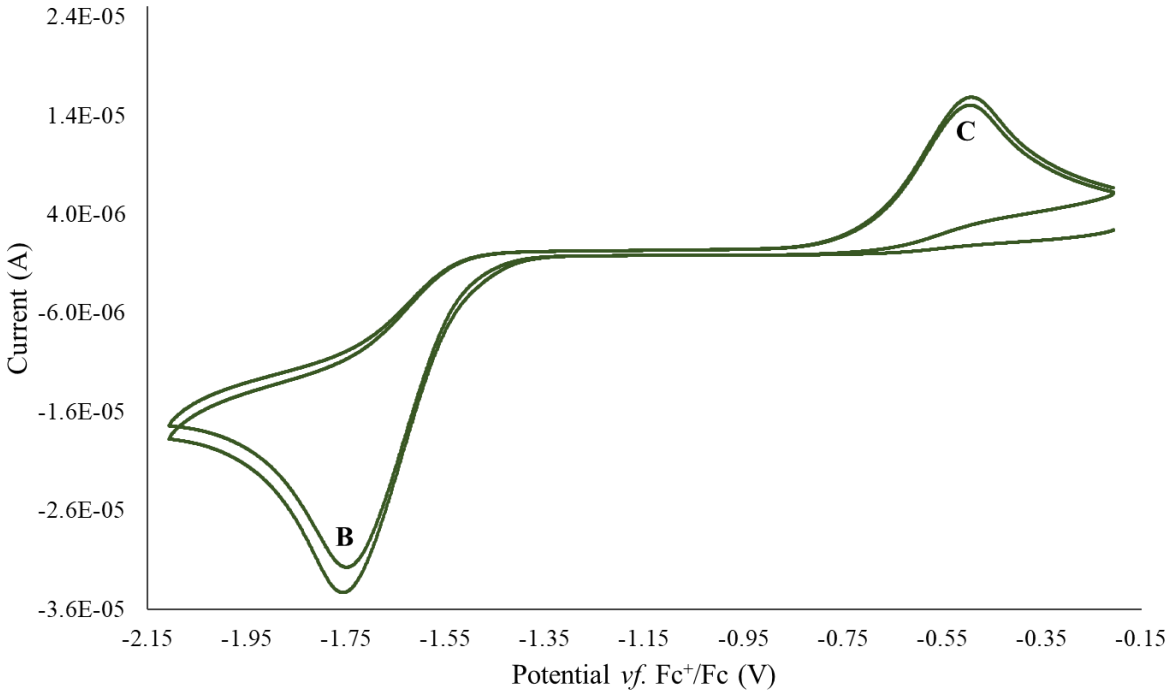

Figure 4·22. Cyclic voltammogram of **IV·18**. Init E = 0.4 V, High E = 0.4 V, Low E = −1.5 V, Scan rate = 0.05 Vs^{-1}. Segment = 4.

The species formed during reduction **B** can be further reduced at −2.27 V vs Fc^{+}/Fc (reduction **A**, **Figure 4·21**). There is no return oxidation process and reduction **A** is therefore both electrochemically and chemically irreversible. This peak may be a reduction of the cobalt centre from Co(I)→Co(0). It is possible that the zero valent cobalt species then decomposes *via* an unidentified pathway to a species that cannot be oxidised. This process also occurs at a potential higher than that of the reducing agent used to synthesise **IV·20**. This could explain why yields of **IV·20** higher than 38% could not be achieved. However, it should be noted that KC_8 also removes the halide anion from the reaction as a stable, neutral compound, KBr, in the synthesis. It may be, therefore, that the intermediate formed in reduction **B** is unable to undergo further reduction, being chemically changed through reaction with K^{+}.

4.3.6 IPr Complexes

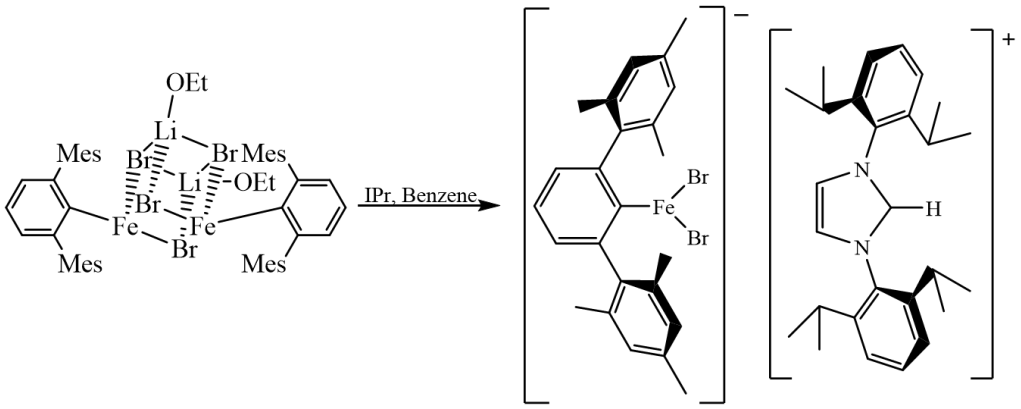

IV·23

Scheme 4·8. The synthesis of [2,6-$Mes_2C_6H_3FeBr_2$][IPrH] (**IV·23**).

Whilst increasing the steric bulk of the *m*-terphenyl ligand was a successful strategy in the stabilisation of **IV·20**, a similar iron complex could not be isolated. The use of IPr [IPr = 1,3-bis(2,6-diisopropylphenyl)imidazoline-2-ylidene], a bulkier NHC, was therefore investigated. One equivalent of IPr was added to a solution of [2,6-$Mes_2C_6H_3MBr]_2$·[$LiBr(OEt_2)]_2$ [M = Fe (**II·39**) and Co (**II·40**)] in C_6D_6. NMR spectroscopic data was collected on the reaction mixtures before crystallisation was induced through the addition of pentane by vapour diffusion.

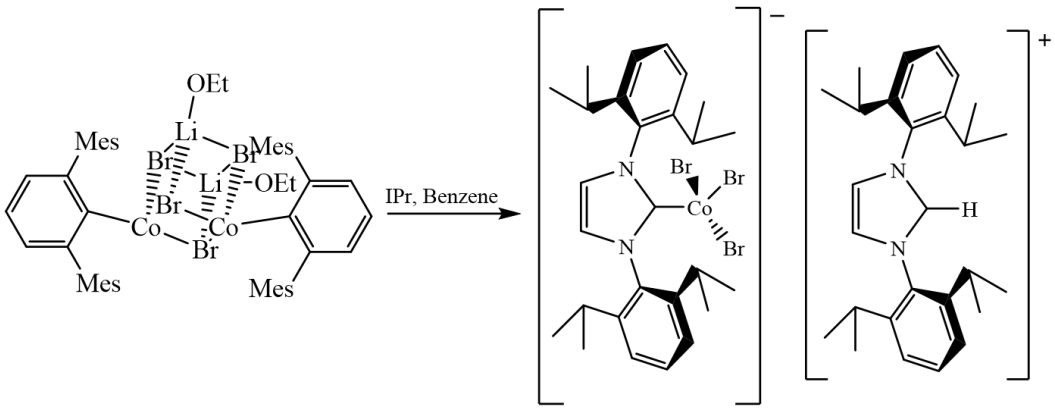

IV·24

Scheme 4·9. The synthesis of [$IPrCoBr_3$][IPrH] **(IV·24)**.

The reaction between IPr and **II·39** afforded yellow crystals of the [2,6-$Mes_2C_6H_3FeBr_2$][IPrH] (**IV·23**, **Scheme 4·8**), through protonation of an IPr moiety and the transfer of a bromide from either LiBr or a [2,6-$Mes_2C_6H_3FeBr$] monomer to the iron centre. The reaction between **II·40**

and IPr afforded [IPrCoBr$_3$][IPrH] (**IV·24**, **Scheme 4·9**) through similar processes the exchange of the cobalt bound *m*-terphenyl with IPr also occurs.

Both complexes were identified through X-ray diffraction studies of crystals isolated from the reaction mixture. **IV·23** crystallises as pale yellow blocks. **IV·24** crystallises as blue pillars alongside colourless plates and small, lime green crystals. The green crystals were not of suitable quality or quantity for X-ray diffraction studies or other forms of analysis. The colourless plates were identified as 2,6-Mes$_2$C$_6$H$_4$.

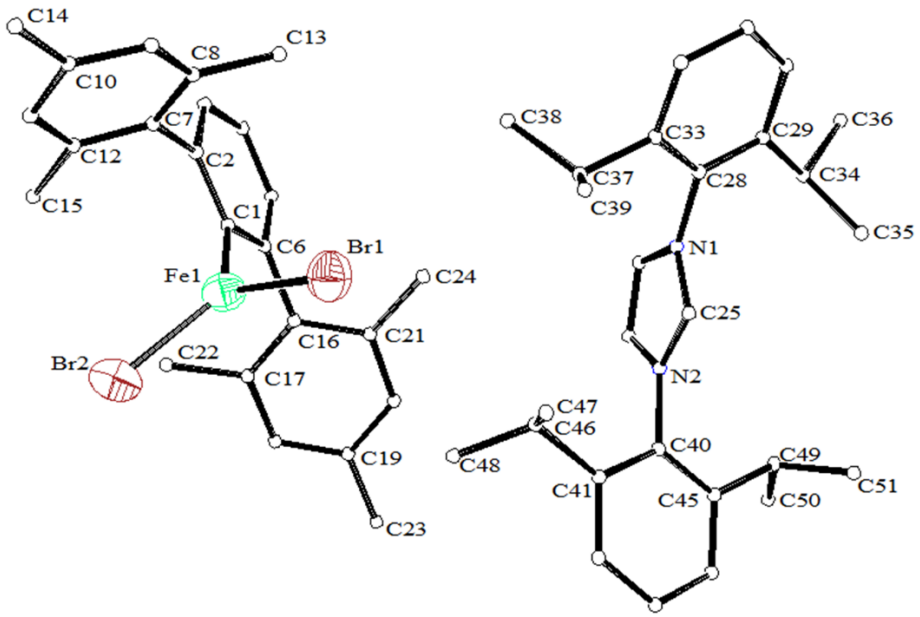

Figure 4·23. The solid state structure of [2,6-Mes$_2$C$_6$H$_3$FeBr$_2$][IPrH] (**IV·23**). Hydrogens have been omitted for clarity and ellipsoids have been set at 50% probability.

Both reactions were performed inside sealed Young's tap NMR tubes and manipulated under a dinitrogen atmosphere in a glove box. The ingress of air was unlikely and thus the protons are likely derived either from the solvent or from the ligand structures. This was also the conclusion of Aldridge *et al*. when they isolated **IV·24** as a product of the reaction between two equivalents of IPr and CoBr$_2$·2THF in THF.[167] The authors do note, however, that the origin of the imidazolium proton in adventitious water in the solvent cannot be conclusively ruled out. The steric strain around the metal centre must cause the decomposition of intermediates, possibly the desired products, in to **IV·23** and **IV·24**. Aldridge *et al*. found that

reducing the steric bulk of the carbene, using IMes instead of IPr, facilitated the isolation of $[IMes]_2CoBr_2$, although some evidence of an IMes analogue of **IV·24** was observed.[167]

Table 4·8. Key bond lengths, angles, and geometric parameters for **IV·23** and **IV·24**.

	IV·23 (M = Fe)		**IV·24** (M = Co)	
	Atom Label		**Atom Label**	
Bond Lengths				
M–C/Å	Fe1, C1	2.054(3)	Co1, C1	2.070(3)
M–Br/Å	Fe1, Br1	2.4064(6)	Co1, Br1	2.4372(6)
	Fe1, Br2	2.4101(6)	Co1, Br2	2.4423(7)
			Co1, Br3	2.4328(6)
H bonds				
CH_3···Br/Å[°]	C13, Br1	2.98(6) [158(4)]	C14, Br2	3.17(11) [155(9)]
Ligand	C22, Br2	3.39(6) [153(4)]	C12, Br2	3.46(6) [134(4)]
	C15, Br2	3.06(6) [144(4)]	C22, Br1	3.49(4) [103(3)]
			C23, Br1	2.97(6) [141(4)]
			C26, Br3	2.91(6) [144(4)]
CH_3···Br/Å[°]	C38, Br1	2.94(7) [174(4)]	C50, Br3	3.09(6) [136(4)]
Protonated	C47, Br1	3.27(5) [148(4)]	C50, Br1	3.46(5) [117(4)]
IPr	C48, Br1	3.12(6) [163(4)]	C49, Br1	3.04(5) [141(3)]
Bond Angles				
C–M–Br/°	C1, Fe1, Br1	118.56(8)	C1, Co1, Br1	114.65(9)
	C1, Fe1, Br2	125.58(8)	C1, Co1, Br2	113.14(9)
			C1, Co1, Br3	103.05(9)
Br–M–Br/°	Br1, Fe1, Br2	115.46(2)	Br1, Co1, Br2	107.00(2)
			Br1, Co1, Br3	110.47(2)
			Br2, Co1, Br3	108.39(2)
Dihedral Angles				
Dipp–$Ar_{central}$/°	C17, C16, C6, C1	79.78(37)	C4, C5, N1, C1	94.77(42)
	C12, C17, C2, C1	81.06(37)	C21, C16, N2, C1	106.95(40)
Ligand CH_3–CH–C–C/°		–	C14, C13, C9, C4	104.35(66)
			C26, C25, C21 C16	132.87(43)
Ligand			C12, C10, C5, C4	137.99(37)
			C23, C22, C17, C16	152.65(36)
Dipp–NHC/°	C45, C40, N2, C25	98.94(32)	C44, C43, N4, C28	76.73(41)
NHCH$^+$	C29, C28, N1, C25	104.35(30)	C36, C31, N3, C28	81.15(41)
CH_3–CH–C–C/°	C50, C49, C45, C40	121.46(37)	C38, C37, C32, C31	70.39(45)
	C36, C34, C29, C28	153.41(30)	C51, C49, C48, C43	97.29(41)
NHCH$^+$	C38, C37, C33, C28	118.80(40)	C54, C52, C44, C43	112.84(43)
	C48, C46, C41, C40	130.12(32)	C41, C40, C36, C31	128.64(44)
Out of plane distortions				
M–$Ar_{Central}$	Fe1, C1	0.2474(53)	Co1, C1	0.3503(59)
Geometric Parameters				
		τ_3 = 0.91		τ_4 = 0.93

Table 4·8 contains key bond lengths, angles, and geometric parameters **IV·23** and **IV·24**. In the solid state (**Scheme 4·23**), **IV·23** has a slightly distorted, trigonal planar geometry around the metal centre (τ_3 = 0.91). The distortion manifests in a larger C1–Fe1–Br2 angle than the idealised 120° [125.59(8)°]. There is a concomitant compression of the Br1–Fe1–Br2 angle to 115.46(2)° and of the C1–Fe1–Br1 angle to 118.55(8)°. The difference between the two angles could be explained through secondary interactions in the complex.

There are short interactions between both mesityl groups and the closest bromide moiety [CH_3···Br = 2.98(6) Å (C13, Br1), 3.39(6) Å (C22, Br2), 3.06(6) Å (C15, Br2)]. Br1, which forms part of the smallest *i*C_{Ar}–Fe–Br angle, is also in close contact with hydrogens from the *i*Pr groups of the IPrH moiety [CH_3···Br = 2.94(7) Å (C38, Br1), 3.27(5) Å (C47, Br1), 3.12(6) Å (C48, Br1)]. These could serve to pull the angle closed in order to maximise the CH_3···Br interactions. There is no shift in the position of *i*Pr groups or the Dipp groups away from an idealised geometry so this theory rests upon CH_3···Br distances derived from X-ray crystallography, which can be inaccurate.[192]

IV·23 provides an opportunity to study a trigonal planar iron complex, stabilised by an *m*-terphenyl ligand, that is less sterically saturated than [2,6-$Mes_2C_6H_3$]FeCl[IPrMe] (**IV·14**). The *i*C_{Ar}–Fe bond lengths are identical in these two complexes [2.054(5) Å (**IV·14**), 2.054(3) Å (**IV·23**)]. This suggests that steric factors and the charge of the complex do not, in this case, have an impact on the nature of this bond. This is not the case for the Fe–Br bonds which are distinctly different [2.3961(11) Å (**IV·14**), 2.4064(6) and 2.4102(6) Å (**IV·23**)]. The out of plane deviation of the iron from the *m*-terphenyl ligand is the same in both complexes [0.202(19) Å (**IV·14**), 0.2474(47) Å (**IV·23**)]. In **IV·14** this deviation was attributed to the sterically saturated space around the iron centre. This is not the case in **IV·23**. In this complex the deviation occurs in the direction of the proposed CH_3···Br interactions which could be the cause.

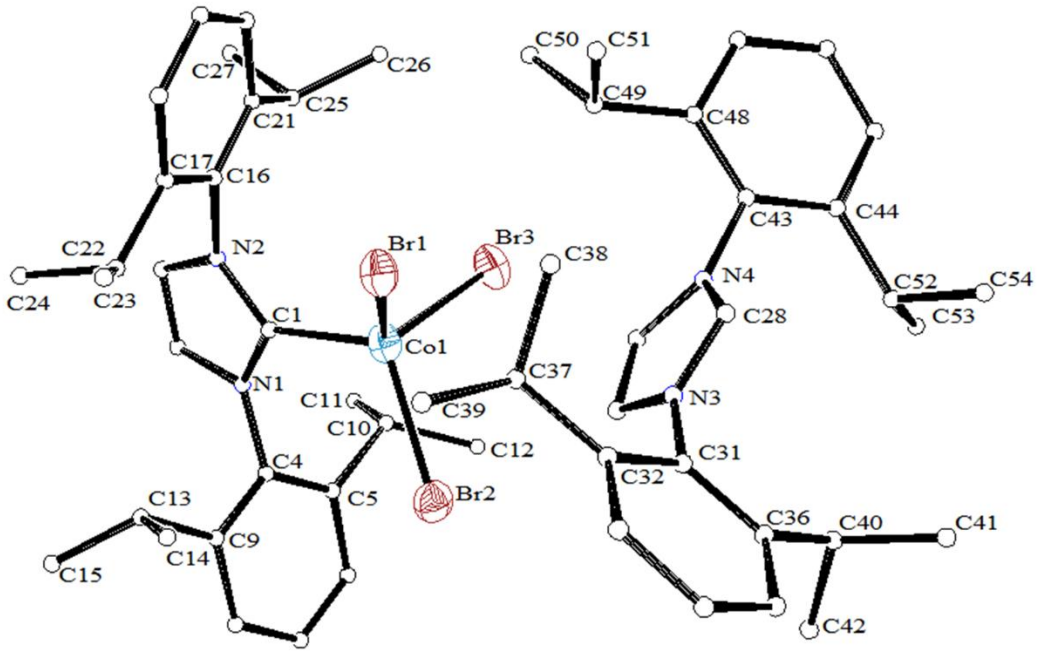

Figure 4·24. The solid-state structure of **IV·24**. Hydrogens have been omitted for clarity and ellipsoids have been set at 50% probability where present. Carbon and nitrogen have been represented as spheres.

The structure of **IV·24** (**Figure 4·24**) obtained by Aldridge *et al*. contained 1.5 equivalents of $C_6H_4F_2$ in the asymmetric unit. In this work the crystal structure obtained of **IV·24** contains no solvent. Despite this the two structures are similar. The cobalt centre in **IV·24** adopts a distorted tetrahedral geometry (τ_4 = 0.93). The largest angles around the metal centre are the C1–Co–Br angles, due to the steric profile of the IPr ligand [115.65(9)° (C1, Co1, Br1), 113.14(9)° (C1, Co1, Br2) and 103.05(9)° (C1, Co1, Br3)]. The outlying value of 103.05(9)° is mirrored in the complex reported by Aldridge *et al*. where the equivalent angles are 116.4(1), 112.9(1) and 100.7(1)°. The reason for this is not immediately obvious but again favourable CH···Br interactions could be involved.

The above experiments indicate that IPr is too bulky to be combined with $[2,6\text{-Dipp}_2C_6H_3]^-$ in three-coordinate, transition metal complexes. Further work, focused on balancing the steric demands of the two organic ligands to provide sufficient steric protection to the metal centre in an isolatable, three-coordinate complex that can be reduced to a two-coordinate complex, is required.

4.3.6 Small Molecule Activation With Mixed Ligand Species

Low-coordinate, transition metal complexes have been shown to be capable of activating small molecules, such as carbon monoxide[142] and carbodiimides[122], and producing synthetically useful molecules. Studies have also shown that such complexes are precursors to catalytic species.[65] As has been alluded to previously, the reactions of several of the complexes described in this chapter with various small molecules were investigated to determine if any unusual or synthetically useful reaction products could be isolated.

On the whole these investigations either showed no catalytic effect or provided an intractable mixture of products. For example, the exposure of **IV·20** to one equivalent of P_4 in benzene-d_6 resulted in a colour change from orange to dark red. The ^{1}H and ^{31}P NMR spectra of the reaction mixture suggested the presence of a range of products that were not starting materials. Attempts to isolate products through vapour diffusion of pentane into the reaction and cooling the resulting mixture to −30°C were unsuccessful.

However, two reactions, presented below, did afford isolatable products, and may suggest future avenues of application for the organometallic complexes involved.

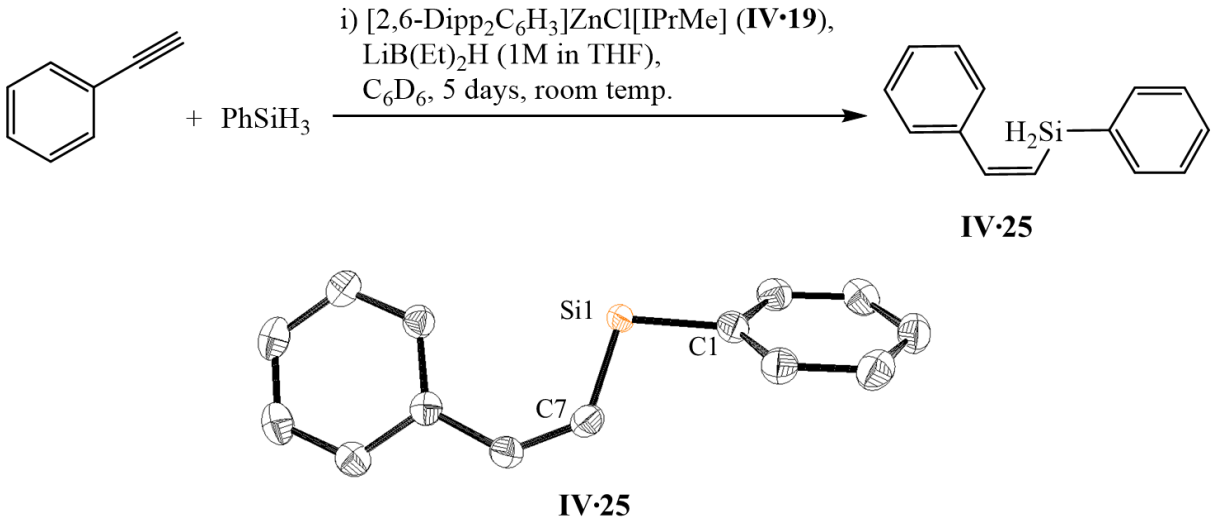

Figure 4·25. The reaction scheme for the synthesis of **IV·25** (top) and the solid-state structure of **IV·25** (bottom). Hydrogens have been omitted for clarity and ellipsoids have been set at 50% probability.

The reaction between phenyl silane and phenyl acetylene in the presence of 0.2 equivalents of $LiB(Et_3)H$ and 0.1 equivalents of **IV·19** afforded a single crystal of phenylstyrylsilane (**IV·25**, **Figure 4·25**) following vapour diffusion of pentane into the reaction mixture and storage of the solution at room temperature under a nitrogen atmosphere for three months. Monitoring of this reaction by ^1H NMR spectroscopy for one week from the start of the reaction gave no evidence of a reaction occurring. This indicates that the formation of **IV·25** is slow.

Zinc complexes have been used as catalysts in the hydrosilylation of a range of substrates.[318,319] Examples include the reduction of carbon monoxide to methane *via* $CH_2(OSiR_3)_2$ reported by Parkin *et al*.,[320,321] and the hydrosilylation of nitriles reported by Nikonov and co-workers. Both reactions are catalysed by a zinc hydride complex,[318] Nikonov *et al*. note, however, that hydrosilylation reactions have been shown to be base catalysed.[322] Therefore $LiB(Et_3)H$, used to generate the zinc hydride, could be the catalytically active species. To ascertain the active species in this work, conditions that increase the rate of the reaction would first have to be found.

The second successful reaction was the synthesis of the hydantoin derivative, 1,3-diphenyl-5-(hexa-ylidene)imidazolidine-2,4-dione (**IV·27**), from two equivalents of phenylisocyanate and one equivalent of hexyne (**Scheme 4·10**). 0.1 equivalents of **IV·20** were employed as a catalyst. The reaction was conducted in benzene-d_6 at 80°C for twenty-four hours.

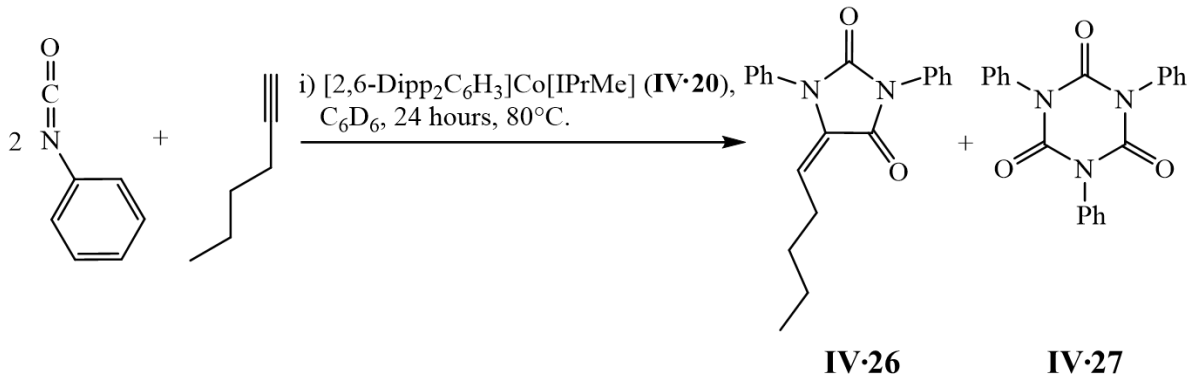

Scheme 4·10. The synthesis of 2,4,6-triphenylisocyanurate (**IV·26**) and 1,3-diphenyl-5-(hexa-ylidene)imidazolidine-2,4-dione (**IV·27**) promoted by **IV·20**.

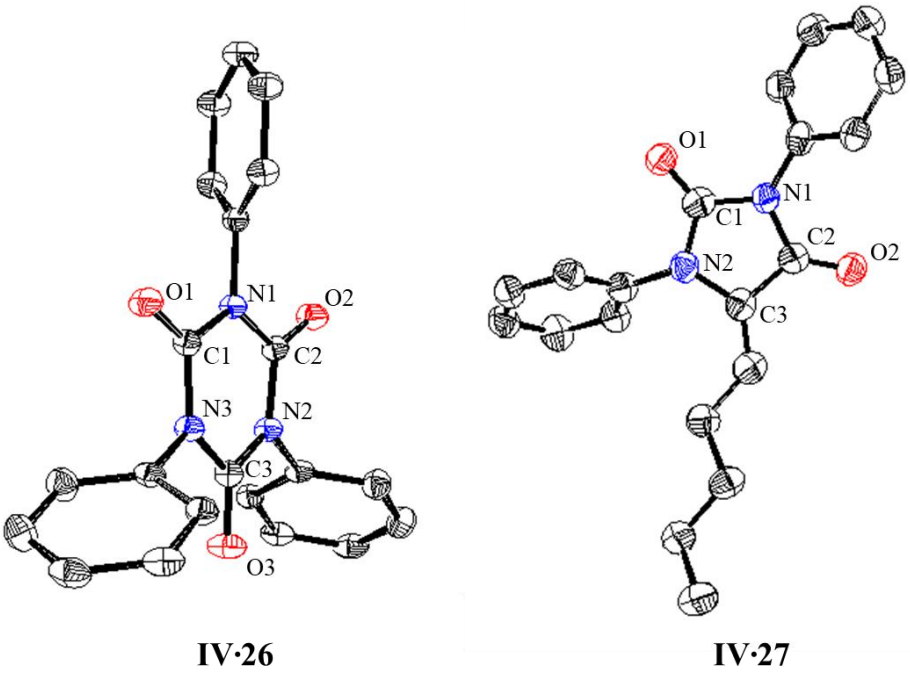

IV·26 **IV·27**

Figure 4·26. The solid-state structures of **IV·26** and **IV·27**. Hydrogens and a molecule of benzene-d_6 (**IV·26)** have been omitted for clarity. Ellipsoids have been set at 50% probability.

A ^{1}H NMR spectrum taken after twenty-four hours revealed a mixture of products and starting material. 2,4,6-triphenylisocyanurate (**IV·25**, **Figure 4·26**) was crystallised from the reaction mixture by addition of pentane and storage at −30°C for two weeks. The reaction mixture was stored under these conditions for a further two months. During this time further crystals developed which X-ray diffraction studies revealed to be the target product 1,3-diphenyl-5-(hexa-ylidene)imidazolidine-2,4-dione (**IV·26**, **Figure 4·26**).

The ^{1}H NMR spectrum taken after twenty-four hours contained a series of signals that can be assigned to the starting materials, phenyl isocyanate and 1-hexyne, and **IV·26**.[323] There are also more peaks in the methyl region than would be expected for 1-hexyne (five signals). These are tentatively assigned to **IV·27**. It should be mentioned that *cis* and *trans* isomers of **IV·26** are can be produced in this reaction, further increasing the complexity of the spectrum. There is a weak signal in the spectrum at 4.91 ppm that could be assigned to the proton of the C=C bond in **IV·26**.[324] The integrals of the peaks in the aliphatic region of the ^{1}H NMR spectrum do not match the integral of this signal. It is therefore possible that there are unknown samples in the

reaction mixture, such as 1,3,5-tripentylbenzene,[121] that overlap with the signals from the starting material and **IV·26**. A ^{1}H NMR spectrum taken after four days simply showed two broad peaks, one in the aliphatic and one in the aromatic regions. This could indicate a greater mixture of products developing over time.

This reaction was inspired by the work of Takai *et al*., in which $MnBr(CO)_5$ was used to promote the same reaction (**Scheme 4·11**).[325] In a later study, Kays *et al*. propose a similar mechanism to that shown in **Scheme 4·11** for the formation of isocyanates catalysed by transition metal, *m*-terphenyl complexes.[65]

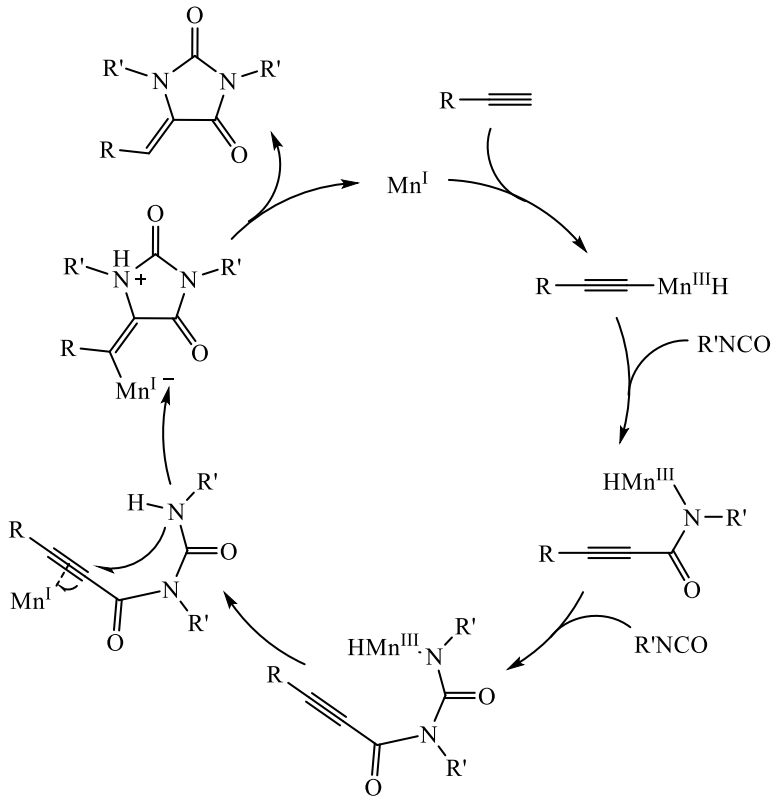

Scheme 4·11. Mechanism for the formation of hydantoin derivatives catalysed by $MnBr(CO)_5$, proposed by Takai *et al*.[325]

The mechanism for the production of **IV·26** and **IV·27** is likely to be similar to those proposed by Takai *et al*. (**Scheme 4·11**)[325] and Kays and co-workers. However, free IPrMe has been shown to catalyse the formation of triphenyl isocyanurate from phenyl isocyanate in moderate yields at room temperature over the time scale of one hour.[326] The involvement of the ligand in the formation of both **IV·26** and **IV·27** cannot be ruled out.

4.4 Conclusions

A series of three-coordinate, Group 12 complexes of the type [2,6-$Mes_2C_6H_3$]MX[IPrMe] [MX = ZnCl (**IV·10**), CdCl (**IV·11**) and HgBr (**IV·12**)] and [2,6-$Dipp_2C_6H_3$]ZnCl[IPrMe] (**IV·19**) were synthesised on a small scale and their structural properties investigated. It was found that **IV·10**, **IV·11** and **IV·19** adopt a trigonal planar geometry, slightly distorted by the steric demands of the ligand. **IV·12** adopts a T-shaped geometry and the Hg–Br distance is significantly lengthened to mimic the linear geometry favoured in mercury(II) complexes. These are rare examples of three-coordinate Group 12 complexes.

[(2,6-$Mes_2C_6H_3$)Mn(μ-Br)(IPrMe)]$_2$ (**IV·13**), [2,6-$Mes_2C_6H_3$]MX[IPrMe] [MX = FeBr (**IV·14**), CoBr (**IV·15**)] and [2,6-$Dipp_2C_6H_3$]MX[IPrMe] [MX = FeCl (**IV·17**), CoBr (**IV·18**)] were also synthesised. **IV·13** was found to dimerise in the solid-state. This observation was tentatively attributed to the larger atomic radius of manganese relative to iron and cobalt. The magnetic properties of the iron and cobalt complexes were investigated. The iron complexes were found to have magnetic moments equal to or lower than the spin only values for a d^6 ion whilst the cobalt centres were found to have higher magnetic moments than the spin only value for a d^7 ion.

Attempts were made to reduce complexes **IV·10**, **IV·14**, **IV·15**, **IV·17**, **IV·18** and **IV·19** with Group 1 metals to afford complexes of the type [2,6-$Ar_2C_6H_3$]M[IPrMe]. The reactions involving the zinc complexes afforded only zinc metal and starting material. The reduction of **IV·14** with KC_8 afforded the iron-oxo complex [(IPrMe)$_2$Fe(μ$_3$-O)]$_2$[(2,6-$Mes_2C_6H_3$)$_2$Fe(μ$_3$-O)]$_2$Fe (**IV·16**) through a reaction with opportunistic oxygen. The reduction of **IV·18** with KC_8 afforded the two-coordinate cobalt(I) complex [2,6-$Dipp_2C_6H_3$]Co[IPrMe] (**IV·20**). **IV·20** is the first example of a neutral cobalt(I) complex supported by ligands binding solely through carbon atoms. **IV·20** was fully characterised and the magnetic moment of the complex was

shown to be almost double the spin only value for a cobalt(I) ion. **IV·20** is one of the lowest molecular weight two-coordinate cobalt complexes in the literature and therefore an in-depth study of its magnetic properties is warranted.

Further study of the formation of **IV·20** using cyclic voltammetry indicated that a further reduction of the cobalt(I) species can take place. This further reduction could explain why **IV·20** could not be isolated in greater than 34% yield.

In an attempt to isolate an iron(I) complex similar to **IV·20**, IPr was used instead of IPrMe. The reaction between the halide bridged dimers, **II·39** and **II·40**, and IPr resulted in the charged species, [2,6-$Mes_2C_6H_3FeBr_2$][IPrH] (**IV·23**) and [$IPrCoBr_3$][IPrH] (**IV·24**), respectively, as opposed to the desired three-coordinate complexes. This was most likely due to the bulk of the IPr ligand being too great to combine with the *m*-terphenyl ligand. Tuning of this steric relationship could provide a route to the targeted three-coordinate complexes in future work.

Initial investigations into the applications of **IV·19** and **IV·20** found that they are potentially active as hydrosilylation catalysts and in the [1+2+2] cycloaddition of 1-hexyne and phenyl isocyanate respectively.

4.5 Future Work

Despite the isolation of **IV·20**, the obvious limitation of this work is the range of metals to which the synthetic method and, therefore the ligand system, can be applied. Changing the steric profile of both the *m*-terphenyl and the NHC to include $[2,6\text{-}(2,6\text{-Xyl})_2C_6H_3]^-$, $[2,6\text{-Tmp}_2C_6H_3]^-$, IMes, IMesPr or any of the other variants available would give an insight into whether this ligand system is capable of supporting any other metal(I) species.

Different methods of reducing the metal(II) species, such as those employed by Deng[129] and Frison[125] should also be investigated. These methods involve the protonation of a ligand, removing it from the iron complex and so different starting materials would be required. To this author's knowledge this has not been trialled for diaryl systems and the generation of dihydrogen involved in both methods may be detrimental to the process. Complexes of the type $[2,6\text{-Mes}_2C_6H_3]_2M$ (M = Mn, Fe and Co), such as those published by Kays[76] or $[2,6\text{-Mes}_2C_6H_3]Co[Ni(SiMe_3)_2]$[63] may make suitable starting materials for the reaction described in **Scheme 4·12**.

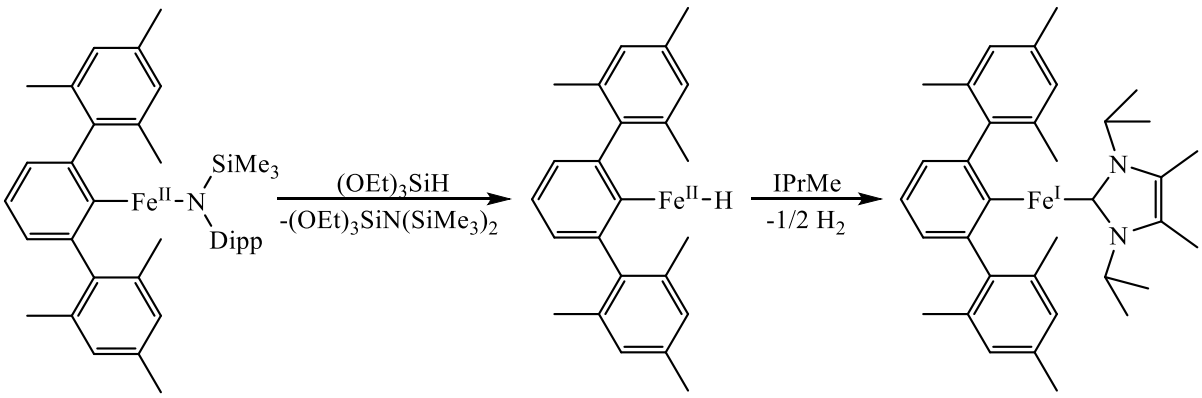

Scheme 4·12. A proposed, alternative reduction toward an iron analogue of **IV·20** based on the work of Deng and co-workers.[129]

Where similar iron(I) complexes have been isolated they feature ligands that bind to the metal *via* a nitrogen.[121,125] It is possible that the electronic properties of this bond are what stabilises these complexes. Therefore, it would be worthwhile investigating other ligands. Whilst the aryl, *m*-terphenyl ligand is somewhat vital to this project, alternatives to the NHC ligand could

be found. Substituted pyridines such as 2,6-lutidine or 2,6-$Mes_2C_5H_3N$ would fulfil the same role as the NHC and offer a steric environment similar to the complexes targeted in Chapter III.[327,328] A ligand that binds to the metal *via* a carbon would fit better with the goal of this work, to isolate heteroleptic, two-coordinate complexes supported by carbon bonding ligands. Cyclic (alkyl)(amino)carbenes (CAACs), developed in 2005 by Bertrand *et al*., are stronger σ donors and π acceptors than their NHC counterparts and, by their nature, have a non-symmetric steric profile.[329] Their ability to coordinate to transition metals has been long established and they have found occupation supporting two-coordinate, metal(0) complexes such as $[CAAC]_2M$ (M = Mn-Zn).[330,331] In this work they could provide an alternate electronic environment to the ligand system employed and allow isolation of complexes such as that shown in **Figure 4·27**.

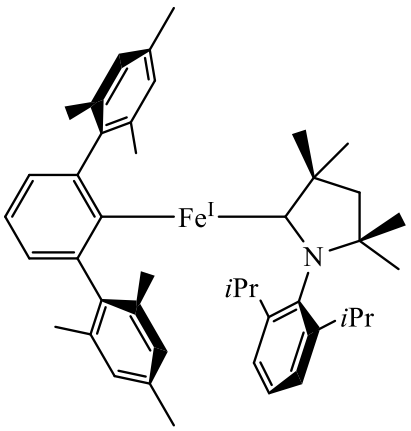

Figure 4·27. A potential iron(I) complex stabilised by a CAAC ligand.

One avenue that was not explored in this work was the replacement of the halide of the three-coordinate complexes with a bulky anion such as $[BAr^F_4]^-$. Such a reaction could afford the two-coordinate complexes desired and would add another dimension to the range of complexes. Such complexes would be similar to the metal(I) complexes isolated by Long,[164] Deng,[126] and their respective co-workers.

Once a method and a ligand system are established that work for a range of metals and allow multiple steric and electronic variations an in-depth investigation into the magnetic properties

of the complexes would be warranted. Evans' measurements of the magnetic moment of **IV·20** demonstrated that it was elevated above that expected of a spin only complex. Due to the almost linear nature of the complex an analysis of the low-temperature magnetic properties of this complex and others in this class would provide an insight into its effectiveness as a single molecule magnet. Further, computational studies into the structures of these complexes could provide an insight into why a co-planar arrangement of the ligands and an almost linear geometry around the metal centre are adopted.

4.6 Experimental

4.6.1 [2,6-$Mes_2C_6H_3$]ZnCl[IPrMe] (IV·10)

To a solution of [2,6-$Mes_2C_6H_3ZnCl]_2$ (22.0 mg, 0.0265 mmol) in C_6D_6 (0.7 mL) was added IPrMe (9.5 mg, 0.0527 mmol) to give a white, cloudy solution. The reaction was stood at room temperature for 16 hrs after which time ^1H and $^{13}C\{^1H\}$ NMR spectroscopic data was recorded. The supernatant was decanted and crystallisation induced by the diffusion of pentane vapour into the solution to give colourless crystals of [2,6-$Mes_2C_6H_3$]ZnCl[IPrMe] suitable for X-ray diffraction studies. 14.5 mg, 46%. ^1H NMR (400 MHz, C_6D_6, 300 K) δ_H / ppm; 0.99 (12H, d, J = 6.8 Hz, CH_3 of *i*Pr group), 1.47 (6H, s, CH_3 of IPrMe backbone), 2.22 (6H, s, *p*-CH_3 of mesityl group), 2.46 (12H, s, *o*-CH_3 of mesityl group), 3.33 (2H, sept, J = 6.9 Hz, CH of *i*Pr group), 6.89 (4H, s, $C_{Ar}H$ of mesityl group), 7.11 (2H, d, J = 7.5 Hz, *m*-$C_{Ar}H$ of central aryl ring), 7.40 (1H, tr, J = 7.5 Hz, *p*-$C_{Ar}H$ of central aryl ring). $^{13}C\{^1H\}$ NMR (C_6D_6, 100 MHz, 300 K) δ_C/ppm; 9.76 (CH_3, Backbone of IPrMe), 20.99 (CH_3, *p*-methyl of flanking mesityl group), 21.56 (CH_3, *o*-methyl of flanking mesityl group), 21.80 (CH_3, methyl of *i*Pr group), 53.86 (CH, CH of *i*Pr flanking group), 125.27 ($C_{Ar}H$, *m*-CH of central aryl ring), 127.09 ($C_{Ar}H$, *p*-CH of central aryl ring), 128.33 ($C_{Ar}H$ of flanking mesityl group) , 125.17 (C_{quat} of the double bond in IPrMe), 134.80 (*p*-C_{quat} of flanking mesityl group), 136.68 (*ipso*-C_{quat} of flanking mesityl group), 144.72 (*m*-C_{quat} of flanking mesityl group), 149.28 (*o*-C_{quat} of central aryl ring), 158.18 (*ipso*-C_{quat} of central aryl ring), 174.08 (*ipso*-C of IPrMe). EI MS: 557.3 (5%) [M – Cl]$^+$, 458.0 (5%) [M – IPrMe + Bu]$^+$, 412.1 (8%) [M – IPrMe]$^+$, 313.2 (100%) [2,6-$Mes_2C_6H_3]^+$, 300.2 (25%), [M – 2,6-$Mes_2C_6H_3]^+$, 180.1 (10%) IPrMe. TOF MS ASAP accurate mass: $C_{35}H_{45}ZnClN_2$ calcd 593.2541 m/z; peak not found. [M−Cl]$^+$ calcd 557.2873 m/z; found 557.2873 m/z. Elemental analysis: $C_{35}H_{45}ZnClN_2$ calcd C 70.70, H 7.63, N 4.71; found C 70.20, H 7.54, N 4.75.

4.6.2 [2,6-$Mes_2C_6H_3$]CdCl[IPrMe] (IV·11)

To a solution of [2,6-$Mes_2C_6H_3CdCl]_3$[$LiCl(OEt_2)$] containing trace [2,6-$Mes_2C_6H_3]_2Cd$ (31 mg of solid therefore 21.2 mg of [2,6-$Mes_2C_6H_3CdCl]_3$[$LiCl(OEt_2)$], 0.0141 mmol) in C_6D_6 (0.7 mL) was added IPrMe (8.9 mg, 0.0494 mmol) to give a white, cloudy solution. The reaction was stood at room temperature for 2 hrs after which time ^1H, $^{13}C\{^1H\}$ and $^{113}Cd\{^1H\}$ NMR spectroscopic data were collected. The supernatant was decanted after 48 hrs and crystallisation induced by the diffusion of pentane vapour into the solution to give XRD quality, colourless crystals of [2,6-$Mes_2C_6H_3$]CdCl[IPrMe], 14.6 mg, 54%. ^1H NMR (400 MHz, C_6D_6, 300 K) δ_H / ppm; 0.97 (12H, d, J = 7.5 Hz, CH_3 of *i*Pr group), 1.43 (6H, s, CH_3 of IPrMe backbone), 2.20 (6H, s, *p*-CH_3 of mesityl group), 2.43 (12H, s, *o*-CH_3 of mesityl group), 3.43 (2H, br, CH of *i*Pr group), 6.89 (4H, s, partially obscured, $C_{Ar}H$ of mesityl group), 7.15 (obscured by solvents and impurities, *m*-$C_{Ar}H$ of central aryl ring), 7.38 (1H, tr, J = 7.5 Hz, *p*-$C_{Ar}H$ of central aryl ring). $^{13}C\{^1H\}$ NMR (C_6D_6, 100 MHz, 300 K) δ_C / ppm; 9.77 (CH_3 of IPrMe backbone), 21.30 (CH_3, *p*-methyl of flanking mesityl group), 21.58 (CH_3, *o*-methyl of flanking mesityl group), 22.49 (CH_3, methyl of *i*Pr group), 53.60 (CH of *i*Pr flanking group), 125.22 ($C_{Ar}H$, *m*-CH of central aryl ring), 125.50 (C_{quat}, double bond in IPrMe), 127.45 ($C_{Ar}H$, *m*-CH of central aryl ring), 128.74 ($C_{Ar}H$ of flanking mesityl group), 135.79 (*p*-C_{Ar} of flanking mesityl group), 136.81 (*m*-C_{Ar} of flanking mesityl group), 145.59 (*ipso*-C_{Ar} of flanking mesityl group), 150.14 (*o*-C_{Ar} of central aryl ring), 162.87 (*ipso*-C_{Ar} of central aryl ring), 179.04 (*ipso*-C of IPrMe). $^{113}Cd\{^1H\}$ NMR (C_6D_6, 88.8 MHz, 300 K) δ_{Cd} / ppm; 509.15. (^1H, ^{13}C, and $^{113}Cd\{^1H\}$ NMR spectroscopic data of the desired product was obtained by comparison with the relevant spectra of the $[Mes_2C_6H_3]_2Cd$ impurity). EI MS: 740.3 (2%) [2,6-$Mes_2C_6H_3$], 607.3 (1%) $[M - Cl]^+$, 506.0 (5%) $[M - IPrMe + iPr]^+$, 329.0 (3%) $[M - 2,6\text{-}Mes_2C_6H_3]^+$, 298.1 (30%) $[2,6\text{-}Mes_2C_6H_3 - Me]^+$, 283.1 (15%) $[2,6\text{-}Mes_2C_6H_3 - 2Me]^+$, 180.1 (7%) IPrMe. TOF MS ASAP accurate mass: $C_{35}H_{45}CdClN_2$ calcd 637.2347 m/z; peak not found. $[C_{35}H_{45}CdN_2]^+$

calcd 603.2614 m/z; found 603.2615 m/z. Elemental analysis: $C_{35}H_{45}N_2CdCl$ calcd C 65.52, H 7.07, N 4.37; found C 65.19, H 7.00, N 4.26.

4.6.3 [2,6-$Mes_2C_6H_3$]HgBr[IPrMe] (IV·12)

To a solution of 2,6-$Mes_2C_6H_3HgBr$ (26.1 mg, 0.0439 mmol) in C_6D_6 (0.7 mL) was added IPrMe (8.5 mg, 0.0471 mmol). ^1H and ^{13}C NMR spectroscopic analysis showed full conversion of the starting materials after *ca.* 1 hour. The reaction stood at room temperature for 16 hrs, during which time large, white crystals suitable for X-ray diffraction studies formed. 14.6 mg, 46%. ^1H NMR (400 MHz, $CDCl_3$, 300 K) δ_H / ppm: 1.21 (12H, d, J = 7.1 Hz, CH_3 of *i*Pr group), 2.06 (6H, s, CH_3 of IPrMe backbone), 2.21 (12H, s, *o*-CH_3 of mesityl group), 2.34 (6H, s, *p*-CH_3 of mesityl group), 3.38 (2H, sept, J = 6.9 Hz, CH of *i*Pr group), 6.89 (4H, s, $C_{Ar}H$ of mesityl group), 7.17 (2H, d, J = 7.5 Hz, *m*-$C_{Ar}H$ of central aryl ring), 7.31 (1H, t, J = 7.5 Hz, *p*-$C_{Ar}H$ of central aryl ring). ^{13}C NMR (100 MHz, $CDCl_3$, 300 K) δ_C / ppm; 10.2 (CH_3 of IPrMe backbone), 21.3 (*p*-CH_3 of mesityl group), 21.4 (*o*-CH_3 of mesityl group), 21.9 (CH_3 of *i*Pr group), 53.9 (CH of *i*Pr group), 126.7 (*m*-$C_{Ar}H$ of central aryl ring), 127.5 (*p*-$C_{Ar}H$ of central aryl ring) , 127.9 (C_{quat}, double bond in IPrMe), 135.9 (*p*-C_{Ar} of flanking mesityl group), 137.0 (*o*-C_{Ar} of flanking mesityl group), 142.3 (*ipso*-C_{Ar} of flanking mesityl group), 147.5 (*o*-C_{Ar} of central aryl ring), 161.8 (*ipso*-C_{Ar} of central aryl ring), 187.4 (*ipso*-C of IPrMe). ^{199}Hg (72 MHz, THF, 300 K) δ_{Hg} / ppm; −545.0. EI MS: 695.4 $[M - Br]^+$, 594.2 (12%) $[M - IPrMe]^+$, 313.2 (100%) [2,6-$Mes_2C_6H_3]^+$, 298.2 (25%) [2,6-$Mes_2C_6H_3$ – Me]$^+$, 283.1 [2,6-$Mes_2C_6H_3$ – 2Me]$^+$, 180.1 (5%) IPrMe. EI MS accurate mass: Mass ion not found. Fragment ion peak ($C_{35}H_{45}N_2Hg$) calcd 695.3284 m/z; found 695.3286 m/z. Elemental analysis: $C_{35}H_{45}N_2HgBr$ calcd C 54.30, H 5.86, N 3.62; found C 54.04, H 5.60, N 3.90.

4.6.4 [2,6-Dipp$_2$C$_6$H$_3$]ZnCl[IPrMe] (IV·19)

To a solution of [(IPrMe)ZnCl$_2$]$_2$ (100 mg) in Et$_2$O (20 mL) cooled to −30°C was added a solution of [2,6-Dipp$_2$C$_6$H$_3$Li]$_2$ (127 mg) in Et$_2$O (20 mL). The colourless solution was allowed to warm to room temperature over 16 hrs. All volatiles were removed *in vacuo* to afford a white solid. This was extracted into toluene (2 × 10 mL) and the volume of the solution reduced to 3 mL before the solution was layered with pentane (15 mL). Storage of this mixture at *ca.* 7°C for 3 d afforded crystals of suitable quality for X-ray diffraction studies. 40 mg, 15%. ^{1}H NMR (400 MHz, C$_6$D$_6$, 300 K) δ_H / ppm; 1.09 (*dd*, J = 4.9 Hz, 6.8 Hz, 36H, overlapping CH$_3$ signals from *i*Pr groups), 1.14 – 1.36 (congested series of peaks, possibly containing CH$_3$ of IPrMe backbone), 2.08 (*s*, 3H), 2.86 (*q*, *J* = 6.8 Hz, 6H, CH of *i*Pr groups), 7.00 – 7.40 (congested series of peaks).

4.6.5 [(2,6-Mes$_2$C$_6$H$_3$)MnBr(IPrMe)]$_2$ (IV·13)

To a solution of [2,6-Mes$_2$C$_6$H$_3$MnBr]$_2$·[LiBr(Et$_2$O)]$_2$ (11.1 mg, 9.11 μmol) in C$_6$D$_6$ (0.63 mL) was added IPrMe (3.2 mg, 0.0178 mmol). The reaction was allowed to stand at room temperature for 16 hrs, during which time no colour change or formation of precipitate was observed. The solution was filtered through celite and crystallisation induced by the diffusion of pentane vapour into the solution. Storage of this solution at −30°C for 1 month afforded crystals of [(2,6-Mes$_2$C$_6$H$_3$)MnBr(IPrMe)]$_2$ that were of suitable quality for X-ray diffraction studies. A yield was not obtained for this product. ^{1}H NMR (400 MHz, C$_6$D$_6$, 300 K) δ_H / ppm; 0.81 (s), 1.63 (s), 2.01 (br, s, $\Delta\nu$½ = 313 Hz), 2.20 (s), 2.59 (s), 2.73 (br, s, $\Delta\nu$½ = 132 Hz), 3.78 (s), 4.55 (br, s, $\Delta\nu$½ = 133 Hz), 7.28 (s), 7.39 (s), 7.52 (s), 7.67 (s), 7.76 (s, partially obscured) 11.69 (br, s, $\Delta\nu$½ = 759 Hz), 13.84 (br, s, $\Delta\nu$½ = 608 Hz), 16.77 (br, s, $\Delta\nu$½ = 1705 Hz), 25.77 (br, s, $\Delta\nu$½ = 595 Hz), 29.15 (br, s, $\Delta\nu$½ = 1274 Hz).

4.6.6 [2,6-$Ar_2C_6H_3$]FeX[IPrMe] [Ar = Mes, X = Br (IV·14) or Ar = Dipp, X = Cl (IV·17)]

To a yellow solution of [2,6-$Ar_2C_6H_3FeX]_2$·[$LiX(Et_2O)]_2$ (A: 200 mg, 0.165 mmol. B: 200 mg, 0.164 mmol) in diethyl ether (10 mL) cooled to −30°C a solution of IPrMe (A: 73 mg, 0.410 mmol. B: 60 mg, 0.333 mmol) in diethyl ether (20 mL) was added dropwise. The solution changed colour to a yellow/beige over 15 min and significant beige precipitate was observed. The reaction was stirred at −30°C for 1 hour before being allowed to warm to room temperature. The reaction was held at this temperature for a further 2 hrs before the solution was filtered and all volatiles were removed *in vacuo*. The reaction was then extracted into toluene (3 mL) to give a yellow solution, leaving behind a white solid. All volatiles were removed *in vacuo* to give a yellow product for analysis.

[2,6-$Mes_2C_6H_3$]FeBr[IPrMe] was obtained as a yellow solid. 131 mg, 63%. Crystals of [2,6-$Mes_2C_6H_3$]FeBr[IPrMe] suitable for X-ray diffraction studies were grown by pentane diffusion into a saturated solution of the complex in benzene-d_6. ^{1}H NMR (400 MHz, C_6D_6, 300 K) δ_H / ppm; −36.73 (br, s, $\Delta\nu$½ = 190 Hz), −31.56 (br, s, $\Delta\nu$½ = 256 Hz), −18.28 (s), −15.64 (br, s, $\Delta\nu$½ = 980 Hz), −7.10 (br, s, $\Delta\nu$½ = 846 Hz), −3.34 (s), −2.22 (s), 0.17 (s), 1.07 (s), 24.26 (s), 35.70 (br, s, $\Delta\nu$½ = 980 Hz). μ_{eff} = 4.79 μ_B. EI-MS $[M]^+$ m/z: 628.2 (17%); Fragment peaks: 314.2 [2,6-$Mes_2C_6H_3]^+$ (100%), 299.2 [2,6-$Mes_2C_6H_3$ − Me]$^+$ (15%), 179.1 [IPrMe]$^+$ (10%). EI-MS accurate mass: $C_{35}H_{45}FeBrN_2$ calcd 626.2162 m/z; found 626.2222 m/z. Elemental analysis: $C_{35}H_{45}CoBrN_2$ calcd C 66.30, H 7.21, N 4.45; found C 66.30, H 7.28, N 4.43. UV/Vis: 2.03 × 10^{-5} M (toluene) λ_{max}/nm (ε/dm^3 mol^{-1} cm^{-1}) 338 (3501).

[2,6-$Dipp_2C_6H_3$]FeCl[IPrMe] was obtained as a yellow/brown solid. 47.6 mg, 18%. Crystals were grown by pentane diffusion into a saturated solution of the complex in benzene-d_6. X-ray diffraction studies of these crystals showed multiple degrees of disorder that rendered a satisfactory solution unachievable. ^{1}H NMR (400 MHz, C_6D_6, 300 K) δ_H / ppm; −59.48 (br, s,

$\Delta\nu_{1/2}$ = 232 Hz), −42.17 (br, s, $\Delta\nu_{1/2}$ = 2161 Hz), −36.04 (s), −28.14 (br, s, $\Delta\nu_{1/2}$ = 1226 Hz), 0.24 (s), 1.09 (s), 2.11 (s), 2.85 (s), 3.74 (s), 28.09 (s). μ_{eff} = 3.42 μ_B. EI-MS: 760.4 (5%) [M – Cl + I]$^+$, 668.4 (10%) [M]$^+$, 633.4 (5%) [M – Cl]$^+$, 524.2 (5%) [M – 4*i*Pr + Me]$^+$, 414.3 (10%), 398.3 (100%) [2,6-Dipp$_2$C$_6$H$_3$]$^+$, 383.3 (40%) [2,6-Dipp$_2$C$_6$H$_3$ – Me]$^+$, 341.2 [2,6-Dipp$_2$C$_6$H$_3$ – *i*Pr – Me]$^+$ (10%), 271.0 (20%) [M – 2,6-Dipp$_2$C$_6$H$_3$]$^+$, 257.1 (25%) [M – 2,6-Dipp$_2$C$_6$H$_3$ – Me]$^+$, 253.0 [M – 2,6-Dipp$_2$C$_6$H$_3$ – Cl + Me]$^+$ (8%), 181.1 (5%) [IPrMe]$^+$, 90.9 (10%) [FeCl]$^+$. EI-MS accurate mass $C_{41}H_{57}FeClN_2$ calcd 666.3743 m/z; found 666.3606 m/z. 4.5 × 10^{-5} M λ_{max}/nm (ε/dm^3 mol^{-1} cm^{-1}) 322 (1513).

Alternative method: To a solution of [2,6-Mes$_2$C$_6$H$_3$FeBr]$_2$·[LiBr(Et$_2$O)]$_2$ (19.8 mg, 0.0136 mmol) in C$_6$D$_6$ (0.63 mL) was added IPrMe (5.9 mg, 0.0327 mmol). An immediate colour change from yellow to yellow/beige occurred. The reaction was allowed to stand at room temperature for 16 hrs, during which time a fine, white precipitate settled. The supernatant was decanted and crystallisation induced by the diffusion of pentane vapour into the solution to give pale yellow crystals of [2,6-Mes$_2$C$_6$H$_3$]FeBr[IPrMe].

4.6.7 [2,6-Ar$_2$C$_6$H$_3$]CoBr[IPrMe] [Ar = Mes (IV·15) or Dipp (IV·18)]

To a solution of [2,6-Ar$_2$C$_6$H$_3$CoBr]$_2$·[LiBr(Et$_2$O)]$_2$ (A: 100 mg, 0.0717 mmol. B: 200 mg, 0.163 mmol) in toluene (10 mL) cooled to −30°C a solution of IPrMe (A: 26 mg, 0.143 mmol. B: 58 mg, 0.322 mmol) in toluene (20 mL) was added dropwise. The solution changed colour (from A: dark green, B: blue/green) to a light green over 15 min. The reaction was stirred at −30°C for 1 hour before being allowed to warm to room temperature. The reaction was held at this temperature for a further 2 hrs before all volatiles were removed *in vacuo*. The reaction was then extracted into toluene (3 mL) to give a lime green solution, leaving behind a blue solid found to be [IPrMe]$_2$CoBr$_2$ by X-ray diffraction studies and ^{1}H NMR spectroscopic

analysis. The green solution was then layered with pentane (20 mL) and stored at *ca.* 7°C for 3 d to afford crystals of suitable quality for X-ray diffraction studies.

[2,6-$Mes_2C_6H_3$]CoBr[IPrMe] was obtained as a crystalline, lime green solid. 36.4 mg, 18%. ^{1}H NMR (400.13 MHz, C_6D_6, 25°C) δ_H / ppm; −48.34 (br, s, $\Delta\nu$½ = 169 Hz), −23.34 (br, s, $\Delta\nu$½ = 39 Hz), −3.62 (br, $\Delta\nu$½ = 2408 Hz), 5.94 (br, s, $\Delta\nu$½ = 162 Hz), 88.19 (br, s, $\Delta\nu$½ = 323 Hz). μ_{eff} = 4.29 μ_B. EI-MS $[M]^+$ m/z: 633.2 (35%); Fragment peaks: 679.2 [(2,6-$Mes_2C_6H_3$)CoI(IPrMe)]$^+$ (7%), 314.2 [2,6-$Mes_2C_6H_3$]$^+$ (100%), 299.2 [2,6-$Mes_2C_6H_3$ − Me]$^+$ (15%), 179.1 [IPrMe]$^+$ (8%).EI-MS accurate mass $C_{35}H_{45}CoBrN_2$ calcd 631.2093 m/z; found = 631.2091 m/z. Elemental analysis: $C_{35}H_{45}CoBrN_2$ calcd C 66.45, H 7.17, N 4.43; found C 66.12, H 7.32, N 4.18. UV/Vis: 1.03 × 10^{-3} Mol λ_{max}/nm (ε/dm^3 mol^{-1} cm^{-1}) 783 (107), broad absorbance 673-480, 658 (166), 482 (171); 3.95 × 10^{-4} M λ_{max}/nm (ε/dm^3 mol^{-1} cm^{-1}) 341 (1134).

[2,6-$Dipp_2C_6H_3$]CoBr[IPrMe] was obtained as lime green crystals. 34 mg, 17%. ^{1}H NMR (300.13 MHz, C_6D_6, 300 K) δ_H / ppm; −66.90 (br, s, $\Delta\nu$½ = 393 Hz), −52.98 (br, s, $\Delta\nu$½ = 148 Hz), −17.36 (br, s, $\Delta\nu$½ = 360 Hz), −2.65 (br, s, $\Delta\nu$½ = 1358 Hz), 14.62 (br, s, $\Delta\nu$½ = 147 Hz), 95.58 (br, s, $\Delta\nu$½ = 385 Hz). μ_{eff} = 5.19 μ_B. ASAP-MS: 740.3 (5%), 717.3 (5%) $[M]^+$, 637.4 (100%) [M – Br]$^+$, 593.3 (60%) [M – Br – *i*Pr]$^+$, 552.3 (5%) [M – IPrMe + Me]$^+$, 498.3 (20%) [M – Dipp]$^+$, 455.2 (40%) [M – IPrMe – Br]$^+$, 397.3 (10%) [2,6-$Dipp_2C_6H_3$]$^+$, 361.0 (10%) [M – 2,6-$Dipp_2C_6H_3$ + *i*Pr]$^+$, 320.0 (10%) [M – 2,6-$Dipp_2C_6H_3$]$^+$, 271.1 (5%) [M – 2,6-$Dipp_2C_6H_3$ – *i*Pr]$^+$, 231.1 (10%) *potential impurity*, 215.1 (10%) *potential impurity*, 181.2 (5%) [IPrMe]$^+$ ASAP-MS accurate mass $C_{41}H_{57}CoBrN_2$ calcd. 715.3037 m/z; found = 715.2040 m/z. Elemental analysis: $C_{41}H_{57}CoBrN_2$ calcd C 68.71, H 8.02, N 3.91; found C 67.83, H 8.01, N 4.14. UV/Vis: 5.30 × 10^{-5} M λ_{max}/nm (ε/dm^3 mol^{-1} cm^{-1}) 781 (133) (shoulder 759 nm), 480 (145); 1.59 × 10^{-5} Mol (toluene) 363 (2258).

Alternative method: To a solution of [(IPrMe)$CoBr_2$]$_2$ (100 mg, 0.125 mmol) in Et_2O (20 mL) cooled to −30°C was added a solution of [2,6-$Dipp_2C_6H_3Li$]$_2$ (101 mg, 0.125 mmol) in Et_2O (20 mL). The blue solution was allowed to warm to room temperature over 16 hrs over which time the colour changed to dark green and some blue precipitate was observed. The reaction was filtered to leave behind the blue precipitate, found to be [IPrMe]$_2CoBr_2$ by ^{1}H NMR spectroscopic analysis, to give a lime green solution. All volatiles were removed *in vacuo* to give a green solid. This was extracted into toluene (2 × 5 mL) and the volume of the solution reduced to 3 mL before the solution was layered with pentane (10 mL). Storage of this mixture at *ca.* 7°C for 1 d afforded crystals of suitable quality for X-ray diffraction studies. 45 mg, 25%.

4.6.8 [(IPrMe)$_2$Fe(μ$_3$-O)]$_2$[(2,6-$Mes_2C_6H_3$)$_2$Fe(μ$_3$-O)]$_2$Fe (IV·16)

To a solution of [2,6-$Mes_2C_6H_3FeBr$]$_2$·[$LiBr(Et_2O)$]$_2$ (100 mg, 0.0819 mmol) in toluene (10 mL) cooled to 0°C was added a solution of IPrMe (29.5 mg, 0.162 mmol) in toluene (10 mL). The reaction changed colour from yellow to a pale yellow. The reaction was stirred at 0°C for 1 hour and at room temperature for 2 hrs. The reaction was cooled to 0°C and added dropwise to potassium graphite (40 mg, 0.324 mmol) over 20 mins. The reaction was allowed to warm slowly to room temperature over 16 hrs. During which time a colour change from pale yellow to orange was observed. The reaction was filtered and all volatiles removed *in vacuo* to afford an orange solid. The reaction was extracted into pentane (10 mL) to give a black/yellow solution. Storage of this solution at −30°C afforded dark red crystals suitable for X-ray diffraction studies.

4.6.9 [2,6-$Dipp_2C_6H_3$]Co[IPrMe] (IV·20)

[2,6-$Dipp_2C_6H_3CoBr$]$_2$·[$LiBrOEt$]$_2$ (104 mg, 0.0756 mmol) and IPrMe (26 mg, 0.144 mmol) were combined and dissolved in toluene (20 mL). A colour change from dark green to a light green/yellow was observed at this point. The reaction was held with stirring at room

temperature for 16 hours during which time a white precipitate formed. This solution was then added dropwise to a suspension of KC_8 (40 mg, 0.296 mmol) in toluene (10 mL) cooled to 0°C. A gradual colour change to orange/red was observed over the course of 6 hrs. Following this the reaction was allowed to warm to room temperature and stirred for 16 hours. The graphite powder was filtered from the reaction and all volatiles removed *in vacuo*. The red solid was then extracted into pentane (2 × 5 mL). Storage of this solution at 7°C afforded deep red crystals of [Dipp$_2$C$_6$H$_3$]Co[IPrMe] suitable for X-ray diffraction studies. 31 mg, 34%. ^{1}H NMR (400 MHz, C_6D_6, 300 K) δ_H / ppm; −78.23 (br, s, $\Delta\nu$½ = 685 Hz), −60.00 (br, s, $\Delta\nu$½ = 205 Hz), −16.14 (br, s, $\Delta\nu$½ = 3074 Hz), −3.31 (br, s, $\Delta\nu$½ = 787 Hz), 110.80 (br, s, $\Delta\nu$½ = 490 Hz), 121.03 (br, s, $\Delta\nu$½ = 341 Hz). μ_{eff} = 4.26 μ_B. ASAP-MS accurate mass $C_{41}H_{57}CoN_2$ calcd. 636.3854 m/z; found 636.3858 m/z. ASAP-MS: 717.3 (2%) [M + Br]$^+$, 636.4 (100%) [M]$^+$, 593.3 (5%) [M – *i*Pr]$^+$, 415.3 (5%) [M – IPrMe – *i*Pr]$^+$, 399.3 (65%) [2,6-Dipp$_2$C$_6$H$_3$]$^+$ (*ligand*), 357.3 (20%) [*ligand* – *i*Pr]$^+$, 315.2 (10%) [*ligand* – 2 *i*Pr]$^+$, 231.1 (5%) *potential impurity*, 181.2 (30%) [IPrMe]$^+$. Elemental analysis: $C_{41}H_{57}CoN_2$ calcd. C 77.33, H 9.02, N 4.40; found C 77.88, H 8.88, N 4.43. UV/Vis: 3.61 × 10^{-5} Mol (Toluene) λ_{max}/nm (ε/dm^3 mol^{-1} cm^{-1}) 681 (453) br, 514 (892), 442 (2308), 374 (3696) (shoulder).

4.6.10 Attempted Synthesis of [2,6-Mes$_2$C$_6$H$_3$]MBr[IPr] [M = Fe (IV·23),Co (IV·24)]

To an NMR tube containing [2,6-Mes$_2$C$_6$H$_3$MBr]$_2$·[LiBr(OEt$_2$)]$_2$ (C: 11.5 mg, 0.0942 mmol, D: 14.7 mg, 0.0120 mmol) in C_6D_6 (*ca.* 0.7 mL) was added IPr (C: 7.3 mg, 0.0187 mmol, D: 9.5 mg, 0.0244 mmol). The reaction was stood at room temperature for 1 hour before ^{1}H NMR spectroscopic data was collected. Crystallisation was induced by the slow diffusion of pentane into the reaction mixture which resulted in crystals of suitable quality for X-ray diffraction.

Crystals of the iron containing product (**IV·23**) were yellow in colour. X-ray diffraction studies found the crystallised compound to be [2,6-Mes$_2$C$_6$H$_3$FeBr$_2$][IPrH]. ^{1}H NMR (400 MHz, C_6D_6,

300 K) δ_H / ppm; −33.83 (s), −23.81 (s), −21.77 (s), −12.25 (s), 0.40 (s), 1.29 (br, s), 1.40 (br, s), 2.18 (*s*), 2.33 (*s*), 3.07 (*s*), 4.53 (br, *s*, Δν½ = 372 Hz), 5.37 (br, *s*, Δν½ = 397 Hz), 6.73 (br, *s*), 6.89 (*s*), 6.98 (*s*), 7.39 (*s*), 15.27 (*s*), 56.46 (br, *s*, Δν½ = 1337 Hz).

The cobalt containing reaction changed colour from dark green/blue to lime green upon the addition of IPr. Three forms of crystal were observed. Small lime green crystals were of insufficient quality and quantity for X-ray diffraction studies or any other technique. Of the two remaining sets both were investigated using X-ray diffraction: colourless plates were found to be protonated ligand and blue pillar crystals were found to be [IPrCoBr$_3$][IPrH] (**IV·24**). ^{1}H NMR (400 MHz, C_6D_6, 300 K) δ_H / ppm; −59.43 (br, *s*, Δν½ = 505 Hz), −43.80 (br, *s*, Δν½ = 422 Hz), −41.13 (br, *s*, Δν½ = 293 Hz), −30.38 (br, *s*, Δν½ = 331 Hz), −28.64 (br, *s*, Δν½ = 225 Hz), −28.06 (br, *s*, Δν½ = 304 Hz), −22.57 (br, *s*, Δν½ = 342 Hz), −13.03 (br, *s*, Δν½ = 872 Hz), −1.32 (br, *s*, Δν½ = 209 Hz), 1.16 (br, *s*, Δν½ = 561 Hz), 2.12 (br, *s*, Δν½ = 243 Hz), 2.97 (br, *s*, Δν½ = 202 Hz), 3.86 (br, *s*, Δν½ = 434 Hz), 5.91 (br, *s*, Δν½ = 252 Hz), 8.03 (br, *s*, Δν½ = 638 Hz), 22.32 (br, *s*, Δν½ = 798 Hz), 43.04 (br, *s*, Δν½ = 463 Hz).

4.6.11 Hydrosilylation of Phenylacetylene Promoted by [2,6-Dipp$_2$C$_6$H$_3$]ZnCl[IPrMe] (IV·24)

To an NMR tube containing [2,6-Dipp$_2$C$_6$H$_3$]ZnCl[IPrMe] (10.1 mg) in C_6D_6 (0.7 mL) was added phenyl silane (16.1mg, 1.49 mmol), phenylacetylene (15.2 mg, 7.16 mmol) and LiB(Et$_3$)H (1 M in THF, 16 µL). The mixture was agitated *via* sonication to encourage mixing of the reagents and held at room temperature for 5 days. The reaction was monitored by ^{1}H, ^{13}C{^{1}H}, ^{11}B and ^{29}Si NMR spectroscopy for 1 week during which time no changes were observed. Crystals of phenylstyrylsilane were grown by vapour diffusion of pentane into the reaction mixture and storage at room temperature for 3 months. ^{1}H NMR (400 MHz, C_6D_6, 300 K) δ_H / ppm; (24 hrs) 0.40 (s, 3H), 1.27 (m, 60H), 1.54 (m, 70H, THF), 1.70 (6H), 2.87 (s, 6H,

CH, *phenyl acetylene*), 3.71 (m, 60H, THF), 4.34 (s, 30H, SiH_3, *phenyl silane*), 5.90 (sept, 2H), 6.97 – 7.11 (m, 13H, $C_{Ar}H$, *phenyl silane*), 7.14 – 7.32 (m, 41H, $C_{Ar}H$, *phenyl silane* and *phenyl acetylene*), 7.45 – 7.46 (m, 39H, $C_{Ar}H$, *phenyl acetylene*).

4.6.12 Synthesis of 1,3-diphenyl-5-(hexa-ylidene)imidazolidine-2,4-dione Promoted by [2,6-Dipp$_2$C$_6$H$_3$]Co[IPrMe]

[2,6-Dipp$_2$C$_6$H$_3$]Co[IPrMe] (10.8 mg, 0.0170 mmol) was added to a solution of 1-hexyne (13.9 mg, 0.169 mmol) and phenyl isocyanate (40.4 mg, 0.339 mmol) in C_6D_6 (588.4 mg). The reaction was heated to 80°C for 24 hrs before a ^{1}H NMR spectrum was collected. The reaction was then held at room temperature for a further three days before a second spectrum was collected. Crystallisation of 2,4,6-triphenylisocyanurate (**IV·26**) was induced from the reaction mixture through vapour diffusion of pentane into the reaction mixture and storage at −30°C for *ca*. two weeks. Crystallisation of 1,3-diphenyl-5-(hexa-2-ylidene)-imidazolidine-2,4-dione (**IV·27**) was induced by storage of the reaction mixture at −30°C for a further two months. ^{1}H NMR (400 MHz, C_6D_6, 300 K) δ_H / ppm; (after 24 hrs); 0.86 (s, 8H), 1.01 (s, 11H), 1.20 (s, 7H), 1.42 (m, 22H), 1.70 (s, 9H), 1.87 (s, 2H), 2.06 (s, 7 H), 2.69 (s, 9H), 3.07 (s, 2 H), 4.91 (s, 1H), 6.71 (s, 34H) 6.95 (s, 63H), 7.15 (s, 6H), 7.24 (m, 18H), 7.37 (s, 7H), 7.58 (s, 4H), 8.70 (s, 1H). (after 4 days); 1.48 (s, b, $\Delta\nu_{½}$ = 1325 Hz) 2.82 (s, b, $\Delta\nu_{½}$ = 606 Hz), 7.37 (s, b, $\Delta\nu_{½}$ = 718 Hz).

Chapter V

Global Conclusions

5·1 Global Conclusions

The aim of this work was to isolate two-coordinate, heteroleptic, transition metal complexes stabilised by *m*-terphenyl ligands. Access to such complexes would expand the range of *m*-terphenyl, transition metal complexes available, potentially improving control over the catalytic applications that have recently been developed by Kays and co-workers[64,65] or enhancing the magnetic properties highlighted by Power and co-workers.[63]

To this end, a series of transition metal and Group 12 complexes bearing one *m*-terphenyl and one halide ligand were prepared for use as intermediates between metal(II) halides and the desired products. Complexes of the type $[2,6\text{-Dipp}_2C_6H_3MI]_2[LiI(OEt_2)]_2$ (M = Mn, Fe or Co), and Group 12 analogues $[2,6\text{-Dipp}_2C_6H_3MI]_n$ (M = Zn, n = 2; M = Cd, n = 2; M = Hg, n = 1) were previously reported by Power and co-workers.[169,170] The methodology that they developed has been extended to afford a wider array of analogous starting materials. These complexes were analysed in the solid state and in solution. The majority dimerised through bridging halides, with the incorporation of lithium halide as observed for similar products in the literature.[169,170,277] The exceptions to this rule were the $[2,6\text{-Ar}_2C_6H_3]HgBr$ [Ar = Mes

(**II·43**) and Tmp (**II·44**)], although long range, intermolecular Hg···Br interactions were observed in the solid state structure of **II·44**.

In the dimeric, paramagnetic complexes (**II·36**–**II·40**), magnetic moments were observed to be lower than the values expected for two of the relevant spin-only ions. This indicated ferromagnetic coupling between the two metal centres. Whether this indicated the existence of metal–metal bonds or superexchange *via* the bridging halides could not be established using the Evans' method, which was employed to measure the magnetic moments of the complexes in this study.

Halide bridged NHC complexes, of the form $[IPrMeMX_2]_2$ [MX = CoBr (**II·30**) and ZnCl (**II·31**)], were also synthesised through the coordination of IPrMe to the metal halide. These complexes also dimerised in the solid-state, though without the incorporation of lithium halide. In the synthesis of these complexes the impurities $[IPrMe]_2MX_2$ [MX = CoBr (**II·32**) and ZnCl (**II·35**)] also formed. These were analysed so that their presence as by-products in future reactions could be identified. The manganese and iron $[IPrMeMX_2]_2$ analogues could not be isolated. Instead multiple attempts resulted in the isolation of $[IPrMeH]_2[MnBr_4]$ and $[IPrMe]_2FeCl_2$, respectively. Similarly, reactions between one equivalent of IPrMe and $NiCl_2$ or $CuCl_2$ afforded $[IPrMe]_2NiCl_2$ (**II·33**) and [IPrMe]CuCl (**II·34**). The former was isolated in a respectable yield, whilst only a single crystal of the latter was obtained.

Once appropriate starting materials were isolated and characterised, the halide bearing, *m*-terphenyl complexes (**II·36**–**II·43**) were further reacted with an equivalent of a different *m*-terphenyl lithium salt.

Four heteroleptic mercury complexes (**III·21**–**24**) were isolated through this approach. These complexes are the first reported examples of two-coordinate complexes supported by two different *m*-terphenyl ligands. Structural studies of **III·21**–**24** demonstrated that the

combination of two different ligands did not possess structural properties that were halfway between the homoleptic analogues, but instead adopted very different conformations in the solid state. There was evidence in the ^{1}H NMR spectra of complexes bearing the [2,6-$Tmp_2C_6H_3$]$^-$ ligand that the ligands interacted through space. The mechanism of this interaction, however, could not be identified using the techniques employed. It is possible that in the two-coordinate complexes the flanking groups are unable to rotate freely; in systems with asymmetric flanking groups, the symmetric flanking groups experience uneven, through space interactions, which gives rise to the unusual splitting of the methyl signals observed in the ^{1}H NMR spectra of these complexes.

Efforts to extend this methodology to transition metals and other Group 12 elements resulted in the isolation of [2,6-$Dcp_2C_6H_3$]M[2,6-$Mes_2C_6H_3$] [M = Mn (**III·30**) and Zn (**III·31**)]. Secondary interactions between the chlorides of the [2,6-$Dcp_2C_6H_3$]$^-$ mean that the complexes are not truly two-coordinate. However, **III·30** is the first example of a quasi-two-coordinate, heteroleptic transition metal complex stabilised by two aryl ligands. **III·30** demonstrates that the synthetic route that affords the synthesis of the Group 12 complexes **III·21–24** can also be applied to certain transition metals, albeit using a very specific ligand system.

Attempts to develop similar complexes encountered several issues. The first was identification: disorder within the crystal structures prevented an accurate structure determination *via* X-ray crystallography. The second was the exchange of the *m*-terphenyl ligands in solution, resulting in a statistical mixture of aryl products.

^{113}Cd{^{1}H} NMR spectroscopic studies suggest that exchange may occur by the establishment of a Schlenk equilibrium during the early stages of the reaction. The identification of this equilibrium, the occurrence of which has not been previously identified, has contributed to the

understanding of how two-coordinate, *m*-terphenyl complexes form. It is hoped that this information will be of use to future researchers in this or related fields.

Reactions between [2,6-$Dcp_2C_6H_3Li]_2$ and iron(II) chloride or cobalt(II) bromide resulted in products containing multiple units of [2,6-$Dcp_2C_6H_3]^-$ cross coupled to one another. These products were 1-[2,6-$Dcp_2C_6H_3$]-7-$DcpC_{12}H_6$ (**III·36**) and [2-{2,6-$(Dcp_2C_6H_3)_2C_6H_3$}-6-$DcpC_6H_3$]CoBr (**III·37**) respectively. The occurrence of cross-coupling reactions provides an explanation for why iron and cobalt analogues of **III·30** could not be isolated. Possible reaction mechanisms for the formation of **III·36** and **III·37** have been proposed, based on mechanisms and catalytic cycles reported in the literature.[244,254] The identification of a limitation to the heteroatoms that can be easily incorporated into an *m*-terphenyl framework of a transition metal complex is a further accomplishment of this study.

The scope for using two different *m*-terphenyl ligands in to one, two-coordinate, heteroleptic transition complex was found to be limited. The study demonstrated that the approach adopted was not suitable for isolating a wide range of readily characterisable complexes in practical yields. It was therefore elected to investigate a different ligand system featuring one *m*-terphenyl and one N-heterocyclic carbene.

To this end, a series of three-coordinate complexes were developed of the general formula [2,6-$Ar_2C_6H_3$]MX[IPrMe]. The intention was to characterise these complexes and then investigate abstracting the halide with a Group 1 metal to afford a two-coordinate, heteroleptic metal(I) complex. The first series of complexes developed was $[(2,6\text{-}Mes_2C_6H_3)MX(IPrMe)]_n$ [n = 1, MX = ZnCl (**IV·10**), CdCl (**IV·11**), HgBr (**IV·12**), FeBr (**IV·14**), CoBr (**IV·15**); n = 2, MX = MnBr (**IV·13**)]. **IV·10**, **IV·11**, **IV·14** and **IV·15** adopted a distorted trigonal planar geometry in the solid state, with an expansion of the angle between the two organic ligands concomitant with a compression of the angle between the organic ligands and the halide. **IV·10** adopted a

T-shaped geometry, which is common in three-coordinate mercury complexes,[332] whilst **IV·11** dimerised, with bromides bridging two manganese centres, resulting in a distorted tetrahedral geometry around the metal centres.

The reduction of (**IV·10**, **IV·14** and **IV·15**) with sodium or potassium graphite did not result in the isolation of the desired metal(I) complexes. $[(IPrMe)_2Fe(\mu_3\text{-}O)]_2[(2,6\text{-}Mes_2C_6H_3)_2Fe(\mu_3\text{-}O)]_2Fe$ (**IV·16**) was the only product isolated from these reactions, formed from the reaction between **IV·14**, potassium graphite, and (presumably) trace oxygen from the solvent. **IV·16** is a rare example of a complex that contains five iron centres in three different chemical environments. Unfortunately, an amount of **IV·16** suitable for further chemical, electronic and magnetic studies could not be isolated.

A series of complexes of the type $[2,6\text{-}Dipp_2C_6H_3]MX[IPrMe]$ (MX = FeCl (**IV·17**), CoBr (**IV·18**) and ZnCl (**IV·19**) was prepared and characterised according to the theory that greater steric bulk around the metal centre may stabilise the desired metal(I) species. The reaction between potassium graphite and **IV·18** afforded $[2,6\text{-}Dipp_2C_6H_3]Co[IPrMe]$ (**IV·20**) as deep red crystals in a moderate yield. In the solid state the complex displayed an almost linear C–Co–C moiety and the ligands adopted a co-planar geometry, in contrast to other two-coordinate complexes in the literature that bear similar ligands.[63,76,126] **IV·20** is the first example of a neutral cobalt(I) complex supported by ligands binding solely through carbon atoms.

Investigations into the magnetism of **IV·20** demonstrated that it displayed a magnetic moment (4.3 μ_B) higher than that of a spin only d^8 ion (2.83 μ_B), which was attributed to a significant spin orbit contribution allowed by the linear geometry around the cobalt(I) centre. **IV·20** is one of the lowest molecular weight two-coordinate cobalt complexes with an elevated magnetic moment in the literature and therefore an in-depth study of its magnetic properties is warranted.

An electrochemical study of **IV·20** demonstrated that the complex can undergo at least two reductive processes, neither of which was electrochemically reversible. The presence of an oxidative process, linked to the higher potential reductive process (**B**), demonstrated that it was chemically reversible. Attempts to reduce **IV·17** and **IV·19** using a Group 1 metal did not yield the target iron(I) or zinc(I) products.

In a further attempt to isolate an iron(I) complex similar to **IV·20**, a bulkier NHC (IPr) was employed. The reaction between halide bridged dimers **II·39** and **II·40** and IPr resulted in the charged species, [2,6-$Mes_2C_6H_3FeBr_2$][IPrH] (**IV·24**) and [IPrCoBr_3][IPrH] (**IV·25**), respectively, as opposed to the desired three-coordinate complexes. It was theorised that the IPr ligand possessed too much steric bulk to form a three-coordinate complex also containing $[2,6\text{-}Mes_2C_6H_3]^-$ as a ligand.

Preliminary investigations into the ability of the complexes developed in this work to activate small molecules or promote reactions between two substrates were conducted. These suggested that **IV·19** and **IV·20** are potentially active as pre-catalysts or catalysts in the hydrosilylation of alkynes and the [1+2+2] cycloaddition of 1-hexyne and phenyl isocyanate respectively.

As is often the case in research, much of the work discussed in this thesis did not afford the expected or desired results. Fundamental difficulties in the isolation and characterisation of two-coordinate complexes bearing two different yet similar ligands were uncovered and often could not be overcome.

Purely *m*-terphenyl ligand systems were developed that alleviated these issues, affording small amounts of two-coordinate, heteroleptic *m*-terphenyl complexes such as [2,6-$Dcp_2C_6H_3$]Mn[2,6-$Mes_2C_6H_3$] (**III·30**).

A new class of three-coordinate complexes, featuring NHC and *m*-terphenyl ligands, has been developed to overcome the above outlined difficulties. These, in turn, have facilitated the

synthesis of the first in a new class of two-coordinate transition metal complexes, [2,6-$Dipp_2C_6H_3$]Co[IPrMe] (**IV·20**).

Overall, the goal of producing two-coordinate, heteroleptic, transition metal complexes has begun to be achieved, despite the difficulties uncovered over the course of this work. Whilst the potential variety and utility envisioned at the beginning of this project has only been glimpsed, it is hoped that the work detailed above will provide a useful contribution for researchers who wish to take this area further.

Appendices

6.1 Appendix A – Solid State Structures of Ligand Scrambled Products

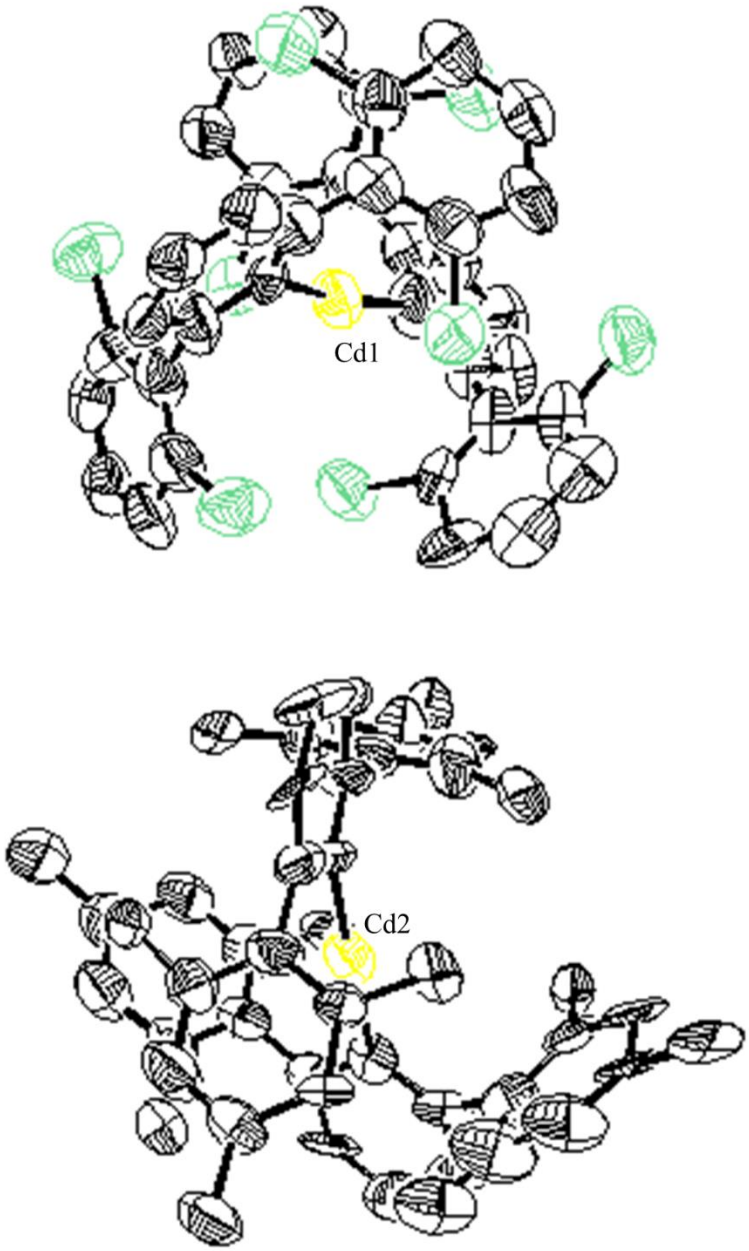

Figure 6·1. The solid-state structure of $[2,6\text{-}Dcp_2C_6H_3]_2Cd$ and $[2,6\text{-}Mes_2C_6H_3]_2Cd$ (**VI·1**), obtained by X-ray diffraction studies, that co-crystallised. The crystal was obtained from the reaction between $[2,6\text{-}Mes_2C_6H_3CdCl]_3LiCl(Et_2O)$ and $[2,6\text{-}Dcp_2C_6H_3Li]_2$.

	VI·1
Code	CDGALF
Formula	$C_{42}H_{34}CdCl_4$
M_w	792.89
Crystal system	triclinic
Space Group	*P* -1
Crystal size	0.089 × 0.082 × 0.041
a (Å)	10.6696(16)
b (Å)	19.510(2)
c (Å)	20.178(2)
α (°)	61.441(11)
β (°)	84.294(10)
γ (°)	89.578(12)
V (Å^3)	3667.1(9)
Z	4
T (K)	120(2)
D_{calc} (g cm^{-3})	1.436
F_{000}	1608
μ (mm^{-1})	7.664
θ range for data collection (°)	4.169 73.761
Max. and min. transmission	0.972 0.941
reflns measd	27857
independent reflns	14213
R_{int}	0.4035
Final *GooF*	0.934
R_1, wR_2 [$I > 2\sigma(I)$]	0.2240 0.3831
R_1, wR_2 (all data)	0.4670 0.4807
min. and max. electron densities (e Å^{-3})	-1.925 1.082

6.2 Appendix B – Crystallographic Tables

	II·30	**II·31**	**II·32**	**II·33**
Code	COGALM	ZNGALM	COGALN	NIGALA
Formula	$C_{22}H_{40}Br_4Co_2N_4$	$C_{22}H_{40}N_2Zn_2Cl_4$	$C_{22}H_{40}Br_2Co\ N_4$	$C_{34}D_{12}H_{40}N_2NiCl_2$
M_w	798.08	633.12	579.33	658.48
Crystal system	monoclinic	monoclinic	monoclinic	monoclinic
Space Group	$P2_1/c$	$P\ 2_1/c$	$P\ 21/n\ 1$	$P2_1/n$
Crystal size	0.345 × 0.196 × 0.131	0.176 × 0.140 × 0.139	0.056 × 0.047 × 0.024	0.369 × 0.338 × 0.248
a (Å)	19.2472(5)	19.0012(3)	11.1236(2)	12.84725(15)
b (Å)	14.5080(4)	14.15029(17)	15.2371(4)	8.62349(11)
c (Å)	11.2499(4)	11.10419(13)	15.5184(4)	16.22803(20)
α (°)	90	90	90	90
β (°)	105.803(3)	105.2982(12)	90.2337(19)	101.9489(12)
γ (°)	90	90	90	90
V (Å^3)	3022.68(17)	2879.82(6)	2630.22(11)	1758.92(4)
Z	4	4	4	2
T (K)	120(2)	120(2)	120(2)	120(2)
D_{calc} (g cm^{-3})	1.754	1.46	1.463	1.243
F_{000}	1576	1312	1188	692
μ (mm^{-1})	14.913	5.589	8.774	2.39
θ range for data collection (°)	7.74-133.19	3.947-76.975	4.066-73.808	4.009-73.443
Max. and min. transmission	-0.782 1.776	0.603 0.515	0.955-0.913	0.559 0.433
reflns measd	28853	20128	14832	7028
independent reflns	5335	5928	5182	3453
R_{int}	0.0808	0.017	0.0393	0.0196
Final *GooF*	1.047	1.082	1.044	1.039
R_1, wR_2 [$I > 2\sigma(I)$]	0.0791, 0.2242	0.0308, 0.082	0.0442, 0.1173	0.0359, 0.0968
R_1, wR_2 (all data)	0.0853, 0.2319	0.0317, 0.0826	0.0505, 0.1225	0.0378, 0.0986
min. and max. electron densities (e Å^{-3})	0.77, 1.79	-0.84, 0.361	-1.384, 0.786	-0.297, 0.683

	II·34	**II·35**	**II·36**	**II·37**
Code	CUGALA	ZNGALW	MNGALG	COGALI
Formula	$C_{11}H_{20}ClCuN_2$	$C_{34}H_{52}Cl_2N_4Zn$	$C_{70}H_{99}Br_4Li_2Mn_2O_{2.50}$	$C_{71.50}H_{96}Br_4Co_2Li_2O_2$
M_w	279.28	653.06	1423.89	1438.86
Crystal system	tetragonal	monoclinic	monoclinic	monoclinic
Space Group	$P\,4_12_12$	$P\,21/c$	$P\,21/n$	$P\,21/n$
Crystal size	0.397 × 0.276 × 0.229	0.27 × 0.234 × 0.144	0.4997 × 0.4362 × 0.2639	0.5391 × 0.2703 × 0.1298
a (Å)	8.0050(4)	9.8434(6)	13.1147(2)	13.03551(15)
b (Å)	8.0050(4)	38.2058(14)	24.7601(4)	24.5998(3)
c (Å)	20.6391(16)	9.8942(6)	22.5251(3)	22.4433(3)
α (°)	90	90	90	90
β (°)	90	105.860(6)	96.3007(15)	96.7914(11)
γ (°)	90	90	90	90
V (Å^3)	1322.54(16)	3579.3(3)	7270.2(2)	7146.42(15)
Z	4	4	4	4
T (K)	120(2)	120(2)	120(2)	120(2)
D_{calc} (g cm^{-3})	1.403	1.212	1.301	1.337
F_{000}	584	1392	2940	2964
μ (mm^{-1})	3.949	2.520	5.696	6.555
θ range for data collection (°)	5.929-77.063	2.313-73.549	3.570-73.669	3.593-73.725
Max. and min. transmission	0.303 0.465	0.970 0.947	3.570 73.669	0.862 0.543
reflns measd	31335	9014	31181	31403
independent reflns	1386	5694	14296	14087
R_{int}	0.0459	0.0214	0.0445	0.0371
Final *GooF*	1.149	1.097	1.038	1.035
R_1, wR_2 [$I > 2\sigma(I)$]	0.0242, 0.0568	0.0379, 0.0950	0.0550, 0.1482	0.0655, 0.1903
R_1, wR_2 (all data)	0.0242, 0.0568	0.0430, 0.0970	0.0571, 0.1505	0.0675, 0.1933
min. and max. electron densities (e Å^{-3})	-0.342, 0.290	-0.402, 0.576	-1.513, 2.397	-2.313, 2.957

	II·36b	**II·37b**	**II·38**	**II·39**
Code	MNGALF	COGALJ	FEGAMF	COGALL
Formula	$C_{60}H_{74}Br_2Mn_2$	$C_{60}H_{74}Br_2Co_2$	$C_{56}H_{70}Fe_2Li_2Br_4O_2$	$C_{56}H_{70}Br_4Co_2Li_2O_2$
M_w	1064.89	1072.87	1220.34	1226.5
Crystal system	triclinic	monoclinic	monoclinic	monoclinic
Space Group	*P* -1	*P* $2_1/c$	*P* $2_1/n$	*P* $2_1/n$
Crystal size	0.2531 × 0.177 × 0.1597	0.358 × 0.158 × 0.088	0.475 × 0.091 × 0.056	0.162 × 0.075 × 0.053
a (Å)	10.6528(6)	13.6774(5)	11.62875(8)	11.6239(2)
b (Å)	14.0813(10)	10.5818(3)	26.00369(19)	26.0995(5)
c (Å)	19.1084(11)	39.1882(13)	18.89732(11)	18.6955(3)
α (°)	91.097(5)	90	90	90
β (°)	90.204(5)	98.837(3)	90.9935(5)	91.4252(15)
γ (°)	96.523(5)	90	90	90
V (Å^3)	2847.2(3)	5604.4(3)	5713.51(7)	5670.02(18)
Z	2	4	4	4
T (K)	120(2)	120(2)	120(2)	120(2)
D_{calc} (g cm^{-3})	1.242	1.272	1.419	1.437
F_{000}	1108	2232	2480	2488
μ (mm^{-1})	5.496	6.555	7.624	8.162
θ range for data collection (°)	3.880-66.598	4.331-74.664	2.891-73.636	3.387-73.763
Max. and min. transmission	0.930, 0.890	0.624, 0.308	0.942 0.676	0.915 0.790
reflns measd	11441	39835	106318	25147
independent reflns	8229	11217	11455	11161
R_{int}	0.0464	0.0487	0.0499	0.0324
Final *GooF*	1.739	1.038	1.038	1.008
R_1, wR_2 [$I > 2\sigma(I)$]	0.1271, 0.3945	0.0824, 0.2518	0.0258, 0.0658	0.0341, 0.0821
R_1, wR_2 (all data)	0.1324, 0.4028	0.0906, 0.2612	0.027, 0.0666	0.0419, 0.0867
min. and max. electron densities (e Å^{-3})	-1.175, 3.953	-1.188, 3.393	-0.699, 0.659	-0.673, 0.931

	II·42	**II·43**	**II·44**	**III·21**
Code	CDGALH	HGGALO	HGGALA	AJSDKC
Formula	$C_{76}H_{85}Cd_3Cl_4LiO$	$C_{24}H_{25}BrHg$	$C_{24}H_{25}BrHg$	$C_{52}H_{58}Hg$
M_w	1500.38	593.94	593.94	883.57
Crystal system	monoclinic	orthorhombic	orthorhombic	monoclinic
Space Group	*C* 2/*c*	*P bca*	*P nma*	*C* 2/*c*
Crystal size	0.533 × 0.433 × 0.359	0.62 × 0.081 × 0.06	0.1612 × 0.1329 × 0.0496	0.1408 × 0.0594 × 0.0276
a (Å)	23.7582(2)	8.9571(3)	7.5114(6)	14.4046(2)
b (Å)	14.7902(2)	16.8354(4)	23.7897(16)	18.0583(3)
c (Å)	41.0392(6)	28.9935(8)	11.6512(8)	16.4319(2)
α (°)	90	90	90	90
β (°)	94.7111(11)	90	90	95.3419(14)
γ (°)	90	90	90	90
V (Å^3)	14372.0(3)	4372.1(2)	2082.0(3)	4255.77(11)
Z	8	8	4	4
T (K)	120(2)	120(2)	120(2)	120(2)
D_{calc} (g cm^{-3})	1.387	1.805	1.895	1.379
F_{000}	6112	2272	1136	1800
μ (mm^{-1})	8.720	14.780	15.519	6.721
θ range for data collection (°)	2.160-66.598	3.048-73.436	3.716-66.551	4.610-73.535
Max. and min. transmission	0.559, 0.029	0.914, 0.600	0.399, 0.061	0.961, 0.863
reflns measd	153327	40830	11675	8364
independent reflns	12715	4360	1888	4163
R_{int}	0.1070	0.0606	0.0636	0.0219
Final *GooF*	1.071	1.090	1.222	1.025
R_1, wR_2 [$I > 2\sigma(I)$]	0.1212, 0.2900	0.0389, 0.0870	0.0699, 0.1862	0.0189, 0.0465
R_1, wR_2 (all data)	0.1246, 0.2924	0.0428, 0.0893	0.0721, 0.1872	0.0197, 0.0470
min. and max. electron densities (e Å^{-3})	-4.766, 5.581	-1.211, 1.473	-2.760, 3.173	-0.713, 0.669

	III·22	**III·23**	**III·24**	**III·30**
Code	HGGALB	HGGALK	AJSDKJ	MNGALA
Formula	C_{46} H_{46} Hg	$C_{42}H_{34}Cl_4Hg$	$C_{52}H_{58}Hg$	$C_{42}H_{34}Cl_4Mn$
M_w	799.42	881.08	883.57	735.43
Crystal system	triclinic	triclinic	orthorhombic	monoclinic
Space Group	*P* -1	*P* -1	*P ca*2_1	*P* $2_1/c$
Crystal size	0.1906 × 0.053 × 0.0295	0.3969 × 0.2346 × 0.1642	0.411 × 0.107 × 0.073	0.3398 × 0.1767 × 0.1331
a (Å)	10.9276(4)	11.4064(3)	20.3099(6)	9.42034(18)
b (Å)	11.5945(4)	11.5770(3)	19.6237(6)	39.1036(5)
c (Å)	15.8062(2)	15.5049(4)	10.5051(4)	10.64933(19)
α (°)	99.841(2)	95.343(2)	90	90
β (°)	95.278(2)	102.375(2)	90	116.147(2)
γ (°)	109.991(3)	109.362(3)	90	90
V (Å^3)	1829.65(10)	1856.60(10)	4186.8(2)	3521.44(12)
Z	2	2	4	4
T (K)	120(2)	120(2)	120(2)	120(2)
D_{calc} (g cm^{-3})	1.451	1.576	1.402	1.387
F_{000}	804	868	1800	1516
μ (mm^{-1})	7.757	4.462	6.832	6.061
θ range for data collection (°)	2.876-74.422	3.358-28.708	4.354-74.356	4.523-75.067
Max. and min. transmission	0.810, 0.502	0.748, 0.555	0.919, 0.739	0.923, 0.850
reflns measd	13226	61639	11748	145094
independent reflns	7205	8920	6297	7218
R_{int}	0.0285	0.0506	0.0245	0.1027
Final *GooF*	1.106	1.090	1.014	1.056
R_1, wR_2 [$I > 2\sigma(I)$]	0.0282, 0.0741	0.0329, 0.0757	0.0273, 0.0645	0.0693, 0.1844
R_1, wR_2 (all data)	0.0307, 0.0757	0.0414, 0.0822	0.0355, 0.0698	0.0700, 0.1850
min. and max. electron densities (e Å^{-3})	-1.452, 1.744	-1.467, 1.135	-1.053, 1.004	-1.259, 2.131

	III·31	**III·32**	**III·33**	**III·35a**
Code	ZNGALF	CDGALJ	JRDWLM	MNGALB
Formula	$C_{42}H_{34}Cl_4Zn$	$C_{48}H_{50}Cd$	$C_{60}H_{74}Cd$	$C_{36}H_{18}Cl_8Mn$
M_w	745.86	739.28	907.59	789.04
Crystal system	monoclinic	triclinic	monoclinic	orthorhombic
Space Group	*P* 21/*n*	*P* -1	*C* 2/*c*	*Pbca*
Crystal size	0.3465 × 0.1344 × 0.0998	0.236 × 0.073 × 0.052	0.241 × 0.189 × 0.087	0.2921 × 0.1835 × 0.1486
a (Å)	15.5024(2)	10.4327(7)	15.6449(3)	19.3853(8)
b (Å)	14.58245(19)	10.6940(9)	15.9444(3)	15.2493(7)
c (Å)	15.9349(3)	19.9847(11)	19.9249(3)	21.9954(9)
α (°)	90	75.706(6)	90	90
β (°)	104.4756(16)	81.501(5)	92.326(2)	90
γ (°)	90	66.680(7)	90	90
V (Å^3)	3487.93(9)	1981.0(3)	4966.14(15)	6502.1(5)
Z	4	2	4	8
T (K)	120(2)	120(2)	120(2)	120(2)
D_{calc} (g cm^{-3})	1.420	1.239	1.214	1.612
F_{000}	1536	772	1928	3160
μ (mm^{-1})	4.019	4.629	3.781	1.091
θ range for data collection (°)	3.558-74.441	4.574-75.340	3.96 73.462	3.017-28.915
Max. and min. transmission	0.339, 0.067	1.000, 0.663	0.93, 0.857	0.984 0.969
reflns measd	62738	18392	10651	110780
independent reflns	7061	7792	4877	8073
R_{int}	0.0475	0.0564	0.0211	0.1054
Final *GooF*	1.073	1.085	1.055	1.048
R_1, wR_2 [$I > 2\sigma(I)$]	0.0366, 0.1021	0.1279, 0.3309	0.0234, 0.0601	0.0471, 0.0922
R_1, wR_2 (all data)	0.0381, 0.1038	0.1390, 0.3407	0.0236, 0.0603	0.0758, 0.1034
min. and max. electron densities (e Å^{-3})	-0.404, 0.472	-1.840, 6.495	-0.492, 0.575	-0.459, 0.405

	III·35b	**III·36**	**III·37a**	**III·37b**
Code	MNGALO	FEGALG	COGALA	COGALK
Formula	$C_{36}H_{18}Cl_8$ Mn	$C_{36}H_{18}Cl_6$	$C_{58}H_{27}BrCl_{10}Co$	$C_{75}H_{51}BrCl_{10}Co$
M_w	789.04	663.20	1217.13	1445.49
Crystal system	monoclinic	triclinic	monoclinic	triclinic
Space Group	*C* 2/*c*	*P* -1	*P* 21/*n*	*P* -1
Crystal size	0.535 × 0.372 × 0.275	0.4131 × 0.2949 × 0.1842	0.0979 × 0.0822 × 0.0441	0.182 × 0.129 × 0.129
a (Å)	19.7369(6)	10.7681(6)	11.8853(2)	11.5612(4)
b (Å)	11.5757(3)	11.5719(11)	24.2581(4)	16.9174(8)
c (Å)	15.0835(5)	12.5845(12)	17.9999(3)	18.2368(6)
α (°)	90	95.732(8)	90	64.274(4)
β (°)	112.251(4)	107.511(7)	104.8447(18)	84.808(3)
γ (°)	90	92.549(6)	90	85.548(3)
V (Å^3)	3189.49(18)	1483.4(2)	5016.44(15)	3197.2(2)
Z	4	2	4	2
T (K)	120(2)	120(2)	120(2)	120(2)
D_{calc} (g cm^{-3})	1.643	1.485	1.612	1.502
F_{000}	1580	672	2428	1466
μ (mm^{-1})	9.753	5.486	8.837	7.030
θ range for data collection (°)	4.522-73.490	3.709-73.705	4.031-74.051	3.843-73.588
Max. and min. transmission	0.650, 0.493	0.658 0.475	0.940 0.895	0.843 0.673
reflns measd	6014	10348	21414	24056
independent reflns	3118	5764	9894	12529
R_{int}	0.0291	0.0336	0.0439	0.0290
Final *GooF*	1.085	1.034	1.036	1.031
R_1, wR_2 [$I > 2\sigma(I)$]	0.0453, 0.1128	0.0345, 0.0888	0.0527, 0.1393	0.0367, 0.0925
R_1, wR_2 (all data)	0.0456, 0.1132	0.0376, 0.0908	0.0584, 0.1459	0.0411, 0.0953
min. and max. electron densities (e Å^{-3})	-0.973, 0.493	-0.521, 0.305	-1.231, 2.056	-0.590, 0.574

	IV·10	**IV·11**	**IV·12**	**IV·13**
Code	ZNGALU	CDGALI	HGGALM	MNGALX
Formula	$C_{35}H_{45}ClN_2Zn$	$C_{35}H_{45}CdClN_2$	$C_{35}H_{45}BrHgN_2$	$C_{75}H_{102}Br_2Mn_2N_4$
M_w	594.55	641.58	774.23	1329.30
Crystal system	tetragonal	tetragonal	orthorhombic	monoclinic
Space Group	$P\,4_3$	$P\,4_3$	$P\,na2_1$	$P\,2_1/n$
Crystal size	0.453 × 0.349 × 0.308	0.699 × 0.565 × 0.425	0.332 × 0.118 × 0.111	0.199 × 0.067 × 0.028
a (Å)	11.78921(4)	11.88175(8)	23.44954(6)	24.0738(5)
b (Å)	11.78921(4)	11.88175(8)	11.75702(3)	12.5868(2)
c (Å)	23.09985(15)	23.2154(2)	11.91455(6)	24.3044(5)
α (°)	90	90	90	90
β (°)	90	90	90	105.034(2)
γ (°)	90	90	90	90
V (Å^3)	3210.54(3)	3277.45(5)	3284.803(19)	7112.5(3)
Z	4	4	4	4
T (K)	120(2)	120(2)	120(2)	120(2)
D_{calc} (g cm^{-3})	1.230	1.300	1.566	1.241
F_{000}	1264	1336	1536	2800
μ (mm^{-1})	2.000	6.256	10.000	4.516
θ range for data collection (°)	1.913-78.946	3.720-74.495	3.710-73.843	3.766-73.725
Max. and min. transmission	0.910, 0.783	0.719, 0.037	0.223, 0.030	0.970, 0.878
reflns measd	86956	101701	261122	34606
independent reflns	6520	6666	6469	14015
R_{int}	0.1553	0.0602	0.0537	0.0284
Final *GooF*	1.201	1.029	1.108	1.039
R_1, wR_2 [$I > 2\sigma(I)$]	0.0291, 0.0758	0.0501, 0.1316	0.0605, 0.1739	0.0348, 0.0863
R_1, wR_2 (all data)	0.0339, 0.0972	0.0501, 0.1317	0.0606, 0.1739	0.0415, 0.0909
min. and max. electron densities (e Å^{-3})	-0.398, 0.374	-1.082, 1.410	-2.489, 2.496	-0.643, 0.463

	IV·14	**IV·15**	**IV·16**	**IV·18**
Code	FEGAMA	COGAMD	FEGALW	COGALQ
Formula	$C_{35}H_{45}BrFeN_2$	$C_{35}H_{45}BrCoN_2$	$C_{92}H_{128}Fe_5N_8O_4$	$C_{41}H_{57}BrCoN_2$
M_w	629.49	632.57	1689.27	716.72
Crystal system	tetragonal	tetragonal	monoclinic	monoclinic
Space Group	$P\,4_3$	$P\,4_1$	$P\,2_1/n$	$P\,2_1/n$
Crystal size	0.380 × 0.360 × 0.309	0.389 × 0.356 × 0.193	0.920 × 0.450 × 0.381	0.237 × 0.225 × 0.135
a (Å)	11.8690(3)	11.78979(10)	15.0365(2)	24.2581(4)
b (Å)	11.8690(3)	11.78979(10)	17.9110(2)	13.84490(19)
c (Å)	23.5143(8)	23.2860(3)	16.5283(3)	24.3602(4)
α (°)	90	90	90	90
β (°)	90	90	93.6961(14)	112.7589(18)
γ (°)	90	90	90	90
V (Å^3)	3312.54(19)	3236.73(7)	4442.12(11)	7544.4(2)
Z	4	4	2	8
T (K)	120(2)	120(2)	120(2)	120(2)
D_{calc} (g cm^{-3})	1.262	1.298	1.263	1.262
F_{000}	1320	1324	1796	3032
μ (mm^{-1})	5.231	5.774	6.797	5.012
θ range for data collection (°)	3.724-76.978	3.749-73.455	3.643-73.680	3.750-66.600
Max. and min. transmission	1.000, 0.344	0.802, 0.672	0.459, 0.140	0.871, 0.793
reflns measd	10072	14115	72176	92861
independent reflns	4995	6329	8896	13303
R_{int}	0.0404	0.0313	0.1022	0.0575
Final *GooF*	1.109	1.063	1.020	1.170
R_1, wR_2 [$I > 2\sigma(I)$]	0.0738, 0.1998	0.0371, 0.0972	0.0552, 0.1488	0.1287, 0.3266
R_1, wR_2 (all data)	0.0751, 0.2011	0.0373, 0.0974	0.0585, 0.1527	0.1304, 0.3271
min. and max. electron densities (e Å^{-3})	-0.554, 1.320	-0.433, 0.835	-0.924, 0.826	-1.375, 2.003

	IV·19	**IV·20a**	**IV·20b**	**IV·24**
Code	ZNGALO	COGALS	COGAMF	FEGALZ
Formula	$C_{41}H_{57}ClN_2Zn$	$C_{41}H_{57}CoN_2$	$C_{41}H_{57}CoN_2$	$C_{51}H_{62}Br_2FeN_2$
M_w	679.60	636.81	636.81	918.69
Crystal system	orthorhombic	monoclinic	triclinic	triclinic
Space Group	*P na*21	*Cc*	*P* -1	*P* -1
Crystal size	0.380 × 0.360 × 0.309	0.268 × 0.192 × 0.104	0.210 × 0.149 × 0.112	0.323 × 0.145 × 0.115
a (Å)	26.8314(3)	9.44161(16)	11.9972(8)	10.6355(3)
b (Å)	13.85669(15)	22.4591(3)	12.3524(7)	12.0097(3)
c (Å)	20.32421(19)	18.1499(3)	14.9842(6)	20.8855(3)
α (°)	90	90	69.124(5)	74.4150(17)
β (°)	90	100.9466(15)	81.637(5)	77.9003(19)
γ (°)	90	90	66.935(6)	69.785(2)
V (Å^3)	7556.44(13)	3778.65(10)	1908.9(2)	2391.12(9)
Z	8	4	2	2
T (K)	120(2)	120(2)	120(2)	120(2)
D_{calc} (g cm^{-3})	1.195	1.119	1.108	1.276
F_{000}	2915	1376	688	956
μ (mm^{-1})	1.767	3.755	3.716	4.732
θ range for data collection (°)	3.590 73.609	3.937 73.604	4.005 77.638	4.015 77.106
Max. and min. transmission	0.717, 0.860	0.925, 0.856	1.000, 0.669	1.000, 0.429
reflns measd	40313	7889	21146	28508
independent reflns	14244	5010	7702	9687
R_{int}	0.0250	0.0144	0.0852	0.0409
Final *GooF*	1.111	1.046	1.069	1.141
R_1, wR_2 [$I > 2\sigma(I)$]	0.0531, 0.1435	0.0291, 0.0767	0.0997, 0.3108	0.0481, 0.1413
R_1, wR_2 (all data)	0.0542, 0.1443	0.0295, 0.0772	0.1144, 0.3258	0.0524, 0.1454
min. and max. electron densities (e Å^{-3})	-0.538, 1.093	-0.357, 0.343	-0.685, 1.012	-0.768, 0.501

	IV·25	**IV·26**	**IV·27**	**IV·28**
Code	COGAME	ZNGALW	MNGALS	MNGALS
Formula	$C_{54}H_{73}Br_3CoN_4$	$C_{14}H_{14}Si$	$C_{27}H_{21}N_3O_3$	$C_{20}H_{20}N_2O_2$
M_w	1076.82	210.34	435.47	320.38
Crystal system	triclinic	monoclinic	monoclinic	triclinic
Space Group	*P* -1	*P* 21/*n*	*C* 2/*c*	*P* -1
Crystal size	0.130 × 0.045 × 0.039	0.478 × 0.395 × 0.238	0.281 × 0.255 × 0.209	0.141 × 0.121 × 0.070
a (Å)	10.3779(2)	9.0909(9)	13.4932(7)	8.0876(10)
b (Å)	13.2389(3)	8.7591(6)	13.5417(7)	10.0423(13)
c (Å)	19.4059(4)	14.5920(12)	12.6047(6)	11.3819(14)
α (°)	89.6924(18)	90	90	81.806(10)
β (°)	83.5878(18)	106.965(10)	97.303(5)	79.589(11)
γ (°)	86.6456(18)	90	90	68.731(12)
V (Å^3)	2644.99(10)	1111.37(17)	2284.5(2)	844.28(19)
Z	2	4	4	2
T (K)	120(2)	120(2)	120(2)	120(2)
D_{calc} (g cm^{-3})	1.352	1.257	1.266	1.260
F_{000}	1114	448	912	340
μ (mm^{-1})	5.474	1.525	0.678	0.655
θ range for data collection (°)	3.344-76.966	5.149-73.297	4.645-74.246	3.963-73.567
Max. and min. transmission	1.000, 0.781	0.931, 0.876	0.977, 0.970	0.986, 0.969
reflns measd	30353	4327	4601	7814
independent reflns	10645	2186	2265	3206
R_{int}	0.0321	0.0256	0.0258	0.0683
Final *GooF*	1.091	1.100	1.035	1.106
R_1, wR_2 [$I > 2\sigma(I)$]	0.0444, 0.1179	0.0544, 0.1536	0.0420, 0.1115	0.0942, 0.2692
R_1, wR_2 (all data)	0.0519, 0.1224	0.0566, 0.1556	0.0447, 0.1145	0.1437, 0.3138
min. and max. electron densities (e Å^{-3})	-0.747, 1.078	-0.793, 0.659	-0.270, 0.214	-0.368, 0.379

6.3 Appendix C – UV/Vis Spectra

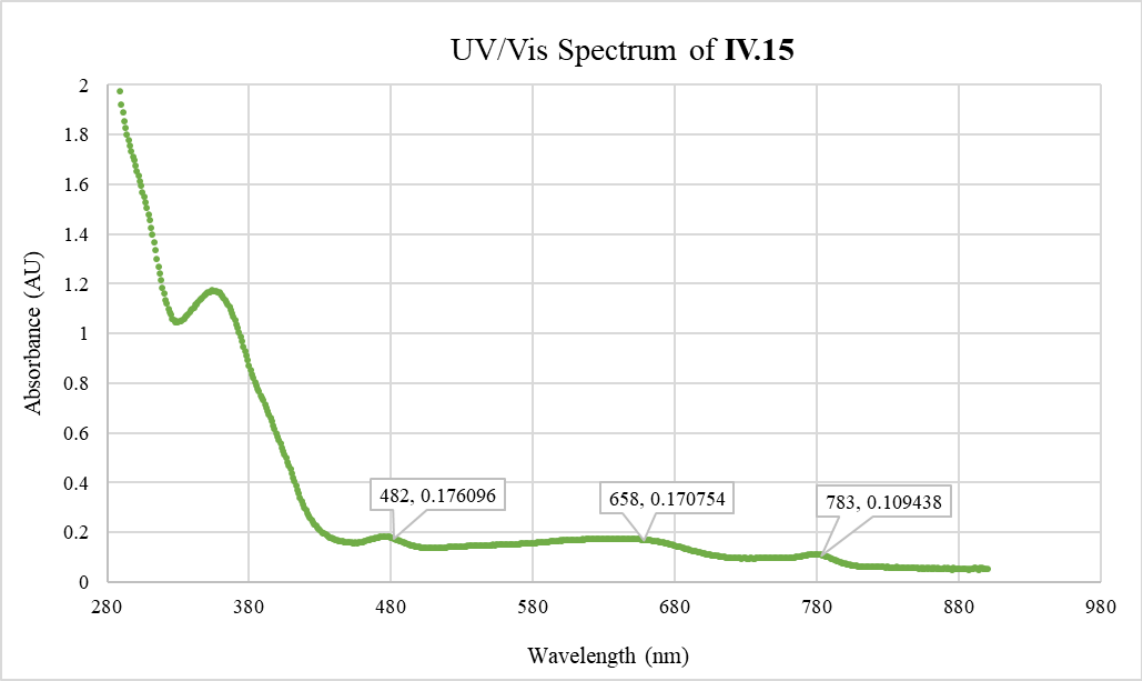

Figure VI·2. A UV/Vis Spectrum of **IV·15**. Concentration of sample solution = 1.03 mM in toluene.

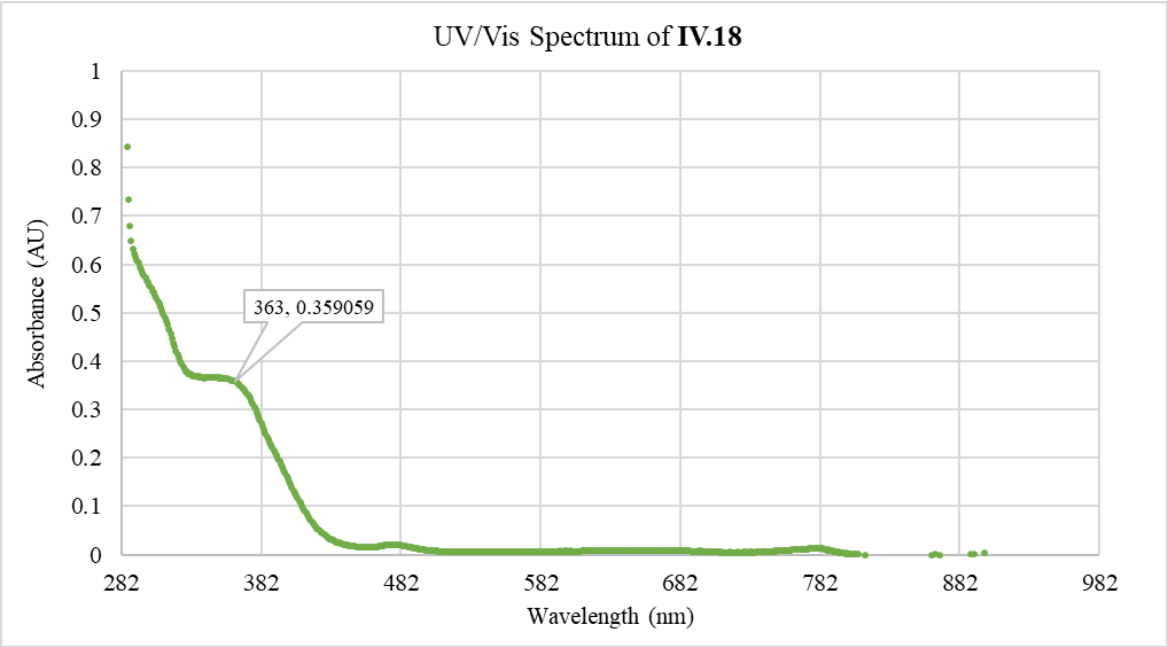

Figure VI·3. A UV/Vis Spectrum of **IV·18**. Concentration of sample solution = 0.159 mM in toluene.

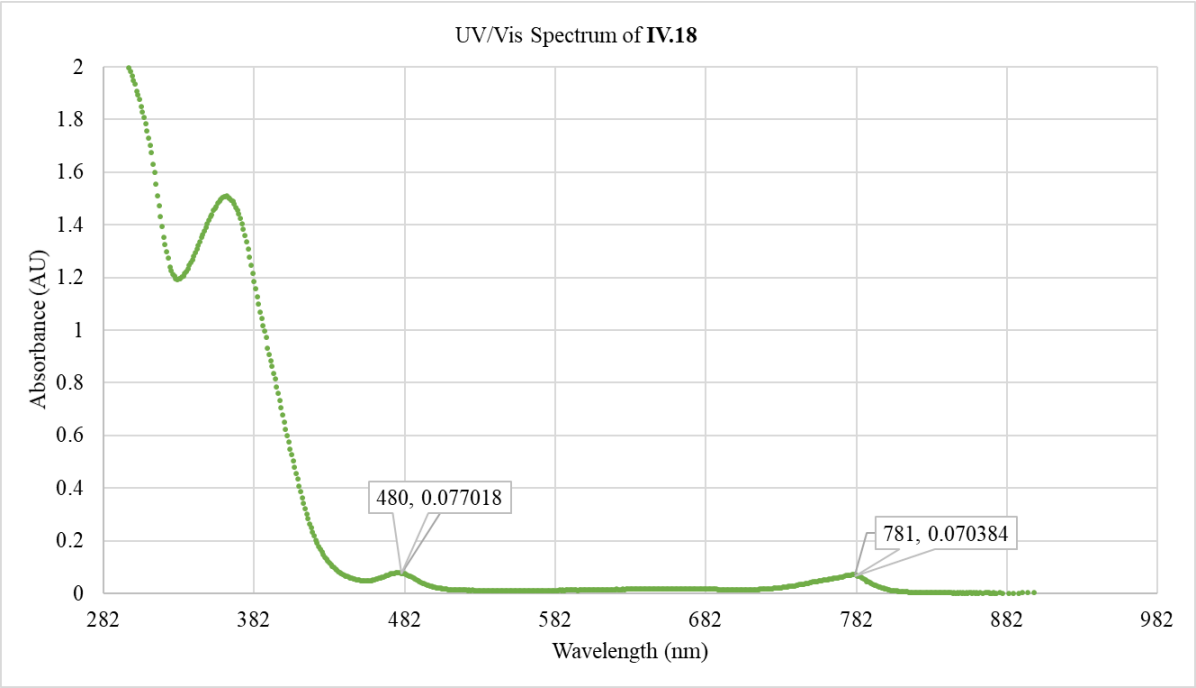

Figure VI·4. A UV/Vis Spectrum of **IV·18**. Concentration of sample solution = 0.530 mM in toluene.

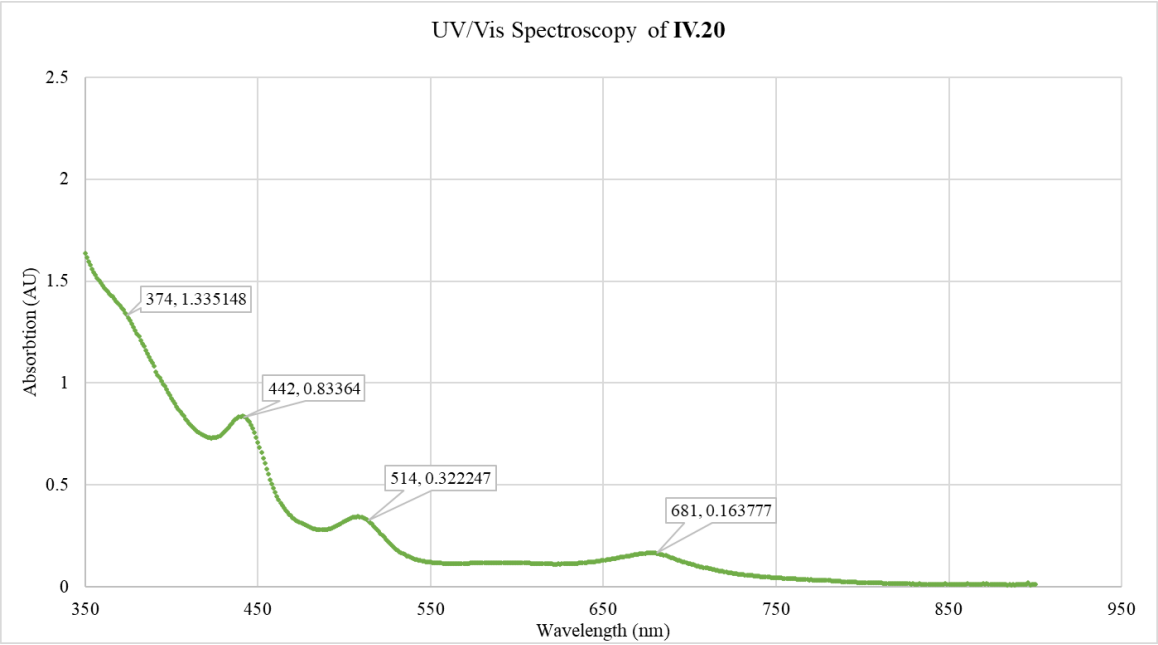

Figure VI·5. A UV/Vis Spectrum of **IV·20**. Concentration of sample solution = 0.361 mM in toluene.

6.3 References

1 *Nobel Prize.Org/nobel_prizes/chemistry/laureates/1963/press.html (Accessed: 15 January 2018)*.
2 M. Scholl, S. Ding, C. W. Lee and R. H. Grubbs, *Org. Lett.*, 1999, **1**, 953.
3 P. Schwab, R. H. Grubbs and J. W. Ziller, *J. Am. Chem. Soc.*, 1996, **118**, 100.
4 G. C. Vougioukalakis and R. H. Grubbs, *Chem. Rev.*, 2010, **110**, 1746.
5 G. C. Bazan, J. H. Oskam, H. N. Cho, L. Y. Park and R. R. Schrock, *J. Am. Chem. Soc.*, 1991, **113**, 6899.
6 J. S. Murdzek and R. R. Schrock, *Organometallics*, 1987, **6**, 1373.
7 S. Baba and E. Negishi, *J. Am. Chem. Soc.*, 1976, **98**, 6729.
8 N. Miyaura and A. Suzuki, *Chem. Rev.*, 1995, **95**, 2457.
9 C. A. P. Goodwin, F. Ortu, D. Reta, N. F. Chilton and D. P. Mills, *Nature*, 2017, **548**, 439.
10 F.-S. Guo, B. M. Day, Y.-C. Chen, M.-L. Tong, A. Mansikkamäki and R. A. Layfield, *Angew. Chem. Int. Ed.*, 2017, **56**, 11445.
11 G. Wilkinson, *Pure Appl. Chem.*, 1972, **30**, 627.
12 P. P. Power, *Chem. Rev.*, 2012, **112**, 3482.
13 R. P. Stewart and P. M. Treichel, *J. Am. Chem. Soc.*, 1970, **92**, 2710.
14 M. C. Baird, *J. Organomet. Chem.*, 1973, **64**, 289.
15 P. S. Braterman and R. J. Cross, *J. Chem. Soc., Dalt. Trans.*, 1972, 657.
16 R. H. Crabtree, *The Organometallic Chemistry of the Transition Metals. Sixth Edition.*, 2014.
17 G. Yagupsky, W. Mowat, A. Shortland and G. Wilkinson, *Chem. Commun.*, 1970, 1369.
18 A. Shortland and G. Wilkinson, *J. Chem. Soc. Chem. Commun.*, 1972, 318a.
19 F. A. Adedeji, J. A. Connor, H. A. Skinner, L. Galyer and G. Wilkinson, *J. Chem. Soc. Chem. Commun.*, 1976, 159.
20 B. D. Murray and P. P. Power, *Inorg. Chem.*, 1984, **23**, 4584.
21 H. Hope, M. M. Olmstead, B. D. Murray and P. P. Power, *J. Am. Chem. Soc.*, 1985, **107**, 712.
22 R. A. Andersen, E. Carmona-Guzman, J. F. Gibson and G. Wilkinson, *J. Chem. Soc. Dalt. Trans.*, 1976, 2204.
23 N. H. Buttrus, C. Eaborn, P. B. Hitchcock, J. D. Smith and A. C. Sullivan, *J. Chem. Soc. Chem. Commun.*, 1985, 1380.
24 T. Viefhaus, W. Schwarz, K. Hübler, K. Locke and J. Weidlein, *Zeitschrift für Anorg. und Allg. Chemie*, 2001, **627**, 715.
25 A. M. LaPointe, *Inorganica Chim. Acta*, 2003, **345**, 359.
26 R. A. Andersen, D. J. Berg, L. Fernholt, K. Fægri, Jr., J. C. Green, A. Haaland, M. F. Lappert, W.-P. Leung and K. Rypdal, *Acta Chem. Scand.*, 1988, 42a, 554.
27 R. a. Bartlett and P. P. Power, *J. Am. Chem. Soc.*, 1987, **109**, 7563.
28 M. B. Hursthouse, D. C. Bradley, K. M. Abdul Malik and M. Reainhold, *Transit. Met. Cham.*, 1978, **3**, 253.
29 R. A. Bartlett, X. Feng, M. M. Olmstead, P. P. Power and K. J. Weese, *J. Am. Chem. Soc.*, 1987, **109**, 4851.
30 H. Chen, R. A. Bartlett, M. M. Olmstead, P. P. Power and S. C. Shoner, *J. Am. Chem. Soc.*, 1990, **112**, 1048.
31 R. A. Bartlett, H. Chen and P. P. Power, *Angew. Chem. Int. Ed.*, 1989, **28**, 316.
32 C. L. Wagner, L. Tao, E. J. Thompson, T. A. Stich, J. Guo, J. C. Fettinger, L. A. Berben, R. D. Britt, S. Nagase and P. P. Power, *Angew. Chem. Int. Ed.*, 2016, **55**, 10444.
33 H. Gilman and J. C. Bailie, *J. Org. Chem.*, 1937, **2**, 84.
34 R. Fischer, M. Gorls, M. Friedrich and M. Westerhausen, *J. Organomet. Chem*, 2009, **694**, 1107.
35 C. Beermann and K. Clauss, *Angew. Chem. Int. Ed.*, 1959, **71**, 627.
36 S. Gambarotta, C. Floriani, A. Chiesi-Villa and C. Guastini, *J. Chem. Soc. Chem. Commun.*, 1983, **1983**, 1128.
37 W. Siedel and I. Burger, *Zeitschrift für Anorg. und Allg. Chemie*, 1977, **17**, 31.
38 K. H. Theopold, J. Silvestre, E. K. Byrne and D. S. Richeson, *Organometallics*, 1989, **8**, 2001.
39 H. Muller, W. Siedel and M. Gorls, *J. Organomet. Chem*, 1993, **445**, 133.

40 B. Machellet, *Zeitschrift für Anorg. und Allg. Chemie*, 1976, **16**, 116.
41 A. Klose, E. Solari, C. Floriani, A. Chiesi-Villa, C. Rizzoli and N. Re, *J. Am. Chem. Soc.*, 1994, **116**, 9123.
42 C. Ni, J. C. Fettinger, G. J. Long and P. P. Power, *Dalt. Trans.*, 2010, **39**, 10664.
43 R. J. Wehmschulte and P. P. Power, *Organometallics*, 1995, **14**, 3264.
44 P. L. Holland, *Angew. Chem. Int. Ed.*, 2011, **50**, 6213.
45 D. L. Kays, *J. Organomet. Chem.*, 2010, 36, 56.
46 H. Fan, D. Adhikari, A. A. Saleh, R. L. Clark, F. J. Zuno-Cruz, G. S. Cabrera, J. C. Huffman, M. Pink, D. J. Mindiola and M. H. Baik, *J. Am. Chem. Soc.*, 2008, **130**, 17351.
47 H. Andres, E. L. Bominaar, J. M. Smith, N. A. Eckert, P. L. Holland and E. Münck, *J. Am. Chem. Soc.*, 2002, **124**, 3012.
48 S. Yao and M. Driess, *Acc. Chem. Res.*, 2012, **45**, 276.
49 J. Li, H. Song, C. Cui and J. Cheng, *Inorg. Chem.*, 2008, **47**, 3468.
50 J. J. Ellison, K. Ruhlandt-Senge and P. P. Power, *Angew. Chem. Int. Ed.*, 1994, **33**, 1178.
51 A. M. Bryan, W. A. Merrill, W. M. Reiff, J. C. Fettinger and P. P. Power, *Inorg. Chem.*, 2012, **51**, 3366.
52 C. Ni and P. P. Power, *Chem. Commun.*, 2009, 5543.
53 J. Hicks and C. Jones, *Organometallics*, 2015, **34**, 2118.
54 J. Hicks, E. J. Underhill, C. E. Kefalidis, L. Maron and C. Jones, *Angew. Chem. Int. Ed.*, 2015, **54**, 10000.
55 J. Hicks, C. E. Hoyer, B. Moubaraki, G. L. Manni, E. Carter, D. M. Murphy, K. S. Murray, L. Gagliardi and C. Jones, *J. Am. Chem. Soc.*, 2014, **136**, 5283.
56 C. A. Tolman, *Chem. Rev.*, 1977, **77**, 313.
57 J. Huang, H.-J. Schanz, E. D. Stevens and S. P. Nolan, *Organometallics*, 1999, **18**, 2370–2375.
58 A. C. Hillier, W. J. Sommer, B. S. Yong, J. L. Petersen, L. Cavallo and S. P. Nolan, *Organometallics*, 2003, **22**, 4322.
59 S. Díez-González and S. P. Nolan, *Coord. Chem. Rev.*, 2007, **251**, 874.
60 A. Poater, B. Cosenza, A. Correa, S. Giudice, F. Ragone, V. Scarano and L. Cavallo, *Eur. J. Inorg. Chem.*, 2009, **2009**, 1759.
61 A. Sattler and G. Parkin, *Organometallics*, 2015, **34**, 1828.
62 T. Nguyen, A. D. Sutton, M. Brynda, J. C. Fettinger, G. J. Long and P. P. Power, *Science*, 2005, **310**, 844.
63 C. Ni, T. A. Stich, G. J. Long and P. P. Power, *Chem. Commun.*, 2010, **46**, 4466.
64 H. R. Sharpe, A. M. Geer, W. Lewis, A. J. Blake and D. L. Kays, *Angew. Chem. Int. Ed.*, 2017, **56**, 4845.
65 H. R. Sharpe, A. M. Geer, H. E. L. Williams, T. J. Blundell, W. Lewis, A. J. Blake and D. L. Kays, *Chem. Commun.*, 2017, **53**, 937.
66 H. R. Sharpe, A. M. Geer, T. J. Blundell, F. R. Hastings, M. W. Fay, G. A. Rance, W. Lewis, A. J. Blake and D. L. Kays, *Catal. Sci. Technol.*, 2018, **8**, 229.
67 C. J. F. Du, H. Hart and K. K. D. Ng, *J. Org. Chem.*, 1986, **51**, 3162.
68 K. Ruhlandt-Senge, J. J. Ellison, R. J. WehmschultE, F. Pauer and P. Power, *J. Am. Chem. Soc.*, 1993, **115**, 11353.
69 A. Saednya and H. Hart, *Synthesis*, 1996, **1996**, 1455.
70 P. Romanato, S. Duttwyler, A. Linden, K. K. Baldridge and J. S. Siegel, *J. Am. Chem. Soc.*, 2011, **133**, 11844.
71 R. C. Smith, T. Ren and J. D. Protasiewicz, *Eur. J. Inorg. Chem.*, 2002, **11**, 2779.
72 M. C. Lipke, R. A. Woloszynek, L. Ma and J. D. Protasiewicz, *Organometallics*, 2009, **28**, 188.
73 T. J. Blundell, *Transition Metal Complexes of Sterically Demanding m-Terphenyl Ligands: Synthesis and Small Molecule Reactivity*, 2015.
74 J. J. Ellison and P. P. Power, *J. Organomet. Chem.*, 1996, **526**, 263.
75 A. Haaland, K. Rypdal, H. P. Verne, W. Scherer and W. R. Thiel, *Angew. Chem. Int. Ed.*, 1995, **33**, 2443.
76 D. L. Kays (née Coombs) and A. R. Cowley, *Chem. Commun.*, 2007, **58**, 1053.
77 A. Schröder, E. Lork and J. Beckmann, *Main Gr. Met. Chem.*, 2014, **37**.

78 E. O. Fischer and A. Maasböl, *Angew. Chem. Int. Ed.*, 1964, **3**, 580.
79 R. R. Schrock, *J. Am. Chem. Soc.*, 1974, **96**, 6796.
80 E. O. Fischer, *Pure Appl. Chem.*, 1970, **24**, 407.
81 H.-W. Wanzlick and H.-J. Schönherr, *Angew. Chem. Int. Ed.*, 1968, **7**, 141.
82 M. N. Hopkinson, C. Richter, M. Schedler and F. Glorius, *Nature*, 2014, **510**, 485.
83 A. Igau, H. Grutzmacher, A. Baceiredo and G. Bertrand, *J. Am. Chem. Soc.*, 1988, **110**, 6463.
84 A. J. Arduengo, R. L. Harlow and M. Kline, *J. Am. Chem. Soc.*, 1991, **113**, 361.
85 D. A. Dixon and A. J. Arduengo, *J. Phys. Chem.*, 1991, **95**, 4180.
86 C. Boehme and G. Frenking, *J. Am. Chem. Soc.*, 1996, **118**, 2039.
87 C. Heinemann, T. Müller, Y. Apeloig and H. Schwarz, *J. Am. Chem. Soc.*, 1996, **118**, 2023.
88 D. J. Nelson and S. P. Nolan, *Chem. Soc. Rev.*, 2013, **42**, 6723.
89 M. S. Collins, E. L. Rosen, V. M. Lynch and C. W. Bielawski, *Organometallics*, 2010, **29**, 3047.
90 S. C. Zinner, C. F. Rentzsch, E. Herdtweck, W. A. Herrmann and F. E. Kühn, *Dalt. Trans.*, 2009, 7055.
91 A. J. Arduengo, J. R. Goerlich and W. J. Marshall, *J. Am. Chem. Soc.*, 1995, **117**, 11027.
92 M. Melaimi, M. Soleilhavoup and G. Bertrand, *Angew. Chem. Int. Ed.*, 2010, **49**, 8810.
93 A. J. Arduengo III, *Patent WO9114678*, 1992.
94 W. a Herrmann, *Angew. Chem. Int. Ed.*, 2002, **41**, 1290.
95 P. de Fremont, N. Marion and S. P. Nolan, *Coord. Chem. Rev.*, 2009, **253**, 862.
96 A. A. Gridnev and I. M. Mihaltseva, *Synth. Commun.*, 1993, **24**, 1547.
97 N. Kuhn and T. Kratz, *Synthesis*, 1993, **1993**, 561.
98 F. E. Hahn, L. Wittenbecher, D. Le Van and R. Fröhlich, *Angew. Chem. Int. Ed.*, 2000, **39**, 541.
99 F. E. Hahn, L. Wittenbecher, R. Boese and D. Bläser, *Chem. A Eur. J.*, 1999, **5**, 1931.
100 J. C. Green, R. G. Scurr, P. L. Arnold and F. Geoffrey N. Cloke, *Chem. Commun.*, 1997, 1963.
101 D. Nemcsok, K. Wichmann and G. Frenking, *Organometallics*, 2004, **23**, 3640.
102 R. H. Crabtree, *J. Organomet. Chem.*, 2005, **690**, 5451.
103 A. M. Magill, K. J. Cavell and B. F. Yates, *J. Am. Chem. Soc.*, 2004, **126**, 8717.
104 D. Bourissou, O. Guerret, F. P. Gabbaï and G. Bertrand, *Chem. Rev.*, 2000, **100**, 39.
105 H. Braband and U. Abram, *Organometallics*, 2005, **24**, 3362.
106 D. Janssen-Müller, C. Schlepphorst and F. Glorius, *Chem. Soc. Rev.*, 2017, **46**, 4845.
107 D. J. Nelson, *Eur. J. Inorg. Chem.*, 2015, **2015**, 2012.
108 Y. Wang and G. H. Robinson, *Inorg. Chem.*, 2014, **53**, 11815.
109 P. L. Arnold and I. J. Casely, *Chem. Rev.*, 2009, **109**, 3599.
110 O. S. Mills and A. D. Redhouse, *Angew. Chem. Int. Ed.*, 1965, **4**, 1082.
111 P. P. Samuel, R. Neufeld, K. Chandra Mondal, H. W. Roesky, R. Herbst-Irmer, D. Stalke, S. Demeshko, F. Meyer, V. C. Rojisha, S. De, P. Parameswaran, A. C. Stückl, W. Kaim, J. H. Christian, J. K. Bindra and N. S. Dalal, *Chem. Sci.*, 2015, **6**, 3148.
112 A. A. Danopoulos, K. Y. Monakhov, V. Robert, P. Braunstein, R. Pattacini, S. Conde-Guadaño, M. Hanton and R. P. Tooze, *Organometallics*, 2013, **32**, 1842.
113 S. Bellemin-Laponnaz and S. Dagorne, *Chem. Rev.*, 2014, **114**, 8747.
114 Z. Wang, L. Jiang, D. K. B. Mohamed, J. Zhao and T. S. A. Hor, *Coord. Chem. Rev.*, 2015, **293**, 292.
115 A. R. Kennedy, J. Klett, R. E. Mulvey and S. D. Robertson, *Eur. J. Inorg. Chem.*, 2011, 4675.
116 R. A. Musgrave, R. S. P. Turbervill, M. Irwin and J. M. Goicoechea, *Angew. Chem. Int. Ed.*, 2012, **51**, 10832.
117 Z. Ouyang, J. Du, L. Wang, J. L. Kneebone, M. L. Neidig and L. Deng, *Inorg. Chem.*, 2015, **54**, 8808.
118 Z. Mo, Z. Ouyang, L. Wang, K. L. Fillman, M. L. Neidig and L. Deng, *Org. Chem. Front.*, 2014, **1**, 1040.
119 P. P. Samuel, K. C. Mondal, N. Amin Sk, H. W. Roesky, E. Carl, R. Neufeld, D. Stalke, S. Demeshko, F. Meyer, L. Ungur, L. F. Chibotaru, J. Christian, V. Ramachandran, J. Van Tol and N. S. Dalal, *J. Am. Chem. Soc.*, 2014, **136**, 11964.
120 G. Ung, J. Rittle, M. Soleilhavoup, G. Bertrand and J. C. Peters, *Angew. Chem. Int. Ed.*, 2014,

53, 8427.
121 M. I. Lipschutz, T. Chantarojsiri, Y. Dong and T. D. Tilley, *J. Am. Chem. Soc.*, 2015, **137**, 6366.
122 L. Xiang, J. Xiao and L. Deng, *Organometallics*, 2011, **30**, 2018.
123 Q. Zhang, L. Xiang and L. Deng, *Organometallics*, 2012, **31**, 4537.
124 X.-N. Yao, J.-Z. Du, Y.-Q. Zhang, X.-B. Leng, M.-W. Yang, S.-D. Jiang, Z.-X. Wang, Z.-W. Ouyang, L. Deng, B.-W. Wang and S. Gao, *J. Am. Chem. Soc.*, 2017, **139**, 373.
125 A. A. Danopoulos, P. Braunstein, K. Y. Monakhov, J. van Leusen, P. Kögerler, M. Clémancey, J.-M. Latour, A. Benayad, M. Tromp, E. Rezabal and G. Frison, *Dalt. Trans.*, 2017, **46**, 1163.
126 Y.-S. Meng, Z. Mo, B.-W. Wang, Y.-Q. Zhang, L. Deng and S. Gao, *Chem. Sci.*, 2015, **6**, 7156.
127 Z. Mo, J. Xiao, Y. Gao and L. Deng, *J. Am. Chem. Soc.*, 2014, **136**, 17414.
128 J. Sun and L. Deng, *ACS Catal.*, 2016, **6**, 290.
129 Y. Liu and L. Deng, *J. Am. Chem. Soc.*, 2017, **139**, 1798.
130 A. A. Danopoulos, P. Braunstein, N. Stylianides and M. Wesolek, *Organometallics*, 2011, **30**, 6514.
131 L. Zhang, Y. Liu and L. Deng, *J. Am. Chem. Soc.*, 2014, **136**, 15525.
132 Z. Mo, D. Chen, X. Leng and L. Deng, *Organometallics*, 2012, **31**, 7040.
133 J. Du, L. Wang, M. Xie and L. Deng, *Angew. Chem. Int. Ed.*, 2015, **54**, 12640.
134 J. A. Przyojski, H. D. Arman and Z. J. Tonzetich, *Organometallics*, 2013, **32**, 723.
135 B. M. Day, K. Pal, T. Pugh, J. Tuck and R. A. Layfield, *Inorg. Chem.*, 2014, **53**, 10578.
136 A. J. Arduengo, S. F. Gamper, J. C. Calabrese and F. Davidson, *J. Am. Chem. Soc.*, 1994, **116**, 4391.
137 P. L. Arnold, F. Geoffrey, N. Cloke, T. Geldbach and P. B. Hitchcock, *Organometallics*, 1999, **18**, 3228.
138 C. A. Laskowski and G. L. Hillhouse, *J. Am. Chem. Soc.*, 2008, **130**, 13846.
139 B. R. Dible, M. S. Sigman and A. M. Arif, *Inorg. Chem.*, 2005, **44**, 3774.
140 C. a Laskowski, D. J. Bungum, S. M. Baldwin, S. A. Del Ciello, V. M. Iluc and G. L. Hillhouse, *J. Am. Chem. Soc.*, 2013, **135**, 18272.
141 C. A. Laskowski and G. L. Hillhouse, *Organometallics*, 2009, **28**, 6114.
142 B. M. Gridley, A. J. Blake, A. L. Davis, W. Lewis, G. J. Moxey and D. L. Kays, *Chem. Commun.*, 2012, **48**, 8910.
143 C. Ni, H. Lei and P. P. Power, *Organometallics*, 2010, **29**, 1988.
144 D. L. Kays, *Dalt. Trans.*, 2011, **40**, 769.
145 H. Lei, B. D. Ellis, C. Ni, F. Grandjean, G. J. Long and P. P. Power, *Inorg. Chem.*, 2008, **47**, 10205.
146 H. Lei, J. C. Fettinger and P. P. Power, *Inorg. Chem.*, 2012, **51**, 1821.
147 E. Clot, O. Eisenstein, N. Jasim, S. A. MacGregor, J. E. McGrady and R. N. Perutz, *Acc. Chem. Res.*, 2011, **44**, 333.
148 T. R. Dugan, X. Sun, E. V. Rybak-Akimova, O. Olatunji-Ojo, T. R. Cundari and P. L. Holland, *J. Am. Chem. Soc.*, 2011, **133**, 12418.
149 Z. Lian, X. Xu, H. Sun, Y. Chen, T. Zheng and X. Li, *Dalt. Trans.*, 2010, **39**, 9523.
150 X. Li, H. Sun, F. Yu, U. Flörke and H. F. Klein, *Organometallics*, 2006, **25**, 4695.
151 A. Staubitz, A. P. M. Robertson and I. Manners, *Chem. Rev.*, 2010, **110**, 4079.
152 W. A. Herrmann and C. Köcher, *Angew. Chem. Int. Ed.*, 1997, **36**, 2162.
153 K. Riener, S. Haslinger, A. Raba, M. P. Högerl, M. Cokoja, W. A. Herrmann and F. E. Kühn, *Chem. Rev.*, 2014, **114**, 5215.
154 S. C. Bart, E. J. Hawrelak, A. K. Schmisseur, E. Lobkovsky and P. J. Chirik, *Organometallics*, 2004, **23**, 237.
155 A. R. Hermes and G. S. Girolami, *Organometallics*, 1988, **7**, 394.
156 Z. Mo, Q. Zhang and L. Deng, *Organometallics*, 2012, **31**, 6518.
157 Z. Mo, Y. Liu and L. Deng, *Angew. Chem. Int. Ed.*, 2013, **52**, 10845.
158 R. A. Layfield, *Organometallics*, 2014, **33**, 1084–1099.
159 F. D. Natterer, K. Yang, W. Paul, P. Willke, T. Choi, T. Greber, A. J. Heinrich and C. P. Lutz,

Nature, 2017, **543**, 226.
160 J. M. Frost, K. L. M. Harriman and M. Murugesu, *Chem. Sci.*, 2016, **7**, 2470.
161 Y. S. Meng, S. Da Jiang, B. W. Wang and S. Gao, *Acc. Chem. Res.*, 2016, **49**, 2381.
162 G. A. Craig and M. Murrie, *Chem. Soc. Rev.*, 2015, **44**, 2135.
163 A. Kumar Bar, C. Pichon and J.-P. Sutter, *Coord. Chem. Rev.*, 2016, **308**, 346–380.
164 J. M. Zadrozny, D. J. Xiao, M. Atanasov, G. J. Long, F. Grandjean, F. Neese and J. R. Long, *Nat. Chem.*, 2013, **5**, 577.
165 J. M. Zadrozny, M. Atanasov, A. M. Bryan, C.-Y. Lin, B. D. Rekken, P. P. Power, F. Neese and J. R. Long, *Chem. Sci.*, 2013, **4**, 125.
166 M. Atanasov, J. M. Zadrozny, J. R. Long and F. Neese, *Chem. Sci.*, 2013, **4**, 139.
167 K. A. Smart, A. Vanbergen, J. Lednik, C. Y. Tang, H. B. Mansaray, I. Siewert and S. Aldridge, *J. Organomet. Chem.*, 2013, **741**–**742**, 33.
168 A. Asadi, C. Eaborn, M. S. Hill, P. B. Hitchcock and J. D. Smith, *J. Organomet. Chem.*, 2005, **690**, 944.
169 Z. Zhu, M. Brynda, R. J. Wright, R. C. Fischer, W. A. Merrill, E. Rivard, R. Wolf, J. C. Fettinger, M. M. Olmstead and P. P. Power, *J. Am. Chem. Soc.*, 2007, **129**, 10847.
170 A. D. Sutton, T. Ngyuen, J. C. Fettinger, M. M. Olmstead, G. J. Long and P. P. Power, *Inorg. Chem.*, 2007, **46**, 4809.
171 T. Nguyen, W. A. Merrill, C. Ni, H. Lei, J. C. Fettinger, B. D. Ellis, G. J. Long, M. Brynda and P. P. Power, *Angew. Chem. Int. Ed.*, 2008, **47**, 9115.
172 R. Wolf, C. Ni, T. Nguyen, M. Brynda, G. J. Long, A. D. Sutton, R. C. Fischer, J. C. Fettinger, M. Hellman, L. Pu and P. P. Power, *Inorg. Chem.*, 2007, **46**, 11277.
173 H. Lei, J. D. Guo, J. C. Fettinger, S. Nagase and P. P. Power, *J. Am. Chem. Soc.*, 2010, **132**, 17399.
174 C. Ni and P. P. Power, *Organometallics*, 2009, **28**, 6541.
175 C. Ni, B. D. Ellis, J. C. Fettinger, J. Long, P. P. Power, G. J. Long and P. P. Power, *Chem. Commun.*, 2007, 1014.
176 R. Wolf, M. Brynda, C. Ni, G. J. Long and P. P. Power, *J. Am. Chem. Soc.*, 2007, **129**, 6076.
177 J. Hicks and C. Jones, *Inorg. Chem.*, 2013, **52**, 3900.
178 S. J. Bonyhady, S. P. Green, C. Jones, S. Nembenna and A. Stasch, *Angew. Chem. Int. Ed.*, 2009, **48**, 2973.
179 P. Atkins, T. Overton, J. P. Rourke, M. Weller and F. Armstrong, *Inorganic Chemistry, Fifth Edition*, 2010.
180 E. Solari, F. Musso, E. Gallo, C. Floriani, N. Re, A. Chiesi-Villa and C. Rizzoli, *Organometallics*, 1995, **14**, 2265.
181 E. O. Wollan and W. C. Koehler, *Phys. Rev.*, 1955, **100**, 545.
182 P. Atkins, T. Overton, J. Rourke, M. Weller and F. Armstrong, in *Inorganic Chemistry*, 2010, p. 601.
183 P. W. Anderson, *Phys. Rev.*, 1950, **79**, 350.
184 J. B. Goodenough, *Phys. Rev.*, 1955, **100**, 564.
185 U. Bossek, D. Nuhlen, E. Bill, T. Glaser, C. Krebs, T. Weyhermuller, K. Wieghardt, M. Lengen and A. X. Trautwein, *Inorg. Chem.*, 1997, **36**, 2834.
186 P. Zhao, Z. Brown, J. C. Fettinger, F. Grandjean, G. J. Long and P. P. Power, *Organometallics*, 2014, **33**, 1917.
187 S. S. Batsanov, *Inorg. Mater. Transl. from Neorg. Mater. Orig. Russ. Text*, 2001, **37**, 871.
188 T. J. Blundell, F. R. Hastings, B. M. Gridley, G. J. Moxey, W. Lewis, A. J. Blake and D. L. Kays, *Dalt. Trans.*, 2014, **43**, 14257.
189 B. M. Gridley, G. J. Moxey, W. Lewis, A. J. Blake and D. L. Kays, *Chem. - A Eur. J.*, 2013, **19**, 11446.
190 P. J. Hore, *Nuclear Magnetic Resonance: 2nd Edition*, 2015.
191 A. Okuniewski, D. Rosiak, J. Chojnacki and B. Becker, *Polyhedron*, 2015, **90**, 47.
192 T. Steiner, *Angew. Chem. Int. Ed.*, 2002, **41**, 48.
193 H. R. Khavasi, F. Norouzi and A. Azhdari Tehrani, *Cryst. Growth Des.*, 2015, **15**, 2579.
194 T. R. Jensen, C. P. Schaller, M. A. Hillmyer and W. B. Tolman, *J. Organomet. Chem.*, 2005, **690**, 5881.

195 D. Wang, K. Wurst and M. R. Buchmeiser, *J. Organomet. Chem.*, 2004, **689**, 2123.
196 J. Louie and R. H. Grubbs, *Chem. Commun.*, 2000, **1363**, 1479.
197 L. Deng, E. Bill, K. Wieghardt and R. H. Holm, *J. Am. Chem. Soc.*, 2009, **131**, 11213.
198 D. F. Evans, *J. Chem. Soc.*, 1959, 2003.
199 A. L. Companion and M. A. Komarynsky, *J. Chem. Educ.*, 1964, **47**, 257.
200 C. M. M. Rohlfing, L. C. Allen and R. Ditchfield, *J. Chem. Phys.*, 1983, **79**, 4958.
201 R. K. Ã, M. Tollinger, G. Kontaxis and B. Kra, *Spectroscopy*, 1999, **982**, 961.
202 W. A. Herrmann, G. Gerstberger and M. Spiegler, *Organometallics*, 1997, **16**, 2209.
203 T. Wagner and U. Englert, *Struct. Chem.*, 1997, **8**, 357.
204 J. B. Waters, R. S. P. Turbervill and J. M. Goicoechea, *Organometallics*, 2013, **32**, 5190.
205 K. Matsubara, K. Ueno and Y. Shibata, *Organometallics*, 2006, **25**, 3422.
206 J. P. Coyle, G. Dey, E. R. Sirianni, M. L. Kemell, G. P. A. Yap, M. Ritala, M. Leskelä, S. D. Elliott and S. T. Barry, *Chem. Mater.*, 2013, **25**, 1132.
207 S. Díez-González, E. C. Escudero-Adán, J. Benet-Buchholz, E. D. Stevens, A. M. Z. Slawin and S. P. Nolan, *Dalt. Trans.*, 2010, **39**, 7595.
208 P. de Frémont, N. M. Scott, E. D. Stevens, T. Ramnial, O. C. Lightbody, C. L. B. Macdonald, J. A. C. Clyburne, C. D. Abernethy and S. P. Nolan, *Organometallics*, 2005, **24**, 6301.
209 P. de Frémont, N. M. Scott, E. D. Stevens and S. P. Nolan, *Organometallics*, 2005, **24**, 2411.
210 P. De Frémont, N. M. Scott, E. D. Stevens, T. Ramnial, O. C. Lightbody, C. L. B. Macdonald, J. A. C. Clyburne, C. D. Abernethy and S. P. Nolan, *Organometallics*, 2005, **24**, 6301.
211 B. Liu, Y. Zhang, D. Xu and W. Chen, *Chem. Commun.*, 2011, **47**, 2883.
212 A. J. Arduengo, H. V. R. Dias, J. C. Calabrese and F. Davidson, *Organometallics*, 1993, **12**, 3405.
213 H. Kaur, F. K. Zinn, E. D. Stevens and S. P. Nolan, *Organometallics*, 2004, **23**, 1157.
214 B. R. M. Lake and C. E. Willans, *Organometallics*, 2014, **33**, 2027.
215 A. O. Larsen, W. Leu, C. N. Oberhuber, J. E. Campbell and A. H. Hoveyda, *J. Am. Chem. Soc.*, 2004, **126**, 11130.
216 J. J. Van Veldhuizen, J. E. Campbell, R. E. Giudici and A. H. Hoveyda, *J. Am. Chem. Soc.*, 2005, **127**, 6877.
217 J. Yun, D. Kim and H. Yun, *Chem. Commun.*, 2005, **942**, 5181.
218 E. L. Kolychev, V. V. Shuntikov, V. N. Khrustalev, A. A. Bush and M. S. Nechaev, *Dalt. Trans.*, 2011, **40**, 3074.
219 Y. Wang, B. Quillian, C. S. Wannere, P. Wei, P. V. R. Schleyer and G. H. Robinson, *Organometallics*, 2007, **26**, 3054.
220 M. H. Al-Afyouni, V. M. Krishnan, H. D. Arman and Z. J. Tonzetich, *Organometallics*, 2015, **34**, 5088.
221 G. R. Fulmer, A. J. M. Miller, N. H. Sherden, H. E. Gottlieb, A. Nudelman, B. M. Stoltz, J. E. Bercaw and K. I. Goldberg, *Organometallics*, 2010, **29**, 2176.
222 J. W. Akitt and a. J. Downs, *Chem. Commun.*, 1966, 222.
223 B. M. Gridley, *m-Terphenyl Ligands in Transition Metal Chemistry*, 2013.
224 M. Tschinkl, R. E. Bachman and F. P. Gabbaï, *J. Organomet. Chem.*, 1999, **582**, 40.
225 M. Kaupp and H. G. Von Schnering, *Inorg. Chem.*, 1994, **33**, 2555.
226 D. Grdenic, *Q. Rev. Chem. Soc.*, 1965, **19**, 303.
227 M. Niemeyer and P. P. Power, 1997, **7333**, 3258.
228 L. Álvarez-Rodríguez, J. A. Cabeza, P. García-Álvarez and D. Polo, *Coord. Chem. Rev.*, 2015, **300**, 1.
229 Z. Zhu, R. J. Wright, M. M. Olmstead, E. Rivard, M. Brynda and P. P. Power, *Angew. Chem. Int. Ed.*, 2006, **45**, 5807.
230 G. A. Bain and J. F. Berry, *J. Chem. Educ.*, 2008, **85**, 532.
231 J. Cosier and A. M. Glazer, *J. Appl. Cryst.*, 1986, **19**, 105.
232 C. O. D. T. U. L. Y. England, .
233 I. . Uson and G. M. Sheldrick, *Curr. Opin. Struct. Biol.*, 1999, **9**, 643.
234 G. M. Sheldrick, *Acta Crystallogr. Sect. A Found. Crystallogr.*, 2008, **64**, 112.
235 G. M. Sheldrick, *Acta Crystallogr. Sect. A Found. Adv.*, 2015, **71**, 3.
236 L. Palatinus and G. Chapuis, *J. Appl. Cryst.*, 2007, **40**, 786.

237 O. V. Dolomanov, L. J. Bourhis, R. J. Gildea, J. A. K. Howard and H. Puschmann, *J. Appl. Cryst.*, 2009, **42**, 339.
238 D. A. Rice, G. W. A. Fowles and R. A. Walton, *J. Inorg. Nucl. Chem.*, 1969, **31**, 3119.
239 J. Huang and S. P. Nolan, *J. Am. Chem. Soc.*, 1999, **121**, 9889.
240 R. Bhatia, J. Gaur, S. Jain, A. Lal, B. Tripathi, P. Attri and N. Kaushik, *Mini. Rev. Org. Chem.*, 2013, **10**, 180.
241 B. Schiemenz and P. P. Power, *Organometallics*, 1996, **15**, 958.
242 C. Ni, J. C. Fettinger, G. J. Long and P. P. Power, *Inorg. Chem.*, 2009, **48**, 2443.
243 M. F. Semmelhack, H. P. M. and G. J. D., *J. Am. Chem. Soc.*, 1972, **94**, 9234.
244 J. A. Przyojski, K. P. Veggeberg, H. D. Arman and Z. J. Tonzetich, *ACS Catal.*, 2015, **5**, 5938.
245 L. Zhang, A. Wang, J. T. Miller, X. Liu, X. Yang, W. Wang, L. Li, Y. Huang, C. Y. Mou and T. Zhang, *ACS Catal.*, 2014, **4**, 1546.
246 I. Colon and D. Kelsey, *J. Org. Chem.*, 1986, **51**, 2627.
247 R. Stürmer, *Angew. Chem. Int. Ed.*, 1999, **38**, 3307.
248 P. Romanato, S. Duttwyler, A. Linden, K. K. Baldridge and J. S. Siegel, *J. Am. Chem. Soc.*, 2010, **132**, 7828.
249 T. Klis, D. R. Powell, L. Wojtas and R. J. Wehmschulte, *Organometallics*, 2011, **30**, 2563.
250 A. E. Carpenter, C. C. Mokhtarzadeh, D. S. Ripatti, I. Havrylyuk, R. Kamezawa, C. E. Moore, A. L. Rheingold and J. S. Figueroa, *Inorg. Chem.*, 2015, **54**, 2936.
251 T. B. Ditri, A. E. Carpenter, D. S. Ripatti, C. E. Moore, A. L. Rheingold and J. S. Figueroa, *Inorg. Chem.*, 2013, **52**, 13216.
252 H. Leitner, A, Furstner, A, Mendez, M, and Krause, *J. Am. Chem. Soc.*, 2002, **124**, 13856.
253 G. Cahiez, A. Moyeux, J. Buendia and C. Duplais, *J. Am. Chem. Soc.*, 2007, **129**, 13788.
254 G. Cahiez and A. Moyeux, *Chem. Rev.*, 2010, **110**, 1435.
255 G. Antonacci, A. Ahlburg, P. Fristrup, P.-O. Norrby and R. Madsen, *European J. Org. Chem.*, 2017, **2017**, 4758.
256 M. S. Kharasch and E. K. Fields, *J. Am. Chem. Soc.*, 1941, **63**, 2316.
257 A. Fürstner, *ACS Cent. Sci.*, 2016, **2**, 778.
258 B. D. Sherry and A. Fürstner, *Acc. Chem. Res.*, 2008, **41**, 1500.
259 A. Fürstner and A. Leitner, *Angew. Chem. Int. Ed.*, 2002, **41**, 609.
260 H. Shinokubo and K. Oshima, *European J. Org. Chem.*, 2004, **2004**, 2081.
261 I. Bauer and H. J. Knölker, *Chem. Rev.*, 2015, **115**, 3170.
262 D. A. Valyaev, G. Lavigne and N. Lugan, *Coord. Chem. Rev.*, 2016, **308**, 191.
263 J. R. Carney, B. R. Dillon and S. P. Thomas, *European J. Org. Chem.*, 2016, **2016**, 3912.
264 H. Takaya, S. Nakajima, N. Nakagawa, K. Isozaki, T. Iwamoto, R. Imayoshi, N. J. Gower, L. Adak, T. Hatakeyama, T. Honma, M. Takagaki, Y. Sunada, H. Nagashima, D. Hashizume, O. Takahashi and M. Nakamura, *Bull. Chem. Soc. Jpn.*, 2015, **88**, 410.
265 A. Fürstner, R. Martin, H. Krause, G. Seidel, R. Goddard and C. W. Lehmann, *J. Am. Chem. Soc.*, 2008, **130**, 8773.
266 M. Nakamura, K. Matsuo, S. Ito and E. Nakamura, *J. Am. Chem. Soc.*, 2004, **126**, 3686.
267 R. B. Bedford, D. W. Bruce, R. M. Frost and M. Hird, *Chem. Commun.*, 2005, 4161.
268 A. Hedström, Z. Izakian, I. Vreto, C.-J. Wallentin and P.-O. Norrby, *Chem. - A Eur. J.*, 2015, **21**, 5946.
269 G. Cahiez, V. Habiak, C. Duplais and A. Moyeux, *Angew. Chem. Int. Ed.*, 2007, **46**, 4364.
270 G. Lefèvre and A. Jutand, *Chem. - A Eur. J.*, 2014, **20**, 4796.
271 R. B. Bedford, *Acc. Chem. Res.*, 2015, **48**, 1485.
272 K. E. Rowland and R. D. Thomas, *Magn. Reson. Chem.*, 1985, **23**, 916.
273 J. C. Hierso, *Chem. Rev.*, 2014, **114**, 4838.
274 F. A. Cotton, G. Wilkinson, A. M. Carlos and M. Bochmann, in *Advanced Inorganic Chemistry*, 1999, pp. 599–629.
275 P. Wothers, N. Greeves, S. Warren and J. Clayden, *Organic Chemistry*, 2009.
276 H. R. Sharpe, *m-Terphenyl Transition Metal Complexes: Catalysis and Small Molecule Activation*, 2017.
277 B. M. Gridley, T. J. Blundell, G. J. Moxey, W. Lewis, A. J. Blake and D. L. Kays, *Chem. Commun.*, 2013, **49**, 9752.

278 A. D. Cardin, P. D. Ellis, J. D. Odom and J. W. Howard, *J. Am. Chem. Soc.*, 1975, **97**, 1672.
279 D. F. Evans and G. V Fazakerley, *J. Chem. Soc. A Inorganic, Phys. Theor.*, 1971, 182.
280 A. J. Blake, J. Shannon, J. C. Stephens and S. Woodward, *Chem. - A Eur. J.*, 2007, **13**, 2462.
281 K. D. Croft, *Ann. N. Y. Acad. Sci.*, 1998, **854**, 435.
282 A. Studer and D. P. Curran, *Angew. Chem. Int. Ed.*, 2016, **55**, 58.
283 L. Wang, L. Hu, H. Zhang, H. Chen and L. Deng, *J. Am. Chem. Soc.*, 2015, **137**, 14196.
284 J. Torres-Alacan and P. Vöhringer, *Int. Rev. Phys. Chem.*, 2014, **33**, 521.
285 R. Martin and A. Fürstner, *Angew. Chem. Int. Ed.*, 2004, **43**, 3955.
286 W. C. Lothrop, *J. Am. Chem. Soc.*, 1941, **63**, 1187.
287 C. D. Campbell and C. W. Rees, *J. Chem. Soc. C Org.*, 1969, 742.
288 B. C. Berris, Y. Lai and K. P. C. Vollhardt, *J. Chem. Soc. Chem. Commun.*, 1982, 953.
289 T. Schaub and U. Radius, *Tetrahedron Lett.*, 2005, **46**, 8195.
290 S.-L. Wang, M.-L. Pan, W.-S. Su and Y.-T. Wu, *Angew. Chem. Int. Ed.*, 2017, **56**, 14694.
291 R. A. Lewis, S. P. George, A. Chapovetsky, G. Wu, J. S. Figueroa and T. W. Hayton, *Chem. Commun.*, 2013, **49**, 2888.
292 Y. Chen, H. Sun, U. Flörke and X. Li, *Organometallics*, 2008, **27**, 270.
293 J. Li, C. Wang, X. Li and H. Sun, *Dalt. Trans.*, 2012, **41**, 8715.
294 P. Knochel and C. Diène, *Comptes Rendus Chim.*, 2011, **14**, 842.
295 C. Perthuisot, B. L. Edelbach, D. L. Zubris, N. Simhai, C. N. Iverson, C. Müller, T. Satoh and W. D. Jones, *J. Mol. Catal. A Chem.*, 2002, **189**, 157.
296 C. A. Laskowski, A. J. M. Miller, G. L. Hillhouse and T. R. Cundari, *J. Am. Chem. Soc.*, 2011, **133**, 771.
297 M. I. Lipschutz and T. D. Tilley, *Organometallics*, 2014, **33**, 5566.
298 C. B. Hansen, R. F. Jordan and G. L. Hillhouse, *Inorg. Chem.*, 2015, **54**, 4603.
299 H. R. Khavasi and A. Azhdari Tehrani, *Inorg. Chem.*, 2013, **52**, 2891.
300 S. J. Grabowski, *J. Phys. Org. Chem.*, 2004, **17**, 18.
301 B. F. Hoskins, R. Robson and E. E. Sutherland, *J. Organomet. Chem.*, 1996, **515**, 259.
302 X. Y. Tang, J. X. Chen, G. F. Liu, Z. G. Ren, Y. Zhang and J. P. Lang, *Eur. J. Inorg. Chem.*, 2008, **2**, 2593.
303 A. Saneei, M. Pourayoubi, A. Crochet and K. M. Fromm, *Acta Crystallogr. Sect. C Struct. Chem.*, 2016, **72**, 230.
304 A. Nimmermark, L. Öhrström and J. Reedijk, *Zeitschrift für Krist. - Cryst. Mater.*, 2013, **228**, 311.
305 M. M. D. Roy, M. J. Ferguson, R. McDonald and E. Rivard, *Chem. - A Eur. J.*, 2016, **22**, 18236.
306 I. S. M. Al-Rafia, P. A. Lummis, A. K. Swarnakar, K. C. Deutsch, M. J. Ferguson, R. McDonald and E. Rivard, *Aust. J. Chem.*, 2013, **66**, 1235.
307 J. Chai, H. Zhu, Y. Peng, H. W. W. Roesky, S. Singh, H.-G. Schmidt and M. Noltemeyer, *Eur. J. Inorg. Chem.*, 2004, **2004**, 2673.
308 A. A. Danopoulos, P. Braunstein, M. Wesolek, K. Y. Monakhov, P. Rabu and V. Robert, *Organometallics*, 2012, **31**, 4102.
309 C. G. Werncke, E. Suturina, P. C. Bunting, L. Vendier, J. R. Long, M. Atanasov, F. Neese, S. Sabo-Etienne and S. Bontemps, *Chem. - A Eur. J.*, 2016, **22**, 1668.
310 C. G. Werncke, P. C. Bunting, C. Duhayon, J. R. Long, S. Bontemps and S. Sabo-Etienne, *Angew. Chem. Int. Ed.*, 2015, **54**, 245.
311 Y. Marcus, *Chem. Rev.*, 1988, **88**, 1475.
312 L. Pauling, *J. Am. Chem. Soc.*, 1927, **49**, 765.
313 D. M. Kurtz, *Chem. Rev.*, 1990, **90**, 585.
314 S. J. Lippard, *Angew. Chem. Int. Ed.*, 1988, **27**, 344.
315 N. Hoshino, A. M. Ako, A. K. Powell and H. Oshio, *Inorg. Chem.*, 2009, **48**, 3396.
316 K. Zhou, S. Roy and C. bin Zhao, *Comput. Theor. Chem.*, 2017, **1110**, 35.
317 A. J. Bard and L. R. Faulkner, *Electrochemical Methods: Fundamentals and Applications*, 2000.
318 C. Boone, I. Korobkov and G. I. Nikonov, *ACS Catal.*, 2013, **3**, 2336.
319 A. K. Wiegand, A. Rit and J. Okuda, *Coord. Chem. Rev.*, 2016, **314**, 71.

320 M. Rauch and G. Parkin, *J. Am. Chem. Soc.*, 2017, **139**, 18162.
321 W. Sattler and G. Parkin, *J. Am. Chem. Soc.*, 2012, **134**, 17462.
322 K. Revunova and G. I. Nikonov, *Dalt. Trans.*, 2015, **44**, 840.
323 M. S. Khajavi, M. G. Dakamin and H. Hazarkhani, *J. Chem. Res.*, 2000, **2000**, 145.
324 P. Mathur, R. K. Joshi, D. K. Rai, B. Jha and S. M. Mobin, *Dalt. Trans.*, 2012, **41**, 5045.
325 Y. Kuninobu, K. Kikuchi and K. Takai, *Chem. Lett.*, 2008, **37**, 740.
326 H. A. Duong, M. J. Cross and J. Louie, *Org. Lett.*, 2004, **6**, 4679.
327 J. R. Hagadorn, J. Que and W. B. Tolman, *Inorg. Chem.*, 2000, **39**, 6086.
328 M. Palusiak, *J. Organomet. Chem.*, 2007, **692**, 3866.
329 V. Lavallo, Y. Canac, C. Präsang, B. Donnadieu and G. Bertrand, *Angew. Chem. Int. Ed.*, 2005, **44**, 5705.
330 M. Melaimi, R. Jazzar, M. Soleilhavoup and G. Bertrand, *Angew. Chem. Int. Ed.*, 2017, **56**, 10046.
331 S. Roy, K. C. Mondal and H. W. Roesky, *Acc. Chem. Res.*, 2016, **49**, 357.
332 T. S. Lobana, Rekha, R. J. Butcher, T. W. Failes and P. Turner, *J. Coord. Chem.*, 2005, **58**, 1369.